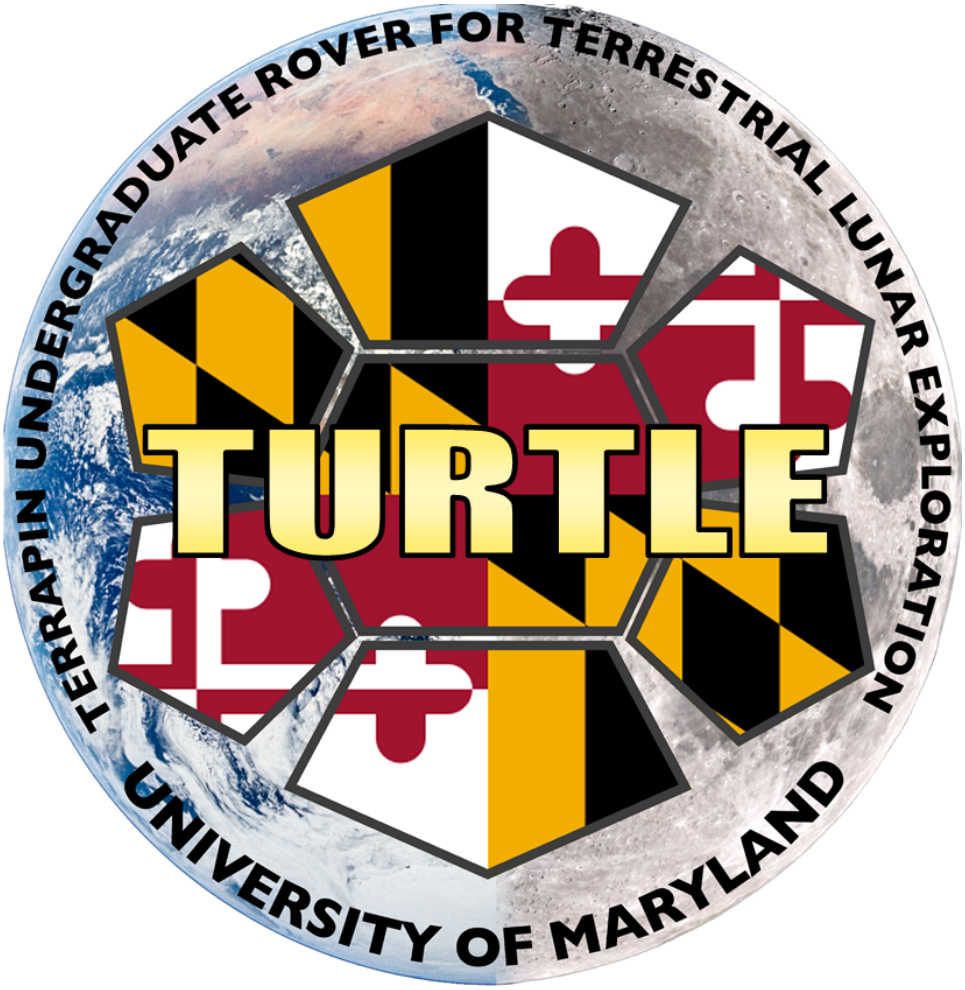

University of Maryland

ENAE484 Senior Design Project

Project TURTLE

Author:
ENAE484 Space Systems Design

Supervisors:
Dr. David L. Akin
Dr. Mary Bowden

May 12, 2008

Authors

Systems Integration

Kanwarpal Singh Chandhok
Joshua Colver
David Gers
Madeline Kirk
Thomas Mariano

Avionics

Andrew Ellsberry
Michael Levashov
Joseph Lisee
Jacob Zwillinger

Crew Systems

James Briscoe
Sara Fields
Ali Husain
Jason Laing
Adam Mirvis
Tiffany Russell

Loads, Structures and Mechanisms

Enrique Coello
Aaron Cox
Stuart Douglas
Ryan Levin
Brian McCall
David McLaren
Omar Manning
Jessica Mayerovitch
Zohaib Hasnain

Mission Planning

David Berg
May Lam
Ryan Murphy
Hasan Oberoi
Matthew Schaffer

Power, Propulsion and Thermal

Jason Leggett
Aleksander Nacev
Ugonma Onukwubiri
Stephanie Petillo
Ali-Reza Shishineh

We would like to thank the following groups for their support:

- Maryland Space Grant Consortium for generously funding our Rover Mock-up
- The Space Systems Lab for providing lab space for construction
- Dr. David Akin and Dr. Mary Bowden for their guidance and support throughout our project

Additional Credit:

- Exterior CAD: Jessica Mayerovitch
- Interior CAD: Jason Laing
- Lander CAD: Thomas Mariano
- Copy Editing: Joshua Colver, Madeline Kirk, Michael Levashov, Thomas Mariano, Ryan Murphy
- Paper Compilation: Ryan Murphy
- Bibliography: David Berg, Ryan Murphy

Contents

List of Tables

List of Figures

Nomenclature

ASLEP	Apollo Lunar Surface Experiments Package
CG	Center of Gravity
CME	Coronal Mass Ejection
DCU	Distributed Computing Unit
DDT&E	Design, Development, Testing, and Evaluation
EELV	Evolved Expendable Launch Vehicle
EVA	Extravehicular Activity
FOV	Field of View
FPGA	Field Programmable Gate Array
FPS	Frames per Second
GB	Gigabyte
GCR	Galactic Cosmic Radiation
GPS	Global Positioning System
HD	High Definition
HDCS	High Definition Camera System
IMU	Inertial Measurement Unit
ISS	International Space Station
LACE	Lunar Atmospheric Composition Environment
LH_2	Liquid Hydrogen
LIDAR	Light Detection and Ranging
LLO	Low Lunar Orbit
LME	Lunar Meteorite Experiment
LOC	Loss of Crew
LOI	Lunar Orbit Insertion
LOM	Loss of Mission
LOX	Liquid Oxygen
LPT	Low Power Transceiver
LRO	Lunar Reconnaissance Orbiter
LRV	Lunar Roving Vehicle

LSAM	Lunar Surface Access Module
LSM	Lunar Seismic Monitoring
LSG	Lunar Surface Gravimeter
LQR	Linear Quadratic Regulator
M	Mass of the Rover
m	Mass of a Part
MB	Megabyte
MCVA	Miniature Coherent Velocimeter and Altimeter
MI	Microscopic Imager
MOS	Margin of Safety
NASA	National Air and Space Administration
NRC	National Research Council
P-D	Person Days
PAF	Payload Attachment Fitting
PCS	PLSS Containment System
PEM	Proton Exchange Membrane
PLSS	Primary Life Support System
PVC	Polyvinyl Chloride
PWM	Pulse Width Modulator
RAM	Random Access Memory
RAT	Rock Abrasion Tool
RTG	Radioisotope Thermoelectric Generator
SEL	Single Event Latchup
SEU	Single Event Upset
SF	Safety Factor
SPE	Solar Particle Event
SSPC	Solid State Power Controller
TLI	Trans Lunar Injection
TRL	Technology Readiness Level
X	CG coordinate in x-direction
x	Coordinate on the rover, referenced from back of rear wheels
Y	CG coordinate in y-direction
y	Coordinate on the rover referenced to left of dust covers
Z	CG coordinate in z-direction
z	Coordinate on the rover reference up from ground

Chapter 1

Introduction

1.1 Project Overview (Madeline Kirk)

During the Apollo missions, the lunar surface was only explored in small localized areas either by walking or using the Lunar Roving Vehicle. To expand surface exploration, a method to allow astronauts to sleep, eat, and be protected as they explore must be developed. This paper describes the design of TURTLE the Terrapin Undergraduate Rover for Terrestrial Lunar Exploration, a pressurized lunar rover for astronauts to live in during sortie missions.

1.1.1 Project Goals and Mission Profile

The overall goal of Project TURTLE is to develop a small, pressurized, lunar rover that will support a crew of two astronauts for two three-day science missions with a two day contingency. On these missions TURTLE will provide transportation, shelter, and life support including food, water, and oxygen in a pressurized vehicle. For each mission the rover will travel 50 km total, traveling approximately 25 km away from the base. TURTLE will also support two-person Extra Vehicular Activity (EVA) with access to the lunar surface directly from the vehicle during the missions.

TURTLE will launch and rendezvous with the crew on the lunar surface. After descent and landing on the lunar surface TURTLE will perform a self check-out and autonomously disconnect from the lander. TURTLE will then autonomously travel up to 10 km to rendezvous with the four astronauts at the Lunar Surface Access Module (LSAM). Once TURTLE has been safely checked out for a crew mission, two crew members will board the rover and begin three-day independent mission traveling 25 km away from the LSAM. During the mission, crew members will perform several two-person EVAs taking samples and setting science equipment. They will also have the capabilities of driving short distances during EVA through an external driving platform. Astronauts will eat and sleep in the rover as well as perform basic analysis of samples gathered during EVA. After TURTLE returns to the LSAM, the remaining two crew members will board TURTLE for a

second three-day mission. TURTLE is designed to support a crew for eight days, therefore re-supply of the rover is not necessary before the second mission. At the conclusion of both missions, samples will be relocated to the lander ascent stage and return to earth with the astronauts.

1.2 Constellation Program (Kanwarpal Singh Chandhok)

1.2.1 Overview

The Bush administration, after being re-elected in 2004, announced a new vision for exploration to be implemented by the National Aeronautics and Space Administration (NASA). This vision was called The Constellation Program - Earth, Moon, Mars and Beyond. As President George W. Bush said, "This cause of exploration and discovery is not an option we choose; it is a desire written in the human heart." The Constellation Program targets precisely these words. As the caption suggests, it incorporates several different phases ranging from the retirement of the current space transportation fleet to the exploration of other planets.

The loss of the seven brave astronauts aboard the Space Shuttle Columbia on January 14, 2004 marked the aging shuttle fleet and a blurred vision needed a new direction with new hopes, which was the birth of the Constellation Program. Its overall program goals are [20]:

- Implement a sustained and affordable human and robotic program to explore the solar system and beyond.
- Extend human presence across the solar system, starting with a human return to the Moon by the year 2020, in preparation for human exploration of Mars and other destinations.
- Develop the innovative technologies, knowledge, and infrastructures both to explore and to support decisions about the destinations for human exploration.
- Promote international and commercial participation in exploration to further U.S. scientific, security, and economic interests .

These overall goals have many steps involved within themselves in order for them to be accomplished [25].

- The completion of the International Space station with international partners
- Retirement of the Space Shuttle fleet by 2010
- Development of the Crew Exploration Vehicle (CEV), Orion no later than 2016
- Return to the Moon no later than 2020
- Establish a Lunar Base for extended duration missions

- Robotic missions to Mars
- Human missions to Mars

The Constellation Program is driving the development of the next generation launch system, ARES, and Orion, which will be the crew carrying capsule. These developments are under way and the retirement of the Space Shuttle is on schedule.

1.2.2 Constellation Program and Project TURTLE

The question now is how is our Project TURTLE going to fit into the Constellation Program. Well, we target the goal of returning to the Moon and establishing a lunar base for extended duration missions. The plan starts of on the drawing board where we contemplate several important sites on the Moon to be explored. Once we have selected a few, we will initially execute three day sortie missions to those landing sites. These sortie missions will have two parts to them: The TURTLE rover will land on the Moon followed by a crew of two astronauts. The TURTLE rover will then act as a habitability ground for the astronauts as well as a mobility platform, which enables them to cover greater distances from the landing site for research and exploration. The TURTLE rover will prove a very important instrument as it will allow for extended duration sortie missions with minimal astronaut discomfort while covering ground that otherwise would require a whole new mission. As our rover is going to be pressurized, we can also test how the rover behaves as a small habitable environment on the lunar soil. We can also test out technologies like Suit Ports for ease of preparing for Extra Vehicular Activities (EVAs).

Once the sortie missions have yielded a good location to establish a lunar base, then our rover can be reconfigured slightly to serve as a support station while the base is being constructed. The astronauts can come in and take breaks, relax, and even take off their space suits. This will allow the astronauts to work more efficiently and subject them to less fatigue. Along with acting as a base support station, the TURTLE rover will serve as the mobility platform for the stationed astronauts. This will allow for longer duration missions while stationed on the base to explore more of the lunar surface.

1.3 Requirements (Madeline Kirk)

The following are the level one requirements defined at the beginning of the project. These requirements are the driving factors for the lunar rover design that were specified into level two requirements by specific teams.

1. The rover must be capable of launching on a lower-cost launch vehicle, and be a stand alone addition to a constellation sortie mission.

2. The lunar rover, along with all transportation infrastructure, shall be designed to launch on an existing EELV-class launcher or equivalent.
3. The rover shall be capable of autonomous landing on unimproved sites equivalent to those selected for J-class Apollo mission.
4. The rover shall be capable of autonomously off-loading from the lander.
5. The rover shall be capable of autonomously driving no more than 10km to rendezvous with the crew.
6. The rover shall be capable of supporting a three day mission with two crew members.
7. The rover shall be capable of traveling a 50 km radius from the lander with a total travel distance of 100 km between two sortie missions.
8. The rover must be pressurized and capable of surviving in a lunar environment for mission duration of eight days.
9. The rover shall accommodate crew sized ranging from 95th percentile American male to 5th percentile American female.
10. All crew interfaces shall be in accordance with NASA STD-3000.
11. Rover shall provide life support for nominal mission plus 48 hours contingency.
12. Rover shall support nominal two-person EVAs without cabin depressurization.
13. Access to and from the surface shall be compatible with safe transverses by pressurized subjects in Earth gravity.
14. Emergency egress options with pressure suits shall be available at all times.
15. Cabin atmosphere and pressure shall be chosen to provide safe zero-prebreathe egress.
16. Rover design shall ensure sufficient direct sight lines and illumination to allow safe driving in daylight or night conditions.
17. Rover shall have a maximum operating speed of at least 15 km/hr on level, flat terrain.
18. Rover shall be designed to accommodate a 0.5 m obstacle at minimal velocity.
19. Rover shall be designed to accommodate a 0.1 m obstacle at a velocity of 7.5 km/hr.
20. Rover shall be designed to accommodate a 20 degree slope in any direction at a speed of at least 5km/hr with positive static and dynamic margins.

21. Rover shall be capable of being controlled directly, in teleoperation, and autonomously.
22. Rover shall be capable of being driven while depressurized.
23. Rover shall be capable of communicating at HDTV rates direct to Earth.
24. Rover shall provide voice/data/video to and from pressure suits during EVAs.
25. All critical systems shall be two-fault tolerant, with instrumentation for status monitoring.

1.4 Rover Variations (Madeline Kirk)

The TURTLE design is based off of the requirements listed in a previous section. However, due to the flexible nature of the project, modifications were made to the lunar design to account for other programs or functions. The four rovers are the Lunar Rover, Mock-up Rover, Outpost Rover, and Field Rover. While the Lunar Rover and Mock-up are parallel designs that feed one another, the outpost and field rovers are supplimental designs based off the lunar design.

1.4.1 Lunar Rover

The lunar rover, or flight rover, shown in Figure 1.1 is the baseline design for the different rover variations and is derived from a series of level one requirements distributed at the beginning of the semester. The lunar rover will be launched and land on the moon to perform two sortie missions. The lunar rover is designed to survive in the space environment and is entirely self-contained in terms of consumables (i.e., fuel, food, water, air). One of the major defining points is that the lunar rover is a "disposable" rover that is only meant to survive for two three-day sortie missions with a two-day contingency. As such, there are no designed methods for specifically refueling or replenishing the rover for additional missions.

1.4.2 Mock-up Rover

The rover mock-up is a low fidelity mock-up of the lunar rover cabin that was used as a design tool. It was initially derived from lunar rover designs, but through testing influenced TURTLE's final design. The goal of constructing the mock-up was to allow team members to see and feel how the dimensions and placement of interior items influence comfort and ease of use in the cabin. Testing was isolated to console design, interior layout, window size and placement, sleeping options, and suitport operations and functionality. The funds to support the construction of the TURTLE mock-up came from Maryland Space Grant Consortium. As shown in Figure 1.2 the mock-up has a simple exterior and functional interior for focused testing.

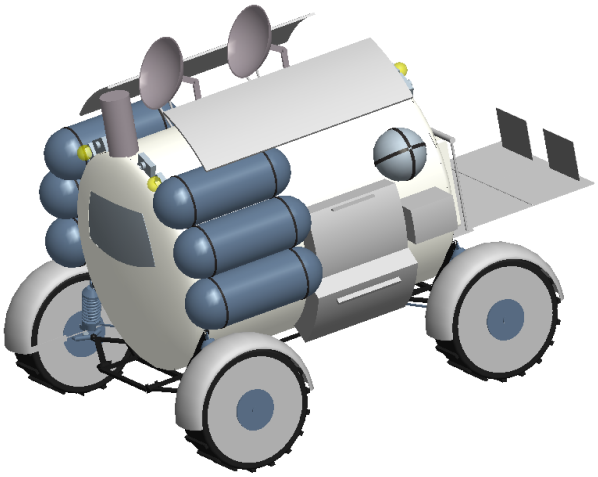

Figure 1.1: CAD Model of Lunar TURTLE

Figure 1.2: Mock-up Rover at Rollout

1.4.3 Outpost Rover

Part of the Constellation Program is to develop a lunar outpost to support long duration missions on the moon. With some modifications, TURTLE can also be used as a support and multi-use rover for the outpost. Similar to the original lunar rover, the outpost rover can, as a minimum, go on three-day missions and support a crew of two people. However, upon return, consumables in TURTLE are replenished and damaged parts are serviceable. Outpost TURTLE will also have a shirt-sleeve entrance so the rover can dock with the outpost and allow easy access for servicing and replenishing the interior of the vehicle. It is designed for multiple missions and an extended life on the lunar surface. The outpost rover will be discussed in Section 11

1.4.4 Field Rover

To test the concept of a pressurized lunar rover for surface exploration, a high fidelity mock-up of TURTLE was designed to provide a means for Earth testing in a simulated lunar environment. The field rover design is based off the lunar rover with modifications to account for changes on Earth including, increased gravity, external atmosphere, and a nearby support team. Unlike the cabin mock-up, the Field TURTLE would be capable of supporting a three-day test mission in the desert with two crew members performing EVAs and living in the cabin. The Field TURTLE also would be capable of independent movement and power generation. Although the hardware is not flight ready, the field rover is a high fidelity mock-up used to test the overall concept and major systems of the rover.

Chapter 2

Science Goals

2.1 Lunar Science (Matthew Schaffer)

2.1.1 Science Objectives

The science objectives for our mission were determined to bridge a connection between TURTLE and NASA's goal of returning to the moon and building a lunar base. It also must conform to NASA's proposed plan in their lunar architecture, which is to model early return missions after J-class Apollo missions 15, 16, and 17 [22]. The objectives decided upon for TURTLE are to:

- Deploy science equipment to enable long-term collection of data
- Collect data that will contribute to the design of the lunar base
- Learn more about the moon's structure and environment
- Obtain samples for study on Earth
- Perform a basic analysis of samples on the lunar surface
- Increase understanding of lunar habitability

Increasing our understanding of lunar hability is one objective that is inherent to the mission. Astronauts will live in TURTLE for a nominal duration of three days per sortie. During this time they will deploy the science equipment, survey the surface, and search for various sites in order to collect a diverse range of samples to be analyzed.

Science equipment will be deployed during the first sortie operation in order to allow adequate time to resolve any issues that arise. These issues could range from simple difficulties in deploying equipment to hardware or software failures that ground control must work to determine whether a workaround solution is available.

2.1.2 Science Package

Table 2.1: Breakdown of the Science Package

Component	Dimensions (cm)	Volume (cm^3)	Mass (kg)
RTG	40.6 x 46.0	59,552	19.6
LSM	23.0 x 29.0	12,049	11.5
LSG	27.7 x 25.4 x 38.4	27,017	12.7
LACE	32.3 x 30.5 x 19.8	19,506	7.4
LME	33.7 x 16.5 x 31.8	17,682	9.1
Total		135,806	60.3

The science package is the main hardware that will be deployed during the mission. The science package consists of devices including the Lunar Seismic Monitoring (LSM), Lunar Surface Gravimeter (LSG), Lunar Atmospheric Composition, and Lunar Meteorite Experiments (LME). It also contains the Radioisotope Thermoelectric Generator (RTG) which is used to power the equipment.

2.1.2.1 Power

While TURTLE has a fully-functional power system, the science package requires its own power source. Acquiring power from TURTLE is not plausible since the equipment must remain stationary. Additionally, TURTLE is not designed to produce power for the long duration necessary for collecting data through these devices.

To fulfill the requirement of powering these devices for years, TURTLE uses a RTG. Radioisotope Thermoelectric Generators generate power from the heat of a radioactive element without moving parts [18]. Model SNAP-27 was used in the Apollo missions to power the Apollo Lunar Surface Experiments Package (ALSEP) and generated between 70 to 80 Watts of power from 3 kg of fuel. An isotope of plutonium, Pu-238, is a radioactive fuel with a long half-life of 87.7 years [18]. Due to the relatively simple nature of RTGs, this makes it an ideal candidate for powering our equipment.

There is a major caveat in the use of RTGs. Pu238 is in limited supply due to its nature. As of a 2005 inventory for the United States supply of Pu238, there is only 39.5 kg available of the fuel source [21]. It may need to be obtained from outside sources such as Russia, unless a new, reliable technology is developed.

Solar power was also considered, but ultimately not used due to several factors. Solar generators require constant exposure to sunlight, which varies depending on location and is also be affected by the topography of the selected site. The dust on the moon also poses a major issue. Dust is perturbed during landing and takeoff, by astronauts during EVA, by the rover, and by meteorites. The dust can settle on the solar panels and diminish its ability to convert sunlight to power. Initially,

this could be handled by allowing the experiments to collect data for a limited range of time, but eventually power would be cut off completely and the experiments would end.

2.1.2.2 Lunar Seismic Monitoring Experiment

The LSM is a seismometer that monitors and measures moonquakes. A study performed from 2004 to 2006 of the data that was collected by the Apollo Passive Seismic Experiment through 1977 found that there were various moonquakes that could be classfied into four categories. Three of the four classifications are vibrations that are considered harmless and result from meteorite impacts, crust expansion when the surface begins to warm after periods of extreme cold, and quakes occuring 700 km beneath the surface [49].

The fourth type of moonquake, shallow quakes, could pose complications to the design of any structure built on the moon. In a five year span leading up to the deactivation of the seismometers, twenty-eight of these quakes were recorded. Each of them lasted longer than ten minutes, a duration five times the duration of the longest earthquake, with some quakes reaching magnitudes comparable to a 5.5 on the Richter scale [49]. Any earthquake with a magnitude greater than five is capable of causing structural damage.

The LSM experiment will renew monitoring of moonquakes focusing on studying shallow quakes to find out more about their frequency and whether there are any warning signs leading up to a quake. With subsequent missions, a new seismic network could be established and allow for pinpointing of any hotspots where seismic activity may be more active. A completely new network of seismometers must be installed, since the devices from Apollo cannot be reactivated due to insufficient power. This was discovered in 1986 when NASA unsuccessfully attempted to reactivate the seismometers [85].

2.1.2.3 Lunar Surface Gravimeter Experiment

The LSG experiment has the same purpose and function as in Apollo. Originally deployed during Apollo 17, the LSG was intended to measure the moon's gravity flux over time to the nearest 10^{-11}g. An error in manufacturing prevented successful operation of the experiment and future repairs were unsuccessful [98].

The main component is a spring balance capable sensing subtle changes in the gravity field around the moon. Through these subtle changes, the LSG is used as a receiver searching for the existence of gravity waves. In conjunction with the LSM, the data obtained through the LSG can be used to study the moon's structure and the tidal effects [98].

2.1.2.4 Lunar Atmospheric Composition Experiment

A version of the Lunar Atmospheric Composition Experiment (LACE) was conducted during Apollo 17. LACE was moderately successful except for the inability to operate during peak sunlight hours

when the surface is at its highest temperatures [98]. This problem was due to insufficient thermal shielding, which is an issue that was prevalent throughout Apollo.

TURTLE will advance LACE by monitoring the composition of the gases during both the lunar day and night to gain a complete set of data as possible. Two spectrometers will be used to complete the experiment; one oriented vertically and a second oriented parallel to the surface. The vertically oriented spectrometer will measure the gases as they appear in the atmosphere and while they exit into space. The horizontal spectrometer will measure gases that escape from beneath the surface and from gases trapped in meteorites and other debris from space that collided on the surface.

2.1.2.5 Lunar Meteorite Experiment

The Lunar Meteorite Experiment (LME) is an adaptation to the Apollo 17 Lunar Ejecta and Meteorites experiment. The experiment is designed to use three sensors to measure characteristics of meteorites and the occurred on impact. During Apollo, it originally appeared to be working correctly, but began picking up anomalous data [98].

The LME will focus on understanding the frequency of meteorite occurrences at a specific location. Sensors will be aligned to detect characteristics such as the meteorite's velocity, which would play a part in designing the long-term meteorite shielding for the lunar base. Verification of meteorite impact will come from the seismometer of the LSM experiment, which will detect the resulting vibration that occurs.

2.1.2.6 Additional Consideration

As the lunar base is designed, it will be necessary to understand the effects of the lunar environment on the materials of the structure. Building a structure that is meant to endure years of the raw environment of the moon will different from something designed to handle last days or months. TURTLE could be used to deploy some of the materials that would be used in the construction of the lunar base. Future missions can then return to the deployment site for these materials and run more advanced tests. Another possibility is to use the remote or autonomous driving systems to leave TURTLE in a location that would allow for a future mission to return and analyze the effects of long-term lunar exposure. This would be especially useful to determine the effectiveness of micrometeorite shielding over a long period of time.

2.1.3 Sampling

As in Apollo, sampling will be a major task for astronauts in the mission. To determine how many samples we can expect the astronauts to collect given their time on the surface of six to eight hour EVAs per day, the number of samples and their total mass had to be examined. As shown in Table 2.2, Apollo missions 15, 16, and 17 were a significant improvement over the earlier missions due to

the use of the Lunar Roving Vehicle (LRV), which increased the distance the astronauts could cover and the mass they could take with them.

Table 2.2: Samples Taken Througout Apollo [43]

Mission	Sample Mass	Samples Taken	Average Sample Mass (kg)
Apollo 11	21	58	.372
Apollo 12	34	69	.498
Apollo 14	43	227	.186
Apollo 15	77	370	.209
Apollo 16	94	731	.131
Apollo 17	110	741	.149

TURTLE can cover 50 km of terrain over a three-day sortie with a total of 100 km traversed over two sorties. This means that the potential exists for astronauts to collect more samples for study. Figure 2.1 shows a plot of samples taken for each Apollo mission from 11 to 17, excluding 13. To provide a basis for samples taken during TURTLE's mission, an exponential regression on the data was performed, which provided a close fit with an R^2value of 0.97. The equation obtained through the regression is $y = .276e^{.447x}$ where x is the mission number and y is the number of samples obtained.

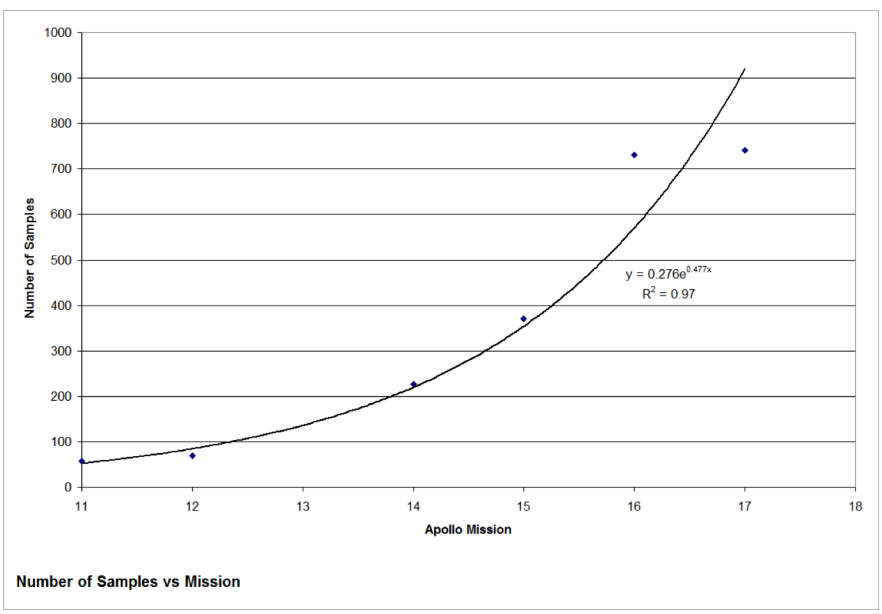

Figure 2.1: Number of Samples vs Apollo Mission

Using this equation, an estimate for the number of samples can be extrapolated for the next mission. Using $x = 18$ as the TURTLE mission, it is predicted that approximately 1480 samples

can be obtained. With an average sample mass of 0.163 kg/sample, which is obtained by averaging the latter three average masses from Table 2.2, this provides a total estimated mass of 240 kg over the duration of the mission.

Astronauts will use the external driving platform to find sites near each EVA location for diverse sampling. A broad range of samples allows more information to be learned about the moon's history and the history of the solar system.

In the current plan for the CEV used to return to the moon, astronauts will be able to return with approximately 100 kg of samples [23]. This means that over the course of the mission, there are many opportunities to study samples that would otherwise be discarded due to mass contraints. To address this, astronauts will be doing basic onsite analysis of samples. Astronauts will use modified versions of the Microscopic Imager (MI) and the Rock Abrasion Tool (RAT), which are currently used on the Mars Exploration Rovers [29]. The RAT exposes the interior of samples by scraping layers off and brushing the surface to allow a clean view of the grain of the sample [93]. The MI can then be used to photograph these samples with a resolution of 1024 x 1024 so that scientists can analyze them on earth without requiring additional mass on the return trip [70].

There are several advantages to performing onsite analysis of samples. Since the samples are not leaving their natural environment, there is no risk of altering them through exposure to other environments. Also, it allows for the study of samples that would otherwise have to be ignored due to mass contraints.

2.1.3.1 Sampling Equipment

An itemized list of sampling equipment can be seen in Table 2.3. The equipment was determined by going through the Apollo catalogue to find what tools were used in the later missions [43] and comparing the number of samples taken in Apollo's three-day period to the amount of samples we can obtain in TURTLEs two three-day missions.

Sampling equipment can be broken down into two categories: tools and containers. Tools enable collection of samples and the containers are used to store the collected samples during the EVAs and return trip. One addition to the tools is the core drill. During Apollo, coring was an arduous process that involved astronauts slowly hammering drive tubes into the surface and then slowly extracting them [98]. A core drill should simplify this process. Modifications will be made to current designs for lunar use, which include the addition of thermal shielding to the motor and the design of a battery power system. The return containers are the same as those used in Apollo for return trips. In Apollo, only two containers were taken to store two sample collection bags each, leaving the rest to exposure in the crew cabin of the lunar module [43]. For TURTLE, the same will have to be done, since the containers are heavy and adding enough for all samples is not feasible. If the containers are stored on the crew lander, then more possibly be added.

Table 2.3: List of Sampling Tools for TURTLE

Qty	Tool	Dimensions (cm)	Volume (cm^3)	Mass (kg)
1	RAT	7 x 10	38.5	0.685
1	MI	10.5 × 7.0 × 7.1	522	0.27
1	Core Drill	~40x15x45	27000	3.2
10	Core Tube	4.4 × 42	2554	0.5
1	Hammer	39 × 16 × 38	2110	1.3
1	Scoop	11.4 × 5.1 × 15.2	2470	0.59
2	Tongs	40x12x24	11520	0.23
2	Extension Handle	Rod x 3: 5.0 x 25.3 Handle: 15.5 x 5 x 10	2762	0.82
1	Rake	29.4 × 29.4 × 32.7	10740	1.5
1	Sample Scale	35 x 3 x 3	315	0.23
12	Sampling Bag Dispenser	6.0 × 23.0	2601	0.44
8	Sample Collection Bag	42 × 22 × 15	13860	0.76
8	Extra Collection Bag	42 × 22 × 15	13860	0.56
4	Return Container	48 × 30 × 20	28800	6.7
		Total:	**120000**	**56**

2.2 Landing Site Selection (David Berg)

2.2.1 Requirements

A few level 1 requirements given at the start of the project were relevant to selecting a landing site for the flight rover.

- The rover shall be capable of autonomous landing on unimproved sites equivalent to those selected for a J-class Apollo mission.
- The rover shall be designed to accomodate a 0.5 m obstacle at minimal velocity.
- The rover shall be designed to accommodate a 20° slope in any direction at a speed of at least 5 km/hr with positive static and dynamic margins.

Extra criteria were derived for the purpose of focusing the selection process.

- No major obstacles should be visible near the landing area in the surface imagery studied.
- Planned mission routes cannot cross any lunar terrain containing a slope greater than 20°.
- Landing site colongitude[1] must be considered when planning the timing between rover landing and crew landing; while the rover does not require sunlight to land safely, the crew does.
- The site must contain multiple science objectives that contribute to human understanding of the Moon.

A general mission plan was also developed which influenced the search for appropriate landing sites.

- TURTLE lands on the Moon after launching on an EELV from Earth.
- A crew of four astronauts lands on the Moon at a maximum distance of 10 km from the rover's position.
- TURTLE autonomously rendezvous with the crew to begin sortie activities.
- Two astronauts stay on station at the crew landing site while the other two board TURTLE and perform their mission objectives for 3 days, driving 50 km to accomplish them.
- The two crews switch places and TURTLE's second crew performs their mission objectives for 3 days, driving another 50 km.
- Approximately 24 hours on the lunar surface are dedicated to preparations for each sortie mission, switching crews, etc.
- The crew returns to Earth and leaves TURTLE on the lunar surface, totaling 7 days of human activity and 100 km of driving on the Moon.

[1] Colongitude is defined as the longitude of the morning terminator.

2.2.2 Site Selection Process

The site selection process began by determining what a J-class Apollo mission was. Research revealed a simple naming scheme that NASA scientists came up with for the different types of missions performed during the Apollo era [106]. Mission types were assigned with the letters A through J, A-class missions being unmanned test flights and J-class missions being extended manned missions with a focus on intense scientific investigation of the lunar surface. The J missions also featured an improved version of the Lunar Module that was capable of larger sample returns and equipped with new science instrumentation [89].

The first research done on landing sites was examining some of the landing sites that were selected for Apollo, but were never explored due to the program being cut short. This was done primarily because the guidelines for site selection were not yet fleshed out and the definition of a J-class mission was still unclear. It was safe to assume that any landing site selected for the later Apollo missions could be classified as a J mission, and as long as the site had enough territory to be explored, it would fit into the mission plan. It was then made clear that the project was geared toward sites featuring multiple science objectives that could be accomplished on two sortie missions. This essentially came to mean the project was going to be integrated into the Constellation program.

Because the mission plan for the TURTLE rover was supposed to integrate into NASA's Constellation architecture, the next step in the site selection process was to research what NASA's science goals are for their return to the Moon. This would help narrow the focus of the search and provide insight to places that NASA may consider in the future. In 2007, the NRC published a document that gave NASA suggestions for science objectives that could be accomplished in their Vision for Space Exploration [53]. The 107 page report identified major long term goals for lunar exploration, as well as some high-priority landing sites that potentially contain critical information to scientific understanding of the formation of the Moon and the early solar system.

To aid in studying the lunar surface and selecting potential landing sites, the 3D space simulator Celestia [31] was used. The default lunar imagery was replaced with an add-on [1] that contains high-resolution mapping obtained from the 1994 Clementine mission.

2.2.3 Landing Sites Considered

Note: all coordinate data in Table 2.4 and all images in this subsection were captured in Celestia unless otherwise noted.

2.2.3.1 South Pole - Aitken Basin

The NRC highlighted the South Pole - Aitken basin as a site that could contain samples of the lower lunar crust and possibly the lunar mantle [53]. Access to these geologic sections of the Moon

[2] coordinate data is for the approximate center of the basin

Table 2.4: Coordinate data for considered landing sites

Site Name	Latitude	Longitude
South Pole - Aitken basin[2]	61.9^{o}S	179.2^{o}E
Schrödinger basin	75.0^{o}S	132.4^{o}E
Gassendi crater	17.5^{o}S	39.9^{o}W
Tycho crater	43.3^{o}S	11.2^{o}W
Mare Nectaris	15.2^{o}S	35.5^{o}E
Copernicus crater	9.7^{o}N	20.0^{o}W
Kepler crater	8.1^{o}N	38.0^{o}W
Tsiolkovsky crater	20.4^{o}S	129.1^{o}E
Mare Crisium	18.5^{o}N	66.5^{o}E
Plato crater	51.6^{o}N	9.3^{o}W
Archimedes crater	29.7^{o}N	4.0^{o}W
Mare Fecunitatis	7.8^{o}S	51.3^{o}E
Aitken crater	16.8^{o}S	173.4^{o}E
Mare Orientale	19.4^{o}S	92.8^{o}W

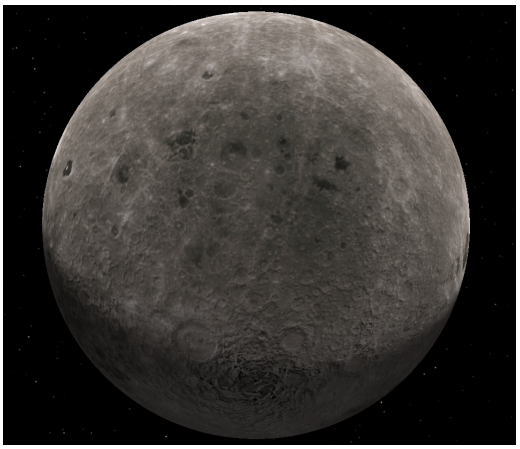

(a) Albedo of SPA

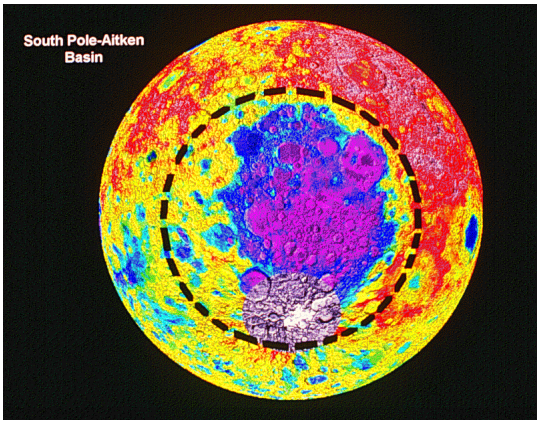

(b) Topography of SPA (NASA image)

Figure 2.2: South Pole - Aitken Basin

could give scientists hints as to what the internal structure of the Moon looks like, and may even provide evidence for the validity of the giant impact hypothesis[3]. Samples from this area can also help determine the age of the basin, which can be used to test the terminal cataclysm hypothesis[4]. Figure 2.2a shows the basin, which is the central region that appears to have a lower albedo than the areas around it. It is the largest impact basin on the Moon with a diameter of roughly 2500 km [53]. Since it is such a large area, sortie routes must be planned carefully to accomplish as much scientifically as possible. The best places to find samples of the lower crust and mantle are in the lowest topographical regions of the basin, which are the dark purple areas of Figure 2.2b.

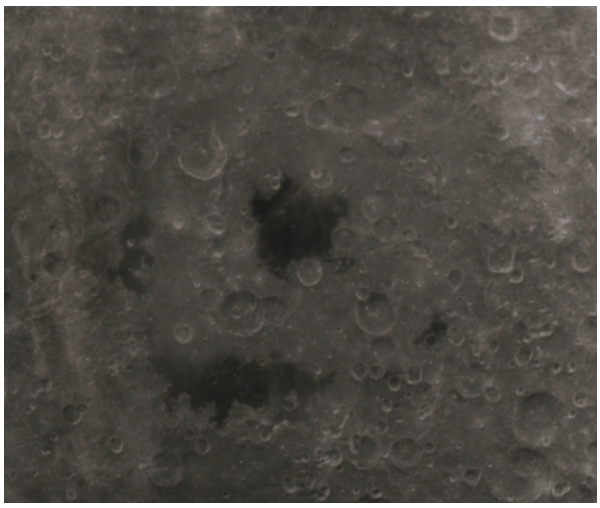

(a) Apollo basin, containing low altitude mare-like areas

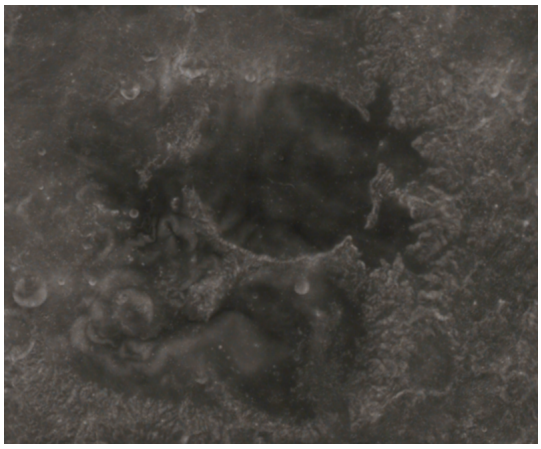

(b) Thomson crater north-east of Mare Ingenii

Figure 2.3: Two low-lying areas in the South Pole - Aitken Basin

Two of the lowest spots as seen in Figure 2.2b are the Apollo impact basin and Thomson crater. Apollo is located at 36.9^{o}S, 151.6^{o}W and is approximately 505 km in diameter [80]. Low areas in Apollo are generally the darker mare-like spots in the crater (see Figure 2.3a). Thomson is located at 33.7^{o}S, 164.9^{o}E, practically right on top of Mare Ingenii, and is about 117 km in diameter [40]. Figure 2.3b reveals that a large amount of ejecta from other impacts has been deposited in the crater, evidenced by the areas with a lighter albedo. Given that finding samples of the lower crust and lunar mantle is the science objective of the highest priority, the mission routes planned for the South Pole - Aitken basin would originate from these low-lying areas.

[3]The giant impact hypothesis is a theory that the Moon was created when another planet that existed in the early solar system collided with Earth. Debris from the impact was ejected into orbit around the wounded Earth and slowly collected to form the Moon.

[4]The terminal cataclysm hypothesis theorizes that the Earth-Moon system experienced a bombardment of meteorites that formed many of the large impact basins on the Moon. The spike in impacts is estimated to have occurred about 4 billion years ago.

2.2.3.2 Schrödinger Basin

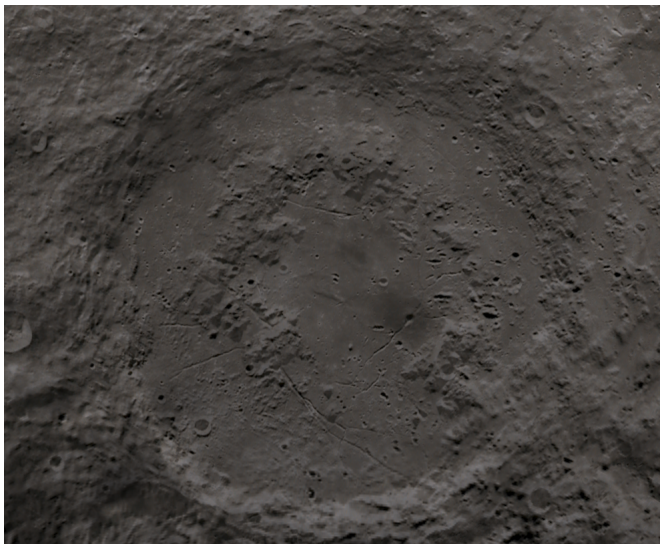

Figure 2.4: Schrödinger Basin

Located relatively close to the lunar south pole, Schrödinger basin may be a possible candidate for a lunar outpost site. The basin is approximately 320 km in diameter and features a unique inner ring of mountain ranges [17]. The area within the inner ring is smooth and flat, which is probably the best location for an outpost. A few rilles blemish the surface, including one inside the inner ring that appears to have spewed volcanic ash onto the regolith[96] (see Figure 2.4). The primary scientific interest here is sampling the mountain ranges for lunar soil that may have been pushed up by the impact, and also the ash ejected from the rille. Another important thing to note is that Schrödinger is actually within the South Pole - Aitken Basin. This could mean that the high-priority science objectives outlined for the South Pole - Aitken Basin can be pursued within Schrödinger basin. According to Figure 2.2b, the lowest area of the crater is in the north-east, which is the best place to look for samples of lunar mantle. If it can be better determined that Schrödinger's topography is low enough for mantle samples to be retrieved, sortie routes would originate from this area. In this case, the route would have to pass through the inner ring in order to sample the volcanic ash. There do appear to be some breaks in the mountain ranges, but the length of the route required to navigate this area may require the landing site to be pushed closer to the inner ring, which is hazardous and should be avoided if possible.

2.2.3.3 Gassendi Crater

Gassendi crater is located on the northern edge of Mare Humorum. It is roughly 110 km in diameter and contains a large system of rilles that run throughout. The crater was an alternate site for Apollo

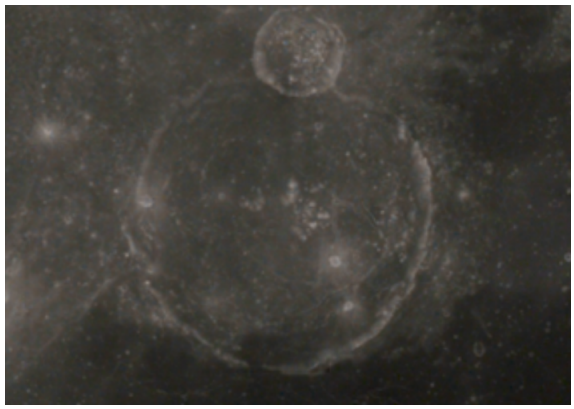

Figure 2.5: Gassendi Crater

17, which deemed its terrain too rough for exploration with the Lunar Roving Vehicle [3]. One of the primary science objectives at this site is to determine the relationship between the auxiliary crater Gassendi M (south-easternmost white spot inside the crater in Figure 2.5) and the parent crater Gassendi [53]. The outcome could affect the crater counts that have been done by scientists in the past, as some craters previously thought to be independent small impacts could be related to bigger impacts [53]. Another objective is to explore and sample the lava rilles in Gassendi's floor. Samples of Gassendi's southern dark spot and Mare Humorum can also be taken for comparison, which may reveal some relation to the age of the two. Finally, the crater wall should be examined, especially in the south where it appears to thin out.

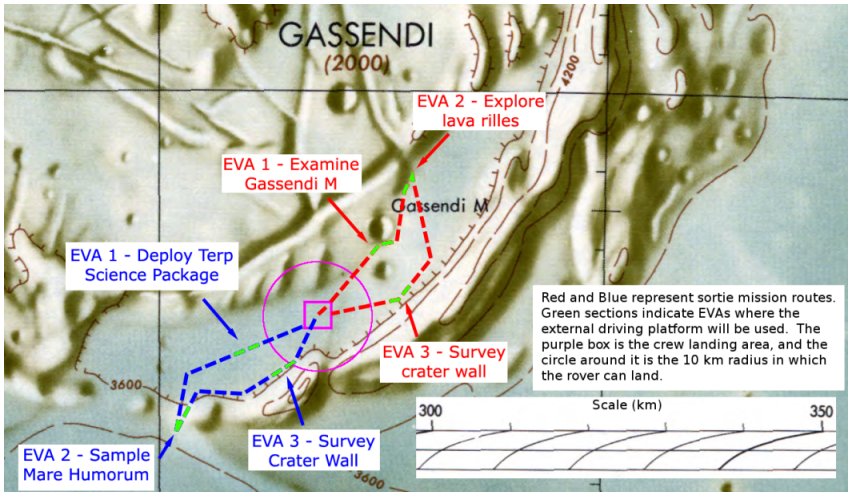

Figure 2.6: Sample Mission Outline for Gassendi Crater

A sample mission outline was created for Gassendi crater, wherein a landing site was chosen,

sortie routes were planned, and EVAs were plotted along the routes (see Figure 2.6). All of the science objectives discussed for Gassendi are addressed in this mission and are noted by the EVA in which the objective is accomplished. The sample mission outline was created to establish a basic idea that could be applied to any site chosen for a mission involving TURTLE. A landing site would be picked, taking into consideration where the crew would land and where the rover could potentially land for that given area. From there, sortie routes are plotted such that the science objectives for the landing site can be addressed. EVAs are then mapped along the routes so that experiments can be performed appropriately and samples can be taken.

2.2.3.4 Tycho Crater

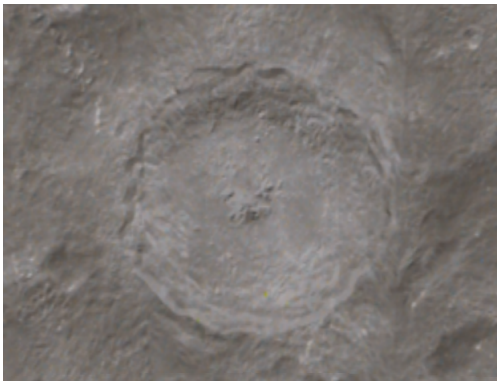

Figure 2.7: Tycho Crater

Tycho crater, one of the most prominent features on the Moon, sits approximately at the half-way point between the equator and the south pole. It is a lunar hot spot, meaning the floor of the crater stays warmer longer than most other parts of the lunar surface [78]. Scientists discovered this when they observed the Moon through infrared telescopes during lunar eclipses. Tycho is approximately 85 km in diameter and is estimated to be about 100 million years old based on samples taken during Apollo 17 [17].

The main scientific interest of this site is determining an accurate age of the impact crater, which will help establish lunar impact chronology that is precise [53]. There is also interest in the central peaks, as Clementine imagery has revealed the soil in the mountains is a different geologic composition than the rest of the crater floor [10]. The terrain within Tycho is variably rough, with the safest place to land being in the southwest close to the central peaks. This is advantageous since the central mountain range is of significant interest. Aside from driving inward to examine and sample the central peaks, numerous samples of the crater floor and surrounding hilly terrain will help accomplish the objective of dating the impact site. Sortie routes must be carefully planned here because of how rough the surface is, even at resolutions slightly below 1 km/pixel. Higher

resolution imagery from NASA's Lunar Reconnaissance Orbiter [7] can better determine whether or not a sortie mission here is feasible.

2.2.3.5 Mare Nectaris

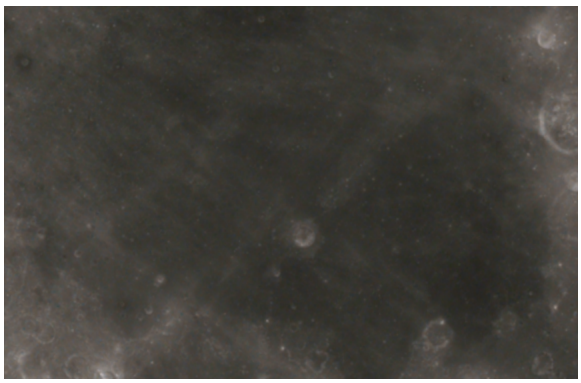

Figure 2.8: Mare Nectaris

Nestled between two other maria on the near side, Mare Nectaris spans a diameter of 333 km [37]. It contains Rosse crater in the south-west, which has been streaked by ejecta from Tycho crater (see Figure 2.8). The terrain is essentially flat throughout, containing small pinhole craters that speck the surface. The main scientific goals of exploring this site is to test the terminal cataclysm hypothesis, as it contains impact-melt rocks that will help determine its age [53]. In the case that Tycho is deemed unsafe for human exploration using TURTLE, the ejecta found in Mare Nectaris could be sampled to contribute another approximate age of the crater. Sortie routes at this site would most likely originate near Rosse crater so it could be examined and sampled on an EVA. This also gives a close proximity to the Tycho ejecta found north-east of the crater.

2.2.3.6 Copernicus Crater

Copernicus crater, about 93 km in diameter, is estimated to be one of the youngest impact craters on the Moon at slightly under 1 billion years old [17]. Its nebulous ejecta system can be seen in Figure 2.9. The crater features a steeply terraced wall and a rocky floor, especially to the south. Scientifically, the goals for exploring Copernicus are similar to Tycho. Because of its relatively young age, it is important to date the impact that formed it, which would anchor the lunar geologic time scale[5]. Again similar to Tycho, samples of the central peaks are desired, as they could contain deep lunar soil that was pushed up from the impact. Mission routes inside of Copernicus crater would likely originate from the northeast where the terrain is fairly flat. The challenge is to find a way

[5]The Moon is currently in the Copernican Era, which is defined by when this impact crater was formed.

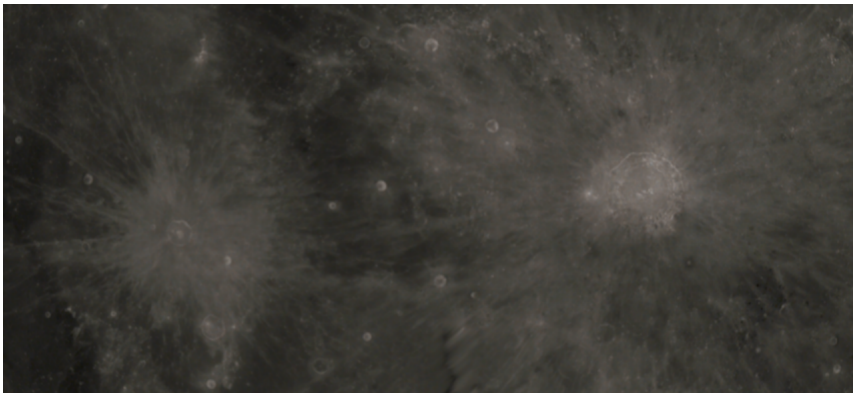

Figure 2.9: Kepler Crater (left) and Copernicus Crater (right)

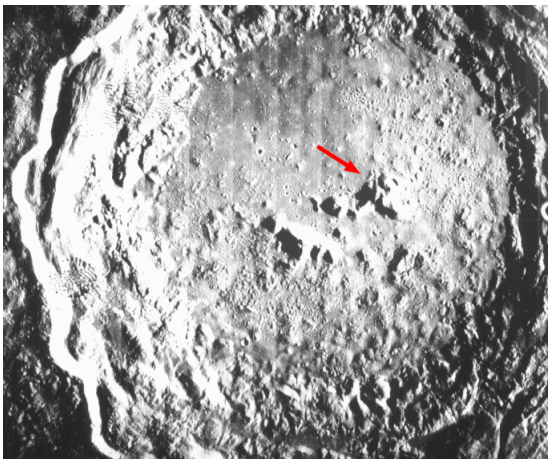

Figure 2.10: Opening in rocky terrain allowing passage to central peak (NASA image)

through the rocky terrain near the central peaks so they can be sampled. There is an opening to the easternmost peak that appears passable from Lunar Orbiter imagery (see Figure 2.10), although it is not certain whether the slope in this area can be navigated by TURTLE.

2.2.3.7 Kepler Crater

Kepler, a crater that spans only 31 km in diameter [28], is found close to Copernicus, giving it the appearance of a younger brother (see Figure 2.9). It is very small in comparison to other craters considered for TURTLE, so small that landing inside of it might be hazardous and would greatly reduce the amount of ground TURTLE could cover. Since this is the case, landing at Kepler would occur outside the impact floor and a study of the crater would be conducted by looking inward. The science to be conducted here would primarily focus on dating the crater to determine its relation to the younger craters on the Moon, such as Tycho and Copernicus. This would be done by sampling its ray system, which has coated the regolith immediately surrounding it. Another objective would be to study the relation of some of the auxiliary craters that surround Kepler, similar to the study in the Gassendi sample mission outline. A landing site about 20 km to the east of the crater would be ideal, since this would put TURTLE within reach of two auxiliary craters, A and B, as well as the crater wall.

2.2.3.8 Tsiolkovsky Crater

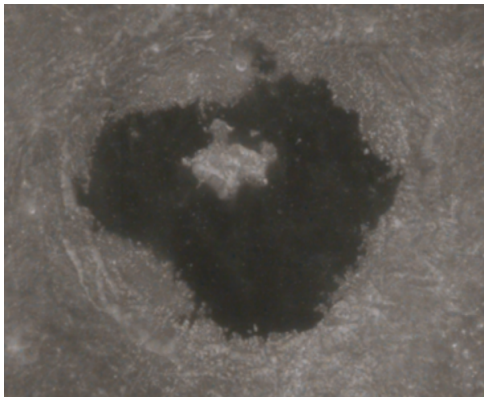

Figure 2.11: Tsiolkovsky Crater

Probably the most unusual crater on the Moon, Tsiolkovsky is a 180 km-wide impact feature on the lunar farside [68]. Its mare-like floor is a rare sight in the midst of a heavily cratered highland area. The interest in this site was determining how the crater formed, as well as the composition of the mountain range and crater wall within. The science objectives are to sample these areas to confirm their geologic structure, as well as examining the slight branch containing dark soil in the

crater wall located in the north-east. Since the floor is fairly flat, landing near the north-east tip of the mountain range would allow TURTLE to access these features within the limits of the sortie routes. The distance between the north-eastern tip of the peaks and the branch in the crater wall is about 40 km, which leaves about 5 km for deviations in each sortie.

2.2.3.9 Mare Crisium

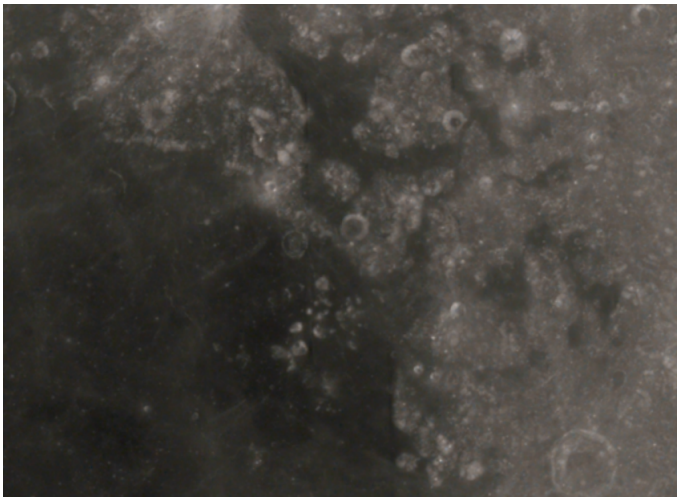

Figure 2.12: Eastern mountainous region on the edge of Mare Crisium

The eastern edge of Mare Crisium hosts an area of high albedo mounds. The primary scientific objective for landing in this area is to study and sample these hills to determine their composition and origin. Samples can also be taken of the mare to confirm its composition. Landing in Mare Crisium should be of little concern, as the entire surface is quite flat. The landing area for the mission in consideration would be just north-west of the hills. Mission routes here would weave throughout the cluster of mounds, one route going counter-clockwise, the other going clockwise.

2.2.3.10 Plato Crater

Plato crater lies just north of Mare Imbrium in the highlands of the nearside. It is 101 km in diameter [66] and has been the subject of intense study by astronomers because of the visual anomalies associated with it [108]. It appears that material from other impacts have sprayed onto the low albedo deposits of Plato's surface, namely on the northern rim and the western rim. The floor is very flat, making landing inside the crater a simple task. Science objectives at Plato are to examine as many of its mini craters as possible and to sample the crater wall. The most efficient place to land for these mission objectives would be close to the pair of mini craters in the northern

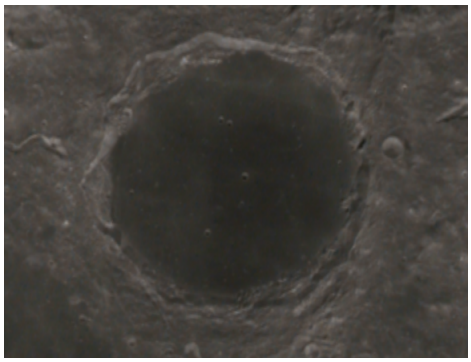

Figure 2.13: Plato Crater

half of the crater floor. Sortie routes would be aimed at the central mini crater in one direction and the crater wall in the other.

2.2.3.11 Archimedes Crater

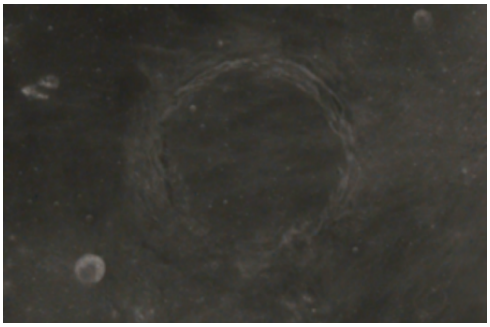

Figure 2.14: Archimedes Crater

Lying within Mare Imbrium, Archimedes crater very much resembles Plato crater in that it features an inner floor completely flooded by lava. It is the largest impact crater in Imbrium, stretching 83 km in diameter [66]. Landing inside of Archimedes should be easy, as the majority of the floor is quite flat. The main scientific objective of this landing site would be to find samples of pyroclastic deposits on the southern rim, which are associated with a low albedo [66]. To accomplish this, landing would occur in the south-west quadrant of the crater floor. One sortie route would be assigned to find pyroclastic samples on the southern rim, while the other route could drive north to examine and sample the formation protruding from the western rim. Higher resolution imagery would again be helpful in determining the feasibility of the latter, as the terrain could actually be somewhat hilly.

2.2.3.12 Mare Fecunditatis

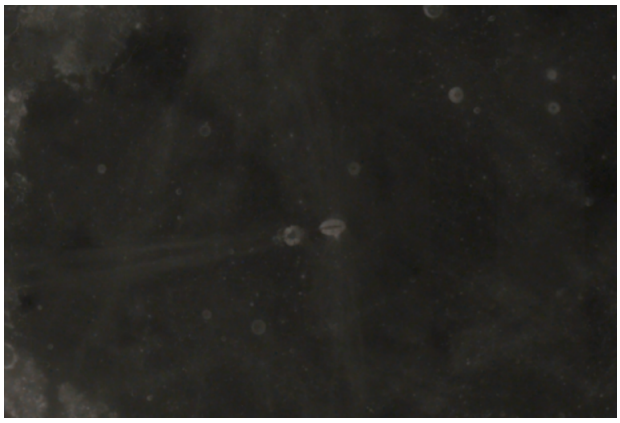

Figure 2.15: Messier A (left) and Messier (right) craters in Mare Fecunditatis

Mare Fecunditatis, sandwiched by Nectaris and Tranquillitatis, stretches out a broad 690 km from north-west to south-east [27]. It contains multiple ghost craters, which is a nickname for craters that have been buried by lunar geologic processes and ejecta from other impacts [107]. The main objective of exploring Mare Fecunditatis is to examine the craters Messier and Messier A (see Figure 2.15). Other features that could be examined are Messier B (above Messier) and the wrinkle-ridge that is approximately 10 km above it. A good place to land to accomplish these goals would be about 10 km above Messier within its ray system. One sortie route would explore the two craters to the south while the second sortie would travel north to examine Messier B and the wrinkle ridge.

2.2.3.13 Aitken Crater

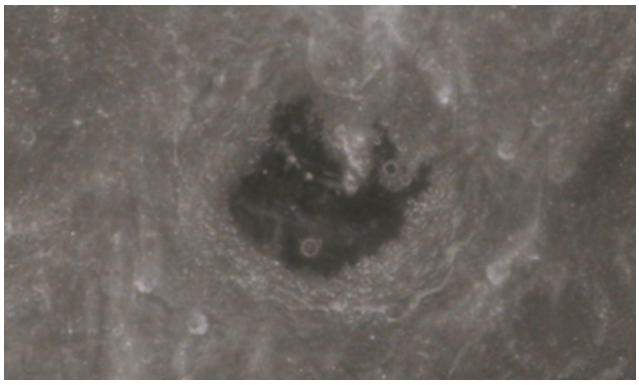

Figure 2.16: Aitken Crater

Aitken crater is 120 km in diameter and features an inner peak and an auxiliary impact crater on its northern wall [99]. This feature marks the northern rim of the South Pole - Aitken Basin, from which the basin got part of its name. The main science objectives at Aitken crater are obtaining samples of the crater floor and the crater wall. The inner peak could also be examined, though it is possible that the terrain is too rough for TURTLE to traverse. Higher resolution imagery from the Lunar Reconnaissance Orbiter will confirm whether or not this is true. Sortie routes would originate at the flat area in the south-eastern part of the crater floor and extend to the south along the crater wall and the north towards the inner peak.

2.2.3.14 Orientale Basin

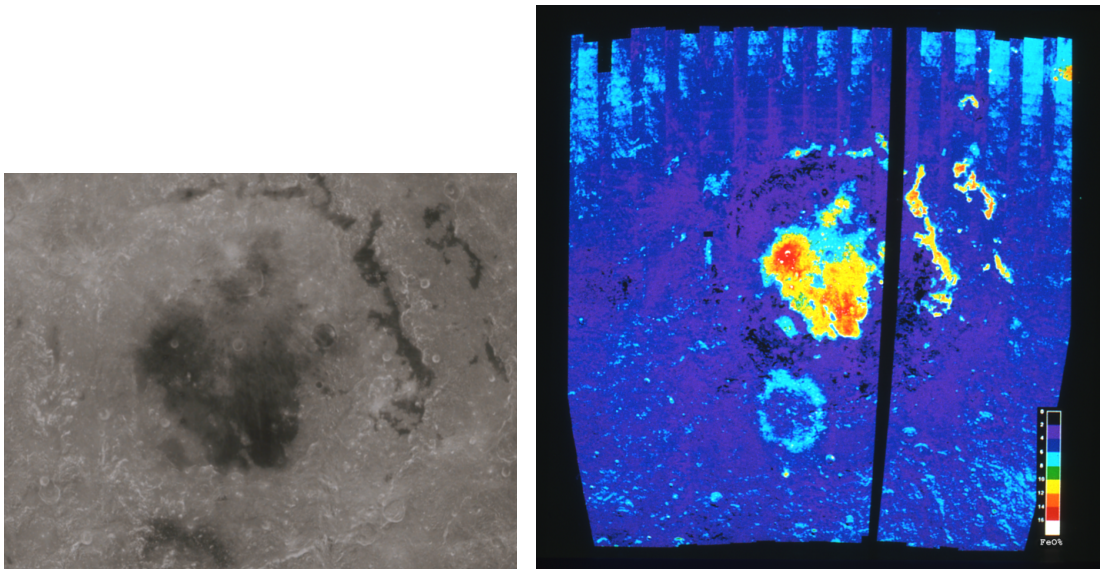

(a) Albedo image of Orientale basin

(b) Iron concentration in Orientale basin (NASA image)

Figure 2.17: Images of Orientale Basin

The Orientale basin is the impact basin that defines the beginning of the Upper Imbrian period on the lunar geologic time scale. It has a diameter of 930 km, the rim being outlined by the Cordillera Mountains [5]. The basin has never been sampled, so the date of the impact is not very accurate. This is the primary scientific objective of this landing site, similar to Tycho and Copernicus. An accurate date of the impact basin will provide another anchor to the Moon's geologic time scale. A good area to land in this basin is in the south-west near the edge of the mare, as there are a variety of rock types in this area [96]. This can be seen in Figure 2.17b as the purple channel on the bottom left of the heavily iron-concentrated area in the middle. The scant black areas in this figure represent places where nearly pure anorthosite can be found [96], which could be preserved

lunar crust [53]. Mission routes at this site would simply accomodate the need to find samples of each soil type.

Chapter 3

Launch and Landing

3.1 Launch Vehicle (May Lam)

3.1.1 Launch Vehicle Trade Study

As part of the Level One Requirements, the rover, and all landing and propulsion infrastructure, must be able to launch on an existing Evolved Expendable Launch Vehicle (EELV). To determine the best choice for the mass and dimensional configurations of our rover, a trade study was done. Several current launch vehicles were considered, excluding ones that had exceedingly small payload masses. As shown in 3.1, the Ariane V and the Atlas V have smaller payload masses and length dimensions than the Delta IV. Additionally, while the Falcon 9 has significantly more mass capability than the other three launch vehicles it has not yet successfully launched system.

Table 3.1: Launch Vehicle Trade Study

Vehicle	Delta IV-H	Ariane V	Atlas V	Falcon 9
Max Payload to LEO (kg)	23,040	21,000	20,050	27,500
Payload Diameter (m)	5	5.4	5	3.6 or 5.2
Payload Length (m)	19.8	4.5	13.1	11.4
Successfully Launched	Yes	Yes	Yes	No

3.1.2 Delta IV Heavy

The Delta IV Heavy consists of three Common Booster Cores (CBC), each with an RS-68 engine. The fairing is 19.8 m in length and 5 m in diameter, and is made of a graphite-epoxy/foam core composite sandwich structure. The main CBC houses the payload and the second stage RL10-B2. Both engines run on LOX/LH_2 fuel. Due to space reserved for the acoustic blankets and fairing envelope, the usable static dimensions for our system are 17.1 m in length and 4.5 m in diameter.

3.1.3 Launch Environment

During launch, there were several factors that were considered in the design of the rover. In the first stage, steady state accelerations on the payload will reach up to 4.8 g's. Also during liftoff and transonic flight, the acoustic environment is at a maximum where the peak sound pressure level reaches around 135 dB. This pressure level represents a 95th percentile average space flight environment. To prevent dynamic coupling between the launch vehicle and payload modes the rover must be designed to produce fundamental frequencies above the minimum axial and lateral frequencies shown in Table 3.2. The acoustic blankets will reach up to a maximum temperature of 115 deg F. This temperature represents a worst-case, hot day launch condition. Generally these blankets will provide adequate protection and shielding for the payload from ascent heating and the radiation environment. The internal pressure decay inside the shroud is about 2.76 kPa/sec the absolute pressure will reach up to 110 kPa [102]. How these critical launch loads directly affected the design of the shell structure is discussed in the Structures section of this report.

Table 3.2: Launch Environment

Steady State Acceleration	1st Stage 2nd Stage	4.8 g 0.8 g
Peak Sound Pressure Level	f = 80 to 350 Hz	135 db
Static Envelope Requirements	Minimum Axial Frequency Minimum Lateral Frequency	30 Hz 8 Hz
Internal Pressure Decay		2.76 kPa/sec
Fairing Absolute Pressure	Minimum Maximum	97 kPa 110 kPa

3.2 Transfer Stages (Ryan Murphy)

3.2.1 Lunar Transfer Orbit

The Delta IV-H payload will launch the payload directly into a trans lunar injection orbit (TLI), with a maximum payload capacity of 10200 kg [102]. By launching directly into TLI, staging in low earth orbit is avoided, which increases the maximum landable mass on the lunar surface. Since mass was one of the driving constraints of the lunar rover design, landing the maximum amount of mass is necessary to sucessfully complete a worthwhile mission. The total time spent in TLI varies from 4-6 days, depending on the mission profile.

3.2.2 Low Lunar Orbit

After traveling through the TLI stage, the retro engine will provide a ΔV of 800 m/s to insert the payload into a low lunar orbit (LLO) of a 200 km nominal altitude. Although braking into LLO decreases the total amount of mass that can land on the moon, it provides a very real advantage to the mission. While in LLO, plane and inclination changes can change the orbit around the moon, creating a different ground track. If the landing site chosen for a particular mission is not on the ground track of the initial orbit, the orbit changes will allow the rover to reach several different landing sites. The rover is designed for up to a one day holding period in low lunar orbit.

3.2.3 Lunar Descent

While in lunar orbit, the rover will prepare for descent to the landing site. Minor corrections to the orbit can occur to accomodate the 10 km landing from the crew before beginning descent. The descent stage follows a Hohmann transfer ellipse to the lunar surface. A ΔV from the retro engine of 135 m/s initiates the descent following the transfer ellipse[1] During the lunar descent, the retro stage separation will occur at a 2000 m altitude.

3.2.3.1 First Descent Stage

During the first descent stage, the rover will reduce altitude from 200 km to 2000 m while following the transfer orbit to the surface. At the 2000 m altitude, braking will begin. During this point on the transfer orbit, the required ΔV to decelerate the rover is 1725 m/s. This large ΔV was the main factor in the retro engine selection. The time prior to braking with the retro engine is one hour, with two minutes required by the retro engine to provide the ΔV.

To separate the first stage from the second stage, several systems are required. The varying avionics systems will determine when separation is necessary. Once it has been determined that the stages must separate, an order is issued to separate the stages. Separation may be done using several technologies, including explosive bolts, diaphragm devices, and thrust reversal devices. To reduce complexity, explosive bolts will be used. However, to ensure staging occurs, linear shaped charge cords will be placed in the beams connecting the two stages and will also detonate (being ignited by the explosive bolt).

3.2.3.2 Second Descent Stage (David Gers)

After separation of the retro engine and associated fuel tanks, only the landing system and rover remain (see Figure 3.1). The reaction control system will then re-orient the lander so its z-axis is aligned with the radial direction of a moon-centered coordinate system. Since the lander will have a

[1]The ΔV of 135 m/s is required for a 200 km altitude orbit. As the altitude changes, the required ΔV will change; however, this effect is deemed insignificant since there is minimum variability for different orbits ($\sim$100 m/s).

horizontal velocity of about 30 m/s, thrusters will immediately begin firing to reduce that velocity to zero and ensure sufficient separation upon landing between the retro engine and the lander. After a short period of free fall, the larger vertical thrusters will fire and slow the lander to a hover at a height of about 1 m above the surface. If obstacle avoidance is necessary the thrusters can translate the rover to a more suitable landing site before turning off and allowing the legs to touch down onto the surface. The total time of descent is 80 seconds with a required ΔV of 80 m/s.

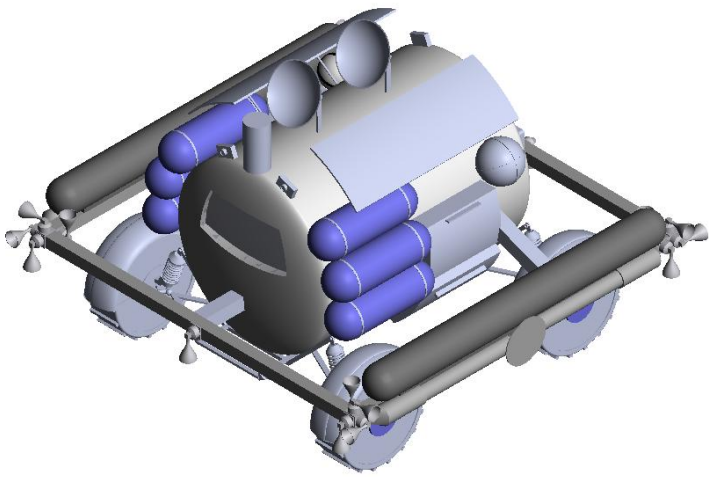

Figure 3.1: Rover in Landing Structure

3.2.4 Landing

The final descent of the rover will slow it down to negligible velocity slightly above the lunar surface. The thrusters will shut off, the landing legs will deploy and the rover and landing structure will drop to the surface (see Figure 3.2). After settling onto the ground, the legs will be blown off the landing structure using explosive bolts. The remainder of the landing structure will then be disconnected from the rover and drop to the surface. Since the rover has the capability of driving over a 0.5 m boulder, it will be able to drive over the landing structure, which will not protrude more than 0.3 m above the ground.

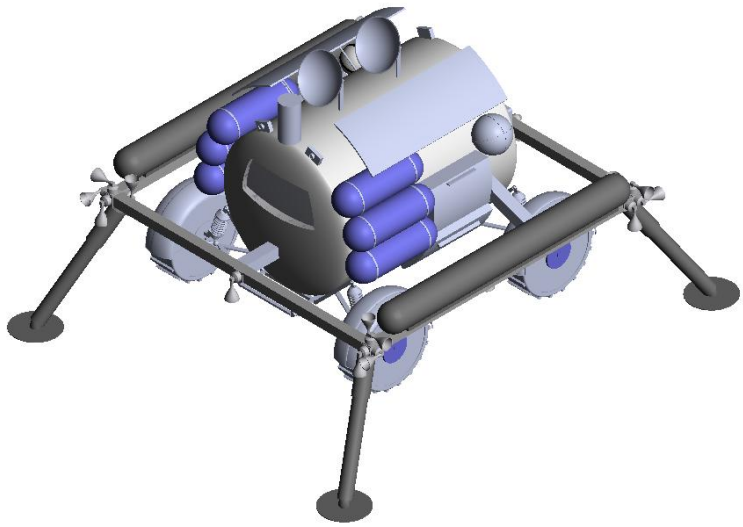

Figure 3.2: Final Landing Stage with Legs Deployed

3.3 Launch Vehicle Payload (Ryan Murphy)

3.3.1 Payload Overview

The payload carried on the launch vehicle can be divided into two distinct stages. The first stage consists of a retro engine and its associated fuel tanks and structure. The second stage consists of the rover and the landing system. To accommodate the dimensions of the payload, the government version payload shroud (5 m diameter, 19.8 m length) will be used. The 1575-5 payload attachment fitting (PAF) will be used as the attachment fitting in the Delta IV-H. The PAF integrates the launch vehicle with the payload through a circular interface measuring 1.575 m in diameter and is appropriate for the 5 m diameter payload shroud [102]. Although the Delta IV-H offers a total payload mass of 10200 kg [102], the PAF has a mass of 420 kg, reducing the usable payload mass to 9780 kg. Figure 3.3 shows the full payload structure inside the shroud, with the structural clutter removed. Details of the structure are presented in Section 3.3.5.

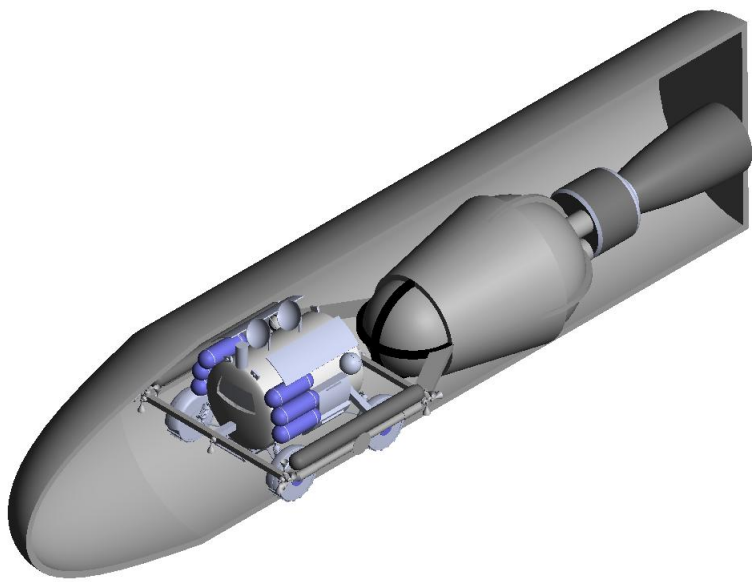

Figure 3.3: Payload in the Delta IV-H.

During flight and landing, avionics will determine position and make necessary course adjustments. The avionics and the propulsion systems, along with any other systems requiring power, will be powered by fuel cells. Solar arrays were the inital concept for power on flight, however, complications would arise if the payload system left sunlight and still require fuel cells. Thus, the amount of fuel cells was increased to account for the power lost by dropping solar arrays.

3.3.2 Stage One

The first stage of the payload structure will include a retro engine, the Pratt & Whitney Rocketdyne RL10A-4-2. Some characteristics of the RL10A-4-2 are described in Table 3.3. The retro engine trade study is covered in Appendix A.1. The retro engine and fuel tanks will be fully supported during launch. Figure 3.4 depicts the first stage of the landing system.

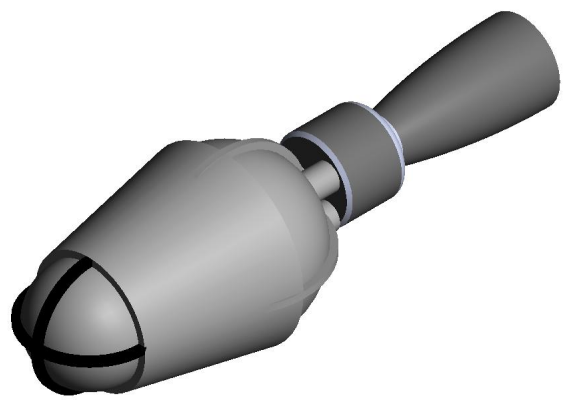

Figure 3.4: First Stage of the Landing System

Table 3.3: RL10A-4-2 Specifications

Thrust	99.1 kN
Mass	167 kg
Fuel/oxidizer	Liquid hydrogen (LH_2)/Liquid oxygen (LOX)
Mixture ratio	5.5:1
Specific Impulse	451.0 s

3.3.3 Stage Two

The second stage consists of the landing system and the rover. During transit, several smaller thrusters will provide reaction control and station keeping, while larger thrusters will provide the necessary thrust to brake the rover. After separation of the first stage, thrusters placed in the horizontal direction will mitigate residual horizontal velocities such that the two stages do not collide during final descent. Figure 3.1 shows the rover and lander configuration during launch.

Since the landing structure and rover constitute one single stage, they must be connected. To reduce the amount of forces applied to the landing structure during launch, the rover and landing structure will be independently supported in the Delta IV-H payload shroud.

3.3.4 Payload Mass

The total payload to TLI on the Delta IV-H is 10200 kg. The breakdown of the total usable payload mass is described in Table 3.4. The fuels for each stage all include a 20% margin to incorporate boil-off and provide extra fuel if required. The structural interfaces to the payload fairing has a 30% margin incorporated into the 685 kg mass. Systems without a margin are those that exist and have a fixed, known mass.

Table 3.4: Launch Vehicle Payload Mass

Component	Mass (kg)
Rover	2500
RL10A-4-2	167
Stage 1 and Launch Integration Structure (30% margin)	685
LH_2 (including 20% margin)	740
LH_2 Tank	416
LOX (including 20% margin)	4100
LOX Tank	382
Landing Structure	350
Landing/RCS Thruster	90
N_2H_4 (including 20% margin)	280
N_2H_4 Tank	70
Total Usable Payload	9780

3.3.5 Attachment Points

Due to the lack of accesible data on the Delta IV-H payload fairings, the structural interfaces to the launch vehicle have been difficult to construct. However, the retro engine, along with all of its fuel tanks, will be supported directly by the payload fairing. The fuel tank support is designed to be a shroud containing both of the fuel tanks. Additionally, the shroud and retro engine will be attached to the payload shroud to help mitigate launch loads. Due to time constraints, these were unable to be modeled in the CAD diagram or effectively analyzed; with further time and experience, a realizable structure based off the design describe above can be created.

The rover and landing system will be isolated on launch. This allows the payload fairing to mitigate the launch loads, as opposed to the landing system handling its loads in addition to the rover loads. A strut structure has been designed and analyzed that effectively mitigates launch loads on the rover. This structure is shown in Figure 3.5 and analyzed further in Section 4.3.2.1 .

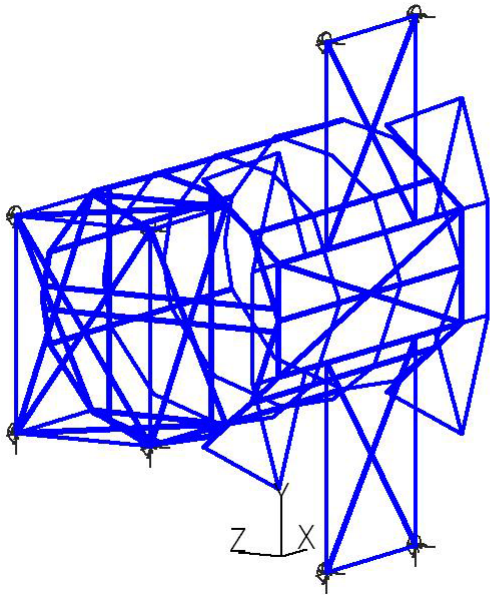

(a) Skew view.

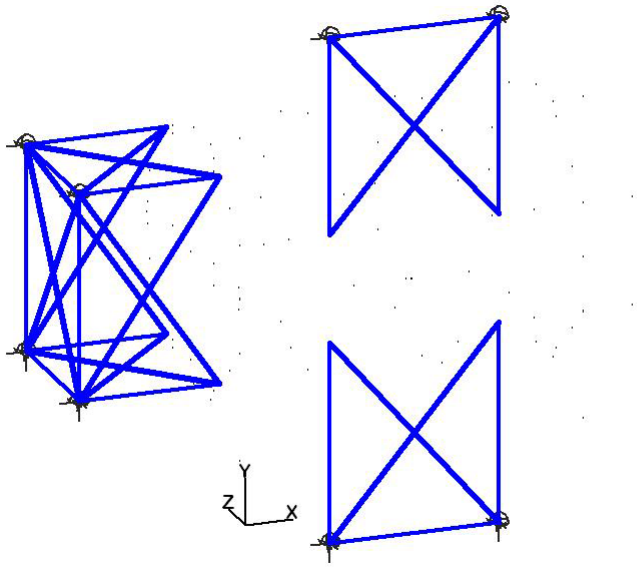

(b) Supports only.

Figure 3.5: Two Views of Attachment Structure

3.4 Landing Avionics (Michael Levashov)

The launch vehicle will inject the rover into a lunar transfer orbit and after that the vehicle on-board systems will be responsible for successful rendezvous with the astronauts. There will be communication with the ground, which will be primarily concerned with monitoring the state of the mission. So, the on-board sensors, actuators and controllers will be responsible for actually delivering the rover to the Moon. The driving parameter in the design is the soft landing, during which a small error can result in a catastrophic failure of the whole system.

3.4.1 Operation During Transfer and Landing

As the rover starts traveling in the lunar transfer orbit, it will monitor its state using a star tracker and by ranging from satellites. If the orbit doesn't match the desired trajectory, the on-board computer will instruct the Reaction Control System (RCS) to make the necessary corrections. In addition, the computer will use the same RCS to control the attitude of the vehicle to maximize the effectiveness of solar arrays, while pointing the directional antenna at Earth.

When the position in orbit reaches a certain point, the computer will use the RCS to re-orient the lander for a burn of the main engine, putting it into a different orbit. The parameters of the new orbit would then be re-acquired using ranging from satellites and a star tracker. After another re-orientation of the vehicle and a small burn, the lander will enter the descent orbit.

In the descent orbit, the rover will again determine its orbital elements from position and attitude measurements and will make small corrections to the course using the RCS. At a certain point in orbit, the lander will rotate itself and start measuring the range to the lunar surface. At a certain altitude above the Moon surface, the vehicle will start to monitor ground velocity and make slight course corrections to make sure it has the desired velocity. As the resolution of the ground sensors increases with decreasing altitude, the vehicle will be able to make finer corrections. Upon reaching a certain point in the descent orbit, the lander will perform its final burn, drop off the main thruster, change orientation and proceed to descend to the ground. During the final descent the velocity and distance to ground will be monitored and corrected by RCS to ensure a soft landing. Finally, at an altitude of about 1 m, the lander will deactivate its engines and drop to the ground.

During all of the burns and changes of orientation, feedback to the thrusters will be provided by an on-board inertial system, consisting of accelerometers and angular rate gyroscopes. The attitude of the vehicle will be carefully monitored throughout the burns, so that the thrust vector is applied in the correct direction. The rover on-board computer will interface with sensors, run the controllers and actuators, and communicate with Earth.

3.4.2 Landing Avionics Requirements

3.4.2.1 Altitude

The landing procedure calls for the lander to turn off all thrusters at about 1 m altitude, to prevent them from excessively kicking up dust, while not letting the rover to fall too far down, generating unnecessary velocity. In order to turn off the engines at about 1 m, the computer needs to know the position more accurately than 1 m. This design assumes that knowing the altitude to within 0.5 m will be sufficient.

3.4.2.2 Vertical Landing Velocity

The structure of the rover is designed to sustain a 1 m/s vertical velocity on contact with the ground. However, because of the uncertainty in the altitude, the vehicle may accelerate over the distance of 1.5 m before it reaches the ground. Just dropping from that distance with zero starting velocity will result in a 2.2 m/s velocity on contact with the ground. To soften the impact, the lander includes collapsable legs, described later in the paper. For the requirements, a 0.5 m/s maximum vertical velocity on landing is assumed. Starting at 1.5 m above the ground and with a vertical velocity of 0.5 m/s down, the vehicle still achieves approximately 2.2 m/s on landing.

3.4.2.3 Horizontal Landing Velocity

Assume that the moment the rover touches the ground, the legs collapse and it is effectively held by the wheels. Also, assume that the wheels get caught and are not allowed to slip. For example, it might have hit a rock.

The rover center of mass is located 1.6 m from the front center of the wheel axis and 1 m above the bottom. In order for the rover to flip, it needs to raise its center of mass by $h = \sqrt{1.6^2 + 1} - 1 = 0.89$ m. The maximum horizontal velocity on landing is then $v_{max} = \sqrt{2gh} = 1.7$ m/s. A requirement of 1 m/s is selected with a 40% margin, allowing to accomodate uncertainties in the center of mass or landing on a slope of up to 13 degrees.

3.4.2.4 Attitude

The directional antennas should be pointed at Earth to within 1 degree for correct operation. Therefore, the attitude of the rover needs to be known to within 1 degree for most of the time.

The lander performs a number of burns during the transfer and landing. If the spacecraft is not perfectly oriented, there will be components of the thrust vectors that are perpendicular to the desired direction. This will result in velocity perpendicular to the primary direction. This velocity is not desired, because it will need to removed by the RCS system once the offset is detected.

Assume that a 5 m/s extra velocity is not acceptable for the main engine final burn. Then, the angle error must stay below 0.12°. This combines the error before the final burn and the

accumulated error during the burn. Before the burn, a good star tracker can easily measure an angle to within 0.1 degrees. Then, to first approximation, the drift error in the gyroscopes can't exceed 0.76 $^\circ/hr$.

The IMU will also be used when driving. It would be beneficial to go 1 hour before having to fix position using the star tracker. At the same time, the antennas should be pointed at Earth to within 1 degree. Therefore, it would be good to have a drift of less than 1 $^\circ/hr$ for the purposes of driving.

3.4.2.5 Landing Accuracy

The vehicle has to be within a few kilometers of the rover on landing. However, a smaller landing radius is preferable not only because it minimizes the drive distance, but because it allows to pick a good, rock-free landing spot. A number of previous and future lunar lander designs were used to determine a reasonable landing radius requirement. Both Apollo 16 and 17 landed with approximately 200 m accuracy. Selene-B, a Japanese lunar landing mission, will be able to land to within 100-200 m accuracy. Based on these values and assuming access to similar or better technology a landing accuracy of 200 m was selected for this mission.

There are two parameters limiting the accuracy of the landing:

1. The initial information about the spacecraft position relative to the moon
2. The integrated errors of the accelerometers and rate gyros during the descent

The position and orientation of the lander will be relatively well known from ranging and the star tracker up until the main engine burn. It is assumed that after that until touchdown, new measurements are not available.

The state of a spacecraft in a geosynchronous orbit can be known to within 1 m and 1 m/s [88]. Using the Deep Space Network, even better estimates are possible. In addition, ground velocity sensors can be effective up to 5 km in altitude, with velocity estimates of down to 10 cm/s. But even assuming that they these are not used to improve velocity estimates, a 1 m/s error in orbit for a two minute landing results in a 120 m landing error.

Subtracting this in quadrature from 200 m gives 160 m. This is how much the accelerometer can drift over two minutes and still statistically end up within 200 m. This gives a maximum of $0.02m/s^2 = 2mg_\circ$ drift in the accelerometers. Doing the same calculation with 80 m gives $1mg_\circ$

Therefore, if the accelerometer drift is less than $2mg_\circ$ the rover will probably land within 200 m of the target site. If it is less than $1mg_\circ$ the rover is guaranteed to land within 200 m of the target. Note that this is how well the lander knows about its position. It is assumed that since the state is being continuously monitored and adjusted with RCS during the descent, the rover can actually reach the location that it calculates to be the target.

3.4.3 Devices

3.4.3.1 Inertial Measurement Unit

The lander will use gyroscopes and accelerometers integrated into an Inertial Measurement Unit (IMU). Commercial IMU's of TRL 9 are easily available. Many of the IMU's also include internal redundancy, which allows to greatly increase their lifetime. Some sample IMU performance specifications include 0.0003 °/hr gyro stability, 0.996 reliability over 15 years and 300 $\mu g_\circ$ to 3 $mg_\circ$ bias repeatability. 1 $mg_\circ$ desired bias stability is within the available range and the gyroscope stability far exceeds the 1 $°/hr$ requirement.

Over a 30 day mission, which includes some contingency period for sitting on the ground, the reliability becomes 0.9999. So, a single IMU is sufficient to meet the reliability requirements.

The IMU is located inside the rover and remains connected after the rover leaves the lander. This allows it to be used for estimating the vehicle position and orientation while driving.

3.4.3.2 Star Tracker

Commercial star trackers of TRL 9 are available. Typical characteristics include 0.004° roll accuracy and 0.001° pitch and yaw accuracy. Some available star trackers are also robust to vehicle motion of more than 20 °/s and take less than 3 seconds to acquire the attitude.

Although one star tracker meets the reliability requirements, with 0.999 reliability over 30 days, a second one might be placed on the lander for the case that the first star tracker is damaged.

3.4.3.3 Ground Velocity Sensing and Obstacle Avoidance

Some sort of a system is necessary to directly measure the vehicle velocity relative to the ground during landing. A number of possible solutions are investigated below.

Landing Radar Radar systems have been previously used on landings, mostly for measuring the altitude. The Mars Science Laboratory will use a phased-array terrain radar for landing and obstacle avoidance. However, that radar is large, heavy (25 kg) and consumes 200 W of power [110]. For the next generation of missions JPL is developing a lighter and more efficient radar [58].

The radar system is not sensitive to dust accumulation. The radar also can measure the altitude of the system and provides enough pixel resolution to do obstacle avoidance.

The processing requirements on the system are moderate, because it needs to manipulate large amounts of data to extract the lander ground velocity.

If obstacle avoidance is implemented, the processing requirements grow much larger, as they do for all other systems.

Landing LIDAR LIDAR is being considered for use in spacecraft landing applications [57]. Currently, it is extensively used in topographic mapping. LIDAR measures the reflection of laser beams to create a 3D map of the surrounding environment. Dimensions and weight of space LIDAR systems were estimated from their ground-based counterparts with a margin for space-rating the device.

Unlike the radar, dust on the LIDAR screen may cause problems with its operation. However, dust is not going to be a concern up until it is kicked up by the engines up close to the ground. The horizontal velocity should reach zero by that point and the LIDAR will still be able to get a reasonable value for the altitude.

The processing requirements for the LIDAR are similar to that of the radar, both have to convert a series of two-dimensional maps into velocity vectors.

Visual System A visual system has been used on landing of the Spirit and Opportunity Exploration Rovers, which used three adjacent pictures to estimate the lateral velocity of the lander. Algorithms for obstacle avoidance are also being developed [60]. Although the cameras necessary for the visual system can be small and light, the system also requires a radar altimeter, because cameras cannot be used to estimate the altitude.

As the LIDAR, the system can be affected by dust settling on the lens, but that should not be a problem until a low altitude. However, the visual system is also sensitive to lighting conditions, so it can only be used for day landings. In addition, if obstacle avoidance is implemented, there may be problems with obstacles hiding in the shadow of other obstacles.

The computational requirements for the visual system are the largest, because they require analysis of a stream of images.

Miniature Coherent Velocimeter and Altimeter A Miniature Coherent Velocimeter and Altimeter (MCVA) system is being developed by NASA for planetary landings [59]. It uses a number of small lasers located at different points on the lander to get the range and the range rate. From the range rates, the velocity vector of the lander is extracted.

The MCVA lasers are small, lightweight, and are easy to position on the lander structure. In addition, mounting a few additional units allows one to easily incorporate redundancy. To have sufficient redundancy for all other systems requires essentially two copies of them.

The lasers can be affected by dust and are sensitive to vibration, so there may be issues with the system when the hydrazine thrusters are firing during the final stage of descent.

The computational power requirements for these units are small, since there are only a few data channels.

Overview and Selection Table 3.5 shows a side by side comparison of these systems. All of them can meet the requirements on vertical and horizontal landing velocities.

Table 3.5: Ground Velocity Sensor Comparisons

System	Landing radar	Landing LIDAR	Visual system	MCVA
Altitude resolution	0.1 m	< 0.5 m	Radar(0.1 m)	0.1 m
Velocity resolution	0.1 m/s	< 0.5 m/s	< 0.5 m/s	0.1 m/s
Obstacle avoidance	Yes	Yes	Yes	No
Environment	Any	Low-dust	Low-dust, Well-lit	Low-dust
Size	27 cm dish	25 cm box	15 cm box	6 boxes, 5x2x2 cm
Mass	< 9 kg	10 kg	< 10 kg	6 kg total
Processing requirements	Medium	Medium	Large	Small
TRL	6	4	8	5
Fault tolerance	None	None	None	Double

It was decided to implement obstacle avoidance on the lander to increase the probability of landing success. This eliminates the MCVA system from the possible candidates.

Based on this, as well as on the performance and technology readiness level, a radar system was selected for the landing. Its major drawbacks are the mass and power draw. However, the radar needs to be active only for a few minutes during the landing.

3.4.4 Reaction Wheels

Reaction wheels provide a very fine and smooth attitude control, while using small amounts of fuel. They are well-suited for satellites that spend a long time in orbit and need to maintain their orientation.

However, for this project the lander spends less than a week in space, during which time it needs to point its antenna to a 1° accuracy. Also, there is no requirement for smoothness during attitude corrections and most of the finer attitude adjustment happen during the engine burns, when the reaction wheels are not usable.

So, all the attitude adjustment can be achieved by the RCS with small amounts of fuel, without a need for reaction wheels, which mass in at more than 20 kg for a full set.

3.5 Controller Design

Figure 3.6 shows a simplified layout of the sensors, the control system and its connection to the RCS.

On the diagram, $\ddot{x}$ and $\dot{\theta}$ represent the vehicle acceleration vector and the rotation vector, respectively.

These values are integrated to obtain the position and velocity of the vehicle. The absolute position for the integration is obtained from ranging off satellites. The attitude is obtained from

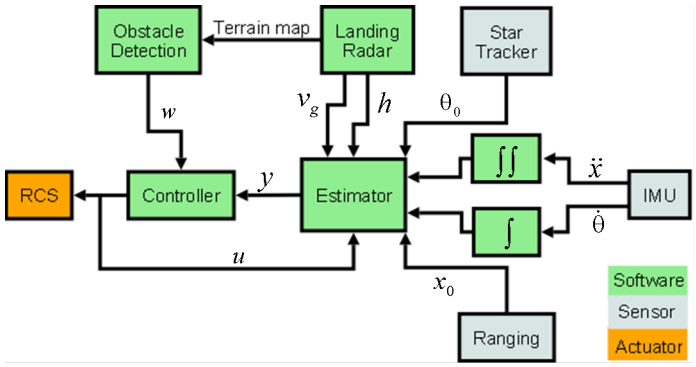

Figure 3.6: Control of the landing system

the star tracker. Absolute positions are used when available and are estimated by integration when they can't be measured directly.

The values are filtered by the estimator that outputs the rover state y, which is used by the controller to calculate the thruster commands u.

When the lander starts descending to the lunar surface, the landing radar begins to measure the altitude h and the ground velocity vector v_g. The estimator uses these values in addition to x and θ to estimate the vehicle state y. In addition, the terrain map is analyzed by an obstacle detection algorithm that outputs the weights, w, corresponding to different landing locations.

A specific controller and estimator were not yet selected. Linear Quadratic Regulator (LQR) and Kalman filter are a possible choice. However, their performance needs to be carefully measured, because the nonlinear dynamics and model uncertainty may cause the system to become unstable.

3.6 Lander Staging (David Gers)

3.6.1 Overview

The ideal launch configuration, both in terms of size constraints and structural loading issues, required that the retro engine and its associated fuel tanks be mounted to the rear of the rover, as opposed to underneath or around the rover structure. This configuration meant the retro engine would be unusable at too low of an altitude in order to allow for the rover to land upright. Since leaving this engine attached while another system performed the final descent would add significant mass to the system, and thus require significantly more fuel, it was necessary to separate the two stages. However, since the large retro engine is far more efficient than any smaller engine or thruster system, it is also desirable to use it for as long as possible. Therefore it was necessary to find an optimal staging height that would minimize the mass of fuel required.

3.6.2 Staging Altitude Trade Study

One requirement on this staging height is to ensure that the retro engine does not pose a hazard to the rover upon landing. Therefore, a minimum safe distance of 1 km was set as the ideal distance between the landing site of the rover and impact site of the retro engine. This provides a safety margin so that if the separation does not go as planned, there is still little chance of the retro engine posing a landing hazard. Figure 3.7 shows the separation distance between the lander and retro engine as a function of height, and the staging height must be above the intersection with the red line representing the minimum safe distance of 1 km.

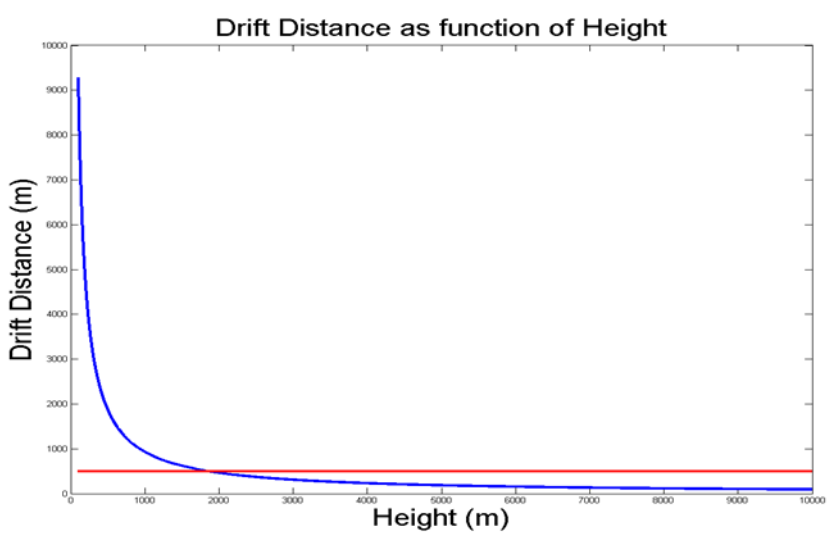

Figure 3.7: Drift Distance as Function of Height

Another requirement on this staging altitude is the time to reach zero horizontal velocity. Since the lander is not designed to land with any transverse velocity, it must slow to zero horizontal velocity in less time than it takes for the vertical descent. Figure 3.8 shows the vertical and horizontal stopping times as a function of height.

The final factor in selecting a staging height is to minimize the fuel mass required. Figure 3.9 shows the horizontal, vertical, and total fuel requirements as a function of height. Although there is a minimum on the graph, it is an altitude too low to meet the other two requirements. Since the curve only increases from the single minima, to minimize fuel mass it is necessary to choose the minimum height that meets the two other requirements. Since all three of these studies depend on the thrust in the vertical and horizontal directions, the ideal staging height can also be affected by changing the number of thrusters. However, several test cases showed that adding many additional thrusters did not significantly lower fuel mass, yet would increase complexity and lower reliability. Therefore, a descent thruster configuration of eight 1600 N vertical thrusters and two 1600 N

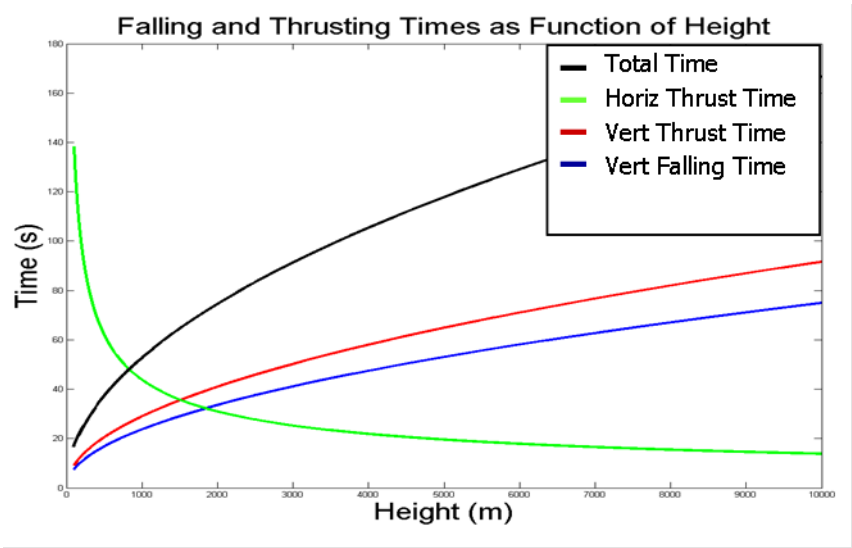

Figure 3.8: Falling and Stopping Time as Function of Height

horizontal thrusters was chosen. By using more powerful thrusters than required for simple reaction control, additional redundancy was added while minimizing the total number of thrusters needed. In the vertical direction, two thrusters could fail, and assuming these failures could be detected early enough in the descent process, the lander would still be capable of a successful landing.

3.6.3 Staging Altitude Selection

Given the chosen thruster configuration, a staging altitude of 2 km was chosen as the ideal height above the surface for retro engine separation. This minimizes fuel requirements while allowing some margin for errors in the engine separation, thrust, or sensor measurements.

3.7 Landing (May Lam)

3.7.1 Landing Leg Requirements

The final stages of landing places importance on the design of the legs. Three main events are to occur: once the thrusters start firing the legs are to deploy, the lander will land and the legs will "crush", explosive bolts will blow the legs off and the rover will drop to the lunar surface. Given this landing scenario there were two general requirements in the design of the landing legs. First, the rover should be able to withstand the forces upon landing without transmitting significant loads to the rover. Two, upon crushing, they must allow for a safe drop to the ground after collapsing. An understood requirement is that they must fit into the shroud and within the mass constraints.

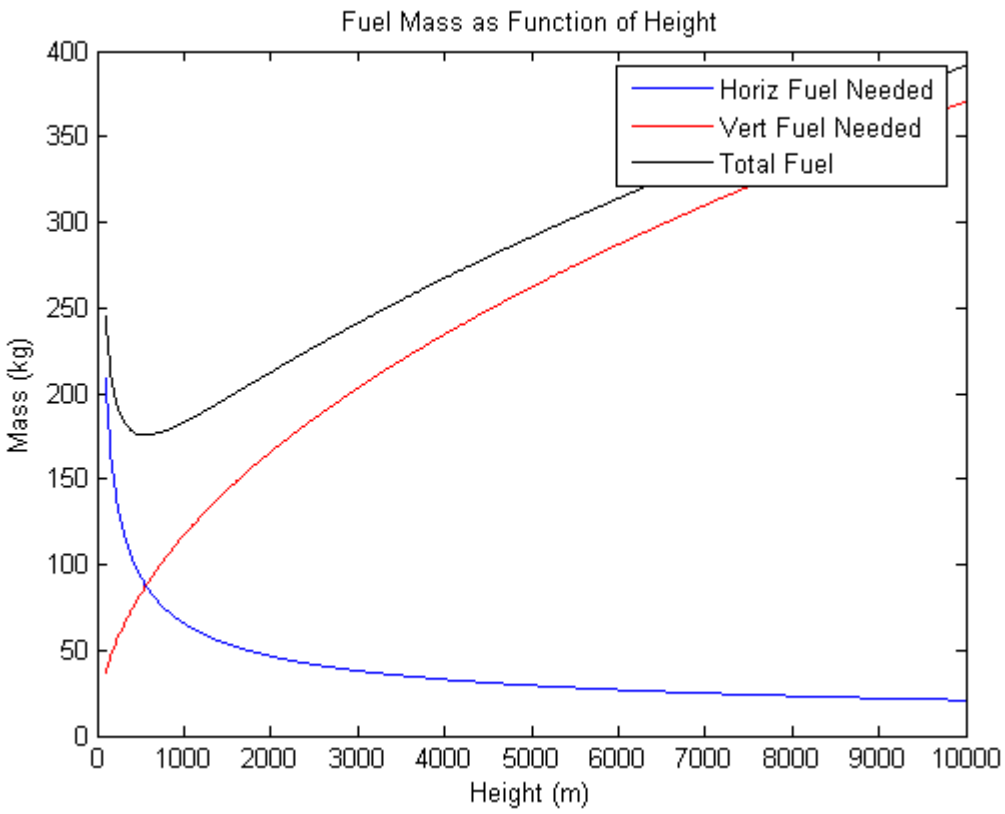

Figure 3.9: Fuel Mass Requirements as a Function of Height

3.7.2 Landing Legs and Lunar Surface Impact

The landing legs consist of three primary sections: the upper strut, the lower strut and a pivoting landing pad. Each strut is essentially a cylinder with no bottom end cap. The struts and the landing pad are constructed of Aluminum 7075 T-6. Encased in the upper strut are crushable honeycomb inserts. Upon landing, the lower strut will telescope into the upper, crushing the honeycomb. The pivoting landing pad allows for the accomodation of various terrain or if the lander were to land on a slope. The upper strut was sized to meet the requirement of enclosing the honeycomb inserts. The exact dimensions of the landing legs are shown in Table 3.6. The total length of the leg is the addition of the landing pad, the honeycomb and the lower (secondary) strut. Figure 3.10 shows a computerized model of the landing legs.

Table 3.6: Landing Leg Dimensions and Mass

	Length (m)	D_o (cm)	D_i (cm)	Total Mass (kg) (4 Legs)
Hexcel Tube-Core Honeycomb	0.44	17	14	1
Primary Strut	0.46	20	19	15
Secondary Strut	0.63	17	16	19
Landing Pad	0.02	30	-	16
Total	1.09	-	-	51

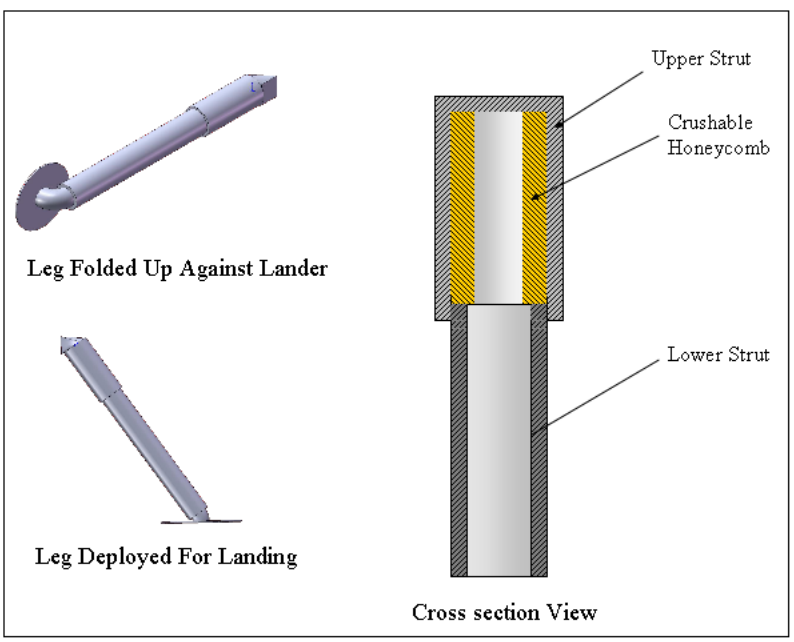

Figure 3.10: Landing Leg Diagram

Crushable honeycomb inserts have been widely used in past landing missions to absorb impact forces including the Apollo landings and the Mars Global Surveyor. The Hexcel Corporation manufactures crushable honeycomb products, specifically their Tube-Core brand that is designed for space applications. They are ideal for this landing system because of their high crush strength to weight ratio, reliability, high fatigue resistance and ability to absorb large energy loads [71]. As seen in Figure 3.11, the honeycomb will initially crush and and the deflections will settle out so vibration loads here should not be a factor.

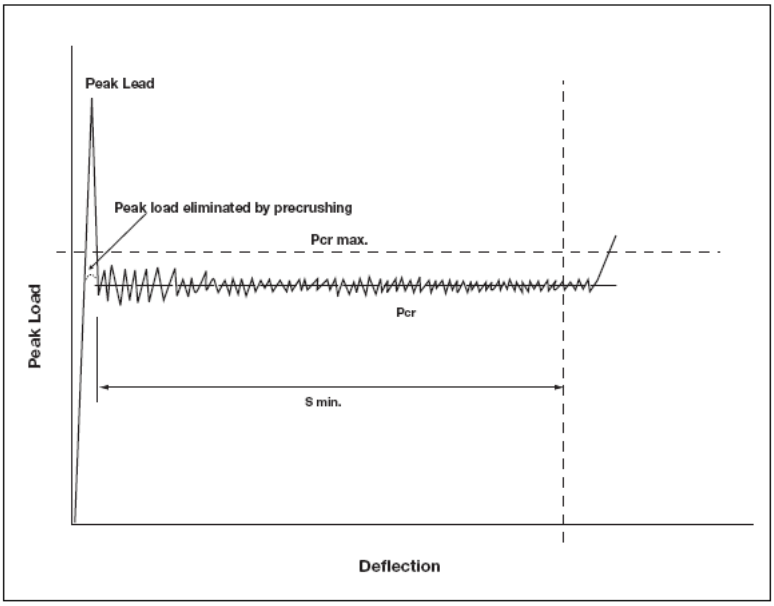

Figure 3.11: Honeycomb Crush Strength

The optimal case would be for the lander to have a zero horizontal velocity and land on all four legs. But given even the best avionics system, this most likely will not happen. The worst case would consider landing velocities in both directions and if only one leg were to crush. If this were to happen, there is a possibility the other three would remain completely uncrushed offsetting the balance of the rover.

The force upon landing assuming no significant horizontal velocity was modeled as an impulse force. The maximum possible landed mass is $m = 3000$ kg and the impact velocity $v_i = 1$ m/s. Using Equations 3.1 and 3.2, the total dynamic force is calculated to be 9000 N. The time of this impulse, 0.33 seconds is calculated by the time it takes for the honeycomb to crush which is given by Equation 3.4 where the final velocity v_f =0 m/s. The stopping distance s, is the crush level for the honeycomb and is found by Equation 3.3. To minimize the amount of force going straight into the legs and to provide better stability, they are angled at 45°. As a result, the actual dynamic force on the landing legs upon impact is 6400 N. The total amount of energy that the legs must

absorb is the kinetic energy of the system and is thus $1.5KJ$.

$$I = mv_i \tag{3.1}$$

$$F_{dyn} = \frac{I}{t} \tag{3.2}$$

$$s = \frac{v_i^2}{2 \cdot a} \tag{3.3}$$

$$t = \frac{2 \cdot s}{v_i + v_f} \tag{3.4}$$

Crush Strength is the amount of force that is required to crush a certain amount of honeycomb and is a material property. Nominally, Tube-Core has a crushing efficiency of 70% meaning that it will crush this percentage of its initial length. Given the worst case of landing on one leg, each leg must withstand 6400 N of force. The thickness or, more intuitively, the length of honeycomb needed was found using Equation 3.5 where

v_i = initial velocity

K_s = crush efficiency

a = deceleration of the lander upon impact

For the given parameters, $t_c = 44$ cm, allowing for a maximum crush stroke of 31 cm. Tube-Core Honeycomb is produced with a minimum crush strength of 150 psi. Using Equation 3.6 where f_{cr} is the crush strength, the required crushed area was calculated. Tube-Core, as its name suggests, is a tube and so the inner and outer diameters needed to be determined. The outer diameter of the honeycomb was found using Equation 3.7 which was derived from Equation 3.6 and the reaction force per leg where ε is the strain of the honeycomb and g_m is the gravity of the moon. The outer diameter was calculated as 17 cm. The amount of force actually placed on the legs was much less than critical buckling force of and thus was not an issue.

$$t_c = \frac{V_i^2}{2 \cdot K_s \cdot a} \tag{3.5}$$

$$A_{cr} = \frac{F_{dyn}}{f_{cr}} \tag{3.6}$$

$$D_o = \frac{m \cdot g_m}{\pi \cdot f_{cr} sin(\theta) \cdot \varepsilon} \tag{3.7}$$

The landing structure was designed so that it would attach to the rover at the center of its wheels. With a wheel diameter of 1 meter, this causes them to stick out a half meter under the structure. The initial design of the legs allowed for at least 0.5 m of clearance after the legs crushed.

This assumed that the bottom of the wheels would be at least 0.5 m off of the ground after crushing. This height was unacceptable because it placed loads on the suspension system that would compress more than it was designed for. It was then accounted for that the chassis of the rover is already at this minimum height and the legs did not need to be at its original height of 1.7 m. The rover was then redesigned to drop from a shorter drop height of 5 cm allowing for an overall post-crushed leg length of 78 cm. The crushable honeycomb inserts chosen are designed only to crush given a normal force and thus shear forces on the legs were not considered.

The static stability conditions of climbing a slope should not exceed 50 deg or a side to side slope of 49.1 deg. The maximum angle that the legs can hit the ground were determined through these stability conditions. In the worst case of only one leg crushing completely and the other three completely uncrushed, the rover would be stationed at an angle of 11°.

The material properties for Hexcel are shown in Table 3.7 and those of aluminum 7057 T-6 are shown in Table 3.8

Table 3.7: Hexcel Tube-Core Honeycomb Properties

Material Property	Value
Density (g/cm^3)	0.14
Crush Strength (kPa)	1030
Crushing Efficiency (%)	70

Table 3.8: Aluminum 7075 T-6 Properties

Material Property	Value
Elastic Modulus (GPa)	71.7
Density (g/cm^3)	175
Yield Strength (MPa)	503

3.7.3 Landing Leg Deployment

The legs are initially folded up against the side of the landing structure because the width constraints in the payload fairing are not adequate for them to be initially deployed. They are deployed in the final stage once the thrusters start firing. This introduces another risk in the landing system. Failure of the landing legs to deploy is a function of the reliability of the actuators and spring mechanisms. If any of these parts were to fail, this would mean a loss of mission. The suspension system currently would not be able to withstand the loads were it to land on its wheels.

3.7.4 Landing Structure Detachment

Assuming the lander has landed safely onto the lunar surface, the legs are to collapse off using pyrotechnic fasteners. When this occurs, the landing structure will detach from the center of the wheels and along with the hydrazine thrusters and fuel tanks will free fall to the ground. Simultaneously, the rover, with a mass of 2500 kg will drop 5 cm to the ground. The load on the wheels when it hits the ground was found to not to damage the rover or its suspension system because it was calculated that the total force on all of the wheels is 4900 N as shown in Figure 3.12. The time until impact of 5 milliseconds was found through the modeling of the suspension system. At this force, the suspension system will compress a maximum of 11 cm, less than the 15 cm it is designed to take. This is less than the force of 3000 N per wheel that it is designed were it to hit a boulder at a speed of 7.5 km/hr. After this, the rover will autonomously drive over the landing structure and rendezvous with the crew.

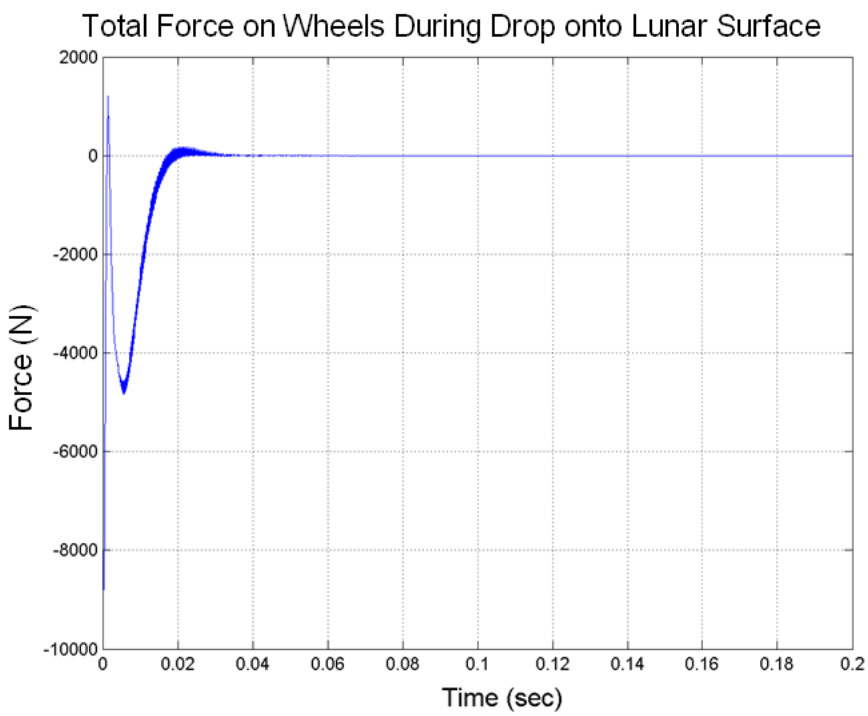

Figure 3.12: Force on Wheels During Drop to Lunar Surface

Pyrotechnic fasteners have widely been used in space missions and are extremely precise and controlled devices. They have a high reliability but given the off chance they will not fire the rover would not be able to free itself from the landing structure. Depending on its landing site distance from the outpost base, the astronauts might be able to recover the rover manually.

To simulate the a more realistic model of the complexities of the landing dynamics further analysis should be done. The dynamic stability upon landing and rover detachment should also be further analyzed to account for the residual horizontal velocities. Additionally a type of ramp for the rover to drive off of after landing would be ideal as this would eliminate the loads on the rover upon dropping. Crushable Honeycomb inserts having been widely used in space applications and are at a TRL 9. Collapsible legs are at a TRL 3 as they have not been fully demonstrated.

3.8 Lander Reaction Control System (David Gers)

3.8.1 Thruster Overview

A reaction control system is required to control lander orientation during transfer stages to the moon and during descent. In order to control all six degrees of freedom, four thrusters were placed at each corner of the lander. An additional four thrusters, providing thrust in the +z direction, are also considered part of the reaction control system, but are essentially used only during descent. Several types of thrusters were examined, and all seemed to produce between 1-1600 N of thrust. Almost all were throttleable across their full range of operation, and were fairly small, within 10-100 cm in length. Typically, thrusters utilizing monopropellants were slightly smaller (approximately 20 cm shorter in length) than those using bipropellants, a factor which led to the decision to use mono-propellant hydrazine thrusters.

3.8.2 Propellant Trade Study

Before finalizing a decision on which type of propellant to use, a trade study was conducted comparing monopropellant hydrazine with a bipropellant combination of MMH and N_20_4 as the fuel and oxidizer, respectively. The bipropellant thrusters offer a higher I_{sp} of around 320, compared with the monopropellant thruster I_{sp} value of around 240. However, bipropellant thrusters require twice the structure of monopropellants, requiring separate tanks for the oxidizer and the fuel, along with the required piping connecting each tank to all of the thrusters. Figure 3.13 shows a trade study comparing the fuel and structure mass required as a function of staging height for both a monopropellant and bipropellant. As the graph shows, despite the increased structure mass, there is still a slight mass savings by using a bipropellant. However, since space on the lander structure is limited, additional structure will likely need to be added to accomodate the additional tanks and fuel lines needed for a bipropellant system. The additional fuel lines and pumps will not only add additional complexity (and therefore additional points for failure) but could possibly also add more mass than what was taken into consideration. Since the mass savings of the bipropellant is only around 15 kg at the optimal staging height, this led to a decision to use monopropellant hydrazine as the fuel source for the reaction control system.

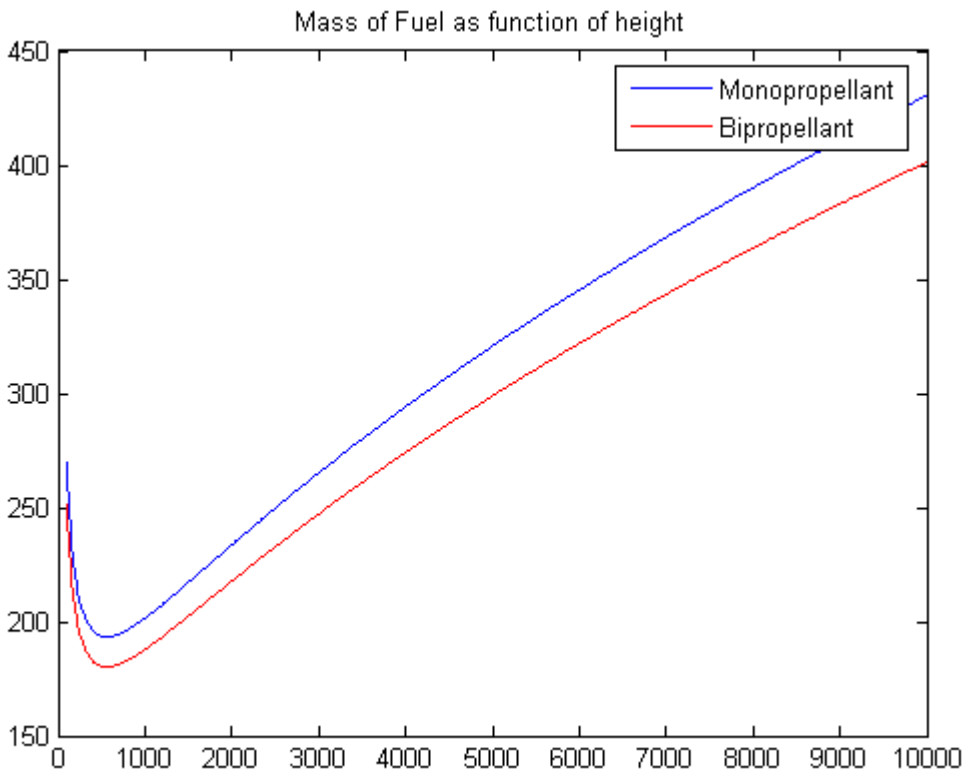

Figure 3.13: Comparison of Monopropellant and Bipropellant Fuels

3.9 Launch and Landing Reliability (Ryan Murphy)

The total reliability for the launch and landing system has been assumed to be 90.0%. As designed, the rover will be used for an independent sortie mission. Although the sortie mission would provide a great chance for lunar exploration and experimentation, it would not jeopardize the astronauts or the overall lunar mission if the rover cannot be used. Since the sortie is not part of the overall mission, a 90.0% reliability for crew rendezvous is reasonable. Additionally, crew will not be aboard the vehicle during launch and landing stages, relieving the 99.9% requirement for crew survival. The full launch and landing reliability is given in Table 3.9[2].

Table 3.9: Reliability for Launch and Landing Stages

Stage	Reliability
Launch	0.970
Lunar Orbit Insertion	0.990
Hohmann Descent Burn	0.990
Retro Stage Braking and Jettison	0.990
Final Descent Stage and Landing	0.965
Unloading Lander	0.995
Crew Rendezvous	0.995
Total	0.900

3.10 Lander CAD Development (Thomas Mariano)

3.10.1 Software Choice

For the development of the trans lunar stage and the lander CAD, the software program SolidWorks was used. This specific package was the most familiar and was able to import the existing rover model for full integration. This software allowed for the development of the landing structure to be built based off of the actual rover design with a minimum amount of time spent learning new software. SolidWorks' ability to export images to a transparent background for seamless integration into presentations was also a deciding factor in the software choice.

3.10.2 Design Process

Initial drawings were made after meeting with the team working on the landing and trans lunar stages. After gathering information as to the shape and dimensions, initial drawings were made of the landing strucuture. These images were then sent to the team and input was given to help refine

[2]The hydrazine thruster reliability is assumed to be 99.9% per thruster. The landing assumes a 1.5% chance of hitting a large, unavoidable rock on landing

the design. This took place several more times and helped to eliminate problems such as fits and clearances of different components.

The biggest issue that was remedied by the development of the CAD drawings was that it was able to be shown that the landing structure and trans lunar stage would fit inside of the launch vehicle. This size constraint also helped decide how to move the landing structure relative to the rover so that the entire strucutre fit in the launch vehicle. This design constraint then led to the beginning development of the attachment points to the rover of the landing structure.

To make the final drawing, the finalized rover drawing had to be completed first. This file was then imported into SolidWorks and integrated with the landing and trans lunar systems. The final drawing was then moved to the requested angles and views and photos were captured and exported.

3.10.3 Future Work

In the future, these models may be used for finite element analysis. With a finer level of development of the dimensions and the system, FEA may be used to help determine if the structure is sound. Also, it may be used to determine the attachment sizing and locations. FEA would also determine where some structure may be removed and where it should be added and may reduce the mass of the system overall. With more detail on the design, more of the drawing can be made and it will more accurately represent the final design of the system and allow for much more accurate design tools to be used.

Chapter 4

Structures

4.1 Structural Requirements (David McLaren)

For the design of the rover's structural components, certain conditions must be observed. Firstly and most importantly, every single piece of structure in the rover must have a margin of safety greater than zero. The safety margin for every component is determined using Equation 4.1 where SF is the safety factor.

$$MOS = \frac{Load_{allowable}}{Load_{applied} * SF} - 1 \tag{4.1}$$

A safety factor of 3 is used for pressure vessels. Composite structures require a safety factor of 2. For metallic structures, a safety factor of 2 is appropriate, but under some crucial conditions, a safety factor of 1.4 is used to save mass. [84]

For ease of fabrication and handling, metallic components are required to have a minimum thickness of 1 mm. Composites must have a minimum thickness of 2 mm, and sandwich structures 12 mm.

All components must survive two severe loading conditions. The most crucial loads for most pieces of structure are launch loads. The worst case accelerations on launch are 6 g in the axial direction and 2 g laterally. The forces induced by these accelerations are often worse than the loads a piece will actually experience during regular use on the lunar surface. Thermal loads are the other major source of design loads for the flight rover. Temperatures on the lunar surface can vary by 240 K between day and night.

In addition, the suspension system must be designed to absorb the shock of the rover passing over a 0.1 meter obstacle at a velocity of 7.5 km/hr. The resulting forces drive design of some chassis members as well.

4.1.1 Mass Balance (Jessica Mayerovitch)

4.1.1.1 Coordinate System

The origin of the coordinate system for the rover is located in the back right corner at the ground. This is referenced from the back right wheel when it is straight forward and under nominal loading on even ground. With the exception of the external driving platform during driving configuration, all coordinates on the rover will therefore always be positive. The z axis is vertical with respect to the rover sitting on perfectly flat ground. The x axis runs along the length of the rover and is positive toward the front. The y axis is positive toward the left side of the rover (see Figure 4.1).

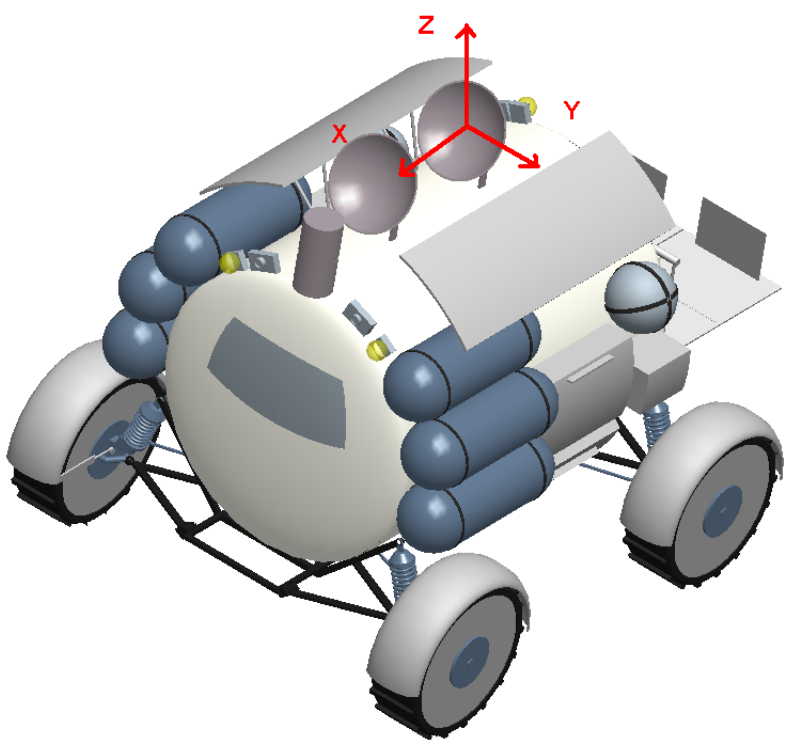

Figure 4.1: Coordinate System

4.1.1.2 External Layout Determination

To ensure that the rover is stable enough to handle its projected driving conditions, the masses of all internal and external parts and equipment had to be placed into a table with their coordinates on the rover. Many parts in the rover which fixed positions, while others vary with time.

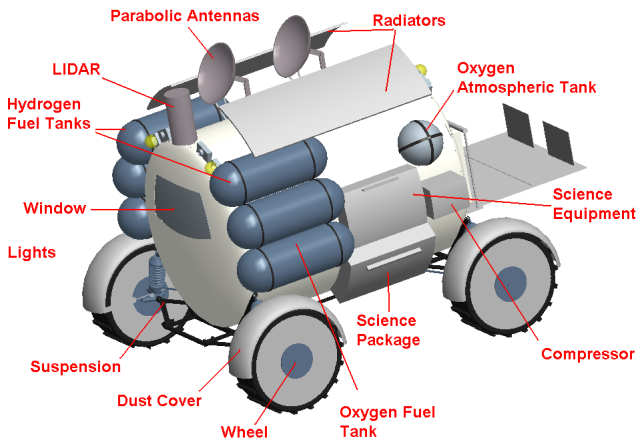

(a) Front view

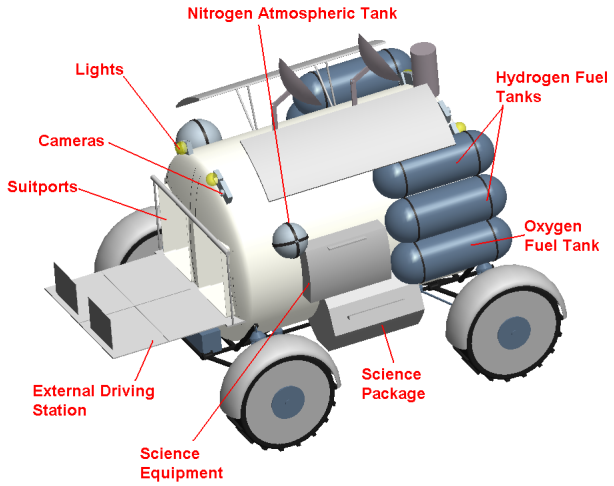

(b) Back view

Figure 4.2: External Layout

- The locations of the internal equipment are driven by space and habitability requirements.
- The suitports, which constitute about 10% of the base mass of the rover, are located in the rear.
- The astronauts, which at a maximum will be 180 kg, will also often be located in the back of the rover.
- The science package must be accessible by the astronauts, therefore, the two science packages are placed in-between the wheels.
- The sampling equipment must be readily accessible by the astronauts during EVAs, therfore, the two equipment boxes are located in-between the wheels, at a height that places them directly in front of a standing astronaut.

There are several other constraints which limit the locations of equipment on the exterior of the rover.

- All items must be mounted above .5 m while in the driving configuration, so that the rover can meet its requirement to clear .5 m obstacles.
- Objects must not interfere with the movement of the wheels, therefore large objects can't be located between the cabin and the wheels.
- All equipment must be located where it can be secured to the chassis, not just the cabin.
- Equipment vital to the mission shouldn't be placed on the front, below the astronaut's line-of-sight, in case of a collision.
- The parabolic antennas for communication need to have a clear line-of-sight to the horizon.

With these constraints in mind, the equipment is placed on the exterior of the rover as low to the ground and as balanced around the x and y axes as possible. To do this, the parts are modeled in ProE (see Figure 4.6) and placed onto an assembly of the rover. Their CGs are calculated and placed along with their masses into Table 4.1.

4.1.1.3 Rover Center of Gravity

Many of the masses on the rover change throughout the course of the mission. In order to determine the static stability margins for the rover, the following changes are taken into account:

- The rover drives both with and without the astronauts, and with the astronauts in two different driving conditions

- The two atmospheric tanks are expended.
- The fuel tanks are expended, one oxygen tank at a time and one hydrogen tank at a time.
- The science package is dropped on the first sortie.
- Samples are collected from the lunar surface.

Table 4.1: Initial Mass Balance

Component	Initial Mass (kg)	x-coord (m)	y-coord (m)	z-coord (m)
External Platform	45	0.2	1.6	1.1
Chassis	160	1.5	1.6	1.2
Suspension/Motors/Gears	291	1.7	1.6	0.6
Pressure Shell	240	1.7	1.6	1.4
Window	54	3.0	1.6	1.7
Radiators	54	1.7	1.6	2.5
Compressor	30	0.8	2.7	1.4
Fuel Cells	39	0.3	1.6	0.6
O2 Fuel Tank 1*	116	2.5	0.4	1.3
O2 Fuel Tank 2*	116	2.5	2.8	1.3
H2 Fuel Tank 1*	14	2.5	2.7	1.7
H2 Fuel Tank 2*	14	2.5	0.5	1.7
H2 Fuel Tank 3*	14	2.5	2.5	2.1
H2 Fuel Tank 4*	14	2.5	0.7	2.1
Circuit Breaker	8	0.1	1.6	1.4
Star Trackers	8	1.7	1.6	2.8
HD Cameras	15	1.7	1.6	2.2
LIDAR	27	2.9	1.6	2.7
Parabolic Antennas/Amplifiers	62	1.7	1.6	2.8
O2 Atmospheric Tank	17	0.9	2.63	1.9
N2 Atmospheric Tank	3	0.9	0.6	1.9
Science Package 1*	40	1.7	0.7	0.7
Science Package 2*	20	1.7	2.4	0.8
Sampling Equipment	56	1.7	1.6	1.7
Samples*	0	1.7	1.6	1.7
Astronauts**	0	0.3	1.6	1.4
Internal Equipment*	293	1.8	1.6	1.2
Total Initial Mass and CG	1752	1.8	1.6	1.3

* Mass is variable

** Location is variable

The following equations are utilized in a version of Table 4.1 in Microsoft Excel so that the CG shift can be analyzed at different times during the mission. This also allows the time that certain events occur to be modified for optimization of stability.

- Atmospheric Tanks

  There are only two atmospheric tanks, one for oxygen and one for nitrogen. They are used continuously.

  $m_{t=time} = m_{i-}\dot{m}_{atm} * t$

- Fuel Tanks

  There are two oxygen fuel tanks and four hydrogen fuel tanks. Only one oxygen tank and one hydrogen tank are utilized at a time.

  - First Fuel Tank

$$m_{t=time} = \begin{cases} m_{i-}\dot{m}_{fuel} * t > tankmass & m_{i-}\dot{m}_{fuel} * t \\ m_{i-}\dot{m}_{fuel} * t \leq tankmass & tankmass \end{cases}$$

  - Second Fuel Tank

$$m_{t=time} = \begin{cases} m_{i-}\dot{m}_{fuel} * t > tankmass & m_i \\ m_{i-}\dot{m}_{fuel} * t \leq tankmass & m_{i-}\dot{m}_{fuel} * (t - \frac{(m_i - tankmass)}{\dot{m_{fuel}}}) \\ 2m_{i-}\dot{m}_{fuel} * t \geq 2tankmass & tankmass \end{cases}$$

- Science Packages

$$m_{sciencepackage1} = \begin{cases} t < t_{drop} & 40 \\ t \geq t_{drop} & 0 \end{cases}$$

$$m_{sciencepackage2} = \begin{cases} t < t_{drop} & 20 \\ t \geq t_{drop} & 0 \end{cases}$$

- Astronaut Masses/Locations

$$m_{astronauts} = \begin{cases} t < t_{sortie} & 0 \\ t \geq t_{sortie} & 180 \end{cases}$$

  - Since the CG is only considered for driving, the two possible astronaut locations are considered.
  - Both astronauts inside at front driving station
    - x = 2.9 m
    - y = 1.6 m
    - z = 1.4 m
  - Both astronauts on external driving station

    * x = 0.3 m
    * y = 1.6 m
    * z = 1.4 m

- Internal Equipment

  When the astronauts enter the rover, their suits add 110 kg to the overall mass

$$m_{internal} = \begin{cases} t < t_{sortie} & 293 \\ t \geq t_{sortie} & 403 \end{cases}$$

$$x = \begin{cases} t < t_{sortie} & 1.8 \\ t \geq t_{sortie} & 1.5 \end{cases}$$

$$y = \begin{cases} t < t_{sortie} & 1.6 \\ t \geq t_{sortie} & 1.6 \end{cases}$$

$$z = \begin{cases} t < t_{sortie} & 1.2 \\ t \geq t_{sortie} & 1.2 \end{cases}$$

4.1.2 Stability Analysis

4.1.2.1 Geometric Center

The geometric center of the rover is located in the center of the cylindrical-shaped cabin (Figure 4.3). This serves as a reference point for the CG in determining the best configurations, because the ideal is to have the X and Y coordinates as close to the geometric center as possible. For stability, the Z coordinate should be as low as possible.

Geometric Center Coordinates:

x = 1.7 m, y = 1.6 m, z = 1.4 m with the geometric center denoted by the green circle in Figure 4.3.

4.1.2.2 Worst-Case CG Scenarios

Changing the times at which events occur and analyzing the resulting CG shift allows the worst-case scenarios for stability to be calculated.

- Worst-case scenario in the y-direction, left side
  - The worst-case for side-to-side stability is the case when the science package is dropped at the exact time that the oxygen fuel tank on the right has been completely expended, but the left is still full. This creates an imbalance to the left side of the rover, because the larger of the two science packages is also on the right side (Figure 4.4).

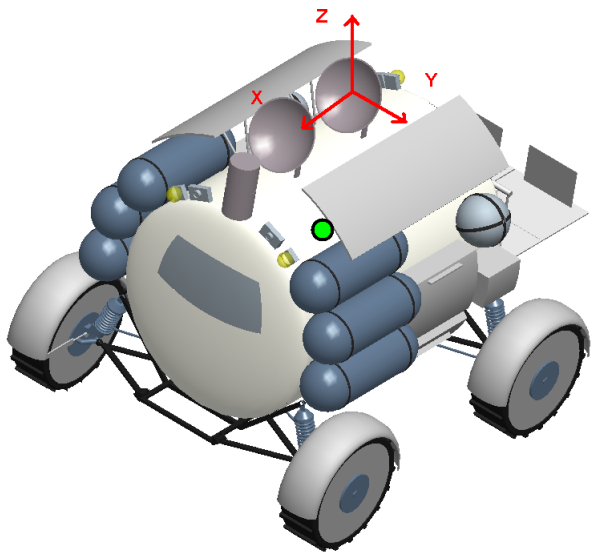

Figure 4.3: Geometric Center

- X = 1.6 m
- Y = 1.7 m
- Z = 1.4 m
- M_{rover}= 1928 kg

- Worst-case scenario in the y-direction, right side
  - Since the rover will always be slightly unbalanced to the left, but never more than 10 cm, the worst-case scenario tilted to the right would be when CG is directly at the geometric center but lower to the ground. This occurs at the very beginning of the mission before the astronauts are there.
  - X = 1.6 m
  - Y = 1.6 m
  - Z = 1.3 m
  - M_{rover}= 1752 kg
- Astronauts inside, driving forward, worst-case scenario in the x-direction
  - The first worst-case for front-to-back stability is the case where both astronauts are in the front of the rover early on in the mission. Due to the fuel tanks being full and

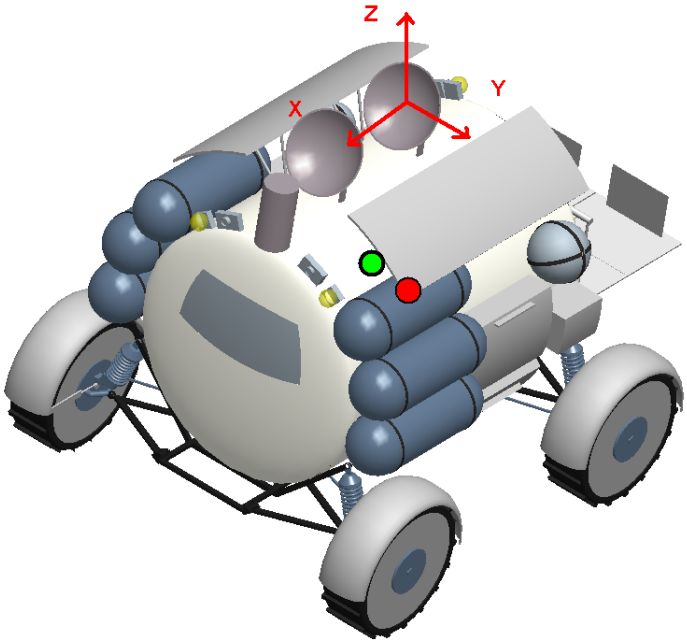

Figure 4.4: Left Side Stability
Green Circle is Geometric Center
Red Circle is the CG

located toward the front of the rover, this causes the rover to be unbalanced to the front. However, the science package has not been dropped at this point, therefore, the CG will also be lower. (Figure 4.5)

- X = 1.9 m
- Y = 1.6 m
- Z = 1.3 m
- M_{rover}= 2039 kg

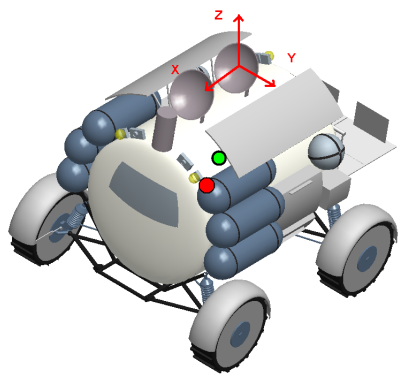

Figure 4.5: Front Stability

- Astronauts outside, driving in reverse, worst-case scenario in the x-direction
  - The second worst-case scenario for front-to-back stability is the case where both astronauts are seated on the external driving platform toward the end of the mission. Because a majority of the fuel has been used up at this point, this scenario causes the rover to be unbalanced to the back. This situation is likely to occur after the science package has been dropped, so the CG is higher than the previous scenario.
  - X = 1.5 m
  - Y = 1.6 m
  - Z = 1.4 m
  - M_{rover} =1863 kg

4.1.2.3 Static Stability

The static stability margins are calculated using the worst-case scenarios. In Table 4.2 the equations used to find the critical angles of stability. A wheelbase of 3.16 m and a wheelspan of 2.42 m were used for the calculations.

Table 4.2: Static Stability Limits

Tilt Direction	Equation	Critical Angle
Left	$\theta_{critl} = \arctan\left\{\frac{\left[\frac{1}{2}wheelbase-(Y-1.6)\right]}{Z}\right\}$	48°
Right	$\theta_{critr} = \arctan\left\{\frac{\left[\frac{1}{2}wheelbase-(1.6-Y)\right]}{Z}\right\}$	50°
Forward	$\theta_{critf} = \arctan\left\{\frac{\left[\frac{1}{2}wheelspan-(X-1.7)\right]}{Z}\right\}$	38°
Backward	$\theta_{critb} = \arctan\left\{\frac{\left[\frac{1}{2}wheelspan-(1.7-X)\right]}{Z}\right\}$	37°

4.1.3 Suspension Design

Because the rover was designed to have four wheels, independently steered and powered, it also needs to have independent suspension. Each wheel is connected to the rest of the rover through a simple Macpherson strut. (Figure 4.6)

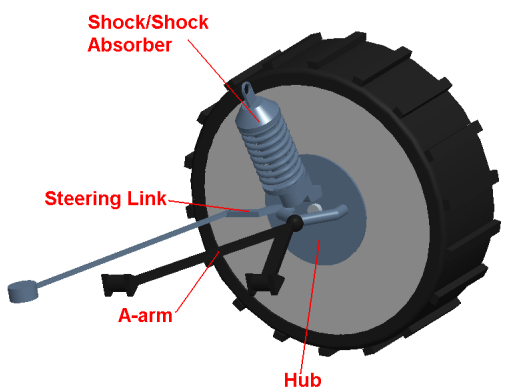

Figure 4.6: Suspension System: Isometric View

- Shock Absorber - This part connects the lower portion of the suspension to the chassis. It moves in and out like a piston, damping out the impact forces. There is a pin connection between the top of the shock absorber and the chassis, giving the suspension system a degree of freedom around the x-axis. Under static loading conditions, the angle of the shock absorber is 20°from vertical.

- Shock - A simple spring coiled around the outside of the shock absorber. It expands and contracts along with the shock absorber.
- Hub - The circular piece of the suspension which connects the shock and shock absorber to the rest of the wheel. The shock/shock absorber can rotate independently of the hub, which gives the wheel the freedom to turn.
- Steering Link - The extension of the hub which connects to the linear actuator used to turn each wheel. The steering link is offset from the center of the wheel so that the linear actuatory can create a torque. There is a pin connection between the the steering link and the linear actuator with a degree of freedom around the z-axis.
- A-arm - The wishbone-shaped piece which connects the hub to the lower portion of the chassis. It is connected to the hub via a stiff ball joint connection. The freedom of motion around the x-axis allows the wheel to remain upright while the A-arm swings up and down with the motion of the rover. The freedom of motion around the z-axis allows the wheel to turn. The A-arm is connected to the lower portion of the chassis via two stiff pin connections, with a degree of freedom around the x-axis.

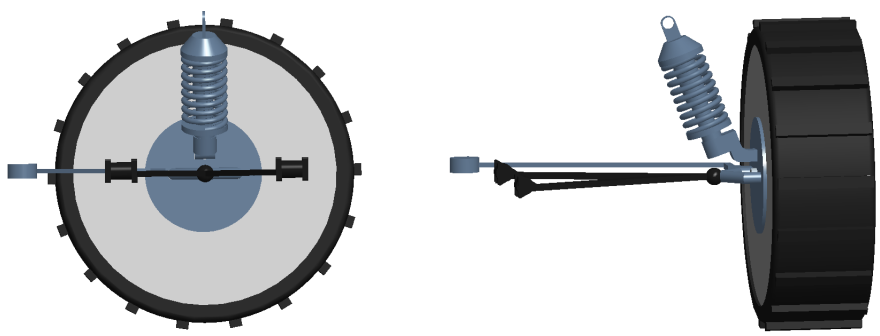

(a) Front view (b) Side view

Figure 4.7: Suspension System

4.1.4 Chassis Design

The chassis (Figure 4.8) is designed to take loads from four major sources. The first is static loads during driving configuration. The chassis needs to be able to support the unsprung weight (everything except the wheels and suspension below the shock and shock absorber) of the rover. Because the cabin of the rover is cylindrical and the internal equipment is distributed across the

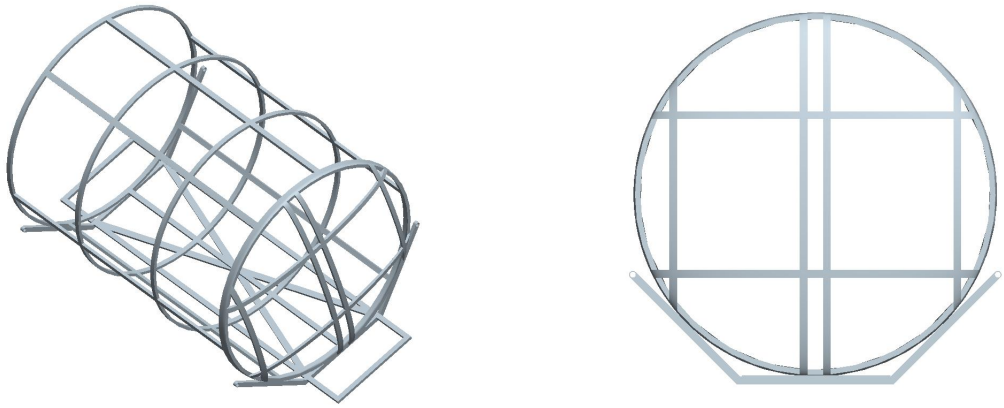

(a) Front (b) Back

Figure 4.8: Chassis

interior, a circular chassis design was chosen. Having circular shaped struts on the bottom provides the best distribution of the weight loads and also increases the stability the chassis provides to the cabin. Because these struts conform to the shape of the cabin, they also waste less external space. It also allows the internal and external equipment to be attached to the same part of the structure.

With a cabin length (not including the endcaps) of 2.43 m, it was determined that four circular struts along the length of the cylinder would be ideal. This creates a distance between struts of .81 m, which is approximately the length of the fuel tanks.

Since much of the internal and external equipment has to be attached to the top of the rover, such as the avionics and the potable water supply, the circular struts extend all the way around the rover.

The second major source of loads on the rover is driving loads. The chassis is designed to incorporate the four MacPherson strut suspension systems on each wheel. In order to incorporate the suspension, a flat lower portion is added to the circular struts of the chassis. This part of the chassis consists of two struts running parallel to the x-axis of the rover. These struts transfer the sprung weight of the rover down to the A-arm so that not all of the weight is being supported by the shock and shock absorber. Two additional struts are placed diagonally across the two parallel struts in order to provide torsional stability.

A shock tower is located at the front and back and end of the chassis to take the impact loads from the wheels. These support the rest of the chassis only at the bottom and along a 45°angle along the sides. This is designed to keep the impact loads during driving from going directly into the cabin of the rover.

The third major load source, and the one which produces the largest forces, is launch. During launch, the x-axis is pointing up; the rover is standing on its back end. Because of this configuration,

it will experience large axial loads along its x-axis during launch. To handle the launch loads, seven struts running in the x-direction encircle the rover. These struts are designed to handle the large axial loads and are spaced so that the largest pieces of equipment can connect directly to them, instead of just to the circular struts.

4.2 Suspension (Enrique Coello)

4.2.1 Trade Study on How to Model Suspension Dynamics

4.2.1.1 Quarter Vehicle Model

For the quarter car vehicle model (Figure 4.9), the suspension was initially assumed to have average values of a regular passenger vehicle. The spring and damper constants were changed to accommodate the weight of the quarter mass of the rover. [92]

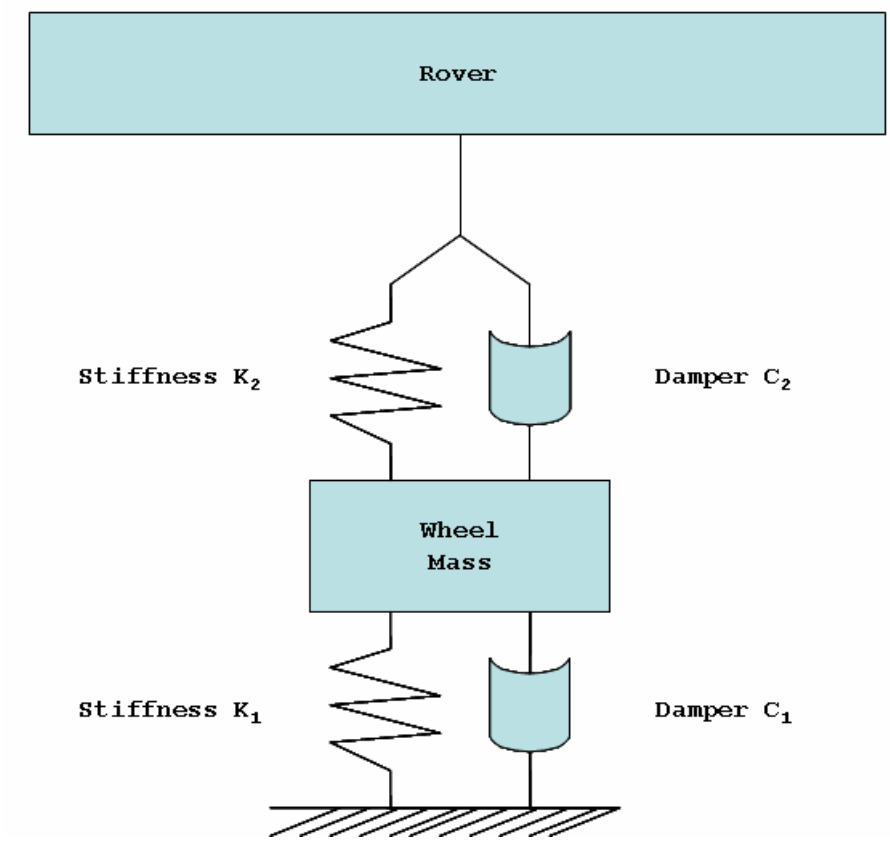

Figure 4.9: Modeling of quarter vehicle suspension system

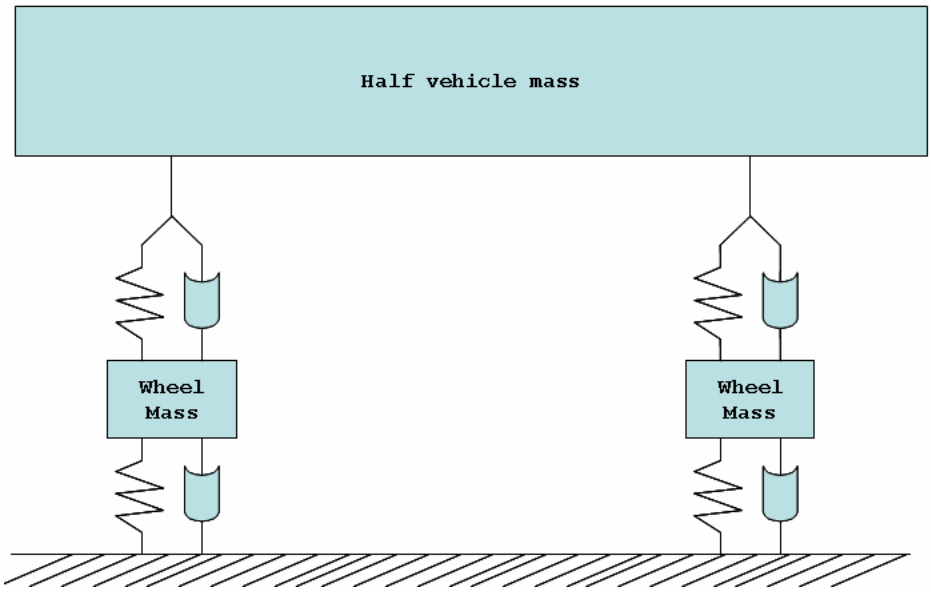

Figure 4.10: Modeling of Half Vehicle Suspension System

4.2.1.2 Full Vehicle Model

The full vehicle model (Figure 4.11) is similar to the quarter vehicle except for it includes roll and pitch through the center of gravity. This model is much more accurate because it was implemented and tested with two different inputs. The input that was used to taste the suspension system's reaction was a random generation of what the lunar ground. The lunar ground was modeled for a range of eight meters. The variations of the ground level range from zero to ten centimeters allowing the suspension to be constantly reacting to the limit of the impact we needed the suspension to take. The suspension was also tested by driving on a flat terrain and encountering a ten centimeter boulder at the speed of 7.5 km/hr [92].

4.2.2 Modeling of Suspension as One Degree of Freedom

The suspension was solved using two different algorithms for our two cases: driving over a boulder and landing the rover on its wheels.

4.2.3 Methods of Solving the Suspension Design Problem Using Vehicle Dynamics

To solve the problems, we tried to approach the problem in different ways to see which solution yielded fast results and as accurate as to the expected results for a vehicle on Earth.

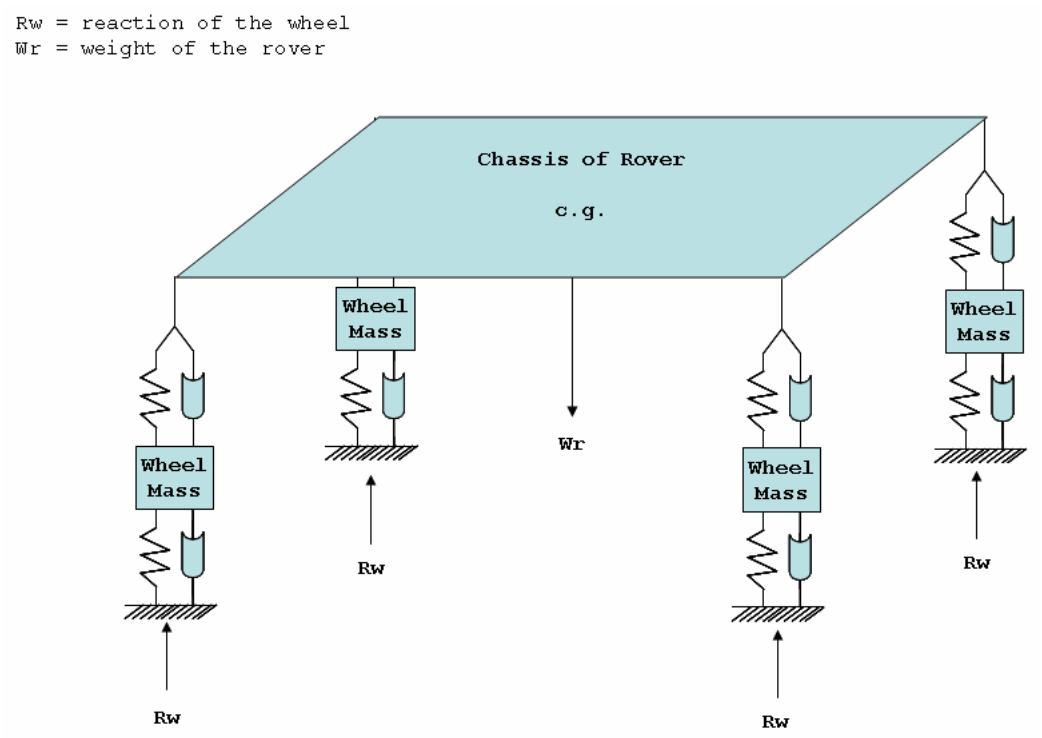

Figure 4.11: Modeling of Full Vehicle Suspension System

4.2.3.1 Solving System Numerically

Using the dynamics of the system, we were able to come out with two equations of motions and solve them for a range of time that demonstrates how the suspension reacts to landing on its wheels and how the oscillations die out. We were also able to find how much compression the suspension undergoes and whether the suspension supports the landing loads. For landing, the rover was assumed to land with a constant speed of 1 m/s.

Another algorithm was implemented to solve for the reaction of the suspension system to support the impact of one of the front wheels of the rover on a ten centimeter boulder at a constant speed of 7.5 km/hr.

4.2.3.2 Solving System Using Transfer Functions

To find the reaction of the suspension to different inputs, the suspension was tested using a transfer function (Equation 4.2). This method allowed us to visualize and get a quick feel for how the suspension was reacting to input but did not return accurate results for a full vehicle model so it was discarded.

The m represents a quarter of the rover's mass, c and k are the damping and spring coefficients. [63]

$$G(s) = \frac{1}{ms^2 + cs + k} \tag{4.2}$$

4.2.3.3 Solving System Analytically (Work Done by Zohaib Hasnain)

For the case of driving over a 10 cm boulder (Equation 4.3), the suspension model was simplified to a single mass, spring and damper system. The following are the equations used to solve the problem.

Equation used to model the boulder as a parabola is:

$$y = -(3.5x - 5)^2 + (3.5x - 5) - 0.15 \tag{4.3}$$

Where x and y are the range and height of the boulder

The differential equation (eq. 4.4) that was solved for the motion of the suspension has y as the position of the rover and q is the position of the suspension

$$\left(\frac{M_r}{4}\ddot{y}\right) = -1000\dot{y} - 75000y + 1000\dot{q}_1 + 75000q_1 \tag{4.4}$$

The force (eq. 4.5)on the suspension due to impact with the boulder was calculated as:

$$SF = k(y_f - y) + \left(\frac{M_r}{4}\right)\left(\frac{g_e}{6}\right) \tag{4.5}$$

Where SF is the spring force, $y_f$and y are the positions of the rover and the suspension respectively, $M_r$is the mass of the rover and $g_e$is the gravity of the Earth

4.2.3.4 Solving Dynamics Using MATLAB

See appendix for code on how the suspension was solved numerically. The numerical solution was solved using numerical integration of matrices using the Central Difference Scheme. The equations used were the following: [56]

This equation shows the relationship of the suspension's parameters (Equation 4.6) with the two bodies in motion (the rover and the wheels)

$$\mathbf{M}\ddot{\mathbf{q}}_\mathbf{n} + \mathbf{C}\dot{\mathbf{q}}_n + \mathbf{K}\mathbf{q}_\mathbf{n} = \mathbf{F}_\mathbf{n} \tag{4.6}$$

Where the M is the mass matrxi (Equation 4.7), C is the damping constant matrix (Equation 4.8) and K is the spring constant matrix (Equation 4.9):

$$\mathbf{M} = \begin{bmatrix} M_w & 0 \\ 0 & M_r \end{bmatrix} \tag{4.7}$$

$$\mathbf{C} = \begin{bmatrix} c_1 - c_2 & -c_2 \\ -c_2 & c_2 \end{bmatrix} \tag{4.8}$$

$$\mathbf{K} = \begin{bmatrix} k_1 - k_2 & -k_2 \\ -k_2 & k_2 \end{bmatrix} \tag{4.9}$$

The position vector (eq. 4.10) that holds the position of the wheels and rover is:

$$\mathbf{q} = \begin{bmatrix} q_1 \\ q_2 \end{bmatrix} \tag{4.10}$$

Expanding the equation of motion of the system (eq. 4.6) we get eq. 4.11:

$$\begin{bmatrix} M_w & 0 \\ 0 & M_r \end{bmatrix} \begin{bmatrix} \ddot{q}_1 \\ \ddot{q}_2 \end{bmatrix} + \begin{bmatrix} c_1 - c_2 & -c_2 \\ -c_2 & c_2 \end{bmatrix} \begin{bmatrix} \dot{q}_1 \\ \dot{q}_2 \end{bmatrix} + \begin{bmatrix} k_1 - k_2 & -k_2 \\ -k_2 & k_2 \end{bmatrix} \begin{bmatrix} q_1 \\ q_2 \end{bmatrix} = \begin{bmatrix} 0 \\ 0 \end{bmatrix} \tag{4.11}$$

Using the Central Difference Scheme (eq. 4.12) and solving for $\mathbf{q_{n+1}}$

$$\left[\mathbf{M} + \frac{\Delta t}{2}\mathbf{C}\right]\mathbf{q_{n+1}} = \mathbf{M}\left[2\mathbf{q_n} - \mathbf{q_{n-1}}\right] + \frac{\Delta t}{2}\mathbf{C}\mathbf{q_{n-1}} + (\Delta t)^2\left[\mathbf{F_n} - \mathbf{K}\mathbf{q_n}\right] \tag{4.12}$$

The vector $\mathbf{q_{n+1}}$contains the postions of the wheels and the rover, therefore, the difference between the two vectors is the amount of displacement of the suspension.

4.2.4 Suspension Design

4.2.4.1 Scenario 1: Driving Over a Ten Centimeter Boulder (Work Done by Zohaib Hasnain)

As mentioned above, the rover has been modeled to support the impact on a boulder of 10 centimeters in height. Using this crude model, our estimated impact force on one of the front wheels is about 5200 N. This force was used to solve other structural designs like the chassis and the thickness of the rover. Eventually those designs were analyzed after BDR with more accurate models of the suspension and other structural components.

Properties The properties of the suspension were simplified for the design of driving a 10 centimeter boulder. For the solution of this scenario, the stiffness and dampness of the rover's tire were assumed to be very large compared to the suspension system's counterparts.

Assumptions The mass that each suspension is assumed to support is a quarter of the total mass. The mass is 750 kg. The spring constant is 50 kN/m and the damper's constant is 100 N-s/m.

Boulder Figure 4.12 is an approximation of a boulder. The curve was assumed to be parabolic. The dimensions are about 15 centimeters wide and 10 centimeters in height. The model of the suspension system is assumed to not slip while driving over the boulder.

Actual Displacement When driving over the boulder, the suspension's expands about one centimeter at the peak of the boulder (Figure 4.13) and compresses about five millimeters after driving over the width of the boulder.

Forces Acting on Rover The reaction forces on the suspension range between -4000 N and +5200 N (in expansion and compression respectively). There are spikes at the point of impact with the boulder and when landing, that is, right after driving over the boulder (Figure 4.14). This spikes show that there are acceleration changes affecting the rover's suspension and therefore impulses as well.

4.2.4.2 Scenario 2: Landing Rover on Moon on Four Wheels

Landing on all four wheels is the ideal case and the least likely. The reaction of the suspension is distributed on all four wheels creating equal stress on the chassis. This case allows for minimal torques on the vertical direction on the rover's shell as well as torsion around the axial direction.

The velocity ranges in the vertical direction are between -5 and +5 m/s at the point of impact and after driving over the boulder creating a change in velocity of about 10 m/s.

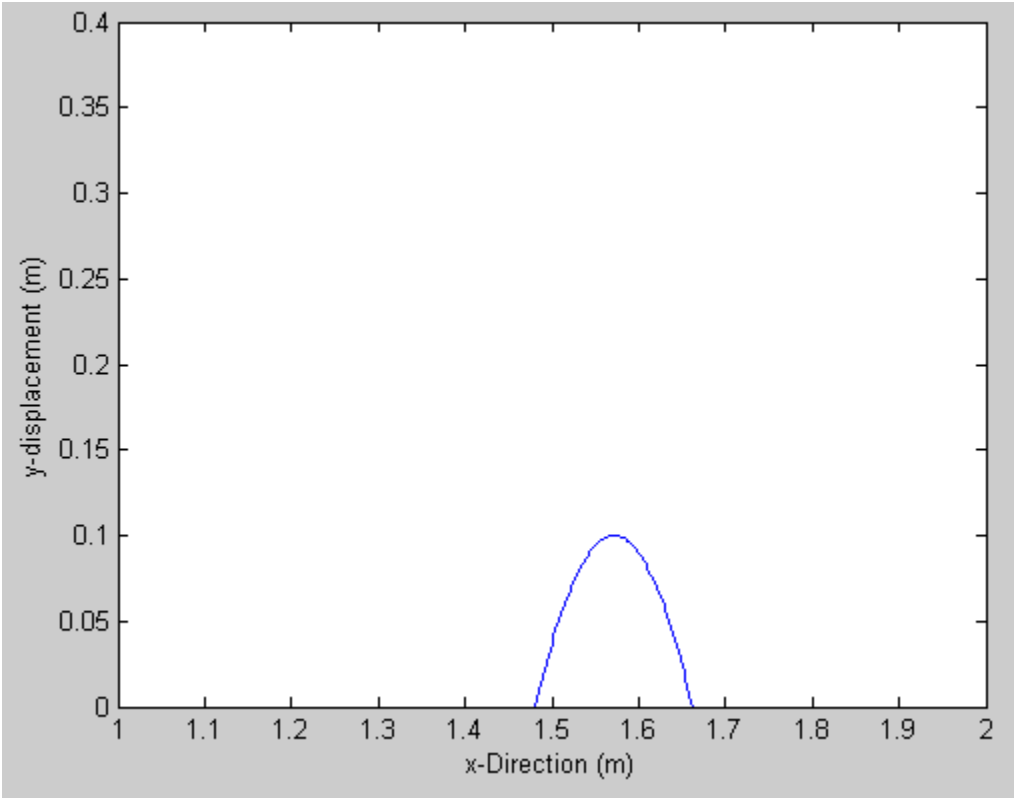

Figure 4.12: Boulder Modeled as a Parabola

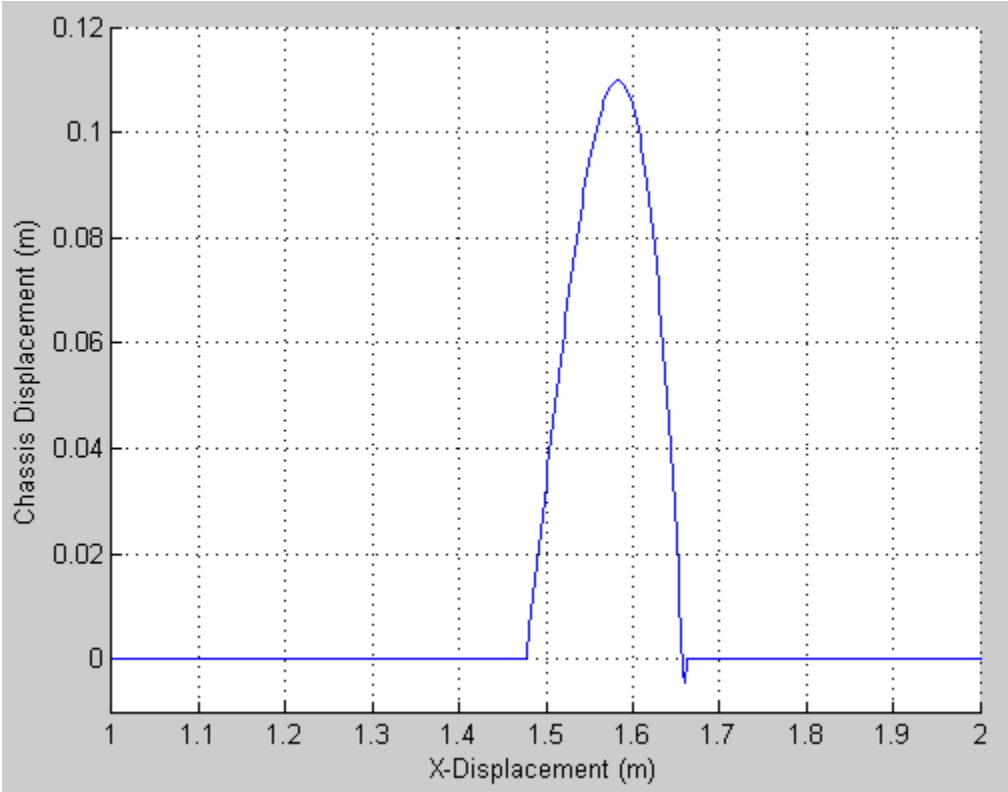

Figure 4.13: Rover's Position Driving Over a 10 cm Boulder

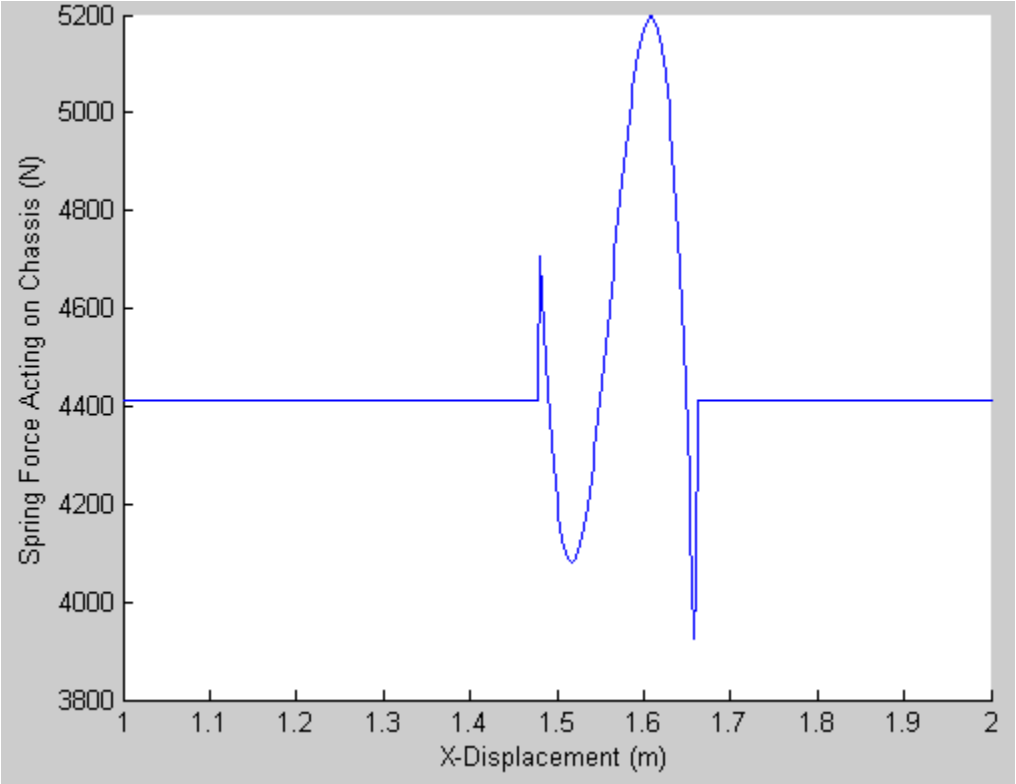

Figure 4.14: Reaction Force of Suspension

Properties For the numerical solution of landing the rover on its four wheels the mass of each wheel was taken into account. The mass of the rover was assumed to be its total mass; that is, 3000 kg. The suspension's spring constant was set to 70 kN/m and the damping constant was set to 2 kN-s/m (Shown in Figure 4.15). Landing on its wheels, the rover's tires were modeled as another set of mass-damper-spring system. The spring constant for the tires was 190 kN/m and the damping constant 12 kN-s/m.

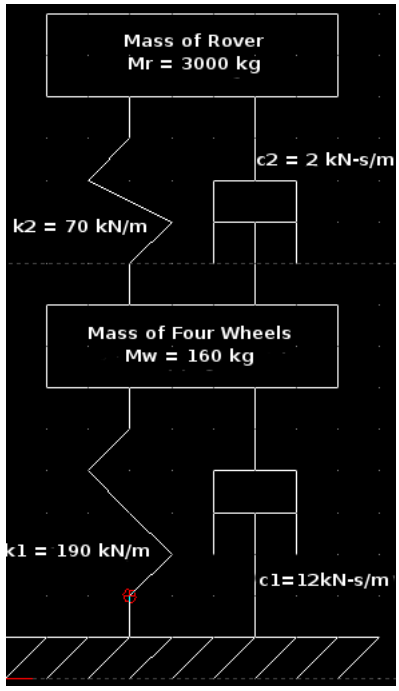

Figure 4.15: Properties of Suspension System for Landing the Rover on the Moon

Positions The suspension's compression was plotted using the position of the center of the tires and the rover's chassis (Figure 4.16). The forces applied to the wheels create a compression on landing of about 10 cm. The suspension can compress up to fifteen centimeters before deformation. This compression is the limit of how much the suspension system was designed for. The rover should not be overloaded to ensure that the suspension supports landing on its wheels.

Combined Forces The forces acting on the rover's suspension system get distributed over the damper and spring, each one taking some of the reaction and creating a damped oscillation that eventually allows the vertical motion of the rover to die out to zero after a few very short period of time (Figure 4.17). The damper takes a maximum force of about 1000 N and the spring takes about 8000 N. Both maximum forces occur in compression creating a total compressive force on

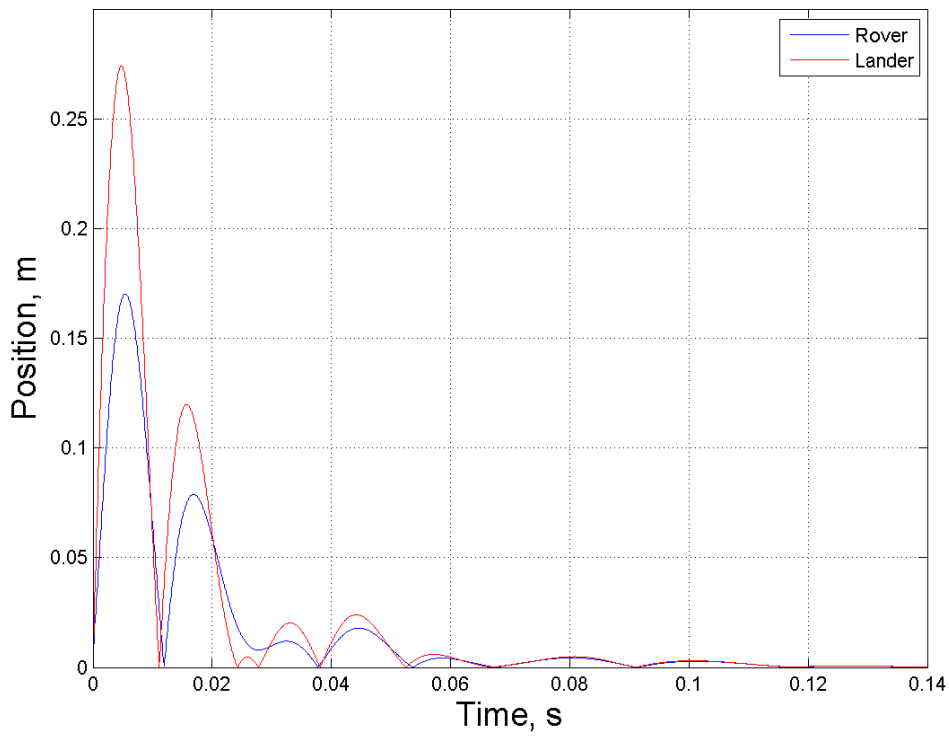

Figure 4.16: Displacement of Suspension and Rover Showing Suspension Compression

the wheels of about 7854 N and a displacement in the compression of the suspension of about ten centimeters.

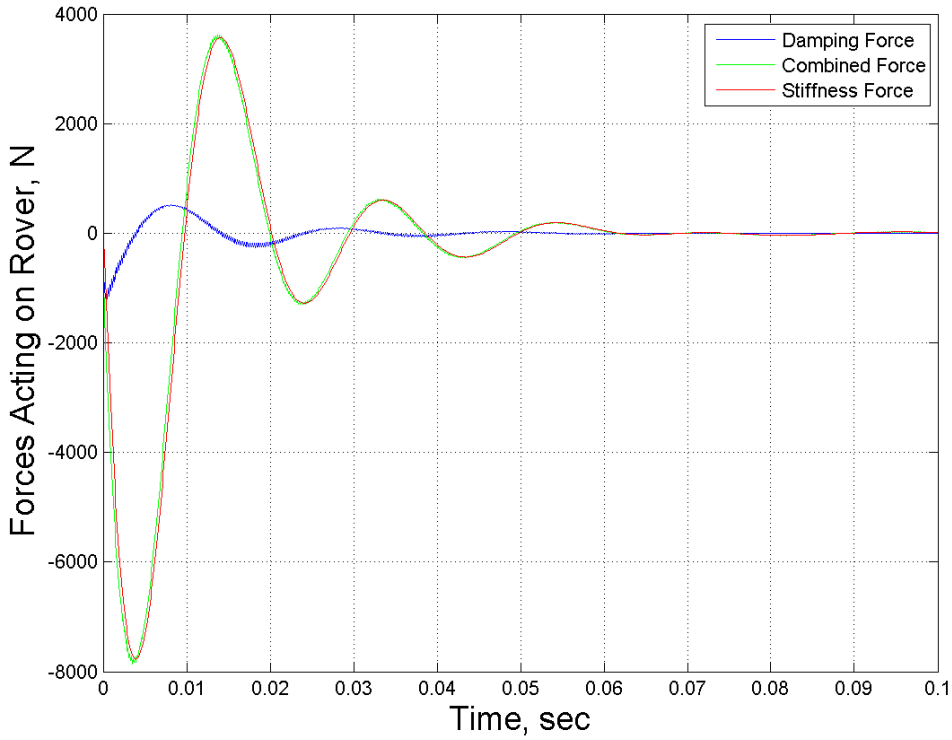

Figure 4.17: Combined Forces Acting on Suspension for Landing Rover on Four Wheels

4.2.4.3 Scenario 3: Landing Rover on Moon on One Wheel

This was the worst case scenario for landing the rover on its wheels, or rather on one wheel. The entire weight of the rover varies depending on the roll and pitch angles at which the rover is landing with. The very worst case scenario for stability is to land the rover on one wheel and have the opposite end wheel be at the most at forty centimeters above ground lever. While there is stability in that the rover will not tip, the amount of weight transferred to the one suspension compresses it past its design.

Properties As mentioned above, the rover lands on one wheel at the same speed of 1 m/s using thrusters attached to the rover. In this case, the rover is assumed to land on one wheel before the other three do and the maximum force the suspension can take is solved for. The model assumes the entire rover's weight is acting down and the reaction of the wheel is acting upward. The maximum height of the opposing wheel can be forty centimeters before the suspension breaks. Having a greater inclination when landing would then break the suspension of landing wheel and end crew mission.

Positions and Forces Landing the rover on one wheel in the worst case creates a maximum compression of the rover's suspension of 15 cm (shown in fig. 4.18), which is just about the maximum compression allowed. and the combined forces of the damper and spring are about 28 kN (shown in fig. 4.19). The damping force clearly shows how the suspension tries to dampen out while the spring creates an oscillation. The forces die out after a tenth of a second.

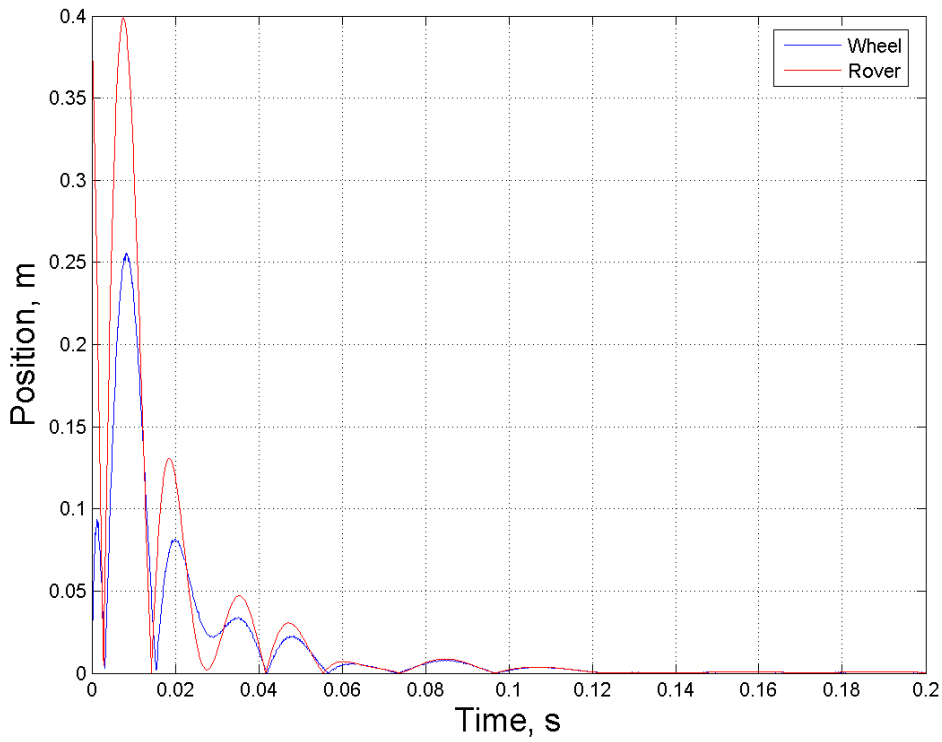

Figure 4.18: Displacement of Suspension and Rover Showing Suspension Compression

4.2.5 Suspension Modeled for Crew Comfort

For the CDR, we were allowed to implement a more accurate model of the rover. The full-vehicle model was used to include roll and pitch about the center of gravity (shown in Figure 4.20) while driving over a terrain defined with random oscillations [50].

4.2.5.1 Smooth Ride

The suspension was redesigned for a smooth ride. The properties of the previous models for landing the rover on its wheels and impact with a ten centimeter boulder were discarded and replaced with smaller constants for the spring and damper.

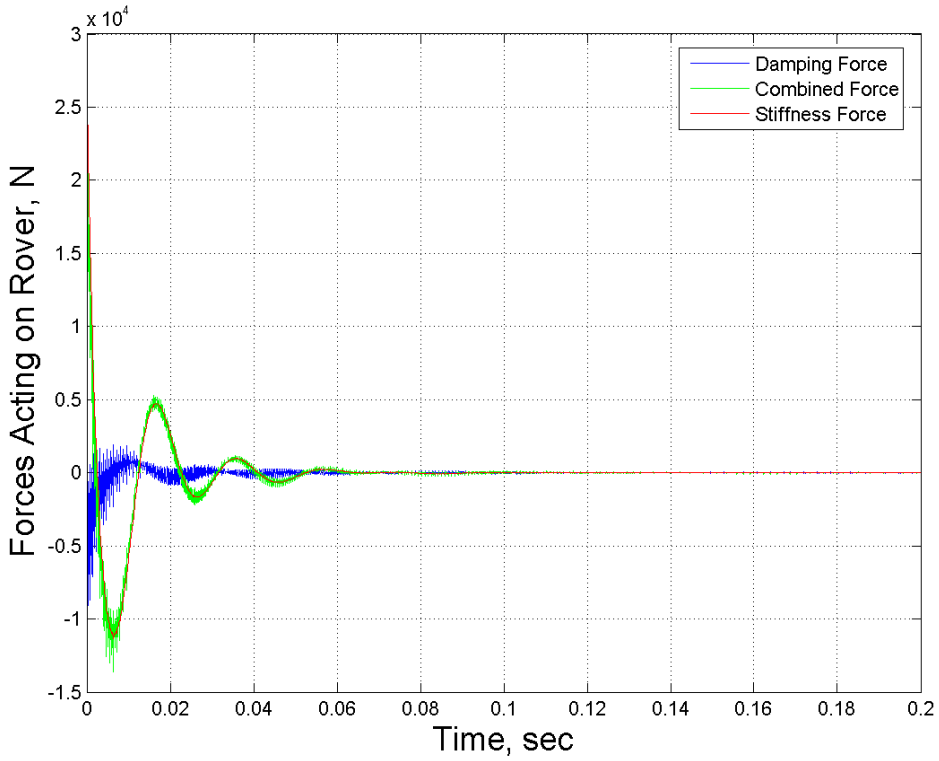

Figure 4.19: Combined Forces Acting on Suspension for Landing Rover on One Wheel

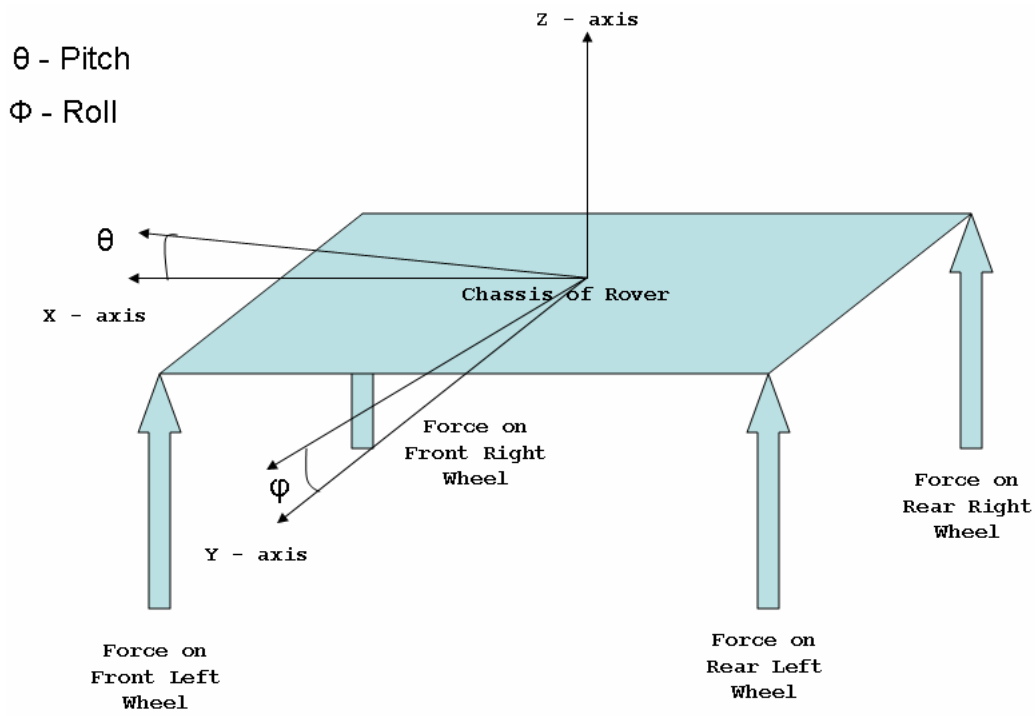

Figure 4.20: Model of Rover with Four Independent Suspensions Taking Into Account Roll and Pitch About the Center of Gravity

4.2.5.2 Low Rotating Angles

The pitch (shown in Figure 4.21) of the rover is the rotation about the x-z plane and impedes proper visualization of the terrain while driving. The roll (shown in Figure 4.22), which is the rotation of the rover about its y-z plane, needs to be low to not make the crew become nauseous when driving over rocky or bumpy terrains.

The suspension as a result was designed to create quick decay of oscillations on the z-axis, that is, the vertical direction when the terrain heights range between zero and ten centimeters.

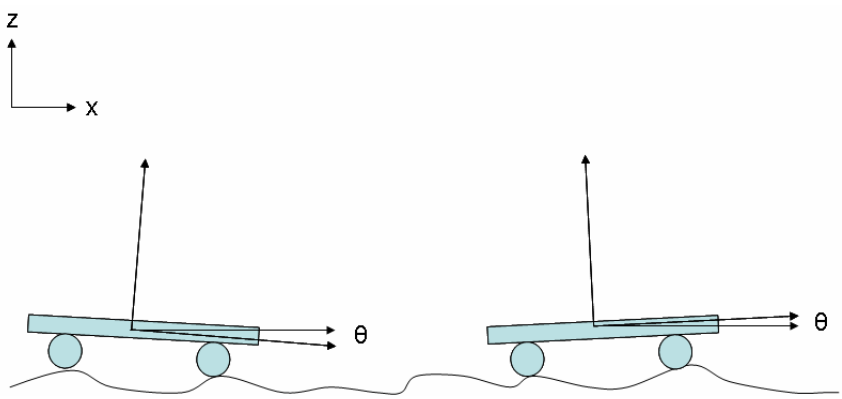

Figure 4.21: Change of Pitch of the Rover when Driving Over Lunar Terrain

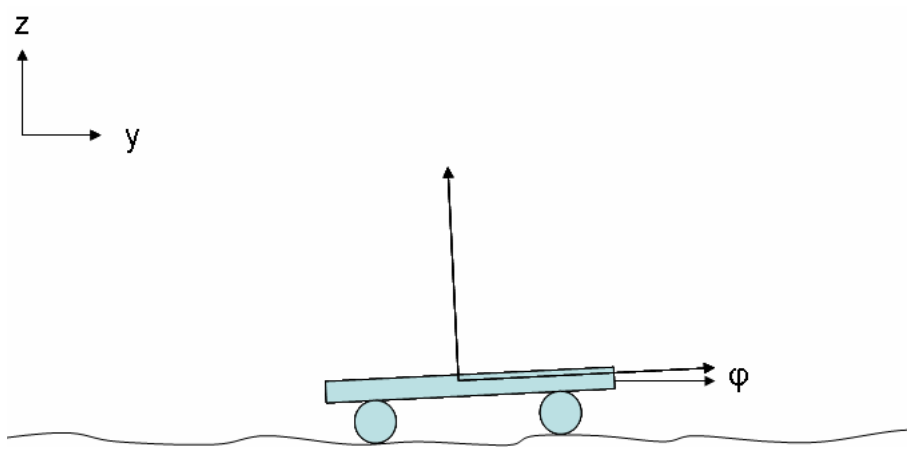

Figure 4.22: Change of Roll of the Rover When Driving Over Lunar Terrain

4.2.6 Suspension Properties

The suspension on each wheel was modeled as a the model for the quarter vehicle suspension. The mass that each suspension takes is about a quarter of the rover's total mass. The rover was assumed

to have a mass of 2500 kg without the crew inside when landing. The dampers of the suspension are 1 kN-s/m and the springs constants are 35 kN/m, while the quarter mass of the rover is about 625 kg.

4.2.7 Lunar Surface Modeling

The surface of the lunar ground was modeled for a traveling distance of eight meters. This distance is arbitrary and can be changed for further study to find fatigue on chassis and shell structural parts. The surface was modeled to have heights ranging ten centimeters (shown in fig. 4.23). While driving over a bumpy terrain was not in the requirements, this model of the lunar surface helps to confirm that the reaction on all four wheels oscillate from the static reaction by about 100 N, therefore confirming that the suspension system model used is accurate and correct. [91]

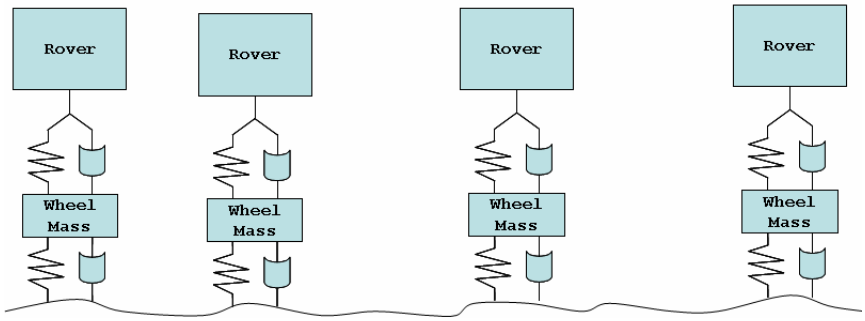

Figure 4.23: Suspension Designed for Crew Comfort (Minimal Vertical Motion When Driving Over Rocky Surfaces

4.2.7.1 Typical Model Reaction for Each Wheel (Work Done by Enrique Coello and Zohaib Hasnain)

The rover's suspension was plotted against the lunar terrain model and a line was used for comparison to note how much the suspension was being displaced (shown in fig. 4.24). The suspension was plotted in red and the lunar terrain was plotted in blue. The analysis shows that the suspensions reaction and displacement is smooth compared to the input, therefore giving a smooth ride to the crew on board.

4.2.7.2 Roll and Pitch About the Center of Gravity

To find the roll and pitch on the rover, all four suspension reactions were put together to find a final roll and pitch about the center of gravity. The roll was calculated using the rear tires and the front tires independently because all four wheels experience different terrain heights (shown in fig. 4.25). Therefore, the roll on the front of the rover and the rear are different. The pitch of the rover

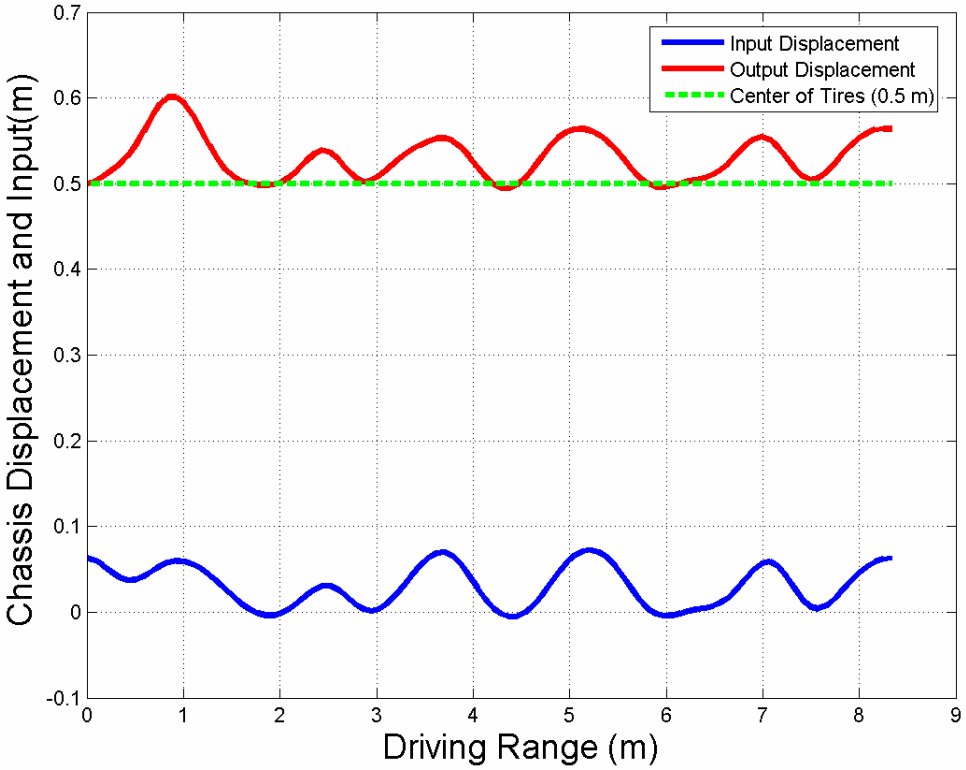

Figure 4.24: Reaction of Suspension to Lunar Terrain Model

was also found using the same idea. The pitch on the left wheels and the right wheels gave different angle changes with respect to the center of the rover. Putting together the rear and front rolls, we can find the roll about the center of gravity. The same is done with the pitch. The rover's pitch and roll angles are less than three degrees from the center of gravity (shown in fig. 4.26). [46]

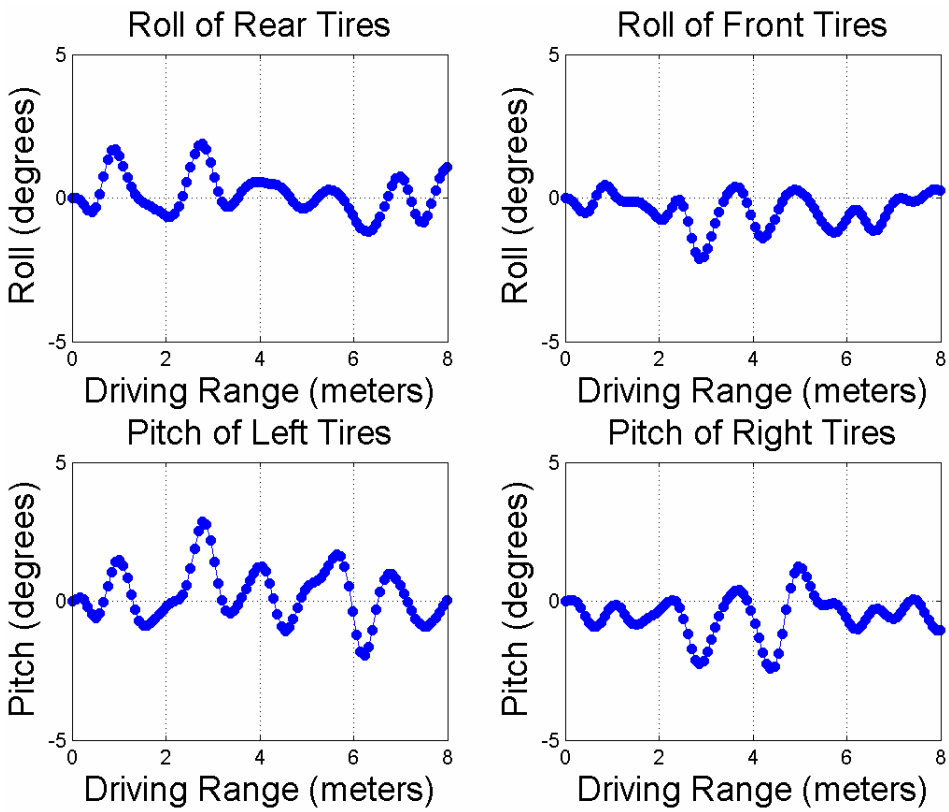

Figure 4.25: Rotation of Roll and Pitch About the Extremes of the Rover

The reaction forces on all four wheels when driving at a velocity of 7.5 km/hr on lunar terrain range from 3500 N to 4500 N. This averages a reaction force of about 1000 N on each wheel and is about a quarter of the total static reaction of the rover when not driving.

The reaction forces (show in eq. 4.13) for each suspension system (that is, for each wheel) were calculated from the equation:

$$\mathbf{F} = \mathbf{M}\ddot{\mathbf{q}} + \mathbf{C}\dot{\mathbf{q}} + \mathbf{K}\mathbf{q} \tag{4.13}$$

The total reaction force of the wheels is the sum of the four reaction forces on the wheels and the average is a quarter of the sum. The value of the total reaction force and the average vary due to the amount of variations in height of the terrain where the rover is driving over but overall is about the same as the static force. [54]

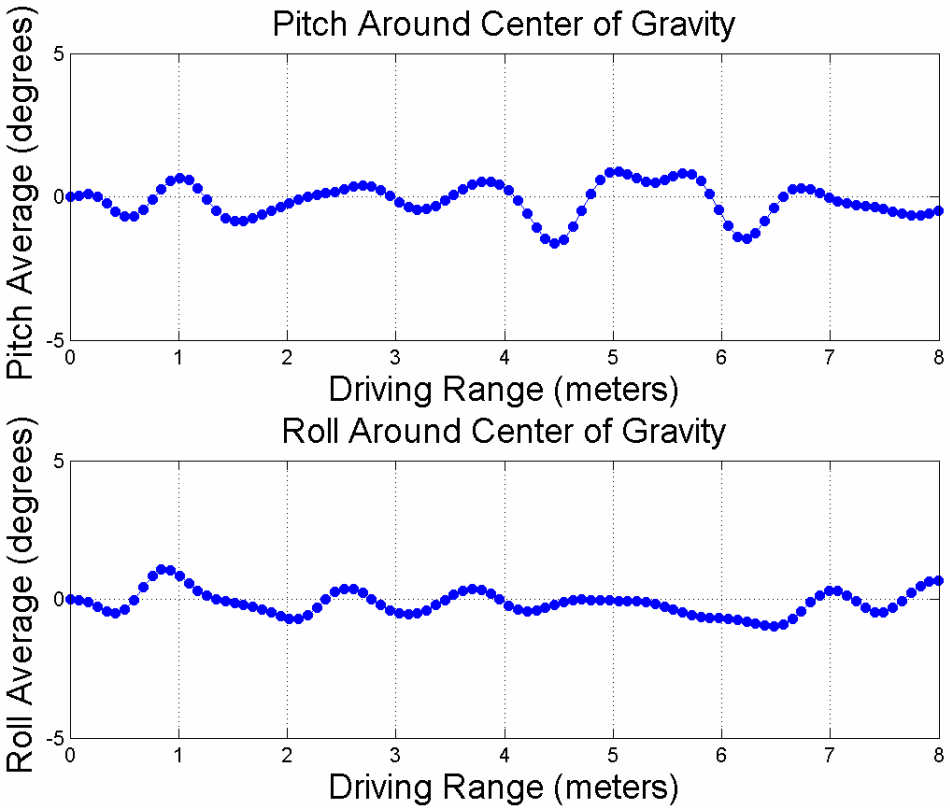

Figure 4.26: Roll and Pitch Change When Driving at a Speed of 7.5 km/hr

Lastly, varying the input to a flat level ground with a bump to simulate a boulder of ten centimeters in height (shown in fig. 4.28), the total reaction force on one suspension is about 6500 N (shown in fig. 4.27). This reaction force value is well below the limits of what the suspension was designed for while the rest of the wheels take in about 900 - 1100 N that settle back to about 1000 N after less than a second allowing a smooth ride and comfort of the crew when a boulder is not seeing while driving.

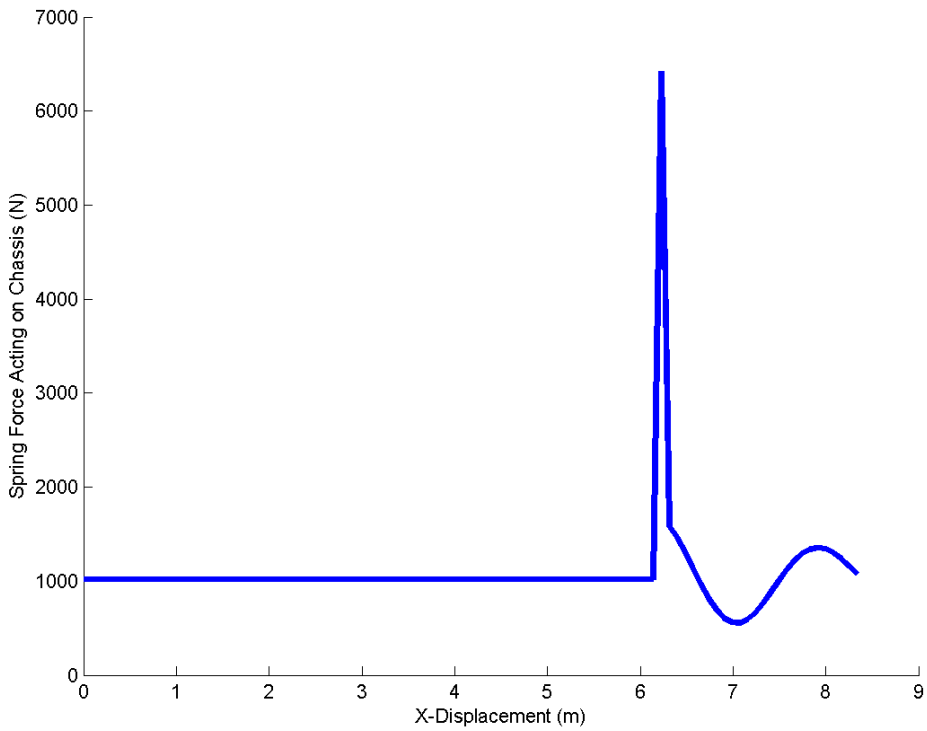

Figure 4.27: Force Transfered to Suspension When Hitting a 10 cm Boulder

4.2.8 Future Work

The suspension was designed for landing on its legs at the speed of 1 m/s for the BDR and then the suspension had to be redesign for driving over different lunar terrains when a lander was used to drop the rover on the surface of the moon for the CDR. The problem with the CDR is that the rover's suspension was assumed to be able to support a drop of fifty centimeters from the lander with initial speed of 0 m/s. The problem here is that when the a three thousand kilogram rover is dropped half a meter, its going to pick up speed. The suspension for the CDR was not designed to accomodate for this type of impact. We need to either redesign the suspension's properties, that is, the spring and damper coefficients or implement a platform on the lander design to allow the rover to drive off after landing on the moon using some type of ramp.

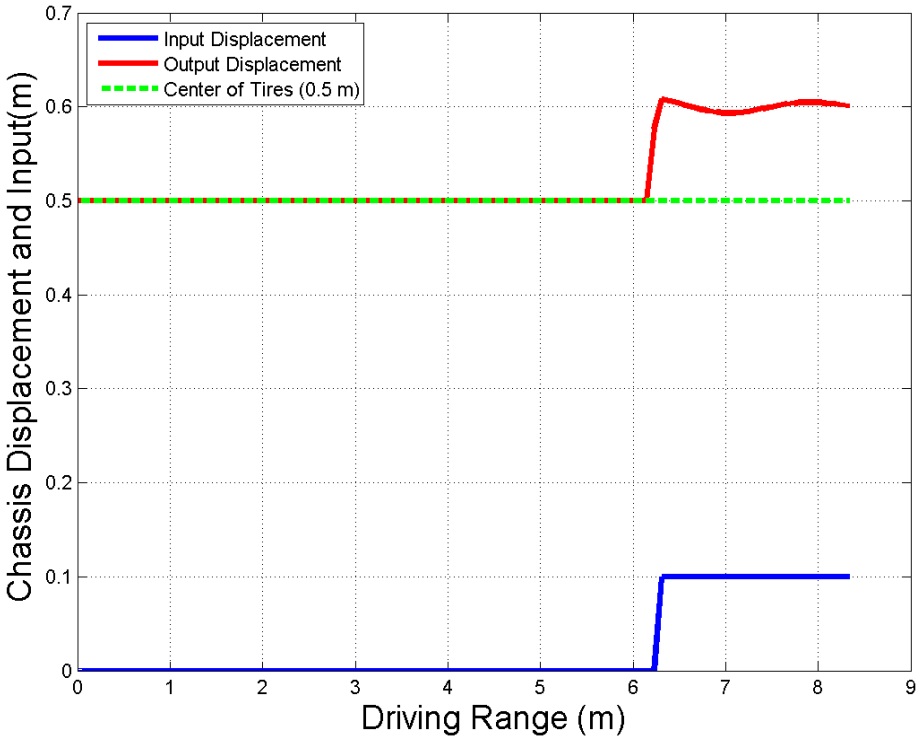

Figure 4.28: Displacement Reaction of Suspension When Hitting a 10 cm Boulder

4.3 Flight Rover Chassis Analysis

The method of analysis and the results from this analysis were the product of several iterations that occurred in earlier stages of the development of the chassis model. These earlier iterations are detailed in the Appendix. The current analysis used the aid of a computer software program called Visual Analysis. In addition, the results from Visual Analysis were compared to the results obtained from the first-cut analysis to assess the validity of.

4.3.1 Chassis Model (Aaron Cox)

Visual Analysis was used to draw the members of the chassis. Each member was distinguished by the nodes at its endpoint. In all, 90 members were created with the purpose of mirroring the CAD model of the chassis as closely as possible; however, since Visual Analysis is only capable of drawing straight beams, some sections in the chassis model are approximated. For instance, the four rings present in the CAD model had to be simplified in Visual Analysis by making an approximate ring out of 12 separate members. In addition, some bent members in the CAD model that were a single, solid piece had to be approximated by using two separate members. For example, in the CAD model, the "shock tower" was a single member that bends upward in the positive z direction near both of its endpoints. In Visual Analysis this single member was drawn by breaking the member into three pieces. All other members were exactly modeled as the CAD model of the chassis. The lengths and the geometry of each member were modeled exactly as designed in the CAD drawings.

4.3.2 Loading Cases (Aaron Cox)

Loading cases were determined by observing the possible situations during the field rover's operation that may cause substantial stresses on the members of the chassis. Three major loading cases became apparent: launch, landing, and driving. Specifically, for the driving scenario, an investigation was made into the loads applied to the chassis while hitting a rock with one wheel.

4.3.2.1 Launch

During launch, the rover was oriented so that its axis of motion is aligned parallel with the launch vehicle's axis of motion. The chassis was attached to the launch vehicle at eight different locations. These locations are distinguished in Figure 4.29 by the nodes C1-C8. These nodes were fully constrained, meaning they were not allowed to rotate or translate in the model.

Under launch, the chassis was subjected to an axial acceleration of 6g's and a lateral acceleration of 2g's. These accelerations were applied to the mass of all the components attached to or contained within the chassis. These masses under acceleration created by inertial loads on the rover chassis during launch. The table in Figure 4.29 lists various load sources and describes the location of these load sources on the chassis by a color code. In addition, the table depicts the magnitude and

direction of the loads and shows which load sources were considered either a point or distributed load in the model. The chassis model in Figure 4.29 also shows the distributed inertial loads experienced during launch.

If a load source spanned a large portion of the chassis, then it was considered a distributed load. For example, the water for the radiation protection spanned the upper half of the ring structure and also ran along the length of the cabin. Components with significant mass that spanned a small area were considered point loads. For example, fuel tanks attached to the sides of the rover were point loads.

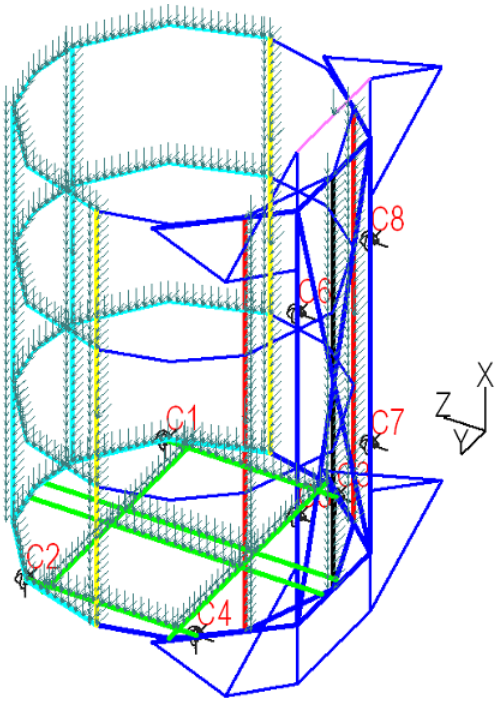

Load Source Legend

Color	Load Source	Load Type	Force X	Force Y	Force Z
Light Blue	Water	Distributed	-10.5 kN/m	3.5 kN/m	0
	Avionics	Distributed	-7.9 kN/m	2.6 kN/m	0
	Radiators	Point	-1.6 kN	0.53 kN	0
Light Green	Suitports	Distributed	-9.3 kN/m	3.1 kN/m	0
	External Platform	Point	-3.2 kN	1.1 kN	0
Black	Cabin Weight	Distributed	-9.6 kN/m	3.2 kN/m	0
Red	Cabin Weight	Distributed	-4.8 kN/m	1.6 kN/m	0
	Science Package	Point	-5.0 kN	1.7 kN	0
Pink	Fuel Cells	Point	-5.0 kN	1.7 kN	0
Yellow	Fuel Tanks	Point	-21.4 kN	7.1 kN	0

Figure 4.29: Launch Loading Case

4.3.2.2 Landing

The landing scenario analyzed the loads that were transferred from the landing structure to the chassis during the impact with the lunar surface. The chassis is oriented with the x-y plane of the body frame parallel to the lunar surface. The landing load case is shown in Figure 4.30. Similar to the launch loading case, the table in the figure shows the loads with their corresponding colors and load types. The inertial loads that were present in the launch case were also present in the landing case; however, the direction of all the inertial loads were in the negative z direction as opposed to the x and y direction. The constraint nodes are shown on the bottom portion of the chassis and are

labeled C1-C4. Nodes C1-C4 were fully constrained again, but there were four constraint locations as opposed to eight. These constraints represented attachment points to the landing structure during landing. The members that contained these attachment locations were color coded gray. These were the members that experienced the impact force in the positive z direction upon landing. The landing force was 6.9 kN in magnitude.

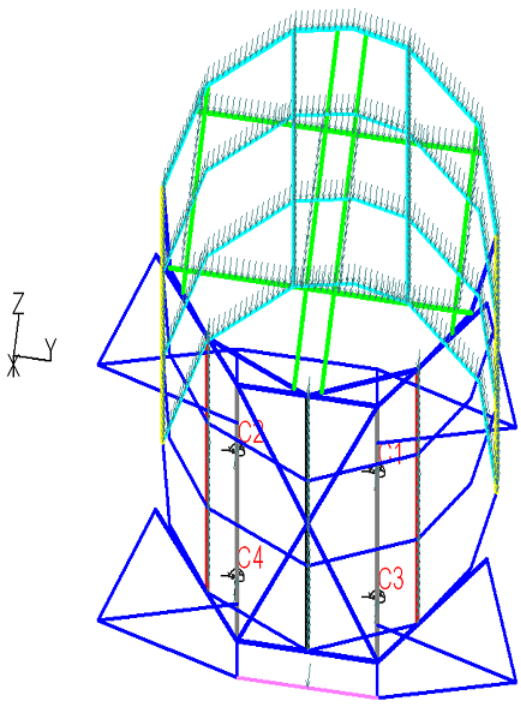

Load Source Legend

Color	Load Source	Load Type	Force X	Force Y	Force Z
Light Blue	Water	Distributed	0	0	-290 N/m
	Avionics	Distributed	0	0	-220 N/m
	Radiators	Point	0	0	-45 N
Light Green	Suitports	Distributed	0	0	-260 N/m
	External Platform	Point	0	0	-90 N
Black	Cabin Weight	Distributed	0	0	-270 N/m
Red	Cabin Weight	Distributed	0	0	-130 N/m
	Science Package	Point	0	0	-140 N
Gray	Landing Impact	Point	0	0	6.9 kN
Pink	Fuel Cells	Point	0	0	-140 N
Yellow	Fuel Tanks	Point	0	0	-600 N

Figure 4.30: Landing Loading Case

4.3.2.3 Rock Collision

The loading case in this scenario was very similar to that of the landing load case. The orientation of the rover in the rock collision case was identical to that of the landing case; however, the conditions that created the external applied load were different.

The rover was modeled to be moving at 7.5 km/hr and striking a 0.1 meter tall rock with its right, forward wheel. The rock impact applied a load of 0.45 kN in the positive y direction and a 1.11 kN force in the positive z direction. Temperature effects were also taken into consideration for the model by assuming that a 240 C temperature change was being applied to all of the members of the chassis while the rover was striking the rock.

Figure 4.31 shows the loading case for this scenario. Figure 4.31 shows the different load sources and load types along with their location in the chassis as designated by the different colors. All the

inertial load magnitudes and directions were identical to the inertial loads present in the landing load case. The constraints are shown by nodes C1-C4 located on the chassis. These locations represented the wheel attachment points to the chassis. The gray colored member in the figure shows the member that experienced the applied force due to the rock impact.

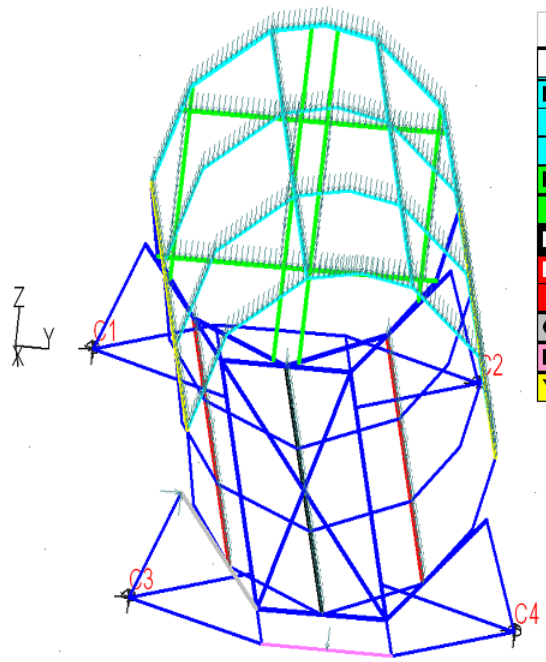

Load Source Legend

Color	Load Source	Load Type	Force X	Force Y	Force Z
Light Blue	Water	Distributed	0	0	-290 N/m
	Avionics	Distributed	0	0	-220 N/m
	Radiators	Point	0	0	-45 N
Light Green	Suitports	Distributed	0	0	-260 N/m
	External Platform	Point	0	0	-90 N
Black	Cabin Weight	Distributed	0	0	-270 N/m
Red	Cabin Weight	Distributed	0	0	-130 N/m
	Science Package	Point	0	0	-140 N
Gray	Rock Impact	Point	0	0.45 kN	1.11 kN
Pink	Fuel Cells	Point	0	0	-140 N
Yellow	Fuel Tanks	Point	0	0	-600 N

Figure 4.31: Rock Collision Loading Case

4.3.3 Method of Analysis (Aaron Cox)

The chassis was analyzed by treating the model as a 3D space frame. Using Visual Analysis, external loads were applied as described in each of the three loading cases. In each load case, the external loads were used to calculate the reaction forces at each constraint node. Using static analysis, the reaction forces in each individual member was determined. Specifically, the forces were determined at the endpoints (i.e. the nodes) of each individual member.

Once the reaction forces in each member were known, several section cuts were made along the length of each member. The internal forces at each of these section cuts were then determined. This allowed the axial force, shear forces, torsion, and bending moments to be found in each of the 90 members that created the chassis model.

4.3.4 Results (Aaron Cox)

Visual Analysis created a complete report detailing all of the internal forces found at each section cut in all 90 members. These results were obtained for all three loading cases. A sample of these results is shown in Figure 4.32. The six highest stressed members from each loading case are shown along with their general location in the chassis in Figure 4.32. In addition, the highest internal load for axial, shear (Vy and Vz), torsion, and bending moments (My and Mz) are highlighted in the figure below.

The complete report detailing the internal forces in all 90 members was used as the basis for member sizing. Each member was sized so that it would not fail when subjected to these loading cases. The results showed that overall, the launch loading case was the source of the critical loads for the majority of the chassis members.

Launch: Member Maximum Internal Forces

Member	Location	Axial (N)	Vy (N)	Vz (N)	Torsion (N-m)	My (N-m)	Mz (N-m)
1	S-port Ring	-2100	260	-9400	370	2300	0
2	S-port Ring	1600	-8400	2800	-470	-120	-250
3	S-port Ring	2400	1400	1400	540	-800	100
4	S-port Ring	-5700	2400	11000	270	400	270
5	Upper Strut	-8000	-4200	1800	-80	-950	2100
6	Bottom	11000	5500	-80	110	-70	770

Landing: Member Maximum Internal Forces

Member	Location	Axial (N)	Vy (N)	Vz (N)	Torsion (N-m)	My (N-m)	Mz (N-m)
1	Bottom	-450	240	-70	-60	-20	-30
2	Bottom	-660	20	-1000	10	-270	10
3	Rear	-1100	-70	630	50	-150	20
4	Front	-1300	140	-600	-40	140	10
5	Ring	-240	220	100	10	40	80
6	Ring	1100	10	40	0	-10	10

Rock Collision: Member Maximum Internal Forces

Member	Location	Axial (N)	Vy (N)	Vz (N)	Torsion (N-m)	My (N-m)	Mz (N-m)
1	Bottom	-8800	20	60	0	-50	-10
2	Bottom	3700	50	10	0	0	-10
3	Bottom	570	1900	-300	-40	40	-10
4	Rear	490	-450	0	0	0	210
5	Rear	600	610	10	-10	0	-290
6	Lower Strut	-270	60	-240	10	90	-30

Figure 4.32: Member Internal Forces Results

4.3.5 Chassis Sizing Analysis (David McLaren)

4.3.5.1 Design Parameters

Based on information from NASA-STD-5001, a safety factor of 1.4 is used to size the chassis members[84]. The lowest possible safety factor is needed to minimize the chassis mass.

Aluminum alloy 6061-T6 is used as the material for the chassis. It is a very commonly used alloy with a yield strength of 275 MPa and density 2700 kg/m^3, giving it a high strength-to-weight ratio. Its shear strength is 205 MPa, modulus of elasticity is 69 GPa, and Poisson's ratio is 0.33[30]. An additional advantage of this alloy is that it is weldable, simplifying connections between chassis members.

4.3.5.2 Goals

The goal of the sizing process is to find the lightest cross-sectional shape to withstand expected loading conditions, with positive margins of safety. Internal loads in different pieces of the chassis were found and written to files using the Visual Analysis software package. Since it was not possible to optimize the sizes of individual members using that program, MATLAB code files were written to expedite the process.

The chassis is modeled with 90 unique pieces. The scale of this model, and the time constraints for the task, make it sensible to pursue an overall estimate of what the chassis would look like. The first goal of the analysis is to obtain a realistic estimate of the required piece dimensions and mass for the current design and load conditions. At this stage, it is sensible to limit the process to selecting the best hollow square or circular cross section for each piece.

The second goal of the analysis is to identify the pieces which are in need of optimization– those which need the greatest cross-sectional area and mass to survive loads in the current design. Identifying these members would lead to suggestions for improving the truss design to re-distribute loads. Where needed, further optimization could then be obtained through the use of cross sections other than the basic square and circular shapes. An automated, "one size fits all" solution to this problem is not meant to give perfect results for every piece, so much as a good approximation for the overall system. The current iteration of the sizing analysis is intended to give a reasonable first estimate of chassis size, and identify areas for improvement.

4.3.5.3 Fundamental Equations

Every piece is sized to withstand normal stress, shear stress, and buckling due to compressive forces. Each piece is designed to experience stress limited to

$$\sigma_{allowable} = \frac{\sigma_{yield}}{SF^2} \tag{4.14}$$

in order to have a positive safety margin when tests are applied from different loading conditions. Note that the safety factor is squared because of the definition of margin of safety used in Equation 4.1; sizing a piece while allowing any more stress would produce a negative margin of safety. Allowable shear load is determined using a similar equation. Yield strength of the materials is used in this calculation.

Maximum normal stress is determined using

$$\sigma_{max} = \frac{Mc}{I} + \frac{F}{A} \tag{4.15}$$

where M and F are the absolute values of the internal moment and axial force, A is the cross-sectional area of the piece, c is the distance from the neutral axis, and I is the area moment of inertia. This calculation gives the magnitude of the stress at the most severely loaded point under combined loading.

Similarly, maximum shear stress is determined using

$$\tau_{max} = \frac{Tc}{J} + \frac{kV}{A} \tag{4.16}$$

where T and V are the magnitude of torque and shear loads, c is the same distance to neutral axis, and J is the polar moment of inertia. The parameter k varies with the shape of the cross-section. This is an estimate of the max shear stress occuring on a particular piece.

For buckling analysis, most pieces in the chassis can be analyzed under fixed-fixed conditions, since they are constrained at both ends. Only those pieces connected to the wheel hub are free to rotate at one end. The critical buckling load can be determined as

$$P_{cr} = \frac{c\pi^2 EI}{L^2} \tag{4.17}$$

where c depends on the boundary conditions, L is the length of the piece, and E is the elastic modulus for the material. The actual compressive load is compared against this critical load to determine margin of safety against buckling. The test is disregarded in cases where axial loads are tensile, not compressive.

For some particular thickness value, the required width of a piece under the given conditions could be determined, and tested against shear stress and buckling. If the piece did not have positive margin of safety against one of these types of loads, it was resized to withstand it. Required widths were rounded up to the nearest millimeter.

4.3.5.4 Procedure

Developing methods to size the chassis was a long and iterative process. Methods to perform this task were at first derived and performed on paper. However, the need for automation was identified early. For the baseline design review, a program was written to display the dimensions and cross-sectional area of a piece sized against given loads, as its thickness was varied. This method was used to find the sizes of two of the most heavily loaded pieces in the chassis. This work was a building block for what would come later; the fundamental process and equations would not change

much, but in order to obtain information on every single piece of the chassis, the process had to be completely automated.

This was achieved by the critical design review. For every piece in the chassis, the program solved the equations for normal stress to produce a first estimate of the cross-section's thickness and width. This was tested for integrity against shear forces, as well as for buckling under compressive loading. If either condition was not met, the piece was resized to pass the failed test with positive margin of safety.

The heuristic used to size pieces is to select one with outer width 5% greater than the smallest observed width. As the wall thickness increases, the outer diameter needed to carry the loads does not decrease significantly. To illustrate the reason for this selection, plotted output from a circular example piece with internal moment 3000 N-m and axial force 9200 N is shown in Figure 4.33.

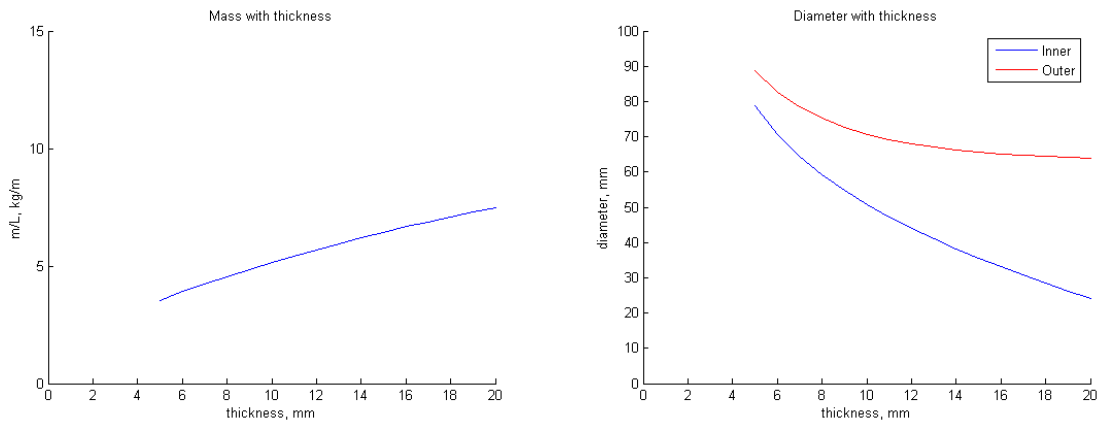

(a) Mass trend

(b) Diameter trend

Figure 4.33: Trends in Mass and Dimensions as Thickness Increases

The software tests loading conditions for each piece against hollow square and circular cross sections. However, since chassis members are expected to experience forces from many different directions, it is preferable to use circular cross sections. Thus, these are used to obtain size estimates for the final iteration of the sizing procedure.

To further optimize the size of pieces, it would make sense to try more uniquely shaped cross sections (rectangular, elliptical, etc.), to better distribute loads. The intention is to obtain an overall design for all chassis members, not try to optimize every single one of them for its unique loading conditions.

4.3.5.5 Software Program Structure

The software program is arranged to perform two separate functions: sizing and testing. One module reads input parameters including piece names and applied load magnitudes from a report

provided by the Visual Analysis program, then finds working sizes for each piece and stores these in a file. The second module loads the stored piece information, and then tests each piece to see if it has a positive margin of safety against the forces resulting from each individual test case (launch, landing, rock hit).

All pieces for the rover design are initially sized to withstand launch conditions. Intuitively, this seems to be the worst case expected for most pieces. The corresponding sizes are then tested against the other two loading cases: driving while hitting a rock (with temperature effects on the lunar surface included), and landing. Any pieces found to have a negative margin of safety against one of these loading conditions are then resized. In practice, driving loads required that 5 of the 90 pieces be resized, and landing does not require any of them to be scaled up.

4.3.5.6 Selected Results: Main Chassis

The main chassis structure, shown in Figure A.3, includes the central "box" consisting of M19-21, and M5-8 in the figure. This is the base of the rover, supporting the cabin during the lunar sortie and holding it together during launch. The wishbone structures (such as M18 & M17) can be seen jutting out to the sides.

The critical loads all occur during launch. Hollow, circular cross sections are used. Required dimensions and masses are shown in Table 4.3.

Table 4.3: Safety Margins for Selected Main Chassis Members

Member	M5	M6	M7	M19	M20
Crit. Load Type	Combined	Buckling	Combined	Combined	Buckling
Axial Force (N)	-6100	-19000	+41000	-10000	-35000
Moment (N-m)	320	270	270	680	150
Inner/Outer Width (mm)	20/34	28/44	16/36	26/44	34/52
Unit Mass (kg/m)	1.6	2.4	2.2	2.7	3.3
Margin of Safety	0.35	0.29	0.25	0.36	0.25

Members M8 and M21 were excluded from the table. The loading conditions and resulting shapes are very similar to M5 and M19, respectively.

The 6g axial acceleration during launch requires that the two members M6 and M20 be sized by buckling conditions. The effective length of these two pieces could be reduced by adding another horizontal piece in the middle, increasing the critical buckling force on these pieces. This would require a smaller moment of inertia, smaller area, and thus lower mass in each piece. If the addition of these new pieces could reduce the mass of this section sufficiently, the overall chassis mass could be reduced. This is one particular opportunity identified for improving the overall design of the chassis. This suggestion was not implemented due to time constraints.

4.3.5.7 Selected Results: Rear Ring and Suitport Supports

There are four circular ring structures wrapping around the cabin, spaced along the chassis. They are also connected by longitudinal struts, shown in Figure A.7. In finding loads in the Visual Analysis program, the ring shapes were approximated by straight lines.

The ring at the rear of the rover, shown in Figure A.4, is where astronauts will enter and exit through the suitports. It is also where external supports will be added during launch to support the rover in the payload shroud. Extra members are present in this section of the chassis to support the suitports during launch and EVA events, rather than putting the associated loads directly on the shell.

Table 4.4: Safety Margins for Selected Rear Ring Members

Member	M41	M43	M80	M83
Axial Force (N)	2800	-5200	-5700	2200
Shear Force (N)	8300	9400	11000	8900
Moment (N-m)	1900	2300	1500	530
Inner/Outer Width (mm)	34/58	36/62	34/56	24/40
Unit Mass (kg/m)	4.7	5.4	4.2	2.2
Margin of Safety	0.21	0.23	0.32	0.40

All members must be sized by combined loads during launch, where they experience significant moments and shear forces. These members are the largest pieces in the entire chassis on a per-length basis. The mass of the suitports pushing down, and the connections to launch support structure, require these members to be very strong.

The addition of more structure to support the rover in the payload shroud during launch could allow the size of these pieces to be decreased. There is a tradeoff between adding more structure solely for the launch phase, and bulking up members in the rover chassis. A more detailed analysis would have to be conducted to determine the optimum external support structure, and how much overall mass can be saved for the system.

A 600 N instantaneous force was applied on piece M83 in a test to simulate loads experienced during astronaut ingress/egress. This produced a 600 N axial force, 40 N-m moment, and 800 N shear force internally. Comparing with Table 4.4, it can be seen that these forces are minor compared to those experienced during launch. The resulting margin of safety is 10 for this type of load.

4.3.5.8 Overall Results

Forces for all 90 chassis members are tabulated in Appendix A.4. The resulting dimensions, masses, and margins of safety are tabulated in Appendix A.5. To clarify the piece names, figures showing

the model used to obtain internal forces are shown in Appendix A.3.

Using this procedure, a mass estimate of 163 kg is obtained for the rover chasis. This could be improved by implementing the changes discussed for the two subsystems above. One other possible way to improve the mass is to switch the design material to titanium alloy, a material with an even higher strength-to-weight ratio.

4.4 Pressure Shell

4.4.1 Shell–Cylinder (Stuart Douglas)

The shell is the structure that creates the habitat and protects the astronauts from the harsh lunar environment. It will need to sustain the internal pressure necessary for crew life support and external loads from the many stages of launch, landing and driving.

4.4.1.1 Material Selection

The shell was designed for optimum strength to weight ratio. It is the largest structure on the rover and mass was a concern. Composite material became an option based on its agreeable material properties, and lower density compared to metals. Several NASA missions have utilized graphite/epoxy, therefore the material is a TRL 9.

The composite material was chosen based upon the largest loads the shell must support. The shell was modeled in two sections, a cylinder and endcaps, and the stress was treated as such. In certain cases, FEA analysis, smeared properties were used. The term smeared refers to the combination of both lateral and transverse moduli and ultimate strength. In order to choose a specific graphite fiber and epoxy, a material property reference had to be established.

After preliminary study, internal pressure was found to be the limiting factor for design. Using Equation 4.19 for a hoop stress of a pressure vessel, the stress was determined as a function of thickness. Using known Young's modulus' from various sources as a reference, the thickness was optimized.

$$\sigma = E\epsilon \tag{4.18}$$

$$\sigma = \frac{Pr}{t} \tag{4.19}$$

The elastic modulus (Equation 4.18) and thickness were then used as the starting point for material selection. The elastic modulus was determined from the hoop stress and strain was treated as the modulus in the longitudinal direction (Equation 4.20). Using basic composite equations (Equation 4.21, 4.22) the fiber volume and transverse elastic modulus were determined[69]. See Table 4.5.

$$E1 = EfVf + Em(1 - Vf) \tag{4.20}$$

$$1 = Vf + Vm \tag{4.21}$$

$$\frac{1}{E2} = \frac{Vf}{Ef} + \frac{Vm}{Em} \tag{4.22}$$

Table 4.5: Calculated Material Properties

E1 (GPa)	Em (GPa)	Vf	G12 (GPa)
146	10.6	0.62	4.5

The known material properties gave way to a specific selection of carbon fibers and epoxy resin. Examination of NASA documents and technical reports led to a graphite/epoxy laminate of T300/934.

A NASA study[1] focused on testing tensile, compressive and shear strength in both longitudinal and transverse direction under radiation in a space environment [61]. The report states that based on low CTE and high tensile strength and elastic modulus the material is ideal for aerospace applications. The relevant results of the report are as follows:

- Temperature was found to significantly affect compressive properties of T300/934. Properties generally improved at cryogenic temperature (-250° F; -157° C) and degraded at elevated temperature (2500° F; 121° C).
- Irradiation degraded properties at all three temperatures and this degradation was most severe at elevated temperature.

Conducting further research yielded manufacturers[2] properties. It should be apparent that Cytec unidirectional prepreg T300/934 properties closely mirror the required properties. The manufacturer also includes ultimate strength of the material which is important in determining margins of safety [101]. This can be seen in Table 4.7

4.4.1.2 Classical Laminate Plate Theory

In order to better understand the effects of an anisotropic composite, it was imperative to learn more on composite materials. Several resources were used in discovering which calculations would

[1] NASA Technical Report 19870016722_1987016722. Space Environmental Effects on Graphite Epoxy Compressive Properties and Epoxy Tensile Properties

[2] Cytec Engineered Materials

Table 4.6: Manufacturer's Material Properties

E_1(GPa)	E_2 (GPa)	Vf	$G_{1,2}$(GPa)	CTE_1	CTE_2
148	9.65	0.6	4.5	.6e-6	12e-6

Table 4.7: Manufacturer's Ultimate Strength

Ultimate Tensile Strength$_1$(MPa)	1314
Ultimate Tensile Strength$_1$(MPa)	1220
Ultimate Tensile Strength$_2$(MPa)	45
Ultimate Tensile Strength$_2$(MPa)	168
Ultimate Tensile Strength (MPa)	48

be necessary to determine the stresses in the material[3]. Fiber reinforced materials are used most frequently by stacking multiple layers, often referred to as ply, to form a laminate. The ply can have a large value range, but often are limited to the size of the fibers, which for T300 is about 0.127 mm. The number of plys determines the thickness of the laminate. In this case the shell thickness is t = 8.4mm. This thickness determines a mass of m = 177 kg. The orientation at which each ply is arranged determines its reaction to forces [73].

Optimization is the key to finding the right amount of material to use and the orientation of each individual ply. Using Algorithm 1, a custom computer program was employed to incorporate classic laminated plate theory. The program has the inputs of the number and orientation of each ply as well as the loads, thermal loads, and moments that the laminate will experience in every direction. The program creates stiffness and bending matrices based on the material properties and outputs the stresses in the axial, transverse and shear directions for each individual ply.

The orientation of each ply and the final layup of the laminate was determined in an effort to minimze material thickness and stress. Layup symmetry was used because it eliminates bending and strecthing coupling [69]. Initially, it was assumed that $\pm 45^o$ ply would be needed to support torque forces. However, it was observed that the $\pm 45^o$ ply increased the stress in the transverse and shear directions and thus the thickness. It was decided that $\pm 45^o$ plys would not be needed and that the torque forces could be handled adequately by the 0° and 90° plys. The final layup of the laminate is $[0_{11}/\ 90_{23}]_s$.

4.4.1.3 Loads

The loads the shell will be facing determine the layup orientation of each ply. In every case the shell will be taking loads in more than one direction. Since a composite is not an isentropic material, the strength of the material depends on the direction. A laminate is strongest in a fiber axial direction under a tensile force; however, the laminate will face axial as well as shear and transverse forces

[3]See references

1. Enter basic lamina properties (E_1, E_2, $G_{1,2}$, $v_{1,2}$).
2. Compute ply stiffnesses, $[Q]_{1,2}$, referred to its principal material axes.
3. Enter orientation of principal material axes, θ_k, of layer k.
4. Calculate transformed layer stiffnesses $[Q]^k_{x,y}$ of layer k referred to laminate coordinate system (x,y).
5. Enter through-the-thickness coordinates h_k and h_{k-1} of layer k surfaces.
6. Calculate laminate stiffness matrices [A], [B], and [D].
7. Calculate laminate compliance matrices [a], [b], [c], and [d].
8. Enter mechanical loading, i.e., forces $[N]_{x,y}$ and moments $[M]_{x,y}$.
9. Calculate reference plane strains $[\epsilon^o]_{x,y}$ and curvatures $[K^o]_{x,y}$.
10. Calculate thermal and layer strains $[\epsilon]_{x,y}$ and curvatures $[K]_{x,y}$.
11. Calculate layer stresses $[\sigma]^k_{1,2}$referred to layer principal axes (1,2)

Algorithm 1: Classic Laminate Plate Theory

during critical stages of the mission and it will need to withstand the stresses it will be facing. The importance of examining applied loads at launch, landing and driving provides knowledge of mission critical loads.

Launch During launch the shell will be facing a variety of loads. The first and most obvious of these is the axial load that the shell will take upon launch. The shell will also be required to withstand the lateral accelerations of the launch vehicle. Random vibration also produces critical stresses. The shell will not take pressure upon launch. Thermal stress was not accounted for during launch, but was accounted for in later stages of the mission. The launch vehicle will have a maximum acceleration upwards of 6g's. There will be lateral accelerations that will reach maximums of 2g's. For a better understanding of the launch vehicle accelerations see Figure 4.35. These loads were treated statically in calculations and dynamic loads were not taken into account, but were considered. Upon takeoff the shell will face a compressive force from inertial accelerations. The composite is considerably weaker in compression, but remains within the limit of the ultimate compressive stress. Initially, skin buckling was a concern. For this structure it will occur at $\sigma = 1.5$ GPa and it is apparent the stress will not reach critical buckling values. See Table 4.9.

$$\sigma_{buckling} = \frac{1}{\sqrt{3}} \frac{E}{\sqrt{1-\nu^2}} \frac{t}{r} \tag{4.23}$$

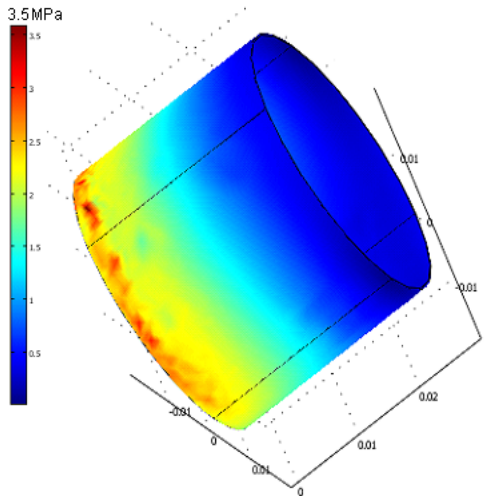

Figure 4.34: Finite Element Analysis of Shell under Launch Accelerations

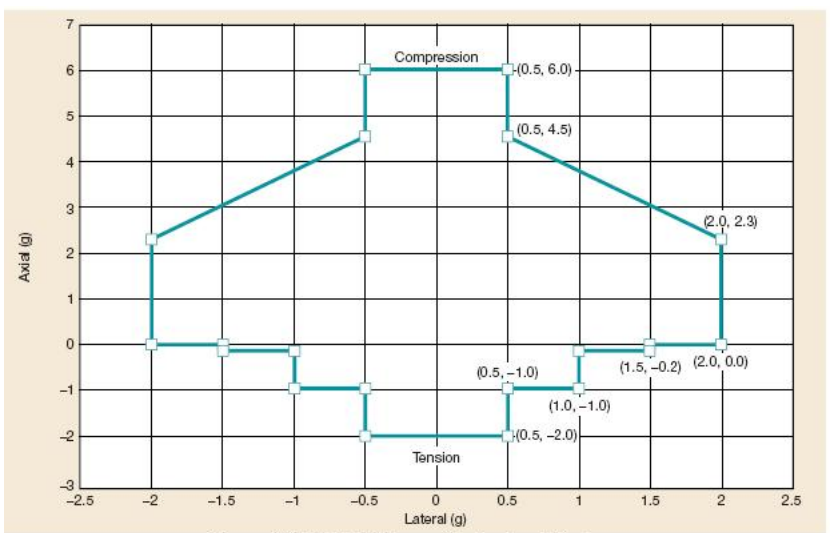

Figure 4-30. Delta IV Heavy Design Load Factors

Figure 4.35: Delta IV Heavy Accelerations

The vehicle will also face stress from random vibration. In order to roughly account for the vibration during flight, a simple stress calculation was employed to determine an order of magnitude that the shell will face. The shell itself will have a very high frequency based on its light weight and large size, however, much of the vibration will be damped out by the surrounding structures. Using Table 4.8 the damping ratio was determined and using Figure 4.36 the power spectral density was determined. The random vibration acceleration (Eq. 4.23)of the shell will be approximately RFL = 6.5g at a frequency (Eq. 4.24) f = 60Hz, which is a rough, but conservative estimate. The vibration accerleration (RFL) was used and then added to the other stresses. See Table 4.10.

Table 4.8: Damping Ratio Based off of Random Vibration Frequency of the Shell

f	ξ
$<$ 150 Hz	0.045
150 - 300 Hz	0.020
$>$300 Hz	0.005

Figure 4.36: Launch Vehicle Vibration Environment

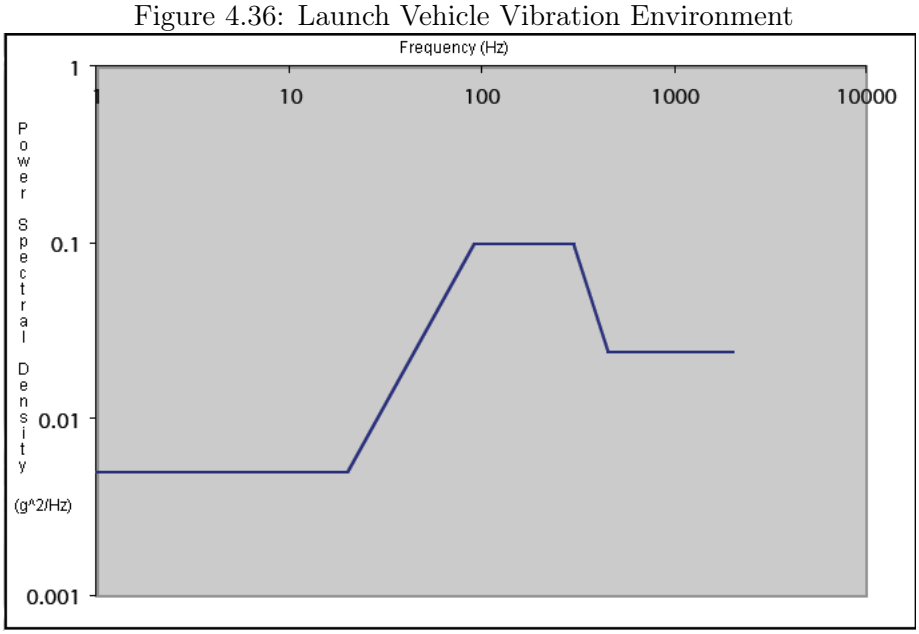

$$RLF_{\mathrm{n}} = \sqrt{\frac{\pi f_{\mathrm{n}} PSD}{4\xi}} \tag{4.24}$$

$$f_1 = \frac{1.732}{2\pi}\sqrt{\frac{EIg}{0.236Wl^3}} \tag{4.25}$$

Table 4.9: Launch Stresses with Axial and Transverse accelerations

Ply in Degrees	σ_1(MPa)	σ_2(MPa)	σ_3(MPa)
0	-2.9	0.022	0
90	1.5	-0.24	0

Table 4.10: Launch Stresses with Acceleration Loads and Vibration

Ply in Degrees	σ_1 (MPa)	σ_2(MPa)	σ_3(MPa)
0	-5.9	-2.9	$\pm$2.96
90	4.1	2.8	$\pm$2.96

Landing Landing was modeled as a beam under a distributed load with reaction forces at either end. Using static equations, an internal moment was derived. This was not the case and the soft landing from the suspension and landing system keep the internal moment from becoming critical.

The landing acceleration at contact will be approximately 1 m/s^2. This is a conservative estimate. The symmetric distributed load created an internal moment greatest at the center of the structure with an approximate value of 6 kN-m. Critical moment occurs approximately at 11MN-m (Equation 4.25), thus skin buckling during landing is not a critical load [111]. Based on where the support attachments are located the shell will take a shear force that will propagate along the hoop of the cylinder. The landing stresses are the smallest of the three critical load scenarios which is apparent in Table 4.11.

$$M_{cr} = K\frac{E}{1-\nu^2}rt^2 \tag{4.26}$$

Table 4.11: Landing Stresses with Induced Bending Moment

Ply in Degrees	σ_1(MPa)	σ_2(MPa)	σ_3(MPa)
0	-0.08	0.65	0.04
90	3.7	0.02	-0.04

Driving Driving loads turned out to be the critical of the three stages examined. The internal pressure needed for life support, worst case situations for driving, and thermal stress were all accounted for. Upon landing, the rover will become pressurized, the internal pressure of the module will be 8 psi or 55 kPa. The internal pressure was identified as the critical load of the shell. It determined the thickness of the hull, and the ply orientation. The stresses from the internal pressure in each ply were on the order of hundreds of MPa. The stress in the transverse direction was very high, and required a thicker laminate to counter balance the effects of the critical load. Since the

rover will be in motion as well as pressurized, a scenario was designed to account for the greatest loads. The input force into the suspension from the wheel at 7.5 km/hr over a 0.1 m obstacle is approximately 8 kN. Assuming that all of the force from the obstacle is transmitted to the shell, a shear force would be created from torque along the exterior of the shell similar to landing. The thickness of the shell was designed to withstand the combined loads of the internal pressure and torque generated from an obstacle (see Table 4.12).

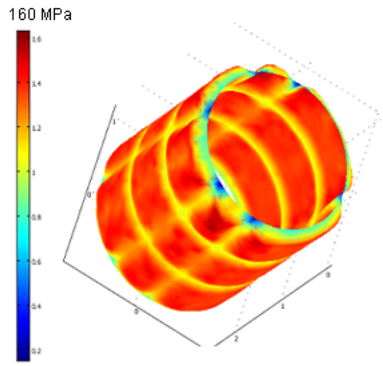

Figure 4.37: Finite Element Analysis of Driving Stress

While being on the moon the structure is required to withstand the temperature of the lunar day at 120°C and lunar night -120°C. Thermal stresses will be generated as the composite is subjected to large changes in temperature. Unlike metals, the coefficient of thermal expansion is low for composites. The coefficient of thermal expansion is also different in the longitudinal than in the transverse directions due to the anisotropic properties of the composite. In order to account for the added thermal effects, computer code was added to the classical laminate plate theory [73]. The thermal stress was very large and counteracted the effects of the internal pressure. The thermal stress was added to the other driving stresses to get a complete understanding of forces the shell will take during this stage (see Table 4.13).

Table 4.12: Driving Stresses with Pressure and a Torsion Stress from Obstacles

Ply in Degrees	σ_1(MPa)	σ_2(MPa)	σ_3(MPa)
0	176	15	0.16
90	191	15	-0.16

4.4.1.4 Margin of Safety

NASA STD-5001 states that all manned pressure vessels must have a factor of safety (SF) of 3 [84]. Based on this requirement, three times the stress in each ply must not be more than the ultimate

Table 4.13: Driving stresses with Combined Loads as Well as Thermal Loads

Ply in Degrees	σ_1(MPa)	σ_2(MPa)	σ_3(MPa)
0	150	-13	0.16
90	160	-15	-0.16

strength. This was a driving factor in determining the thickness of the shell. The internal pressure during driving created large stresses in the transverse direction (σ_2). Increasing thickness minimized the magnitude of the transverse stresses until an optimum value was found. It may seem that the structure has been grossly overdesigned, but in order to acheive a Margin of Safety (MOS) zero or greater the thickness was increased and the other loads became increasingly insignificant. Attention should be given to the stresses with the smallest margin of safety. A summary is presented in Table 4.14.

Table 4.14: Margin of Safety

Load	Highest Stress (MPa)	SF	Stress with SF (MPa)	MOS
σ_1				
Launch	5.9	3	9	147
Landing	3.7	3	6	236
Driving	190	3	570	1
σ_2				
Launch	2.9	3	4	37
Landing	0.65	3	2	22
Driving	15	3	45	0
σ_3				
Launch	2.9	3	4	10
Landing	0.04	3	0	399
Driving	0.16	3	0	0

The shell was designed for optimum strength to weight ratio. Launch, landing, and driving loads were examined critical situations. Driving loads were determined as the limiting load due to a combination of internal pressure, thermal stresses, and obstacle induced stresses. Using stress and strain equations and basic composite theory, graphite epoxy T300/934, closely matched the properties required. Graphite epoxy T300/934 has been studied and used in space flown hardware, therefore the material is a TRL 9. Classic Laminate Plate Theory was used to determine the stresses based on all three load situations. To minimize principle stresses, analysis was used to determine the $[0_{11}/90_{23}]_s$ orientation of the symmetric plys. A 8.4 mm thickness was required to achieve this ply layup, which amounts shell mass of 177 kg.

4.4.2 Pressure Vessel End-Cap Design (Zohaib Hasnain)

4.4.2.1 General Geometry Selection

The end cap geometery was selected with the basic idea of minimizing weight for the given loading conditions. Constraints are in place due to interior space requirements from other groups. In order to minimize weight an elliptical design was chosen over a hemispherical one.

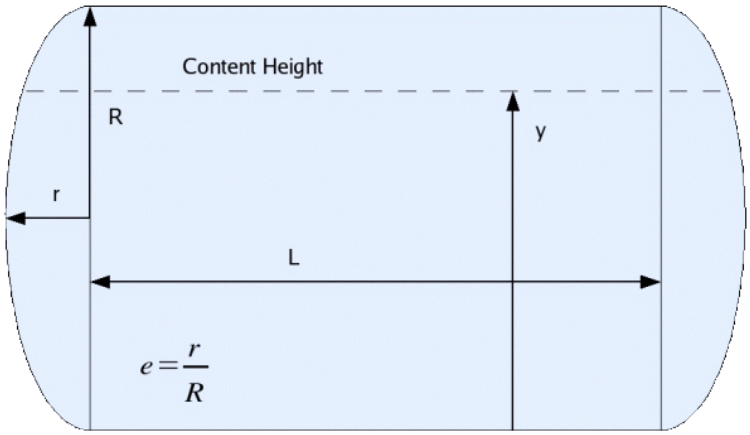

Figure 4.38: End-Cap Dimensions

The length of the semi-minor axis, r, is 0.325 m. This dimension was chosen in compliance with constraints presented by other groups such as Avionics. The semi-major axis, R, is 1.830 m. This dimension was constrained by the shell radius which is also equal to R. Both distances are given from origin to the inner-surface of the end-cap.

4.4.2.2 Material and Modeling

The material selected for both the front and rear end-cap was Graphite Epoxy (same as that used for the shell) with yield/failure strength of 1800 MPa. It has a density of 1600 kg/m^3. Although the material is not perfectly isotropic, uniform properties are assumed in all directions due to the insignificant variation in material properties in various directions. The coefficient of thermal expansion is 20 x 10^{-6}m/K. In accordance with NASA standards a safety factor of 3 was chosen and used through out the analysis.

All the modeling was done using COMSOL Multiphysics. For the specified CAD a mesh was generated consisting of tetrahedral, hexahedral, and prismatic (with triangular base) Lagrange (isoparametric, i.e the mapping functions were the same as the shape functions) elements. A linear static solver with a tolerance of 1 x 10^{-6} was used to solve the resulting equilibrium equations. Mesh details varied for every model and are provided with detailed model analysis. Due to computational power constraints symmetry was utilized in various models which will be discussed with

each individual model. The following figures show the initial CAD drawings of the front and rear caps. The x-axis points out of the rover along the cylindrical axis. The details of the drawing and assembly process will be described when analyzing each model seperately. All dimensions depicted in figures are in meters.

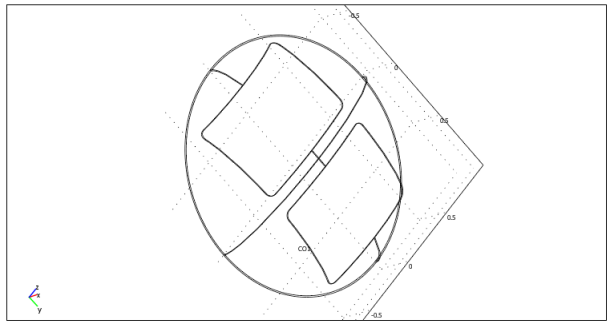

Figure 4.39: Rear End Cap with Suit Port Holes

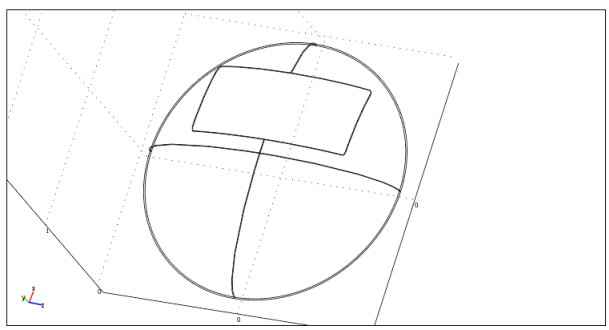

Figure 4.40: Front End Cap with Window Hole

4.4.2.3 Geometric and Physical Properties of Models

The geometric and physical properties of the end cap model were analyzed using COMSOL as well. The original intent was to perform a vibration analysis to determine loading response to dynamic situations. However, due to limitations on computational resources, the models had to be simplified using symmetry and hence a vibrational analysis using COMSOL was not possible.

Front End-Cap The thickness was chosen to be uniform, at 10 mm for purposes of analysis. Based on the volume calculated and the density of Graphite Epoxy the mass of the front end-cap came out to be 38.83 kg. Relevant properties have been calculated with respect to the axis orientation shown in the original CAD drawing.

Subdomain properties

Volume:	0.023533 m^3
Surface area:	5.177912 m^2
Center of mass:	(-0.081771, 0.162797, -7.930954e-4)
Moment of inertia:	Tensor
J_{xx}	0.00635 $m^2 \cdot kg$
J_{yx}	1.485992e-4 $m^2 \cdot kg$
J_{yy}	0.011983 $m^2 \cdot kg$
J_{zx}	6.956958e-6 $m^2 \cdot kg$
J_{zy}	-2.673877e-6 $m^2 \cdot kg$
J_{zz}	0.00598 $m^2 \cdot kg$

Figure 4.41: Geometrical Properties for Front End Cap with Window Hole

Rear End-Cap The chosen thickness was again a uniform 10 mm. Based on the volume and density, the calculated mass came out to be 27.85 kg. As for the previous case, the relevant geometric properties have been calculated with respect to the axis orientation shown in the original CAD drawing for the rear end-cap.

Subdomain properties

Volume:	0.016881 m^3
Surface area:	3.781163 m^2
Center of mass:	(0.133895, 4.746472e-4, -3.951745e-4)
Moment of inertia:	Tensor
J_{xx}	0.010192 $m^2 \cdot kg$
J_{yx}	4.414098e-7 $m^2 \cdot kg$
J_{yy}	0.00588 $m^2 \cdot kg$
J_{zx}	-7.659518e-7 $m^2 \cdot kg$
J_{zy}	-1.372532e-6 $m^2 \cdot kg$
J_{zz}	0.004528 $m^2 \cdot kg$

Figure 4.42: Geometrical Properties for Rear End Cap with Suit Port Holes

4.4.2.4 Front End-Cap Detailed Analysis

Design Process and Assembly The original model was created by rotating the area difference between two quarter ellipses of appropriate dimensions about the vertical axis. The dimensions of these ellipses were chosen such that the thickness of the model remain uniform at 10 mm. The following figure shows the cross-section that was rotated to form a complete end-cap which originally had no cutaway sections.

The rotated 3-D figure was then projected in the y-z plane, in which essentially came out to be a circle of radius equal to the semi-major axis of the ellipse. In this plane a rectangular cutaway was

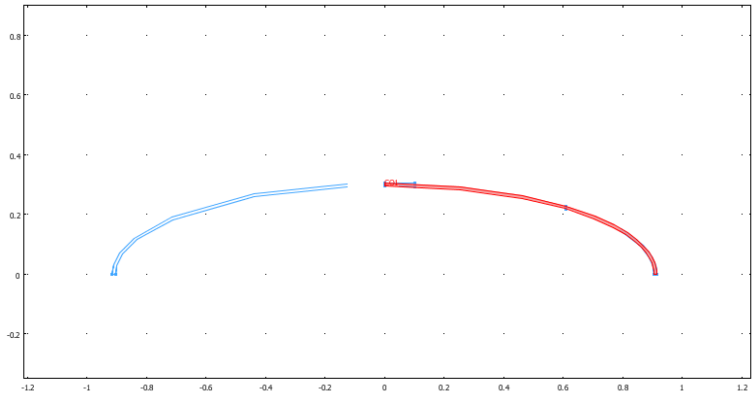

Figure 4.43: Cross Section of End-Cap (X-Z View)

made with dimensions as shown in the figure below. This represents the window hole with accurate dimensions and placement.

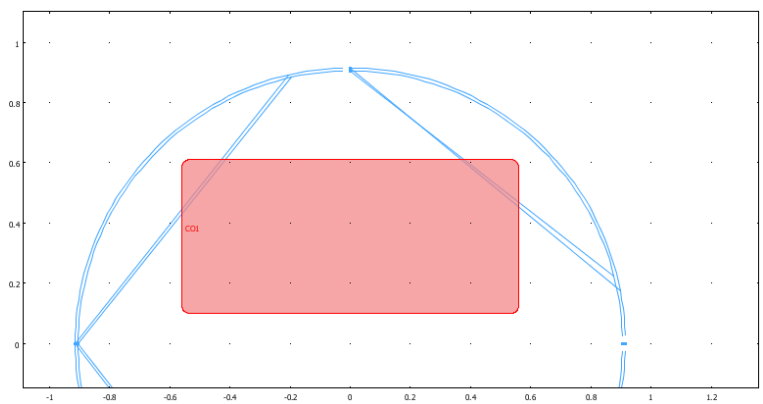

Figure 4.44: End-Cap with Window Hole (Y-Z View)

As visible in the above figure, the corners of the rectangle were replaced with fillets. The radius of curvature of these fillets is 25 mm and it was selected after repeatedly processing the model for varying radii and examining stress concentrations at these points. This radius was the minimum radius that allowed an acceptable stress concentration.

This resulted in a complete end-cap with a window cutaway. However, this model had to be further simplified due to constraints on available computational resources. The original model was meshed such that it had 31688 elements with a total of 180327 degrees of freedom, with 3 degrees of freedom at each node. The large number elements demanded more system memory then was available during matrix assembly. The problem was addressed by simplifying the model about

the only available axis of symmetry. Hence, only half the end cap was actually used for analysis purposes. The simplified model is shown in the figure below.

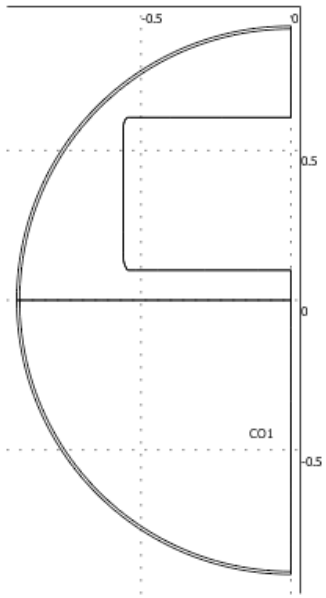

Figure 4.45: Simplified Front End-Cap Model

Loading, Boundary Conditions and Stress Analysis The new half model was meshed such that it had a total of 25155 elements, with a total of 152991 degrees of freedom. Each element node had 3 degress of freedom. All elements were tetrahedral.

For the above shown model the arc edges were fixed (prescribed displacement was set equal to zero). Similarly the edges of the window were also fixed. The internal surface was then subjected to a 53 KPa pressure which corresponds to the load experienced due to pressurization. Due to temperature variations on the lunar surface, accounting for thermal loading was also critical. The initial analysis, without any thermal loading was performed at a temperature of 298.15 K. Using an emissivity value of 0.8 and absorptivity value of 0.2, and assuming radiative equilibrium the equilibrium temperature upper bound was determined to be 380 K. Hence a thermal load corresponding to a 60 K temperature change was applied to the model.

Solver parameters were the same as the ones described earlier. The thickness of the model, as mentioned earlier, was 10 mm. This thickness was determined by analyzing the model as a surface subject only to tangential loads (no normal loads). This allowed processing the model several times while varying the thickness each time to determine what thickness permits acceptable stress concentrations. The stress analysis of the model is summarized in the following figures.

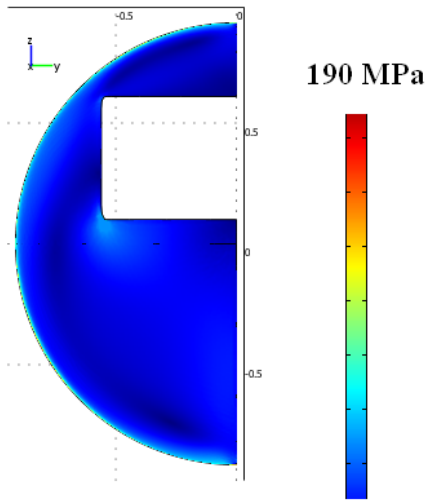

Figure 4.46: Stress Analysis on Front End Cap (Y-Z) View

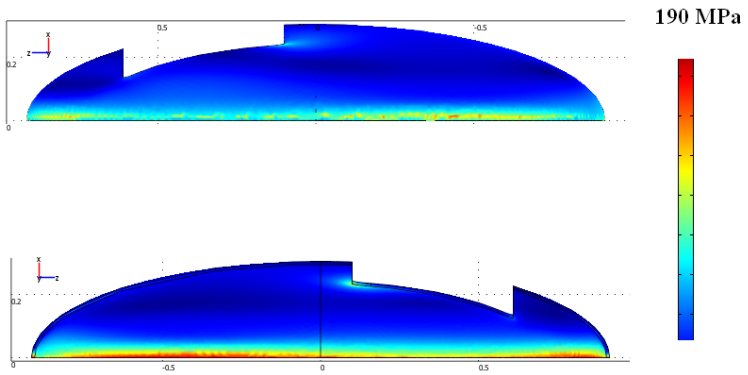

Figure 4.47: Stress Analysis on Front End Cap (X-Z) View

As determined using COMSOL the maximum stress due to all the previously described loads was 190 MPa. Stress concentrations can be seen along the arc edges which is expected given the applied boundary conditions of fixed edges and the applied thermal loading. Another feature worth noticing is the higher stress concentration on the inner arc edge which indicates the effect of applied pressure. Using a safety factor of 3, the calculated margin of safety for this member is 0.05.

4.4.2.5 Rear End-Cap Detailed Analysis

Design Process and Assembly The original model was created by rotating the area difference between two quarter ellipses of appropriate dimensions about the vertical axis. The dimensions of these ellipses were chosen such that the thickness of the model remain uniform at 10 mm. The process for creating the 3-D end-cap was exactly the same as the one used in creating the front end-cap. The only difference was in the cutaway sections. The dimensions of the suitports were different then that of the window. Also, there were two suitport holes instead of one and hence there had to be some structural support in between. The model was created by projecting the solid end-cap onto the the y-z plane and removing rectangles of specific dimensions from appropriate locations. The following figure shows the projection and the cutaway sections.

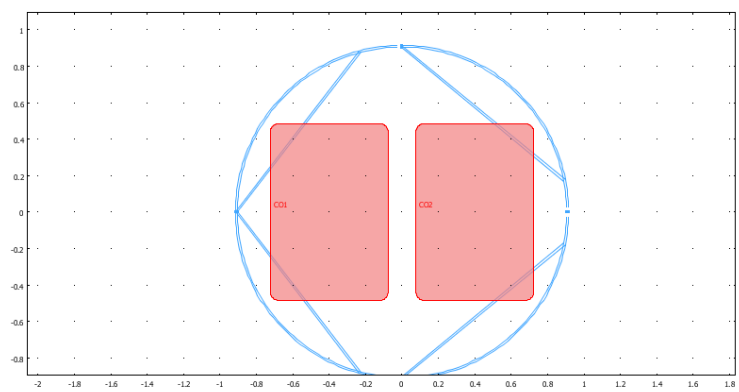

Figure 4.48: Projection of Rear End-Cap with SuitPort Cutaway Sections

Notice again that the edges of the suitport holes have been rounded to avoid stress concentrations. The rounding of these edges was done in a similar fashion to the rounding of the window hole edges. Fillets with radius of curvature 25 mm were placed at the corners. The radius of curvature was also determined using the same technique as for the window hole fillets.

This entire model was meshed to have 35320 elements with 215487 degrees of freedom. Like with the front end-cap the solver ran out of memory while performing a matrix assembly and hence the model had to be simplified. The simplification was done around the vertical axis of symmetry

and resulted in the following structure. The new model had 17401 elements, with 106980 degrees of freedom. All elements were tetrahydral.

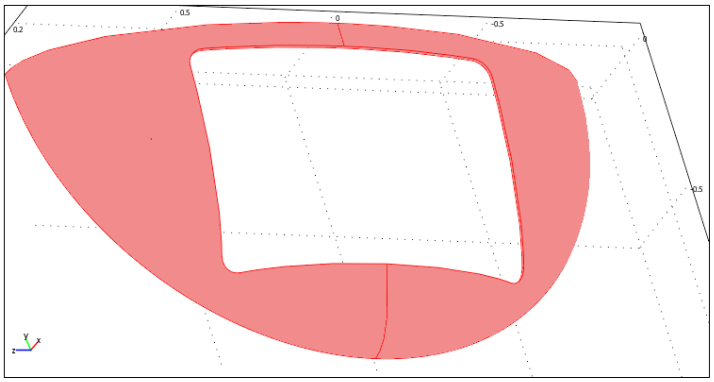

Figure 4.49: Rear End-Cap Simplified

Loading, Boundary Conditions and Stress Analysis For the above shown model again, the arc edges were fixed (prescribed displacement was set equal to zero). Similarly the edges of the suitport hole were fixed. The internal surface was then subjected to a 53 KPa pressure which corresponds to the load experienced due to pressurization. A thermal load corresponding to a 60 K temperature change was applied to this model as well.

Solver parameters were again the same. The thickness of the model, as mentioned earlier, was also 10 mm. The significant difference between this end-cap and the front end-cap was the loads experienced to the attached suitports. This corresponds to 150g load. For the lunar surface this came out to be about 245 N distributed over the edges of the suitport cavity. The total surface area of the edges was calculated to be 0.324 m^2. Hence edges were subjected to an additional load of 757 N/m^2in the - z direction. The results are summarized in the figures below.

For this case, significant concentrations are evident on the inner arc edges, due to thermal expansion and internal atmospheric pressure. The maximum stress in this case is 198 MPa. This results in a margin of safety of 0.01.

4.4.3 Micrometeoroid Protection (Joshua Colver)

Once the minimum shell thickness for the main cylinder and end caps was determined based on pressure and loading requirements, it is necessary to calculate whether or not additional material is needed for micrometeoroid shielding. The process involves analyzing the lunar meteoroid flux model and then comparing several types of shielding to determine the optimal configuration for the

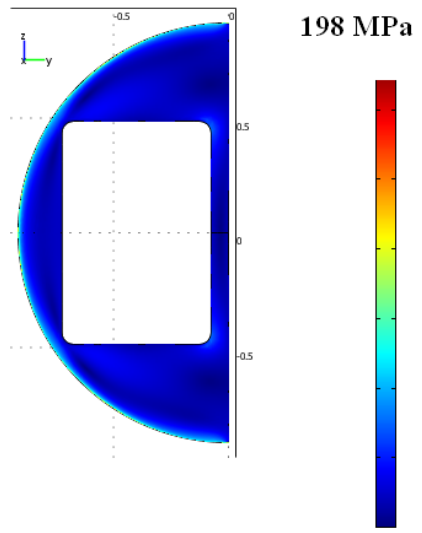

Figure 4.50: Rear End-Cap Stress Analysis (Y-Z View)

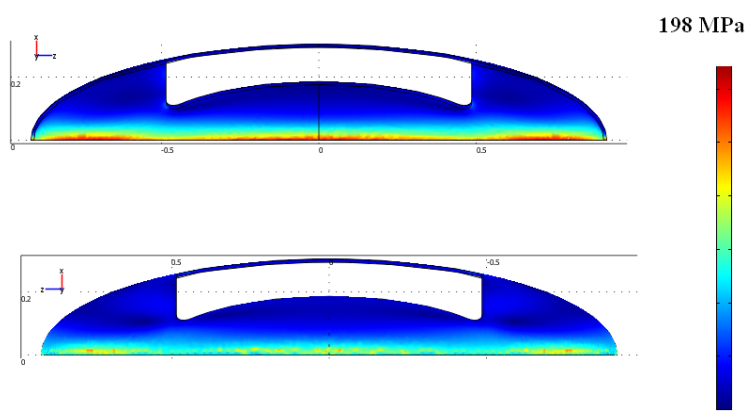

Figure 4.51: Rear End-Cap Stress Analysis (X-Z) View

rover. There were several criteria used in evaluating various protection models. These included mass, simplicity, and how easily it incorporates into the rest of the rover design.

4.4.3.1 Lunar Meteoroid Flux Model

The first step in determining the necessary meteoroid protection is to analyze the lunar meteoroid flux model. The lunar flux model details the relation between the diameter of a particle and the frequency at which it impacts a certain area over a specified time. The flux can be calculated using three pieces of information: rover surface area, mission duration, and number of critical hits allowed. After subtracting out the area of the window and the suitports, the surface area of the rover is 18.12 m^2. The mission duration was chosen to be 10 days. This includes two three-day missions as well as two-day contingencies for each mission. The number of critical hits is the number of particles that are allowed to penetrate the shell over the course of the mission. This number needs to be small, as any shell penetration will lead to loss of crew. For this analysis, the number of critical hits was chosen to be 0.001 hits. Using this information the flux was calculated to be:

$$Flux = \frac{.001\ hits}{(18.12\ m^2)(\frac{10}{365}\ years)} = 2.0 \times 10^{-3} \frac{hits}{m^2 \cdot year}$$

According to the graph shown in Figure 4.52, the calculated flux from above corresponds to a critical particle diameter of 2.0 mm [19].

This means that the shell must protect against any particle that has a diameter less than or equal to 2.0 mm. Assuming a particle mass density of 1.5 g/cm^3 and a spherical shape, the particle mass was calculated to be $m = 6.3 \times 10^{-3}\ g$. These particles were assumed to be traveling at 30 km/sec upon impact with the shell. Each particle was assumed to impact the shell perpendicularly, making this a worst-case scenario assumption. One final piece of information needed for the subsequent shielding models is the material constant, K. It is a number that quantifies the combination of the shell material's strength, density, ductility, and thermal properties. For graphite epoxy, $K = 0.4$.

4.4.3.2 Single Layer Model

The first option for micrometeoroid shielding is simply increasing the thicknesses of the shell and end caps enough to provide adequate protection. The necessary shell thickness is governed by the following Equation 4.27 [6]:

$$thickness = K \cdot \rho^{0.167} \cdot m^{0.352} \cdot V^{0.875} \tag{4.27}$$

Thus, each part of the shell must be at least 14 mm thick in order to shield against micrometeoroids. To summarize from the previous sections, pressure and launch loads require the main cylinder and end caps to have at least the thicknesses as described in Table 4.15.

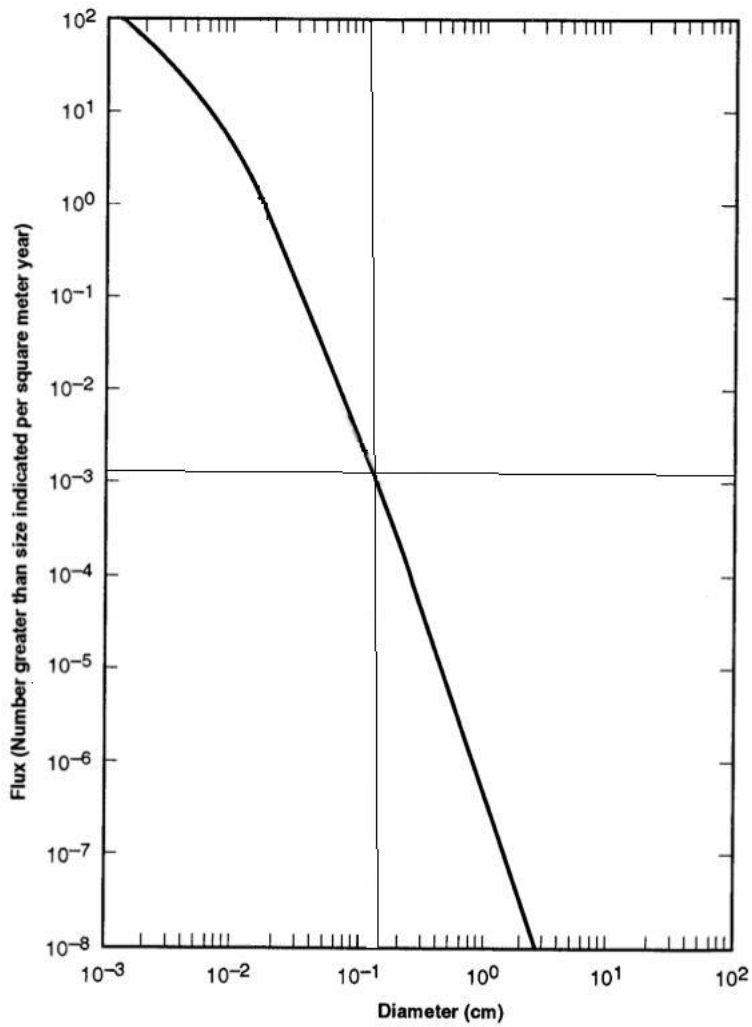

Figure 4.52: Lunar Meteoroid Flux Model

Table 4.15: Pressure Thickness for Micrometeoroid Protection

Part	Thickness (mm)
Main Cylinder	8.4
Front End Cap	10
Rear End Cap	20

Using these figures yields a total pressure shell mass of 226 kg prior to any micrometeoroid protection. Increasing the main cylinder and front end cap thicknesses to 14 mm produces a total pressure shell mass of 346 kg. Given the very tight mass constraints, 120 kg strictly devoted to micrometeoroid shielding is unacceptable. Next, a multi-layer model was analyzed in an effort to reduce the mass of the shielding.

4.4.3.3 Multi-Layer Model

A multi-layer model involves encasing one shell inside of another and generally results in more mass efficient designs for shielding. There are two layers of material separated by a vacuum. The outer shell is thin and is designed to either stop meteoroids completely or break them apart should they penetrate through the shell. After being slowed and broken apart by the outer shell, the meteoroid debris disperses while in the vacuum between the two layers. These particles then impact the main shell as smaller, slower, and thus more benign meteoroids. The chosen model uses the same parameters (material constant, particle mass density, particle mass, and particle velocity) as that of the single layer model, but is significantly more complex [19]. It allows for the main shell thickness and the layer spacing to be varied in order to optimize the model. One provision the model does not account for is the shield layer thickness. According to NASA standards, the minimum manufacturable thickness for composite materials is 2.0 mm. As a result, the shield layer was set to be 2.0 mm thick. Next, various combinations of main shell thicknesses and layer spacings were analyzed to determine the optimal configuration. Figure 4.53 shows a graph of the necessary main wall thickness and layer spacing. Any thickness and spacing combination above the curve is sufficiently thick to shield from micrometeoroids.

As the layer spacing is increased, the main wall can be made thinner. However, there is a decreasing marginal benefit for increasing the layer spacing and there comes a point at which additional layer spacing is detrimental due to added structure that would be necessary to hold the layers together. Additionally, choosing a layer spacing that is too small may interfere with the struts circumferencing the exterior of the main wall. As a result, the layer spacing was chosen to be 35 mm. This spacing ensures that the circular struts are not compromised and that minimal additional structure is needed to mount the shield layer. Once again looking at Figure 4.53, a 35 mm spacing coupled with at least an 8.4 mm main wall provides more than adequate micrometeoroid protection.

Thus, the design for the multi-layer model is to place a 2.0 mm thick shield layer around the main cylinder and front end cap. The rear end cap needs no additional shielding since it is already thick enough due to loads placed upon it by the suitports. The micrometeoroid shield layer results in an additional 45 kg of mass added to the rover. In comparison with the single layer model mass estimate of 120 kg, the multi-layer model saves 75 kg of mass and is the optimal choice for micrometeoroid protection.

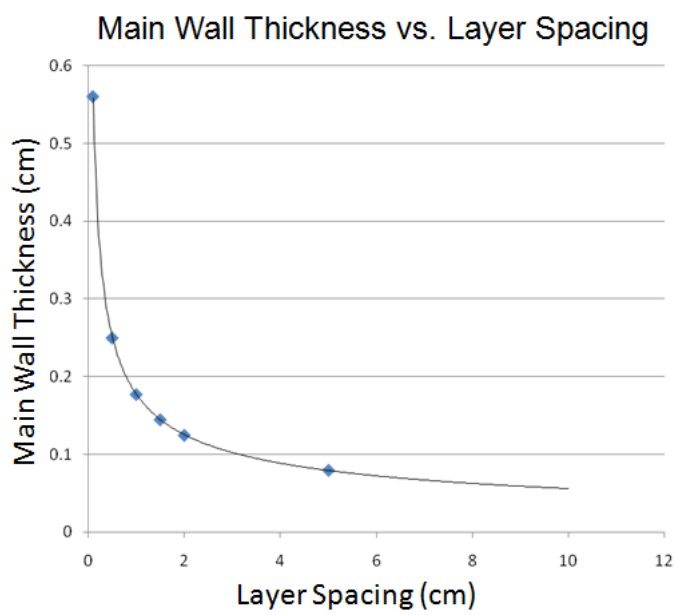

Figure 4.53: Main Wall Thickness vs. Layer Spacing

4.5 Driving Window (Adam Mirvis)

4.5.1 Requirements and Assumptions

The requirements for the main driving window were derived from the following level one requirements [41]:

- The vehicle must accommodate crew members ranging in size from a 5th percentile American female to a 95th percentile American male.
- The vehicle must be capable of traveling on slopes as great as 20°.

Several assumptions were made in designing the shape of the main driving window:

- The driver will require a symmetrical field of view to the left and right.
- The driver will need to be able to see all terrain lying in the path of the rover at some time before it is encountered.
- The driver will be able to shift up to 15 cm (6 in) left and right in their seat in order to briefly expand the field of view offered by the window. This estimate was kept conservative pending human subject testing.

- Rising terrain features in the path of the rover will be visible near the center (vertically) of the driver's field of view at some point prior to being encountered by the rover. This assumption is justified as follows:
  - Features which rise above the horizon will be visible when approaching from far away, thus, they will be at a low sight angle.
  - Positive slope transitions which are not visible above the horizon, such as the far wall of a valley, will pass across the vertical center of the driver's field of view when the rover begins to descend the near side of the valley. These two cases are illustrated in Figure 4.54.
- The driver will be able to make some use of external cameras for obstacle avoidance during low speed maneuvers.

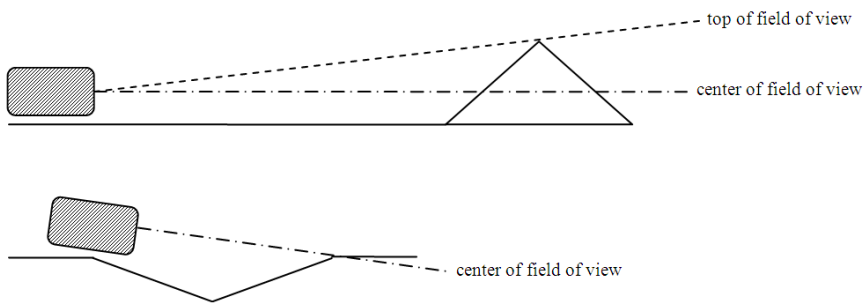

Figure 4.54: Rising Terrain Cases for Field-of-View Upper Limit Requirement

4.5.2 Driver Posture and Position

Several driver postures were considered in order to reduce the necessary area of the window, thus reducing the mass of the rover. The first posture considered was a normal seated posture, with the driver's knees and waist bent at approximately 90° and the driver seated as close to the front of the rover as possible, *i.e.* with their toes touching the front end cap. This posture has the advantage of comfort when driving for significant periods of time, but carries the disadvantage of locating the driver's head a significant distance from the front of the cabin, thus requiring a larger window. The second posture considered was a standing driving position. This would allow the driver's eye to be closer to the front of the cabin, reducing window size. However, the size restriction placed on the cabin by other design restrictions, particularly the overall mass of the vehicle, eliminates this posture as an option. Finally, a lean-forward driving position was considered, in which the driver's weight is supported on their shins, buttocks, chest, and forearms, with their head close to the front

of the cabin, as illustrated in Figure 4.55. This posture would reduce the necessary window area; however, the comfort of this design has not been assessed for long periods of time. Therefore, the normal seated posture was selected.

Figure 4.55: Lean-Forward Driving Posture

In addition to posture, two driver positions were considered – a center-seated driver, and a left- (or right-) seated driver. Each of these positions was incorporated into a complete interior cabin layout, and these layouts were tested with human subjects in the physical mock-up for comfort and utility to both the driver and passenger (See Section 8.2). In the left-seated configuration, the structural transition region between the front end cap and the cylindrical portion of the cabin pressure shell interfered with the space which could be occupied by the driving window, thus reducing the allowable window area to that side. Based on this testing and on the assumption that the driver will require a roughly symmetrical field of view to the left and right, a center-seat driver position was chosen for TURTLE.

In the selected driver position and orientation, the driver's eye is located 79.8 cm (31.4 in) behind the tip of the front end cap. The tallest driver's eye will be 43.9 cm (17.3 in) above the center of the cabin, and the shortest driver's eye will be 62.7 cm (24.7 in) above the center of the cabin. The driver's eye will be located roughly on the horizontal centerline of the rover.

4.5.3 Field of View

The field of view angles were derived from the level one requirements, design assumptions, and field testing. The "look down angle", or the angle from the center of the driver's field of view to the bottom edge of the window, is 20°. This is based on a worst case scenario in which the rover is situated at the edge of a plateau whose sides are sloped at 20°. This is the maximum slope the rover is required to be able to drive on. Therefore, for slopes less than the maximum, the driver must be able to see a point along the descending slope, to confirm that the terrain is within acceptable driving limits (See Figure 4.56). It is assumed that with a 20° look down angle, obstacles in the

rover's path large enough to present a danger to the rover will be visible above the bottom of the window long enough for the driver to identify the obstacle as such and to have enough visual information on which to base a course of action – either braking, turning, or a combination of these.

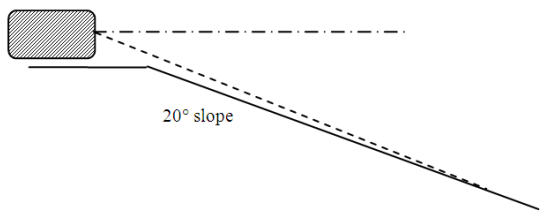

Figure 4.56: Descending Terrain Case for Field-of-View Lower Limit Requirement

Based on the assumption that rising terrain features will be visible near the vertical center of the driver's field of view at some point before being encountered, the "look up" angle is much shallower at 5°.

4.5.3.1 Field Testing

In order to determine an initial guess at the required horizontal field of view, low fidelity field testing was conducted. A test subject was seated in the front passenger seat of a car driving at 15 k/hr (9 mph) along residential streets. The subject held a rectangular cardboard window in front of their face, adjusting the "aspect ratio" and the distance of the window from their eyes until they acheived what was subjectively assessed as a comfortable driving field of view. The distance and dimensions of the window were then measured, and the field of view angles calculated.

This testing was useful in gaining a general impression of what sort of field of view would be required; however, the low fidelity of the testing made the significance of the numbers generated somewhat dubious. To generate more useful test data, field testing would have to be conducted with numerous test subjects actually controlling a vehicle with dynamics and stability similar to those of the TURTLE, in a lunar simulation environment with obstacle size and frequency and terrain similar to the geology of the selected landing site(s), and with the test subjects assessing the difficulty of navigating and avoiding obstacles on a Cooper-Harper scale.

For the purposes of the current level of analysis, a horizontal field of view of 45°to either side was selected.

4.5.4 Window Dimensions and Placement

The driving window has a minimum field of view of 45° to the left and right, 20° down, and 5° up for all drivers within the size range specified by the level one requirements. The window area was

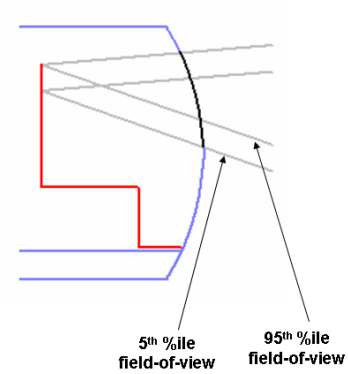

Figure 4.57: Vertical Field of View Limits for Full Range of Driver Sizes

determined by finding the intersection of the designed field of view limits with the pressure shell end cap. The top of the window was defined by the intersection of a plane containing the location of the tallest driver's eye and sloping up 5° toward the front of the rover, and the bottom was similarly defined by a 20° downward sloping plane containing the location of the shortest driver's eye. The left and right sides of the window were defined by vertical planes angled out at 45°, with the left-side plane shifted 15 cm to the right and vice versa to account for the ability of the driver to shift in their seat. The resulting window is roughly rectangular, 1.09 m wide at the widest point, and 0.51 m tall at the tallest point. It is centered horizontally on the front end cap of the cabin, and begins 0.87 m above the floor, as illustrated in Figure 4.58.

4.6 Window (Omar Manning)

4.6.1 Introduction

The primary factors with the selection of a window for the TURTLE were based on the lunar surface's maximum and minimum surface temperatures and cabin pressure. Compressive, shear, and impact forces acting on the window were also taken into account. The TURTLE window was modeled after the NASA Space Shuttle windows because these materials have been proven in the space environment. The NASA Shuttle uses a three-pane window concept combination of fused silica and aluminosilicate glass with infrared reflection and anti-reflective coatings. The outer pane acts as a heat shield. The inner pane is the primary pressure containing pane and the middle paine serves as a redundant member for both the outer heat shield pane and inner pressure pane. The Shuttle windows have a proof pressure of 8600 psi at 115 degrees C. The three-layer model of the NASA Shuttle was reduced to two layers because the outer most layer of the Shuttle is primarily used as a heat shield for re-entry plasma deflection. A 76-page shuttle window testing report was

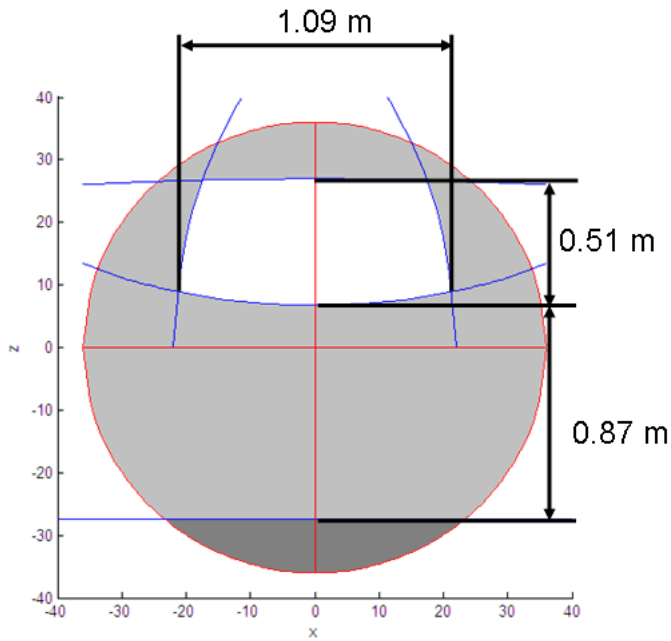

Figure 4.58: Position and dimensions of driving window

generated by NASA in 1973. In this report the testing and results of the Shuttle glass-seal-frame interfaces were described. [67]

4.6.2 Fused Silica

Fused silica's infrared transmission is limited by its strong water absorption in the infrared spectrum. Its low coefficient of thermal expansion (5.5 x 10-8 m/m-K) allows fused silica to withstand large temperature changes. Fused silica has an operational temperature of 1175 K. Fused silica has a hardness of 5.3 to 6.5 on the Mohs Scale. The tensile strength, compressive strength and elastic modulus are 48.3 MPa, 1.1 GPa, and 71.7 GPa respectively. Fused silica has a low coefficient of thermal expansion, it has great optical clarity (1.459 refractive index). Calculations of micrometeorite impact resistance involved applying the force due to impact against the material properties and size of the exterior fused silica window. Calculations were done in COMSOL using a mass of $6 * 10^{-3}$ kg and velocity of 30 km/s. This windowpane thickness was based off meteorite impact. At a windowpane thickness of 12.7 mm the deflection of the window was $10 * 10^{-5}$ m (near zero deflection). [32]

4.6.3 Aluminosilicate Glass

Aluminosilicate glass is a low-expansion glass that has been proven to provide maximum mechanical strength. Aluminosilicate glass contains 17 percent aluminum. This is the key element in this glass that strengthens it when compared to fused silica. Aluminosilicate glass has an elastic modulus of 88 GPa (20 percent higher than fused silica), and a maximum service temperature 950 K. Aluminosilicate glass also protects against scratches due to handling and debris, it has a low coefficient of thermal expansion, as well as great optical clarity (1.53 refractive index). Calculations of window thickness based off 100000 Pa cabin pressure are shown below. These calculations were made using COMSOL 3-D modeler stress strain software. The window thickness of 20 mm was chosen for a near zero deflection. The coordinate system for the window are: x is width, z is height and y is thickness. See Table 4.16 for window sizing and deflection data. [32]

Table 4.16: Table of Window Size and Deflection Due to Cabin Pressure

Fused Silica Pane			
x	1.09	m	
y	0.02	m	20 mm thick
z	0.51	m	
Stress	1740000	Pa	
Deflection	.0000018	m	no deflection
Aluminosilicate Pane			
x	1.09	m	
y	0.0175	m	17.5 mm thick
z	0.51	m	
Stress	34050000	Pa	
Deflection	0.000435	m	.4 mm deflection

4.6.4 Anti Reflection Coating

A multi layer silica anti reflection coating will be used on the outside window for near zero light reflection allowing the TURTLE astronauts to have maximum visibility of the outside environment. The Renssealer Polytechnic Institue has designed a multi layer silica coating that has a refractive index close to 1.05 (close to that of air). This coating was determined the best option due to the physical strength and temperature properties of silica. [94]

4.6.5 Infrared Reflection (IRR)

Infrared reflection coating will increase the IRR properties already present in the fused silica window. The IRR coating will reduce the amount of heat transferred though the window to the TURTLE cabin. This method is in use on the space shuttle.

4.6.6 Window Frame

Vitreloy (Liquidmetal.com) will be used as the primary material for the window frame. The physical properties of Vitreloy are superior to those of aluminum, steel, and titanium. One of the most unique characteristics of Liquidmetal alloys is the availability of its superior mechanical properties in as-cast form. This is in distinct contrast to conventional metals where the as-cast forms have inferior mechanical properties compared to their wrought and forged forms, which limits the fabrication of intricate and sophisticated designs. The yield strength of vitreloy is $1.8 * 10^9$ Pa with a hardness of 50 Rc and Youngs modulus of $1.8 * 10^{12}$ Mpsi. The density and Poisson's ratio are 6.1 g/cc and .39 respectively. The window frame will disperse/carry all loads from the end cap using shear flow, thus the window will not be affected by the max loads exerted onto the end cap or the window frame. The Vitreloy frame can be forged without welding to a perfect fit thus securing the cabin and crew.

4.6.7 Window Seal

The window seals are Viton fluoroelsatomer O-rings (Dupontelastomers.com). Fluoroelsatomer O-rings provide good slippage capability and can be pre-cured prior to installation to prevent out-gassing at specified temperatures. Viton allows elastic recovery after thermal exposure from 250 K to 477 K. Since the maximum temperature on the lunar surface is 360 K, the seal is within its operational parameters. Each window pane has a designated seal.

4.6.8 Meteorite Impact

The study conducted by NASA regarding meteorite impact on the Shuttle found that the probability of no windshield failure form meteoroid damage was .9991. Given the similar surface area of the TURTLE window it is safe to assume the same probability or higher. Calculations were made to determine the thickness of the outside windowpane based on the mass ($6.3 * 10^{-3}$), velocity (30 km/s) and size (2 mm diameter) of micrometeorites impacting the lunar surface. Using COMSOL software the force of impact was applied to the 12.7 mm fused silica windowpane. Deflection was determined to be $1 * 10^{-5}$ m, virtually zero. The NASA shuttle-viewing window has a thinner fused silica pane than TURTLE.

4.6.9 Regolith Build-up

Regolith will be a problem for many components of the TURTLE especially the cabin window. Many options have been considered for regolith buildup removal. The first option is a brush that can be used to wipe down the window manually. This brush could be stored on the external surface of TURTLE. The second method would be the use of a windshield wiper constructed of a stiff metallic rod with a fluoroelsatomer O-ring wrap and a soft material wrap on top to prevent scratching. This

wiper may be magnetized or charged in a way that it would grab or repel the maximum amount of dust from the window.

4.6.10 Radiation Considerations

The TURTLE window will require radiation protection for its crewmembers, however radiation on the moon as related to human health still needs further study. The Lunar Reconnaissance Orbiter (LRO) is the first mission in NASA's vision for space exploration. The LRO will launch in late 2008 with the objectives to finding safe landing sites, locate potential resources, characterize the radiation environment, and demonstrate new technology. With this new radiation data, radiation protection can be fine tuned. As for now we can assume that the inside of the outside window panel will have a coating consisting of a mixture of lead infused silica to assist in blocking radiation.

4.6.11 Window Summary

In summary, the window chosen for the TURTLE was a two-pane window with the outer window material being fused silica (12.7 mm thick) and the inner pressure pane window material Aluminosilicate glass (20 mm thick). The windowpane set is approximately .51 m in height and approximately 1.09 m in length. The window seals will be redundant fluoroelsatomer O-rings allowing elastic recovery after exposure to maximum and minimum lunar temperatures. The inside of the outer window will be coated with anti-reflection coating and the outside of the inner window will be coated with IRR to reduce heat transfer. Testing must be conducted to determine the best method for removing regolith from the window. See Figure 4.59 for a full diagram on the window structure.

4.7 External Driving Platform (Brian McCall)

4.7.1 Configurations

4.7.1.1 Launch Configuration

Figure 4.60 shows the configuration of the platform during launch. Note the origin at the lower left of the figure shown in blue. Noting the image at the top right, the arrow pointing to the right is pointing away from the rear of the rover. The arrow pointing up is pointing towards the top of the rover.

The platform is located on the aft section of the rover and is attached to the spars of the frame supporting the suit-ports. Note that all of the actuators are hinged and free to rotate in their respective planes. Also note that the support rods from each spar that meet with the platform are to be jettisoned upon landing by means of explosive bolts. The purpose of the support rods is to ensure the actuators are undamaged during launch since they were designed for use in lunar gravity and would fail under launch loads.

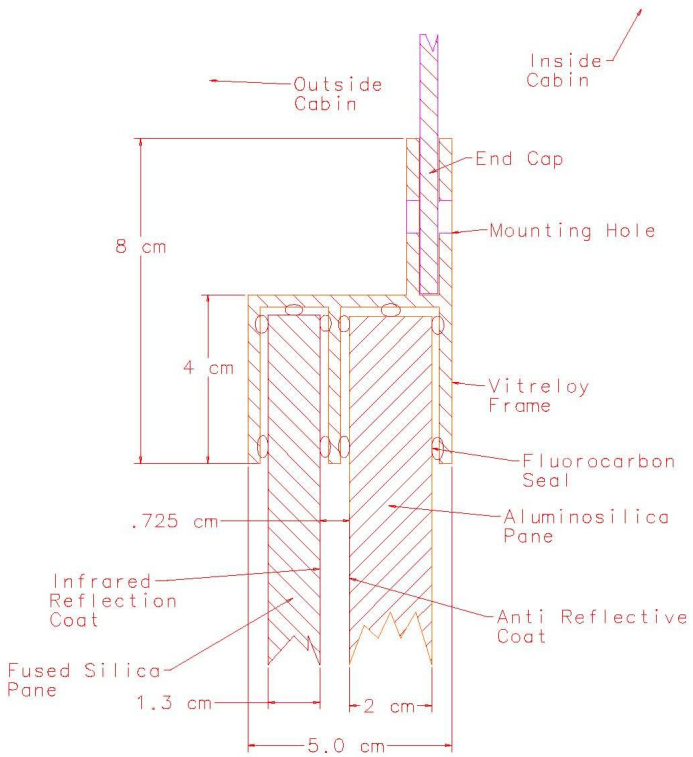

Figure 4.59: Window and Frame

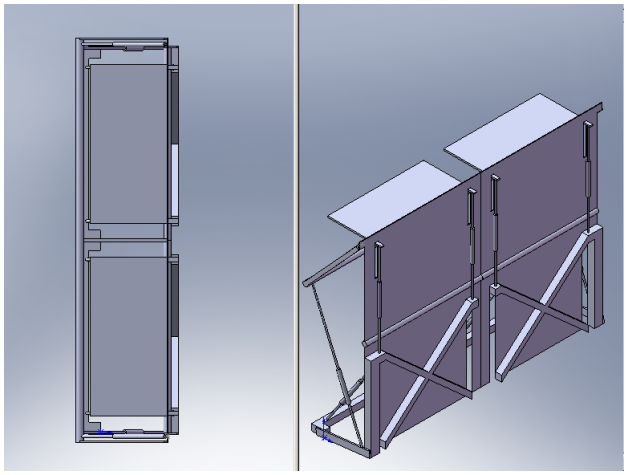

(a) Top and Isometric Views

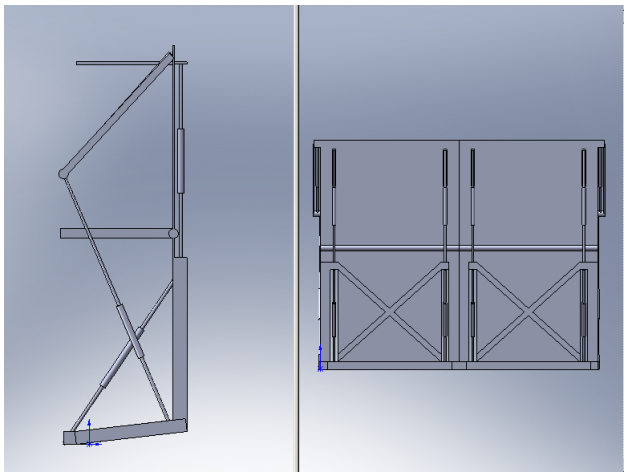

(b) Aft and Side Views

Figure 4.60: Platform in the Launch Configuration

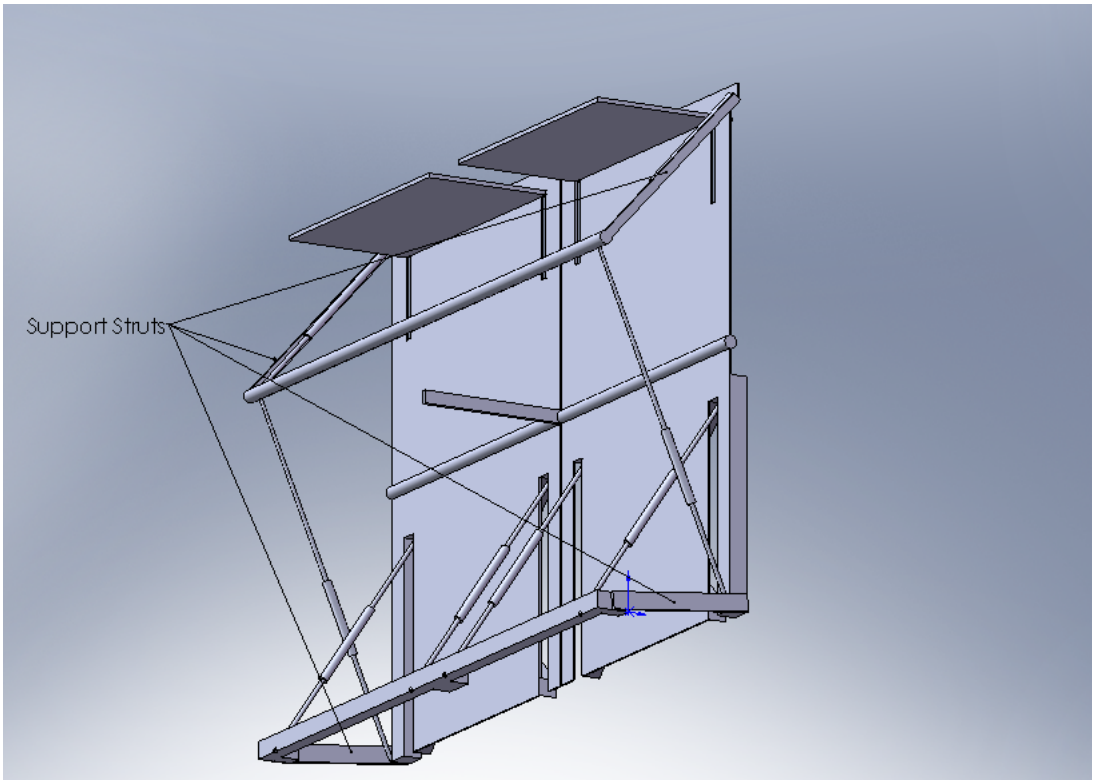

Figure 4.61: Locations of Launch Support Struts

4.7.1.2 Suit Storage and Internal Driving Configuration

Figure 4.62 shows the position the platform will take during extended internal driving sessions and autonomous driving sessions during the mission. Note that the platform is parallel to the ground and the vertical actuators are contracted allowing for maximum ground clearance. This configuration is only used when the suits are vacant or absent due to the lack of conformity to a relaxed human stature.

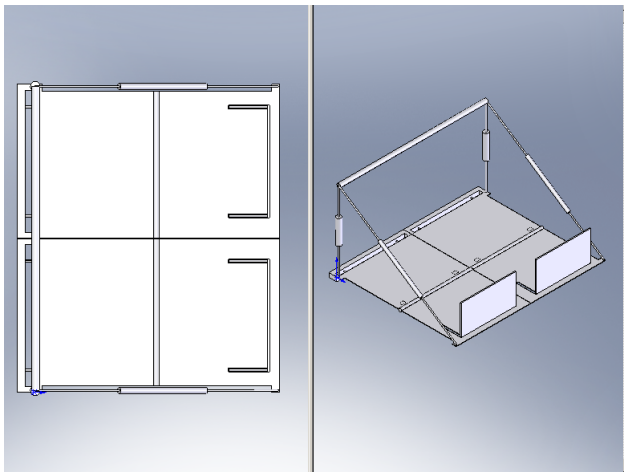

(a) Top and Isometric Views

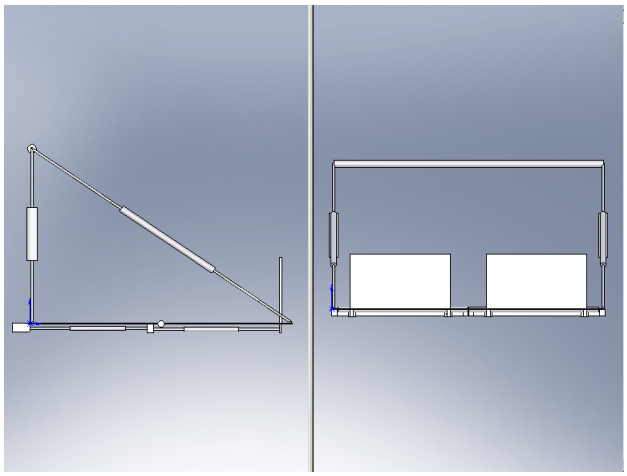

(b) Aft and Side Views

Figure 4.62: Platform in the Suit Storage and Internal Driving Configuration

4.7.1.3 Seated Configuration

Figure 4.63 shows the position the platform will take to accommodate external driving sessions and internal driving sessions while one or both of the suits are occupied. The foot platform has an

adjustibility of 10 cm to accommodate 95th percentile American males and 5th percentile American females. The knee hinges have a limited adjustibility of approximately 10 degrees to accommodate astronauts during extended driving sessions with the platform in use and varies from 35 to 45 degrees below the horizontal.

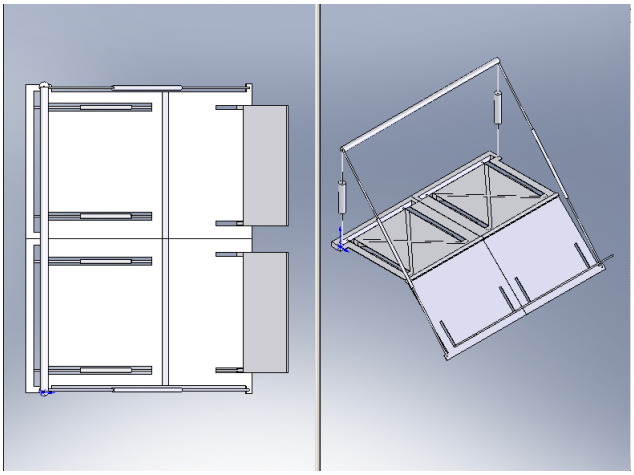

(a) Top and isometric views

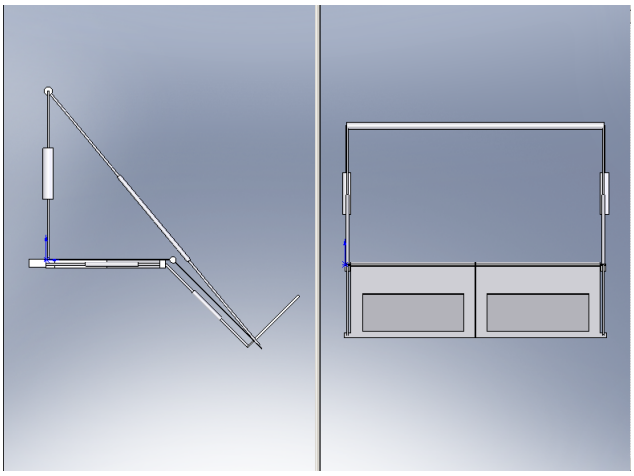

(b) Aft and Side Views

Figure 4.63: Platform in the Seated Configuration

4.7.1.4 EVA and Suit Entry/Exit Configuration

Figure 4.64 shows the position the platform will take when an astronaut embarks on an EVA and during entry and exit of the spacesuits. Due to the geometry of the human body, it was found that the suits must be in the standing position to accommodate entry and exit because the leg must be bent in a way that would be impossible in any other configuration. As a result of this and based

on our requirement of 0.5m ground clearance, suit entry and exit can only occur while the rover is stationary.

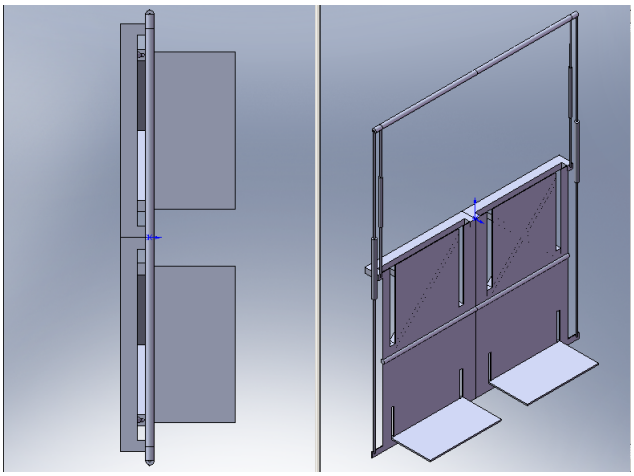

(a) Top and Isometric Views

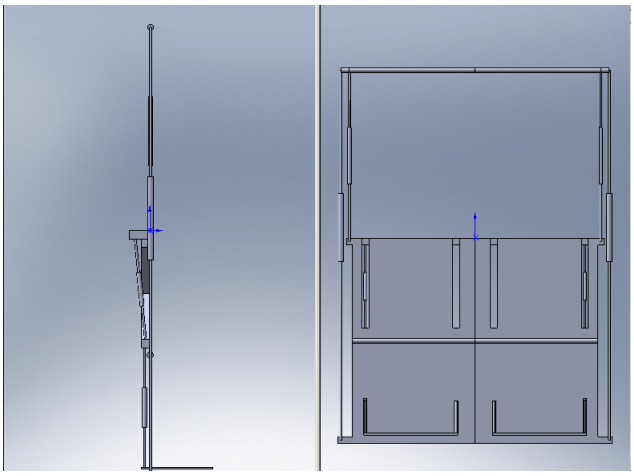

(b) Aft and Side Views

Figure 4.64: Platform in the Suit Entry/Exit Configuration

4.7.2 Design

4.7.2.1 Parts Overview

Figure 4.65 depicts the platform in the EVA and suit entry/exit configuration with parts labeling and terminology used to describe the platform and the design analysis. Figure 4.65 also includes the actuator number designation for reference. The platform consists of four sheets of aluminum alloy 6061-T6, approximately 0.6 m in length and 1.0 m in width, referred to as sub platforms. The thickness of the sub platforms was determined to be approximately 5 mm and the foot platform

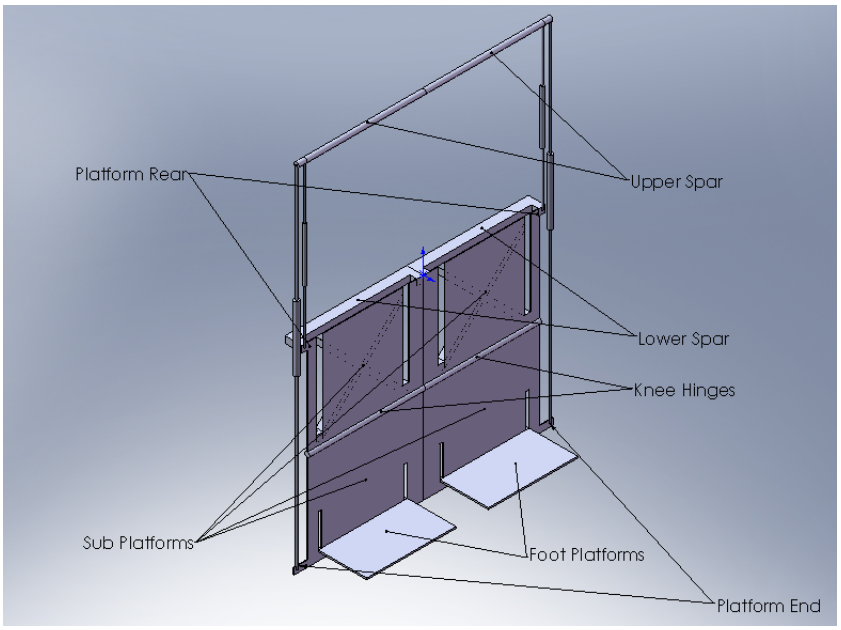

(a) Labeled Parts

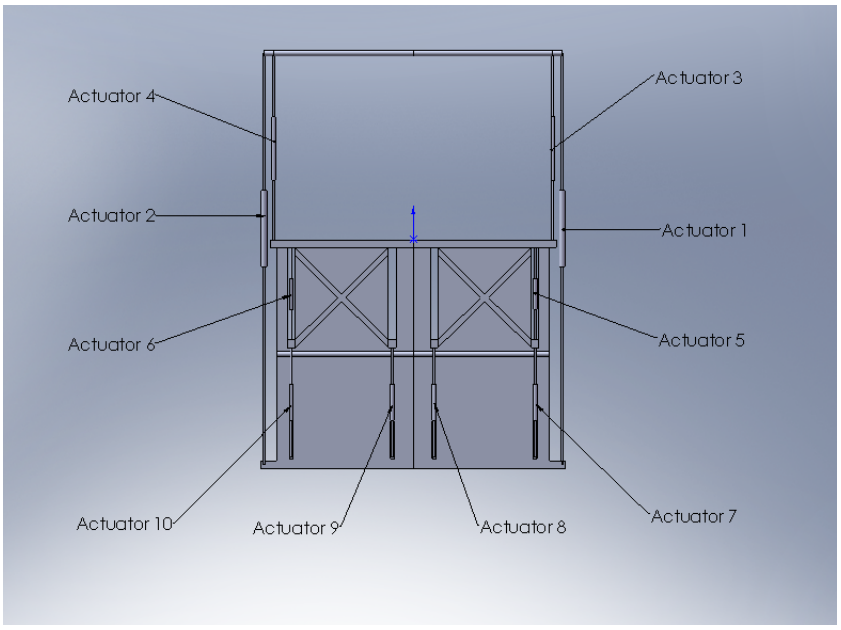

(b) Actuator Positions

Figure 4.65: Platform Parts Labeling and Reference

thickness was determined to be approximately 8 mm. The platform in its entirety is designed to accommodate two 95th percentile American males sitting in a side by side configuration. As a whole the platform is 2 m wide and 1.2 m long. This size provides approximately 20 cm of width on each side of each astronaut. This spacing provides adequate clearance between the shoulders of each astronaut and the actuators connecting to the top spar. Additionally, this spacing provides adequate freedom of movement of the arms in the center for reaching external controls.

The knee hinges are located 0.6 m from the platform rear and 0.6 m from the platform end. The data used to determine these dimensions was gathered from NASA standards. The angle at which the platform resides in the seated configuration was determined based on NASA standards and can be adjusted between 45 and 35 degrees from the horizontal plane. Adjustability by means of additional actuators not crucial to the movement of the platform to and from the differing configurations were added to accommodate 5th percentile American females, intermediate astronaut geometries and variations of the lunar landscape. These are actuators 3, 4, 7, 8, 9, and 10 in Figure 4.65. These actuators provide adjustable distances in the vertical and horizontal directions only and the ranges of motion are listed in the tables below, detailing the loads on each actuator in the different configurations.

There is a 10 mm wide cut along the length of the platform. Due to redundancy requirements and the 99.9% crew survivability requirement, the platform has the capability for each half to operate independently in the event of a partial failure. Movement of the platform is accomplished by ten electrical linear actuators powered by direct current. Movement of the platform can be controlled from the interior of the rover and from external controls by use of the space suits.

The thicknesses of the platform and foot platforms were chosen based on critical loads determined during the expected use of the platform and the configuration in use during which these loads occurred. Presuming humans were present, the calculations to determine critical loads in configurations assumed a suited astronaut has a mass of 125 kg. Since the platform is a side by side seating arrangement, a total mass of 250 kg was used to determine worst case loads when both humans are present. Configurations analyzed in which humans were present, included EVA and suit entry/exit configuration and the seated configuration. Analyzing the loads on the platform when humans were assumed not present, included a mass of 70 kg to account for the presence of the two vacant space suits on the platform. The configuration analyzed assuming humans were not present but space suits were present, was the suit storage and internal driving configuration. In addition to the expected loads occurring from the presence of space suits and astronauts, the platform itself has an assumed mass of 35 kg. This mass was also factored into the analysis involving the internal loads effecting the actuators. The maximum load maintained by the platform on the lunar surface was determined to be 535 N.

Analyzing the loads imparted on the platform during launch did not include the mass of astronauts or the space suits and only involved the 35 kg assumed mass of the platform. The requirements

of the mission dictated that the platform withstand 6g's of acceleration during the launch phase to transit from Earth to the Moon. Analysis showed the amount of mass and area inertia required to counter this force and the stresses it produced was well beyond a minimalistic design of the platform in terms of mission applicable operability. As mentioned previously, the maximum load imparted on the platform during its expected use on the lunar surface was 535 N. This is significantly less than the 2058 N force that is experienced during launch.

It was determined that the best means of countering an over design issue was to reinforce the platform during launch and maintain the minimalistic approach to design during mission time spent on the moon. This was deemed necessary upon consideration of the added mass and power requirements that would accompany a configuration using only the actuators to support the platform during launch. The solution was to reinforce the platform with five struts to absorb and channel the launch loads onto the chassis to protect the actuators from buckling and the platform itself from deforming due to bending. In Figure 4.65, note the locations of the struts at each end of the lower and upper spars and a strut situated in the center of the platform. Analysis dictated that these struts incorporate a hollow cross section and be 8 mm x 40 mm with a thickness of 2 mm. The struts are to be jettisoned upon landing on the lunar surface by means of 10 explosive bolts. These as well as all other components of the platform were designed with a safety factor of 2 and margins of safety on the order of 0.01 - 0.03. A safety factor of 2 as opposed to a safety factor of 1.5 was used because the loads imparted by human dynamics needed to be accounted for.

4.7.2.2 Actuator Loading and Power Requirements

Figure 4.65 depicts the numbering of the various actuators for reference with the tables. The loads on each actuator in the different configurations appear in the tables below. Based on a trade study done on linear actuators, the voltages and amperage needed to power each actuator can be found in the table below. Figure 4.65 shows the location of each actuator and its corresponding number used in the table. Hyphenated actuator lengths correspond to actuators which are adjustable to compensate for differing astronaut geometries.

Based on the analysis, the maximum axial loads on the actuators occurs in the EVA suit entry/exit configuration while both astronauts are assumed to be on the platform. Based on a linear actuator trade study, actuators 5 and 6 will require 12 V and run on 3 amps of current each. Actuators 1 - 4 and 7 - 10 will require approximately 5v and 2 amps each. It was also determined that the platform will take approximately 15 seconds to fold from the suit storage configuration to the EVA suit entry/exit configuration.

4.7.2.3 Results From the Platform Mock-up

Initially, the design of the platform was quite different. The preliminary design incorporated two independent platforms. After the suit-port construction occurred on the mock-up, it was clear this

Table 4.17: Actuator Loading in the Suit Storage and Internal Driving Configuration

Actuator Number	Axial Loading	Actuator Length	Attachment
1	130 N	1.6 m	Top Spar to Platform End
2	130 N	1.6 m	Top Spar to Platform End
3	84 N	1.0 m-0.8 m	Top Spar to Platform Rear
4	84 N	1.0 m-0.8 m	Top Spar to Platform Rear
5	201 N	0.55 m-0.85 m	Lower Spar to Mid Hinge
6	201 N	0.55 m-0.85 m	Lower Spar to Mid Hinge
7	100 N	0.45 m-0.55 m	Mid Hinge to Foot Platform
8	100 N	0.45 m-0.55 m	Mid Hinge to Foot Platform
9	100 N	0.45 m-0.55 m	Mid Hinge to Foot Platform
10	100 N	0.45 m-0.55 m	Mid Hinge to Foot Platform

Table 4.18: Actuator Loading in the Seated Configuration

Actuator Number	Axial Loading	Actuator Length	Attachment
1	164 N	1.8 m	Top Spar to Platform End
2	164 N	1.8 m	Top Spar to Platform End
3	134 N	1.0 m - 0.8 m	Top Spar to Platform Rear
4	134 N	1.0 m - 0.8 m	Top Spar to Platform Rear
5	96 N	0.55 m - 0.85 m	Lower Spar to Mid Hinge
6	96 N	0.55 m - 0.85 m	Lower Spar to Mid Hinge
7	60 N	0.45 m - 0.55 m	Mid Hinge to Foot Platform
8	60 N	0.45 m - 0.55 m	Mid Hinge to Foot Platform
9	60 N	0.45 m - 0.55 m	Mid Hinge to Foot Platform
10	60 N	0.45 m - 0.55 m	Mid Hinge to Foot Platform

Table 4.19: EVA and Suit Entry/Exit Configuration

Actuator Number	Axial Loading	Actuator Length	Attachment
1	134 N	2.2m	Top Spar to Platform End
2	134 N	2.2m	Top Spar to Platform End
3	134 N	0.8 m - 1.0 m	Top Spar to Platform Rear
4	134 N	0.8 m - 1.0 m	Top Spar to Platform Rear
5	268 N	0.55 m - 0.85 m	Lower Spar to Mid Hinge
6	268 N	0.55 m - 0.85 m	Lower Spar to Mid Hinge
7	134 N	0.45 m - 0.55 m	Mid Hinge to Foot Platform
8	134 N	0.45 m - 0.55 m	Mid Hinge to Foot Platform
9	134 N	0.45 m - 0.55 m	Mid Hinge to Foot Platform
10	134 N	0.45 m - 0.55 m	Mid Hinge to Foot Platform

Table 4.20: Maximum loads on actuators

Actuator Number	Axial Loading	Actuator Length	Attachment
1	134 N	2.2 m	Top Spar to Platform End
2	134 N	2.2 m	Top Spar to Platform End
3	134 N	0.8 m - 1.0 m	Top Spar to Platform Rear
4	134 N	0.8 m - 1.0 m	Top Spar to Platform Rear
5	268 N	0.55 m- 0.85 m	Lower Spar to Mid Hinge
6	268 N	0.55 m - 0.85 m	Lower Spar to Mid Hinge
7	134 N	0.45 m - 0.55 m	Mid Hinge to Foot Platform
8	134 N	0.45 m - 0.55 m	Mid Hinge to Foot Platform
9	134 N	0.45 m - 0.55 m	Mid Hinge to Foot Platform
10	134 N	0.45 m - 0.55 m	Mid Hinge to Foot Platform

approach was not practical due to spacing between the suit-port. When considering the options available in constructing the mock-up platform it became clear the best option was to build one wider platform as opposed to two seperate entities. This simplified the design and helped significantly expedite the design process because the mock-up provided a real world approach to the design. However, it remained clear the platform on the actual mission would need to have the capability of each side operating independently in the event of a partial failure.

4.7.2.4 Contingencies

Due to the requirement that the mission have a 99.9% crew survivability, there are several contingencies in place should part of the platform fail at any time during the mission. It is imperative the platform be operable at all times during the mission as it is the only means the astronauts have of entering and exiting the rover. The actuators are supplemented by a mechanical system that can be used in the event of an actuator failure. In addition to this, the platform includes duplicates of each actuator onboard for replacement. In the event of severe damage, the platform can be removed in its entirety or partially for repair or to access the suit-ports.

4.7.3 Exterior Driving Station (Andrew Ellsberry)

The astronauts have a secondary driving position on the outside of the rover, colocated with the suitports, that allows them to drive without reentering the pressurized cabin. This provides a similar capability to the Apollo LRV and the proposed Constellation unpressurized rovers for extending EVA range. The astronauts will use the external driving station to access the full range of the rovers systems and provide the same capabilities as driving from the interior of the rover.

The overall unit can not be installed prior to arrival on the lunar surface as it would interfere with the stowed position of the external driving platform and will be shipped to the lunar surface in

an external compartment of the rover. The driving station can be broken down into 3 components: display, joystick, and cantilever truss.

The truss will connect to the frame of the vehicle between the two suitports and is used to position the display and the hand controller between the two astronauts so it can be used by either operator. It will rigidly lock into place on the aft bulkhead and will cantilever outwards; it is not supported by or interferes with the exterior driving platform. An integrated umbilical will connect to vehicle and provide the rest of the unit with both power and a direct interface with the vehicle's ARINC 664 networking.

The driving station includes a similar 2-DOF joystick hand controller to the one located inside the rover, but it is protected from the lunar dust as well as optimized for use while wearing a pressure glove. The unit also provides room for a small number of mechanical toggle switches, if needed, but they must be recessed or properly guarded to prevent inadvertent activation by the astronauts during both driving and suitport ingress/egress.

The exterior display is the same basic DU-1310 monitor as used on the interior of the rover. The main difference is that it is oriented in the vertical position that both is more visible on the side of each astronaut's FOV, but also fits well with the workspace for the joystick without protruding further into the area occupied by the astronauts while driving or using the suitports. It is enclosed in a housing to protect it from both the lunar dust and extreme temperatures that it is exposed to on the exterior. The astronauts have access to all the menus and interfaces that they would from the interior including vehicle diagnostics, checklists, and camera control. One of the items that needs further analysis and testing is the need and functionality of a sun hood around the display to improve viewing and to balance that against any issues where it interferes with the display's use as a touch panel.

Chapter 5

Lunar Propulsion

5.1 Terramechanics (Ugonma Onukwubiri)

Terramecanics is the relationship between the soil surface and the wheel. This includes traction and motion resistance. The goal of this analysis is to achieve mobility and trafficability. The trafficability is based on the traction load of TURTLE and the number of wheels. On the other hand, the mobility is the relationship between the driving motor torque and resistance torque on the wheel.

Table 5.1 represents the soil properties that govern TURTLE mobility and trafficability.

Table 5.1: Lunar Soil Parameters

Soil Property	Symbol	Value	Units
Soil Cohesion	C_b	176	N/m^2
Soil Cohesive Modulus	k_c	1400	kg/m^2
Soil Frictional Exponent	k_ϕ	8300	kg/m^3
Soil Deformation Exponent	n	1	
Internal Friction Angle	ϕ	35	$\circ$
Coefficient of Soil Slip	K	0.018	m
Coefficient of Friction	c_f	0.05	
Terzaghi Soil Bearing Capacity	N_c	0.010	
Terzaghi Soil Bearing Capacity	N_n	0.014	
Wheel Slip Ratio	s	0.04	
Soil Density	γ	14500	g/m^3
Soil Adhesion	μ_α	0.0011	

5.1.1 Wheel Sinkage

The amount of sinkage experienced by the wheel depends on the geophysical properties of the soil, the wheel loading, the dimension of wheel and tire. The relationship between the contact pressure, the wheel sinkage for a particular soil property, and the wheel loading provides a parametric equation of the wheel sinkage as a function of the width of the loading area. The equation below can be used to predict the sinkage of a wheel.

The pressure-sinkage relationship can be used to derive the equation of maximum sinkage of a soil wheel in and soil [48]. The depth z depends on the weight of each wheel W_w, the wheel width b, the wheel diameter d, and the soil deformation exponent n.

$$z = \left(\frac{3 \star W_w}{(3-n)bk\sqrt{d}} \right)^{(\frac{2}{2n+1})} \tag{5.1}$$

5.1.2 Motion Resistance

The rolling resistance between the tire and the ground is due to the tire slip, contact patch, deflection of the road surface and energy losses due to adhesion on the road and hysteresis. Rolling resistance varies with the type and material of the tire tread, the velocity of the vehicle and physical parameters of the environment such as temperature, pressure and the amount of water vapor in the soil. For trafficability on unprepared off-road terrain the main mechanisms of energy losses are the wheel's compaction with the soil [47]. In addition to that, bulldozing due to the soil displacement and the soil drag also impacts the motion resistance. The ability to overcome the resistance of an obstacle or slope determines the terrainability of TURTLE. The motion resistance's effects on the performance of TURTLE is accomplished by estimating wheel configuration parameters that minimizes the amount of energy dissipated into the terrain and the forces that opposes the motion of the wheel.

5.1.2.1 Obstacle Resistance

One of the level one requirements of TURTLE was the ability to climb a 0.5 meters obstacle. When TURTLE is climbing an obstacle, a force component of motion resistance is developed at the tire-obstacle interface due to the change in the normal contact force. TURTLE stability changes while climbing an obstacle is due to uneven weight distribution over the wheel. Bekker's equation on obstacle resistance can be use to model two scenarios that depend on the front and rear wheels . One of the scenarios is when TURTLE's front wheels climb the obstacle and the second scenario is when the back wheels climb the obstacle. The minimum force produced by either scenario is the obstacle resistance force.

Therefore, the maximum climbable obstacle is the smaller of the values obtained from the analysis of Ro_f and Ro_b. These values depends on the soil adhesion μ_α, the contact angle α, the obstacle height h_1, and the distance from the center of gravity to the center of the wheel l_1 and l_2.

$$x = 0.5\sqrt{d^2 - (d^2 - 2h_1)^2} \tag{5.2}$$

$$\alpha = \arcsin(\frac{d - 2h_1}{d}) \tag{5.3}$$

$$Ro_f = \frac{W(l_1 + x)(\mu_\alpha - c_f)(c_f \sin\alpha + \cos\alpha)}{\cos\alpha + c_f \sin\alpha - \mu_\alpha \sin\alpha(h_1(\mu_\alpha - c_f) + l_1 + l_2 + x)} \tag{5.4}$$

$$Ro_b = \frac{W(l_2 - x)(\mu_\alpha - c_f)(c_f \sin\alpha + \cos\alpha)}{\cos\alpha + c_f \sin\alpha - \mu_\alpha \sin\alpha(h_1(\mu_\alpha - c_f) + l_1 + l_2 + x)} \tag{5.5}$$

5.1.2.2 Gravitational Resistance

The ground slope adds a component to the motion resistance which is proportional to the component of the total weight parallel to the slope. The gravitational resistance force on each wheel can be estimated assuming that the magnitude of the gravitation load on a wheel is inversely proportional to the distance of the wheel contact from the projection of the center gravity to the contact plane [44].

Equation 5.6 was used to calculate the effect of gravitational resistance on the wheel.

$$R_g = W \star sin\theta_{slope} \tag{5.6}$$

5.1.2.3 Rolling Resistance

Rolling resistance is one of the forces that affects terrainability. The rolling resistance is a combination of the effects of wheel slip and scrubbing at the wheel-soil interface [Apostolopoulos]. The values of both the coefficient of rolling resistance c_f and the weight of TURTLE depend on configuration parameters.

The wheel diameter and tire cross section also factor in the calculation of gravitational and inertial load distribution on the wheels depend on the mass distribution and chassis configuration. Equation 5.7 can be used to model the rolling resistance where W is the weight of TURTLE and $c_f$is the coefficient of friction (typically 0.05 for lunar soil).

$$R_r = W \star c_f \tag{5.7}$$

5.1.2.4 Bulldozing Resistance

Bulldozing resistance is developed when a considerable soil mass is displaced by a wheel. This type of resistance is very common when a wheel compresses the surface layers of the soil and pushes the compacted soil forward and after the tire. The bulldozing resistance on narrow tires is alleviated by the fact that a portion of the soil bulk is pushed of the sides of the wheel.

This takes in account the bearing capacity and various physical parameters of the soil. The bulldozing resistance is directly related to the tire width. It increases with tire width. Soil bulldozing is the most dominant force on traction loss [105].

During the process of determining the parameters of the wheel and tire design for TURTLE, the larger diameter wheel with narrow width developed more traction than smaller diameter but wide wheel width with the same contact patch area and wheel loading. The compromise for more traction was TURTLE's dynamic stability. The Terzaghi soil bearing capacity is used to calculate the bulldozing resistance in Equation 5.12. Based on Bekker's theory, the bulldozing resistance can be calculated using the following equations:

$$K_c = N_c - \tan\phi_b)(\cos^2\phi_b) \tag{5.8}$$

$$K_g = (\frac{2N_n}{\tan\phi_b} + 1)(\cos^2\phi_b) \tag{5.9}$$

$$lo = 2\sqrt{(d - 0.01) \star 0.01} \tag{5.10}$$

$$\alpha = \arccos(1 - 2\frac{z}{d}) \tag{5.11}$$

$$R_b = \frac{b\sin(\phi_b + \alpha)2zC_bK_c + (\gamma z^2 K_g)}{2\sin\alpha\cos\phi_b} + \pi lo^2\gamma\left(\frac{90 - (\phi_b\frac{180}{\pi})}{540}\right) + (C_b\pi\frac{lo^2}{180}) + (C_b lo^2\tan(\frac{\pi}{4}) + \frac{\phi_b}{b}) \tag{5.12}$$

N_c and N_n are Terzaghi soil bearing capacity

5.1.2.5 Compression Resistance

Loss of soil thrust in an unprepared terrain is primarily due to the compaction resistance of the soil. Compaction is equivalent to the vertical work per unit length in pressing a wheel into the ground to a depth of its maximum sinkage [Wong]. Using the simplified model of wheel sinkage proposed by Bekker's theory, the compaction resistance can be calculated using equation 5.14.

In this case both wheel diameter and width influences compaction resistance. As a result, the diameter of a solid wheel enters the compaction equation in a power higher than the width of the tire and that both configuration parameters are inverse proportional to compaction, an increase of

the diameter reduces the compaction resistance by a greater rate than an equal increase of the tire width. The value of the exponent of soil deformation n, the cohesive moduli k_c, and the frictional moduli of soil deformation $k\varphi$ is constant and unique for various soil type and terrain. The soil consistency k, can be calculated in equation 5.13 using lunar soil properties.

$$k = \frac{k_c}{b} + k_\phi \tag{5.13}$$

k_ϕ = modulus of friction for soil deformation

$$R_c = (\frac{bk}{n+1})z^{n+1} \tag{5.14}$$

5.1.3 Soil Thrust and Traction

Traction is obtained at the boundary of a powered wheel with the ground. The maximum tractive force is limited by the thrust H produced by the soil which is also proportional to the mechanical strength of the soil. The amount of thrust required to move forward that is developed at the tire-soil interface depends on the geometry of the tire. In order to improve traction, grousers are added onto tires.

In order to calculate the tractive force, the length of the contact patch was calculated using Equation 5.15. This is the tire-soil interface that depends on the tire dimension.

$$l = \frac{d}{2}\arccos(1 - \frac{2z}{d}) \tag{5.15}$$

Equation 5.16 is the equation of tractive force with grousers.

$$H = \left[blC_b(1 + \frac{2h}{b})N_g + W\tan\phi_b(1 + 0.64\frac{h}{b}\arctan\frac{b}{h})\right]\left[1 + \frac{K}{sl}(1 - e^{\frac{-sl}{K}})\right] \tag{5.16}$$

Equation 5.17 is the equation of tractive force without grousers.

$$H = [blC_b + W\tan\phi_b]\left[1 - \frac{K}{sl}(1 - e^{\frac{-sl}{K}})\right] \tag{5.17}$$

h=height of grouser
N_g= number of grouser in contact with the ground
bl = contact area
C_b = soil/wheel cohesion
ϕ_b = wheel/soil friction angle
s =wheel slip ratio
K = coefficient of soil slip

5.1.4 Drawbar Pull

The drawbar pull is the difference between the motion resistance and the soil traction. It is the force which is available to pull or push an additional payload until the maximum available traction is reached. In other words it determines if TURTLE can be able to climb a slope or an obstacle while accommodating the effects of motion resistance. It is a significant performance parameter in mobility and trafficability because it involves wheel and tire configuration and soil properties. Equation 5.18 is used to calculate the drawbar pull for TURTLE.

$$D = H - R_c - R_r - R_o - R_b - R_g \tag{5.18}$$

5.2 Wheel and Tire Design (Ugonma Onukwubiri)

In order for TURTLE to be able to climb a 0.5 meter obstacle, the wheel had to be at least the height of the obstacle. That resulted in a wheel diameter of 1 meter. The number of wheels was determined using Bekker's theory as mentioned in the previous equations. Trade studies were done on the number of wheels, the width of the wheel, the number of grousers and the maximum climbable slope. This was done to achieve a positive drawbar pull with the minimum mass required.

5.2.1 Wheel Dimension and Number of Wheels

The wheel width and number of wheels was determined from analysis that involved using the Bekker's equations and the lunar soil parameters. The maximum climbable slope from the requirements was 20 degrees. During the analysis, TURTLE did not achieve a positive drawbar pull on a 20 degree slope, therefore grousers were required to give more traction. In Figure 5.1, TURTLE achieved a positive drawbar pull with 8 wheels and 2 grousers on a 20 degree slope. More grousers were added to improve traction on 6 and 4 wheels.

The addition of more grousers to the tire improved the drawbar pull for all wheels. In Figure 5.2, TURTLE achieved a positive drawbar pull on all wheels with 8 grousers and height of grouser is 0.015 meters. The mass constraint was minimize and optimize the drawbar pull, the number of wheel for TURTLE was 4 wheels.

Using 4 wheels, the analysis on the wheel width was done to optimized the drawbar pull and stability while minimizing the mass. In Figure 5.3 , a positive drawbar pull as achieved at a wheel width of 0.30 meters. Although increasing the wheel width improves TURTLE's dynamic stability, the increase in negligible.

The power draw increase as the wheel width decreases. The wheel width is 0.3 meters.

Once the number of wheels and dimension was determined, the wheel and tire were designed to represent the dimensions in Figure 5.4 . TURTLE will have non-pneumatic tires, thus an issue. The tire is fused into the wheels. It decrease shock absorbsion and rolling resistance. The wheels

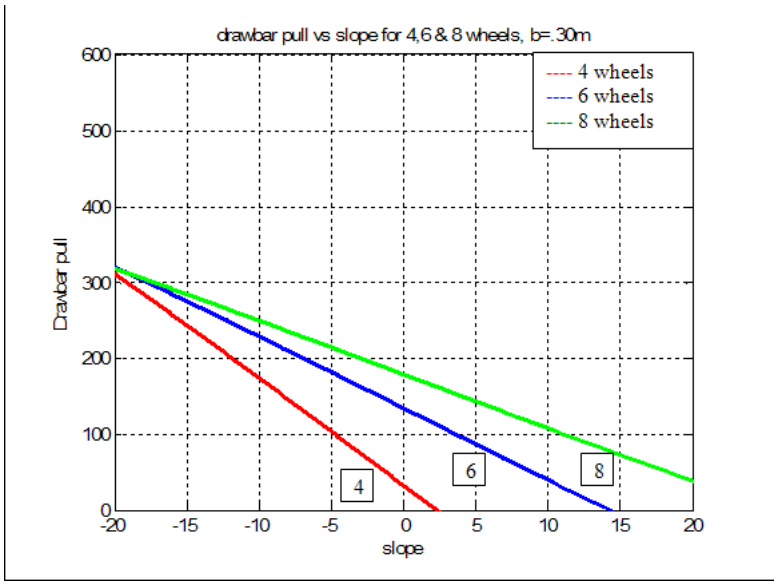

Figure 5.1: Drawbar Pull vs Slope with Two Grousers

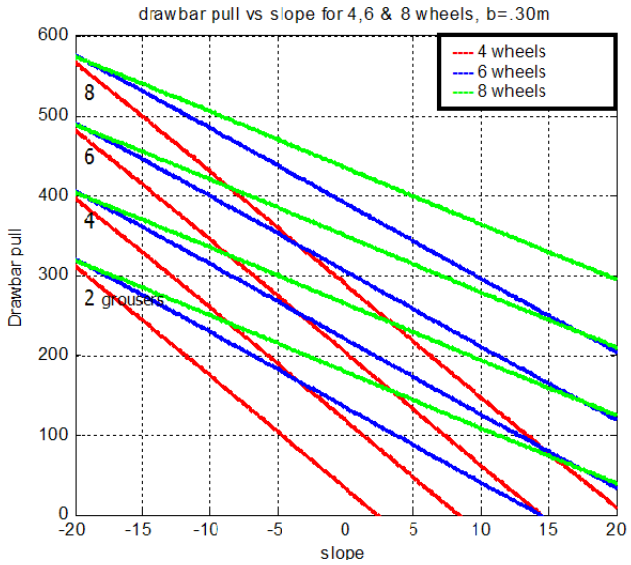

Figure 5.2: Drawbar Pull vs Slope

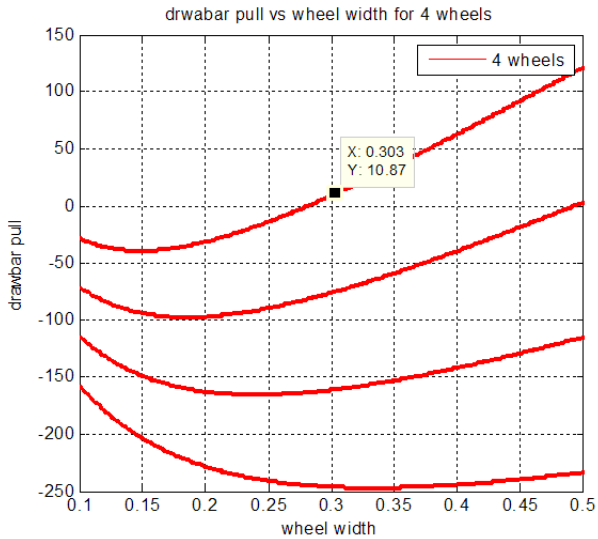

Figure 5.3: Drawbar Pull (on 20 deg. slope) vs Wheel Width

Table 5.2: Summary of trafficability for all wheel configurations

Performance	4 wheel	6 wheel	8 wheel	% change 4 to 6	%change 4 to 8
sinkage [m]	0.46	0.35	0.29	↓24%	↓37%
soil thrust [N]	927	732	634	↓21%	↓32%
total resistance [N]	918	527	339	↓ 42.5%	↓ 63%
drawbar pull [N]	10	204	295	↑ 95%	↑ 96.6%
maximum slope [◦]	20	40.5	60	↑ 63%	↑ 67%

are made out of Aluminum-2024 T351. The wheel material was chosen because of its high specific heat. For dust control, brushes will be inserted into the fenders to keep dust off grousers and wheel.

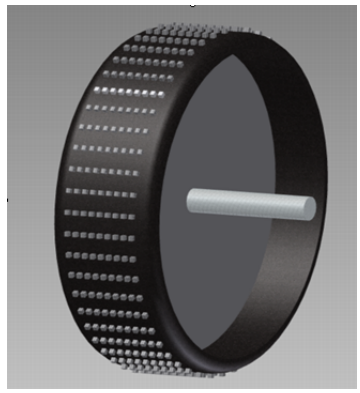

Figure 5.4: Wheel and Tire Design

The final result for wheel, tire and grouser dimension are listed in Table 5.3.

Table 5.3: Wheel and Tire Dimension

	Value
Wheel diameter	1.0 m
Wheel width	0.3 m
Number of grousers	8
Grouser height	0.015 m

5.3 Braking (Ugonma Onukwubiri)

TURTLE uses a dual braking system to achieve the desired stopping distance. To be able to climb a 0.5 meter obstacle safely, TURTLE has to be able to stop or slow down quickly enough to climb the obstacle at minimum speed. The minimum stopping distance for TURTLE depends on the maximum distance the crew can see ahead. This analysis is based on the window sizing and placement. Magnetic and friction brakes will be used to achieve the desired stopping distance. The friction brakes are used for emergency stops only.

5.3.1 Friction Brakes

Due to the climbable obstacle requirement, TURTLE will be using friction brakes. Friction brakes have difficulty dissipated heat due to a alck of environment. Therefore, to compensate for that, TURTLE will be using disc brakes which will be made out of titanium carbide ceramic. Titanium

carbide has a high specific heat constant and stores more heat during braking without failure. Figure 5.5 show a model of the friction brake system. The dimensions are 1.95 cm thickness and 20 cm radius.

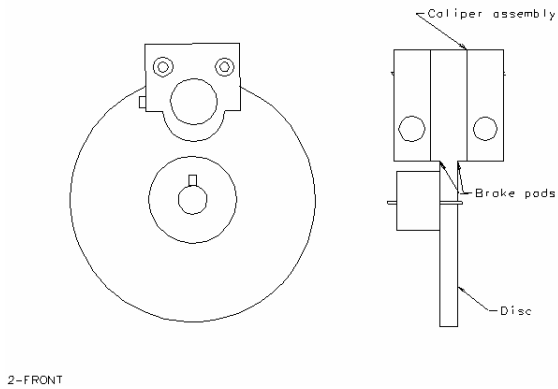

Figure 5.5: Brake System

Table 5.4 shows the material properties of titanium carbide.

Table 5.4: Disc Brake Material Properties

Material property for TiC	Value	Units
Heat Capacity	882	J/Kg
Density	4900	kg/m^3
Thermal conductivity	5.64	W/m/K
Yield strength	20	Gpa

5.3.2 Stopping Distance

The stopping distance, stop time and deceleration rate were calculated using the minimum distance the crew can see ahead. The dual braking system enables TURTLE to decelerate at a desired rate that achieves the stopping distance. Since the desired stopping distance and velocity is known, the stop time and deceleration rate were calculated using Equation 5.19

$$s = \frac{1}{2}at^2 \tag{5.19}$$

When TURTLE is traveling on flat ground and at the speed of 15 km/hr, the stopping distance, stop time, and deceleration rate for TURTLE are shown on Table 5.5. This also includes the brake force.

Table 5.5 shows the stopping distance, stop time, and deceleration rate for TURTLE. As well as the brake force when TURTLE is traveling at the speed of 5 km/hr on a 20 degree slope.

Table 5.5: Stopping TURTLE on Flat Ground at 15km/hr

Stopping TURTLE	Value	Units
Stopping Distance	4.34	m
Stop Time	2.1	s
Deceleration Rate	2.0	m/s^2
Brake Force	4000	N

5.4 Stability and Turning (Ugonma Onukwubiri)

Analysis was also done on TURTLE's stability while turning. The wheel base was directly related to turning stability. Therefore, it is the distance between the front tires. The smaller the wheel base, the tighter the turn that is possible. The steering gear box also factors into the turning radius by translating the turning of the steering wheel to the front wheels.

5.4.1 Static Stability

The static stability was analyzed based on the center of gravity location of TURTLE on a 20 degree slope. The worst case is when sitting crosswise on a slope known as the critical angle. The static stability is shown on Table 5.6. The center of gravity on TURTLE is off front the geometric center by 0.175 meters to the front and 0.28 meters to the left relative to the driver.

Table 5.6: Static Stability

Static Stability	Value
Critical angle, right	49.1°
Critical angle, front	50°
Critical angle, left	53.2°
Critical angle, back	55.6°

5.4.2 Turning Radius and Wheel Angle

The wheel width determines the turning radius of TURTLE. The turning radius was calculated from the worst case scenario which was determined by the center of gravity. The turning radius also depends on the travel velocity, the acceleration due to gravity g. The maximum turning radius was calculated using Equation 5.20

$$R = \frac{v^2}{tan\theta_{crit}g} \tag{5.20}$$

The inboard steering angle is the wheel inside the turn. This depends on the wheelbase which is the distance from the front axle to the rear axle, the turning radius and the track width.

Equation 5.21 is used to calculate the minimum wheel angle.

$$\theta_{min_{in}} = \arctan(\frac{w}{R - \frac{t}{2}}) \tag{5.21}$$

The outboard steering angle is the wheel outside the turn. It was calculated using Equation 5.22.

$$\theta_{min_{out}} = \arctan(\frac{w}{R + \frac{t}{2}}) \tag{5.22}$$

Table 5.7: Turning Radius and Wheel Angle at 15 km/hr

Turning	Value	Units
Max Turning Radius	9.2	m
Inboard Steering Angle	18	∘
outboard Steering Angle	13	∘

5.5 Propulsion System(Jason Leggett)

In designing a propulsion system for the rover that is consistent with the requirements, a top level analysis must include all Level 1 Requirements directly relating to the lunar propulsion elements. This includes

- Travel at 5 km/hr up a 20 degree slope
- Capacity to travel 100 km in 3 days
- Capacity to prevent loss of crew during two-motor failure
- Maximum velocity of 15 km/hr

These top-level design requirements will be translated into relevant requirements for the motors themselves, which then will be used to set guidelines about which the smallest, lightest, and most fuel-efficient propulsion system will be designed via a series of trade studies and logical design parameters.

5.5.1 Translation to Level 2 Required Features

In this section, the baseline requirements for the propulsion system will be defined in terms of how the Level 1 requirements relate to lunar conditions.

5.5.1.1 Torque

Total system torque output can be found by summing the relevant forces on the rover as noted in Terramechanics (Section 5.1), and multiplying by wheel radius as per Equation 5.23.

$$T = \sum (F_{gravity} + R_{compress} + R_{roll}) * r \tag{5.23}$$

The force of gravity is normal to vehicle motion, except when traveling on a slope. Plugging in the numbers calculated in the terramechanics section yields the following results:

- 512 N-m torque required for travel on flat travel
- 1202 N-m torque required at maximum for travel up a 20° slope

These will encompass the minimum requirements for motor torque output. It should be noted that each of these as applied to the motor is inversely proportional to gear ratio—the higher it gets, the lower the torque requirement for the motors gets.

5.5.1.2 Energy Requirement

In order to travel 100 km in 3 days, the rover is rated for an "average" velocity, to be seen as the nominal speed throughout the trip. Although it is unlikely that most motion will occur at this nominal speed, it is useful for the purposes of calculation of power draw and hence fuel use. To complete the trip in 72 hours, an average speed of 1.83 km/hr is required. In terms of energy, the total mechanical energy required can be calculated (assuming 100% efficiency) as in Equation 5.24

$$E = \frac{T * RPM}{5252} * \frac{.752kW}{Hp} * 72h \tag{5.24}$$

Plugging all the numbers in, and recognizing that combining torque and RPM for the mechanical energy equation will cancel out the influence of the gear system (since gears simply swap RPM for torque at some efficiency loss), the minimum energy requirement for the entire trip is 53.79 kWh.

5.5.1.3 Reliability

In order to meet the Level 1 requirement that loss of crew does not occur during two system failures, two important traits of the system must be established. The first is that the propulsion system is required to be designed as a series of individual, independent operating systems, rather than a single design. This instantly rules out any sort of central drive system, and means there must be several individual motors operating independently.

Fortunately, due to lunar conditions, no further Level 2 requirements are placed on the propulsion system. Due to the heavy weight of the rover, uphill travel already demands more than twice the torque of travel on flat ground. Due to the location selection of rover landing points, all of which

allow for sufficient flat ground to be traversed back to the safety of the Crew Exploration Vehicle, it is acceptable to simply require the rover to be capable of traversing flat ground. Thus the previous Level 1 requirement already provides sufficient coverage of this mission requirement. Regardless, for acceptable reliability it is impossible to use any interdependent propulsion system such as a central drive, and a wheel-mounted system must be relied upon. Finally, loss of a single motor does not yield loss of mission; however, it does pose a serious crew hazard as maximum speed and power efficiency are sacrificed in order to operate at greater individual motor torque levels.

5.5.1.4 Maximum Velocity

Following the RPM equation as calculated previously in Section 5.5.1.2, the maximum required velocity for lunar travel on flat ground is 80*GR. For whatever gearing system is utilized, the motor must be capable of spinning its driveshaft 80 times faster than the applied gear ratio. For example, a 10:1 ratio (increasing torque tenfold) would demand a motor capable of 800 RPM. This requires the selection process to mainly include a series of high-performance engines capable of both exceptional torque and speed, rather than one skewed far to one direction with a system meant to make up for its deficiencies. The required RPM for the motor, at the given Hp rate, is found from Equation 5.25.

$$RPM = \frac{V(km/hr) * GearRatio}{R_{wheel} * .377} \tag{5.25}$$

5.5.1.5 Size

The wheel system of the vehicle has been designed to have a radius of .5m. As such the motor cannot under any circumstances exceed this size in diameter, as doing so would require additional mass to be utilized to hold it up, drawbar length would be extended, and general mass would skyrocket. This is a hard requirement, as for the vehicle to pass over a large obstacle; a motor of size greater than this would be exposed to the ground and would likely suffer irreparable damage. The concept, as explained in Section 5.6, requires the motor to be kept fully off the ground. It is mounted alongside the strut and is moved along with the wheel system, and its mass is accounted for in the suspension design. Loss of one motor does not yield loss of mission but represents a serious crew hazard, and is to be avoided even if this results in higher overall mass. Safety of the crew is a greater priority than optimal mass budget.

5.5.2 Level 3: Optimal System Parameters

5.5.2.1 Mass

The ultimate parameter under consideration throughout the entire design process is mass. No more than 2500 kg can be landed on the moon under any circumstance. Furthermore it is desired to

develop a theoretical rover mass with a 20% margin of error or better, allowing for critical last-minute additions as they become necessary. Most of such additions would fall into the category of Crew Systems/Life Support or Structures, and as such it is in the best interests of this project to meet the Level 1 and 2 requirements as closely as possible and not to expend any extra mass on exceeding them.

5.5.2.2 Power Draw

To optimize the propulsion system, fuel usage must also be minimized in tandem with propulsion system mass. The fuel source is a hydrogen fuel cell with energy density 2.32 kWh/kg. Every excess kWh of energy required by systems less than 100% efficient then requires an additional .43 kg mass in fuel. Maximum and minimum power requirements are considered minor as will be noted in the circuitry section; all wires selected will be rated for more than 20 A of current, which is more than will ever be needed for the system as a whole.

5.6 Propulsion System Overview (Jason Leggett)

The motor, regardless of its composition, is to be fully encased in a thin (.1mm) shell of 2024 Aluminum Alloy. This will protect it from dust particles kicked up by the wheel system. The mass of this shell is virtually negligible, but comes to approximately 1.5 kg each and is included in the mass budget. This does not protect the motor from damage, and thus the Level II reliability requirements are yet unchanged (and indeed, will never change). The motor itself is to be mounted along the strut portion of the vehicular suspension. This section moves upward along with the wheels and as such prevents contact between the motor and the ground. Each individual motor is not especially heavy, as will be noted in the motor trade study analysis in Section 5.7, and as such is more than capable of being held up by the struts. The struts themselves bear the weight of the entire vehicular frame, which is expected to be several times more massive than the propulsion system. A series of miniature struts provides balance to the motor, connect to upper elements of the struts without impeding the suspension in any way, and weigh in at 5 kg each, for a total support system mass of 26kg. The struts are the heaviest element, but they are a part of the suspension and weigh in separately. The motors each extend a 2024 Aluminum driveshaft (5 kg, part of motor mass) into 12-tooth carbon steel helical gears. These gears are 5cm thick in both body and teeth, and as such are very strong and capable of producing substantial gearing up of the torque output. They connect in parallel to a second gear with five times larger a radius, oriented directly at the center of the wheel, connecting precisely to the center of the wheel itself. The second driveshaft extending from the gear to the wheel is a standard automobile carbon driveshaft, and is slightly lighter at 4.5kg, despite being substantially thicker.

The final system design is outlined Table 5.8, and on Figure 5.6 is a rough sketch of the entire propulsion system with all dimensions and all parts labeled. It should be noted that while the strut appears to "bend", it doesn't actually do so. The strut connects around the gear system, rather than under it, but it's impossible to demonstrate this in a non-3D drawing. Also it should be noted that there is a flaw with this design: the magnets actually take up the majority of the space, not the "frame". The magnets should be .2 m in thickness each, not .1.

Table 5.8: Critical Motor Statistics

Nominal Motor Torque	26 N-m
Nominal Efficiency	.91
Critical Motor Torque	62 N-m
Critical Efficiency	.60
Maximum RPM	540 RPM
Average Power Draw	0.821 kW
Maximum Power Draw	6.19 kW
Acceleration Rate	0.230 m/s2
Average Waste Heat	48.6 W
Total Motor Length	.22 m
Motor Radius	.25 m
Total Mass	171.3 kg

The overall mass of the motor is calculated in Table 5.9.

Table 5.9: Propulsion System Components by Mass

Component	Mass
Neodymium Magnets	66.4 kg
Aluminum Stators	20 kg
Large Gears	20.125kg
Small Gears	.805 kg
Strut Fasteners	~25 kg
Carbon Driveshafts	10 kg
Hall Effect Sensors	4 kg
Voltmeter	5 kg
Ammeter	5 kg
Internal Wheel Support	15 kg
Total	171.3 kg

The gears are designed in parallel; each 5cm thick, one of diameter .05 m, with a .025 m gap for the aluminum stator/driveshaft. The second is of diameter .25 m, with a .125 m gap for the carbon driveshaft that connects directly to the wheel. This brings the driving force to the exact center of the wheel, as will be diagrammed.

The length of the system design allows it to fit entirely within the confines of the wheels of the vehicle, without extending out at any point.

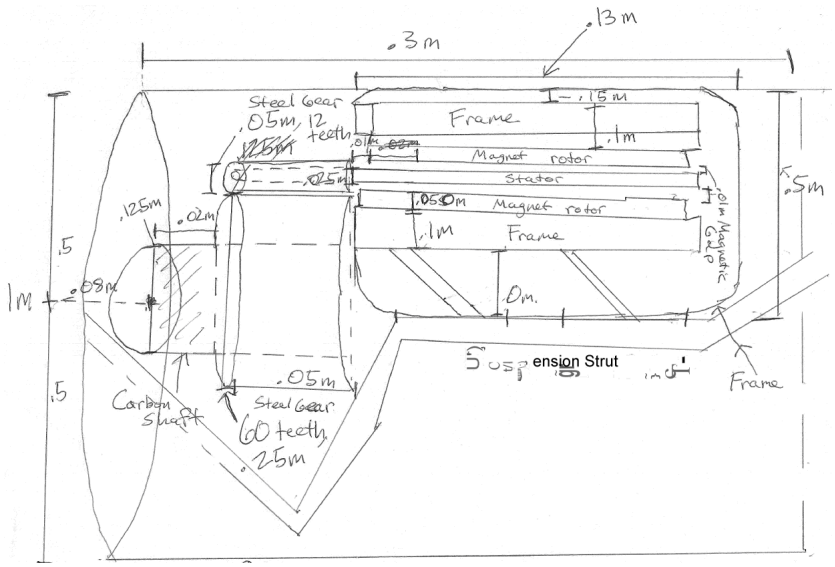

Figure 5.6: Sketch of Full Propulsion System (rough)

5.7 Motor Design (Jason Leggett)

Three primary motor options were considered: the typical vehicular internal combustion engine, and the two dominating forms of DC electric motors: a physically commutated, brushed motor, and the electronic brushless type. Some offered additional qualities that did not directly fall within the bounds of the Level II requirements, often as a side effect of better matching the Level III design parameters (mass and fuel efficiency). These will be discussed within the qualities of each system type.

5.7.1 Motor Types

5.7.1.1 Internal Combustion

The internal combustion motor most useful for this task would be the single-cylinder engine often found in such tools as snowblowers. While individually not very powerful, it is far more compact and efficient than the larger varieties found in automobiles. While typical automobile systems burn gasoline at power efficiencies of approximately 25%, the single-cylinder engine avoids the friction associated with a series of pistons as it only uses one, and as a result can operate at levels as high as 45%, near the peak of combustion engine performance.

5.7.1.2 DC Brushed Electric

The brushed electric motor uses a series of physically commutated brushes to turn its driveshaft. They are powered by the current flow through a series of coils that wrap around the brushes and use electric fields to push it in a circular motion. While the individual parts of the motor are substantially heavier than the brushless design, the brushed motor is simple to control and does not require complex avionics.

5.7.1.3 DC Brushless Electric

The way the DC brushless motor works is simpler than that of the other systems. A current is passed through the aluminum stator, while the field from a series of neodymium magnetic rotors is shifted perpendicular to the stator on both sides. The stator will spin at up to 540 RPM, and will be exposed to torques of approximately 24 N-m per motor. This requires about 10 A of current, which is fairly minor. A close-scale image of an example of the brushless system is shown in Figure 5.7.

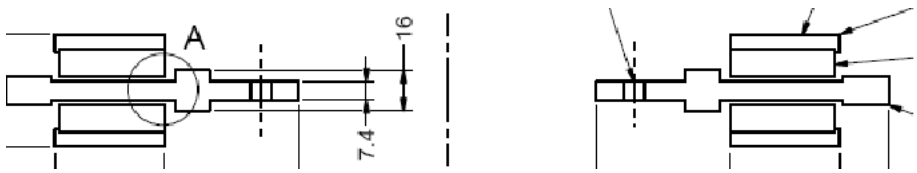

Figure 5.7: Motor Components of Brushless DC Motor[79]

Under normal circumstances, the electronically commutated brushless DC motor would be a poor choice for a propulsion system with minimal mass because of the large amount of equipment necessary to properly control it. However, due to the large amount of sensory equipment already available to avionics, this is not a problem. Much of the monitoring equipment utilized by avionics to track power systems throughout the rest of the rover can double to input a simple controller (most likely a PD control or something equally insignificant) upon the motors. The only additional tools necessary will be a fairly accurate voltmeter and ammeter, in order to assure inputs to the stator and rotor of the motor work properly. The rest of the equipment, a computer to run the control program, and a program to interpret the Hall Effect sensors[79]can simply multitask from life support and science tasks. The control of this motor does not require a huge amount of bandwidth, just several different tools.

5.7.2 Level 3 Investigation with Level 2 Requirements as Controls

A brief overview, with the graph of the results, will be provided in this section explaining how and why the brushless electric system was selected and optimized.

5.7.2.1 Zero-Fuel Mass Analysis

The design properties of each motor made their masses fairly simple to predict. While the brushless permanent magnet's mass was dominated by the neodymium rotor and the associated tracking equipment, the internal parts of the other two systems were far heavier, though easier to control. Because avionics opted to unify their control to some degree, there is mass overlap in the control systems and the brushless system best takes advantage of this. This is why it is the least massive, despite the fact that it would likely outweigh a brushed system if all its control were to be run separately. Figure 5.8 demonstrates the plot of Motor Mass vs Torque.

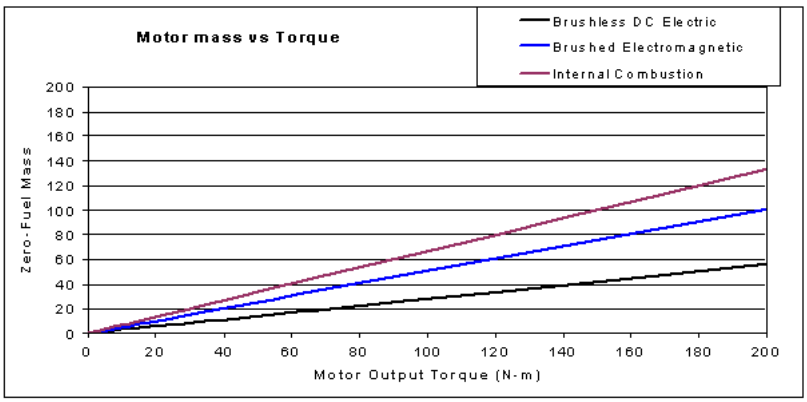

Figure 5.8: Zero-Fuel Mass Plot

5.7.2.2 Fuel Draw Analysis

While at first glance, the internal combustion system might seem like the obvious choice when it comes to the mass of fuel it uses, a natural result of the extreme energy density of gasoline at approximately 12 kWh/kg, but this is not the case in space. While this fuel usage study compares the expenditure of the hydrogen fuel cell system for the electromagnetic and permanent magnet DC systems, it assumes a gasoline-oxygen burning system for the internal combustion engine. For every kg of gasoline burned, 8 kg of oxygen must be burned. Internal combustion simply cannot be relied upon for this mission, and the graph will demonstrate this clearly. Figure 5.9 demonstrates the plot of fuel usage versus time, by motor type. It is worth noting that while the two DC motors don't use substantially different levels of fuel, for an outpost rover that would be in repeated use, the benefits of a more efficient drive improve many times.

5.7.2.3 Sizing Analysis

Having become abundantly clear that the brushless motor will be the selection, as it boasts lower mass at zero-fuel as well as slightly lower fuel usage, because gear system mass will increase expo-

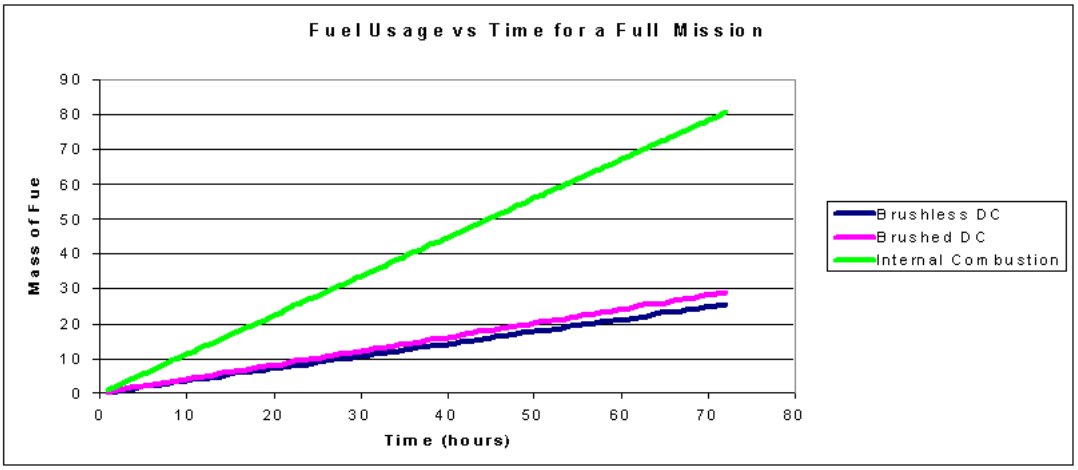

Figure 5.9: Fuel Use over Time

nentially while motor mass only increases linearly, the larger the motor is, the lighter the overall propulsion system will be. As such, the largest acceptable diameter, 50 cm, is chosen. There is no reason to use a smaller motor and bigger gears; the gears become much heavier as the gear ratio rises, and one must trade away efficiency by switching to a different gear system, which is not optimal. Maximizing motor size ultimately minimizes mass. Figure 5.10 shows a plot of just the mass versus torque output of the motor options, and it is this that ultimately leads one to select the brushless drive. It is far more compact than the other options.

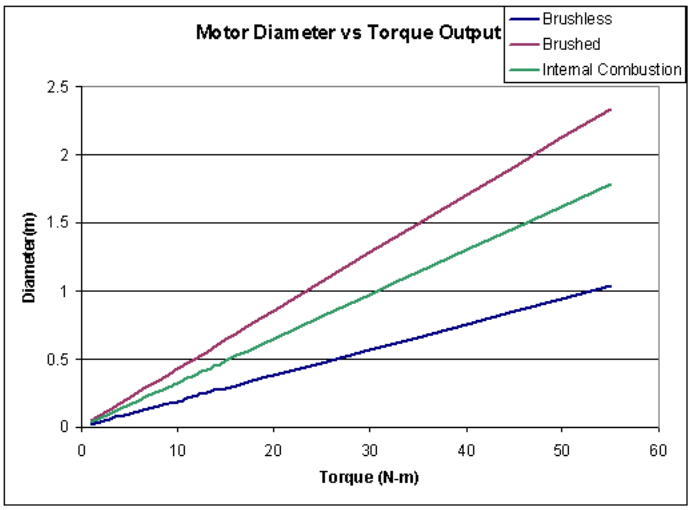

Figure 5.10: Motor Size Capacity

5.8 Motor Control (Jason Leggett)

5.8.1 Hall Effect

The brushless motor is controlled by a series of three Hall Effect sensors implanted in the aluminum stator.

The presence of these sensors allows measurement of microvoltage flux throughout the stator. Essentially measuring the influence of the Hall Effect in the metal, this is in simplest terms the formation of electric potentials around the conductor through which current flows due to a moving magnetic field. The presence of this potential will reflect on how quickly the magnetic field is shifting and thus how much torque is exerted on the stator itself. The stronger the potential is measured to be, the greater the torque on the stator is expected to be as well.

Controlling the brushless motor is far more complicated than controlling a regular brushed or combustion motor. This electronic commutation requires substantially more avionics to control but also can be controlled more closely, which is a vast improvement on the systems inherent to other motor designs. A highly accurate ammeter and voltmeter are necessary to run the stator in the correct manner, as torque and RPM are linearly related to current and voltage respectively[79]. When the current is run through the stator and the magnetic field is switched on, there will be a force pushing perpendicular to the motion of current (as explained in Section 5.8.2). The intensity of the voltage pressed in, as measured by the Hall Effect sensors, will determine how fast the stator, which now acts as the motor's driveshaft, will spin. The key advantage to controlling this motor is that the Hall Effect sensors can directly be connected to the same avionics computing system that handles a multitude of other tasks. In a standard system it would require its own separate control equipment to regulate the flow of voltage and current to the stator and rotor, but because the rover as a whole undergoes a complicated system of automated control, the same devices that control other systems can be multitasked to control the drive as well. Because said devices also have backups, this does not influence the risk of loss of crew or mission. Figure 5.11 and Figure 5.12 show front and side views, respectively, of the sensor system.

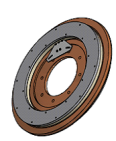

Figure 5.11: Front View: Sensor Positioning[79]

5.8.2 Torque Control

Because the magnetic force equation is of the form $F = I * B$, and because the magnetic field B is of constant magnitude, the current passed through the aluminum stator is the primary source

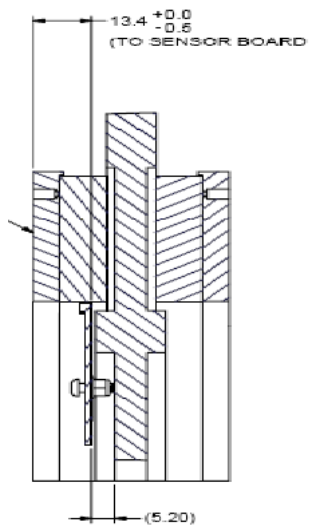

Figure 5.12: Side View: Sensor Positioning[79]

of torque control. Just as the force equation suggests, increasing the magnitude of the current increases the torque in a linear manner. This should come as no surprise as the magnetic field is consistently oriented to be perpendicular to the current, hence creating spin in the stator at the highest possible rate. The torque then linearly relates to current as per thickness of the stator and strength of the B-field. Each motor produces approximately 2.4 N-m of torque per ampere of current. A key element of control of this system is that because current can shift so quickly, the torque is entirely reversible. Using a switch system to reroute the voltage, the motors can be run forward or in reverse, and hence a secondary form of braking[79]using the neodymium magnet to create a magnetic system torque[79]is applicable. This is only 10% of the total braking system so as to minimize damage to the driveshaft; regardless it generates far less waste heat than a physical brake as the motor itself runs at such an efficient rate.easily

5.8.3 RPM Control

In order to establish a standard voltage throughout the rover, RPM control will be accomplished using a voltmeter and high-priority computer response to modify the motor RPM to match the desired vehicular speed. All other systems are rated with standard voltage, however the motors will be kept on their own seperate circuit (necessary for reversability anyway) that has variable voltage. Voltage input to the stator will increase the impact of the magnetic Hall Effect, and will be measured by the sensors. This in turn will increase the speed at which the magnetic field shifts across the rotor[79]but not the strength of the field produced. The neodymium magnetic field is of constant strength and is weak enough that it is not a health risk to the astronauts under any

circumstances. However, increasing voltage input will result in higher RPM for the stator (and hence the driveshaft to the wheel).

5.9 Gearing Optimization (Jason Leggett)

5.9.1 Selection of Best Base Gears

Table 5.10: Relevant Gear Statistics

Type	Maximum Reasonable Gear Ratio	Efficiency
Helical	5:1	.98
Spur	10:1	.75
Worm	100+:1	<.5

Three principal types of gear systems were selected for consideration: Helical, spur, and worm gears. The worm gear system was discounted primarily because the advantages it offered[62]high gear ratio and low space usage[62]were not necessary for this system as the selected brushless motors were within a reasonable range of the necessary torque as outlined in the Level 2 requirements. As such the choice came down between helical and spur gears. While helical gears are impractical at the highest gear ratios because they are not capable of experiencing as much force on their gear teeth, they are far more efficient due to the quiet, low-friction manner in which the gear teeth come together. Because the required gear ratio winds up being fairly low, it is more economical to utilize the helical gear than the stronger spur gears. The difference in mass at lower levels is negligible.

5.9.2 Spacing and Positioning of Gears

Figure 5.13: Parallel Gear Positioning

Because of the moderately large size of the motor, and the fact that the stator exits the motor shaft system .15 m above the center of the wheel, a parallel gear arrangement is used to bring the driveshaft exactly in line with the center of the wheel, where it will connect and exert approximately

130 N-m of torque per wheel when on flat ground; and up to 260 N-m of torque when traveling up a 20 degree slope. The teeth of the gears, as well as the driveshafts, are all rated for such action[62].

5.9.3 Development of Optimal Gear Ratio

$$W = \frac{SFY}{P_N}\left(\frac{600}{600+V}\right)$$

W = Tooth Load, Lbs. (along the Pitch Line)
S = Safe Material Stress (static) Lbs. per Sq. In. (Table III)
F = Face Width, Inches
Y = Tooth Form Factor (Table IV)
P_N = Normal Diametral Pitch
(Refer to Conversion Chart)
D = Pitch Diameter
V = Pitch Line Velocity, Ft. Per Min. = .262 x D x RPM

Figure 5.14: Gear Load Formula[62]

It now becomes clear why the largest possible size for the motor is desirable. In order to reach the target torques as defined by the Level 2 requirements, the gear ratio must ramp up the motor output torque. However, the teeth on the larger gear are thus exposed to the full torque of the motor, which in turn means that they must be thick enough not to break under such stress. Using the helical gear theoretical equation in Figure5.14 it is possible to determine the required thickness: The result is that for the strongest possible gears (1020 Carbon Steel), a tooth thickness (and hence overall thickness) of 5 cm is necessary. Since the gears' mass will increase exponentially with gear ratio, it is in the best interest for conserving mass to use the smallest gear ratio available. As seen below, a 5:1 gear ratio is the all that is required, which yields a relatively low gear weight. There's no way to go lower than this as this gear ratio corresponds to a motor of approximate diameter 50cm, which is as large as it can possibly be. Thus the overall propulsion design in Section 5.6 has been proven.

5.10 Steering Method (Aleksandar Nacev)

The rover suspension system allows for the individual control of each rover wheel to be steered a maximum angle of 60°. Therefore to apply the torque to each wheel forcing turning, a linear actuator is attached to wheel base and the suspension system.

5.10.1 Calculation of Force Required

$$\ddot{\theta} = \frac{2\Delta\alpha}{\Delta t^2} \tag{5.26}$$

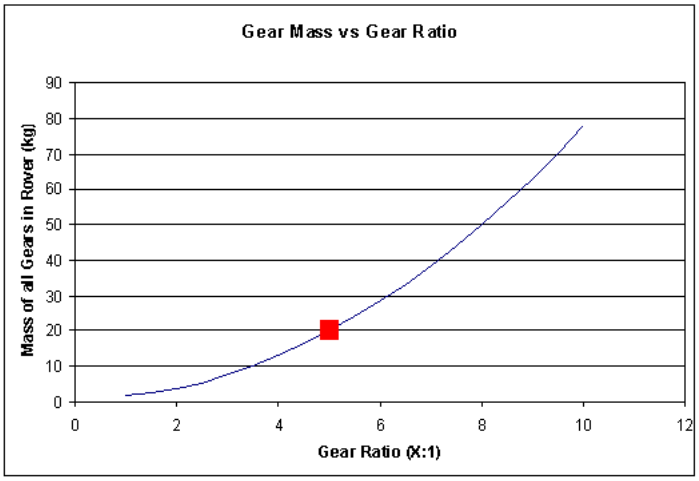

Figure 5.15: Graph of Gear Ratio versus Mass

$$T = I_{wheel}\ddot{\theta} \tag{5.27}$$

$$F_N = \frac{T}{d} + \frac{R_b}{4} \tag{5.28}$$

$$F_{strut} = \frac{F_N}{\cos(\alpha_1)} \tag{5.29}$$

$\ddot{\theta}$	Angular acceleration of the wheel
$\Delta\alpha$	Angle difference that the wheel is turning
Δt	Amount of time for wheel to turn
I_{wheel}	Moment of inertia of one wheel
T	Torque needed to be applied to the wheel from the linear actuator
d	Distance from rotation axis that the force is applied
R_b	Bulldozing resistance for the wheel
F_N	Force applied normal to the wheel surface
F_{strut}	Force applied by the linear actuator to the wheel surface
α_1	Angle the actuator makes with the wheel

To calculate the required force the linear actuator needs to apply to generate the torque on the wheel for turning, the Equations 5.26, 5.27, 5.28 and 5.29 were used. These equations assumed a turning time of 60° in 1 second. This time is the assumed response time of the wheel itself and does not include the response and speed of the linear actuator. The assumption is made that the linear actuator used will be able to respond at similar rates if not faster. Figure 5.16 shows the relationship between the force required by the linear actuator when turning the wheel a certain angle.

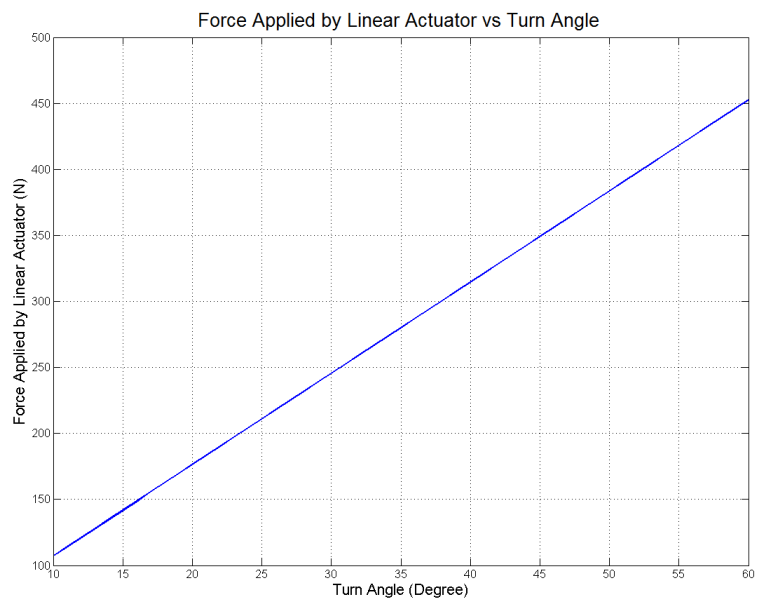

Figure 5.16: Force Applied by Linear Actuator Over Turn Angle

5.10.2 Calculation of Energy Needed

$$E_{max} = 2d \tan(\theta_{max}) \tag{5.30}$$

After knowing how much force the linear actuator needs to exert in order to turn the wheel, the energy required to supply to the linear actuator was also calculated. The energy required is related to the distance the actuator moves and is shown by Equation 5.30. This energy can then be converted into a power draw for each wheel actuator by averaging it over the time required to turn. Figure 5.17 shows how the power draw changes over the turning angle. This power draw was then averaged over the driving time to obtain a worst case scenario and added into the power budget.

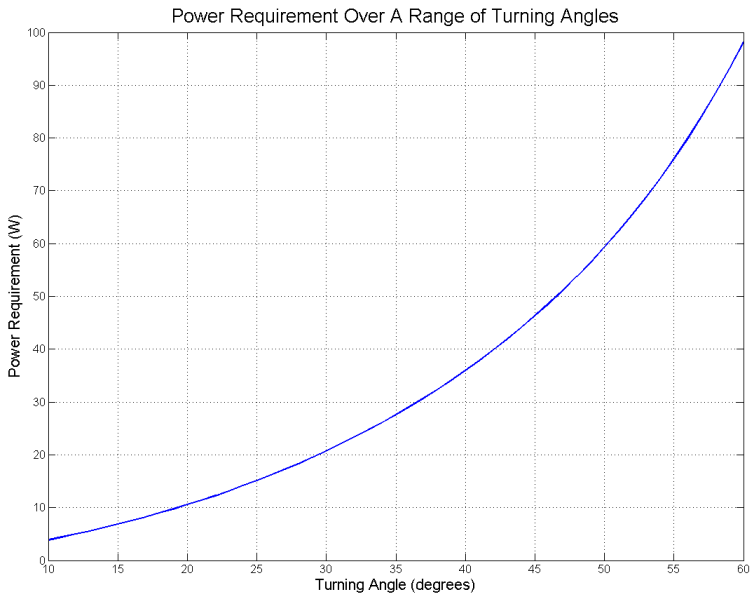

Figure 5.17: Power Draw From a Given Turning Angle

Chapter 6

Power

6.1 System Overview (Stephanie Petillo and Aleksander Nacev)

The overall power system designed for TURTLE is simple, yet effective. As outlined in Figure 6.1, the primary (and only) power supply is the array of three fuel cells contained on the outside of the rover. Any single fuel cell could supply enough power to the rover for the duration of the mission, but tri-fold redundancy of this system has been included as fault tolerance, because it is vital to the survival of the crew. Due to this redundancy, the fuel cells must be low mass. At any given time, at least two fuel cells will be active to safeguard against a complete power shutdown in the unlikely event that one fuel cell fails.

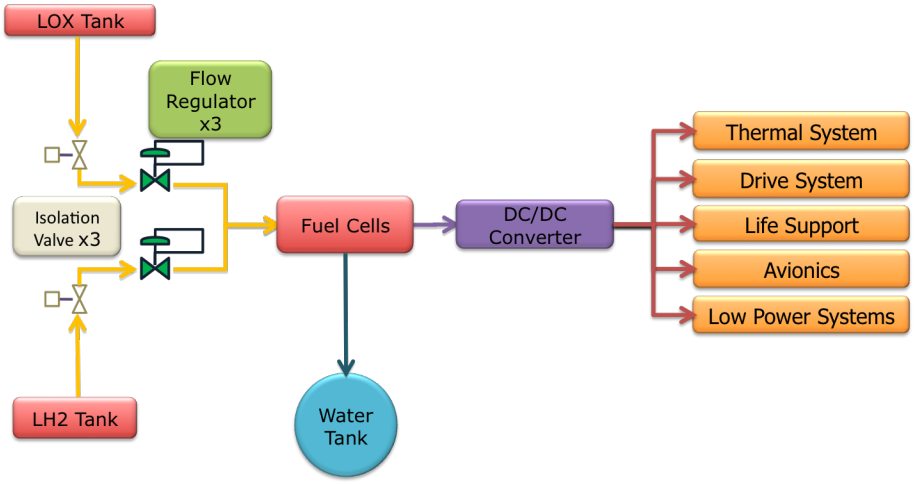

Figure 6.1: Overview Diagram of the Rover Power System

The fuel cells are supplied with cryogenic reactants of liquid hydrogen (LH_2) and liquid oxygen (LOX) stored in insulated composite tanks on the outside of the rover. When the reactants flow into

the fuel cells and react, potable water is produced and stored for use by the astronauts throughout the mission.

With the reactants flowing through the fuel cells, the power generated by the chemical reaction of hydrogen and oxygen to form water is used to power the various systems of the rover. To achieve the proper supply voltage, a DC/DC converter is connected between the fuel cells and the rover systems.

6.2 Critical Power Distribution (Stephanie Petillo and Aleksander Nacev)

There are four levels of failure that may result from the power loss to various rover systems, as outlined in Figure 6.2

A "crew critical" failure will result in loss of the crew within minutes. If power to life support fails, the crew may run out of air, or the cabin may depressurize or quicky become dangerously hot or cold. A crew critical failure would also occur if all three fuel cells fail because they are the only system that provides power to the rover. However, if two fuel cells malfunction, one fuel cell will be able to power the entire rover.

A "crew hazard" failure does not put the crew into immediate danger, but they will only have a matter of hours or days to get back to the lunar base before the failure becomes life-threatening. Loss of power to the drive system is hazardous to the crew because, even though they could continue to live in the rover for a few days, they would have to perform an EVA and walk back to the lunar base before the Personal Life Support System (and rover) run out of power and supplies.

A "mission critical" failure does not affect the survival of the crew, but will result in the loss of the mission. Communications is one such system that requires power in order to determine the positioning of the rover and remain in contact with earth and the lunar base. If comunications fail, it will be dangerous and near impossible to determine where to drive to complete a sortie mission, and the crew should return to the lunar base immediately to avoid risking getting lost or caught off-guard by driving an unfamiliar path.

An "acceptable failure" constitutes such failures that do not jeopardize the sortie mission or the crew's lives. Loss of power to low-power rover systems may cause some discomfort or inconvenience to the crew, but will not be detrimental to their survival or to the completion of a sortie mission.

6.3 Power Requirements and Generation (Stephanie Petillo and Aleksander Nacev)

The power needed over the duration of the lunar mission varies over five stages. Fuel cells were selected as the power supply to optimize for meeting power generation, mass, power density, and

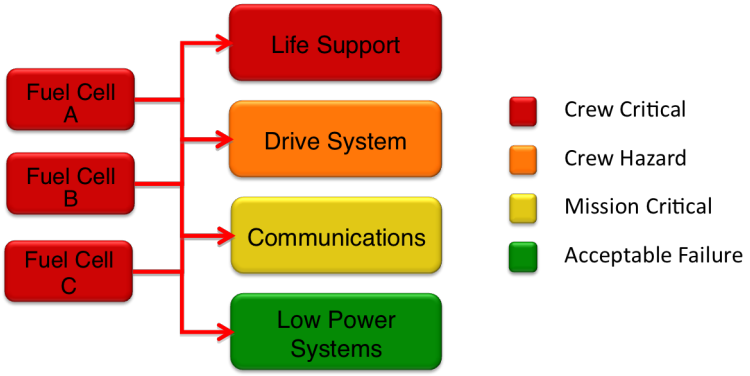

Figure 6.2: Overview Diagram of the Critical Power Distribution throughout the Rover

supply duration requirements.

6.3.1 Power and Energy Needed for Components

During each stage of the mission there are different components running on the rover. This causes a wide variation in the amount of power that needs to be supplied such that it is more efficient and accurate to separate the power requirements for each stage of the mission between the Earth and moon, rather than average the power over the entire mission. In doing this, the following power breakdowns were developed.

6.3.1.1 Lunar Transfer Stage

During lunar transfer, power must be supplied to avionics systems for running communication systems, cameras, and positioning and attitude sensors. Due to limited space in the payload shroud of the Delta IV Heavy, the power for the rover during lunar transfer is provided by the rover's fuel cells. These fuel cells will be providing a total of 290 Watts for about seven days (48.4 kWhr of energy) during the lunar transfer stage. A breakdown of the power distribution during lunar transfer is given in Table 6.1.

6.3.1.2 Descent and Landing Stage #1

The first part of the lunar descent and landing stage takes place over a period of about 55 minutes, in which the retro engines are burning and the compressor to the thermal system is running to regulate the rover temperature. The fuel cells continue to run at this stage and are producing water that will be ready for the crew to use once they rendezvous with the rover. Throughout this stage, 1,328 Watts of power are needed on average (1.217 kWhr) to run avionics tracking equipment, communication

Table 6.1: Lunar Transfer Stage Power Distribution

Active Components	Number of Components	Total Power (W)
Star Tracker	1	20
IMU	1	38
Rad750	1	25
Interface Box	1	25
Memory Idle	1	20
Communications	1	40
Cameras	1	18
Compressor	1	104
Total Power (W)		290
Time of Transfer (days)		6.958
TOTAL ENERGY (Whr)		48430

transmission equipment, attitude sesnors, and HD cameras on the rover. A breakdown of the power requirements for this stage is shown in Table 6.2.

6.3.1.3 Descent and Landing Stage #2

The second part of the descent and landing stage has a duration of about 5 minutes, in which the retro engines are ejected. At this point, the fuel cells are powering the avionics systems, communications and landing thrusters as the rover makes its final descent to the lunar surface. As totalled in Table 6.3, the overall average power needed for this stage is 1,068 Watts (89 Whr of energy).

6.3.1.4 Standby Stage

The rover is put into a low-power standby mode during the maximum of seven days that it is on the moon before its rendezvous with the astronauts and for the two days betwen the two sortie missions, for a total of nine days in the standby stage. In this mode, only the systems necessary for cabin pressurization, comunications, computer memory, avionics system-monitoring sensors, and components in an idle configuration are running in order to save on power and fuel consumption while the rover is not in use. This requires 426 Watts of power on average (92.0 kWhr), as distributed in Table 6.4. The source of power for this stage is provided by fuel cells on board the rover.

6.3.1.5 Sortie Mission Stage

Completing two sortie missions requires three days for each mission, plus two days of contingency, for a total duration of eight days or power required. The fuel cells will also be used for this stage to provide the nominal power of 3,240 Watts (622.2 kWhr of energy) to avionics, driving, life support,

Table 6.2: Descent and Landing Stage Power Distribution using Solar Panels

Active Components	Number of Components	Total Power (W)
Star Tracker	1	20
IMU	1	38
Radar	2	20
HD camera	3	45
RAD750	3	75
Interface Box	1	25
LIDAR	2	40
Mass Memory	1	50
S-Band LPT	2	100
Ka-Band	2	94
Pointing Device	1	100
Retro Engine	1	350
Compressor	1	371
Total Power (W)		1328
Time of Transfer (days)		0.0382
TOTAL ENERGY (Whr)		1217.3

Table 6.3: Descent and Landing Stage Power Distribution using Batteries

Active Components	Number of Components	Total Power (W)
Star Tracker	1	20
IMU	1	38
Radar	2	20
HD camera	3	45
RAD750	3	75
Interface Box	1	25
LIDAR	2	40
Mass Memory	1	50
S-Band LPT	2	100
Ka-Band	2	94
Pointing Device	1	100
Compressor	1	311
Thrusters	10	150
Total Power (W)		1068
Time of Transfer (days)		0.0035
TOTAL ENERGY (Whr)		89

Table 6.4: Standby Stage Power Distribution

Active Components	Number of Components	Total Power (W)
IMU	1	38
HD Camera	6	18
RAD750	1	25
Interface Box	1	25
Mass Memory	1	10
Communications	1	40
Cabin Air Control	1	60
Hubs	4	40
Compressor	1	170
Total Power (W)		426
Time of Transfer (days)		9.00
TOTAL ENERGY (Whr)		92016

thermal control, and all other cabin systems, as shown in Table 6.5. To drive the rover, inhabit the rover and complete EVA's, this nominal power must be supplied throughout the duration of the eight-day mission and contingency.

Nominal power usage is highly impacted by the compressor of the thermal system, which is used to regulate the cabin environment as well as the temperature of the internal electronics and the fuel cells on the rover exterior. The 1.30 kWatts consumed by the compressor is over a third of the total power required by the rover during this stage. This is due to the iterative process that marks the tradeoff between power usage of the compressor and the thermal radiation of the cooling loop, which will be described in Section 7.2.2.3 concerning the compressor's roll in the active thermal system.

6.3.2 Power Generation

6.3.2.1 Criteria

In order to determine the best way to power the lunar rover, the overall mass and power density of the various types of power supplies are taken into account. Due to mass restrictions on the rover, the method of power generation chosen is based on the lowest achievable power system mass.

6.3.2.2 Power Generation Methods

Four types of power supplies were analyzed for use on the lunar rover throughout the voyage to and on the moon. Proton Exchange Membrane (PEM) fuel cells, lithium-ion batteries, alkaline batteries, and solar arrays were all compared, as described in Appendix A.8, to determine the most mass- and power-efficient power supply.

Table 6.5: Sortie Mission Stage Nominal Power Usage Distribution

Active Components	Number of Components	Total Power (W)
IMU	1	38
Radar	2	20
HD camera	6	90
LIDAR	1	20
RAD750	3	75
Interface Box	1	25
Mass Memory	1	50
S-Band LPT	2	100
Ka-Band	2	94
Display	3	75
Pointing Device	1	100
Optical Encoders	1	4
Buttons	1	10
Hubs	4	40
Interior Supplimental Lighting	4	60
Ambient Lighting	2	80
Exterior Lighting	4	200
Motors	4	821
Compressor	1	1300
Turning Linear Actuators	4	38.4
Total Power (W)		3240.4
Time of Transfer (days)		8.00
TOTAL ENERGY (Whr)		622156.8

6.3.2.3 PEM Fuel Cells

The PEM fuel cells with cryogenic reactants of liquid hydrogen (LH_2) and liquid oxygen (LOX) were chosen to suppy power throughout the lunar mission (13.2 kW at 300 A and 48 V, though the voltage will be limited to 28 V for most rover systems). This allows for potable water production as the reactants are used, which adds to the water supply available to the crew. One example of such a fuel cell is the Mark 9 SSL by Ballard[39]. This PEM system is shown in Figure 6.3, and will be adapted so that the reactants of gaseous hydrogen and oxygen from the air can be replaced by cryogenic LH_2 and LOX. A system efficiency of 60% for the fuel cells is used in this case. PEM fuel cells were also selected for adaptation because of their low mass (13 kg each). Three fuel cells will be used to maintain tri-fold redundancy, since the functionality of the power system is critical to crew survival [34].

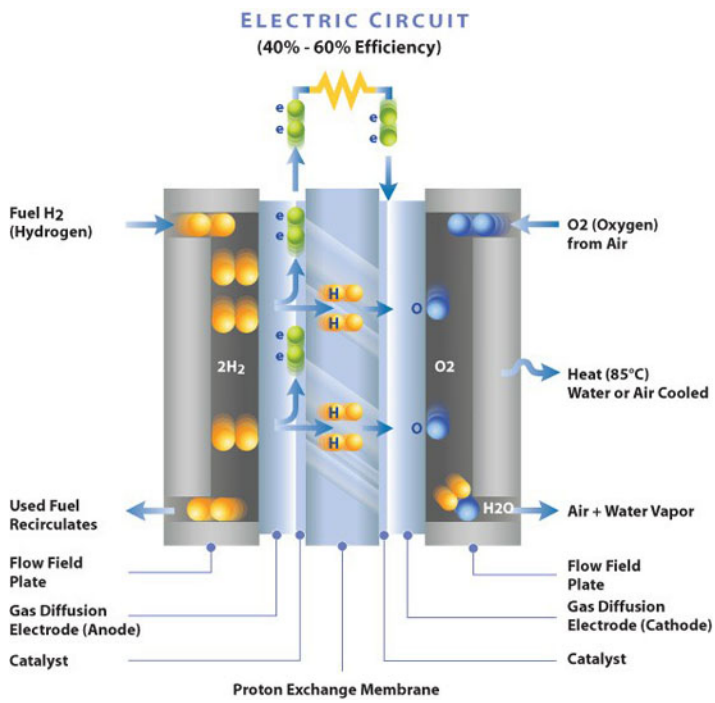

Figure 6.3: PEM Reaction Schematic

6.3.3 Fuel Cell Reactants

To determining the amount of LH_2 and LOX needed to react and provide power to the rover, the total energy required for each stage of the mission was determined by finding the average power per stage and providing that power for the duration of each stage.

6.3.3.1 Gibbs Free Energy

The mass of each reactant required to produce this energy is calculated using the Gibbs Free Energy equation (Equation 6.1). Where ΔG is the free energy of reaction, ΔH is the change in enthalpy of the system, T is the temperature in units Kelvin, ΔS is the entropy of the system, n is the number of moles of each product, and m is the number of moles of each reactant [8].

$$\Delta G = \Delta H - T\Delta S \tag{6.1}$$

$$\Delta H = \sum nH_{products} - \sum mH_{reactants} \tag{6.2}$$

$$\Delta S = \sum nS_{products} - \sum mS_{reactants} \tag{6.3}$$

This calculates the mass energy density of LH_2 and LOX in the reaction, based on the reaction chemistry, fuel cell efficiency, and reaction temperature given in Table 6.6. The working reaction of hydrogen and oxygen to form water is shown in Equation 6.4.

$$2H_2 + O_2 \rightarrow 2H_20 \tag{6.4}$$

Table 6.6: Fuel Cell Reaction Properties

	H_2	O_2	H_2O	$H_2 + \frac{1}{2}O_2 \rightarrow H_2O$
Moles	1	0.5	1	—
ΔH_f (kJ/mol)	0	0	-285.83	-285.83
ΔS (J/K)	130.68	205.14	69.91	-163.34
T (K)	—	—	—	290
ΔG (kJ/mol)	—	—	—	-238.46
ΔG at 60% Overall Efficiency (kJ/mol)	—	—	—	-171.69
Molar Mass (g/mol)	1.00794	15.9994	18.01528	—
Mass Energy Density (kJ/kg)	—	—	—	-9530.36

For an ideal chemical reaction in which all energy is conserved, $\Delta G = \Delta H_f$, but due to chemical inefficiencies through heat loss, taken into account by the subtraction of the $T\Delta S$ term, this chemical reaction is only about 83% efficient. The remaining inefficiency is a result of the 72% mechanical efficiency of the fuel cell components, resulting in an overall fuel cell reaction system efficiency of about 60%. From the mass energy density derived from by the Gibbs Free Energy calculation, the mass of each reactant is calculated for each stage based on the energy required. Over the course of the 24-day mission, a total of 29.69 kg of LH_2 and 236.12 kg of LOX are needed to supply all required power.

6.3.3.2 Boil-Off Considerations

Due to the warming from the sun, boil-off effects on the cryogenic reactants will cause a certain percentage of the reactants to vaporize and become unusable. As such, a certain percentage of extra reactants must be added to the system along with Multi-Layer Insulation (MLI) covering the reactant tanks to decrease the absorption of energy from the sunlight. In addition, the sizing of the reactant tanks affects the boil-off. As tank size decreases, boil-off decreases due to less surface area of the reactant exposed as the reactants are used.

Optimization of the mass of reactants, percentage of extra reactants included, size of reactant tanks, layers of MLI, and total mass of the filled and insulated tanks is deduced from the graphs in Figures 6.4 and 6.5. One of the most important variables driving the selection of the tank sizes is maintaining a low overall mass of the system, due to mass restrictions of the rover. A summary of the results from this analysis are enumerated in Table 6.7.

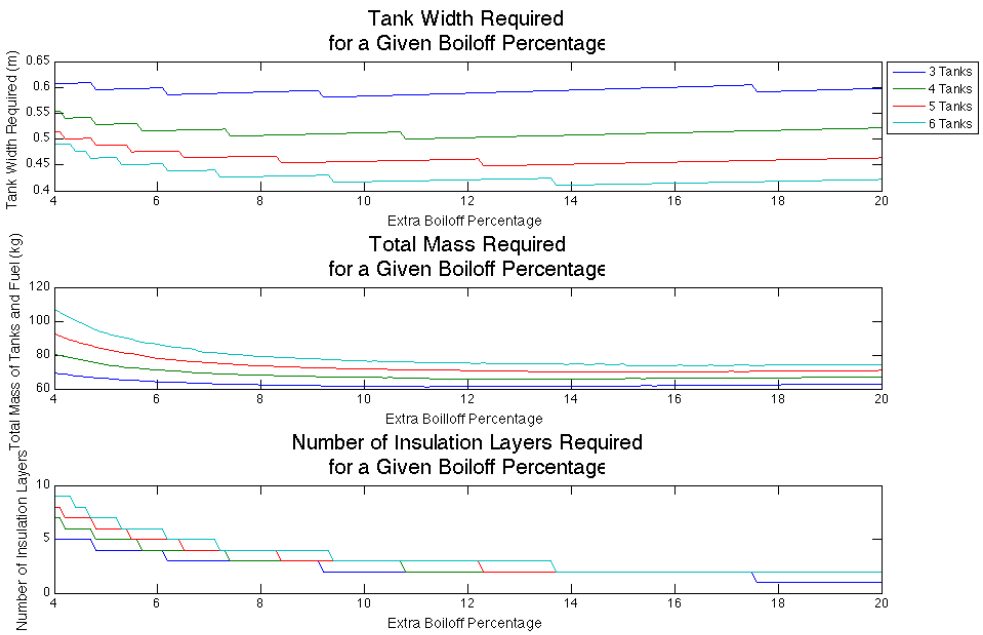

Figure 6.4: Optimization of LH_2

6.3.4 Reactant Tanks

Three types of reactant tanks were considered in selecting the tank materials: aluminum, aluminum-lined composite, and linerless composite. See Appendix A.7 for a trade study of reactant tank materials. Cylindrical carbon fiber composite tanks with hemispherical ends were chosen because

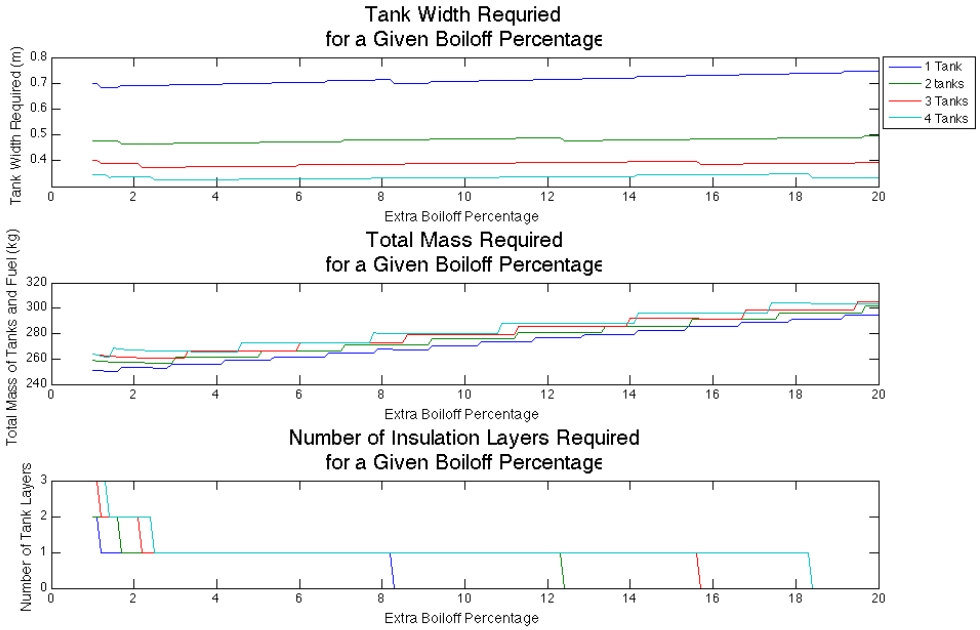

Figure 6.5: Optimization of LOX

Table 6.7: Reactant, Tank and Insulation Optimization due to Boil-off.

Reactant	LH_2	LOX
Number of Tanks	4	2
Length (m)	0.82	0.82
Diameter (m)	0.500	0.464
Number of Layers of MLI	2	1
Total Mass of Reactant (kg)	32.9	243.0
Extra Reactant Included	10.8%	2.9%
Total Mass per Insulated Tank (kg)	8.4	6.9
Total Mass (Reactant, MLI, Tanks) (kg)	66.52	256.7

they have been widely used to contain cryogenics. Carbon fiber composites are high in strength with low thickness and mass.

6.3.4.1 Specifications

The length of the tanks were constrained by their placement on the rover to 82 cm, while the diameter and thickness were selected to meet constraints set by reactant volumes, boil-off and maximum stresses. The number of tanks was also constrained to a minimum of two tanks per reactant, such that an unforseen failure of one tank will not jeopardize the survival of the crew.

In providing the necessary mass (and volume) of reactants to account for both rover power and boil-off effects (32.9 kg LH_2 and 243.0 kg LOX) while maintaining the minimum number of tanks, 4 tanks of LH_2 with a diameter of 50.0 cm each and two tanks of LOX with a diameter of 46.4 cm each were selected. To prevent boil-off, each LH_2 tank is wrapped in two layers of MLI and carries 10.8% extra reactant, and each LOX tank is wrapped in one layer of MLI and carries 2.9% extra reactant. The percentages of extra reactants result from filling the tanks to prevent boil-off before the fuel cells are turned on.

The minimum thickness of the tanks is determined by the hoop stress of the tanks, since the hoop stress (Equation 6.5) of a thin-walled cylindrical pressure vessel is twice its longitudinal stress (Equation 6.6).

$$\sigma_h = \frac{P * r}{t} \tag{6.5}$$

$$\sigma_l = \frac{\sigma_h}{2} \tag{6.6}$$

Toray high performance graphite fiber is one example of a composite material that is frequently used in lightweight, high-strength pressure vessel applications [52]. Since the tensile strength of such a carbon fiber composite is 3,530 MPa (Toray T-300), the minimum tank thickness necessary is 0.171 mm. However, a thickness of 3.0 mm is being used because composite pressure vessels made of carbon fiber must be wound into layers, resulting in a minimum thickness possible to be manufactured to achieve such high a tensile strength. In this case, the maximum hoop stress that these tanks will see is 200.8 MPa (a factor of safety of 17.6) for cryogenics stored at 2.41 MPa. Given these dimensions and a composite density of 1.8 g/cm^3, the mass of each insulated LH_2 tank is 8.4 kg and each insulated LOX tank is 6.9 kg [24].

6.3.5 Tank Insulation

As previously mentioned, insulation of the cryogenic tanks is necessary to reduce boil-off rates by decreasing the absorptivity and increasing the emissivity of the tanks' surface areas. The tank size is

also important in the layering of insulation, since many thick layers of insulation essentially increase the size of a tank.

Perforated MLI was selected to insulate the cryogenic tanks because it is space-rated (TRL 9), has a low apparent thermal conductivity of 0.09 mW/m-K, and is lightweight (0.72 kg/m^2) and thin for the amount of insulation necessary (7 mm thick per 30-sheet layer). As mentioned above, each LH_2 tank is wrapped in two layers of MLI and each LOX tank is wrapped in one layer of MLI. Again, Figures 6.4 and 6.5 show the tradeoff between the number of MLI layers and the tank diameter. The MLI ensures that the heat absorbed by the tanks will only boil off the extra fuel.

6.4 Circuitry and Wiring (Ali-Reza Shishineh)

6.4.1 Introduction

The power system for TURTLE was designed around four main subsystems: Avionics, Crew Systems, Drive System and the Thermal System. The power system had to accommodate all of the components for each subsystem on a power draw and voltage basis. The circuit design for the rover had to supply sufficient current and voltage to every component. The circuit had to be able to sustain maximum driving voltage during various parts of the mission. The large voltage needed for the drive motors creates a problem in circuitry design. This circuit had to be protected properly in the case of a short. The circuit design also included an internal/external device that had to link all electrical components of the rover. The mission requires the main circuit to have two-fault protection which resulted in about 20 independent circuits.

6.4.2 Power System Design

The power draw for the rover breaks down has been shown in Table 6.8. The rows represent the overall usage of power by each individual component within the lunar design rover. Since the lunar rover will be using three Ballard Mark 9 SSL fuel cells and other various batteries, the current will be strictly DC. In the case of a crew critical systems failure, the last fuel cell will be used to return the astronauts back to base. The power draw for the drive system is increased by a factor of 6 when comparing the lunar to field rover. The buttons are human interface devices and will be continually monitored to ensure protection from electrical shock. There are two suitport actuators on each suit which means that each set can be controlled by an individual circuit. The optical encoders are used for the wheels to convert the actual motion of the wheels into a series of pulses that will be provided with the proper voltage and current per wheel. The motors can use up to a maximum of 6190W during peak driving conditions. While the compressor has a maximum current of 3135W. During standby, the rover will be using minimal systems to conserve power. The active components during standby have been show in Table 6.4.

Table 6.8: Power Draw

Component	#	Avg Power (W)	Avg Power/per	Voltage (V)	Current (A)
Star Tracker	1	20	20	28	0.714
IMU	1	38	38	28	1.357
Radar	2	20	10	28	0.357
HD camera	6	90	15	28	0.5357
LIDAR	2	40	20	28	0.714
RAD750	3	75	25	28	0.8929
Interface Box	1	25	25	28	0.8929
Mass Memory	1	50	50	28	1.7857
S-Band LPT	2	100	50	28	1.7857
Ka-Band	2	94	47	28	1.6786
Display	3	75	25	28	0.8929
Pointing Device	1	100	100	28	3.5714
Cabin Air Control	1	60	60	28	2.1429
Suitport Actuation	4	112	28	14	2.00
Driving Platform #1	6	60	10	5	2.00
Driving Platform #2	4	144	36	12	3.00
Interior Supplemental Lighting	4	60	15	28	0.5357
Ambient Lighting	2	80	40	28	1.7286
Exterior Lighting	4	200	50	28	1.7857
Optical Encoders	1	4	4	28	0.1429
Buttons	1	10	10	28	0.3571
Motors	4	860	215	16.76	12.8282
Compressor	1	3135	3135	28	111.9643
Turning Linear Actuators	4	38.4	9.6	28	0.3429
Hubs	4	40	10	28	0.3571

The circuit design layout is shown in Figure 6.6. The fuel cells are monitored and for the possible outpost mission will be refueled as necessary during an outpost mission. The current goes to a distribution and control center where the voltage and current are divided appropriately. A voltage divider cuts the voltage and distributes it to the appropriate subsystem. The ammeter and voltmeter measure the current and voltage, respectively. The astronauts will have digital measurement records to monitor the current and voltage flow.

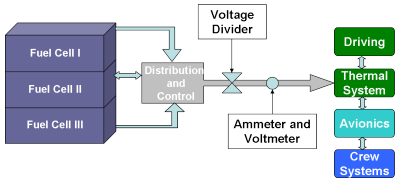

Figure 6.6: Power Flow Chart

The drive system breaks down into four motors. Each motor will nominally use 17 V and 13 A. At maximum speed, each motor can use up to 118 V. When considering the motor system, a pulse-width modulator (PWM) will be implemented. The pulse-width modulator will provide the motors with a constant supply voltage and a varied current draw. The thermal system will use 42 V and 12 A during operation. The avionics system breaks down into 13 components: Sensors, two star trackers, one inertial measurement unit (IMU), six cameras, two light detection and ranging devices (LIDAR), three computers, three S-band low power transceivers (LPT), two S-band amps, a landing radar, two Ka-band radios, two Ka-band amps, three displays and one mass MM. All of the avionics components require 28 V and varying current needs between 0.2-9 A. The external components, (six cameras, S-band LPTs, landing radar, two Ka-band radios) will be internally linked by a K-Series LEMO manufactured connector. The crew systems team required about 94 V and 12 A to power the Suitport actuators.

Crew Systems and Avionics distribution is shown in Figure 6.7.

6.4.3 Mock-up

Crew systems will need power for their mock-up suitport. The mock-up will be using strictly AC. The only components that do not run on 28 volts are the suitport actuators, both driving platforms and the motors. These components will be provided voltage through a voltage multiplier and/or proper voltage divider.

6.4.4 Circuit Protection

The UL 489 (standard) circuit breaker was selected to protect all components. The UL 489 provides branch circuit protection (overcurrent). This breaker also protects the circuit's wiring from fire

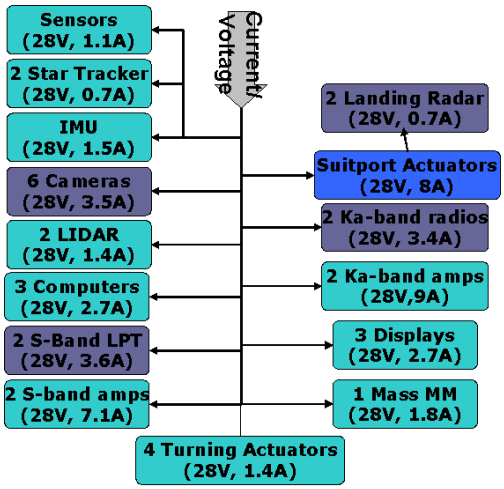

Figure 6.7: CrewSys/Avionics Breakdown

and producing dangerous electrical shocks. The problem with the UL 489 is that it is not current limiting. To current limit the circuit, a supplementary protector was added. The UL 1077 (standard) supplementary protector was used to limit the let through current in the event of a short. When applying a fast current limiting device, the let-through current can be reduced by a factor of seven. This current limiter protects all components in the event of a major short-circuit fault.

To provide two-fault protection, multiple breakers and protectors will be implemented. The astronauts will have control over all breaker switches inside and outside the rover.

6.4.5 External Power Linking

The K-series LEMO external/internal linking device was selected because it has been space tested. The K-series LEMO will be used to link all internal devices to external components and vice versa. The device has full EMC shielding and an airtight connection to maintain pressure and prevent leaks.

6.4.6 Circuit Wiring

Wiring failures can occur due to insulation failure, overcurrent or overvoltage. Through proper overall system wiring, the general power system's reliability and system safety can be improved significantly. In the case of space system design, a simple wiring fault can cause the failure of an entire mission and can put lives at stake. Failures can occur due to inadequate technology, system design, and improper maintenance procedures. Inadequate technology can be described as a short circuit that was caused by poor connection design which was not properly identified by the circuit breaker. In response to a faulty circuit breaker in the previous mission, STS-28, Johnson Space

Center studied various circuit breakers and fuses used in space. Properly tested Remote Power Controllers are a good option to solve this problem.

System design failures have also occurred on the STS-28 mission. The fault here is that the wiring design is the cause of wiring system failure in the first place. A specific example would be the oxygen tank wiring failure on Apollo 13. This failure occurred because the wiring degraded during various ground tests. This failure ultimately caused the oxygen tank to explode and possibly cause a mission critical failure. Although there is no specific way to fix this problem, it proves that there are wiring system failures that can be caused by testing of various systems.

The last group of failures can be caused by improper maintenance procedures. Maintenance during ground testing and during the mission is critical to the survival of any circuit wiring system. Proper circuit breaking and monitoring is an effective way to prevent wiring system failure. Methods for decreasing the number of circuit wiring failures and improving detection include: solid state power controllers, dual-element time-delay fuses, fiber optic current sensor and "intelligent" detection. Solid state power controllers (SSPC) are essentially circuit breakers that trip instantaneously during overcurrent. The SSPC selected for the rover system is the "SSPC535" which is programmable and provides instant or short circuit protection, an on/off reset controller, load current monitor and a built in self test system. The SSPC535's environmental data can be seen in Table 6.9.

Table 6.9: Environmental Data

Test	Limits
Operational Temperature Range	-40C to 85C
Storage Temperature Range	-55C to 122C
Vibration	20g, 20 - 2000Hz
Acceleration	1,000g
Shock	1,000g, 0.5ms
MTBF	150,000 hrs

A safe electrical system for the rover is composed of a well thought out power system design and proper circuit/wiring protection. Proper power draw analysis was performed to implement the most effective circuit protection method. The wiring for this system had to be analyzed further to ensure protection of the overall design.

Chapter 7

Thermal

7.1 Equilibrium Temperature (Aleksander Nacev and Stephanie Petillo)

Thermal conditions of the rover are governed solely by radiative heat flux. Since there is negligible atmosphere on the lunar surface as well as during the transit to the moon, conduction and convection heat flux are ignored. The sources of radiative heat are the sun itself and the lunar surface during the lunar day, reflecting the heat from the sun. Since the rover will have the fuel cells active throughout the entire duration of the mission, the thermal control system will also be active. At low power draws, the thermal control system is capable of supplying heat to the rover in the situation of a partially sun-shaded orientation. All subsequent thermal conditions were done as a worst case scenario when the sun is considered to be at high noon and the rover is at the equatorial plane of the moon. In addition the emissivity of the moon (shown in Equation 7.3) is considered to be a value of 1 for a high end estimate.

The prime variable to consider when regulating the temperature of the rover is the thermal equilibrium temperature. Radiative thermal equilibrium is governed by Equation 7.1.

$$T_{eq} = \left(\frac{q_{sun} + P_{int} + q_{moon}}{\varepsilon \sigma_b A_{rad}} + T_{space}^4 \right)^{\frac{1}{4}} \tag{7.1}$$

$$q_{sun} = I_s A_s \alpha \tag{7.2}$$

$$q_{moon} = \varepsilon_M \sigma_b A_s \alpha T_M^4 \tag{7.3}$$

T_{eq} Equilibrium temperature of the rover

q_{sun} Heat flux from the sun

P_{int}	Internal power to be dissipated
q_{moon}	Heat flux from the moon
T_{space}	Ambient temperature of space
ε	Emissivity
σ_b	Boltzmann's constant
A_{rad}	Radiation area of the rover
I_s	Solar intensity
A_s	Planar area seen by incoming radiation
α	Absorptivity of rover
ε_M	Emissivity of the moon
T_M	Temperature of the moon

The worst case scenario for the current mission profile was considered: the case of a lunar day at the equator incorporating the radiative heating from the lunar soil and sun. This scenario, assumed over the entire mission duration would allow for the high end estimate of all thermal conditions experienced by the rover. Any conditions the rover experiences with less external heat flux will exert less strain on the system and requires less work from the compressor and other control components. Therefore, by considering the high end estimates of energy use, the system was designed to meet the worst-case scenario energy requirements for all time.

For analysis of the thermal equilibrium, two options were considered: passive and active thermal control. Ideally a completely passive thermal control system would be desirable for maintaining the comfortable cabin conditions for all crew and active components in the rover. Passive thermal control would ensure simplicity and save on mass and space requirements. Unfortunately with the high end power output of the rover, the temperature of the rover would well exceed operating conditions of the fuel cells, avionics and control components and life support ranges. The high end power output would create a cabin temperature of 330K if using a completely passive thermal control system. This is roughly 56 degrees Celsius and way above the desired life support range of a human. Therefore, an active thermal control system was developed.

7.1.1 Passive Control Methods

To augment the active control system, however, some passive components were also implemented. Chiefly among them is the Aeroglaze A276 White Paint. This specific white paint is applied to

the exterior of all rover surfaces to the extent that is operationally possible. The benefit of this paint is the high emissivity, and low absorptivity. This ratio directly affects the thermal equilibrium temperature from radiative heating. As seen in Equation 7.1, 7.2 and 7.3 the $\frac{\alpha}{\varepsilon}$ ratio can reduce the effective heat flux from any external radiative component by lowering how much heat is absorbed.

Another passive thermal regulation technique is the MLI insulation on the cryogenic fuel tanks. The cryogenic temperatures required are too low to actively control with a cooling system locally on the rover. Therefore passive techniques must be employed to insulate the fuels from ambient radiative heat flux. A detailed analysis of this technique is described in the section detailing the design of the fuel tanks.

7.2 Active Thermal Control (Aleksander Nacev and Stephanie Petillo)

7.2.0.1 Heat Loads

As mentioned earlier, passive regulation techniques are incapable of balancing the thermal environment of the rover at acceptable temperature ranges. Therefore an active system was developed for handling the thermal loads present in the rover. The thermal loads of the rover come from the external heating of the sun and moon, and the internal heating elements from the fuel cells, avionics, crew members and interior lighting. Table 7.1 shows the breakdown of all thermal load components inside the rover during driving conditions. This heating load has to be removed from the internal environment by the active system. In addition, since it was assumed that the fuel cells would be 60% efficient, the other 40% of energy from the reactants is released as heat and must be removed from the system. All other components, lights, computers, etc. are considered to release all power supplied to them as heat. This is a very conservative high end estimate of the heat input present in the cabin of the rover because the power supplied to all internal components is used for doing work but the efficiency of all components is not known. Therefore to ensure thermal system capability, high end estimates are assumed.

7.2.0.2 Coolant Choice

To expel this amount of heat from the rover, a gas exchange radiation system was designed as seen in Figure 7.1. A helium gas exchange system was chosen for its simplicity and robustness to wide temperature and energy load variations. The system is a one phase gas exchange system, allowing for large variations in the heat loads due to the fact that the helium gas will not change phase throughout the thermal control loop. Helium was used for its lightness, high specific heat compared to other noble gases and its inert properties. However, it was not the only gas considered. Table 7.2 shows the possible gases that work for the system. In addition Hydrogen was analyzed and it contained superior thermal control properties. Unfortunately the combustibility of Hydrogen made the gas an incompatible choice for a working gas. As a previous iteration for the thermal

Table 7.1: Heat Loads Present in the Rover

Component	Quantity	Total Heat Produced (W)
IMU	1	30
RAD 750 Computer	3	75
Sensor Interfaces	1	25
Mass Memory	1	50
Buttons	1	10
Hubs	4	40
Interior Supplemental Lighting	4	60
Ambient Lighting	2	80
Displays	3	75
Crew	2	300
Cabin Air Control	1	60
Total Heat Produced		**813**

exchange process, R12 and other freon gasses were considered for heat exchange. However, due to the phase change requirement to obtain the optimal properties of these coolants, the system lost its robustness. It was very difficult to design a thermal control system which would be able to handle the large variation in internal power dissipation demands. In order to develop this multiphase system, more variables, such as the pressure ratio would have to have been variable. This system was too complex with more varying parts and hence the single gas exchange system was chosen. The main components of the single phase system include the radiator to expel the heat, the compressor to compress the gas flowing to the radiator, and the internal cooling coils running throughout the rover and fuel cells.

Table 7.2: Coolant Options Considered

Properties	Helium	Butane	R-12	Hydrogen
$\rho \left[\frac{kg}{m^3}\right]$	0.1615	2.52	5.11	0.085
$c_p \left[\frac{kJ}{molK}\right]$	0.02	0.096	0.074	0.029
γ	1.664	1.091	1.1388	1.384
$\mu \left[Pa \cdot s\right]$	0.0000186	0.0000068	0.0000116	0.0000086
$k \left[\frac{W}{mK}\right]$	0.1426	0.03383	0.00946	0.1805

7.2.0.3 Overview

The system works by absorbing heat through the inner coils with cold uncompressed Helium gas (stage T_4 to T_1) and arriving at a cabin temperature of 295K (stage T_1). Then the compressor compresses the gas to a set pressure ratio of 2.5 which creates a high temperature of 426 K at

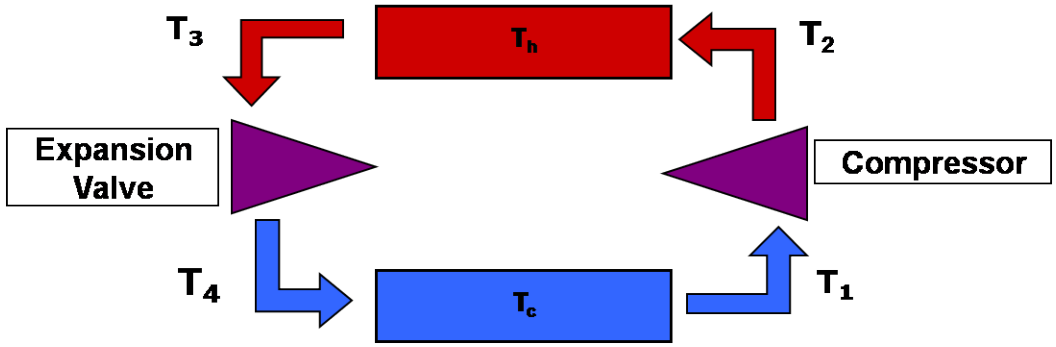

Figure 7.1: Overview of Helium Gas Exchange Cycle

stage T_2. For this specific gas compression system the two pressures were chosen to be 2.5 atm and 1 atm for simplicity, but the ratio of the two pressures is the more important factor. This high temperature compressed gas then flows through the radiator to release its heat to the environment through radiation. The gas then reaches the radiative equilibrium temperature at stage T_3. The colder gas then flows through an expansion valve where it decreases in pressure and temperature shown by stage T_4 again. Important to note on this heat exchanger cycle is that T_1 is fixed at the desired cabin temperature. Also T_3 is fixed and is dependent solely on the equilibrium temperature which is a function of the heat that needs to be dissipated.

Table 7.3: Table of Typical Thermal Control Quantities

Variable	Standby Power	Average Power	Max Power
T_1	295 K	295 K	295 K
T_2	426 K	426 K	426 K
T_3	285 K	345 K	415 K
T_4	211 K	240 K	288 K
Q_L	0.482 kW	2.97 kW	9.4 kW
Q_H	0.652 kW	4.27 kW	13.1 kW
$\dot{m}$	0.001 kg/s	0.01 kg/s	0.25 kg/s
W	0.17 kW	1.3 kW	3.7 kW

7.2.1 Radiator

The radiator was designed to maximize radiative area, be lightweight and remove the heat from the incoming pressurized gas. For this reason an aluminum radiator was designed in the shape of equilateral right triangles to maximize the amount of area an almost flat plate can radiate. Figure 7.2 shows the CAD model of the radiator. For simplicity, the radiator is assumed to only radiate outwards through the top away from the lunar surface.

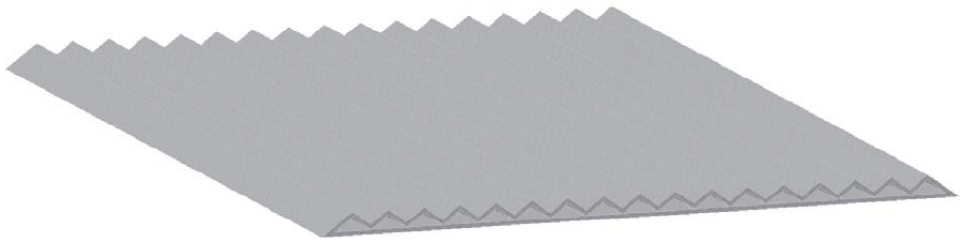

Figure 7.2: CAD Model of the Radiator Design

Figure 7.3 shows the relative dimensions of the radiator chosen. The triangles can be almost any height when constrained only by the total required radiation area. However, the triangle height was chosen by observing the heat transfer properties of the radiator. The heat transfer film coefficient was determined for the radiator triangle cross sections and then the total heat transfer coefficient was determined for the system using the thermal properties of the radiator (aluminum material) and the heat transfer cycle. A code was developed to determine how the thickness of the aluminum radiator impacted the thermal heat transfer properties and consequently the triangle heights. Equations 7.4, 7.5, 7.6, 7.7, 7.8, 7.9 and 7.10 show how the film transfer coefficients and the total heat transfer coefficients for the fluid flow rate can be determined from the geometry of the radiator and the fluid flow parameters.

$$Q = h_{tot} A_{contact} \Delta T \tag{7.4}$$

$$h_{tot} = \frac{1}{\frac{1}{h_{film}} + \frac{t}{k_{aluminum}}} \tag{7.5}$$

$$h_{film} = Nu \frac{k_{gas}}{D_H} \tag{7.6}$$

$$Re = \frac{\dot{m}\, D_H}{\mu A_x} \tag{7.7}$$

$$Pr = \frac{c_{p_{gas}} \mu}{k_{gas}} \tag{7.8}$$

$$Nu = 0.023 Re^{0.8} Pr^{0.3} \tag{7.9}$$

$$D_H = \frac{4A_x}{U} = \sqrt{2} \tag{7.10}$$

A_x Cross sectional area of the triangular radiator tubes

$A_{contact}$	Surface area of contact for heating
D_H	Hydraulic diameter - for this specific cross sectional geometry it is constrained to $\sqrt{2}$
Re	Reynold's number of gas flow
μ	Viscosity of gas
Pr	Prendalt number of gas flow
$c_{p_{gas}}$	Specific heat of gas
k_{gas}	Thermal conductivity of gas
Nu	Nusselt number of gas - in this formula the Prendalt number is raised to the 0.3 power for the cooling effect
h_{film}	Film transfer coefficient
U	Wetted perimeter of the cross section

Figure 7.4 shows the necessary height of the radiator triangular cross sections given a specific radiation area, temperature difference, and mass flow rate while varying the radiator thickness. The graph shows how the required height of the radiator is not impacted much by the thickness of the radiator walls. Therefore, the triangle height was chosen to minimize the mass needed, while still taking into account the manufacturing limitations. A thickness of roughly 2 mm was chosen with a total mass of 40 kg which forces the height of the triangles to be 3.7 cm.

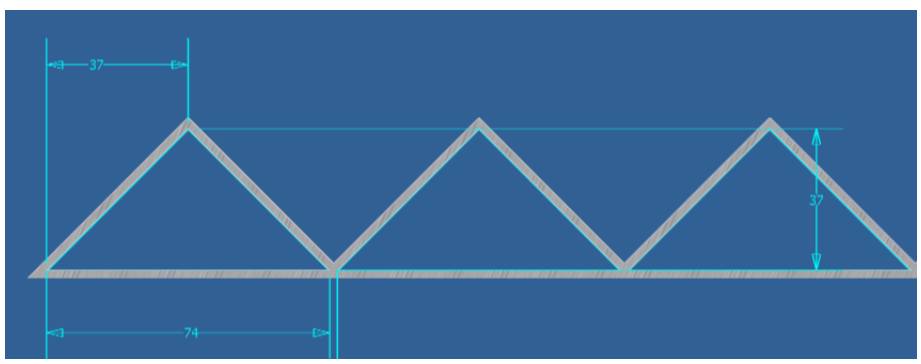

Figure 7.3: Radiator Dimensions (mm)

The surface area of the radiator was chosen so that the entire thermal control system would be able to radiate a sufficient amount of heat effectively. The more surface area there is to radiate heat, the more efficient the thermal system becomes. However, there is a trade-off between mass and space requirements. The radiator is constrained by the amount of space the top section of the

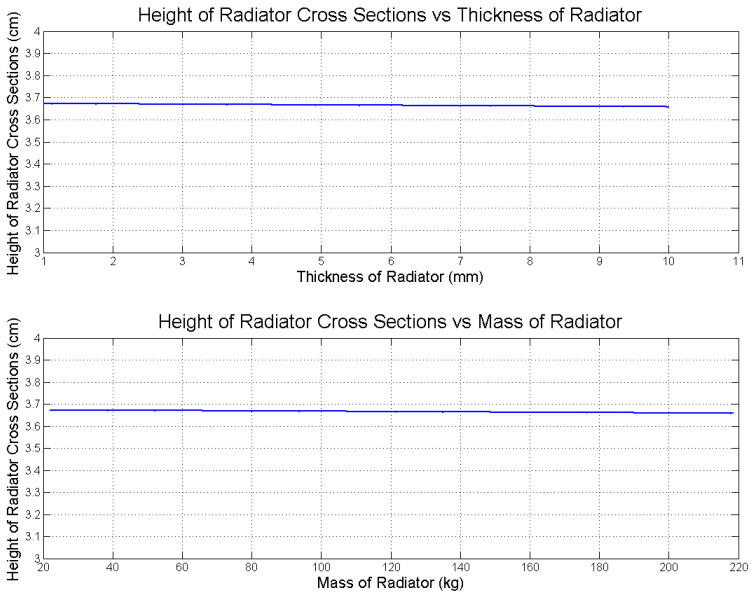

Figure 7.4: Radiator Triangle Height Determination

rover can hold. One requirement is to ensure that there is enough distance between the radiator and the communication devices located on the top of the rover. The communication devices lose efficiency at higher temperatures and are designed for a colder environment, hence the farthest possible distance from the radiators is optimal. Therefore, the radiator has to be small enough not to encompass the entire top half of the rover. In addition the larger the radiator is the more mass it will contain. The structural and thermal groups worked together to determine an acceptable upper bounds on the radiator size. Currently the size is designed to be 8 meters squared radiative area measuring a 2-dimensional planar surface dimension of 2 m $\times$ 2.86 m. This radiator design is divided in two width-wise halves, which are placed near the top on the sides of the rover.

Using this radiation area and the heat loads present in the rover, the thermal equilibrium temperature of the radiator can be determined. It is important to note that this initial calculation is simply a beginning estimate of the equilibrium temperature present on the exterior side of the radiator. The active thermal system contains a compressor which will in turn add its own heat needed to be expelled through the radiator. The nonlinear iterative technique for compensating for this phenomena is described in Section 7.2.2.

7.2.2 Compressor

7.2.2.1 Overview

The compressor is the main element in the thermal control system. It compresses the incoming heated helium to a higher pressure and temperature. Since the helium is at a higher temperature, it is able then to radiate its heat to the surrounding environment at a faster rate than it would otherwise. This allows for the interior side of the rover to be set at any specific temperature given the correct temperature setting of the helium gas used to transport the excess energy. The pressure ratio $\frac{P_2}{P_1}$was set in order to maximize the mass flow rate and the efficiency of the heat transfer system. The main energy loss in the gas exchange system comes from the compressor exerting work on the system to compress the incoming air to a higher pressure. This work requirement became a large energy loss in the system. Having the fluid at a higher pressure ratio allows for a smaller range in mass flow rates; however, the higher pressure also created a less efficient heat transfer system forcing more power to be used by the compressor and hence more fuel. Therefore the pressure ratio was determined to accommodate the following factors: realistic compression, realistic mass flow rates, and lowest possible power consumption.

$$T_2 = T_1 \left(\frac{P_2}{P_1}\right)^{\frac{\gamma-1}{\gamma}} \tag{7.11}$$

$$T_4 = T_3 \left(\frac{P_2}{P_1}\right)^{\frac{\gamma-1}{\gamma}} \tag{7.12}$$

$$\dot{Q}_L = q_L \dot{m} \tag{7.13}$$

$$\dot{Q}_H = \dot{m} c_{p_{fluid}} \left(T_2 - T_3\right) \tag{7.14}$$

$$W = Q_H - Q_L \tag{7.15}$$

γ	Ratio of specific heats
$\dot{Q}_L$	Amount of power absorbed by internal radiator
q_L	Amount of heat absorbed
$\dot{m}$	Mass flow rate of gas
$c_{p_{fluid}}$	Specific heat of gas
$\dot{Q}_H$	Amount of power expelled by external radiator

W Work done by compressor

7.2.2.2 Calculation of Thermal Variables

The solution of the complete thermal system began with the calculation of the thermal equilibrium temperature (T_3) shown by Equation 7.1 based upon the specific power needed to be expelled by the radiator . This was then combined with the cabin temperature (T_1) and the designated pressure ratio to calculate the remaining two temperatures, given by Equations 7.11 and 7.12. With all four temperatures solved for, the power absorbed by the system can be calculated from Equation 7.13. Then the power expelled from the system can be calculated from Equation 7.14. With the two heat flux variables, the work done by the compressor can be determined from Equation 7.15. This system has a cyclic, iterative process built into the calculation method. The thermal equilibrium temperature depends upon the work done by the compressor. To solve for the system variables, the solution method was iterated until the work done by the compressor and the value used for the compressor variables in the thermal equilibrium temperature equation were equal to each other. This process ensured an accurate depiction of the thermal system.

For a more detailed analysis of the system, Figures 7.6, 7.7 and 7.8 quantify the temperature ranges experienced in the thermal system for a given heat load that needs to be expelled. All temperatures experienced in the radiator are within acceptable ranges of the aluminum material that was chosen for radiator structure.

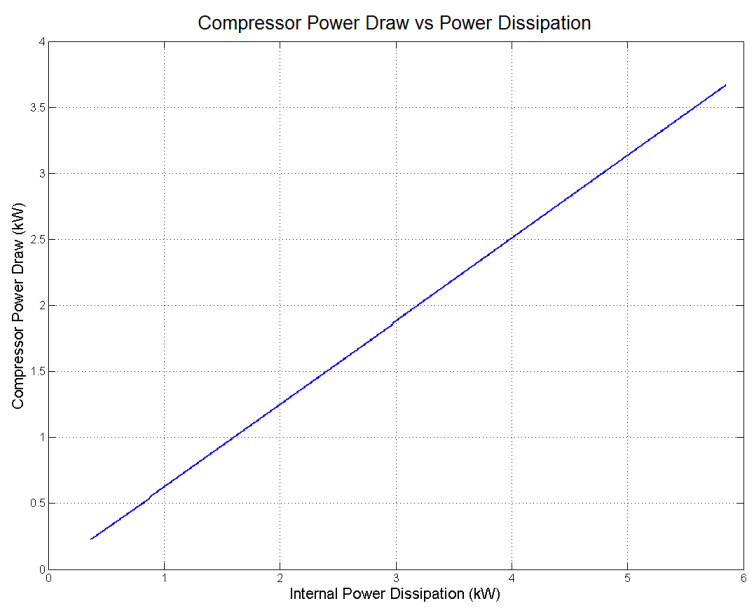

Figure 7.5: Compressor Power Draw versus Power Dissipation

7.2.2.3 Compressor Power Requirements

Figure 7.5 shows that the relationship between the internal power needed to be absorbed and the work the compressor inputs into the system is linear. This is an important realization when it comes to determining the energy requirement for the compressor. Since the relationship is linear, the average required compressor power equals to the average power dissipation of the components. The system should be able to handle the maximum compressor draw; however, an averaged power draw over the duration of the mission is sufficient to calculate the required energy.

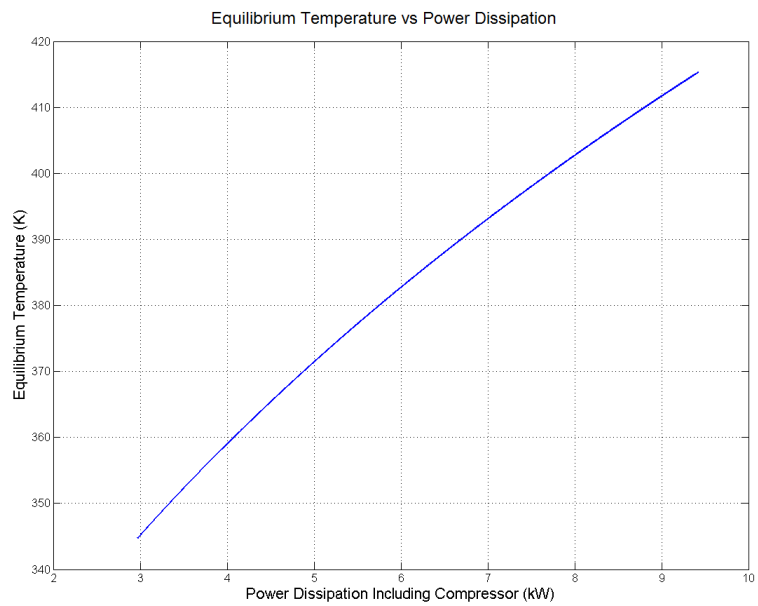

Figure 7.6: T_3 versus Power Dissipation

7.2.2.4 Mass Flow Rate Parameter

Figure 7.9 shows how the mass flow rate of the compressor can be varied to control the different power loads. The pressure ratio was chosen so that the mass flow rate stayed within realistic bounds. As can be seen on Figure 7.9, the mass flow rate has an asymptote at some internal power. Changing the pressure ratio changes the location of the assymptote and thus decides whether the mass flow rate required to expel the internal power increases to infinity. Increasing the pressure ratio decreases the change in the mass flow rate needed over the desired power range, but the efficiency of the thermal system decreases as well. Thus the mass flow rate was designed to stay within a lower asymptotic bound. The numeric limiting factor that the system was designed for was to keep the volumetric flow rate below 50 cubic feet per minute ($0.024\frac{m^3}{s}$). This volumetric flow rate was chosen

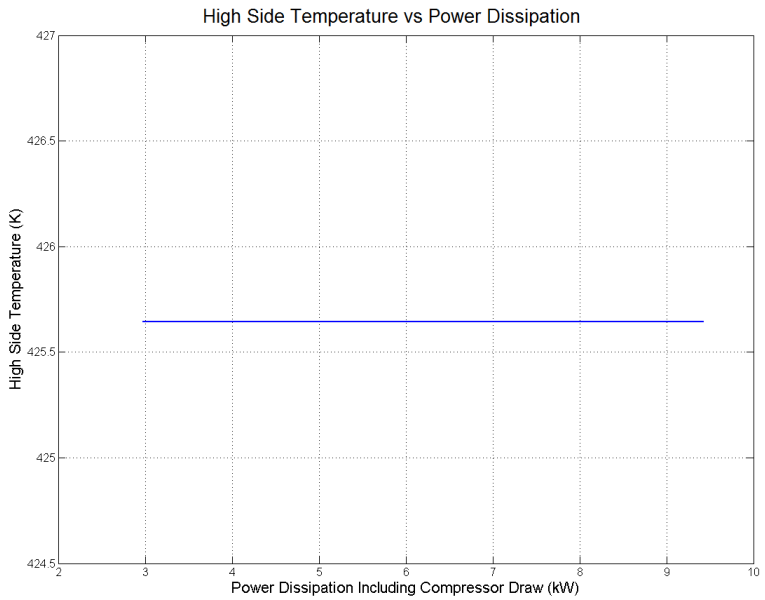

Figure 7.7: T_2 versus Power Dissipation

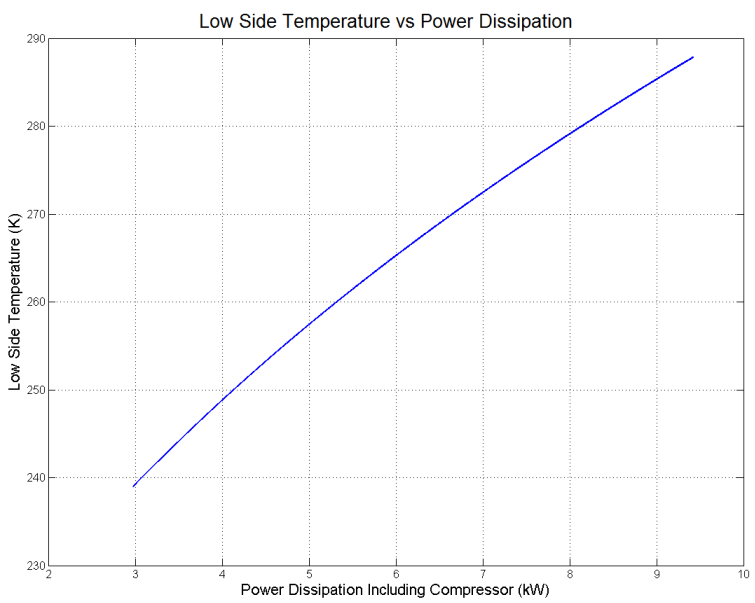

Figure 7.8: T_4 versus Power Dissipation

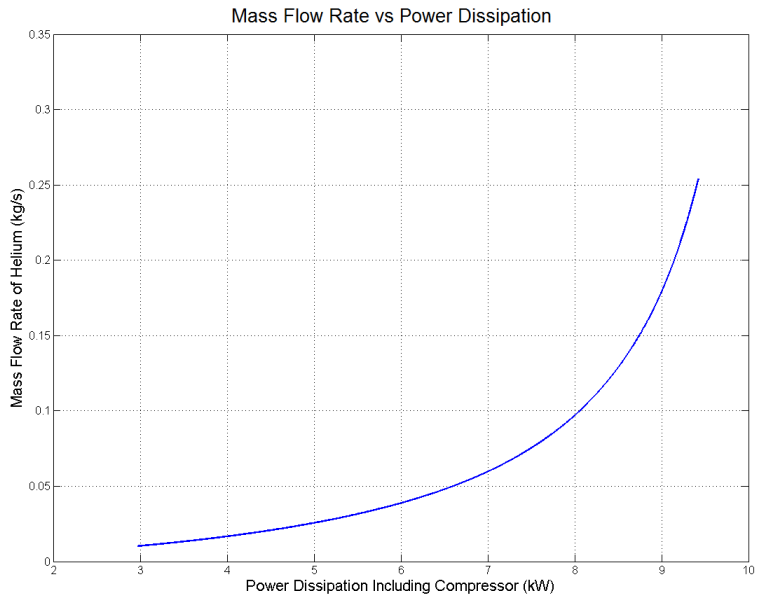

Figure 7.9: Mass Flow Rate ($\dot{m}$) versus Power Dissipation

based upon existing high end compressors and the mass flow rate ceiling was calculated using this volumetric flow rate parameter. Another key point to take away from the mass flow rate is that the rover internal cabin temperature can be managed and changed by varying the mass flow rate as well. This allows for a completely variable system able to handle many power loads and internal temperatures.

7.2.2.5 Efficiency

$$\beta = \frac{Q_L}{W} \tag{7.16}$$

The coefficient of performance for this thermal exchanger system can be calculated by using Equation 7.16. The coefficient of performance is constant over the range of internal power levels and maintains a constant 2.2. This compares to the idealized Carnot refridgeration cycle coefficient of performance as seen in Figure 7.10. One can see that the efficiency of the Carnot cycle decreases rapidly over the power range and yet the coefficient of performance for the engineered system is still beneath the ideal cycle.

7.2.3 Internal Heat Exchanger

The third component of the heat exchanger system is the internal heat exchanger. This section contains the helium gas at a low temperature and pressure. As the gas passes through it, the

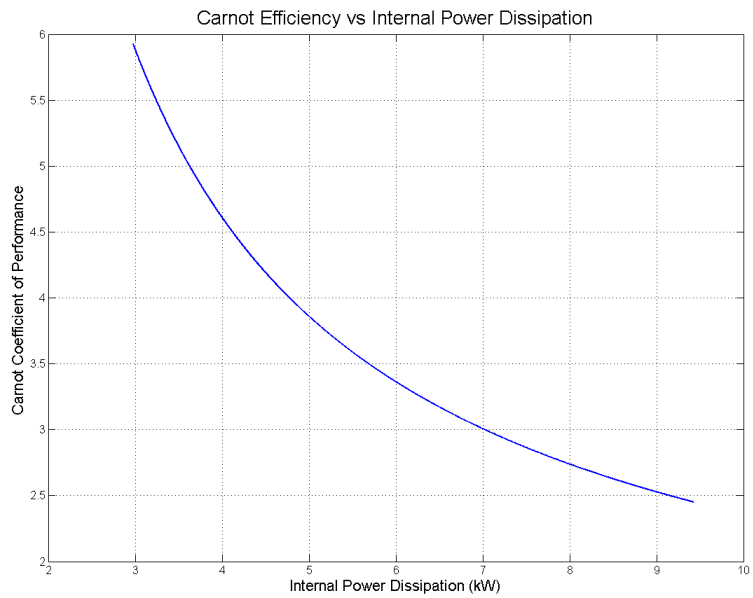

Figure 7.10: Carnot COP versus Internal Power Dissipation

exchanger absorbs the heat from the surrounding environment. The main section of the internal heat exchanger is designed to be copper pipes carrying helium gas such that the surrounding air would flow over the pipes causing the gas in the pipes to pick up heat. The helium gas would also flow through the fuel cells to remove the excess heat from them. Copper was the chosen material due to its high specific heat. The pipe geometry was chosen because the circular cross section works well in creating a high film transfer coefficient as well as reducing the mass required for the desired area. Different materials can be used for the internal heat exchanger but the following calculations are done using the material properties of copper.

$$A_x = \pi \left(\frac{d_i}{2}\right)^2 \tag{7.17}$$

$$Re = \frac{\dot{m}\, d_i}{\mu A_x} \tag{7.18}$$

$$Pr = \frac{c_{p_{gas}} \mu}{k_{gas}} \tag{7.19}$$

$$Nu = 0.023 Re^{0.8} Pr^{0.4} \tag{7.20}$$

$$h_{film} = Nu\frac{k_{gas}}{d_i} \tag{7.21}$$

A_x	Cross sectional area of the pipe
d_i	Inner diameter of pipe
Re	Reynold's number of gas flow
μ	Viscosity of gas
Pr	Prendalt number of gas flow
$c_{p_{gas}}$	Specific heat of gas
k_{gas}	Thermal conductivity of gas
Nu	Nusselt number of gas - in this equation the Prendalt number is raised to the 0.4 for the heating effect
h_{film}	Film transfer coefficient

The length of the copper tubing needed for the internal heat exchanger can be determined by first calculating the film transfer coefficient for the copper tubing (Equation 7.17, 7.18, 7.19, 7.20 and 7.21). This transfer coefficient is then used in Equation 7.22 to determine the total heat transfer coefficient for the gas absorbing energy through the copper pipes. The heat transfer coefficient can then be used in Equation 7.23 for determining the necessary length of copper tubing for the system. Figure 7.11 shows the relationship between the required length of tubing and the heat loads. To be able to handle the maximum heat load, an internal radiator with the maximum length of 21 m was chosen. This length can then be folded upon itself, with spacing so that incoming air can flow over the pipes and deposit the heat into the pipes.

$$h_{tot} = \frac{1}{\frac{1}{h_{film}} + \frac{d_i \log\left(\frac{d_o}{d_i}\right)}{2k_{copper}}} \tag{7.22}$$

$$L_{tubing} = \frac{Q_L}{h_{tot}\left(T_1 - T_4\right)\left(2\pi\frac{d_i}{2}\right)} \tag{7.23}$$

h_{tot}	Total heat transfer coefficient
d_o	Outer diameter of tubes
k_{copper}	Specific heat of copper tubes
L_{tubing}	Length of tubing necessary

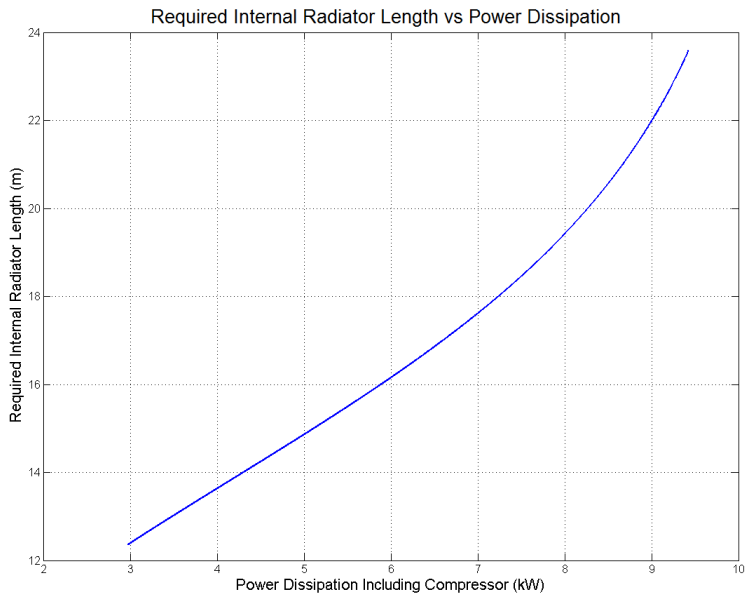

Figure 7.11: Required Internal Radiator Length versus Power Dissipation

Chapter 8

Interior

8.1 Rover Mock-up

8.1.1 Concept (Ryan Levin)

The idea of a pressurized rover that has to support a crew of two for three days, allow for multiple EVAs, and is as small as possible is a complex problem. This concept requires testing certain aspects of the proposed design to see if it is even feasible. The suitport is a concept that has never been used on a spacecraft before and it has to be tested with humans to determine the ease of this method for suit entry and exit. It is also necessary to show that two people can successfully coexist in a cramped environment for an extended period of time. Other scenarios to test include sleeping arrangements, driving station setup, and window placement.

8.1.2 Final Product

The rover mock-up structure is composed of various components. The physical enclosure is composed of a 1,350 gallon industrial water tank 71 in diameter by 88 in height. This closely models the lunar rover which is 72 in diameter by 96 in height. The tank is supported by five wooden ribs (See Appendix Mock-up Structure) instead of a chassis and wheels due to time and cost limitations. Inside the tank, there is a floor similar to the design for the lunar rover that it is at the correct height of eight inches from the bottom and spans 45 inches wide. There are six floor panels, which showed that more sections are required. A driving consol with three monitors sits in the rounded end of the tank. The driving station sits at 26 inches above the floor. This height allows for testing of monitor angles during a driving situation. The two chairs are at a height of 18 inches and each have backs that recline flat to allow for sleeping arrangements. The 18 inch height is exactly the height of the chairs in the lunar rover. One chair is set back from the other, which is on a track to move side to side. A bed is affixed to one side of the rover and a hammock to the other to test

which set-up works better for the astronauts involved. The hammock stows in a storage container while the bed folds up and stores against the wall.

Moving parts in the mock-up are the suitport and external driving platform. The suitport container is constructed out of plywood and attached to a track actuator with supports for smooth motion. The external driving platform is able to support a seated astronaut and also folds flat to allow entry and exit from the suit. Additional non-functioning structures include the food and clothing storage containers, sink, LiOH containers, IMU, AED, fire extinguisher, and first aid kit.

Further details on the development and construction of this mock-up can be found in the appendices.

8.2 Mock-up Testing (Kanwarpal Singh Chandhok)

8.2.1 Purpose

The purpose of building the mock-up was to determine if the interior cabin design for the lunar rover is effective. The cabin design involves variables that cannot be tested with equations. Therefore, testing with a rover mock-up will help determine the most efficient and effective design. To perform testing on humans, the Institutional Review Board (IRB) must approve all procedures and tests. However, the IRB committee was not able to approve the testing proposal in time for official documented testing. To effectively use the mock-up without IRB approval, team members documented their opinions of positioning in the rover on an informal basis. The IRB is now approved assuming minor modifications for safety concerns which opens up new testing opportunities for later classes.

8.2.2 Description

Several questions that needed to be answered through testing included:

- Driving configuration
- Location and angle of instrument panel and monitors
- Location and size of driving window
- Overall mobility inside the cabin
- Configuration of chairs to allow bed/hammock to be deployed
- Location of internal items such as fire extinguisher, first aid kit, toilet, sink, LiOH canisters, and other small support items

Each of the tests listed above are simple and self explanatory except for the driving configuration. While designing the interior layout for the lunar design, a question was raised about whether the

driver should be seated at the center or to the left in a side by side seating arrangement. Two different interior layout plans were constructed for testing purposes. The first configuration seats the driver and the passenger side by side at the instrument panel and allows for the left astronaut to drive the rover. The second configuration places the driver front and center at the instrument panel with the passenger behind the driver and offset to the right. Seven test subjects from the class volunteered to give their opinions on the two interior layout configurations. The testing facility was located in the high bay of the Space Systems Lab in the Neutral Buoyancy Research Facility building on campus.

There were two test divisions: left driving configuration and center driving configuration. Both tests focused on the following areas:

- Head room for the driver's and passenger's seat
- Leg room for the driver's and passenger's seat
- Window size: sight line analysis
- Instrument panel size, location and angle: Is it accessible and viewable from seating positions? If a warning beacon went off, would the astronaut be able to see it in their peripheral vision?
- Configuration from sitting to sleeping: Is it reasonable to sit in the chair, fold down the backrests, and then open the bed or hammock?
- Sleeping method: Would astronauts prefer a traditional style bed or a hammock in which to sleep?
- Mobility around cabin: Is it possible for two astronauts to move around the cabin and reach all of the storage bins and the suitports?

The majority of these tests were done with only one test subject inside the cabin; however, one test was conducted with two test subjects. The subjects were asked to perform a series of tasks that included reaching storage bins, moving about the cabin, changing from sitting to sleeping configurations, and preparing for emergency egress. The following sections will summarize the test results from each of the test subjects.

8.2.3 Testing the Left Driving Configuration

Figure 8.1 shows a picture of the left driving configuration. Subject 1 is siting in the passenger's seat with the toilet (blue) positioned behind his chair. There is a sink behind the driver's seat which is not shown in the picture. The markings on the front end cap show the two window sizes for each of the driving configurations. Below are the summaries from each of the test subjects.

Figure 8.1: A test subject in the left driving configuration.

8.2.3.1 Subject 5

- While seated in the driver's chair:
  - The head room is sufficient.
  - The leg room is sufficient.
  - The window size is acceptable, but the driver may need more visibility on the left side.
  - The control panel location and view angles are acceptable.
- While seated in the passenger's chair:
  - The subject's head bangs against the first-aid kit.
  - The leg room is sufficient.
- The passenger side bed configuration is acceptable.
- The hammock may be okay to use if secured properly, but an astronaut will likely need help getting into it to sleep.
- The center LiOH canister, next to light, is too close to the subject's head. Restraints are needed to secure the astronaut so he/she will not hit the canister during driving conditions.

8.2.3.2 Subject 3

- While seated in driver's chair:
  - The head room is sufficient.
  - The leg room is sufficient.
  - The subject's left knee hits the control panel supports.
  - The window size is acceptable, but may need to be raised a bit to see below. Possible alternatives are adjustable seat heights and ability to lean the chair forward.
  - The control panel is acceptable.
  - The control stick could be placed on an armrest for comfort.
- While seated in passenger's chair:
  - The head room is cramped due to the first aid kit.
  - The leg room is adequate.
- The bed is acceptable, but there may need to be improvisations for astronauts with restless leg syndrome because they might kick the control panel.

- The hammock is not advisable.
- The mobility is adequate.

8.2.3.3 Subject 6

- While seated in the driver's chair:
  - There is not enough leg room. The subject's left leg hits the control panel support.
  - The control panel height is acceptable.
- While seated in the passenger's chair: the head room is acceptable if not for the first-aid box.
- The bed is easy to deploy and retract.
- The hammock may be feasible.
- Mobility about the cabin is sufficient. The subject can reach around most of the cabin while seated.

8.2.3.4 Subject 2

- While seated in the driver's chair:
  - The head room is sufficient.
  - The leg room is cramped.
  - The window sizing and placement is acceptable.
  - The control panel is adequate.
- While seated in the passenger's chair:
  - The head room is sufficient.
  - The leg room is cramped.
- The bed is acceptable.
- Mobility about the cabin is adequate.

8.2.3.5 Subject 1

- While seated in the driver's chair:
  - The head room is sufficient.
  - The leg room is acceptable.
  - The window placements makes it difficult to see out of the left side.
  - The control panel is acceptable.
- While seated in the passenger's chair: the observations were similar to those while in the driver's seat.
- The bed is better choice for sleeping.
- Mobility is adequate, but the subject would like more foot room between seats.

8.2.3.6 Subject 4

- While seated in the driver's chair:
  - The head room is amazing.
  - The leg room is amazing.
  - The subject's left knee strikes against the control panel structure.
  - The window sizing and placement is sufficient.
  - The control panel is sufficient.
- Passenger side comfort is similar to the driver's seat comfort.
- It is very easy to switch to the sleeping position.
- The bed is a good sleeping choice and is comfortable.
- The hammock may be used if it function properly.
- Mobility is amazing. The subject did not have to get in any awkward positions to move about the cabin.

8.2.3.7 Subject 7

- While seated in the driver's chair:
  - The head room is acceptable.
  - The leg room is slightly cramped.
  - The window is sufficient but the subject would like tiny side windows.
  - The control panel is adequate.
- While seated in the passenger's chair: comfort is 5/10, head and leg room is similar to that of the driver's seat.
- The bed is better than the hammock because it might be hard to climb into it. The subject suggested possibly installing handrails.
- Mobility is acceptable.

8.2.3.8 Combined Test: Subjects 1 & 2

Subjects were asked to do a series of tasks which required them to move around inside the cabin. These tasks included changing from sleeping configuration to sitting to use the toilet, accessing different storage areas of the rover, and swapping astronaut seating positions. They reported that all of the tasks were relatively easy to accomplish and adequate room was present to complete the required tasks.

8.2.4 Testing the Center Driving Configuration

Figure 8.2 shows a picture of the center driving configuration. A test subject is siting in the driver's seat and the passenger's seat is offset to the right. The toilet is now located under the passenger chair. There are a set of computers in the space towards the left of the driver and the position of the sink is the same as in the left driving configuration. The markings on the end cap show the window border. Here, we will use the right markings on either side as the border for the driving window. Below are the summaries from each of the test subjects.

8.2.4.1 Subject 6

- While seated in the driver's chair:
  - Head room is very good.
  - Leg room is very good.
  - The control panel height is acceptable.

Figure 8.2: Test subject in the center driving configuration. Passenger chair is at the bottom right.

  - The window is adequate.

- While seated in the passenger's chair: head and leg room are adequate.
- The bed is sufficient.
- Mobility is insufficient. The astronaut needs to be thin and flexible to move around the cabin. The fire extinguisher is in the way and jumping over the sink is not practical. Accessibility of interior cabin items is not an easy task.

8.2.4.2 Subject 2

- While seated in the driver's chair:
  - Head room is acceptable.
  - Leg room is acceptable.
  - The window is adequate.
  - The control panel is sufficient but warning beacons are too far away.
- While seated in the passenger's chair: head room is adequate but leg space is awkward.
- The bed is acceptable.
- The sleep mode configuration is relatively easy to set up.
- Comfort is about 6/10 (better than layout 1).

8.2.4.3 Subject 1

- While seated in the driver's chair:
  - Head room is acceptable.
  - Leg room is acceptable for short term driving. The subject suggests there is a need to be able to stretch your legs for long duration driving.
  - It is difficult to see out of the left side of the window.
  - The control panel is acceptable.
- While seated in the passenger's chair: it is more comfortable than the driver's chair.
- The bed is better to sleep in than the hammock.
- Mobility is not very good. If driver's chair were moved to the left, it would allow more mobility room inside the rover.

8.2.4.4 Subject 4

- While seated in the driver's chair:
  - Head room is sufficient.
  - Leg room is sufficient.
  - Side buttons on the control pane are not optimal.
  - The window is adequate.
- While seated in the passenger's chair: the transition to the passenger seat is not good and is uncomfortable. The chairs crash into themselves.
- The bed is a good choice and is comfortable.
- the hammock may be used if works properly.
- Mobility is very bad. The subject had to get in awkward positions to move around from the passenger's seat.

8.2.4.5 Subject 7

- While seated in the driver's chair:
  - Head room is sufficient but there needs to be restraints to prevent from hitting the LiOH canisters on the top.
  - Leg room is sufficient.
  - The window is not good. The subject would like two small side windows and a smaller main window.
  - The control panel is sufficient. Touch screen monitors need care against accidental button pressing. The touch screen should be reconfigurable for left and right handed astronauts.
- While seated in the passenger's chair: Head room is not that good and leg room is cramped and not as comfortable (3/10).
- Sleep mode conversion was acceptable and not overly-complicated. The subject may accidentally kick monitors while sleeping.
- The bed is better than the hammock because it might be hard to climb into the hammock. The subject suggested possibly installing handrails.
- The cabin needs handles to move around to keep from losing balance and falling on the floor.
- Mobility can improve with grab handles on the side walls and the ceiling.

8.2.4.6 Combined Test: Subjects 3 & 5

They were asked to do a series of tasks which required them to move around inside the cabin. Including changing from sleeping configuration to sitting in order to use the toilet; access different storage areas of the rover; swapping astronaut seating positions. They reported that all of the tasks were not very easy to perform and mobility was nearly impossible. A solution to the problem can be if the driving seat can slide towards the left, which will introduce more room to walk around in. This configuration does seem a little bit more comfortable relative to Layout 1.

8.2.5 Conclusions from Testing

The conclusions drawn from this testing were not straight forward. The chosen layout from testing is the center driving layout with the option of a sliding driver seat. This was the most comfortable layout according to test subjects. The sliding chair will take some of the compactness away and will allow more empty space inside the cabin. This means that for the driver to get into his seat, he will have to sit in his seat and then slide over to the center of the cabin. When he needs to exit, the chair slides back to the left and over the computers. The computers originally stowed under the passenger seat will now be stacked against the end cap below the instrument panel. If the passenger needs to enter or exit his seat, he can move the driver's chair to the left to allow for easy entry and exit. The other points to note were that the fire extinguisher and first aid mock-ups need to be relocated. The computers at the bottom of the passenger's seat need a new location to be mounted. The suit ports are accessible and both astronauts can use the suit ports simultaneously. If the seat cannot slide, then the second choice is a side by side configuration. This is acceptable as it is very efficient in accomplishing internal tasks but is not a comfortable layout.

8.2.6 Mock-up Cost (Thomas Mariano)

The team was granted 6000 dollars to construct our rover mock-up. This money was generously funded by the Maryland Space Grant Consortium. The money was spent at various online and home supply stores to purchase the materials needed to fully construct the mock-up. The entire construction project cost 2845 dollars. This leaves us with a surplus of 3155 dollars. The remaining funds are to help with the transport of the mock-up to the RASC-AL competition in Cocoa Beach, Florida.

8.3 Cabin Interior

8.3.1 Interior Layout (Sara Fields)

To satisfy the Level 1 requirement of supporting a two-person crew for three day missions, the interior of the rover cabin must accomodate all possible crew members and all activites that they

Table 8.1: Mock-Up Cost Summary

Structures	
Preliminary Mock-Up	$50
Cabin	$500
Understructure	$355
Casters	$117
Crew Systems	
Bed	$76
Hammock	$45
Chair	$9
Water Tank	$180
Waste Water Tank	$10
Foam/Brackets	$33
Lighting	$53
External Driving Platform	
Driving Platform	$161
Miscellaneous	$30
Avionics	
Computer Supplies	$391
Monitors	$180
Suitport	
Suitport Actuator	$267
Suit	$60
Miscellaneous	
Paint Supplies	$62
Hardware	$93
Final Details	$163
Total Cost	$2845
Remaining	$3155

will be expected to perform. The rover must support crew members ranging from a 95th percentile male to a 5th percentile female and have space for activities including driving, eating, sleeping, and ingress/egress. The measurement data for the 95th percentile male and 5th percentile female comes from NASA STD-3000, Reference [82]. The physical configuration of the rover interior has been designed for optimally efficient use of the limited available space and crew comfort.

The process of identifying the optimal configuration began by considering the designs presented during the Fall 2007 Concept Design Review, as well as several additional ideas developed afterward. There were a few key layout choices where those designs diverged. Sleeping arrangements included hammocks, chairs that recline into beds, and independent cot-style beds. Passenger chair locations varied from next to the driver with a center aisle, next to the driver with aisles along each side wall, behind the driver and to the side, and directly behind the driver. Ingress/egress options included airlocks and suitports located at the sides or rear of the rover. Early in the design process, a few of these options were eliminated.

- The option of chairs that recline into beds was eliminated because of the need to minimize the size of the pressure shell. The width of a simple chair is dictated by the maximum hip breadth of its possible occupants (42.3 cm for the 95thpercentile male). The width of a bed should be greater than the maximum arm breadth (61.5 cm). By limiting the width of the chairs, the required width of the floor decreases, which directly affects the size of the rover.

- Placing the passenger seat directly next to the driver's seat with aisles running down each side wall was also eliminated to keep a minimal floor width. With two 45.7 cm wide chairs and aisles measuring 22.9 cm each (chosen based on the width of two 95thpercentile feet), using only a single central aisle is a direct savings on structural mass.

- Placing the passenger seat directly behind the driver was also eliminated, because the passenger's view out the window would be almost entirely obscured by the driver. During a bumpy drive in a small enclosed vehicle, this can lead to motion sickness.

- An airlock is prohibitively large and massive for this mission.

- Placing suitports on each side of the rover requires enough unoccupied space in the center of the cabin for two 60 by 90 cm doors to open. This arrangement also requires the suitports to fit between the front and rear wheels of the rover. However, on the rear end cap, there is space large enough for two suitports that does not interfere with the drive system, and because the rover can be operated in reverse, a rear-facing suitport can double as the external driving station.

Based on these eliminating factors, the remaining ideas formed the set of layouts constructed and tested in the mock-up. Two primary choices were yet to be made: whether to use side-by-side chairs

or a centered chair with the passenger chair behind and to the side, and whether to use beds or hammocks for sleeping. Since these options are not wildly different, it was possible to determine the necessary dimensions of the cylindrical pressure shell, to begin construction of the mock-up rover and detailed design of the lunar rover. A diameter of 1.8 meters and length of 2.43 meters was chosen for the lunar design; this allows crew members ample headroom when seated, and although some will not be able to stand to their full stature in the cabin, they will be able to stretch out fully when sleeping.

The testing and evaluation of interior layout configurations conducted in the mock-up rover is described in Section 8.2. The test subjects determined that a centered seat is ideal for driving because it provides a symmetric field of view, but that it was difficult to move around the cabin with this configuration. A simple way to solve this problem is to allow the driver's chair to slide on rails to the side of the cabin when the crew needs to move around. During driving the chair locks in place centered in front of the window. Although the option of a hammock was not fully tested in the mock-up due to structural concerns, the test subjects found that the cot-style bed was comfortable, and felt that a hammock would probably require handholds to increase their feeling of security.

With these decisions made, placement of components in the cabin interior was finalized as follows.

8.3.1.1 Chairs

The chairs are shown in Figure 8.3. The chairs measure 45.7 cm wide and 45.7 cm deep, and the seat is 45.7 cm high. These values were selected to accomodate the widest possible hip breadth of 42.3 cm and average values of buttock-popliteal length and popliteal height, which vary from 37.9 to 55.5 cm and 34.7 to 48.1 cm respectively. To confirm that a 45.7 cm cube is reasonable for the base of a chair, a wide variety of commercially available chairs similar to the desired design were measured.

The seat of each chair consists of a leaf spring covered in padding and fabric to provide a smoother ride when the rover travels over bumpy terrain. The backs of the chairs are 45.7 cm high, and they fold flat, parallel to the floor, on single hinges when the beds are deployed as seen in Figure 8.4.

The driver's chair is secured on tracks that allow it to slide between two possible positions: in the center of the cabin (29.3 cm from the front end cap to allow room for the 95^{th}percentile foot), and against the left edge of the floor. With a sitting eye height range of 68.1 cm to 89.6 cm, this places the driver's eyes at 113.8 cm to 135.3 cm above the floor, which was used along with sight line angles to calculate the necessary window dimensions.

The passenger's chair is located against the right-side edge of the floor and directly behind the driver's chair.

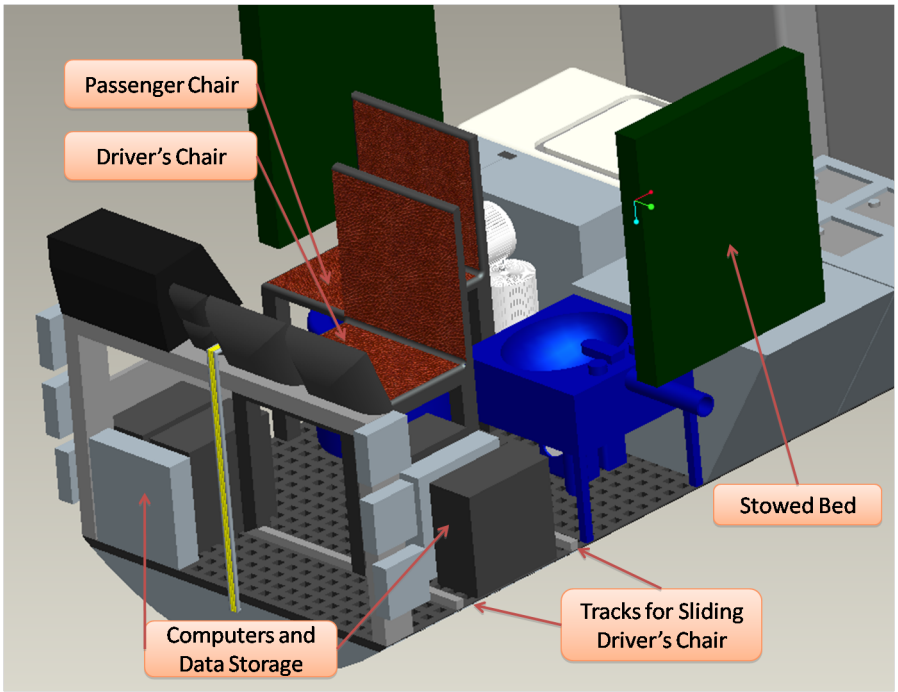

Figure 8.3: The driver and passenger chairs

8.3.1.2 Beds

The beds, shown deployed in Figure 8.4, measure 73.7 cm wide and 190.1 cm long. Since not all possible crew members will be able to stand up straight in the cabin, the bed length was set to allow the crew to stretch out fully when sleeping. The beds are 45.7 cm above the floor when in use, and they are supported by other furniture in the cabin as well as hooks along the side walls. The crew sleeps with their feet toward the rear of the cabin, so that their feet do not damage any control interfaces located at the front of the rover.

The beds are composed of three sections each approximately 63.4 cm long, so that when not in use, as shown in Figure 8.3, the beds can be folded and stowed against the wall. The hooks along the side walls hold the bottom edge of the beds in place, and a latch holds the top.

8.3.1.3 Health and Safety

As shown in Figure 8.5, the toilet is located underneath the passenger seat, which is hinged to lift up. The sink is located directly across the aisle from the toilet, and the four toiletry packs, one for each crew member during the two sorties, are stored under the sink. The contents of the toiletries kits are shown in Table 8.2. A curtain is available, which hangs on hooks that separate the driver's seat at the front of the rover from the rest of the cabin. This provides some privacy when one crew member needs to change clothing or use the toilet.

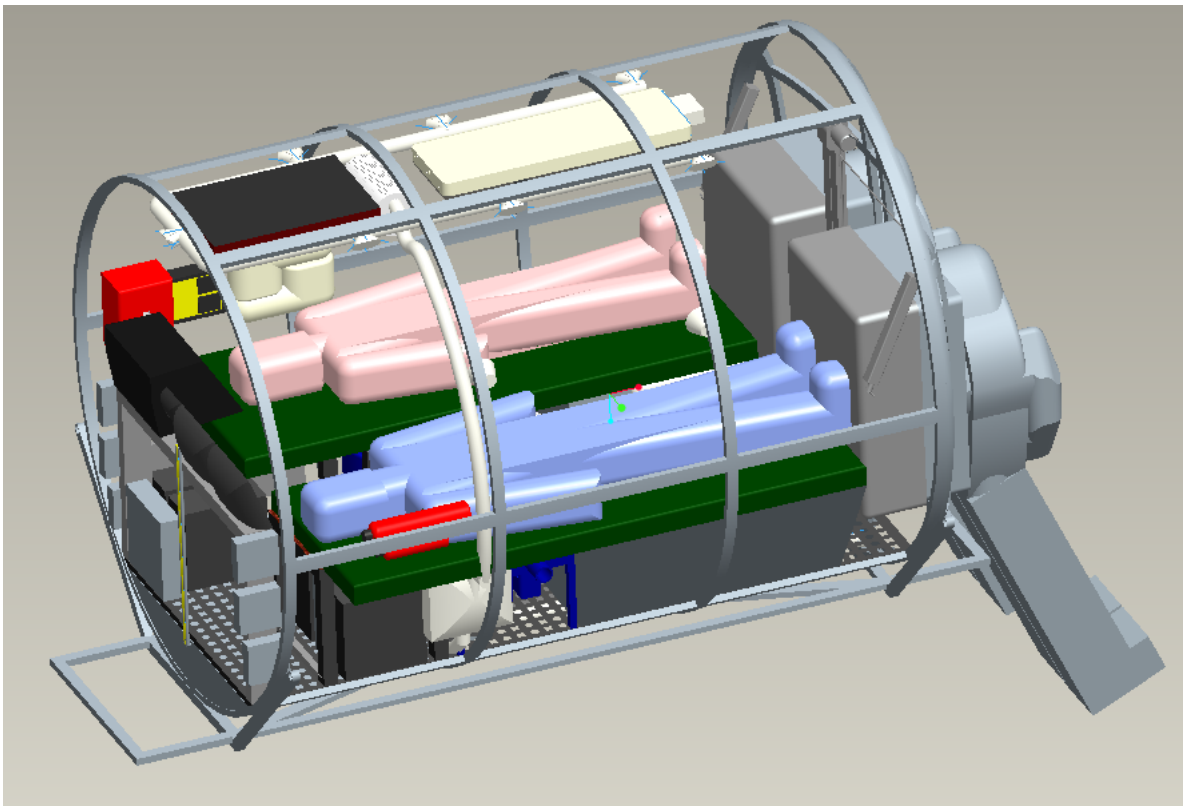

Figure 8.4: Beds deployed

Table 8.2: Toiletry Kit Contents (Jason Laing)

Item	Mass (kg)	Volume (m^3)
Rinseless shampoo	0.032 kg	3.2e-5
Toothbrushes	0.014 kg	3.2e-5
Toothpaste	0.034 kg	4e-5
Soap	0.0565 kg	7.5e-5
Towels (small)	0.22 kg	0.0018
Deodorant	0.05 kg	1.5e-4
	Total = 0.4065 kg	Total = 1.991e-3

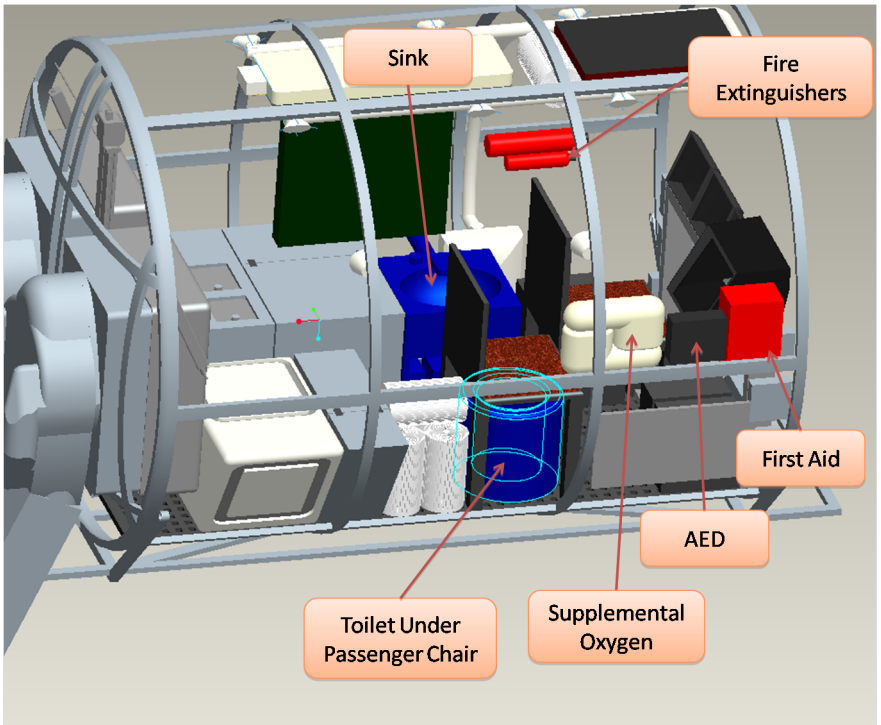

Figure 8.5: Health and Safety Items

Emergency items such as fire extinguishers, an Automatic External Defibrilator (AED), supplemental oxygen, and first aid kits are located along the side walls, at the cabin's widest point so that they do not interfere with movement about the cabin. They are secured in place using Velcro straps, which are strong enough to hold these items in place, but easy to reach and remove in an emergency.

8.3.1.4 Storage

The TURTLE mission requires 0.128 cubic meters of food, including packaging, to be stored in the cabin. This is contained in a trapezoidal storage container which is 45.7 cm high, 48.8 cm wide, 45.7 cm deep at the floor, and 73.7 cm deep at its top. This container includes two compartments separated by a flexible barrier; as the food is consumed, the empty packaging goes into the sealed waste compartment.

The clothing storage requires approximately 0.06 cubic meters with the use of "space bags" to cut down on volume. As with the food containment, the clothing is stored in a trapezoidal bin which is divided into two sealed compartments, one for clean clothes and one for used clothes. The container is 45.7 cm high, 22 cm wide, 45.7 cm deep at the floor, and 73.7 cm deep at its top.

The clothing storage requirements breakdown is shown in Table 8.3. There is also a set of general storage lockers, trapezoidal in shape, for stowing miscellaneous items.

Table 8.3: Clothing Storage Requirements (Jason Laing)

Item	Lifetime (days)	Mass (g)	# Needed	Subtotal Mass (g)	Volume (m^3)
Shirt	2	110	4	440	0.0052
Jacket	14	370	2	740	0.00972
Pants	7	370	2	740	0.003332
Shorts/underwear	1	57	8	456	0.006336
Tshirt/brassiere	1	40	8	320	0.0104
Socks	1	14	8	112	0.0033
Handkerchief	2	7	4	28	0.003168
Sleep/exercise shorts	3.5	85	4	340	0.004992
Sleep/exercise shirt	3.5	110	4	440	0.0052
Slipper socks	90	85	0	0	0
			Total:	3.616	0.051648

A miniature airlock allows the crew to pass small items, such as scientific samples or camera equipment, between the cabin and the outside of the rover. Its dimensions (45.7 cm high, 45.7 cm wide, 45.7 cm deep at the floor, 73.7 cm deep at its top) were determined by the amount of space made available when mock-up testing determined the amount of floor space needed for suitport operation, which was smaller than expected. The airlock door opening is 33.0 cm by 27.9 cm.

As shown in Figure 8.6, the food container and general storage lockers are located on the left side of the aisle, behind the sink. The clothing container and airlock are on the right of the aisle, behind the toilet and the five inactive LiOH canisters. The active sixth canister is located on the ceiling, where it interfaces with other air circulation equipment.

The potable water tank, shown in Figure 8.7, is being continuouly supplied by the fuel cells for drinking and sanitation purposes, and also serves as a layer of radiation protection. It is stored in a hemicylindrical-shell-shaped tank which covers the top half of the rover cabin interior. This tank is about 2.5 cm thick and extends the length of the rover. The internal heat exchanger (60 by 40 by 5 cm) is also located on the ceiling, as is the active LiOH canister.

The waste water tank, approximately 0.065 cubic meters, is stored underneath the floor, toward the front of the rover, underneath both the sink and the toilet. The tank is shaped to fit the curvature of the cabin. The solid waste tank, measuring 0.0036 cubic meters, is also stored under the floor. The circuit breaker, which is 96.5 by 22.2 by 17.8 cm, is stored under the floor along the aisle, and can be accessed by opening panels in the floor.

There are four computers and two data storage devices, which are located in two groups at the front of the cabin as shown in Figure 8.3. The IMU, or inertial measurement unit, is secured in

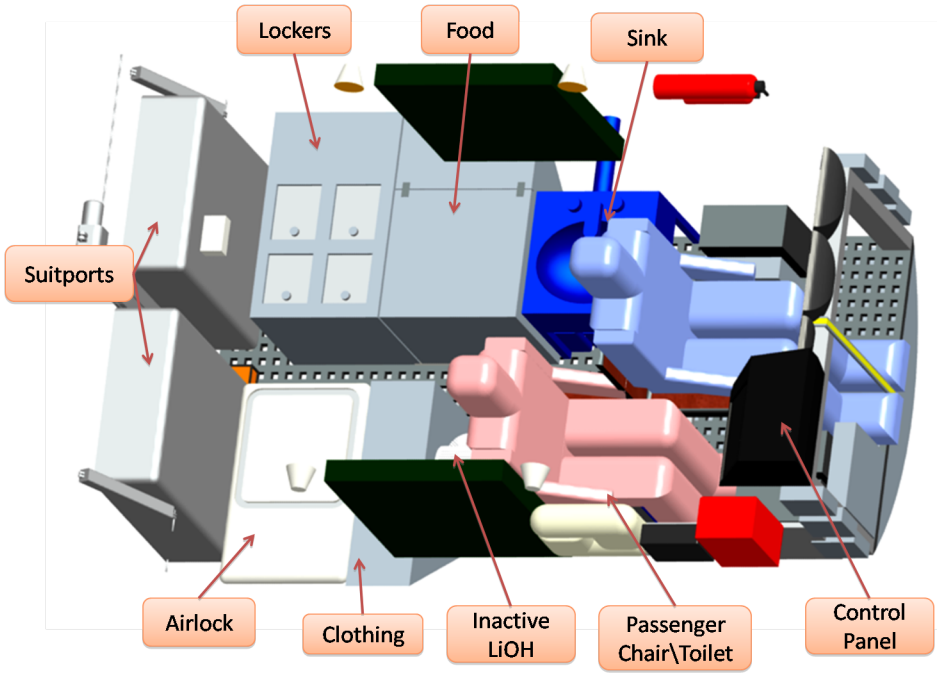

Figure 8.6: Storage Containers

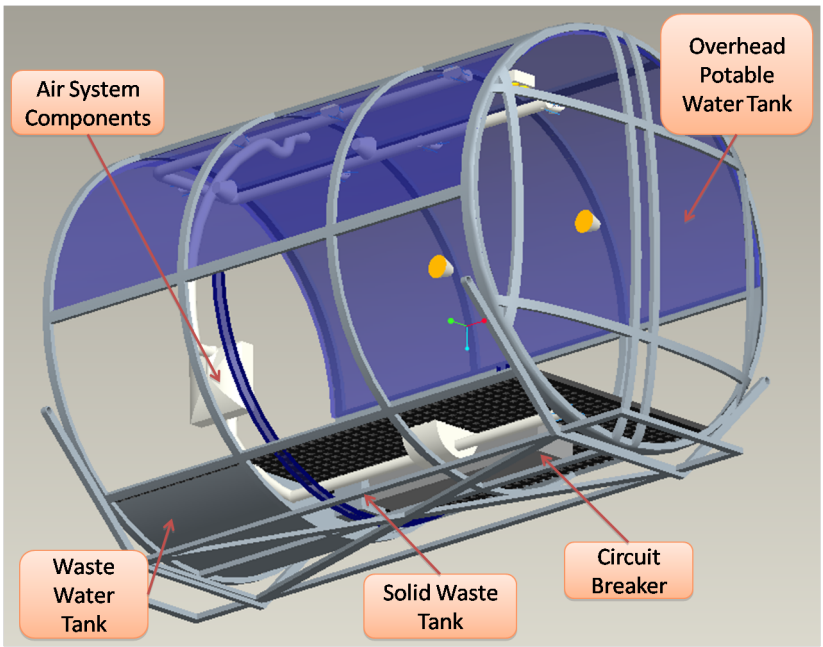

Figure 8.7: Water Tanks

place at the back of the cabin on the floor, underneath the suitport openings. This location places the IMU as close as possible to the center of the rover/lander during landing.

For more information on the items stored in the cabin and their dimensions, see Appendix C.2.

8.3.2 Flooring (Ryan Levin)

8.3.2.1 Requirements

Based on studies from Crew Systems, the floor must run the entire length of the rover at 115 cm (45 in) wide and a uniform height where the center of the floor is 20 cm (8 in) above the lowest point in the tank. The floor should be as thin as possible while not deflecting when weight is applied to it. Also, the floor design should allow for easy access to components underneath the floor. Other floor design constraints were that the floor should be light enough to be manipulated by the astronauts on the moon and choosing a versatile design.

8.3.2.2 Rover Floor

Fiberglass grated flooring works well in terms of fulfilling the requirements listed above. The floor contains eight equal sized panels, each 57.2 cm x 61 cm (1.9 ft x 2 ft) and 2.54 cm thick. Specific information about the grating can be found in Figure 8.8 and Figure 8.9.

Resin Type	Resin Base	Description	Corrosion Resistance	Flame Spread Rating ASTM E84	Available Colors	Max.Oper. Temp.
Type V	Vinyl Ester	Superior Corrosion Resistance and Fire Retardant	Excellent	Class 1, 25 or less	Dark Grey Orange	230˚F

Figure 8.8: Chemical Properties

Grating Thickness	Mesh (Bearing Bar Ctr)	Bars Per Ft.	Bar Thickness (Top x Bottom)	Standard Panel Size	Est. Wt. In Lbs.		Lb. Per Sq. Ft.		Open Area	Min. Glass Content	
					I	V*	I	V*		I	V*
1″	1-1/2″ square	8	.25″ x .20″	4′ x 12′	121	115	2.5	2.4	68%	37%	39%

Figure 8.9: Physical Properties

As seen in Figure 8.10, the span is only 61 cm (24 in) so the maximum deflection on the moon given a maximum weight of 45 kg (100 lbs) will be 0.1 mm (0.029 in). The floor is uniformly supported along the length of the tank by a bar support on either side of the floor area and the center is supported by supports similar to those shown below in Figure 8.11. Removable bands will be used to hold the floor in place during launch. All floor panels will be removable to access the components stored under the floor.The floor is also non-magnetic as well as corrosion, fire, and impact resistant.

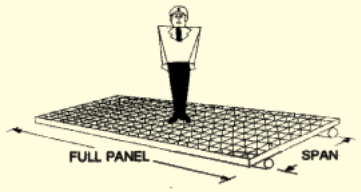

CONCENTRATED FULL PANEL LOAD - 4' x 12'

Deflection in Inches

1" Thick x 1-1/2" Square Mesh x 4' x 12'							
SPAN	POUNDS						
Inches	100	250	500	750	1000	1500	2000
18	0.010	0.027	0.061	0.085	0.105	0.164	0.206
24	0.029	0.065	0.125	0.182	0.241	0.359	0.477
36	0.070	0.175	0.347	0.518			
48	0.116	0.297	0.593				

Figure 8.10: Deflection Data

Figure 8.11: Supports

8.3.2.3 Reference

All of the above data and pictures were acquired from documents available from American Grating, LLC. Actual test data is represented by the data listed in this report.

8.3.3 Lighting (Tiffany Russell)

The lighting arrangement in the rover must be able to provide illumination at all times during the mission. To decrease energy demands, all interior lighting fixtures will use fluorescent light bulbs that are able to dim and have no flicker. The exception to the fluorescent bulbs are the emergency lighting and self illumination markers during low light. The design minimizes shadows, reflections, and glare as well as provides a wide range of light for all tasks that do not exceed the luminance ratio of 5:1.

8.3.3.1 Supplemental Lighting

The lighting arrangement in the rover will provide an illumination of 108 Lux during all lunar operations besides sleeping. During the night hours, the rover will have interior illumination of 54 Lux provided by the self illuminating driving station displays, four supplemental lights, and glow guides located on the emergency equipment, floor, and suitports. The glow guides are stripes that reflect light. Supplemental lighting fixtures are located 0.75 m and 1.5 m from the front interior end cap on each side of the rover and 0.50 m height from the floor. The front light to the left of the driver is located outside of the visual center by 60° for a 95th percentile American male. Since the lights are permanently mounted to the wall, they can adjust to any 180° left to right and 90° up down position. Four 15 W compact fluorescent bulbs are the light source that are can be dimmed to 54 Lux during sleep hours and 108 Lux during performance of localized tasks. The bulbs will provide a clear white light of full spectrum with a color temperature greater than 5000 K.

8.3.3.2 Ambient Lighting

One main lighting fixture of two 40 W fluorescent bulbs will be placed in the center of the rover on the ceiling. It will be 2 ft in length and 1 ft wide located 0.90 m from the interior front end cap. This light will provide white, full spectrum light and have a color temperature of 5000 K. There will be a dimmer capability and a direct connection to the emergency light system. In case of power failure while the ambient light is on, the emergency light will turn on automatically and last for 12 hours. The ambient and supplemental lighting configurations are shown in Figure 8.12.

8.3.3.3 Exterior Lighting

Four 50 W halogen lamps will provide exterior illumination during driving and EVA operations. Each lamp will provide white light at a 45° beam spread. Therefore, two lamps will be mounted

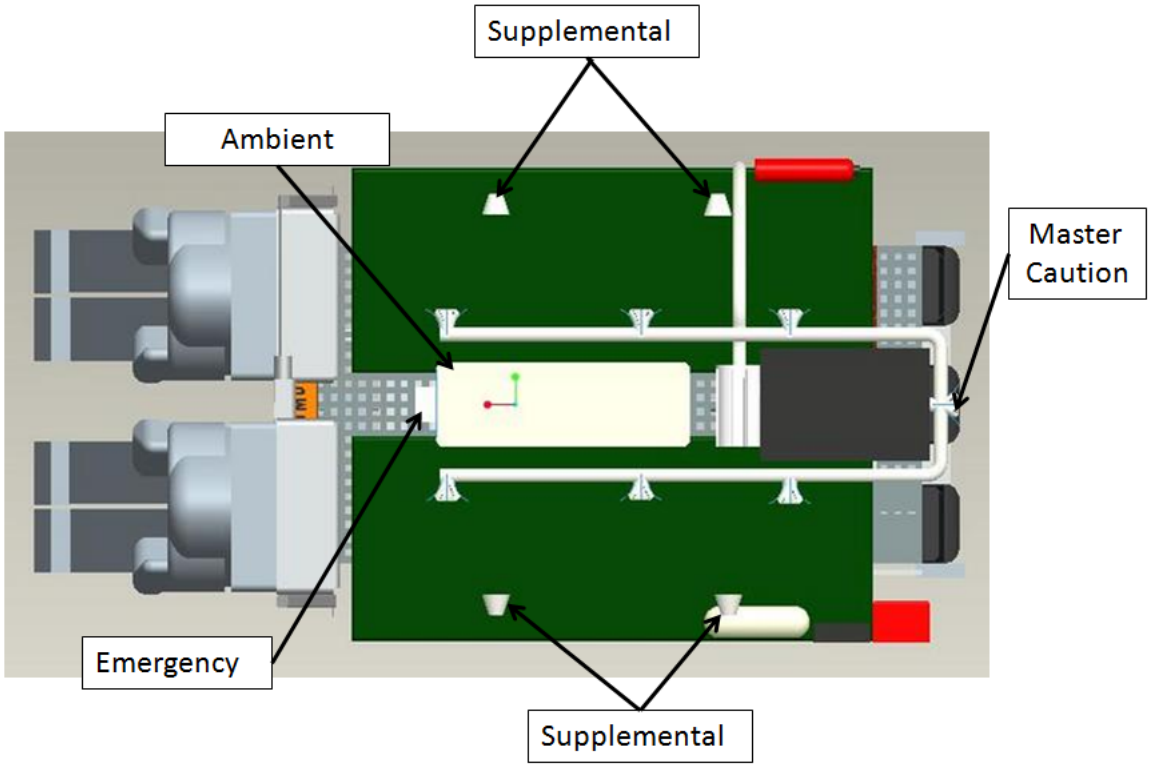

Figure 8.12: Ambient and Supplemental Lighitng Configuration

to the front of the rover, located between the avionics equipment and hydrogen tanks to provide driving illumination. For suitport ingress and egress, two halogen lamps will be mounted directly above the center line of each suitport.

8.3.3.4 Tasks and Power Draw

Table 8.4 shows the particular tasks and power draw for the varying sets of lights.

Table 8.4: Task Designation and Power Draw

Type	Purpose	Location	Color	Power (W)
Emergency	Self sustain in case of power failure	Ceiling above suitports angled down	White	30, external battery
Reading/Sleep	Reading and emergency egress from sleep position	Within reach of 5^{th}percentile female while fully reclined	White	60
Ambient	Gross illumination of the entire cabin	Along the ceiling, not pointed toward any crew member station	White	80
Supplemental	Local task illumination	Local work stations	White	15
Displays	Self illumination of screens, control panel	Driving station, any other control station	White	15
Exterior	Assist during driving and EVA's	Two above driving window, two above suitports	White	

8.3.3.5 Master Caution and Warning System

The warning system is designed to alert and inform crew of potential and imminent hazards. This system is integrated into the avionics network of sensors and control panels. Once a vulnerability within the rover is detected that is vital for crew survival, one of the driving displays will change over to the Master Caution and Warning program. The screen will show CO, CO_2, and radiation levels as well as total cabin pressure. The system will perform a full diagnostic test of the critical crew life support system and provide real time data on all systems to pinpoint the vulnerable system. The audio and visual component of the system is located 0.20 m above the interior driving station and consists of a flashing red light and audio indicator. The alarm can be shut off once the issue has been acknowledged in the program.

8.4 Suitport (James Briscoe)

8.4.1 Concept

The next section describes the design for the suitport concept to enter and exit TURTLE. The suitport concept has never been proven in space and has only minimal design work from NASA Ames. [90] Besides this design and the prototype built by NASA Ames, however, there is relatively little research to use as precedent. For TURTLE, the main goal is to outline the big picture in terms of the suitport mechanism, components, connections, and seals, as well as to build a prototype to demonstrate and test the operation of the suitport.

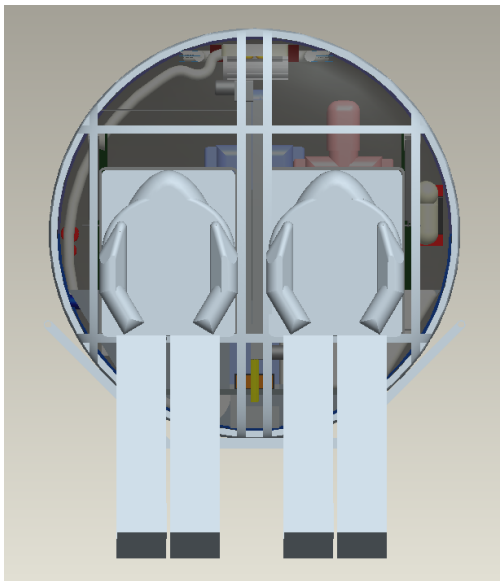

Figure 8.13: View of Suitport From the Rear of Rover

In general, a suitport refers to a system where the space suit is stored outside the rover cabin and the astronaut is able to climb in and out of the rover through a hatch in the back of the suit. After EVA when the suit is backed into the rover, the connection between the suit and the Portable Life Support System (PLSS) is released. The PLSS is then held and carried by the PLSS Containment System (PCS) out of the way so the astronaut can climb into the rover. The suitport is extremely efficient in terms of cabin volume, power and mass allowances, as well as lunar dust containment. There are five connections and seals involved with the suitport system to be discussed in a later section. These interfaces are between the suitport structure and the cabin shell, between the suit and the suitport, between the suitport and the PCS, between the PLSS and the PCS, and finally between the suit and the PLSS.

One assumption that was made for the suitport design was that it should be sized to match the current ILC Dover-developed Mars I-Suit, which is a rear entry suit and thus is ideal for application

to the suitport concept. Going into the design process it was clear that for the suitport to be applied to a real world spacecraft, a new suit or a modified currently existing suit would have to be developed. Despite this, the I-Suit, shown in Fig. 8.14, is a good choice for the concept design because it is relatively lightweight and still in development. The design for the II-Suit and future generations hopefully will be more tailored for suitport applications. [64] The PLSS for the I-Suit is still in development, so the size was estimated based on the size of the I-Suit prototype hatch held in the Space Systems Laboratory at the University of Maryland. The dimensions of the PLSS are: 76.2 x 61.0 x 17.5 cm. The PCS was sized to be slightly larger at 78.7 x 63.5 x 22.9 cm.

Figure 8.14: Mars I-Suit

8.4.2 Trade Studies for Suitport Design

The suitport concept is currently at a TRL level of two, but was the clear choice for a manned rover with EVA capabilities. The decision was made to design a suitport following a trade study between the suitport concept and the proven airlock design, which is currently the only space tested ingress/egress method. A comparison was made between the Quest Joint Airlock of the ISS with the mass and volume estimates of the suitport as shown in Table 8.5.[72] The suitport values include the masses and volumes of the suitport structure, defined to be the beams primarily carrying the suitport loads, the PCS, suit, and the PLSS for both suitports. The I-Suit prototype built by ILC Dover weighs 30 kg without the PLSS [87]. Since the PLSS for the I-Suit is still in development, the weight of the Shuttle PLSS was used, at 15 kg. [103] The PCS is estimated at 9 kg assuming an aluminum alloy with density 2700 kilograms per cubic meter and a thickness of 3 mm. The suitport structure, as described earlier in the structures section, has a total mass of 37 kg. This includes the beams surrounding each opening as well as the underlying beams used to support the loads on the suitport, as illustrated in Fig. 8.18. These values give a total mass of about 145 kg for the pair of suitports.

The suitports are 40 times less massive and occupy 140 times less volume than the airlock In fact, the ISS airlock is twice as massive as the entire lander stage for TURTLE. Even a significantly lighter and smaller airlock would place far too many design constraints on both the mass budget

Table 8.5: Trade Study between Airlock and Suitport

	Mass (kg)	Volume (m^3)
Suitport (x2)	145	0.25
Quest Joint Airlock of ISS	6064	34

and available cabin volume. For these reasons, the suitport is the chosen method for TURTLE despite the low technology readiness level.

The next major decision concerns how the suitport door would open. Another trade study was initiated between a garage door style and a hinged door design. The garage door style suitport uses actuators to push the PCS upwards and rotate into the cabin to allow the astronaut to perform ingress/egress underneath. The hinged door design is much simpler in terms of the design and the necessary components, but uses significant cabin volume. The sweep of the hinged suitport requires about two square meters of unoccupied cabin space while the suitport is being operated. A garage door style suitport, however, would only need the volume of the PCS (about 0.11 m^3). In addition the garage door style places the PCS and PLSS up near the ceiling of the rover where space is more available in general. The major difficulty with the garage door style design is that it requires the design of a new suit with a fully detachable PLSS as no current suit has this feature. There are some suits which currently have hinged PLSS connections, though a redesign would still most likely be necessary. It was assumed from the start that a new suit would have to be designed; therefore, this was not the deciding factor. By this analysis, the decision was made to develop a garage style suitport for ingress/egress, shown in Fig. 8.15.

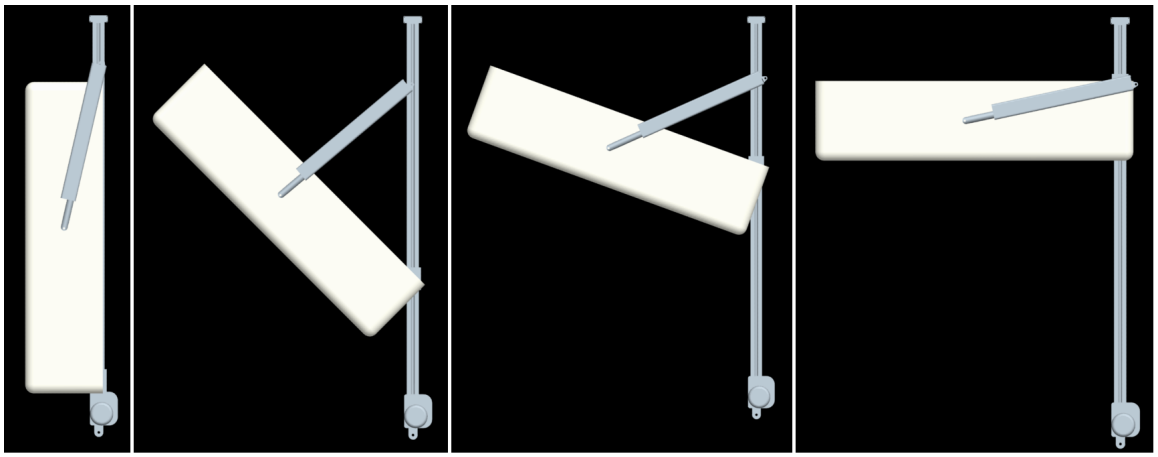

Figure 8.15: Illustration of Garage Door Style Suitport Mechanism

8.4.3 Components

The next section describes the components needed in the design of the garage door style suitport, primarily the two actuators. The first is a 102 cm long track actuator which is bolted to the lower corner of the PCS closest to the center of the rover and pushes the PCS vertically upward. A comparable track actuator built by Firgelli Automation has a maximum load of 900 N, capable of holding the PCS and PLSS together. The actuator moves approximately five centimeters per second depending on the applied load and takes about two amps at 28 Volts DC. Attached to the opposite side of each PCS is a sleek actuator which can adjust its length along its line by 22.9 cm, with a minimum length of 36.8 cm and a maximum of 52.1 cm. The sleek actuator helps rotate the PCS into the cabin ceiling and can produce enough force to push 18.1 kg at five centimeters per second or to hold 45 kg at rest. The sleek actuator is attached to the shell 20 cm above the PCS and 6.5 cm in from the rear end cap. At the other end the actuator is attached to the PCS 27 cm down and 20.5 cm in from the rear end cap. The power draw for the sleek actuator is the same as the track actuator, but at 12 VDC. [36]

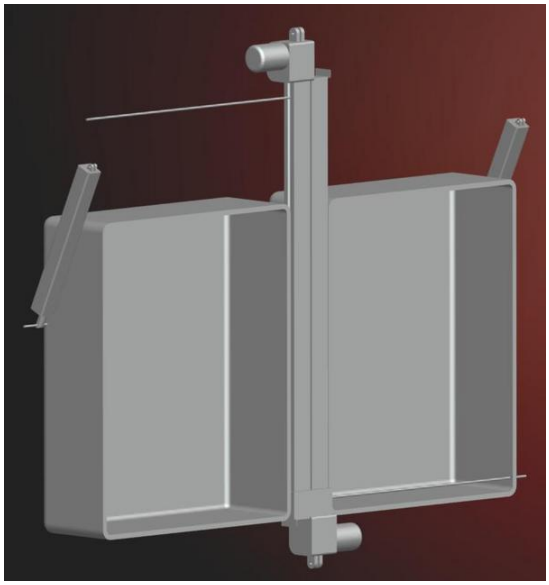

Figure 8.16: View of Suitport Components

Testing from the mockup demonstrated the need to add more components to help balance the forces and moments placed on the PCS during operation. First a non-actuated track on the opposite side from the track actuator helps guide the PCS upwards. The track became obviously necessary early on during the construction of the mockup to counteract the imbalanced actuation of the PCS. Testing also showed that two cables surrounding the PCS were necessary to help balance forces. In later sections the test plan is to be discussed with a more detailed look at the design modification

process.

8.4.4 Connections

As previously stated there are five critical connections and seals between the various components: between the suitport structure and the cabin shell, between the suit and the suitport, between the suitport and the PCS, between the PLSS and the PCS, and finally between the suit and the PLSS, as illustrated in Fig. 8.17. At the start, a few general design guidelines were placed on these connections. For equal functionality, passive mechanisms are preferred over active ones to keep the power draw at a minimum and the design as simple as possible. For all connections and seals, redundancy is key to prevent mission or crew critical failures.

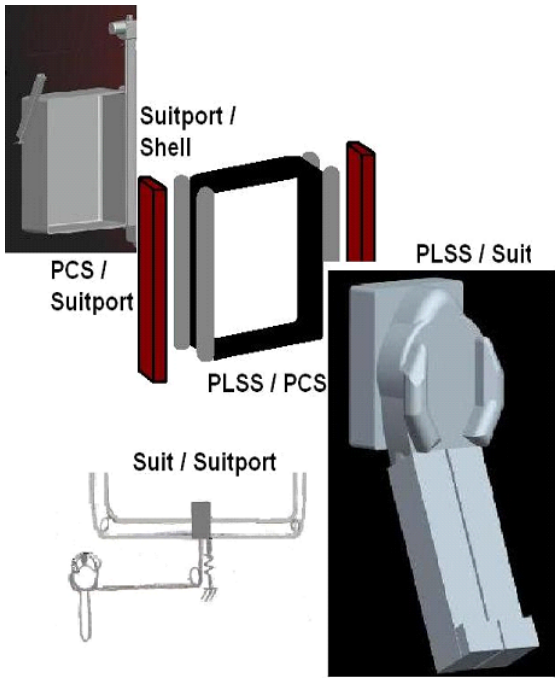

Figure 8.17: Illustration of Suitport Connections and Seals

The first connection is between the structure of the suitport and the rear shell end cap of the rover. There is some complicated geometry involved with fitting the rectangular suitport into the ellipsoidal cabin end cap. The rear end cap has two holes which are rectangular in cross section but curved. The suitport structure is flush with the hole on all sides, with the side closer to the center of the rover deeper than the other to support a PCS which is uniformly thick. The suitport structure also has perpendicular ribs on both sides of the shell. A bolt is put through the ribs and shell to hold the suitport structure in place. For each suitport there are 18 bolts to help prevent areas of heavy load concentration, with five bolts on each side and four on the top and bottom. The

suitport structure is one of the most heavily loaded areas throughout the mission, and especially during launch. The structure must support the weight of the suit, PLSS, and PCS together, about 145 kg of mass. Refer to the structures section for a more detailed analysis of the critical loads and sizing of the members in the suitport structure, shown in Fig. 8.18

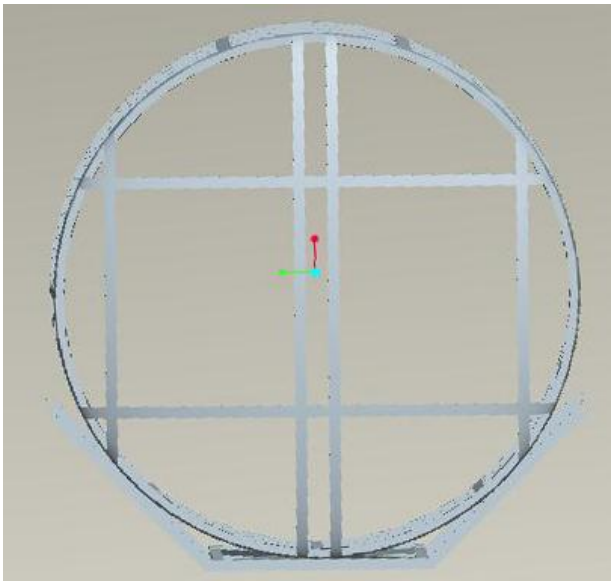

Figure 8.18: CAD Drawing of Suitport Structure

The next connection is between the PCS and the suitport structure. For this connection the decision was made to use a spring-triggered pneumatic lock. A very small spring is placed on the suitport structure which detects whether the PCS is in place. When the spring is compressed by the PCS a pneumatic controller triggers a sliding lock which holds the PCS against the suitport when not in use. For redundancy there are a few options. First the pressurization inside the cabin actually helps push the PCS out against the suitport alleviating a lot of the load. Also a simple chain and hook, as built for the mockup rover, would be easy and simple for the astronaut to clip on once inside the rover after ingress. A combination of the above methods is sufficient to hold the PCS against the suitport.

Next to be discussed is the interface between the PLSS and the PCS. After the suit is backed into place, the PLSS is detached and held by the PCS. Another very similar pneumatic locking mechanism was selected for this connection. A spring in the PCS detects the presence of the PLSS and triggers sliding bolts to lock the PLSS. For redundancy, gravity will keep the PLSS inside the PCS. The PCS opens face up and therefore it is near impossible for the PLSS to get out of the containment tub even without the use of the pneumatic lock.

Another connection is the interface between the suit and the suitport. This connection is a passive mechanism that uses two spring loaded bolts for each suit to hold it to the suitport. The

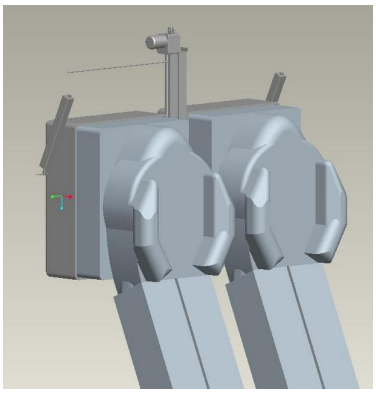

Figure 8.19: PLSS and PCS Interface

tension in the springs keep the bolt in its locked position when unloaded. Rotational levers located on the outside of the rover are attached via a pulley to these bolts. The lever is within arm's reach of the astronaut and is rotated to pull the bolt into its unlocked position. The bolt is held unlocked with the use of a casing and spring loaded pin attached to the lever. A curved casing around the lever has an opening for the spring loaded pin to push through to hold the bolt unlocked. To lock the suit again, simply push the pin through the opening and rotate the lever back to the locked position. As stated, there are two such locks for each suitport for redundancy.

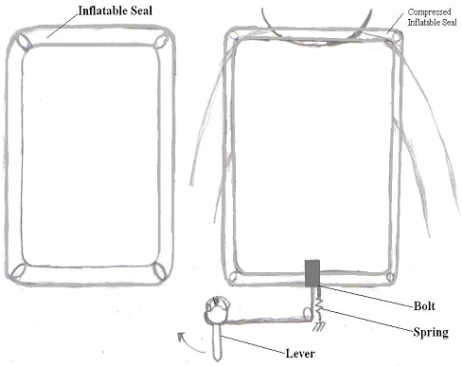

Figure 8.20: Drawing of Suit and Suitport Interface

The final connection, and the most complicated, is the connection between the PLSS and the suit. As previously stated, one of the main difficulties with the suitport design is the fact that no current space tested suit has a fully detachable PLSS, which is necessary for the garage style suitport. A new suit would have to be designed and therefore a full high fidelity design of this connection was not developed. The interface between the suit and PLSS would have to be extremely reliable to ensure crew safety while EVA. One possible concept to allow a fully detachable PLSS is a actuated

lock which rotates multiple hooks in the back of the suit around small metal bars in the PLSS. Current space tested methods of interfacing the air supply and carbon purging could be applied to a detachable PLSS design as well. The Mars I-Suit is the closest thus far to meeting the design demands for a suitport and hopefully a more applicable suit design will be developed soon.

8.4.5 Seals

One of the key benefits of the suitport over other ingress/egress methods is dust mitigation. The suitport keeps the inside and outside environments completely isolated, so dust filtration inside the cabin is not an issue. To ensure dust mitigation seals are necessary in the interfaces between all the various components involved.

The first seal is between the suitport and the shell. As previously stated the suitport structure has ribs which surround the shell end cap. To keep dust from getting in between the shell and suitport simple weather strip style sealants are placed both on the inside and outside of the rover. The weather stripping also has dust shields to prevent damage to the seal itself from lunar dust.

Inflatable seals are becoming more frequent in space applications, and prove useful in the design of TURTLE. Inflatable seals are made of an isomeric material which is extremely strong as well as extremely flexible, and are great options for filling gaps between doorways. For this reason, inflatable seals are used between the suit and suitport as well as between the PLSS and PCS. An inflatable tube is attached on the inside of the suitport structure and the PCS around on all sides. The suit and PLSS are inserted and the tube is inflated to fill any holes. The power draw of these inflatable seals is very small, consuming on the scale of milliamps. For the suit and suitport, testing demonstrated the need for ramps to guide the PLSS into place. These ramps also serve as dust shields for these seals to prevent damage. [38]

Finally, the seal between the PCS and the suitport is designed based on a NASA Ames o-ring sealing system. The system is specifically tailored for pressurized environments and therefore is perfect for application on TURTLE. The PCS is tapered outward towards the rear of the rover and surrounded by an o-ring. As the pressure inside the cabin increases, it pushes against the o-ring, causing it to roll up the ramp created by the tapered PCS. As the o-ring rolls up the PCS it makes a more pressure tight seal between the PCS and the suitport. The seal is illustrated in Fig. 8.21. This proves to be a very elegant design which uses the pressurization inside the cabin to keep the rover pressure tight. Dust shields are not an issue in this seal because the o-ring is not exposed at all to the outside environment as it is blocked by the PCS and suitport structure. [100]

8.5 Mock-up Suitport (James Briscoe)

The focus for the mock-up suitport is to demonstrate the process of ingress/egress as completely as possible and as high fidelity as possible with the resources and time available. In this light a simpler

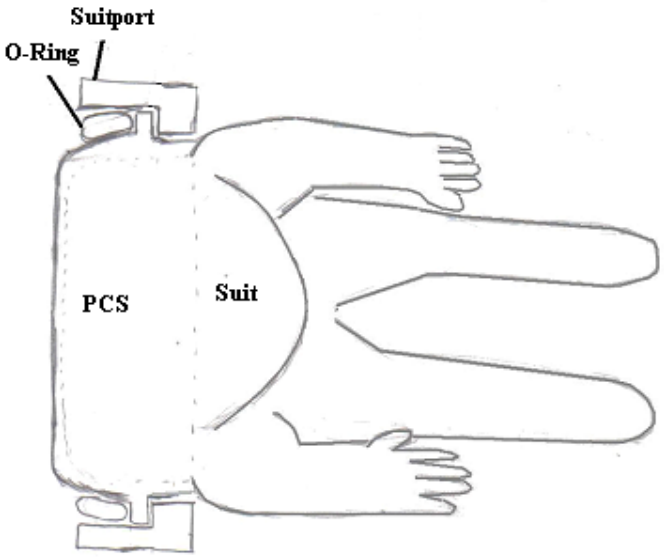

Figure 8.21: Seal between PCS and Suitport

design means a better one for equal functionality. Sealing was ignored to maintain the focus on the operation of the suitport. The test plan focuses on using mock-up for human factors involved with the operation, particularly spatial needs, i.e. how much cabin volume is consumed by the sweep of PCS as well as how much volume is needed by the astronauts to maneuver ingress/egress. Other factors included in the test plan are ease and comfort and what kind of supports are needed, e.g. handrails, pull-up bar, etc.

8.5.1 Components

For the mock-up rover, two holes were cut to match the PCS dimensions, but only one suitport was built. The other opening was used for access for people and objects, and a Plexiglas hinged door was built to cover the hole. The components for the mockup suitport are low fidelity models exactly matching the theoretical design. The exception is the high fidelity track actuator purchased from Firgelli Automation. The track actuator also shared the same design specifications as the flight rover, with a length of 102 cm attached near the bottom corner of the PCS closest to the center of the rover. The track actuator has a maximum load of 900 Newtons and a speed of 2.5-6.3 centimeters per second. The exact location of the attachment point is two centimeters away from the corner in both directions. [36]

Opposite the track actuator a slotted two by four was screwed into the rear shell to help guide the bottom corner of the PCS closer to the side of the rear end cap of the rover. A plastic slider piece is bolted through the PCS, held with washers and a nut, and fitted into the slot of the two

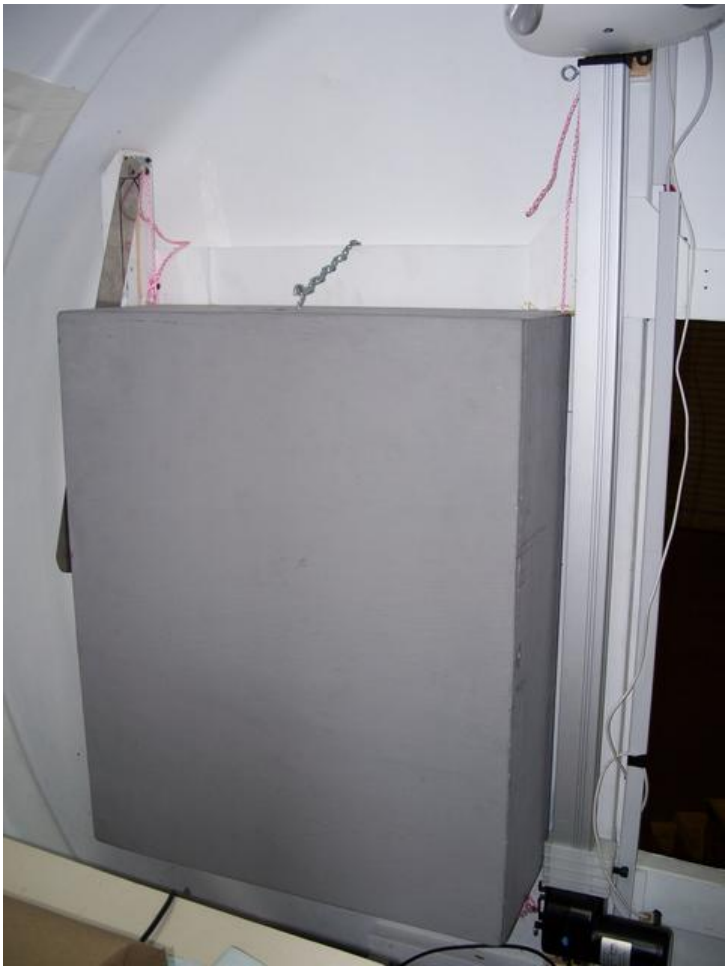

Figure 8.22: Picture of Mock-up Suitport

by four. This serves as a mock-up of the non-actuated track in the flight and field rover. Actuating both sides at the same time would be quite difficult to synchronize and would most likely tear the PCS apart.

To mock-up the sleek actuator a flat metal bar was slotted and attached to the side of the PCS on the side of the rover. A threaded metal piece was screwed through the side of the PCS and the slot of the metal bar allowing it to slide 6.4 cm for a maximum length of 54.6 cm and a minimum of 48.2 cm. The sleek actuator mock-up was sized to match as closely as possible the theoretical sleek actuator. The top attachment point was 20 cm above the PCS and 6.5 cm in from the rear end cap. At the other end the bar was attached to the PCS 27 cm down and 20.5 cm in from the rear wall. Test results predict that the addition of another identical mock-up sleek actuator on the opposite side might help make the suitport move more smoothly.

Testing also showed the need for cables surrounding the PCS to help balance the forces. Two thread cables were added attached above the PCS, one on each side, and ran the length of the PCS on two sides. An eyebolt was also screwed into the top of the PCS and hooked to a chain. The chain could be hooked onto another eyebolt screwed into the suitport structure above the PCS to hold up the PCS when not operating the suitport.

For the mock-up of the PLSS and PCS, low fidelity rectangular models were constructed sized to match the theoretical design. Plywood and two by four squares were used to build the mock-up PCS, sized to match the theory, at 78.7 x 63.5 x 22.9 cm. The PLSS was composed of particle board and cardboard and sized slightly smaller than the theoretical design to allow it to slide more easily into the PCS. The dimensions of the PLSS are 74.0 x 57.0 x 18.0 cm.

Figure 8.23: Picture of Mock-up Suit Docked to Rover

The final aspect to the mock-up suitport is the connection between the PLSS and the suit. Our mock-up budget included provisions for purchasing two training hazardous material suits, one large and one extra large. Holes were cut into the back of the suit sized to the hatch of the I-Suit. The hatch itself was mocked up with the use of PVC pipe which was heated and shaped into an ellipse which is flatter on the bottom than the top. The semimajor axis of this ellipse is 62 cm and the semiminor is 54 cm. A sheet of particle board was cut and bolted through the suit and PVC hatch as well. Four eyebolts were screwed into the particle board which mate with corresponding hooks on the PLSS. This connection is the lowest in fidelity as it is only portion of the ingress/egress process that required the assistance of another person inside the rover. In a real setting the connection would be motorized and actuated by the astronaut performing ingress/egress.

(a) Suit without PLSS (b) Suit with PLSS

Figure 8.24: Mock-up Suit

8.5.2 Suitport Testing (Jason Laing)

Through the use of the mock-up rover as a design aid, the suitport concept was tested to a certain degree. Two students were present at each testing session, with one acting as the astronaut preparing to explore the lunar surface, and another operating and/or assisting the movement of the PLSS Containment System, as well as spotting problem areas. Verbal cues were used to prevent damage to the suitport, as the test subject could not see the PCS or notice problems. These EVA simulations demonstrated the following procedures.

1. Start from within the cabin and raise PCS (containing PLSS) to full height.

Using the hand controller on the track actuator, a test subject "astronaut" actuates the PCS from inside the cabin. This is an operation that takes approximately 30 seconds to complete, assuming that the actuation occurs smoothly and without any problems.

2. Enter suit through rear entry, adjusting all straps and fittings as necessary.

   Using the mock-up storage containers and folded-flat chair inside the cabin, the "astronaut" slides into the mock-up suit that is hanging on the open suitport. The track actuator and guide track serve as hand-holds. Once standing inside the suit, the subject tightens his or her backpack straps in preparation for the load of the mock-up PLSS.

3. Lower PCS into place and make sure that the PLSS is properly attached to suit.

   The hand controller is made accessible through the access door , and with verbal cues from the assistant inside the cabin, the "astronaut" lowers the PCS. Hooks in the rear of the mock-up suit match up with loops in the mock-up PLSS for a solid connection.

4. Detach suit from rover and simulate EVA.

   The suit, previously held to the cabin with simple sliding latches, is detached. The "astronaut" steps forward and down off the external platform, sliding the PLSS out of the PCS. The test subject is then able to walk freely outside of the cabin.

5. Back PLSS into PCS and attach suit to rover, which simulates sealing.

   Using the exterior standing platform as a visual placemarker, the "astronaut" then walks backwards, pushing the PLSS into the PCS. A physical guide below the suitport aids with vertical positioning. The sliding latches are locked into the closed position, holding the suit firmly in place.

6. Raise PCS (containing PLSS) to full height.

   Again using verbal cues from the assistant inside the cabin, the "astronaut" actuates the PCS into the open position inside the cabin.

7. Enter cabin from rear access of suit.

   The "astronaut" exits backwards through the suit, again using the actuator and guide track as handholds. Once the test subject's head and shoulders are inside the cabin, the subject is required to use mostly upper body strength to lift him or herself into a sitting position on the edge of the hatch. From there, the "astronaut" uses both arm and hip movements to slide back onto the mock-up storage units and chair inside the cabin.

8. Lower PCS completely, and return to normal cabin operations.

   Finally, the test subject lowers the PCS using the hand controller. As the PCS iss lowered, hooks on the suit and loops on the PLSS are connected automatically, allowing for the testing

process to be carried out again later. The cockpit chair back is raised into the upright position, simulating normal cabin conditions.

Because the mock-up version of the suitport is rather low fidelity, some alterations needed to be made from the theoretical suitport operation that would be occuring as a part of a real EVA. Many of the procedures associated with operation had to be completed manually. When the suitport is in the closed position, a small chain is used to hold the face of the PCS tight to the wall of the cabin. After the mock-up suitport design was finalized, the moments placed on the PLSS container caused it to "freeze up" during unassisted operation. To fix this, a downward force was exerted on the top corner of the PCS closest to the center of the rover. This caused the opposite corner to be pushed up, allowing for smooth motion. As the PCS reached the fully open position, a length of rope was used to connect the top edge of the PCS to the ceiling of the cabin. This allowed the PLSS Containment System to be held in the open position without placing unnecessary strain on the actuator, linkages, or guide track. Finally, because the movement of the closing PCS was downward, and the tub was then pushed closed (pivoting about the lower edge of the PCS), the top pair of hooks on the suit did not properly connect with the loops on the PLSS. To fix this, the assistant inside the cabin connected these hooks by hand.

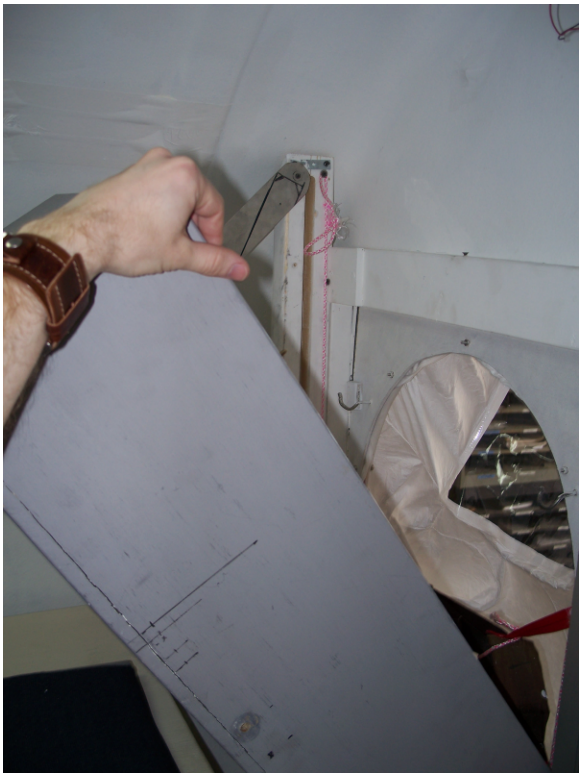

Figure 8.25: Applying a downward force to the upper PCS corner.

Figure 8.26: Misaligned Suit/PLSS Hooks

8.5.3 Suitport Modifications

Despite the low fidelity of the suitport mock-up, testing still gave insight into the potential problems that could arise as a result of using a suitport for EVAs. As soon as testing began, it was noted that the original lifting mechanism had difficulties keeping the PLSS Containment System in a workable orientation. Simplifying the PCS to a 2D model, the source of the problem is made evident. As can be seen in Figure 8.27, as θ increases, Ra must increase dramatically to maintain a constant component in the vertical direction, thus increasing Rax as well. In addition, since the PCS is not orthogonal to the guide track, Rax results in downward motion along the guide track, causing the PCS to become twisted and finally lodged in place.

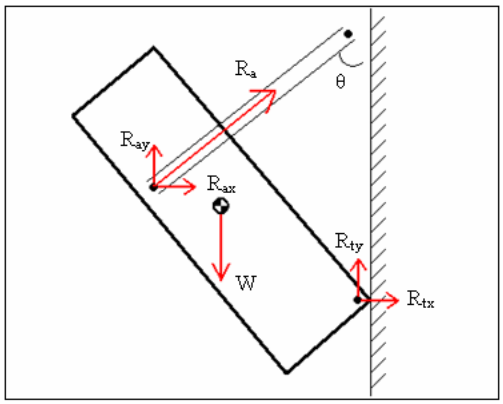

Figure 8.27: 2D PCS Free Body Diagram

A number of methods to fix these conditions were investigated. By using another track actuator opposite the original, both bottom corners could be set to the same height throughout the actuation process, but this creates other problems. In the current configuration, there is not enough room for another track actuator: the curvature of the cabin provides exactly enough room for the PCS to reach the required 0.99 meters of travel; in addition, the rotating linkage takes up the space required for this second actuator. Instead, a pair of cables could be installed through the outermost bottom edge of the PCS, as shown in Figure 8.5.3. When tension is applied to these cables, any rotation in the PCS is countered by an increase in the corressponding cable. For example, in Figure 8.5.3, when the PCS rotates counterclockwise, the red cable's tension increases, and the blue cable counters a clockwise rotation. For the mockup, approximately 90 Newtons of tension was applied to each cable, resulting in the desired effect. Using cables instead of another actuator has other advantages as well. In addition to reducing the power draw to the suitports, this technique would increase the safety of the suitport concept, because cables would be simpler to repair or replace in case of a failure, and replacements would take up less mass than a replacement actuator.

When the PCS is in the open position, a moment of approximately 260 N-m is incident upon

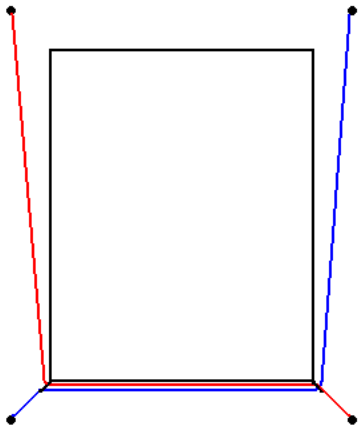

Figure 8.28: Crossed Cable Stabilizer

the lower edge of the PCS. During testing, this resulted in damage to the guide track and structure around the suitport after an extended period of time. To remedy this, a ratcheting support cable should be installed and connected to the top of the PCS, so that this load is shared between the guide track, the track actuator, and the ratchet.

As stated above, the motion of the PCS as it closes is a downward and then rotating closed movement, and likewise, while opening the PCS rotates open first, then lifts up out of the way. While this is acceptable when there are no seals involved, this movement does not meet the requirements for proper PCS mating and seals. A real suitport would first have to slide out of the seals in a completely horizontal motion and then begin rotating to open, and the reverse to open. In order to achieve this, an angled track adapter can be placed on the slider of the track actuator to translate vertical motion into horizontal motion as the PCS just begins to open or just finishes closing. To slide out the PCS a distance of 3 cm, a 4.25cm adapter would need to be installed at an angle of 45degrees. To achieve the same motion on the opposite side, the guide track would need to be curved inward the required 3 cm at the bottom of its length.

A number of changes needed to be made in the suitport design in order to accomodate the astronaut carrying out an EVA. While backing the PLSS up to the suitport, testing showed that it was difficult to insert the PLSS into the PCS based on visual cues alone. To make the process easier, a set of small guide ramps should be installed around the opening of the suitport, allowing for small errors in alignment. While entering and exiting the cabin, handholds were absolutely neccessary to help the astronaut slide into place and lower him or herself into the suit safely. In addition, a completely level floor made ingress and egress much easier. By installing locking hinged shelves onto the aft-most storage containers, the flat surface created by the storage units in the cabin can be extended to the opening of the hatch. Each shelf would have a mass of approximately 0.2 kg.

Chapter 9

Life Support

9.1 Atmosphere (Adam Mirvis)

9.1.1 Requirements

The requirements for the atmosphere for the TURTLE were derived from the following level one requirements [41]:

- The vehicle shall be capable of supporting a crew of two for two three-day sorties.
- The vehicle shall be able to provide for the crew for a 48-hour contingency period.
- The vehicle shall be capable of supporting zero pre-breathe EVAs.
- All design specifications shall be in accordance with NASA STD-3000.

Based on these requirements, the following level two requirements were derived:

- The atmosphere shall provide oxygen at a partial pressure sufficient for crew respiration.
- The atmosphere shall include inert diluent gas(es) sufficient to reduce the flammability of the cabin environment to a tolerable level.
- The atmosphere shall provide an R-factor of 1.2 or lower upon ingress to a 4.3 psi, pure oxygen atmosphere.
- Carbon dioxide shall be maintained at a partial pressure at or below the NASA STD-3000 operational limit of 0.058 psi.
- Particles larger than 0.5 μm shall be removed from the cabin atmosphere.
- Offensive odors shall be removed from the cabin atmosphere.

- The flow rate of cabin air at inlets and exits to which the crew may be exposed shall not exceed 0.2 m/s.
- The atmospheric composition shall be maintained automatically.
- The crew shall be notified of potentially hazardous atmospheric conditions.

9.1.2 Atmospheric Composition and Pressure

To provide adequate life support, the cabin atmosphere must contain sufficient oxygen for crew respiration. To eliminate the need for aclimatization, the partial pressure of oxygen in the atmosphere will be 21.3 kPa (3.09 psi), identical to the oxygen partial pressure in the Earth's atmosphere at sea level. The oxygen must be diluted with inert gas to reduce the flammability of objects inside the cabin, thus reducing the risk of fire to the crew. NASA STD-3000 recommends that the concentration of oxygen in manned spacecraft atmospheres not exceed 30% [82].

To allow for zero pre-breathe EVAs, the atmosphere must present a negligible risk of decompression sickness. The risk of decompression sickness is measured by the R-factor, defined as:

$$R = \frac{pp_{N_2,cabin}}{pp_{O_2,suit}} \tag{9.1}$$

Lower R-factors correspond to a lower risk of decompression sickness, and less severe symptoms. The R-factor of astronauts transitioning from the Space Shuttle to EVA in the EMU spacesuit is 1.67, including a pre-breathe period [55]. This has been found to be acceptable for decompression sickness in microgravity; however, it has been suggested that the physical impacts of a partial gravity environment on joint tissue, which results in more nucleation of absorbed gases in the blood, may require a more conservative choice of R-factor [104]. Assuming the spacesuit used in conjunction with the TURTLE is a pure O_2 suit, the R-factor will be solely dependent on the partial pressure of nitrogren (or other inert gas species) in the cabin atmosphere. Therefore, it is desirable to minimize the partial pressure of any single inert gas species, while still providing flammability protection by keeping down the concentration of oxygen.

One possible way to achieve both these requirements is to use a tri-mix atmosphere – one consisting of oxygen, nitrogen, and a third inert diluent, most likely neon. However, the tri-mix approach significantly increases the complexity of monitoring and maintaining a consistent atmospheric composition. While the partial pressure of oxygen can be directly measured and compared to a measurement of the total atmospheric pressure, one cannot use a simple sensor to directly measure the relative concentrations of two inert gases, such as nitrogen and neon. Therefore, a two gas atmosphere, consisting of oxygen and nitrogen, is used in the rover.

The partial pressure of nitrogen will be 33.9 kPa (4.92 psi). This results in an oxygen concentration of 34%, near the 30% concentration recommended by NASA. The resultant R-factor is 1.14.

The total atmospheric pressure is 55.2 kPa (8.0 psi), identical to the atmospheric pressure selected by NASA for the Altair lander as part of the Constellation infrastructure.

9.1.3 Storage

9.1.3.1 Cryogenic vs. Gaseous Storage

The primary design question with regard to storage of atmospheric gases is whether to use cryogenic storage. Cryogenic storage allows for lower tank mass, but also results in a high rate of boil-off of atmospheric constituents. Given the rover must carry enough atmospheric gases for the two nominal three day missions, plus the 48-hour contigency period, the amount of boil-off must be precisely known and accounted for. Given that the rover is expected to land some time before the crew, and that the exact period before the arrival of the crew is unknown, the rover would be required to carry enough oxygen and nitrogen for the longest possible waiting period. This makes cryogenic storage the more massive of the two options. Cryogenic storage also requires additional power to vaporize th gas before it can be used in an atmosphere. Therefore, the atmospheric components will be stored non-cryogenically.

9.1.3.2 Tank Material and Pressure Selection

The thickness of the spherical pressure vessels was determined according to Equation 9.2 [9]:

$$t = SF \times \frac{pr}{2\sigma} \tag{9.2}$$

in which t is thickness, p is storage pressure, r is the radius of the vessel in the middle of the shell, σ is the yield strength of the material, and SF is a factor of safety.

Two materials were compared for construction of the pressure vessels: aluminum and steel. Aluminum tanks would require 0.003 m^3 more external volume than steel tanks, which was considered a negligible cost. However, steel tanks would be 13.3 kg more massive than aluminum tanks. Therefore, aluminum was chosen as the material for the pressure tanks.

The mass and size of the storage tanks were examined over a range of storage pressures from 16 MPa to 36 MPa (2500 psi to 5000 psi). The mass of the storage tanks was not greatly affected by storage pressure over the range considered. Over this range, tank mass was found to be a nearly linear function of storage pressure, with a positive slope of 0.0253 kg/MPa, as illustrated in Figure 9.1. At a storage pressure of 31.0 MPa (4500 psi), the tanks would weigh 0.26 kg more than at a storage pressure of 20.7 MPa (3000 psi), which is a negligible difference. The total length of both spherical tanks stored next to each other as a function of pressure can be linearly approximated with a slope of -1.0cm/MPa over the range of pressures considered, as illustrated in Figure 9.1. At a storage pressure of 31.0 MPa (4500 psi), the tanks would be 10.4 cm longer, laid end to end, than at a storage pressure of 20.7 MPa (3000 psi). To minimize the area taken up on the outside of the

vehicle, a tank pressure of 31.0 MPa (4500 psi) was chosen. This is the upper end of the pressure range which can practically be achieved with this type of storage.

9.1.4 Atmospheric Maintenance

9.1.4.1 Carbon Dioxide Adsorption

A CO_2 output of 1 kg of per crew member per day was assumed [42]. This translates into 16 kg of CO_2 which must be absorbed during the duration of the mission. Due to the short mission duration and the mass restriction of the launch vehicle, it was decided to use an open-loop system for CO_2 adsorption. Two technologies were considered – lithium hydroxide canisters and alkali superoxides (KO_2)**.** Each of these reactions is exothermic, thus, no power source is required for the systems to operate.

The lithium hydroxide system captures atmospheric carbon dioxide by the following reaction [55]:

$$2LiOH + CO_2 \longrightarrow Li_2CO_3 + H_2O \tag{9.3}$$

In the superoxide system, potassium dioxide reacts with water vapor and carbon dioxide in the cabin atmosphere in the following series of reactions:

$$2KO_2(s) + H_2O(v) \longrightarrow 2KOH(s) + \frac{3}{2}O_2(g) \tag{9.4}$$

$$2KOH(s) + CO_2(g) \longrightarrow M_2CO_3(s) + H_2O(l) \tag{9.5}$$

$$2KOH(s) + 2CO_2(g) \longrightarrow 2MCO_3(s) \tag{9.6}$$

Superoxides generate oxygen for use in the cabin atmosphere, reducing the amount of oxgen which must be carried from Earth. However, the superoxide system is more massive than LiOH canisters for the same capacity of CO_2removal.

An off-the-shelf passive LiOH canister, the Micropore ExtendAir, was considered in the trade study. This product is specified as having an adsorption capacity of 0.75 kg of CO_2 per kg of LiOH. The LiOH is packaged in 4.6 kg canisters containing 3.9 kg of LiOH each [4]. Six such canisters would be required to meet the necessary total $\mathbf{CO_2}$ adsorption total for the mission, for a total system mass of 27.6 kg.

Based on heuristics from past applications, potassium dioxide was assumed to have a capacity of 0.31 kg of CO_2 per kg of KO_2, excluding packaging. The system was assumed to generate 0.38 kg of $\mathbf{O_2}$ per kg of KO_2 [55]. Based on these numbers, the KO_2 system would weigh 51.6 kg, and generate 19.6 kg of usable O_2over the duration of the mission. Because this is more O_2than is required for

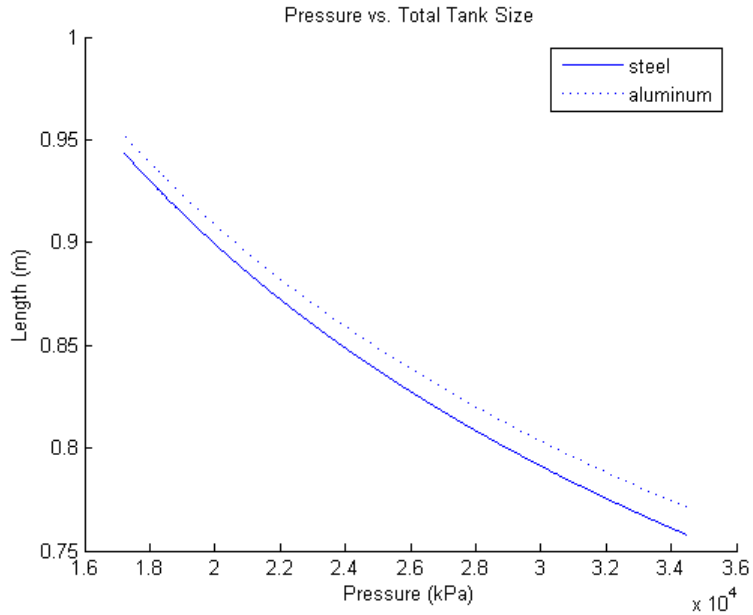

(a) Tank Length

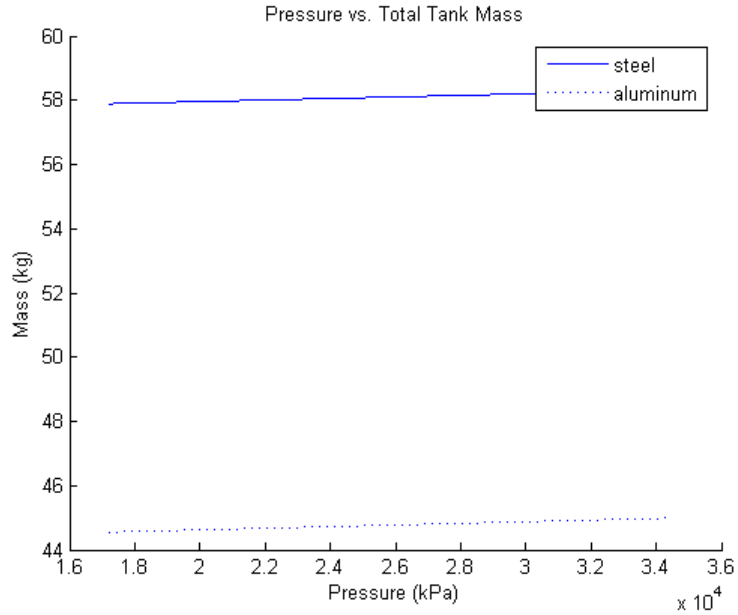

(b) Tank Mass

Figure 9.1: Total Tank Length and Mass as a Function of Pressure

the mission, the KO_2system can only be considered to save the entire required O_2mass, or 18.1 kg. Subtracting the mass saved by oxygen generation, the potassium dioxide system was found to add 33.5 kg to the launch mass of the rover. Thus, the LiOH system was found to represent a mass savings of 5.9 kg over the alkali superoxide system, even with the exclusion of the mass of packaging for the superoxide system, and the fact that a LiOH system based on the off-the-shelf product would carry slightly more CO_2 adsorption capacity than the mission requirements dictate, because of the need to carry a discrete number of canisters.

At the nominal CO_2 output rate, each LiOH canister has a lifetime of 35 hours. The LiOH canisters are used one at a time, with the active canister installed manually by the crew into the air handling system described in section 9.1.4.2, and the full and empty canisters stowed in the cabin. Because the LiOH canisters do not have to used in their entirety at one time, canister replacement can be scheduled to conveniently coincide with daily scheduled crew tasks. For the nominal six-day mission, the crew will exchange the active LiOH canister every 24 hours, stowing the canisters with remaining capacity for use at the end of the mission, if necessary.

9.1.4.2 Air handling

The TURTLE air handling system is responsible for CO_2, odor, and particulate removal, and maintenance of a comfortable temperature inside the crew cabin. Odor removal is accomplished by means of an activated charcoal filter. Particulate control is accomplished by means of a HEPA filter, in order to remove particles as small as 0.5 μm as required by NASA STD-3000 [82]. Excess heat is removed by a heat exchanger located in the ceiling of the cabin. The air handling system is diagrammed in figure 9.2. Figure 9.3 illustrates the location and layout of the air handling system in the cabin. The air flow rate through the air handling system is dictated by the requirements of the CO_2 scrubbing system.

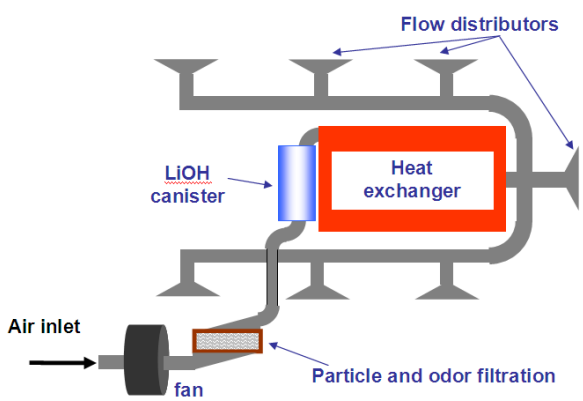

Figure 9.2: Air handling system

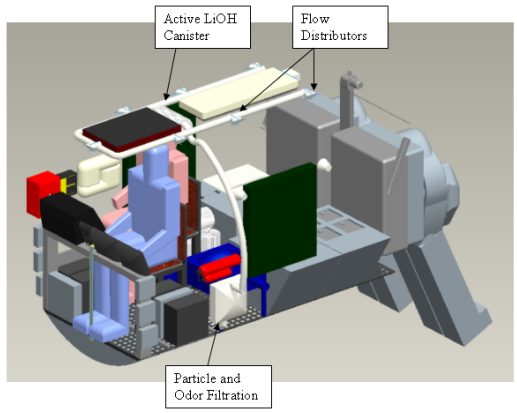

Figure 9.3: Air handling system layout in cabin

CO_2removal is handled by means of the LiOH system described in section 9.1.4.1. NASA STD-3000 recommends an operational maximum CO_2partial pressure of 0.40 kPa (0.058 psi) [82]. Based on the 55.2 kPa (8.0 psi) atmosphere in the cabin, and applying a safety factor of 2, the TURTLE will operate with a CO_2 concentration of 0.36%. The use of a safety factor allows variations in CO_2 output, such as may occur after EVAs, when the crew has just spent a significant period of time exerting themselves, and are likely to be breathing at an increased rate.

Based on a heuristic of 1 kg of CO_2 produced per crew member per day [42], the LiOH system must remove 2.315×10^{-5} kg of CO_2 per second from the cabin atmosphere. The mass flow rate through the air system can be found by the following equation:

$$\dot{m} = \frac{\dot{m_{CO_2}}}{f_a \times conc_{CO_2}} \tag{9.7}$$

where $\dot{m_{CO_2}}$ is the mass flow rate of CO_2 produced by the crew, f_a is the fraction of CO_2adsorbed by the LiOH canister as air is passed through it, and $conc_{CO_2}$ is the concentration of CO_2 in the cabin atmosphere. For an adsorption fraction of 0.25, the mass flow rate through the air system is 2.55×10^{-2} kg/s. The volumetric flow rate can be found by the following equation:

$$\dot{V} = \frac{\left(\frac{\dot{m}}{M}\right) RT}{P_{tot}} \tag{9.8}$$

where M is the average molar mass of the cabin atmosphere, R is the ideal gas constant, T is the cabin temperature, and P_{tot} is the total pressure of the cabin atmosphere. To maintain the desired CO_2partial pressure, the volumetric flow rate through the air handling system is 0.0388 m^3 per second.

NASA STD-3000 requires that air velocities not exceed 0.2 m/s at inlets and outlets which the

crew may be exposed to. To meet this requirement, the inlet of the air handling system is located below the floor of the rover, where it is inaccessible to the crew.

To determine the power required for the blower fan, a heuristic was generated from a selection of fans with similar volumetric flow rates [2]. The data is displayed in table 9.1. The power required for the fan as a function of the volumetric flow rate was found to be approximated by the function $P = 150.5\dot{V} + 10.2$, where P is the power of the fan in watts, and $\dot{V}$ is the volumetric flow rate in m^3/s.

Table 9.1: Fan data used to generate power heuristic

Power (W)	**Flow rate (CFM)**	**Flow rate ($\times 10^{-2}$m^3/s)**
8.05	21	0.99
19.55	23	1.08
11.5	36	1.70
23	36	1.70
13.8	45	2.12
11.5	52	2.45
8.05	59	2.78
11.5	79	3.73
20.7	80	3.78
10.35	56	2.64
11.5	71	3.35
18.4	106	5.00
16.1	106	5.00
17.25	121	5.71
26.45	159	7.50

Based on this heuristic, the air entering the system will need to be accelerated to the necessary flow rate by a 16.0 W fan. The air then passes through an activated charcoal odor filter and 0.5 μm particle filter, through the active LiOH canister, through the heat exchanger, and is then released into the cabin by a series of distributors.

The distributors are designed to accomplish two goals – first, to promote circulation and mixing of the cabin atmosphere (thus minimizing CO_2pooling), and second, to reduce the velocity of the air to 0.2 m/s as required by NASA STD-3000. The exit velocity from the air handling system is found by the equation $v_{ex} = \frac{\dot{V}}{A_{ex}}$, where $\dot{V}$ is the volumetric flow rate through the air handling system, and A_{ex} is the total cross-sectional area at the exit of the distributors. With a series of seven distributors throughout the ceiling of the cabin, each distributor must have an area of 0.0242 m^2.

9.1.4.3 Monitoring and Control

The atmospheric composition is monitored by redundant pressure sensors, O_2 sensors, CO_2 sensors, and sensors for toxic gases such as carbon monoxide which may be generated by equipment in the cabin. The computer is responsible for monitoring these sensors, and adjusting the regulators on the atmospheric gas storage tanks as necessary to maintain the nominal composition. The computer will alert the crew to potentially dangerous levels of carbon dioxide or toxic gases. The computer will also monitor pressure sensors inside the storage tanks, and will alert the crew if the pressures in the tanks are below the expected levels at any point during the mission.

9.2 Radiation Environment (Tiffany Russell)

The lunar surface is bombarded with radiation from Galactic Cosmic Ray's (GCR) and Solar Particle Events (SPEs). The GCR is a constant, low dose of radiation that is present above the lunar soil. Chronic exposure for long durations can cause health concerns and must be within career dose limits set by the National Council on Radiation Protection (NCRP) as defined in Table 9.2 [45]. SPEs are mostly a result of Coronal Mass Ejections (CMEs) from the Sun. They are a source of large amounts of high energy heavy particles and depending on intensity, immediate exposure can cause severe health issues. The SPEs can travel through body tissue and mutate the genetic structure. These mutations, given time, can develop into various cases of cancer. In order to protect from the majority of radiation exposure expected on the lunar surface, the rover must consist of high density materials to block the GCR and an additional layer of a high density substance to protect against a SPE. The astronauts will be required to carry a dosimeter that displays the current radiation levels and accumulated mission exposure. According to the NCRP, career exposure is dependent upon the gender and age of the astronaut as shown in Table 9.3 [45]. Therefore, each dosimeter will be custom designed to monitor the levels of a particular astronaut. On a ten day mission on the lunar surface, it was calculated that the astronauts are expected to be exposed to 21.3 cSv worth of GCR and solar energetic particles without any shielding. (See Table 9.4 [45]) For a 25 year old female, who has the lowest allowable radiation dosage limit, she will have been exposed to 25% of her career dosage limit. Therefore, the amount of radiation exposure during the mission will be within limits regardless of radiation shielding.

Table 9.2: Dose Equivalent Limits, NCRP recommendations (Sv)

	Blood Forming Organs	Bone Marrow	Eye	Skin
Career	Age Dependent	0.5	4.0	6.0
1 year	0.5	0.5	2.0	3.0
30 days	0.25	0.25	1.0	1.5

Table 9.3: Career Dose Equivalent Limits (Sv)

Age	25	35	45	55
Male	1.5	2.5	3.2	4.0
Female	1.0	1.75	2.5	3.0

Table 9.4: For 10 days on the lunar surface (cSv)

Type	With Shielding	Without Shielding
GCR	0.3	0.8
SEP	7.5	20.5
Mission	7.8	21.3

9.3 Radiation Protection (Ali Husain)

According to the manned systems integration standard [82] the requirement to limit radiation exposure falls under the generalized ALARA (as low as reasonably achievable) principle. As such the design considerations that were involved do not necessarily represent an optimum however they are dictated by practical considerations.

The presence of galactic cosmic radiation (GCR) and its potential for latent effects (i.e. long term cancer) is a primary concern for astronauts on the lunar surface. To mitigate these effects the potable water tanks were placed in a hemi-cylindrical shell on the roof on the interior of the cabin. The 2.5 g / cm^2 areal density reduces the radiation absorption to well within career limits [75]. Although this measure seems redundant since even unshielded astronauts would not violate their career exposure limits on the lunar surface the motivation was that even the 30% decrease in dose equivalence (cSV) [75] would be sufficient to warrant the design change.

The problem of solar particle events (SPE) is more involved. SPE are a known issue with regard to manned spaceflight and an accurate forecast model is a near term goal for NASA [81]. Without sufficient warning of an impending coronal mass ejection (CME) astronauts risk being caught unaware of potentially lethal circumstances.

The TURTLE midrange rover does not posses sufficient mass and energy margins to adequately shield against a $+3\sigma$ SPE. However since the statistical likelihood of a SPE occurring during a nominal 1-week mission during times of peak solar activity is 0.4% [26] it cannot be certified that the crew has a 99.9% chance of survival. This dictates the requirement of contingency scenarios in the event of an SPE.

The two general contingency scenarios are dependant on the location of the sun with respect to the lunar horizon. If the sun is high in the sky the contingency solution for the astronauts requires them to exit the rover and climb underneath the chassis. This will provide them with an

estimated 20 g/cm^2 of areal density and greatly increases their chance of survival. Of course the high radiation dose would require them to abort the remainder of the mission and return home at once.

The second scenario provides better protection for the crew. If the sun is at low angles on the horizon the crew needs to find large boulders, cliffs or craters for protection. A depth of 50 cm of idealized lunar regolith would provide sufficient attenuation against even an August 1972 class CME; the worst on record [45]. Assuming an average density of 1.5 g/cm^2 the fluence rate of energized solar particles would be reflected or stopped in the lunar regolith. Figure 9.4 illustrates this concept.

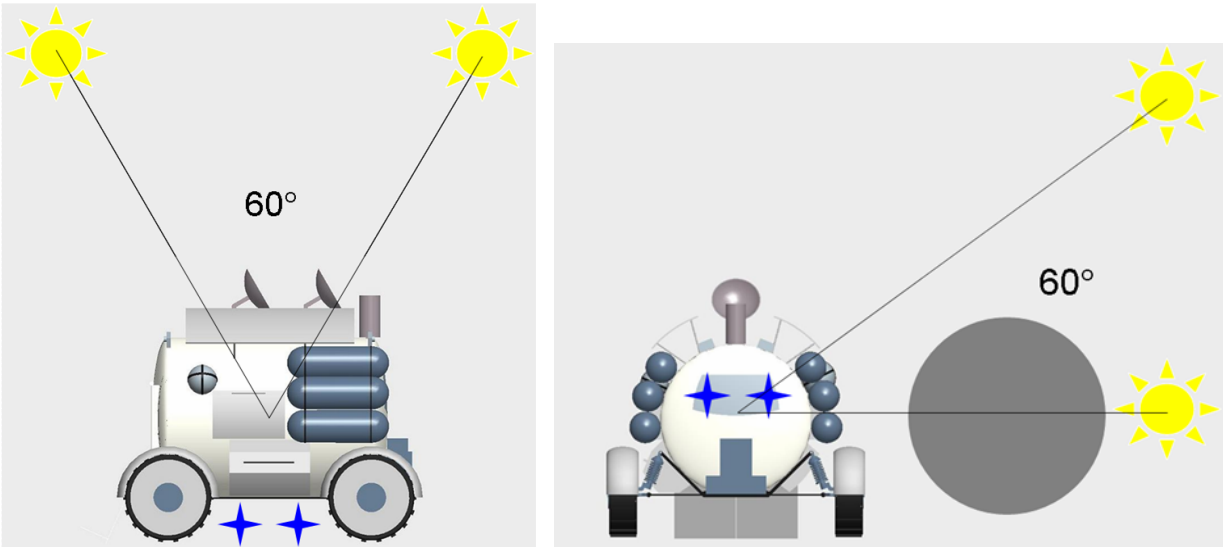

(a) High Angles.

(b) Low Angles.

Figure 9.4: Sun at Different Angles

In addition to the aforementioned considerations, the flight schedule dictates a launch in 2020 which corresponds to an 11-year solar activity minimum [81]. Although this provides further justification for the TURTLE expedition this fact was not a driving design consideration.

9.4 Safety (Jason Laing)

While designing the interior of the rover, safety of the crew was always held in highest regard. All systems were designed to meet NASA-STD-3000. Within these guidelines, four main areas of concern existed: Fire risks, electrical hazards, mechanical or material hazards, and procedural hazards.

When investigating the fire hazards within the cabin, the atmospheric makeup was one of the first areas of scrutiny. In order to meet the zero-prebreathe requirement for entering and exiting

the cabin, partial pressure of oxygen was determined to be greater than the NASA-reccomended value of 30%. Currently, the lander designed for use with the constellation program has a similar atmospheric makeup. While this atmosphere is not ideal for reducing flammability, other measures can be taken to reduce the overall fire risk within the cabin. For example, clothing used by astronauts can comprised of cottons treated with borates such as $NaBO_2$ or $Na_2B_4O_7$. Unlike synthetics such as nylon or polyester, cotton will not fuse to skin upon burning, and a borate treatment will greatly reduce flammability [51]. While such a borate treatment will wear off after repeated washings, clothing within the rover will not be subjected to laundering. Lighting within the cabin is low heat emitting fluorescent bulbs, reducing the risk of fire due to materials accidentally coming into contact with bulb surfaces. Finally, fire detectors will be incorporated into the cabin warning system, and sensors on atmospheric particulate filters will monitor for smoke. In addition, procedures have been laid out for astronauts to follow in case of a fire within the cabin.

In the event that a fire breaks out within the cabin, the size of the fire will dictate the procedures to be followed by the crew. A small fire, such as one with a volume less than a few cubic inches would be best extinguished by the crew. In this case, supplemental oxygen masks would be donned by the crew, and the proper fire extinguisher (as described below) would be retrieved from its storage location. After extinguishing the fire, a towel would be used to clean residue from the cabin interior, and an evaluation of cabin equipment can begin. All damaged items would have to be noted and a summary of all damage would be conveyed to a ground crew to begin returning the cabin to safe operating conditions. A fire larger than a cubic foot, or a fire that is especially fast moving, would require crew members to take more drastic measures. Again, supplemental oxygen masks would be donned, but in this case astronauts would move immediately to the suitports and begin EVA procedures. Supplemental oxygen masks would be removed before closing the PCS, and astronauts would evacuate the rover. From the exterior, the crew would deactivate the oxygen supply to the interior of the cabin, and using the small supplemental airlock, the cabin would then be vented to vacuum. While this measure would not prevent extensive damage from occuring within the cabin, it would extinguish any small lingering fires that could pose a danger to the crew upon re-entering the cabin. Upon reactivating the oxygen supply to the cabin, indicators placed externally would indicate if a proper pressure differential had been established, and if particulate levels within the cabin were acceptible. If so, astronauts could then re-enter the cabin and carry out the same evaluation procedure used in case of a small fire. If the interior of the cabin was not safe for re-entry, the crew would attach to the external driving station and make their way back to the lander or outpost.

NASA-STD-3000 indicates that CO_2, Halon 1301, and water vapor extinguishers are good choices for space vehicles [82], but the situations described in the standards document do not perfectly match up with the circumstances that TURTLE will be subject to. STD-3000 plans mostly for microgravity situations, such as vehicles in low earth orbit, with larger volumes than this rover.

The small size of the rover makes CO_2 a poor choice, as increasing the carbon dioxide inside the cabin would place a strain on the LiOH filtering system. Halon 1301 is primarily designed for situations where an entire area can be flooded with the gas, such as experimental chambers on ISS. In extinguishing fires, Halon 1301 also gives off harmful gasses, including hydrogen bromide and hydrogen fluoride. A water vapor fire extinguisher would be an appropriate choice for class A given that the mist emitted is fine enough to not cause any adverse reactions with electrical systems. A potassium bicarbonate or sodium bicarbonate extinguisher would be ideal for class B and C fires (liquids and electronics), and a water based foming agent (such as Fireade2000, given appropriate flight testing) would be ideal for class A and B fires (combustibles and liquids). Potassium bicarbonate or sodium bicarbonate are minimally toxic, causing only mild and temporary eye irritation. A water based foaming agent such as Fireade2000 is nontoxic and non-corrosive.

Electrical systems on TURTLE are safe for human use, as they are insulated and covered properly, and all cabin components exposed to the crew are at ground potential. Circuit breakers are available for the crew to access beneath the walkway of the rover and on the exterior, allowing for components to be shut down for repair or maintenance or rebooted in case of failure. Any system with currents and voltages are above "let-go thresholds" have three independant controls to drop currents below these levels when a crew member is exposed to the circuit.

All mechanical systems inside the cabin are designed for crew safety, with curved, rolled, or filleted corners and edges, secure storage measures, and warnings around any moving parts. However the cable modifications that have been made to the suitports are energy storing devices, and are therefore undesirable. However, some factors mitigate this situation. The crossed cables used for suitport leveling can be almost entirely contained within the mechanism of the suitport, and the ratcheting cables are located above the PCSs, and are only under strain when the suitport is in use. In this situation, the astronaut would be below the PCS, shielded in the event of a cable breakage.

9.5 Medical Support (Tiffany Russell)

The rover will be able to support all minor injury and medical complications that may occur during the mission for two astronauts. The medical materials will be a smaller replica of the medical materials carried on the current Space Shuttle. Unless an injury is deemed mission terminating, all medical procedures will be performed in the rover. The mass of the medical kit will be 5 kg for the main unit and 2.5 kg for the Emergency Automated External Defibrillator (AED). The kit and the AED will be located at the front of the rover to the right of the driving station and mounted onto the wall. However, the kit and AED are portable by releasing the locked wall mounts. See Figure 9.5

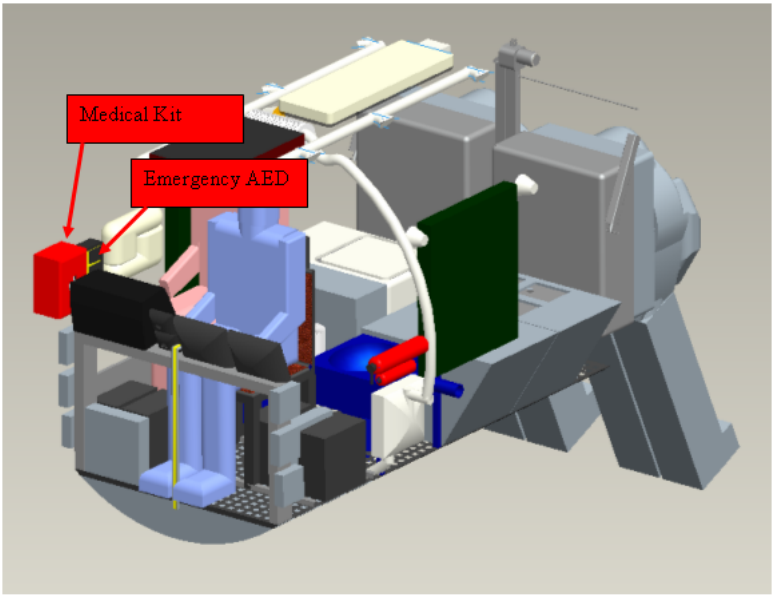

Figure 9.5: Medical Equipment Location

9.5.1 Medical Kit

The kit will house all medical supplies for basic first aid, sterilization and medicinal applications. The sterile materials include suture materials and several various sized syringes. Aspirin, ibuprofen, and local anesthetics will be used to relieve pain and antihistamines will be on hand for allergic reactions. For more extensive injuries, there will be splints, braces, and small oxygen masks. An additional emergency ophthalmic bulb will be available in the lighting storage unit in case of additional lighting needed to perform medical tasks. This light bulb can be substituted into any of the four supplemental lighting fixtures that are adjustable.

Both astronauts will be trained to handle emergency medical conditions that may occur during the mission. The two most common forms of ailment that are expected on the mission are decompression sickness, radiation exposure, and dehydration. The atmospheric composition and pressure is designed to minimize the occurrence of decompression sickness during ingress and egress between the pressurized rover and the EVA suit. In case of radiation exposure, anti-emetics for nausea and vomiting will be available. Even in the case of a large radiation dose, the symptoms of radiation poisoning occur at least 24 hours after the initial exposure. Therefore, the astronauts should be in transit back to Earth to receive proper medical treatment.

Due to the extraneous physical activities of EVA's, extra fluid will be on hand to treat mild to severe cases of dehydration. In case of heart failure, the crew will be expected to perform cardiopulmonary resuscitation (CPR) and the basic life support ABCs: airway, breathing, circulation.

9.6 Nutrition (Ali Husain)

With the exception of very early spaceflights, there has been a need to provide adequate nutrition to astronauts for the duration of their mission. The sophistication of nutritional systems has evolved from simply providing calories to give the astronauts energy to diverse food selection and customized nutrient schedules.

Some of the challenges that have plagued food systems in the past are obviously mass and weight. However food systems are highly configurable by changing basic parameters such as hydration level or food variety. The top level design considerations for the food system were minimizing mass and volume and providing ample nutrition for the generalized lunar mission.

When considering the design for the TURTLE expedition the overall architecture was modeled after Space Shuttle food system. This was for two primary reasons: feedback from astronauts indicated that for short and medium duration missions the variety of foods available were satisfactory, and the mass and volume requirements were within tolerable limits. Shuttle-type food systems require 1.8 kg / person-day at 4,045 cm^3 / p-d while ISS-type systems require 2.38 kg / p-d and 6,570 cm^3 / p-d. The added volume is the result of some fresh produce available to the ISS and long-duration considerations result in a higher package mass. [76]

Although in future planetary missions bioregenerative food systems (i.e. simple crops) will likely be integrated into food systems the sortie style of the TURTLE expedition prohibits consideration of crop cultivation and harvest. Initial investigation demonstrated the volume and energy requirements to be orders of magnitude higher than what is available.[77][55]

When considering hydration level of the foods a trade study was performed to determine the most efficient solutions. The two variables were mass savings and time required by the crew for food preparation. Unless the food is fully hydrated the time crews spend for food preparation is unchanged with the hydration level. Meaning the time penalty for preparing 80% hydrated food as opposed to 20% in negligible. With this in mind it was decided that a hydration level of 9% would be optimal and result in a mass savings of 33 kg, if considering fully hydrated food. Lower hydration levels are impractical and sacrifice the overall quality of food. [76]

The nutrient profile for the sortie mission was constructed using the World Health Organization's recommendations for a 95th percentile male with a high physical activity level (PAL). The basal metabolic rate consists of 40-70 percent of energy expenditure in humans. A conservative value corresponding to males age 18-30 was used and considered with a PAL of 2.4. Although astronauts are generally older and high PAL values are difficult to maintain over long durations this analysis was deemed sufficient for this level of design because of its conservative nature. Furthermore, these values are for earth-based lifestyles and do not take into account the rigors of EVA. The above parameters result in an overall energy requirement of 11,906 kJ/p-d. The nutrient summary is shown below [86].

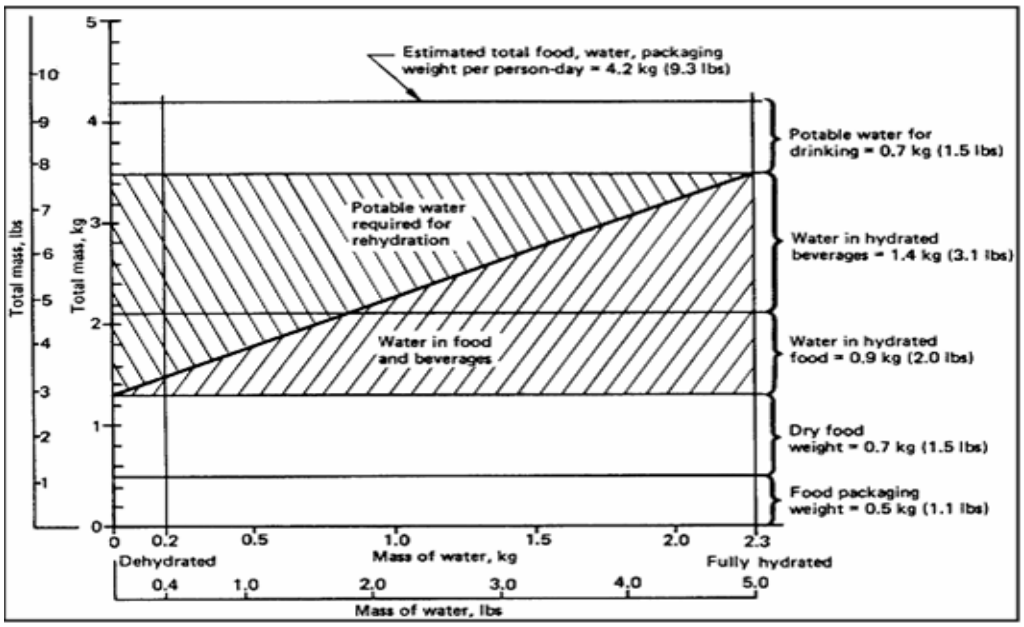

Figure 9.6: Hydration Level and Overall Mass of Food System.[82]

Table 9.5: Nutrient Summary

energy	11906	[kJ/d]	
protein	111	[g/d]	15.50%
carbohydrates	413.3	[g/d]	58.10%
fat	83.2	[g/d]	26.40%
calcium	900	[mg/d]	
magnesium	350	[mg/d]	
potassium	3500	[mg/d]	
phosphorous	900	[mg/d]	
Vitamin A	3	[mg/d]	
Vitamin E	30	[mg/d]	
Vitamin C	150	[mg/d]	
Folic acid	0.2	[mg/d]	
Beta-carotene	15	[mg/d]	
Rutin	75	[mg/d]	

Micronutrients and antioxidant supplements were included in order to reduce the oxidative stress of the lunar radiation environment. Ionizing radiation introduces free radicals in organisms which can damage DNA transcription mechanisms and cell nuclei. The effects of radiation can be ameliorated with additive antioxidants to reduce the radiosensitivity of human cells. Recent studies have shown that the above combination of nutrients is protective in the deep space environment [86].

Chapter 10

Avionics

10.1 Command and Data Handling (Michael Levashov)

The Command and Data Handling system connects together every device in the rover that needs to transmit data or to be controlled by the computer.

10.1.1 Data System Requirements

A failure in communication between the rover devices can result in loss of rover functions, loss of the mission, or the loss of crew. This places very strict requirements on the reliability of the system. The architecture of the system should be optimized to achieve reliable operation. The system needs to be radiation hardened, so that radiation will not introduce significant noise or damage the electronics. It is preferable to stay away from chain configurations, because a failure of a link in the chain would result in overall system failure. Master/Slave configurations are not optimal, because they rely on reliable operation of the Master.

In addition, the network is used to control the vehicle during landing, for which fast-rate, predictable communication is desired. To ensure optimal performance of the controller the data should come in at predictable intervals, the network should be deterministic (real-time).

Finally, the command and data handling is responsible for the high-bandwidth communications, including recording and transmitting HDTV video. Doing this requires between 10 and 100 Mbps data rates.

10.1.2 Interface Bus Selection

(Michael Levashov and Dru Ellsberry)

A number of candidates were investigated for use as the system architecture. Table 10.1 shows some of the alternatives.

Table 10.1: Network Solutions

	Bandwidth (Mbps)	Real Time	Topology	Fault Tolerance	Master/ Slave	Used in Spacecraft
AFDX (ARINC-664)	100 (1000)	Yes	Hub	Yes	No	Planned
FireWire	800	Yes	Chain	No	Yes	Planned
MIL-STD 1553(1773)	1	Yes	Chain	Yes	Yes	Yes
Ethernet	100 (1000)	No	Hub	No	No	No
USB	480	No	Hub	No	Yes	No
SpaceWire (IEEE 1355)	200 (400)	Yes	Chain	Yes	Yes	Yes

Only the AFDX system, also known as ARINC-664 satisfies the bandwidth, real-time, and reliability requirements. The only problem with this system is that, unlike many of those listed, it has never been flown to space before.

10.1.3 AFDX Description

AFDX or ARINC-664 is a real-time variation of Ethernet with a built-in quality of service[109]. It was originally developed for use in aviation and is employed on the new generation of commercial aircraft, including both the A380 and Boeing 787. The system is currently being investigated by NASA for use in space systems. It is a decentralized system, where the nodes are physically connected together by two sets of copper wires and actually send the commands over both wires simultaneously. This creates a layer of redundancy not typically seen with Ethernet, which is what makes the system well-suited for aerospace applications.

All of the devices in the rover are connected to one of four AFDX switches in a way that attempts to minimize wiring. Each device in the rover has its own AFDX interface either integrated into the device or next to the switch location. A device can communicate with any electronic device in the system by referring to a unique address assigned to each element on the network.

Note that because of the hub style of the network a failure of a single device or AFDX interface will not bring down the whole network, the computers will just have to refer to a different address of its backup. However, this does rely on the successful operation of the AFDX switches. Over a 30 day period, the reliability of an AFDX switch is 0.993 [74]. This is below the requirement of 0.999 total for crew survival. In addition, the TRL is approximately 5, since the system has only been tested in Earth high-altitude conditions However, since the system is being adapted by NASA for use with space applications including manned missions, both the reliability and TRL are expected to go up. It is assumed that in the timeframe of this project the system will improve to reach the necessary reliability levels or another system of equivalent performance will be available.

Spare switches are available to replace the active ones in case of failure.

10.1.4 Distributed Computing Units

Many systems inside the rover require active low-level control, whether high or low bandwidth, and are only affected by other systems in emergencies. Intercorrelated error rates can be decreased, overall reliability improved, and some of the load can be taken off the AFDX bus if the control loops are run locally. Therefore, certain systems, in particular those critical to crew health, are directly run by a number of Distributed Computing Units (DCUs). These include:

- Air circulation and partial gas pressures
- Internal temperature
- Fuel cell and power control
- Motor control

Each one of the units consists of a redundant pair of radiation-hardened FPGAs and interface boards which contain A/D and D/A converters as well as digital interfaces. Recent advances in FPGA technology allow them to withstand radiation doses above 300 krads, making them suitable for almost all space applications. FPGAs were chosen for the controllers, because they are highly adaptable for the task, to minimize the amount of power needed to run each control loop. The main computer can monitor the systems by requesting the current state. It can also adjacent parameters of the control loop as constants in the DCU memory.

In each pair, the FPGAs constantly monitor each other and report on any failures. In case of a failure, spare units are available and are easily replaceable from the inside of the cabin. For the periods of FPGA failure, the main computer is capable of taking over the control of their systems. In addition, a panel with hard-wired switches can be used to override the control of some life-critical functions of the systems in case a DCU fails.

10.1.5 Command and Data Handling Diagrams

As mentioned, all of the devices are connected to one of the four switches inside the rover. For presentation purposes the following figures show only parts of the network. The location of the AFDX switches is indicated in each figure. The position of each device in the gray square roughly corresponds to its position inside the rover, with the rover front being at the top of the page.

10.1.5.1 High Bandwidth Devices

Figure 10.1 shows the connections between the highest-bandwidth devices inside the rover.

All of the CPUs are connected to one switch so that they can communicate almost directly to minimize the information flowing through the network. On the same switch are the Ka-band transceiver, which are the high data rate communications with Earth and the Mass Memory. The

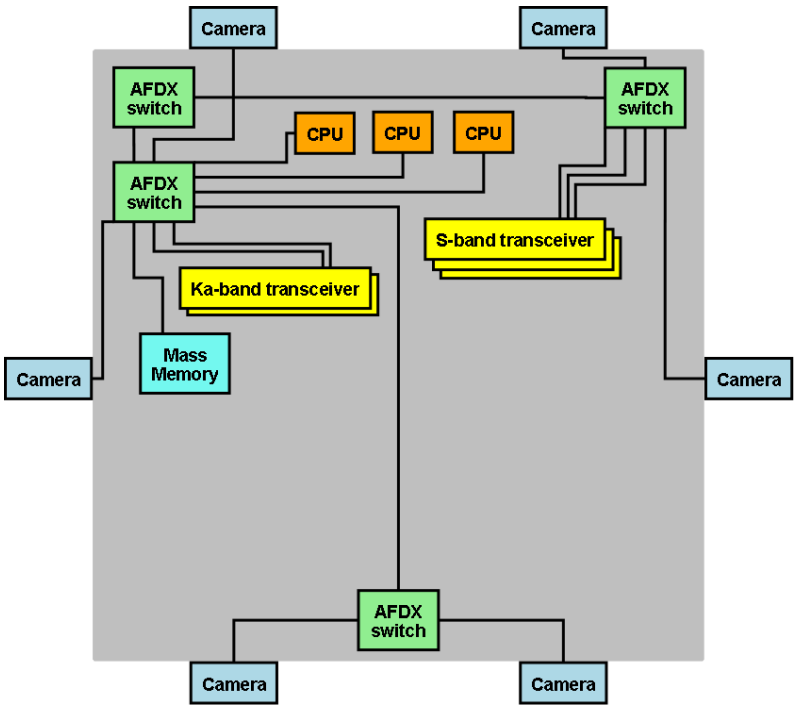

Figure 10.1: High Bandwidth Devices

Mass memory is used to store large amounts of data from the cameras before it can be transmitted to Earth.

The black lines connecting all devices in the figure are the redundant AFDX data cables. The connections between the AFDX switches are suppressed in all of the following diagrams.

10.1.5.2 Life Support

Figure 10.2 shows the life-critical systems being run by the DCU's.

Black lines are AFDX cables, as before. Green lines are analog shielded cables. Blue lines are for digital data, although specific types of digital communication were not selected. Note that a single box might represent multiple sensors or actuators and a single line to them might actually be multiple cables.

The DCU in the top left is responsible for controlling the fuel cells. It reads the tank pressures of Oxygen and Hydrogen, senses the valve positions and flow rates from the tank and through the fuel cell, measures the voltages and power output by the cell and the DC/DC converter. It then controls the valves in the tanks and the fuel cell, as well as the DC/DC converter to keep the rover supplied with power.

The DCU on the top right is responsible for maintaining the temperature inside the cabin. It monitors the radiator, heat exchanger and cabin temperatures and runs the compressor to keep the

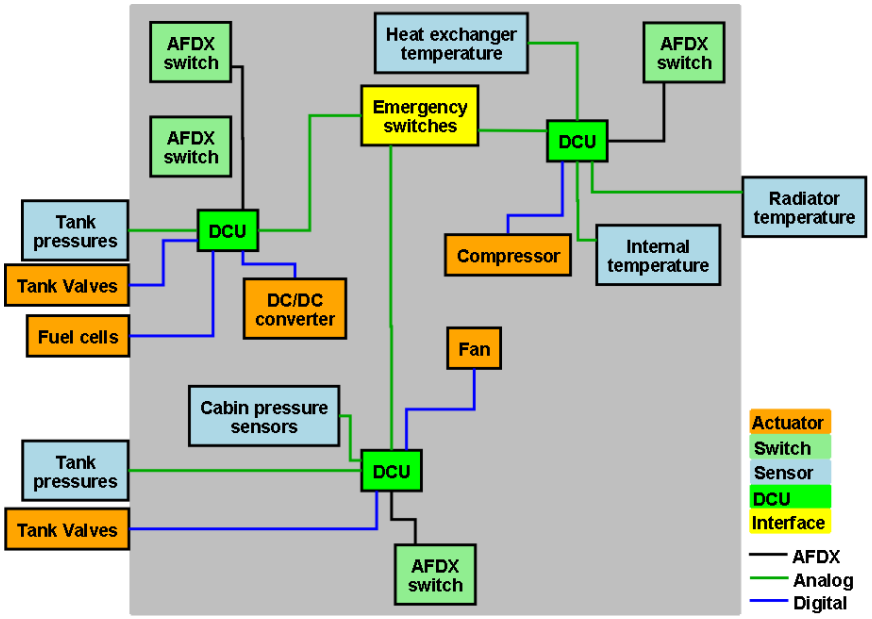

Figure 10.2: Life-critical systems

internal temperature as close to the desired value as possible, while keeping radiator temperatures within operating range.

The bottom DCU maintains the optimal atmosphere within the cabin. It monitors the tank pressures as well as the internal partial pressures and controls the fan as well as the oxygen and nitrogen tank valves.

Note that all 3 DCU's are connected to electrical switches, which are capable of overriding DCU commands in case of an emergency.

10.1.5.3 Motor System

Figure 10.3 shows the connections between the motors and the motor drivers in the system.

The red lines are power wires to the motors. The blue lines are digital lines either to the Hall sensors, which have a local A/D or to the motor drivers from the DCU.

There are 6 motor drivers in the vehicle for redundancy. The DCU sends commands to four of them and uses them to monitor whether the command gets executed properly. If not, it selects another motor to send the command to and uses the high-power multiplexer to reconnect the motor drivers to their respective motors.

The system relies on the reliability of the high-power multiplexer, which shouldn't be a problem, because it is not a complex device.

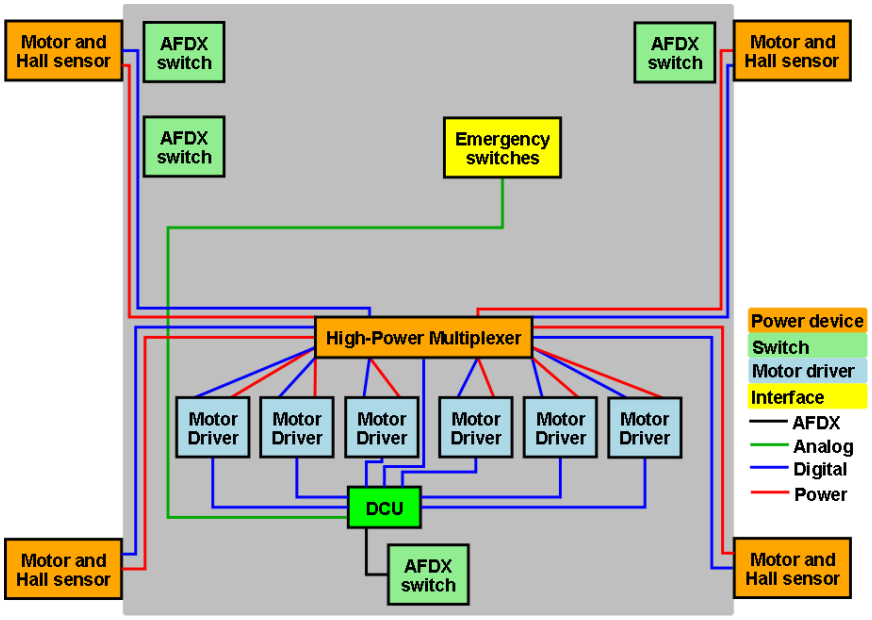

Figure 10.3: Control of motors

Not shown here is the steering system, which runs directly parallel to the driving system. It uses the same DCU, but it uses a set of motor controllers instead of motor drivers to run a servo motor next to each one of the wheels.

Electrical switches are attached to the DCU for emergency shutdown of the system.

10.1.5.4 Human Interfaces

Figure 10.4 shows the human interfaces inside the rover.

The figure shows the location of the CPU's to indicate that the displays are connected to them directly. This is to avoid the high bandwidth video data from being constantly sent across the network. The displays are still attached to the AFDX network to control their settings, get feedback from touch-screens as well as to send data in the case of a CPU-display connection failure or of a CPU failure.

There is a joystick and 2 keypads indicated in the diagram, although the final number of keypads may changes depending in adjustments in console configuration.

The joystick and the display at the bottom of the figure are for the external driving platform.

10.1.5.5 Other Sensors and Actuators

Figure 10.5 shows a variety of sensors used for landing and driving (yellow) as well as vehicle state monitoring (light blue).

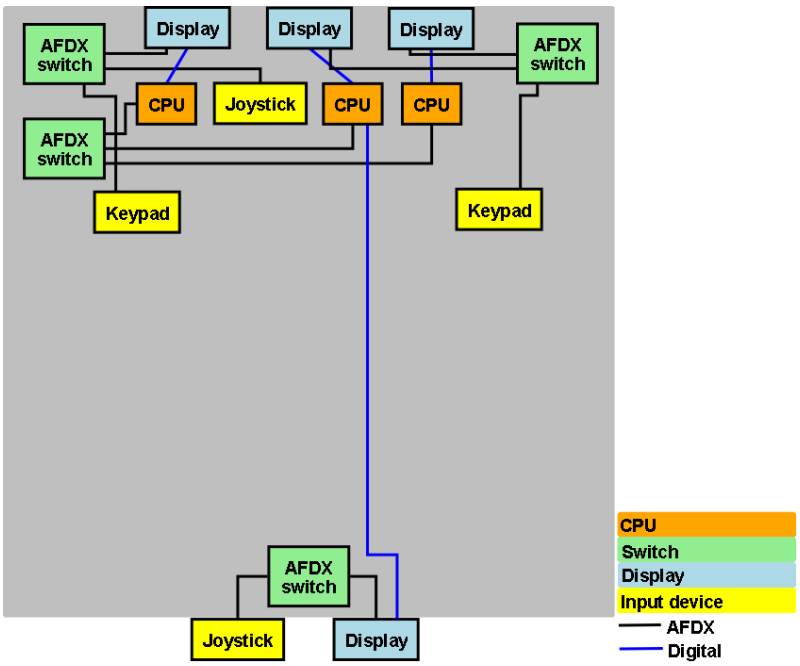

Figure 10.4: Human interfaces

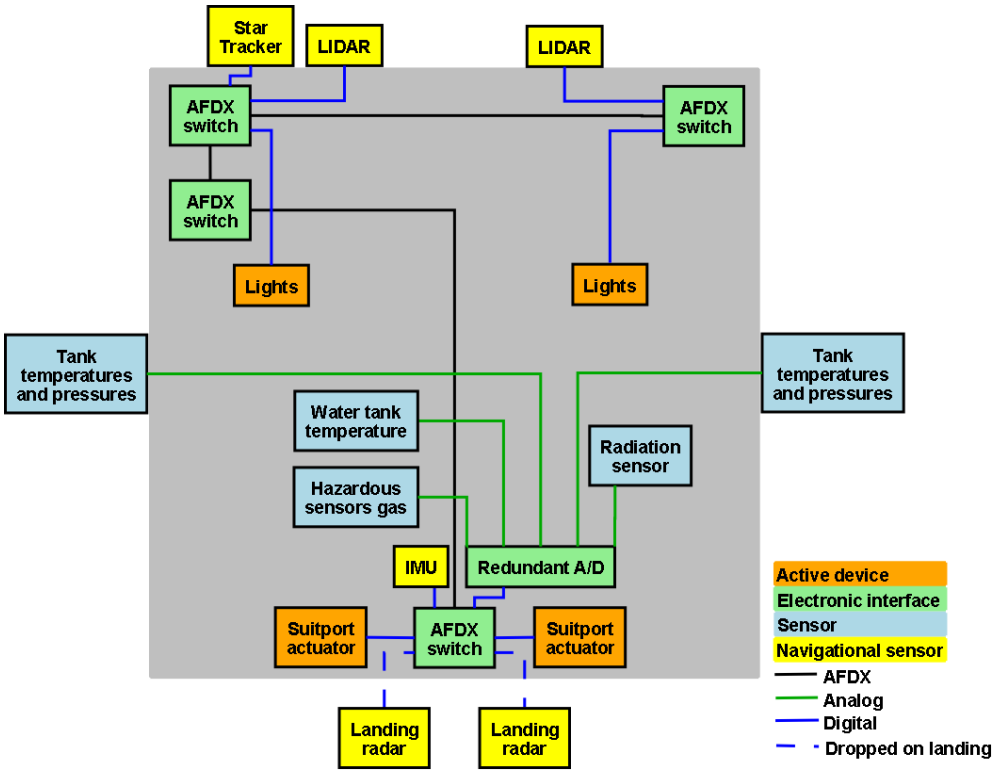

Figure 10.5: Other Sensors and Actuators

The dashed blue lines next to the landing radars indicate that the sensors are used during the transfer to the Moon, but are de-attached once the vehicle separates from the lander.

As before, a light blue box might actually represent multiple analog sensors. They are read by an A/D converter. Redundancy is achieved by having multiple sensors and multiple A/D channels for each reading. A number of alarms in the vehicle can be activated based on the reading of these sensors.

The suitport actuators as well as the internal and external lights are also shown in the figure and are directly controlled by the CPU's. Manual buttons controlling the suitport are not indicated in the figure.

10.1.6 Data Storage

High data rate communications with Earth will not always be available, in particular when the vehicle is in motion. During that time the data from the cameras and the logs of all systems in the vehicle will be recorded to memory. Once the vehicle has stopped and high data rate communication is established, the data will be transferred to Earth.

Temperature, pressure, valve position, voltage data and all other data logged about the state of the rover has a relatively low data rate compared to the amount of space occupied by constantly taking video with the cameras. A conservative estimate gives 50 kbits/s upper bound on the amount of data generated by logging all sensors at up to 50 Hz rate. This comes out to 180 Mbits/hour and 21.6 Gbits for the entire mission.

In contrast, constantly taking video with 6 HD cameras can generate 210 Gbits in just an hour. This is a data rate of 58 Mbits/s and can be managed by the AFDX bus. Assuming a worst-case scenario of an equivalent of 2 hours of constantly taking video with 6 cameras gives 430 Gbits of data to transmit. If one camera is operating on average, it will take 12 hours to accumulate that much data.

Note that the vehicle may be stopping more often, but it might not be able to transmit all of the data in one stop. Much of the data transmission might need to happen when the astronauts are asleep. To make the mission not constrained by the amount of storage available, 500 Gbits of Mass Storage was selected to satisfy these requirements.

Space-rated data storage cards with 256 Gbits per card at only 800 g and 8 Watt peak power consumption and a 0.9997 reliability over 30 days are available. These satisfy the performance requirements at a reasonable mass and power cost.

10.2 Driving System (Joseph Lisee)

10.2.1 Requirements

The following sub-sections go into the requirements which determined the driving system design. They then review the applicable level one requirements, define and justify the resulting level two requirements.

10.2.1.1 Applicable Level One Requirements

The main requirements for the design of the driving system is the rover's need for the capability to autonomously rendezvous with the crew once they have landed. The rover also must be able to navigate 100 km of lunar terrain successfully.

In order to rendezvous with the crew the rover must be able to drive over 10 km of lunar terrain without any outside assistance. This means the rover must be capable of sensing the outside world, turning that information into a model of the world, and then using that model to navigate the terrain to reach the lander and the crew.

Once with the crew the rover's driving system must assist them to accurately cover the path that has been outline by the mission planners. This requires the use of some of the same sensors needed for autonomous driving mode, but only enough to determine the rovers position accurately enough to reach science objectives.

10.2.1.2 Derived Level Two Requirements

From the two above requirements more detailed were derived so the design of the design driving could be done more precisely. These requirements also draw from other high level rover requirements the specify that the rover's ability to handle obstacles and at certain speeds. The derived requirements follow:

1. The rover must know its position within 30 m
2. The vehicle must be able to avoid obstacles larger then 0.1 m while driving at a speed 7.5 kph or less.

The first requirement stems from both the level one requirements listed in section 10.2.1.1. Both require the vehicle to know its position in order for the requirement to be successfully met. The first requirement only needs the rover to be within line of sight of the lander to successfully navigate to it. The general horizon distance formula is $d = \sqrt{2Rh + h^2}$, where R is radius and of the moon, and h is the height of the observer. For the moon $R = 1737km$ and for our rover $h = 2.93m$, where with the resulting h is determined by the height of the rover's antennas. This results in the horizon being 3.19 km away.

For the rover to successfully navigate autonomously in a timely manner it needs to be able to plan an overall path which avoids larger obstacles. The existing lunar map and data created by the Lunar Reconsisance Orbiter (LRO) will have an accuracy of 1 m with a precision of ±0.1 m[95]. This is enough to determine where things like craters and boulder fields are between the rover and its objective. Without an accurate positional fix, the rover would not be to be able to plan an official path around these obstacles ahead of time. The rover would be forced to use local navigational sensors to traverse them at a slower speed or take an even longer path around the edge of the obstruction. The requirement of 30 m provides an accurate enough position to be use the mapping data, but low enough to be feasibly implemented by the system described below.

The second level two requirements is based upon the level one requirement for safe rover operations when driving over obstacles. It is the only hard limit set on the rover for speed and obstacle size. Since this is the only defined obstacle criteria it was chosen as the minimum performance level for the driving system.

10.2.2 Position Determination

10.2.2.1 Purpose

The purpose of the position determination system is to find the location of the rover on the lunar surface within 30 m of its actual position. This meets the limit defined by the first level two requirement.

10.2.2.2 Trade Study

There are several different methods for determining the position of the rover on the moon, the 10.2 table provides a high level overview of these different methods.

Table 10.2: Position Determination Trade Study

Method	TRL	Accuracy	MIPS Required	Use While Moving
Satellite	9	∼10 m	<1 MIPS	No
On board estimation	8	N/A	1 MIPS	Yes
Terrain contour matching	4	∼2 m	1000 MIPS	Yes

The satellite position determination method uses the orbiting lunar relay satellites and earth based systems to triangulate the position of the rover. To get an accurate position fix the rover must be stationary for an extended period of time.

On board estimation use an initial position fix as a starting point and then updates that position with an estimate of how much the rover has moved. This is a standard odometry system. To estimate the how much the rover has moved. The rover determines how much it has moved based its known

heading, turning angle, and how many turns the wheels have done. This system is very susceptible to wheel slip and orientation error. This leads to a drift in the position of up to 4.6 m/min when traveling at 7.5 kph. The computational overhead of this system is low enough that it is done fifty times a second, the same rate as the driving control loop.

Terrain contour matching uses the current estimate of the rover's position, a generated map of the local terrain, and reference map of the surrounding terrain. It uses the generated local map to find where the vehicle is in the reference map. This systems accuracy is determined by the resolution of the reference map. The systems computation overhead is high enough that is run only twice a minute. For complete discussion of terrain contour matching see section 10.2.2.4.

10.2.2.3 Overall System

No single system described in section 10.2.2.2 is enough to meet derived level two requirements. So a combination the three utilizing the strengths of each system was developed.

A satellite position fix is made when the rover first lands. This fixes the rover with 10 m. This must be done because none of the other system function without an initial position. This will provide a good initial estimate for the other position determination methods to work off of. These position fixes will happen infrequently, but at minimum the rover needs a satellite position fix after landing. They can happen also happen if the rover drifts so far that the terrain contour matching system can't updated the vehicle's position.

Working from an initial position the rover uses on on-board estimation to determine the rovers position. This has very low computational overhead so its done at 50hz and the rover always has an update to date estimate of its current position. To correct the build up of error from the odometry based estimation the terrain contour matching system is used. It is run every thirty seconds to get a new position to start the estimating off of. This allows only a maximum of 2.3 m of error to occur for rover's position estimate is corrected. The position derived from the terrain contour matching will be accurate to within 2 m meters.

10.2.2.4 Terrain Contour Matching

The terrain contour matching system is similar to method used by cruise missiles to navigate in the absence of a global positioning system (GPS). The cruise missile's terrain contour matching system is called TERCOM. It compares contour maps of the route and its surrounding terrain with a local map built from a downward looking RADAR. It then matches the map it built to a location in the surrounding terrain. A simple example of this can be seen in figure 10.6. The process is sped up by using the missile's estimated position as the point in which search in the reference map begins.

Terrain contour matching for the rover is slightly different in its implementation but uses the same principal as TERCOM. The reference map for mission areas and the landing zone is derived

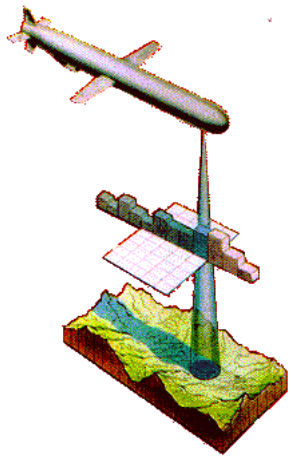

Figure 10.6: TERCOM positioning example

from LRO data and stored in the computer's on-board non-volatile memory. The reference location from which the search is started is the odometry based position estimate.

The differences between TERCOM and the system used on the rover are that the rover generates its map of the surrounding terrain using its scanning LIDAR instead of RADAR. Also the resulting map is a two dimensional high resolution map, not a lower resolution, one dimensional map. The rover's autonomous speed is 1% of what a cruise missile using TERCOM travels at. This mean that it scans a much smaller portion of terrain in the same time interval. At a lower resolution this would result in more then one possible match in surrounding terrain, resulting in no meaningful position estimate. So in order to provide unique matches to a location in the reference map, the resolution of the rovers system is much higher, see section 10.2.4.2 for details.

10.2.3 Orientation Determination

The purpose of the orientation determination system is to enable the the on-board odotmetry based position estimation system. Without accurate knowledge of orientation the performance of the odometry system goes down drastically. For example when traveling at 7.5 kph a heading of error of 1° creates a positional drift of 2 m a minute. The rover's driving system uses the same sensors at the landing avionics system.

10.2.4 Obstacle Detection

In order for the rover to successfully rendezvous with the crew it must cover up to 10 km of lunar terrain. The terrain is only mapped a 2 m resolution and the rover cannot handle boulders larger then 0.5 m. Even if the terrain were mapped to this high an accuracy level, the rover would not

always knows its exact position within that map. The goal of obstacle avoidance system is to detect these obstacles soon enough for the rover to be able to steer around them.

10.2.4.1 Trade Study

All obstacle avoidance system work by detecting the distance from the vehicle to the environment outside it. They do this through either direct or indirect distance measurement. Stereo vision is the most common indirect distance measurement method, while lasers, radar, and sonar are used for direct distance measurement. We will not consider sonar because there is no medium for sound to propagate through while on the moon. Table 10.3 provides a comparison of these methods different obstacle detection methods.

Table 10.3: Obstacle Avoidance Trade Study

Method	TRL	Resolution	MIPS Required	FOV	Range
RADAR	8	1 m	150 MIPS	10°	350 m
Scanning LIDAR	4	0.1 m	1500 MIPS	360°	50 m
Stereo Vision	8	0.1 m	4000 MIPS	90°	100 m

As you can see from table 10.3 scanning LIDAR matches the resolution of stereo vision while having less computation overhead and a wider overall field of view. RADAR cannot be used because of the low field of view per sensor. The low field of view requires a prohibitive amount of sensors to get the needed coverage around the rover.

10.2.4.2 Scanning LIDAR

The scanning LIDAR is the rover's sole obstacle detection system. It replaces a large group of conventional LIDARs which would have to be spread over the vehicle exterior with two rotating sensors mounted on the top front of the rover. The second sensor is for redundancy, only one sensor is needed to autonomously operate to rover. As you can see in figure 10.7 the data from sensor results in a 360°view of the surrounding terrain.

The scanning LIDAR sensor itself is a single rotating unit which houses multiple conventional LIDAR sensors. It is housed in a dust tight, but optically clear, enclosure to prevent lunar dust from interfering with its rotation. All sensors measure the the distance from the unit to the surrounding terrain simultaneously while spinning. The raw range data is transferred over the rover's internal network to the computers processing. The data processing determines which areas are passable and which are obstacles.

Since only one such sensor currently exists, and it will have to be heavily re-engineered to work in the lunar environment, the systems actual performance can be designed to meet the requirements of rover navigation.

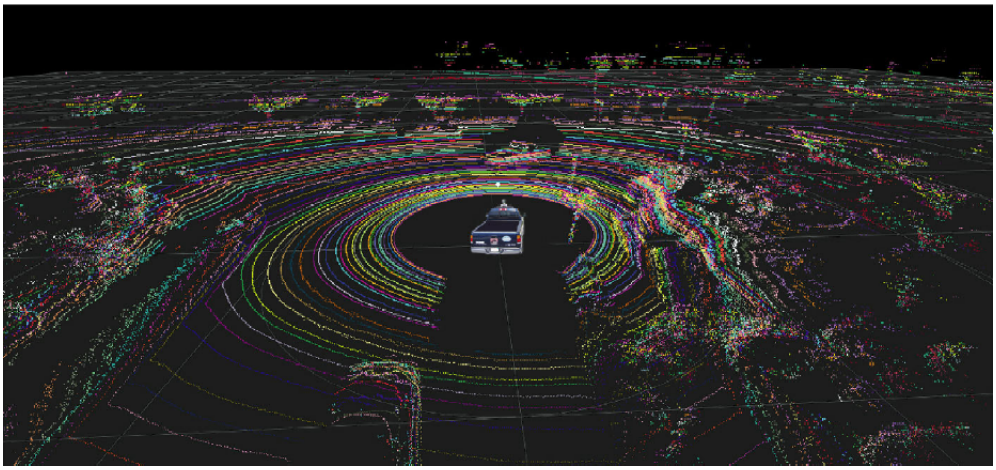

Figure 10.7: LIDAR Point Cloud

10.2.5 Path Planning

Once the world around the rover is known the rover needs to plan a path through it. The rovers world representation is a map grid of the surrounding terrain with areas marked passable and not passable as it current speed. The 10.2.4 section describes how this map is built. The resolution of the map grid is 10 cm. As described in the section 10.2.1.2, anything larger than 10 cm needs to be driven around. So 10 cm is the smallest size object we are concerned with.

The D* path finding algorithm is applied to the map grid to plan a path from the rovers current position to its next objective [97]. The D* algorithm allows efficient updating of an already planned path. This is important because the rover will plan a path through terrain that has only been mapped from orbit, and will need to updated that path once its LIDAR has scanned the area. In figure 10.8 you see a basic example of the map grid and a planned path through it.

10.3 Computers

10.3.1 Computational Requirements

In order to choose the computer all the different computational modes have to be considered. There are three different modes at which the computer can operate: autonomous, manual, and minimal. Each mode provides greater functionality but takes more MIPS.

The modes progress from minimal functionality to fully autonomous operations. The minimal mode operates the computer systems which are associated with power management, life support and communications. This mode is only used when there not enough computation power for other modes. The manual mode activates the position estimation and terrain contour mapping system.

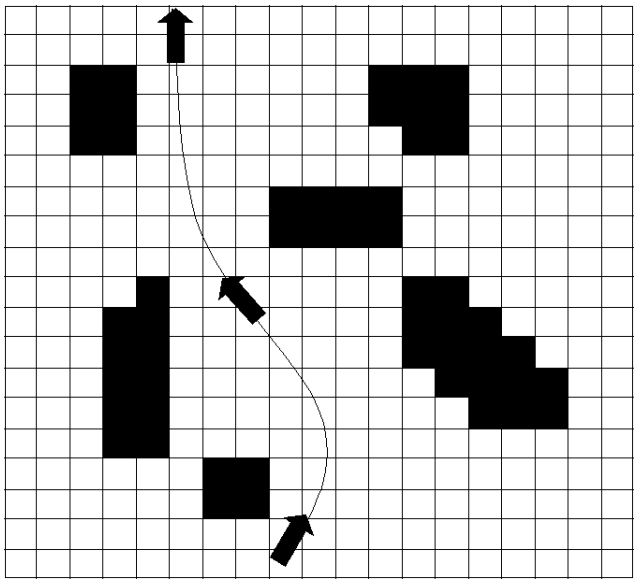

Figure 10.8: Example obstacle map and planned path

The last mode is the fully autonomous mode, which adds obstacle detection and path planning systems. The computational requirements for each mode are listed in table 10.4.

Table 10.4: Computational Requirements

Task	MIPS	Autonomy	Manual	Minimal
Standard Operations	500	Yes	Yes	Yes
Position Estimation	1	Yes	Yes	
Terrain Contour Matching	1000	Yes	Yes	
Obstacle map building	3000	Yes		
Path Planning	500	Yes		
Total	5000	5000	1500	500

The standard operations category is all the processing needed for communications, and keep the rover's other vital systems like life support and power management. The position estimation computations are the computations needed by the odometry based position estimate system. Terrain contour matching is an expensive item because of the type of computations needed and desired precise result, see section 10.2.2.4 for more information. The obstacle map building, section 10.2.4, and the path planning, section 10.2.5, are only needed while the rover rendezvous with the crew.

10.3.2 Required Computer

From the computation requirements shown in table 10.4 we need a computer with at least 5000 MIPS of computation power. The current top of the line space rated computer is the RAD750 by Honeywell, but it only produces 500 MIPS. This shortfall is made up in two ways. The first is by the natural growth in space based computational power. Currently the speed of space rated computers goes up by a factor of ten every five years. The second is by using multiple computers.

The rover uses three next generation RAD750s. Each with 2000 MIPS, four times the computational power of the current generation. This is conservative estimate of the growth in computation power between now, and the time the rovers are built. At the given 2000 MIPS per computer computer system has a total computational power of 6000 MIPS and an overall 17% margin. The reason for using multiple computers is for redundancy and its explained in further detail in section 10.3.3.

10.3.3 System Redundancy

Redundancy in the main computers is achieved in a few ways. The first is the excess processing capacity available when the is operating in manual or minimal modes. In both those modes a single computer is capable of meeting all processing demands. This allows for two computer failures and the crew will still be able to navigate home. The second method of redundancy is that the computers use the excess computational power to check the results of the computations they do. This lets the system identify a bad computer and take it out of the system.

In the event of a computer failure during the autonomous phase, the over speed of the rover can be dropped so that workload is low enough for two computers to handle it. This is approximately 2/3 of the max autonomous speed, or 5 kph.

10.4 High Definition Camera System (Jacob Zwillinger)

Camera systems have played an integral part of rover designs and operations from the Apollo era until the present day. For unmanned rovers, cameras function much like the human eye would, but camera systems still play a valuable role for manned missions, such as the high definition camera system (HDCS) on TURTLE. The HDCS serves many goals; chief among them is the ability to aid astronauts with navigation during lunar traverse. The field of view out of the window is fairly limited, and is supplemented by the HDCS. The camera system will help with determining the traverse path, obstacle avoidance, and turning. The HDCS also has the capability of tracking astronauts while they are performing EVAs, something that will be useful to NASA for monitoring the health of their astronauts and for increasing public awareness. Additionally, the cameras can be used for determining scientific areas of interest, if, for example, the cameras pick up interesting seleneographic features outside the direct field of view (FOV) of the astronauts.

10.4.1 Camera Specifications and Components

The cameras were designed to a weight requirement of 3 kilograms, and have power use of approximately 20 watts / camera during operations, and 5 watts / camera during standby. A pan and tilt head allows for 360° degree of freedom (DOF) along the y axis, and 180° along the z axis. A standard field of view was incorporated, which is equivalent to 37.8° x 54.4°, and the 3x zoom can increase this to a maximum FOV of 13.0° x 19.5°. Table 10.5lists the components included within the HDCS, as well as description and approximate power draw and weight. Technology readiness levels (TRL) are included as well.

Camera Component	Purpose / Description	Power Draw (Watts)	Weight (grams)	TRL Level
Optics	Capture Images	7-10	500	7
Casing	House the optics, dust and radiation prevention	0	1000	8
Thermal Insulation	Keep HDCS temperature within range	0	250	8
Pan and Tilt Head	Allows camera to pan and tilt	0-5	500	7
Electrical Heater	Heat HDCS to keep within temperature range	0-3	100	8
Thermostat	Monitor temperature	1	100	8
Data and Power Wiring	Connect HDCS to main data and power systems	0	N/A	6
Acquisition Buffer	Short term data storage within HDCS	2	300	6

Table 10.5: HDCS Components

It should be noted that since the Data and Power wiring is not an internal component, its weight is not included towards the HDCS's weight.

10.4.2 Design Requirements

The only relevant level one design requirement for the HDCS was the "Rover shall be capable of communication at HDTV rates direct to Earth". This requirement was fairly vague and thus derived level two requirements were necessary. They are as follows:

1. Image resolution shall be no less than 1280 x 720 pixels.

2. Frame rate shall be no less than 24 frames per second

3. Cameras shall be able to fit through the rover airlock system
4. Cameras shall have the capability of recording EVAs
5. Cameras shall assist astronauts with low-speed maneuvering as necessary
6. Power consumption for the camera system shall be no more than 60 watts any point per system.
7. The HDCS shall weight no more than 20 kilograms

Derived requirement (1) comes out of the characterization of high definition. Typically, high definition means any resolution greater than 1280 x 720, but can go as high as 1600 x 1200. For the purposes of this design, there was no reason to increase the resolution over the minimum required. Requirement (2) has a similar characterization. Video feeds can have frame rates of between 24 frames per second (FPS) to 60 frames per second. The minimum necessary is sufficient for this design. Requirement (3) relates to the issue of dust mitigation, which will be discussed in section 10.4.7 . Requirements (4) and (5) follow from the primary purposes of the camera system, while design requirement (6) and (7) were derived from the the power and propulsion team and the system integration team, respectively. It should be noted that based on requirement (7) and the 3 kilogram per camera weight, six cameras can be placed on TURTLE. Also, based on requirement (6), two cameras can be operational at any time, while the remaining four must be kept on standby.

10.4.3 Camera Hertiage

It is important to consider some of the HDCS heritage to understand how it compares and improves on those on other Lunar missions. Since there have been no Lunar missions since the Apollo era, camera systems from Martian rovers have also been examined. The data is summarized in Table 10.6.

It is important to note that TURTLE will have the first rover camera system capable of HD, as well as the first to incorporate dust prevention. While both the mass and power show significant increase over other camera systems,

10.4.4 Camera Placement

Given that six cameras can be placed on TURTLE, the next step was determining the optimal layout of the cameras.

Restrictions There are numerous restrictions on the placement of the cameras. The cameras can not be placed on the radiators, as it would interrupt the heat dissipation as well as causing the cameras to overheat. The cameras can not be placed on any of the external tanks, as this would

	Hasselblad Data Camera	Ground Commanded Television Assembly	MER Pan-Cam	MSL Mast Cam	TURTLE
Used On	Moon	Moon	Mars	Mars	Moon
Year Used	1969-1972	1968-1970	2003-?	2009 (est.)	2020 - ?
Frame Rate (FPS)	N/A (Film)	20	< 1	10	24
Resolution	N/A (Film)	~ 200 x 200	1024 x 1024	1600 x 1600	1280 x 720
HDTV	No	No	No	No	Yes
Dust Prevention	No	No	No	No	Yes
Mass (kg)	1.83 kg	8.3	1.5 (est.)	2	3
Power (w)	Batteries	16.65	2.15	13	20

Table 10.6: Comparison of Relevant Camera Systems

prevent the changing or removal of the tanks, as well as damaging the integrity of the tanks should the cameras be mounted to them.

Rationale Given these constraints, the following options were considered.

Layout 1: Three front, three rear Layout 1 has three cameras placed in the front of TURTLE, and three cameras placed on the back, as shown in figure 10.9 (cameras displayed as red circles). The top camera on the front and the top camera on the rear wold be used primarily for navigating while driving straight, and the four cameras on the sides (two in the front, two in the rear) would be used to assist with low-speed turning maneuvers. The four turning cameras could also be used to determine obstacle avoidance, if TURTLE is so close to a boulder or other obstacle that it can not be determined if there is sufficient clearance from looking out the primary windows.

Strengths Layout 1 has very good coverage of the surface directly in front and directly behind the rover. Should any of the cameras fail, there is significant overlap within the camera's FOV to allow an adjacent camera to cover the same terrain. Placing the cameras higher up, in a fairly unobstructed place, would limit the amount of dust reaching the HDCS.

Weaknesses This option has very poor coverage of the side areas of TURTLE. While having two banks of three cameras would be useful for redundancy purposes, it leaves significant waste in

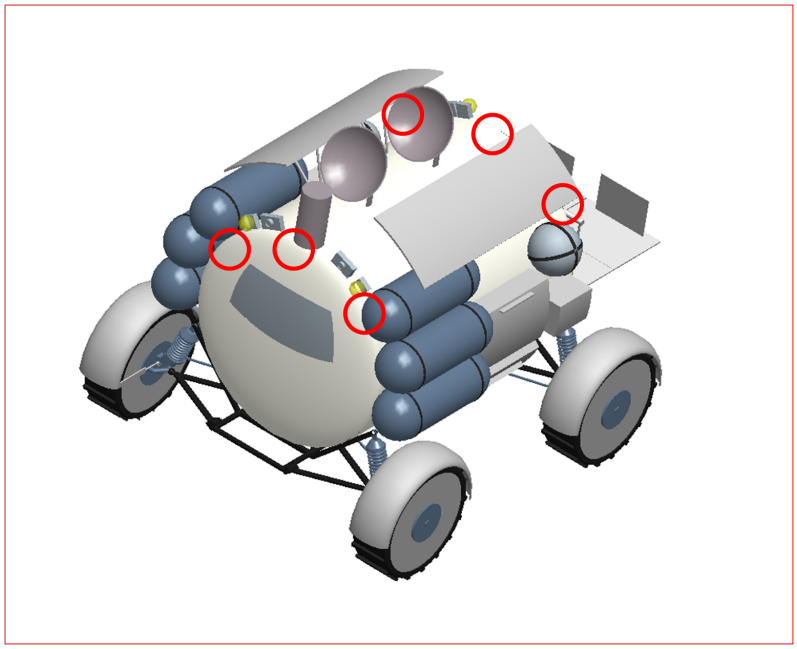

Figure 10.9: Camera Placement Option 1

terms of the amount of terrain not covered. Additionally, the line of sight for the two cameras in the front might be obstructed by the external tanks.

Conclusion Not an optimal layout, given the Lunar surface to the sides of the rover that is not covered.

Layout 2: Horizontal two front, two rear, two side Layout 2 modifies Layout 1 by moving the top camera in the front and rear to the left and right side, respectively, as shown in figure10.10. The two cameras in the front and the two cameras in the rear can still be used to assist with turning, but they can also be used to see the area directly in front and directly behind TURTLE.

Strengths Layout 2 has good coverage of all areas surrounding TURTLE. There is still some overlap with the two front cameras and the two rear cameras, which is useful for redundancy purposes. The cameras are also placed higher up, which would limit the amount of dust reaching the HDCS.

Weaknesses The side cameras have a lot of external equipment which could limit their FOV (radiators, external tanks, external storage).

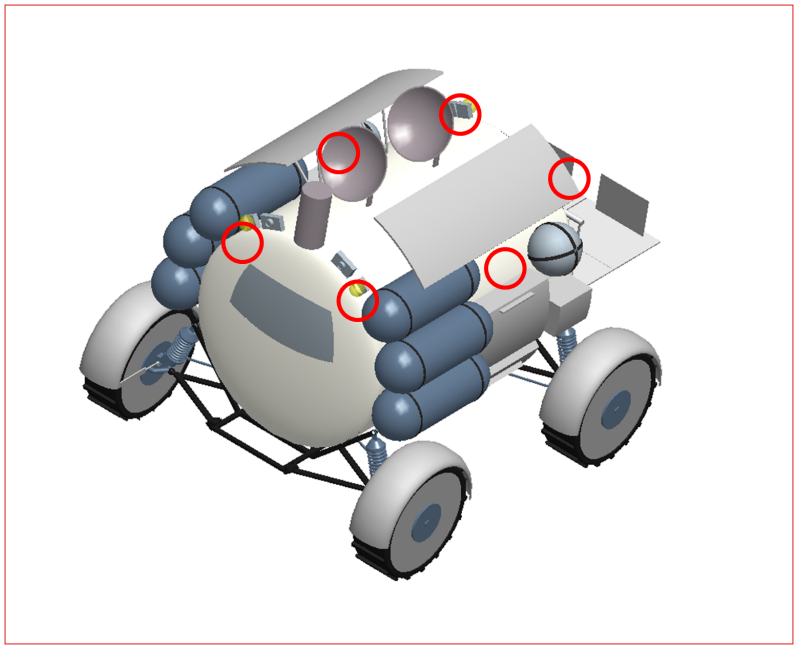

Figure 10.10: Camera Placement Option 2

Conclusion This layout does a good job optimizing visibility around the rover, and is a strong candidate for integration into TURTLE.

Layout 3: Vertical two front, two rear, two side Layout 3 modifies Layout 2 by switching the front and rear camera positions from a horizontal layout to a vertical layout. (The 6th camera, not visible in Figure 10.11, is placed directly below the top rear camera).

Strengths Layout 3 has good coverage of all areas surrounding TURTLE. The lower cameras can give a better view of areas of interest directly in front of the rover and areas in front of the wheels.

Weaknesses The two cameras towards the bottom of the rover (one in the front, one in the rear) will receive more dust and damage. The side cameras have a lot of external equipment which could limit their FOV (radiators, external tanks, external storage).

Conclusion This layout does not have significant improvements over Layout 2. Additionally, the extra dust coverage that the lower cameras will receive makes it a less viable choice than Layout 2.

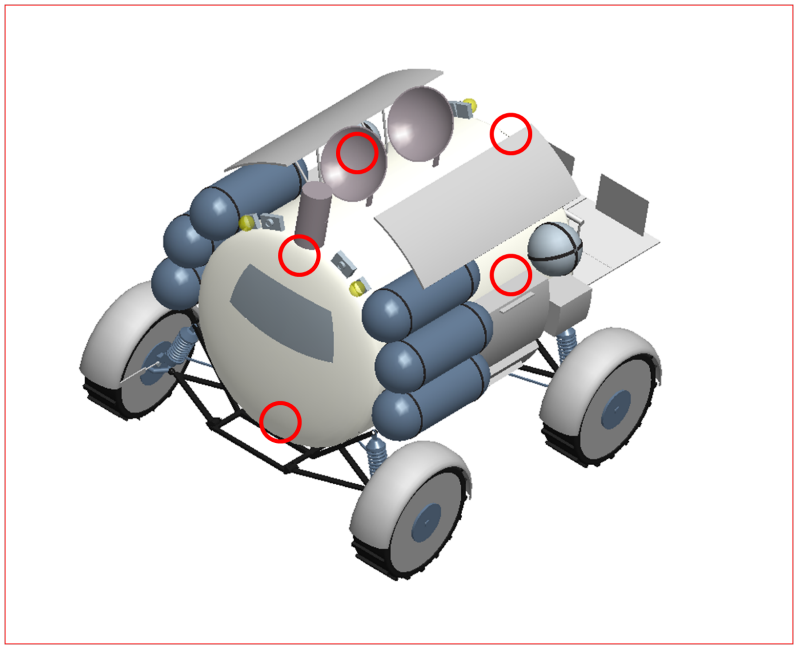

Figure 10.11: Camera Placement Option 3

Layout 4: Four wheels, one front, one rear Layout 4 is a significant deviation from the previous three. It places one camera on each of the four wheels, as well as one camera on the top front and one camera on the top of the rear.

Strengths Layout 4 has very good coverage of all areas surrounding TURTLE. By placing the cameras on the wheels, there are no obstructions which would block or limit the FOV. The two upper cameras (one front, one rear), could be used for objects further in the distance.

Weaknesses Placing the cameras on the wheels has some downsides: they are more prone to dust and vibration, and would be useless if a large boulder were to obstruct the path.

Conclusion While this layout presents excellent coverage, the weaknesses outweigh the strengths.

Option 5: Four wheels, two side Layout 5 is very similar to Layout 4, except instead of cameras in the front and rear, they are placed on the left and right side, as seen in Figure 10.13

Strengths Layout 4 has very good coverage of all areas surrounding TURTLE. By placing the cameras on the wheels, there are no obstructions which would block or limit the FOV. The two side cameras could be used for objects fitter in the distance.

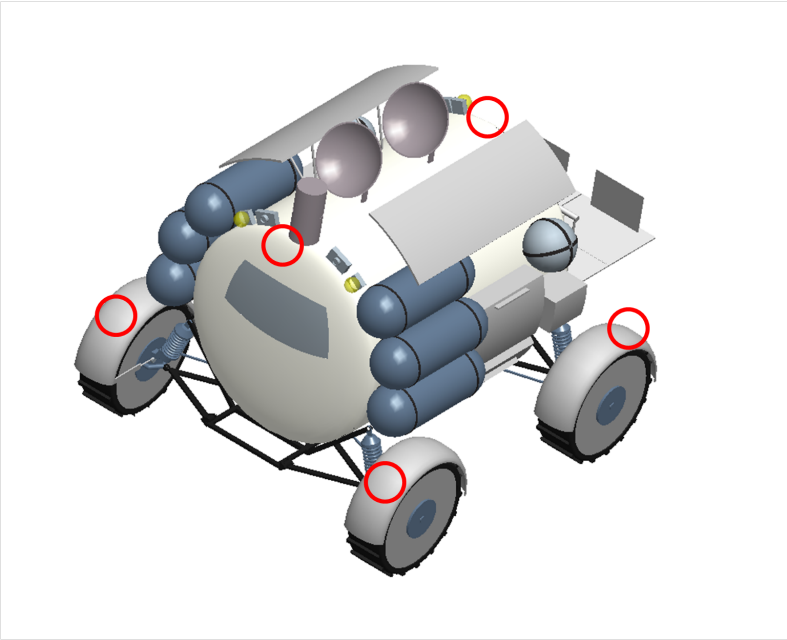

Figure 10.12: Camera Placement Option 4

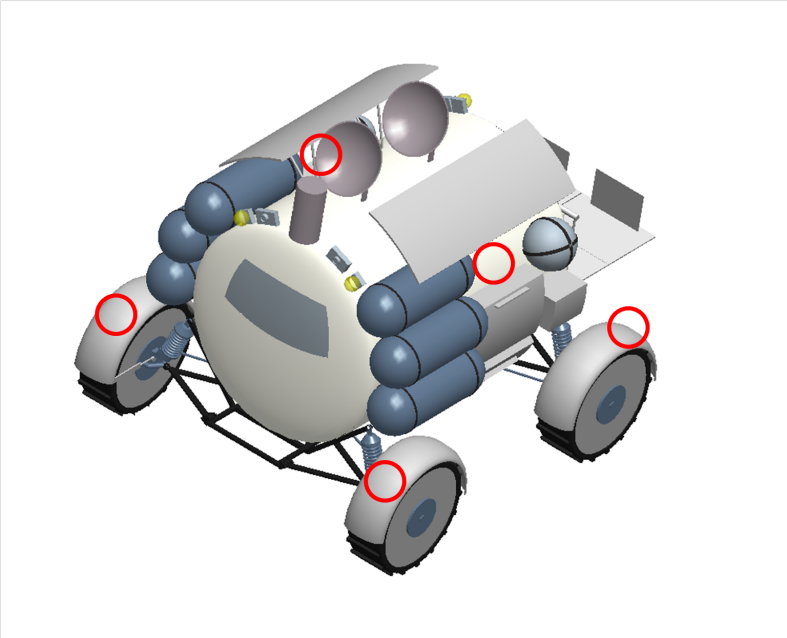

Figure 10.13: Camera Placement Option 5

Weaknesses Placing the cameras on the wheels has some downsides: they are more prone to dust and vibration, and would be useless if a large boulder were to obstruct the path.

Conclusion This option does not provide any advantage over Layout 4, and not having cameras in the front and rear make it a weaker choice.

10.4.4.1 Final Camera Placement

The two strongest options were Layout 2 and Layout 4. With what is currently known about the lunar dust (see section 10.4.7), placing cameras on the wheels will probably be problematic. Thus, Layout 2 is what will be incorporated into TURTLE. However, should field-testing indicate that the issue of dust mitigation can be solved, Layout 4 would be a strong candidate for inclusion.

10.4.5 Data Rates and Transmission

A large portion of the HDCS is data storage. This is especially true for multi-day missions, where the cameras can be running for up to 16 hours a day, producing video that must be stored. Current Earth-based data compression allows for HDTV to be stored at a rate of approximately 10 to 20 Megabits per second (Mbps). (For example, many common television channels have a broadcast rate centered around 15 Mbps.) This type of compression typically uses MPEG-2 or MPEG-2 derivative compression rates, the current standards. Future advances in compression, such as the H.264 compression standard, will dramatically improve compression rates. It is thus likely to assume that by 2020 compression rates should be as good as 5 Mbps, if not better. This correlates to a 3-day mission producing approximately 800 Gb (or 100 GB) of data. This data will be acquired through an acquisition buffer (described below), and then transferred, via ARINC-664, to the interior of TURTLE, where it will be stored for later transmittal. Based on available communication uplinks, the rover may only transmit data while the rover is stationary. While this would indicate that the rover would only need to store the data for a maximum of 4-8 hours, it is best to design the HDCS for the scenario where the rover is not able to establish communications for the course of a standard three day mission. Additionally, it may seem useful to store multiple data streams of HD video simultaneously; however, the extra processing power required is a larger factor than the marginal gain.

10.4.5.1 Potential Data Storage Issues

Two primary issues arise when dealing with data storage in the space environment: they are single event upsets (SEUs) and single event latchups (SELs). They will be discussed in turn.

Single Event Upsets (SEUs) An SEU is when a change of state caused by low-energy ions, or electromagnetic or nuclear radiation interferences strike to a sensitive node in a micro-electronic

device, such as in a microprocessor, semiconductor memory, or power transistors. Because the lunar surface is exposed to constant solar radiation, there is the possibility of an SEU causing the data stream to become corrupted. The solution to this scenario is to store multiple copies of the data. In the event that the data does become corrupted, the data streams can be compared, and the data stream can be restored and then broadcast to Earth. This scenario requires three copies of the data; if only two copies were present, it would not be possible to determine which data was uncorrupted and which data was corrupted. With three copies, if one set of data becomes corrupted, the other two sets of data will still be viable and can be used to replace the corrupted data.

Single Event Latchups (SELs) Another potentially calamitous problem is Single Event Latchups (SELs). An SEL is a condition that causes loss of device functionality due to a single-event induced current state. SELs are hard errors, and unlike SEUs, may cause permanent damage. The SEL results in a high operating current, above device specifications. The latched condition can destroy the device, drag down the bus voltage, or damage the power supply. An SEL can be cleared by a power off-on reset; Lunar testing will be required to determine the amount of necessary shielding to prevent SELs from permanently destroying the HDCS. Beyond standard safety precautions, there are currently no proven methods of fully preparing for and preventing against SELs.

10.4.6 Camera Heritage

In determining how best to implement HD cameras, four different solutions were considered, each of which will be examined in turn:

1. Modifying an Earth-based Commercial, off-the-shelf (COTS) HD Video Camera;
2. Modifying a current space rated HD video camera;
3. Designing an HD camera system from scratch; or
4. Modifying current space-rated non-HD cameras.

Modifying an earth based COTS HD camera. Initially, this method seems promising. As of 2008, there are dozens of COTS HD cameras that meet the requirements. One such example is the Panasonic HDC-SD1, which weights .43 kilograms, uses 8 Watts of power, and has dimensions 7.4 x 6.9 x 14.2 centimeters. Power and weight could be reduced by removing the LCD display monitor, viewfinder, and other unnecessary components. However, significant additions would have to be made: the COTS HD camera would need to be radiation hardened, the power and data connections would need to be modified, and the cameras casing would need to be modified to withstand the temperature fluctuations, and launch, landing, and operational stresses. With all the modifications considered, it is clear that modifying an earth based COTS HD camera would require significant amounts of work.

Modifying a current space rated HD video camera. As of 2008, there is only one active space-rated camera capable of high definition. This distinction belongs to Selene, a Japanese Space Agency (JAXA) instrument currently in lunar orbit. Selene is capable of high resolution pictures and videos, and thus might seem to be a good choice to base the cameras on TURTLE. Using the SELENE hardware would be problematic as well: it has a prohibitive size, (46 x 42 x 28 centimeters); mass (16.5 kilograms) and power draw (50 watts). By reducing these systems to match the requirement of TURTLE would require a complete overhaul of the instrument, and would not be a significant improvement over the following option.

Designing an HD camera system from scratch. The benefits of this option would be the ability to design the HDCS to the exact requirements of TURTLE. The downsides of this method would be a dramatic increase in development cost, development time, project complexity, and ignoring viable technologies (both in use and in development), which could aid in developing the HDCS. While this option might be viable, the last option offers the best possibility. \

Modifying current space-rated, non-HD cameras. There are currently camera systems in use now that would serve as a good baseline on which to design the camera system for turtle, such as the Mars Science Laboratory Mastcam. The Mars Science Laboratory is a Martian rover with a planned operational date of 2009; additionally, the rover has significant heritage from the previous generation of Mars Rovers, the Mars Exploration Rovers. There are many qualities of the Mars Science Laboratory Mastcam that makes it an attractive choice. Chief among them are its capability of taking 1600 x 1600 pixel resolution images, and the ability to store 10 FPS video for approximately two hours. The Mastcam is radiation hardened, can withstand significant variations in temperature, is space-rated, and is designed to withstand launch, landing, and operational loads. Using the Mastcam serves as the best option on which to model TURTLE's HDCS.

Modifications Required Certain modifications would need to be made to the MSL Mastcam to allow it to serve as the HDCS on TURTLE. The first change would be reducing the image quality from 1600 x 1600 pixels to 1280 x 720 pixels. While having a high resolution might ultimately prove useful, it would be wasteful, as it is greater than the design requirements. Another modification necessary would be to modify the data storage. The Mars Science Lander Mastcam has two data buffers: a 256 MB DRAM acquisition buffer and an 8 GB flash RAM mass memory buffer. The acquisition buffer (which serves primarily as short-term storage) governs how fast the cameras can take pictures. The mass memory buffer (which serves primarily as long-term storage) governs how much data can be stored; it acts much like a standard hard drive on a desktop computer, for example. To scale the system up to satisfy the requirements for TURTLE, dual channel 8 GB DRAM acquisition buffer will be included, and 250 GB of storage will be reserved on-board to store

the data in case transmittal to Earth is not possible. Additional minor modifications would also need to be made, such as using ARINC-664 as the primary method for communication.

10.4.7 Dust Control

One of the primary concerns with any system exposed to the lunar regolith is dust mitigation. On the daylit side of the Moon, solar ultraviolet and X-ray radiation is so energetic that it knocks electrons out of atoms and molecules in the lunar soil. Positive charges build up until the tiniest particles of lunar dust (measuring 1 micron and smaller) are repelled from the surface and lofted anywhere from meters to kilometers high, with the smallest particles reaching the highest altitudes. Eventually they fall back toward the surface where the process is repeated over and over again. On the night side the dust is negatively charged by electrons in the solar wind. Since the HDCS will carry electronic components and will thus have a charge, preventing dust from clinging to the optics – which in turn can abrade the surface and limit FOV – is critical to the success of HDCS. Four methods of dust mitigation are incorporated.

Fenders and mechanical blocks The primary defense mechanism for preventing dust getting to the cameras is fenders placed around the wheels. This limits the amount of dust that will reach the lens. In-field testing will determine if simple mechanical blocks placed around the physical camera system are necessary.

Brushes The second method of dust mitigation is using a brush to wipe off the lens. The brush will be kept in the external storage compartment and can be used to remove dust should it build up.

Transparent "tear-offs" The third method of dust mitigation is placing disposable, transparent "tear-offs" over the lenses. Such a system has been successfully implemented in automobile racing and industrial plants. The "tear-offs" amount to the equivalent of space-rated ceran wrap placed around the cameras. Should dust accumulate over the "tear-offs", they can be removed and a new "tear-off" can be placed over the HDCS. Supplies for the "tear-offs" can be kept sealed in the external storage bins.

Wet wipes / vacuum The fourth method of dust mitigation amounts to bringing the cameras inside and cleaning them with wet wipes, or if the dust buildup is significant, a low-powered vacuum cleaner. For transport of the HDCS from the exterior of TURTLE to the interior, the cameras must be unplugged from their power and Ethernet connectivity and placed in the external equipment airlock. After the cameras are cleaned, the cameras can then be brought to the surface and re-installed.

10.4.8 Summary

Cameras play an important role in any planetary rover, and TURTLE is no exception. With the use of the HDCS, astronauts will have an easier time determining a traverse path, will be able to perform obstacle avoidance, and will significantly increase the astronauts FOV. The HDCS continues off of camera systems from previous interplanetary missions and rovers, and no doubt the data returned from the HDCS from TURTLE will be used to plan further missions.

10.5 Communications (Andrew Ellsberry)

10.5.1 Constellation Comunications Infrastructure

TURTLE will be a component of a much larger sortie or outpost mission that will include many other Constellation "systems," including the Orion CEV, ALTAIR lander, space suits and lunar relay satellites that all need to function together. Being a secondary system, the TURTLE rover must be able to communicate with all the existing systems without having to modify them for the purpose. The communications plan for Constellation is standardized so that every system should be able to communicate with any other system without major changes or reconfiguration. TURTLE complies with the relevant portions of the command, control, communication, and information (C3I) interoperability standards in order to guarantee this interoperability.

10.5.2 Frequency Selection

The frequency selection process for the radio communications on turtle was constrained by the limited frequencies available for supporting a manned mission on the moon by the International telecomunications Union or ITU (frequencies and bands are set aside for specific uses) as well as the requirement that TURTLE be capable of communication with other constellation systems. Based especially on the Constellation requirements, S and Ka bands were selected to meet the low and high speed communications requirements. The S-band link allows communication with a large number of systems including all Constellation systems, the Space Network (TDRSS) for launch and transit, the Deep Space Network, and the planned lunar relay satellites.

10.5.3 Lunar Relay Satellites

While a network of ground stations on earth can provide continuous coverage of most of the near side, polar regions and the far side of the mood will have intermittent or no contact with earth. To compensate for this, NASA intends to launch a number of "Lunar Relay Satellites" (LRS). These satellites will fill a similar roll to the Tracking and Data Relay Satellite System (TDRSS) which orbits earth and provides continuous communications coverage to a number of manned and unmanned systems in earth orbit. Like TDRSS, the Lunar Relay Satellites will provide both low

speed communication to multiple users (spacecraft, science stations, astronauts on EVA and the like) as well as high bandwidth communications to a single user, which will usually be a manned or complicated unmanned (TURTLE while uncrewed) system, comparable to the "Single Accesses" antennas on TDRSS. Lower speed communications can also be provided by multiple existing and planned lunar orbiters including LRO and the CEV that brings the astronauts.

The design and deployment details of the LRS are still being decided on but for analysis, a baseline design was created. This baseline, is based when possible on details that NASA has released (at least in preliminary designs or proposals) and similar systems when details are not available. This baseline combines the proposed orbits from that NASA has released with the communications capabilities of an existing TDRS. The most recent plan for the LRS deployments is to launch both to share the same orbit with a semi major axis of 6100 km and an eccentricity of 0.6. The satellites will take 12 hours to orbit the moon and will oppose each other so that one will be at perigee while the other is at apogee. The TDRS properties are based on the receive capability if the more recent I, J and K units that support Ka-band communications.

One of the major considerations while relying on the LRS for a polar or far side mission is that the SA antenna will need to be shared with the LSAM which will also be occupied by 2 astronauts. It would be unreasonable to assume that TURTLE will receive continuous use of the Ka-band SA antenna. Fortunately, TURTLE only requires the high bandwidth link while stationary and for large data downlinks and live HDTV broadcasts.

10.5.4 Deep Space Network

While the distances are longer, near side missions can take advantage of earth based antennas that will have higher availability than the Lunar Relay Satellites. It is also completely conceivable that early sortie missions may be launched before the rest of NASA's planned infrastructure, including the Lunar Relay Satellites, and would only be able to send communications directly back to earth.

The Deep Space Network (DSN) was built during the early space program to support missions outside of earth orbit. It is composed of 3 sites located in Goldstone California, Canberra Australia, and Madrid Spain, each located approximately 1/3 of the way around the earth to provide continuous coverage to most of the solar system. Each site has a combination of 26m, 34m, and 70m antennas, the gain properties of each are described in the Table 10.7.

Table 10.7: DSN Antennas

Antenna	Gain S-Band	Gain Ka-Band
26m	51 dBi	-
34m HEF	55 dBi	-
34m BWG	56 dBi	79 dBi
70m	63 dBi	-

The TURTLE rover utilizes the 34m Beam Wave Guide (BWG) antennas as they are the only DSN antennas that support Ka-Band and they have a significantly cooler thermal noise levels when pointed at the moon than any of the other antennas. It should be noted that although they provide exceptionally high gain for S-band reception, the 70m DSN antennas are prone to failures and the reality that only one is located at each of the three sites means that there is no alternative in the case of a failure. The 70m antennas are potentially useful in an emergency situation should they be needed, but relying on them for continuous mission support is not practical.

10.5.5 Thermal Effects

There was no modeling of thermal effects and instead, empirical data from the DSN and TDRSS for communicating while pointed at the lunar surface (for DSN) or the earth's surface (for TDRSS) and their operationally determined G/T values were used. There will be some variation in the values for the LRS as compared to TDRSS, but the LRS is in an early stage of development (based on public data) and its design will be optimized for the same considerations.

10.5.6 S-Band Communications

The primary communications link is in the S-band (2.2 GHz) portion of the spectrum. Three identical transceivers, providing 2 fault tolerance reliability, provide continuous transmit and receive capability for crew communications, crew and vehicle monitoring, navigation data, standard definition video and housekeeping data. Additionally, the S-band transceivers are capable of two-way ranging with either the lunar relay satellites or the deep space network, which can be used for initial position determination and periodic updates to supplement the vehicles position estimation. Each unit is capable of transmit and receive data rates at up to 20 Mbps which is the maximum data rates supported over S-band for Constellation.

Two of the transceivers will be connected to both an omni antenna and a 53 cm high gain antenna through a dual pole, single throw (DPST) switch that will allow for use of both antennas when the situation requires. The switch will be fault tolerant in order to make sure that its failure will not prevent the transceiver from being used with either antenna. As each antenna is shared between S and Ka bands, the feed point for the HGA will be offset to one side resulting in a small drop in efficiency on S-band frequencies, but this is less than if the Ka feed horn were offset due to its higher frequency.

A third transceiver is used exclusively with an omni antenna and is nominally used for EVA communications which will also operate in the S-band portion of the spectrum. EVA operations require less than one watt of power due to the extremely short distances involved. However, it is identical to the other 2 transceivers including their 20 watt internal amplifiers in order to provide contingency communications with earth, in the unlikely both of the other transceiver systems fail.

10.5.7 Ka-Band Communications

The TURTLE rover features redundant Ka-band transmitters designed to transmit the vehicle's HDTV video and buffered science data. These transmitters are capable of transmitting QPSK data at rates up to 150 Mbps. This is consistent with the C3I specification for high data rate, 1-150 Mbps, Ka-band transmissions, operating with balanced SQPSK (a standard Space Network implementation of QPSK). TURTLE will never be capable of producing 150 Mbps of data, but as the Ka-band transmissions over the LRS or DSN will compete with the primary mission's (ALTAIR) high speed data links back to Earth as well and the higher data rates allow turtle to transmit the same amount of data from its buffer in a shorter period of receiver time.

Each of the two transmitters will be wired directly to the primary (centered) feed horn of one of the vehicle's high gain antennas. The 53 cm antennas will provide approximately 40 decibels of gain over an isentropic radiator, which will require lower feed power, but will have a very narrow beam width. To communicate with Earth, the HGA will be required to point within approximately 1 degree of earth. In order to point so accurately, the Ka-band transmitters will only be usable while the vehicle is stationary. The Ka-band system is transmit only, as there is a significantly redundant receive capability in the S-band system. Moreover, while there is a significant benefit to transmitting large amounts of data and video in full frame rate HDTV back to the earth, there is neither a requirement nor the requisite storage space to receive similar data or video on the rover.

10.5.8 Link Budget

A simplified link budget is shown in Table 10.8. Detailed link budgets and baseline design configurations can be found in Appendix G.

Table 10.8: Simplified Link Budget

	S-Band DSN	S-Band LRS	Ka-Band LRS	Ka-Band DSN	S-Band LRS (Omni)	S-Band DSN (Omni)
Transmitter						
Data Rate (Mbps)	20	20	120	120	4	.200
TX Power (W)	13	4	2	2	13	13
Antenna Gain (dBi)	21	21	40	40	0	0
Ground Station						
Distance (km)	380,000	3,000	380,000	3,000	3,000	380,000
Link Margin (dB)	3.0	3.0	8.4	9.4	3.0	3.0

Chapter 11

Outpost Rover

11.1 Outpost (Hasan Oberoi)

11.1.1 Outpost Overview

NASA's constellation program entails the establishment of a lunar outpost. The lunar base is part of a long-term plan of missions to Mars and experimentation of lunar elements. The mission lengths will gradually increase over time. The current design plans by NASA range from short four to seven day missions, later gradually increasing from two weeks to two months and ultimately to 6-month missions. The initial seven-day sortie missions will be focused on scientific experimentation, lunar terrain examination and lunar outpost site selection. Currently, the lunar South Pole serves as a potential lunar outpost site. The outpost missions will consist of four astronaut crew. The lunar South Pole has its advantages, as it is high in hydrogen content, sunlight for power generation and the diurnal temperatures are less extreme than other sites. Peary crater, Malapert crater and the Shackelton crater are some sites that are being considered by NASA. The lunar outpost components would be sent in a few separate cargo landers. An incremental buildup plan is being considered to establish the outpost. The astronauts would establish the lunar outpost in short consecutives missions to the moon. Thus, once the lunar outpost is established, the manned missions would increase in duration. Some parts of the rover would need to be redesigned to address the longevity of the missions for the outpost. Thus, the TURTLE outpost rover must be reusable and serviceable. The crew systems, power and thermal systems have been redesigned to address the long duration missions. Connecting the rover with the outpost for material and astronaut exchange needs to be addressed by understanding the current lunar base designs. Currently, inflatable technology is being refined to construct inflatable lunar base designs as well as rigid and other structure formats to study and analyze the best solution for the lunar base that is cost effective, easy to deploy, and weight effective. Johnson Space Center is currently developing lunar habitation modules for the outpost. The basic lunar habitation modules are inflatable making them more adaptable, lighter and robust.

Johnson Space Center has built two different mockups where one is a vertical structure and the other is a horizontal structure. NASA has teamed up with the National Science Foundation (NSF) and ILC Dover to study and design inflatable structures. The current lunar habitation modules cater to an airlock for ingress and egress. However, the habitation lacks a docking mechanism with a pressurized rover. Incorporating a docking system would allow astronauts for a shirtsleeve transfer from the outpost to the rover and vice versa.

11.1.2 Outpost Rover Requirements

The outpost rover is meant to be a reusable rover that will be used for the entire length of each mission. Thus, the rover must be able to withstand long-term fatigue and components must be replaceable or serviceable. The outpost rover is not limited to the strict mass requirements as the sortie TURTLE rover. However, it still must be cost and weight effective. The rover must replenish all crew survival components. Power and thermal systems must be serviceable. The power system should have a regenerative process that allows for onboard supply or in situ generation. The rover must have adequate radiation shielding. The long-term effects of lunar dust exposure on electronics and cameras needs to be addressed along with the reliability of components. Micrometeoroid protection needs to be evaluated for longer missions. Thus, the TURTLE outpost rover would encompass these elements to ensure it is operable in long-term missions. The extra rover parts such as panels, tires, and motors would need to be sent separately to the outpost in the cargo lander.

11.1.3 Outpost-Rover Docking

Several ideas were considered to connect the rover with the outpost. Given that the TURTLE rover is equipped with suitports for ingress and egress, the outpost can be designed to have multiple suitport access points that astronauts can use for access. The outpost can have a suitport access wall where four suitports are attached for the four crew members as seen in Figure 11.1. For supply exchange, the current airlock compartment of the rover was considered. However, a shirtsleeve transfer was not possible through the airlock compartment and larger items could not be moved in or out. Using the suitport as an access port to connect with the outpost was another feasible idea. Using a "tube" like approach the rover can be connected with the outpost. The cylindrical tube like structure would be attached to the outpost that remains pressurized and connects with the rover's back to create a passageway for a shirtsleeve transfer. Two such designs were created to analyze which design would be the best choice to further study. The outpost-rover connection design does require collaboration with the Lunar Architecture Team to devise a feasible transition point for the shirtsleeve transfer. It is being assumed that one astronaut would exit the rover via the suitport and aid in connecting with the outpost while the second astronaut remains inside the rover. Dust mitigation, structural integrity, mass requirements and materials for the transfer tube

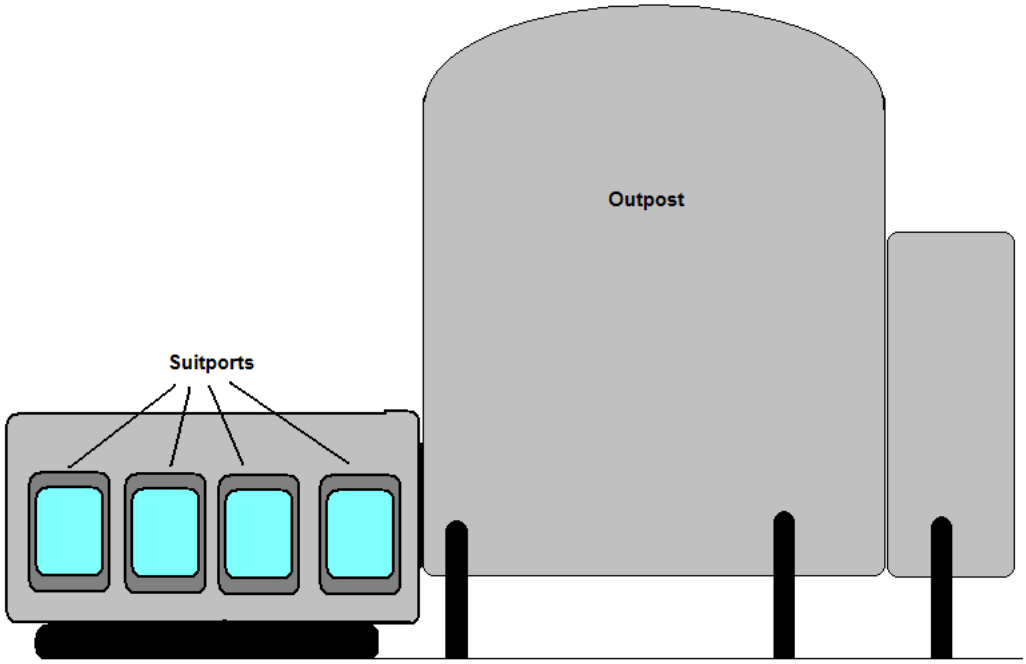

Figure 11.1: Outpost Suitport Access

are still being researched and would depend on the lunar architecture team as the connector is a part of the lunar base and not the rover.

11.1.3.1 Rigid Inflatable Connector Tube Concept

A concept for a shirtsleeve transfer would be to construct a rigid-inflatable tube like structure that is connected with the outpost with a closed end cap on the other side where the rover can dock (see Figure 11.2). The construction material would be similar to the lunar outpost. Currently, the Lunar Architecture Team is also designing a tunnel system that would connect various compartments of the outpost. Once, the design is complete, it can be studied to analyze if the design would meet the requirements for the passageway to connect the rover with the outpost. In this design the tube would be pre-pressurized and have an imitation PLSS on the docking end (see Figure 11.3). For the design, one astronaut would use the suitport and exit the rover. The astronaut would then guide the rover to dock with the outpost connector tube. The imitation PLSS would align with the vacant suitport slot and the two structures would connect forming an airlock seal. Once the imitation PLSS has connected with the rover, the tube would then act as a "space suit" and the astronaut can open the compartment for a shirtsleeve transfer (see Figure 11.4). However, the design requires the entire backend of the rover to connect with the outpost connector, which is not feasible. The

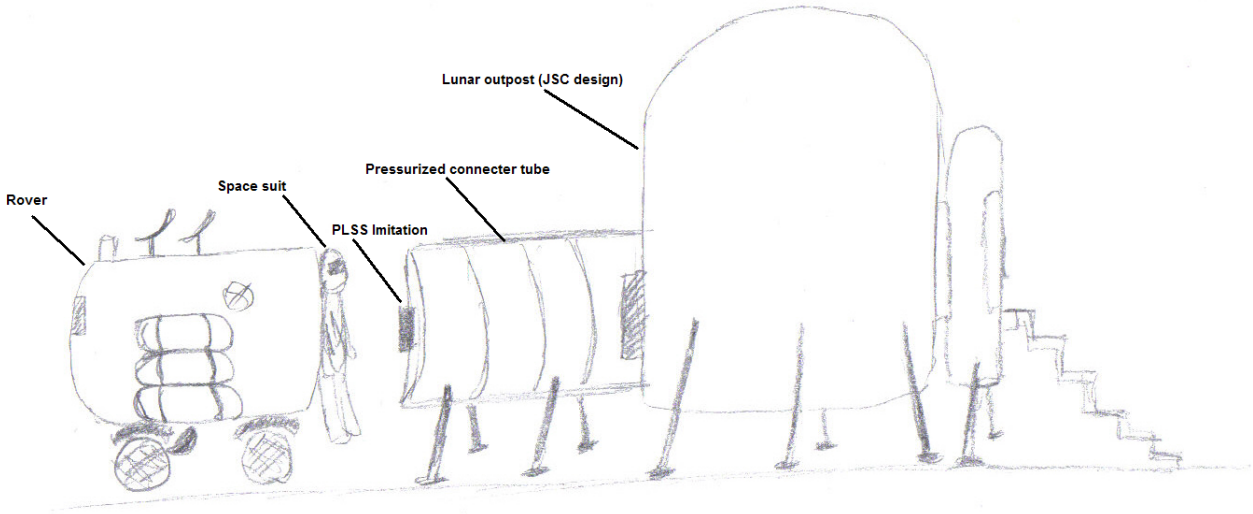

Figure 11.2: Rigid Inflatable Connection Tube Concept

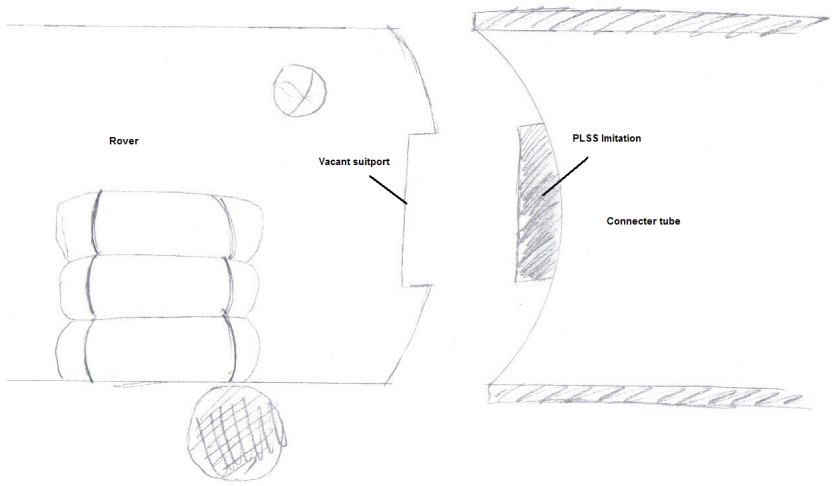

Figure 11.3: Rover-Outpost Docking: PLSS Imitation

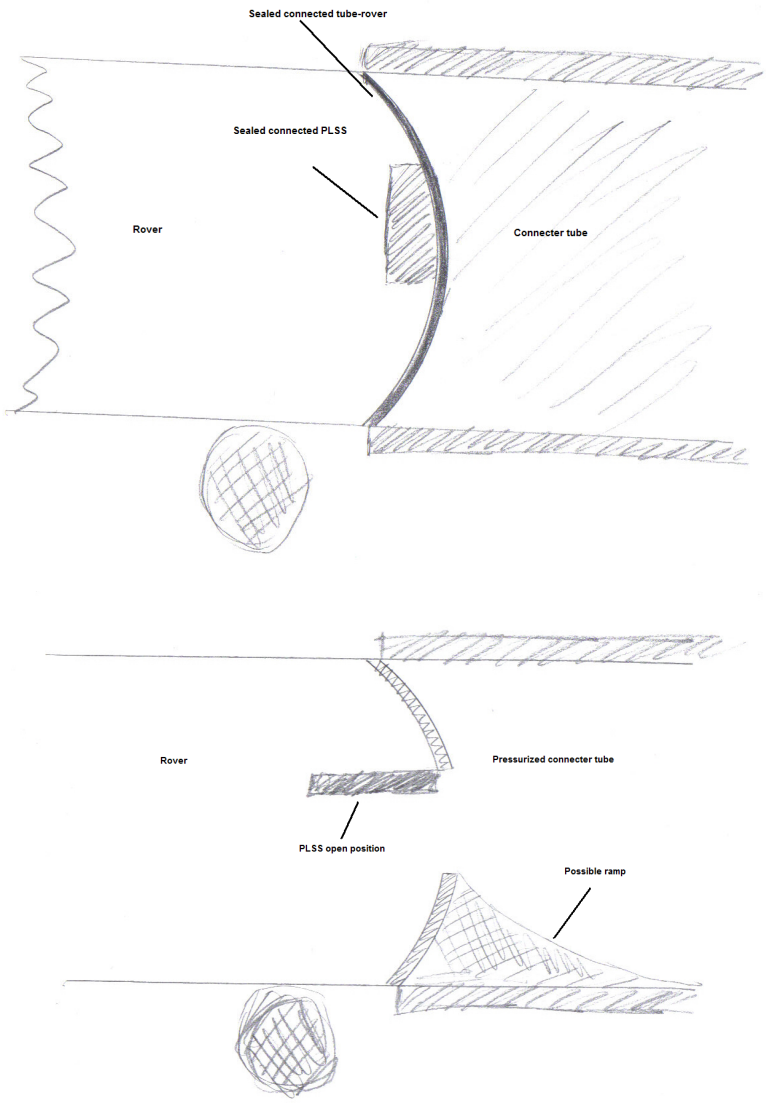

Figure 11.4: PLSS Connection

external platform and the second space suit serve as a major hurdle. In addition, it is a greater area that would need to be sealed.

11.1.3.2 Retractable Docking Concept

On the other hand, a simpler and an effective design would be to have a retractable spring like structure that is attached with the outpost and can be pulled to connect with the rover. The

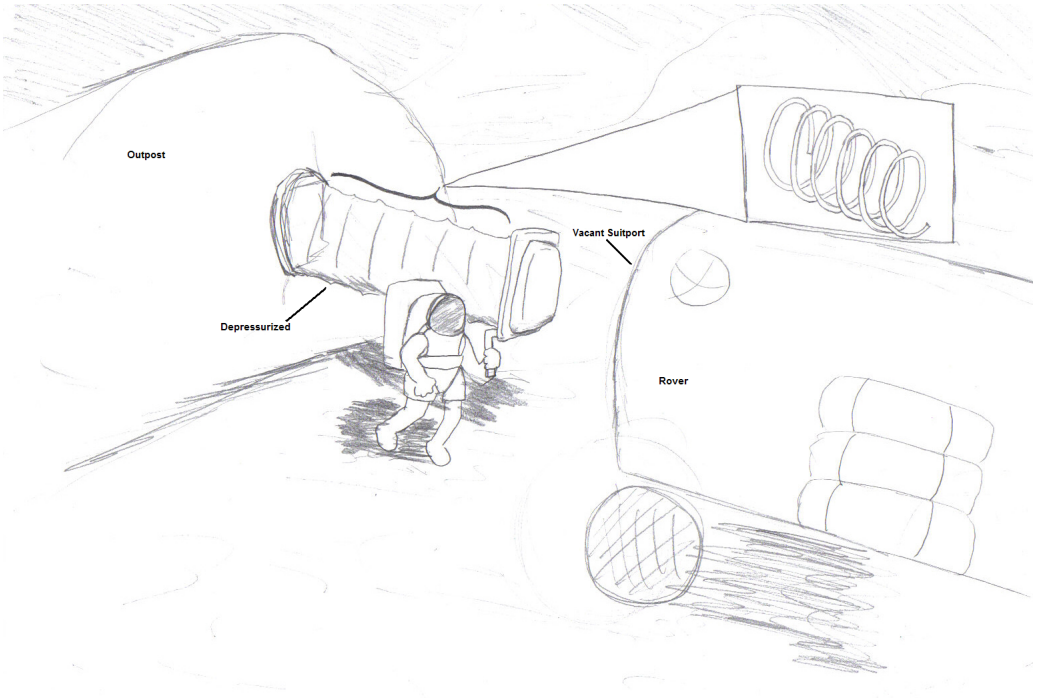

Figure 11.5: Retractable Docking Concept

connector tube would be attached to the outpost and remain depressurized when not in use. In order for the contraption to work, one astronaut would exit the rover from the suitport and pull the connector tube out of the outpost to connect with the rover's vacant suitport as seen in Figure 11.1.3.2. Once the connector tube has sealed with the rover, the astronaut would pressurize the tube. The connector tube would remain depressurized until the astronaut connects it with the rover. Once the tube is pressurized the second astronaut can open the suitport to create a passageway for a shirtsleeve transfer. Once the tube is pressurized, the tube would become rigid (see Figure11.6). The construction material for the connector tube has to be studied to determine the mass budget and the weight limit requirements. The pressurization effects on the tube would also need to be studied to determine the sturdiness of the connector tube and the maximum weight it can withstand.

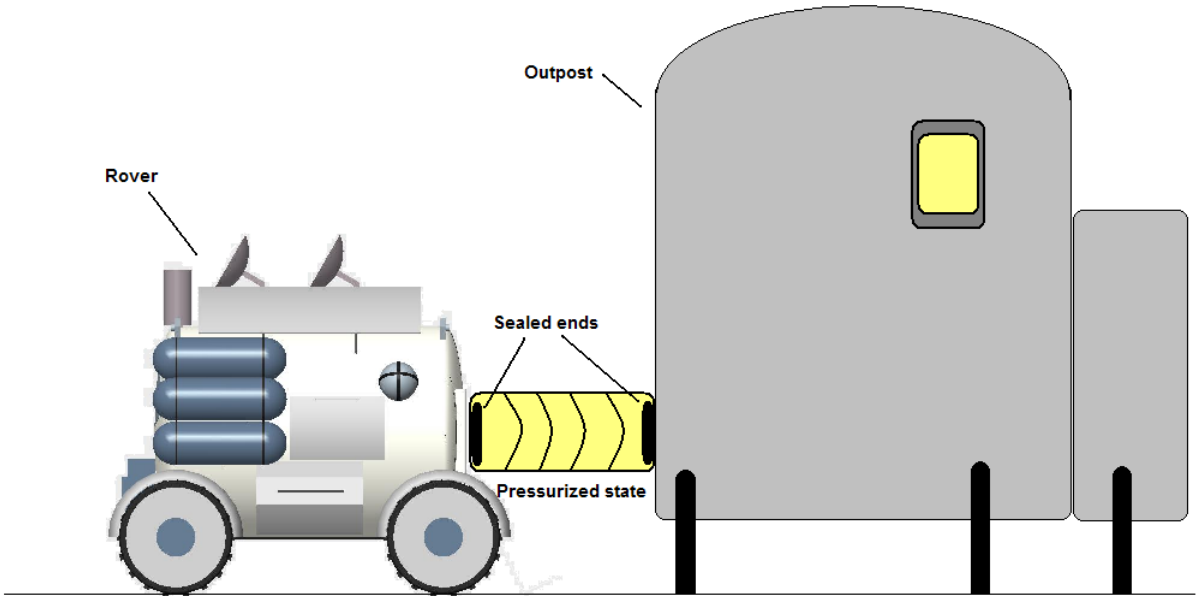

Figure 11.6: Retractable Connection Tube Concept

11.1.3.3 Outpost Rover Ingress/Egress (Jason Laing)

While the sortie rover is designed to allow for EVAs in the most lightweight and space-saving manner possible, using suitports to enter an outpost on the moon would not be ideal. Two equally impractical options exist: using a large garage on the outpost as an airlock for the entire rover, or using a small airlock on the outpost designed for individual astronauts. The former would involve venting and then resupplying more than 32.75 cubic meters of atmosphere in order to completely contain the rover. The latter option would force the astronauts to carry out two transfers: one from TURTLE onto the lunar surface, and one from the lunar surface into the outpost. Instead, a shirtsleeve transfer from the rover into the outpost would be preferred.

Because the aft endcap of the rover is already being used for ingress/egress (and therefore kept free of other technology, storage, or mechanisms), it is an ideal location for the addition of a shirtsleeve transfer (see Figure 11.7). With some small modifications to the rover, this can be achieved. First, a seal would need to be placed on the face of the rear endcap, just past where the knuckle ends. An aluminum ring would be installed around the perimeter of the seal, to which latches on the outpost could clamp, providing a tight seal. These modifications would be attached to members of the chassis, primarily the structure around the suitports.

An inflatable seal system on the part of the outpost colony would be ideal, as the structure needed would be minimal, and the atmospheric volume taken up by the transfer module could be reduced greatly when the module is not in use.

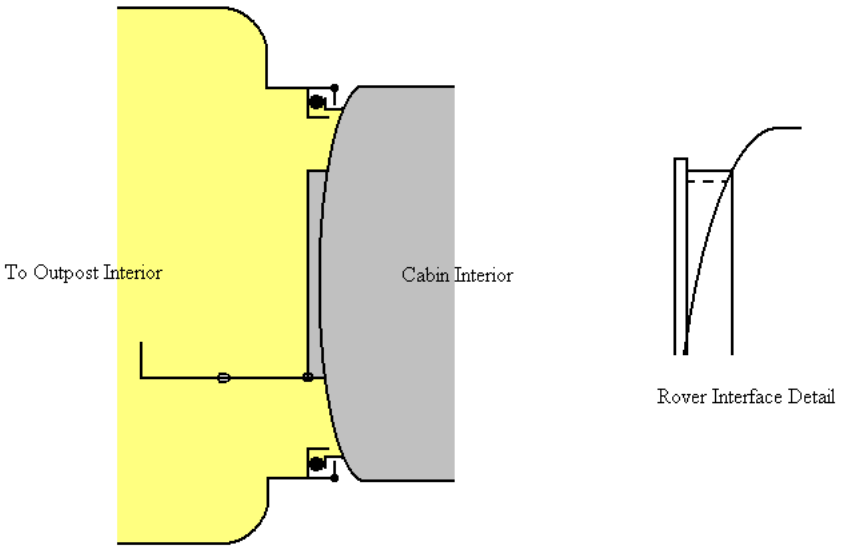

Figure 11.7: Shirtsleeve Transfer Between Rover and Outpost

Because the rover would be approaching the outpost from an exploratory mission, suits would already be attached to the suitports of the rover. This causes a slight complication in using the suitports for shirtsleeve transfer. While the suits would already be in the driving configuration (allowing the rear of the rover to cleanly mate with the transfer module), the suits would need to be detached. Outpost crew would need to assist TURTLE crew in first separating the suits from the rover, allowing the astronauts to exit the cabin. The suits could then be placed aside for inspection, repair, and resupply.

In order to help the TURTLE crew back the rover up to the transfer module for a proper seal, one or more of the cameras placed on the rear of the rover could help with visual alignment, and a set of smooth guide tracks could be installed just outside the transfer module to keep the rover in the correct path (see Figure 11.8). Such guide tracks would start level with the lunar surface and then sink to a depth of .5 meters, the limiting obstacle size for TURTLE. In addition, the use of an inflatable transfer module would mean that there would be a small amount of play in the positioning of the rear of the rover. As the clamps on the outpost module hold tight to the interface on the rover, any inaccuracy would be reduced as the module can slightly adjust its position.

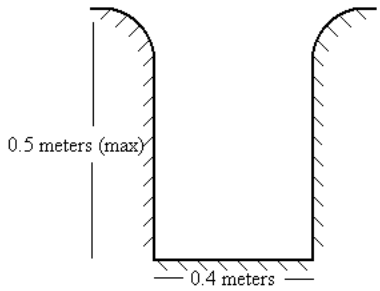

Figure 11.8: Outpost Guide Track, Head-on

Chapter 12

Field Rover

12.1 Field Rover Chassis Analysis (Aaron Cox)

The field rover analysis was very similar to the analysis done for the flight rover. The chassis model that was used in Visual Analysis was identical to the chassis model used in the analysis for the flight rover. Additionally, the method of analysis for the field rover was also identical to the method of analysis carried out on the flight rover. Differences arise in the loading case used to apply external loads to the model which also rendered different results.

12.1.1 Load Case

Only one load case was used in the analysis of the field rover. The scenario applied was almost identical to that of the flight rover analysis of the rock collision. Again, the scenario analyzed was a rock collision; however, the major difference in the load case was that the loads were applied in 1g rather than 1/6g since the field rover was only designed for operation on the Earth. The inertia loads in the field rover case were identical to the inertia loads in the flight rover load case except the magnitude of the forces was higher. The rover was still considered to be moving with a velocity of 7.5 km/hr and considered to be hitting a rock that was 0.1 meters tall. The member that experienced this rock impact was also the same as in the flight rover rock collision load case.

12.1.2 Results

As in the flight rover chassis analysis, Visual Analysis applied the external forces to the model, calculated the reaction forces in each node, and then reported the internal forces in each of the 90 members in the chassis. A sample of the results is shown in Figure 12.1 detailing the six highest stressed members in the field rover chassis. In addition, the figure shows the distributed and point loads applied to the chassis, as well as highlights the highest stressed members in the chassis red.

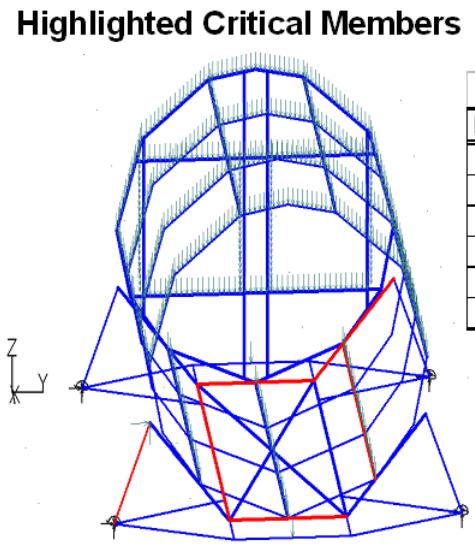

Rock Collision: Member Maximum Internal Forces						
Member	Axial (N)	Vy (N)	Vz (N)	Torsion (N-m)	My (N-m)	Mz (N-m)
M5	4100	300	-1400	-90	290	30
M6	4000	-350	-1800	-230	-200	130
M8	3621	-260	-510	60	90	60
M23	3600	3700	10	-30	10	-1700
M28	6200	1600	50	0	-40	0
M51	-1500	340	-1400	60	500	-180

Figure 12.1: Field Rover Member Internal Forces Results

12.1.3 Conclusion

The rock collision load case created most of the highest stressed in members that were located in the lower portion of the chassis. These member were found in the bottom rectangular section of the chassis. In addition, due to the loads being applied in an environment with higher g's, the member internal forces were higher overall in comparison to the internal forces calculated in the members for the flight rover. Therefore, the chassis members in the field rover will have to be sized larger than the members of the flight rover for the rock collision loads.

12.1.3.1 Field Rover Sizing (David McLaren)

The field rover is sized using the same material (aluminum alloy) and same procedure as the flight rover. The same model is used for its structural members as well.

A safety factor of 2 is used in this case, since minimizing its mass is not as crucial as for the flight rover. The other main difference is that only one loading case is applied: hitting a rock while driving. These loads become much more significant in Earth gravity.

The final mass of the chassis is 140 kg. In general, pieces which bear heavy loads during takeoff in the flight rover are smaller in the field rover. Conversely, pieces which bear the brunt of driving loads are larger in the field counterpart than in the flight rover. For example, the main chassis

member M6 discussed previously in the flight rover section is sized by takeoff loads, and has an outer width of 44 mm. Its field rover counterpart has an outer width of 31 mm. More dimensions are shown in the table.

Table 12.1: Safety Margins for Highly Loaded Field Rover Chassis Members

Member	M5	M6	M8	M23	M28	M51
Outer/inner width (mm)	33/19	31/17	23/11	56/32	48/26	39/23
Unit mass (kg/m)	1.5	1.4	0.9	4.5	3.5	2.1

All members shown are specifically sized to have a 10% margin of safety. They are sized by combined loading from axial forces and moments. None of the pieces are sized by buckling conditions.

12.2 Terramechanics (Ugonma Onukwubiri)

For the earth rover, analysis on terramechanics changes was done due to the distinct difference between the lunar surface and earth surface.

The soil parameter for the earth's surface is shown in Table 12.2.

Table 12.2: Earth Soil Parameter

Dry sand soil property	Symbol	Value	Units
Soil Cohesion	C_b	1040	N/m^2
Soil Cohesive Modulus	k_c	990	kg/m^2
Soil Frictional Exponent	k_ϕ	1528000	kg/m^3
Soil Deformation Exponent	n	1.1	
Internal Friction Angle	ϕ	28	$\circ$
Coefficient of Soil Slip	K	0.015	m
Coefficient of Friction	c_f	0.06	
Terzaghi Soil Bearing Capacity, cohesion	N_c	0.136	
Terzaghi Soil Bearing Capacity, overburden	N_n	0.178	
Wheel Slip Ratio	s	0.02	
Soil Density	γ	15200	g/m^3

The governing equation for the analysis of terrainability, mobility and trafficability is the same for both the field and lunar rover. The only difference is the acceleration due to gravity and the soil parameters. The field rover will not need grousers because it can achieve a positive drawbar pull with 4 wheels and without grousers as shown in Figure 12.2.

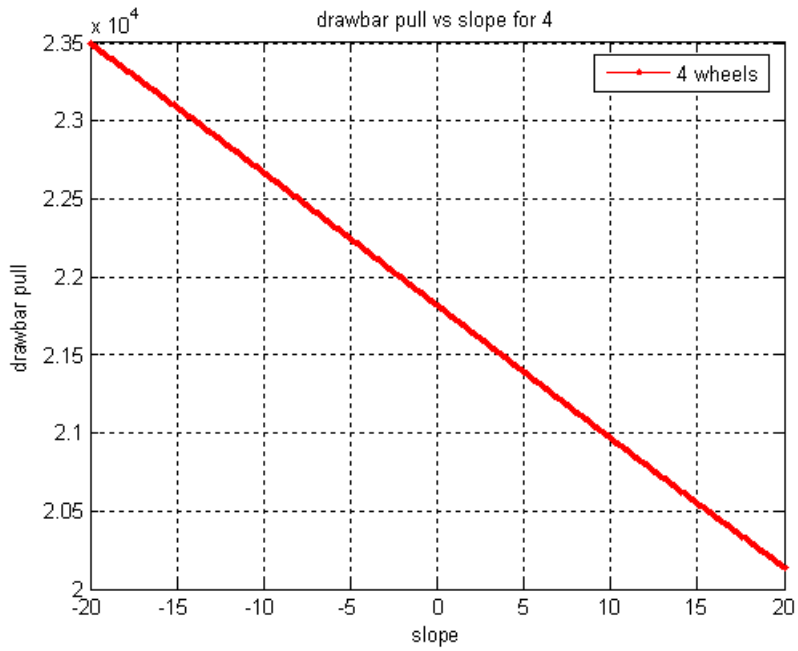

Figure 12.2: Drawpull vs. Slope on Four Wheels

12.3 Wheel and Tire Design for Field Rover

For the field rover, tires will be made out of the tweel technology by Micheline. Its a non-pneumatic tire that proves the concept of the lunar tires that will be using on earth. The dimension for the field rover tires will be same as that of the lunar rover. The non-pneumatic tweel technology is shown in Figure 12.3.

Figure 12.3: Tweel Technology

12.4 Braking System for Field Rover

The field rover will be using dual braking system. This includes magnetic and friction brakes. The friction brakes will be made out of titanium carbide ceramic in order to test the effectiveness of heat dissipation. It will have the same dimension as the lunar rover.

12.4.1 Stopping Distance

The stopping distance, stop time, and deceleration rate for earth is calculated in Table 12.3.

Table 12.3: Stopping field rover at 15 km/hr

	Value	Units
Stopping distance	1.11	m
Stop time	0.5	s
Deceleration rate	7.8	m/s^2
Brake force	15000	N

12.4.2 Stability and Turning

The turning radius and stability envelope is listed in Table 12.4.

Table 12.4: Turning radius and stability

	Value	Units
Turning radius	1.5	m
Critical angle, right	49.1	deg
Critical angle, front	50	deg
Critical angle, left	53.2	deg
Critical angle, back	55.6	deg

12.5 Power System for the Field Rover (Stephanie Petillo and Aleksander Nacev)

12.5.1 Overview

The power system for the field rover aims to remain as consistent as possible with that of the lunar rover design in order to evaluate its effectiveness, durability and feasibility on a lunar sortie mission. It will be based around the same PEM fuel cells used in the lunar rover, which can be bought as off the shelf units. These fuel cells, even as bought off the shelf, use oxygen from the air and gaseous

hydrogen as the oxidizer and fuel reactants to generate power. In the case of the field rover, three fuel cells (max power output of 13.2 kWatts each) are still necessary to attain the peak power draw of 32.62 KWatts and provide the nominal 5.25 kWatts throughout the field testing. A distribution of power requirements for all rover components to be used in field testing is given in Table 12.5.

Table 12.5: Distribution of power requirements during field rover testing.

Active Components	Nominal Power Draw (W)	Max Power Draw (W)
Motors	4419	31790
IMU	6	6
HD Camera	90	90
LIDAR	40	40
GPS	5	5
Computers	75	75
Sensor Interfaces	25	25
Hub	40	40
S-band Antenna	100	100
Ka-Band Antenna	94	94
Interior Displays	75	75
Exterior Lighting	200	200
Ambient Lighting	80	80
Total	5249	32620

12.5.2 Reactants

As previously mentioned, oxygen from the atmosphere will be readily available to the fuel cells since existing PEM fuel cells frequently use oxygen in the air as an oxidizer. Gaseous hydrogen will be used as the fuel of the reaction and will be stored in the six cylindrical pressurized tanks mounted on the sides of the rover. The same size and total number of reactant tanks will be used on the field rover as on the lunar rover in order to keep the distribution of structural loads on the rover as consistent as possible. The only change will be that all six tanks will contain pressurized hydrogen gas to be used throughout the mission, since the air does not need to be stored in tanks. Once the hydrogen in the tanks runs out, the tanks are either refilled or swapped out for new tanks of hydrogen by a ground crew. In this way, the field rover testing can continue with minimal interruption.

12.5.3 Reactant Tanks

To contain cryogenics and keep mass down on the lunar rover, carbon fiber composite tanks are used. For the filed rover, similar non-cryogenic composite tanks are sufficient to contain pressurized

hydrogen gas. In using high-pressure hydrogen gas stored at 35 MPa, the same composite tanks (tensile strength of 3,530 MPa) as designed for the lunar rover can be used, however the tank thickness would be increased to 5.0 mm to provide a safety factor of 2 for the tanks. These tanks will not need to be insulated as much as just shielded from the sun and extreme temperature changes to prevent expansion of the hydrogen.

12.6 Thermal Control System for the Field Rover (Aleksander Nacev and Stephanie Petillo)

12.6.1 Overview

The thermal control system for the field rover is very similar to the control system on the lunar rover. The main objective is still to remove excess heat produced from interior powered components, astronauts, and the fuel cells. However, the main difference is that the field rover can expel heat through convection and conduction using the atmospheric air as the high temperature heat sink. This means that the thermal control system does not need to rely only on radiative heat flux to expel heat to the environment. Therefore the control system can be much smaller and more compact. A traditional off the shelf air conditioning unit (with some modifications) can easily work for this control system. However, this section outlines the requirements of whichever system is built. The following sections will discuss the cooling system in terms of cold and hot temperature sides, the required pressure ratios and the mass flow rates. Again the thermal control system will be a single phase helium exchange cycle. If an off the shelf system were used, it would most likely have a multiphase freon heat exchange cycle. The reason for detailing the helium exchange cycle centers around the fact that if a prototype system were built it would be important to test fidelity of the interior working components of the simple gas exchange cycle. Therefore the choice to either modify an off the shelf system, or to build the single phase gas exchange system is given to the group designing the field rover. Either system would work to expel the excess heat build-up in the rover.

12.6.2 Heat Loads

Even though the rover is pulling in air from the exterior and cooling it, the thermal control system must still be able to supply enough cooling power so that the fuel cells and components will stay at a desired temperature. Table 12.6 shows the heat loads present in the field rover that must be removed. Again the components inside the rover are assumed to expel all power supplied to them as heat. This is again the worst case scenario for heat control in the rover. The fuel cells will also need to be cooled. Since the fuel cells are assumed to be 60% efficient, the other 40% of the reaction energy which is not captured by the fuel cells is assumed to be the heat produced. Therefore the

cooling system will need to absorb and expel the excess reaction energy based upon the power draw of the fuel cells.

In addition the field rover has one slight difference in the system compared to the lunar rover. Since the field rover is an open air environment, meaning it sucks air in from the outside and expels it, the cooling loop will cool the air only as it enters the cabin. Therefore the cooling system absorbs the heat from the fuel cells and then enters a cooling loop that takes heat out of the incoming exterior air. This air must then be cold enough to absorb the required amount of excess heat produced inside the cabin before it exits the rover.

Table 12.6: Heat Loads in Field Rover

Component	**Load (Watts)**
People	300
Ambient Lighting	80
IMU	6
GPS Attitude	5
Computers	75
Sensor Interfaces	25
AFDX Hub	40
Displays	75
Total	**606**

12.6.3 Thermal Cycle

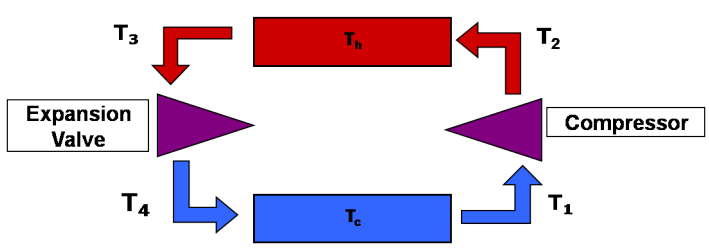

Figure 12.4: Thermal Cycle Overview

The field rover thermal cycle is very similar to the lunar rover thermal cycle. Heat is absorbed between stages T_4 and T_1. Then the gas, which absorbed the heat, is compressed and therefore at a higher temperature (stage T_2). The gas then expels the heat through the radiator system (described in Section 7.2.1 and comes to an equilibrium with the ambient temperature (stage T_3). Then the gas goes through an expansion valve and decreases in pressure and temperature and is ready to absorb more heat from the interior components (stage T_4).

Since the field rover will be on earth, the high equilibrium temperature (stage T_3) will be fixed to the ambient temperature. In addition the cabin temperature (stage T_1) will be fixed to 295 K. For the worst case scenario, the exterior ambient temperature is assumed to be 40 degrees Celsius, or 313 K. In addition the pressure ratio will change from the lunar rover, $\frac{P_2}{P_1}$ is 1.5. The ratio has decreased from the lunar rover system so that the compressor power draw can be much less. The power draw from the fuel cells is significantly higher in the field rover, hence there is more cooling that needs to happen in the field rover. These values allow the thermal system to be completely determined. Table 12.7 shows the temperatures, heat load capacities and mass flow rates of the thermal system. Figures 12.5 and 12.6 show how the mass flow rate and compressor power draw quantities change with the internal power dissipation requirement.

Table 12.7: Ranges of Thermal System Values

Quantity	**Average Power Draw**	**Max Power Draw**
T_1	295 K	295 K
T_2	347 K	347 K
T_3	313 K	313 K
T_4	266 K	266 K
Q_H	5.4 kW	35 kW
Q_L	4.6 kW	29 kW
W	0.94 kW	5.1 kW
$\dot{m}$	0.03 $\frac{kg}{s}$	0.2 $\frac{kg}{s}$

12.6.4 Radiator

The external radiator system will contain a finned radiator system that will have a fan attached to the front of it to promote air flow over the metal fins. This will be similar to the design of a car. It will be capable of expelling the required amount of heat depending on the power draw, seen in Table 12.7. There is no need to have a specific geometry as in the lunar rover, since radiative heat flux will not be the source of energy dissipation. This radiator can be stock off the shelf parts if necessary.

12.6.5 Internal Cooling Loop

The interior cooling loop length is calculated in the same manner that was done for the lunar rover. Figure 12.7 shows the required length of tubing for the system. To assume the worst case scenario, a length of 22.3 m was chosen with a tube inner diameter of 1 cm and a thickness of 1 mm. These have been designed as copper tubing but that material can change. One thing to note, if using copper tubing, a plating of an alloy might be best so that the exterior of the copper tubes does not

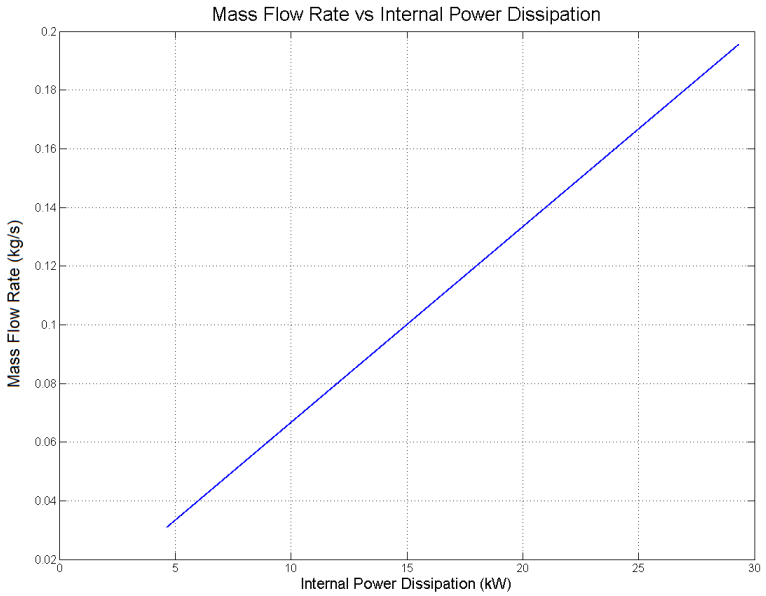

Figure 12.5: Mass Flow Rate vs Internal Power Dissipation

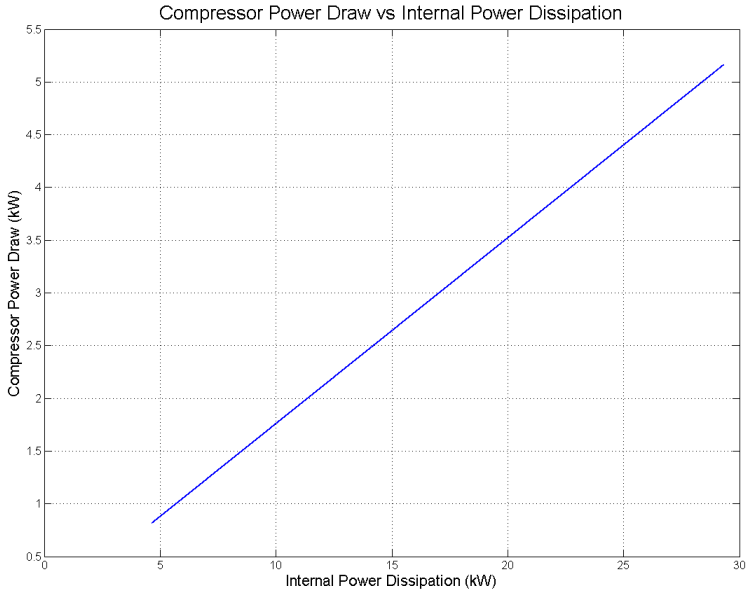

Figure 12.6: Compressor Power Draw vs Internal Power Dissipation

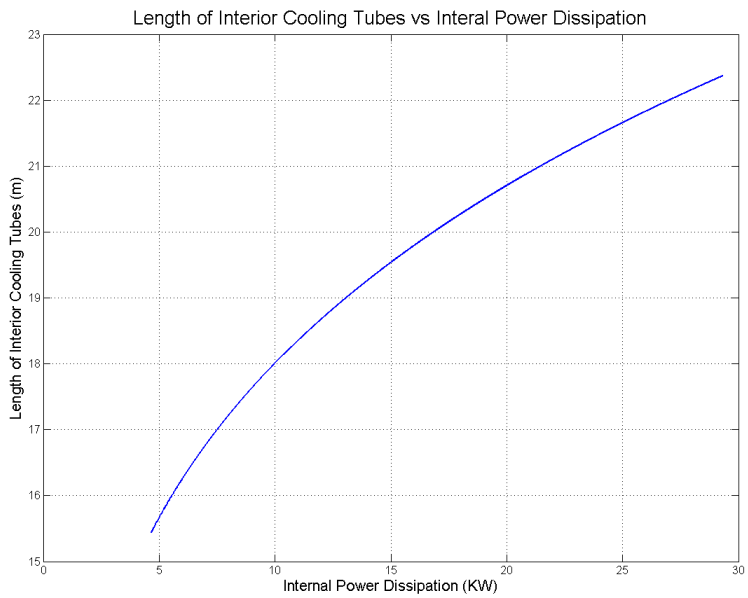

Figure 12.7: Length of Interior Cooling for Internal Power Dissipation

oxidize. These tubes can be bent and formed into a cooling coil that the incoming exterior air will pass over.

12.6.6 Efficiency

$$\beta_{ideal} = \frac{T_L}{T_H - T_L} \tag{12.1}$$

$$\beta = \frac{Q_L}{W} \tag{12.2}$$

The efficiency of the cooling system is determined in the same manner as it was in the lunar rover. Equations 12.1 and 12.2 show the method for determining the coefficient of performance for the ideal system and the designed system. The ideal system has a COP of 16.4 while the designed system has a COP of 5.68.

12.7 Suitport (James Briscoe)

Next to be discussed is the modifications for the suitports from the flight rover for the field rover. The suitport design itself does not change in the slightest. The same components are used as well as the same connections and seals. The only change is the loads felt by the PCS and suitport structure

corresponding to the difference in gravity. The critical loading for the actuators is plenty to handle the weight of the PLSS and PCS while operating on earth, so no design modifications are necessary.

One difference involved with ingress/egress in general is the addition of a hatch in the front of the rover. Despite the suitport design staying unchanged, there is a need to have another way into and out of the rover in case of emergencies. A separate hatch located under the interior driving station would also allow easy transfer of objects and people to the rover without the need to operate the suitport. A similar hatch is to be used for the outpost rover as well.

12.7.0.1 Field Rover Safety (Jason Laing)

In order to keep the test crew completely safe, support crew will be present to provide assistance at any moment. At least one support team member will be trained in CPR, and a fully stocked first aid kit will be on hand. An access hatch will be used if the cabin needs to be evacuated quickly, and class ABC fire extinguishers will be used in case of a fire.

12.8 Communications (Andrew Ellsberry)

The communications implementation for the field rover is composed of 2 major systems: a commercial digital voice and data transceiver and an 802.11G "WiFi" link to interface with the existing DesertRATS infrastructure. The two systems complement each other and provide a mix of simulation capability and operational reliability and safety.

12.8.1 High Data Rate Cmmunications

In previous years, DesertRATS has made extensive use of 802.11 "WiFi" nodes to provide a wireless network for the test area. The individual systems as well as operators and observers can easily connect and transfer data at relatively high speeds. Although there is the newer standard of 802.11N which provides higher theoretical throughput, the majority of the 802.11N units are targeted at consumers and home networking and professional 802.11B/G equipment will usually perform better at anything other than short range.

Both the Field Rover and its support vehicle will be equipped with an externally mounted access point/bridge. This device will be something similar to a Cisco Aironet 1300, an outdoor 802.11B/G access point/bridge which can link our wired vehicle networks to each other and the rest of the DesertRATS network. These units are specifically designed for use on moving platforms and also at temperatures from -30° to +55° centigrade, all of which will be required while driving across the desert. Additionally, the transmit power (100 mw) is still within the legal limits (normally 200 mw) so the units will remain license free, and not require paying FCC licensing fees or certification for the operators.

Both the Field Rover and its support vehicle will utilize the same access point unit so only one spare will need to be carried, but the antennas used will be more specialized. Each access point can utilize 2 separate antennas and the one with the best signal will be used for any given transmission. The field rover will be traversing some rather difficult terrain as part of its trials and will not always remain perfectly horizontal to the ground. For superior coverage even when climbing significant slopes or obstacles, it will utilize a short 3dbi vertical antenna which will provide coverage in all directions and is not highly dependent on the angle of the vehicle to the horizon. Both vehicles will also feature a similar but longer vertical medium gain antenna with approximately 6-9dbi which will provide a faster and longer range link when the vehicles are on relatively flat terrain (the support vehicle will be more likely to be on easier terrain). With the medium gain antennas, it should be possible for the support vehicle to operate from 100-500 meters away, which is probably further than it would normally be located for safety and other reasons (photography, etc). Depending on the infrastructure provided by the DesertRATS team, communications links up to a kilometer may be possible. The second antenna connection on the support vehicle will be used for a high gain parabolic antenna with somewhere from 24-30dbi of gain. The support vehicle and its access point can be configured as a wireless bridge that will retransmit the rovers signals to the DesertRATS network at up to 10 km from the coverage area (once again, this will depend on the NASA equipment). The high gain antenna will need to be pointed within a couple degrees of the other station and will be mounted on a tripod that can be manually deployed at a worksite, but will not be usable for continuous operation while the support vehicle is moving (the rover however can be mobile as long as it maintains communication with the support team).

12.8.2 Backup/Operational Communications

While the 802.11/WiFi communications link provides the best parallel to the actual lunar system (also a high speed wireless IP system), there will be some operational issues that it is not optimal for. The main considerations are that the 802.11 link is not as reliable and depends on the vehicles computer and that the range will be limited, especially if a long range traverse is tested. The secondary radio system will make up for these shortcomings by providing a high reliability, long range, and independent mode of communication. This secondary system is based on the DSTAR (also D*) standard which combines digital voice and data into one signal. A unit such as the Icom ID-1 provides the voice channel as well as 128kbps data in a stand alone, rugged (MIL-STD-810), package.

The DSTAR system operates in the 23cm band of the amateur (ham) radio spectrum. This has the extra requirement that the operators must hold at least a technician class license, which can be obtained by passing a test and in some cases paying a nominal testing fee of less than $15. This price is significantly less than the ~$75 per person required for a GMRS license or the site

costs of a commercial system. Moreover, the operators and test directors will be almost exclusively engineering students and faculty that will have little difficulty with the exam material.

12.9 Display Interfaces (Andrew Ellsberry)

The field rover will require displays that are reliable and effective for driving the vehicle. While the Honeywell DU-1310 displays are available for terrestrial applications, they are only used in aircraft costing tens of millions of dollars and up. While not publicly available, the acquisition prices are likely to exceed the budget for the Field Rover. Additionally, the DU-1310s are designed for use in aircraft and are not the optimal system to interface with the terrestrial computers in the Field Rover. Instead of using aircraft displays, the Field Rover will utilize industrial LCD panels that can be installed right in the consoles (as opposed to the commercial units that were installed behind the panels in the mockup). The critical considerations for these units are that they are sunlight readable, support touch screens, and closely model the size of the planned DU-1310 units. The sunlight readable and touch screen requirements are actually coupled as most (rugged) touch screens are imbedded in a glass pane that sits on top of the monitor and as the displays are at an angle to the viewer, even minor glare from the sun will cause major viewing issues as it passes through the 2 parallel layers of glass. Specially designed sunlight readable (stronger backlights and antiglare coatings) display panels with the touch screens bonded to the display surface will avoid this issue. The other constraint is that the displays should come close to the DU-1310 size planned for the Lunar Rover, which measure 14.1" (36cm) diagonally. The 14.1" monitor is not as common as 15" LCD displays in the standard 4:3 display ratio, (as compared to a 16:9 widescreen ratio) and as in the mock up, using a 15" display may be required as a slightly larger alternative.

12.10 Command & Data Handling (Andrew Ellsberry)

The internal data network for the field rover consists of a simple 1000BASE-T or gigabit Ethernet over copper network. This allows the team to ingenerate any number of devices including computers, existing IP video cameras, and motor controllers. To reduce cable runs, the topology will include 3 switches (hubs): one in the cockpit area, one in the rear of the rover, and one outside the rover. The switches allow devices to operate at different speeds (ie 100 Mbps and 1 Gbps) and also reduce the latency and dropped packets of a hub based system. The exterior switch is an industrial unit that is specified for the higher temperature ranges that it experiences while exposed to the extreme heat and cold, while the internal ones are quality commercial grade units.

Chapter 13

Conclusion

13.1 TRL Summary (Thomas Mariano)

The TURTLE TRL levels were compiled by the team based on clear definitions defined by NASA. These defintions are listed in Table 13.1.

Table 13.1: Technology Readiness Level Definitions

TRL 1	Basic principles observed and reported
TRL 2	Technology concept and/or application formulated
TRL 3	Analytical and experimental critical function and/or characteristic proof-of-concept
TRL 4	Component and/or breadboard validation in laboratory environment
TRL 5	Component and/or breadboard validation in relevant environment
TRL 6	System/subsystem model or prototype demonstration in a relevant environment
TRL 7	System prototype demonstration in the real environment
TRL 8	Actual system completed and "flight qualified" through test and demonstration
TRL 9	Actual system "flight proven" through successful mission operations

Using these definitions, each system was broken down into as many components as possible and then a TRL was determined for each. In some cases, systems as a whole were analyzed due to a lack of specifics on each component included. Items were then placed in each category based on the TRL reported by the teams. According to the teams, these are the highest TRLs for each component and system available. The results can be found in Table 13.2. This table is broken up into three development phases. Phase 1 is the conceptual phase and included TRLs 1 through 3. Phase 2 is the functional phase and includes TRLs 4 through 6. Phase 3 is the space tested phase and includes TRLs 7 through 9.

Table 13.2: Technology Readiness Level Summary

TRL 1-3	TRL 4-6	TRL 7-9
Vitreloy	Science Packages	IMU/Star Tracker
Suitport Components	Window	Propulsion System
Suit	Flooring	Structural Material
Lander legs	Wheels/Tires	LiOH Canisters
Lander Detachment Mechanisms	Brakes	Charcoal/Particulate Filters
Radiator	Motors/Gears	Solar Array
	Thermal Control	Perforated MLI
	Fuel Cells	"LEMO" Connector
	Circuit dreaker	Satellite Based Positioning
	Terrain Contour Mapping	On-Board Estimation
	Laser Ranging	Stereo Vision
	Data Bus	Ka-Band Communications
	Camera Lens	Joystick
	Honeywell Displays	

13.2 Reliability (Joshua Colver)

The reliability analysis for TURTLE focused on two primary events, Loss of Mission (LOM) and Loss of Crew (LOC). Loss of Mission entails a failure that causes the astronauts to abandon the mission, but does not result in any crew casualties. LOM only considers events after the crew rendezvous with TURTLE. Loss of Crew results in at least one crew fatality. Based on the information available and significant uncertainty in component reliability figures, only critical parts were considered in the analysis. Sub-components would only add significant error to the already uncertain results. In addition, all failure events were treated as independent occurrences.

13.2.1 Loss of Mission

Table 13.3 shows component reliabilities for Loss of Mission. There is a 2.8% chance of Loss of Mission over the course of both sorties. The LOM probability for one sortie is simply half this number, or 1.4%. With further research and development, these numbers can be made more accurate and give a truer picture of the primary risks to the mission.

13.2.2 Loss of Crew

Table 13.4 shows the component reliabilities for Loss of Crew. According to NASA, a mission of this nature must have a 99.9% crew survivability rate. Currently, this design does not meet NASA's standards and it is unreasonable to expect it to do so. As more analysis is done and prototypes

Table 13.3: Component Reliabilities for Loss of Mission

Component	LOM Reliability
Suitport Actuators	0.9999
Suitport Wiring	0.9999
Wheels	0.99
Motors	0.999
Suspension	0.99
Chassis	0.9999
IMU	0.9999
Data Bus	0.9995
CPU	0.999
Software	0.999
LIDAR	0.9999
Computers	0.9999999
Fuel Tanks	0.999
Aeroglaze reflective paint	0.999
Batteries	0.999
Thermal Radiation System	0.999
Total	.972

are built, more accurate reliability numbers will be generated. Once this stage is reached, certain design features may be altered to improve the overall reliability of TURTLE.

13.3 Cost Analysis (Thomas Mariano)

Cost Analysis is a vital part of any project. The cost of a project can be the deciding factor as to whether the project continues forward or is canceled. For this reason, the cost analysis must be as accurate as possible. Costs can be divided into two distinct types, non-recurring and recurring costs. Non-recurring costs are associated with design, development, testing and evaluation (DDT&E), and the construction of facilities. Recurring costs are associated with the construction of the vehicle, mission planning and operations as well as launch costs that are present throughout the life of the program.

13.3.1 Overview of Costing

The program consists of supporting missions to the Constellation program. Only three components are necessary and must be developed for the TURTLE program. The rover, the landing structure and transit stage must be developed while the launch vehicle is already developed. The goal of the program is to have an initial flight and landing of the rover on the lunar surface in 2020.

Table 13.4: Component Reliabilities for Loss of Crew

Component	LOC Reliability
Suitport Sealing	0.999
Fuel Cells	0.999999
Suspension	0.999
Chassis	0.9999
Pressure Shell	0.999
Data Bus	0.9996
CPU	0.999
Software	0.999
Air System	0.999
Aeroglaze reflective paint	0.999
Thermal radiation system	0.999
Total	0.992

13.3.2 Assumptions

In order to obtain the an accurate analytical estimate of the cost of the TURTLE program, certain assumptions must be made. The first assumption is that there is no DDT&E on the Launch Vehicle. A Level One Requirement states that the launch must take place on an existing EELV. The launch vehicle has been developed and flight proven. Thus, there is no associated non-recurring costs in the production of the launch vehicle. The second assumption is that the initial flight will take place in 2020. This is concurrent with NASA's planned return to the moon. The third assumption would be that there is an 85 percent learning curve on the construction of the rover. Fourth, the assumed program length is ten missions for the purpose of life-cycle cost estimates. Finally, there are three components that can easily be broken down by mass to estimate their costs: the lander, the trans lunar stage, and the rover.

13.3.3 Inflation

All of the cost models used to develop the cost estimates of each system found the value in 2005 dollars. Using an inflation calculator [65] recommended by NASA, all models were adjusted to account for inflation rates and are in 2008 dollars.

13.3.4 Non-Recurring Costs

The non-recurring costs of each of the required pieces was found using the NASA Advanced Mission Cost Estimator. This estimator was combined with the NASA Spacecraft/Vehicle Level Cost Estimator to help get a more accurate idea of the costs since nothing like this has ever been attempted

before. These models use the costing heuristic of

$$C(\$M) = a\left[m_i(kg)\right]^b, \tag{13.1}$$

where C is the cost in millions of dollars, m is the mass of the part in kilograms, and a and b are adjustable factors [83]. The mass does not include fuel, science packages or consumables. Using the costs found from the cost models on the NASA website, the values for a and b were found. These can be seen in Table 13.5 [83].

The next step was to calculate the mass of the systems. The mass that needs to be found is the mass of the system without any hydrogen, oxygen, consumables or science packages. These masses were all taken from the mass budget. To calculate the rover mass, the mass of the oxygen, hydrogen and all other consumables were subtracted from the maximum mass of 2500 kg. This value came to 2161 kg. The mass of the landing stage is the mass of the structure of the lander not including the mass of hydrazine fuel and was found to be 510 kg. The mass of the trans lunar stage was found to be 1470 kg when not including any fuel for the retro engine. The science package was calculated to be 116 kg. In addition, the calculated masses are shown in Table 13.5.

From these values, all of the costs were found and are listed in Table 13.5.

Table 13.5: Non-Recurring Cost Variables

System	m (kg)	a	b	Cost ($M)
Rover	2161	22.96	.55	1600
Trans Lunar Stage	1470	15.35	.55	850
Lander	510	8.99	.55	280
Science Packages	116	2.29	.50	25

13.3.5 First Unit Production

The first unit of production of the program is the cost to construct and launch the first mission. The same approach that was used for the non-recurring costs was used to find the first unit production cost. Using NASA's Advanced Mission Cost Estimator and NASA Spacecraft/Vehicle Level Cost Estimator, the values for a and b in Equation 13.1 were found. The same masses of each system were used from the non-recurring costs calculations. The variable values, the masses and the final costs are all listed in Table 13.6 [83].

Table 13.6: Recurring Cost Variables

System	m (kg)	a	b	Cost($M)
Rover	2161	.71	.662	120
Trans Lunar Stage	1470	1.11	.662	140
Lander	510	.58	.662	36
Science Packages	116	.39	.7	11

13.3.6 Learning Curve and Cost per Mission

A learning curve is defined to be based on the percentage of construction done by hand and the percentage done by machine processes. As defined by the NASA costing website, a typical value for aerospace projects is 85%. This learning curve is defined as 50% hand assembly and 50% machining [35]. An 85% learning curve is the value that was assumed for all new development items. However, for the EELV, the cost is set at 250 million, thus the learning curve for those are 100%, or no reduction in cost with an increase in quantity built. Figure 13.1 shows the incremental cost for each system per mission in the program.

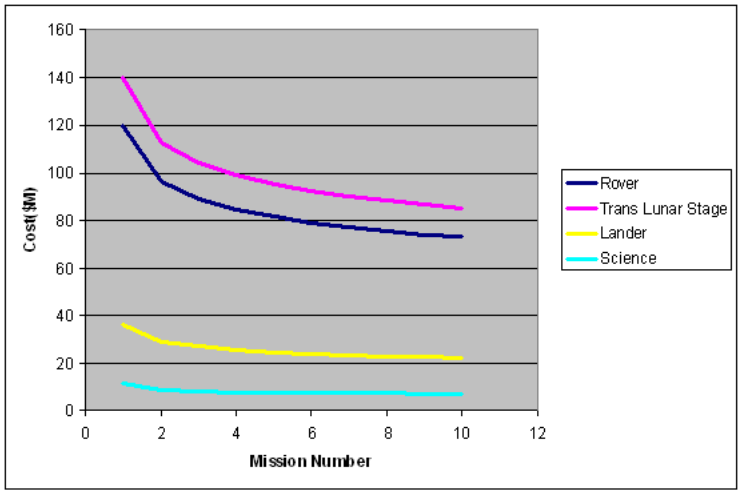

Figure 13.1: Cost of Each Mission

In Table 13.7 the total recurring cost of each system accounting for the 85% learning curve is listed for the ten mission program.

Table 13.7: Ten Mission Cost of Each System

System	Total Recurring Costs ($M)
Rover	850
Trans Lunar Stage	990
Lander	250
Science Packages	78

13.3.7 Cost Spreading

In order to more accurately estimate the yearly cost of the program, the non-recurring costs can be spread out using a standard beta function [33]. This beta curve allows for the cost of the program to be spread out over a definite time frame. For the TURTLE program of ten missions, with an initial flight in 2020 and beginning development immediately, the end of the program would be in 2029. This is the development cycle for the rover, trans lunar stage and the lander. However, the science package is assumed to be completed by the first mission so its non-recurring cost is spread from the present until the first mission. This means that the beta curve is to spread out the non-recurring costs for the next 21 years.

A beta function is based on two specific parameters, alpha (α) and beta (β) , where $0 < \alpha+\beta < 1$. These parameters are shape parameters than choose the shape of the distribution. The original choice for the parameters was $\alpha = .66$ and $\beta = .34$, because that would have over 70% of the DDT&E cost spent before the initial flight of the rover. However, it was suggested that fewer changes be made to the design that far into the program, thus the parameters were changed to spend as much as possible before the initial flight year of 2020. This led to the parameters being changed to $\alpha = 1$ and $\beta = 0$. Figure 13.2 shows the non-recurring cost beta function and how the cost is spread over the program life.

13.3.8 Life Cycle Cost

The life cycle cost of the program is how much the entire program will cost. The total cost of the program is the non-recurring plus recurring plus the launch vehicle costs. These costs are all listed in Table 13.8.

The total life cycle cost of the TURTLE program comes to 7.4 billion dollars. Due to the accuracy of these estimates, all values have been rounded to two significant figures. Figure 13.3 shows the spending over the life of the program with each item shown. The red line that goes up shaprly at 2020 is the total cost of the program. As can be seen in Figure 13.3 the majority of DDT&E spending is done before the launches begin. Thus in 2020 and beyond, the primary expenditure is contruction of the TURTLE system and the Delta-IV Heavy launch vehicle.

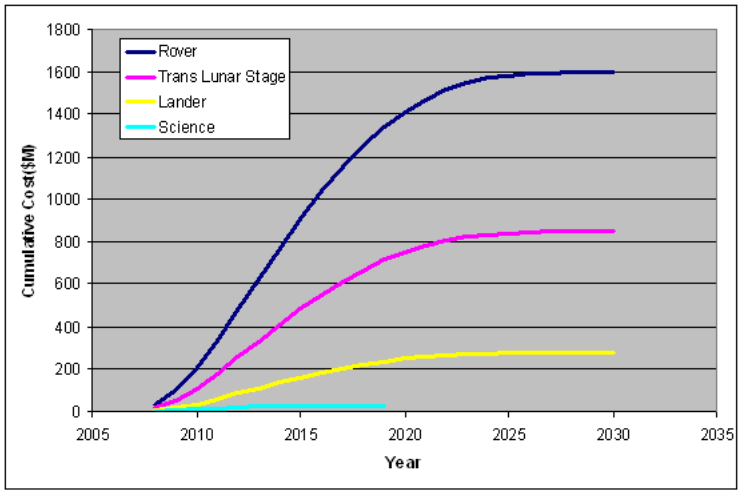

Figure 13.2: Beta Curve with $\alpha = 1$ and $\beta = 0$

Table 13.8: Total Cost of Program

System	Non-Recurring ($M)	Recurring ($M)	Total ($M)
Rover	1600	850	2450
Trans Lunar Stage	850	990	1840
Lander	280	250	530
Science Packages	25	78	103
Delta-IV	-	2500	2500
Total	2800	4700	**7400**

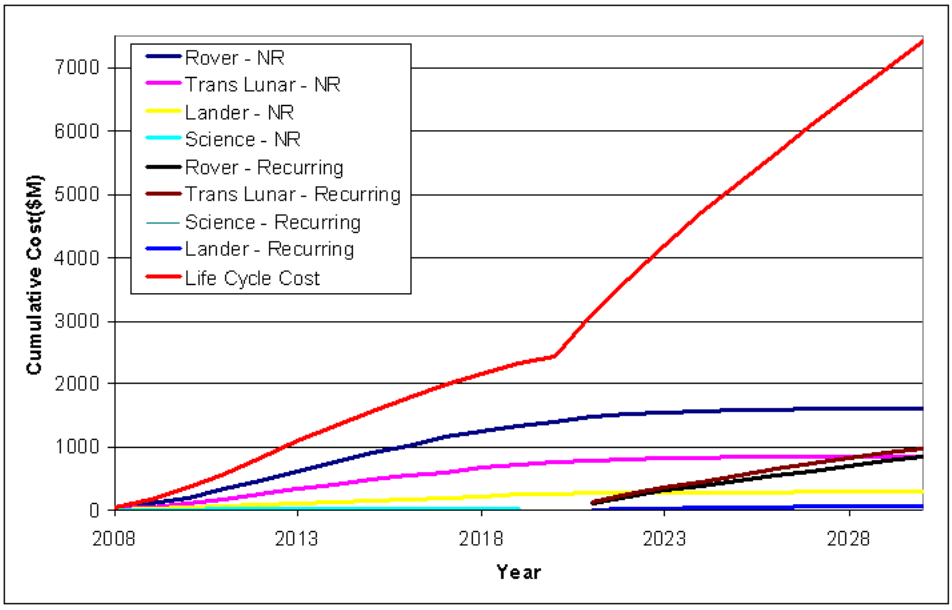

Figure 13.3: Life-Cycle Cost

13.3.9 Cost Readiness Level

Cost readiness level is defined by NASA's costing webpage to be as shown in Table 13.9 [83].

Table 13.9: Cost Readiness Levels

CRL	Description
9	End of project cost
8	Cost fit for very firm engineering and very firm budget commitments (+/- 5%)
7	Cost fit for firm engineering and firm budget commitments (+/- 15%)
6	Cost fit for PDR engineering decisions and PDR budget use (+/- 25%)
5	Cost fit for preliminary engineering decisions and preliminary budget decisions (+/- 35%)
4	Cost fit for very preliminary engineering decisions and very preliminary budget decisions (+/- 45%)

This cost eastimate is at a CRL of 4. This means that this estimate is very preliminary and also is within 45% of actual costs. Thus, the true cost of the program can be estimated to be within the bounds of 4.7 billion dollars and 11 billion dollars. This cost estimate is a very preliminary estimate and needs more analysis to get a better estimate of the true cost involved in the life cycle of the program.

13.4 Outreach (Madeline Kirk)

Engineering outreach is an important aspect of engineering projects for various reasons. It is necessary to publicize the project and encourage new ideas through outreach to the technical community. Outreach can also get the university and general public interested in space and lunar exploration when they see what a group of 34 students have done in the past year. Arguably one of the most important aspects of outreach is to students in elementary, middle, and high school. Many students are not introduced to engineering until late in high school when it is much harder to take the necessary classes to prepare for college engineering.

The outreach goal for this semester was 100% participation with a supplemental goal of 100+ hours of outreach, both of which were achieved. Our outreach was accomplished through a variety of small programs rather than one or two larger programs. The series of programs included University of Maryland Open House presentations, elementary, middle, and high school events, design reviews, and Maryland Day demonstrations.

13.4.1 Open House

The open house programs were run through the University of Maryland Aerospace Engineering Department as part of a prospective student open house day. Project TURTLE was presented by a group of 3-4 team members as part of the Aerospace Engineering presentation. In addition to discussing the overall TURTLE design, we spoke about how the design process for a large scale project works. The presenting students also remained after the presentation to answer questions from prospective students and parents. The open house presentations gave the team a chance to show high school students and parents what is possible in aerospace engineering at Maryland. We participated in four open house sessions with fourteen different student presenters.

13.4.2 School Presentations

The school presentations were one of the biggest priorities of TURTLE outreach. We visited four high schools and two middle schools in the Maryland/Virginia area and had ten team members present between the six schools. We also had one elementary school visit the Space Systems Lab where we gave them a tour of the lab, including the TURTLE mock-up. The high school presentations introduced the basic concept of engineering and design process in addition to the TURTLE Project. Students asked questions about the specifics of the rover and how it comes together as a whole. Although a few were engineering classes, most were regular science classes or science clubs. We took a slightly different approach for the middle school presentation. Because middle school students often have a shorter attention span and less technical knowledge, it was important to design a presentation that was interactive and presented information on their level. To engage the class, the presentation was centered on students responding to questions and developing what engineering is

through their answers. Students learned how many types of engineering are important in aerospace engineering and "designed" a space capsule by determining what each type of engineer would design in the project. After showing the rover design and mock-up pictures there were many questions from the students about TURTLE specifics including "How do you use the bathroom with less gravity?" These school presentations play an important role in developing engineering interest at a young age. Without these presentations, many students may not be exposed to engineering until high school or even college.

(a) Walter Johnson High School (b) Marshall High School

Figure 13.4: Presentation at Walter Johnson and Marshall High Schools

(a) Answering questions (b) Looking in the rover

Figure 13.5: Drew Elementary School Tour

13.4.3 Design Reviews

To create project milestones and receive feedback on our design, we had a series of design reviews that were open to the public. In the fall we had a Preliminary Design Review which was open

to only a few guests due to space limitations. In the spring, however, we had two major design reviews, the Baseline Design Review and the Critical Design Review. Both reviews were open to the public and well attended. At BDR we hosted approximately five individuals from aerospace industry in addition to UMD professors, and several aerospace graduate students. At the Critical Design Review we hosted approximately 30 people outside of the class including industry professionals, members of the Space Automation and Robotics Technical Committee, Aerospace professors, aerospace graduate students, as well as family and friends. The critical design review also provided an opportunity to demonstrate the testing capabilities of the mock-up rover. There was an interior layout demonstration as well as a functional suitport demonstration with full ingress and egress. An interior camera displayed the internal activity on a monitor outside the rover for visitors to view.

Another major event was the Rover Rollout. Similar to rollouts in aerospace industry, we invited professors and affiliated professionals to view our rover for the first time with a suitport demonstration and short presentation describing the structure and interior of the rover. Visitors were also encouraged to go inside the mock-up and sit in the driving and sleeping configuration.

(a) Crowd at rollout (b) Mock-up interior

Figure 13.6: Rover Rollout

13.4.4 Other Activities

There were several other small presentations and events including a presentation for a UMCP-AIAA general body meeting, the Aerospace Advisory board, and the Aerospace Banquet. We also provided tours of the University of Maryland labs for visitors of the AIAA student conference this spring including a tour of the Space Systems Lab where the mock-up rover was constructed.

The largest outreach event was our participation in Maryland Day. Maryland Day is a university sponsored day where the campus is open to the public with activities and presentations from most of the colleges and departments. There was an estimated 70,000 people in attendance. To demonstrate the capabilities of our mock-up and show off the aerospace engineering department, we had a number

of activities. There were suitport demonstrations every hour and a few people were let inside the rover when crowds were low. A poster display showed the construction process and flight design CAD model and a space simulation program called Celestia was available for users to travel through a simulated solar system. For younger children, we provided a variety of candy to design and create a candy lunar rover. Our students also helped out at a variety of other aerospace related programs throughout the day including a mini wind tunnel demonstration with Sigma Gamma Tau, the Aerospace Honor Society, and staffing the Aerospace Engineering informational table.

In 13.10 is a summary of the outreach events and class participation. We had a total of 143 man-hours of outreach, 18 events, and 100% participation from the class. A detailed chart of student outreach participation is located in the Appendices.

Table 13.10: Summary of Outreach Activity

	Man-Hours	Team Members	Events
School Visits	25	10	6
Open Houses	17	13	4
Rover Rollout	2	20	1
Baseline Design Review	3.5	33	1
Critical Design Review	4.5	34	1
Maryland Day	82	22	1
Other	9	8	4
Totals	143 hours	100%	18

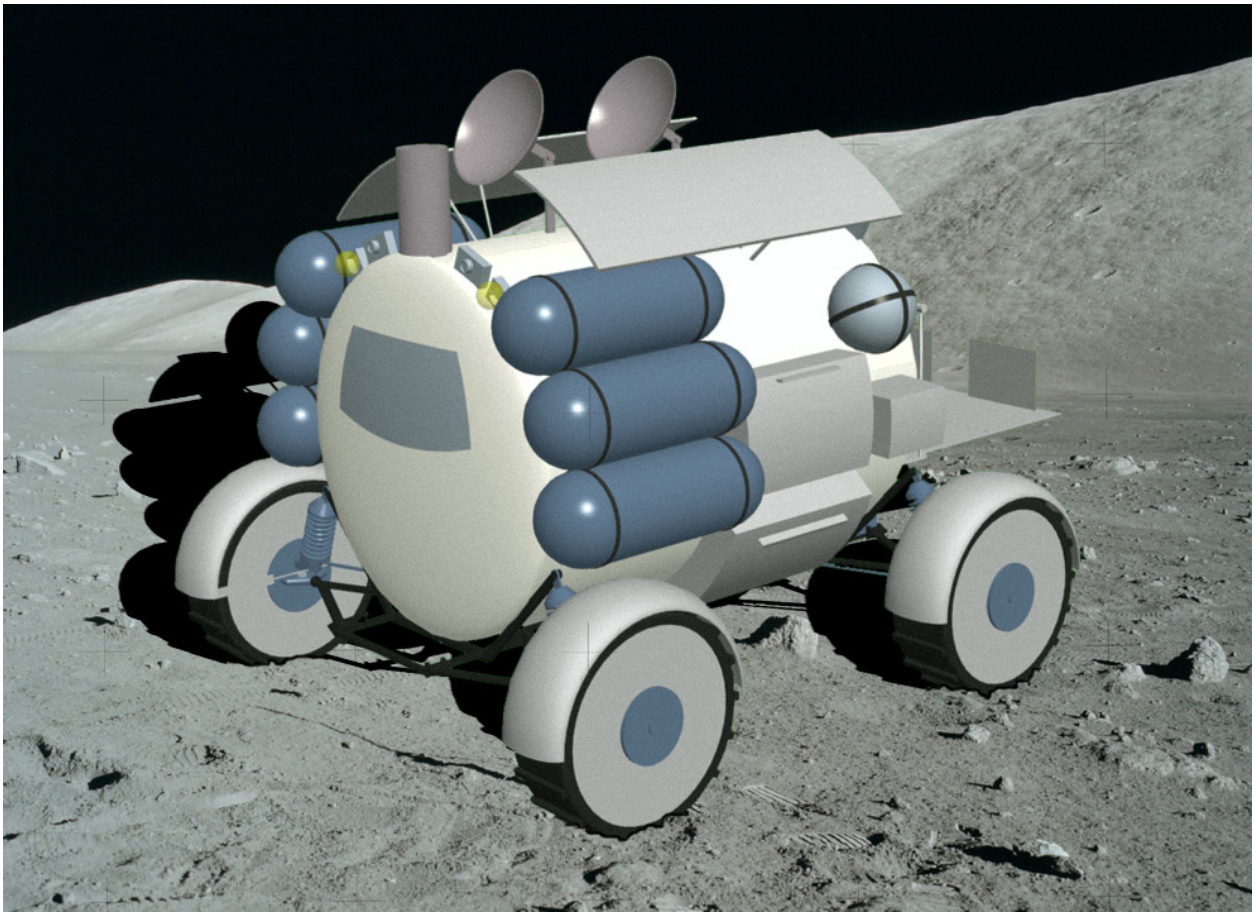

Figure 13.7: Conceptual Illustration: TURTLE on the Lunar Surface

Appendix A

Trade Studies

A.1 Retro Engine Trade Study (Ryan Murphy)

The retro engine is required to brake the payload into a lunar orbit, begin lunar descent, and provide a significant thrust to slow down the landing system during the initial descent to the surface. As such, the retro engine must be restartable. Additionally, the retro engine must fit within the payload shroud of the Delta IV-H (5 m by 19.8 m) along with the structure, fuel tanks, rover, and landing system.

Several options were considered and compared as shown in Table A.1. Since the HM7B is not restartable it was eliminated from consideration, leaving the RL10B-2, RL10A-4-2, RL10A-3-3A and the VINCI engines.

Table A.1: Comparison of Possible Retro Engines

	RL10B-2	RL10A-4-2	RL10A-3-3A	HM7B	VINCI
Isp (s)	462	451	444.4	444.2	465
Mass (kg)	301.5	167	140.6	165	280
Mixture Ratio	5.8:1	5.5:1	5:1	4.8:1	4.84:1
Restartable	Yes	Yes	Yes	No	Yes

A thorough analysis of the engines given the mission parameters was conducted. Assuming an 800 m/s burn into LLO at 200 km, the remaining burns were determined using the exact quantities required to descend from the 200 km altitude through a Hohmann transfer ellipse to 2000 m above the surface[1]. The graph in Figure A.1 shows that the RL10A-4-2 is the best choice for landing the most mass on the moon. However, the other engines are comparable and able to land within 70 kg

[1]The 2000 m separation was determined through an analysis of the landing system to maximize the mass landed on the surface

of the mass landed by the RL10A-4-2. Thus, the RL10B-2, RL10A-3-3A and VINCI are alternatives to the RL10A-4-2 and can be used without drastically changing the rover size or mass.

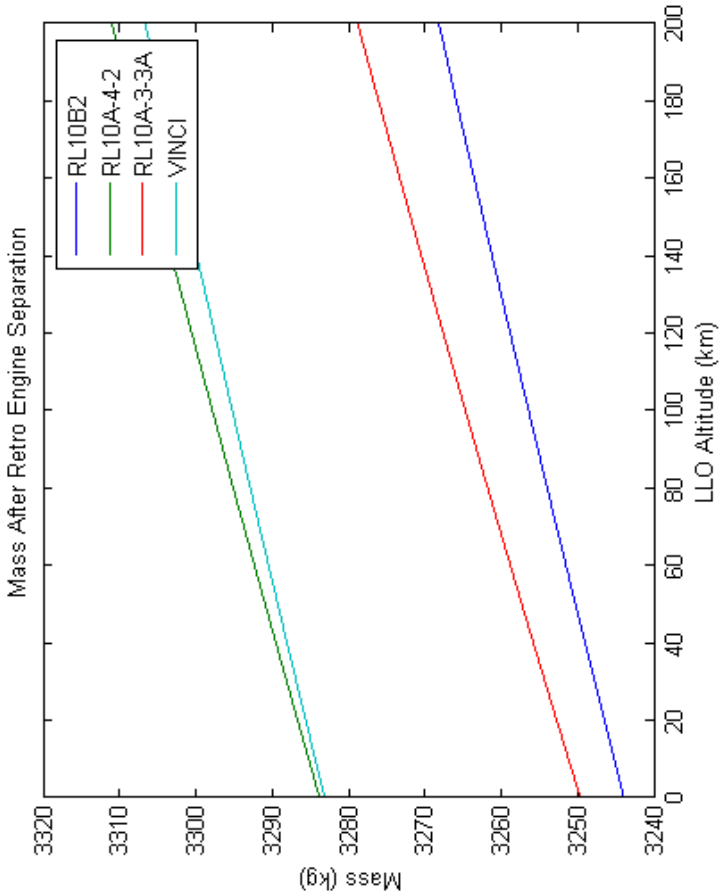

Figure A.1: Total Lunar Landing Mass for the Retro Engines

A.2 Initial Chassis Analysis of the Flight Rover (Aaron Cox)

Analysis done on the chassis was not originally carried out with Visual Analysis or any other computer software program. Instead the analysis was initially done using hand calculations on a much simpler version of the chassis. The goal of this approach was to obtain a relatively quick, rough first cut analysis of the chassis members. The results obtained from this analysis ideally were expected to be within an order of magnitude of the results that would later be obtained using a

more accurate and extensive chassis model. The idea was to use these initial results as verification that the results later obtained with the aid of a computer software program were sensible.

A.2.1 Chassis Model

The original model was hand drawn only contained the lower portion of the rover chassis as seen in Figure A.2. The nodes at each endpoint distinguished each member. The four rings contained in the upper portion of the model were not present. In addition, the suit port supports were also not present in the model. Specifically, the lower rectangular section of the chassis consisting of two diagonal cross members (i.e. members LD and CK) was modeled along with the "shock tower". Where, for instance the front "shock tower" consisted of members BC, CD, and DE. Furthermore, this initial model did not depict the wishbone members completely. Instead the connection between the wheel and chassis was viewed as a single member (i.e. member AC) rather than two members. The suspension was modeled as a beam rather than a spring and damper in this analysis. In all, this model of the chassis consisted of 18 members compared to the 90 total members that were modeled and analyzed in the later chassis model.

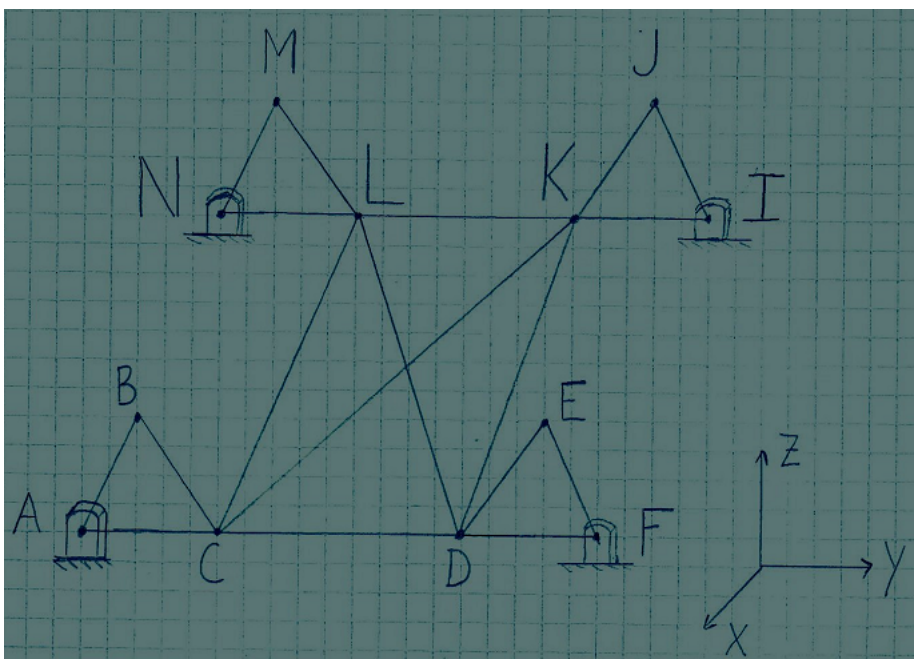

Figure A.2: Initial Chassis Model

A.2.2 Loading Cases

Two load cases were analyzed in this model. At this point of the analysis, launch loads were not considered. Instead, the two scenarios considered were landing onto one wheel and hitting a rock with one wheel while driving.

A.2.2.1 Landing

The landing scenario modeled the stresses that occurred from hitting the lunar surface with one wheel. Specifically the impact was applied in the positive z direction through the right, forward wheel that was attached at node A in the chassis model. The magnitude of the landing impact was derived using a custom made MATLAB code. As a rough estimate, the entire suspension system was considered a spring and damper. Essentially, the rover was modeled as a mass attached to a spring. Rough estimates were made for the values consisting of rover mass, spring constant, and damping constant. In addition, the velocity upon impact with the lunar surface was known to be roughly 1 m/s. Using this information, equations were derived for the displacement, velocity, and acceleration of the rover which modeled the oscillations of the rover mass over time after it impacted the lunar surface.

The derivation of the acceleration equation along with the known rover mass, allowed the force applied to the rover during landing to be quantified. The MATLAB script was used to plot the force vs. time after impact. The maximum value for the applied force was then determined directly from this plot to be roughly 9000N. The inertia loads were also rough estimates. They were applied as point loads at six different locations on the chassis. They were applied in the negative z direction at nodes L, K, C, and D. In addition two more point loads were applied in the negative z direction halfway between member LK and member CD. These point loads were meant to represent the weight of all the components being supported by this lower portion of the chassis. The total weight being supported was divided evenly among these six locations. At this stage of the analysis, the locations of these inertia loads were approximated as the connection points to the upper portion of the chassis structure which included the four circular rings.

A.2.2.2 Hitting a Rock

This loading scenario addressed the loads applied to the chassis while driving on the lunar surface. This scenario was very similar to that of the landing load case. For instance, the inertia loads were modeled identically to the inertia loading described in the landing load case scenario. Again, the external load applied from the rock impact was applied to the right, forward wheel in the positive z direction at node A. The only major difference in this load case was the magnitude of the applied force due to the rock impact. As before, a MATLAB code was created to model the oscillations of the rover after striking the rock. The rover was considered to be moving at 7.5 km/h and the rock

was considered to be 0.1 meters tall above the surface. Using this information, the magnitude of the impact was determined to be roughly 4000N.

A.2.3 Method of Analysis

Several iterations were required to obtain the optimal method of analyzing the chassis members. Initially, the chassis was approximated as a truss structure, then as a space frame. Both methods were carried out with hand calculations. Ultimately, the analysis was carried out with the aid of a software program.

A.2.3.1 Truss Structure

The chassis was considered to consist of three major trusses for this analysis. One section was considered the front, another section was considered the rear, and the third section was considered to be the bottom of the chassis. A front view and a rear view of the chassis (i.e. a y-z plane view) were used to form a free body diagram to help determine how the truss structure was going to be analyzed. Both views essentially equated to the same FBD since the chassis was symmetric about the z-axis. As seen in Figure A.2, the front and rear view shows two triangular sections on the left and right side of the chassis which represent the suspension and wheel attachments. For example, members AB, BC, and AC form one triangular section at the front of the rover, and members DE, EF, and DF form the other triangular section at the front of the rover. A horizontal member represented the center of the chassis which connected these two triangular sections (i.e. member CD at the front of the chassis). Similarly, the truss considered to be the rear of the chassis contained members NM, NL, ML, LK, KJ, KI, and JI. The third section of the chassis that was modeled as a truss was the bottom rectangular portion. A top view (i.e. a x-y plane view) was used to set up the FBD in this perspective. This section consisted of members LC, KD, CD, LK, LD, and KC.

The truss analysis was initially done using hand calculations on paper. With the external force applied at node A, and with the lengths and geometry of each attached member known, the method of joints was used to determine the forces present at each node in the model. The forces at the node A experiencing the external force were first calculated, and then the method of joints allowed the propagation of this applied external force on the remaining nodes to be calculated.

A major drawback with this method of truss structure analysis became apparent. Although treating these three major sections of the chassis as a truss allowed quick and relatively simple calculations to be carried out, the analysis did not fully model all the internal stresses that were occurring in each member. Only the forces at the endpoints of each member were being considered. Also, the axial forces in each member were effectively being analyzed with this method but torsion, bending moments and shear forces were being neglected. Another iteration in the analysis process was required to account for these other internal forces in each member.

A.2.3.2 3D Space Frame

Treating the chassis as a frame allowed for additional internal forces to be calculated. Once the external loads were applied for the loading case under consideration, the reaction forces were calculated at the constrained nodes located at nodes A, F, N, and I. Again, these nodes represented the connections between the chassis and the wheels. With the reaction forces at each of these nodes determined, the reaction forces at the endpoints of each member could also be calculated. For instance, with the reaction forces known at node A, the reaction force in member AB at node B can be calculated. Member AB, in addition to the other 17 members, under considered to be static in this analysis. Therefore, the sum of the forces applied to the member AB must be equal to zero, and the reaction forces in node B must be equal and opposite to those reaction forces in node A. Similarly, this method was applied to the remaining members to obtain the reaction forces.

Once the reaction forces at the endpoints of every member was known, each member of the chassis was treated as a beam. The constraints at the endpoint of each member varied. Many of the members were completely fixed at both of its endpoints; however, the members that were connected to the wheel locations were not fixed at both endpoints. Instead, for instance, member BC was allowed to rotate about the x axis at node B. Similarly, members NM, JI, and EF were allowed to rotate about the x-axis at nodes M, J, and E respectively. Also, member AC was allowed to rotate about the x-axis at node C. Again, similarly, members NL, KI, and DF were allowed to rotate about the x-axis at nodes L, K, and D respectively.

The applied forces in each beam were then taken into consideration. Some beams were considered two-force members where on the reaction forces at their endpoints were applied (i.e. member AB). Other beams had multiple forces applied to them due to the inertia loads in addition to the reaction forces at the endpoints of the beam. In the two-force members, a single section cut was made at a location between the endpoints. The internal axial force, shear force, and bending moment were then calculated at this section cut. In the other beams with multiple applied forces, multiple section cuts were taken. The location of these cuts were placed in between the endpoint and the applied load along the length of the beam. The internal forces at each section cut were calculated in these members.

A MATLAB code was created to streamline the process of calculating the internal forces in each member. The hand-derived equations that determined the reaction forces and the internal forces in each member were included in the code. The MATLAB script used the external loads from each loading case as inputs and then used the equations to output the internal forces in each member.

A.2.4 Results

The internal forces in each of the 18 members were used as a launching point for member sizing. Each loading case created different magnitudes of internal forces in each member of the chassis. The

results allowed the critical load in each member to be determined by comparing the internal loads in each member for each load case and then determining the maximum internal load that occurred.

This method of analysis was an improvement on the truss analysis; however, some undesirable results were still apparent. At this stage of the analysis, the calculated shear force only represented the shear in the one direction. The calculated bending moment represented only the bending moment about one direction as well. The shear in the additional direction, as well as the additional bending moments and torsion had been neglected.

A.2.5 Conclusion

The frame analysis was the optimal method to enforce for the chassis analysis. The hand calculations and the MATLAB script that utilized these calculations had made the process quicker but not necessarily more accurate. Additional components of the internal forces in each member needed to be accounted for. Therefore, another major iteration in the analysis process was consequently required.

A.3 Rover Analysis Model (David McLaren, Aaron Cox)

These figures show the model created in the Visual Analysis program to determine forces in chassis members. It is a close approximation of the structure designed in CAD. Forces for each piece and the resulting sizes are tabulated in Appendix A.4 and Appendix A.5, respectively.

Figure A.3 is a top view of the chassis section which supports the pressure shell and other rover components. The chassis members referred to in the sizing analysis section are those in the center, M5-8 and M19-21. These comprise a box with cross-pieces inside of it.

The rear ring of the rover (Figure A.4) is on the side where astronauts enter and exit through the suitports. Hence, additional structure is added to bear these loads during launch, and also during ingress and egress.

The other three rings are identical and do not need extra supports. The ring shown in Figure A.5 is the next one up from the rear ring. For the next ring closer to the front, all corresponding pieces are numbered MX-1, and those in the front ring are numbered MX-2 (Figure A.5), where X is any of the piece numbers from this figure.

The front and rear of the chassis are shown in Figure A.6. In these sections, the center piece is one of the rigid chassis members. The next two out from that are the shock towers, and the two at the outer edge are the pieces going to the wheel hubs.

The struts shown in Figure A.7 run along the length of the rover from ring to ring.

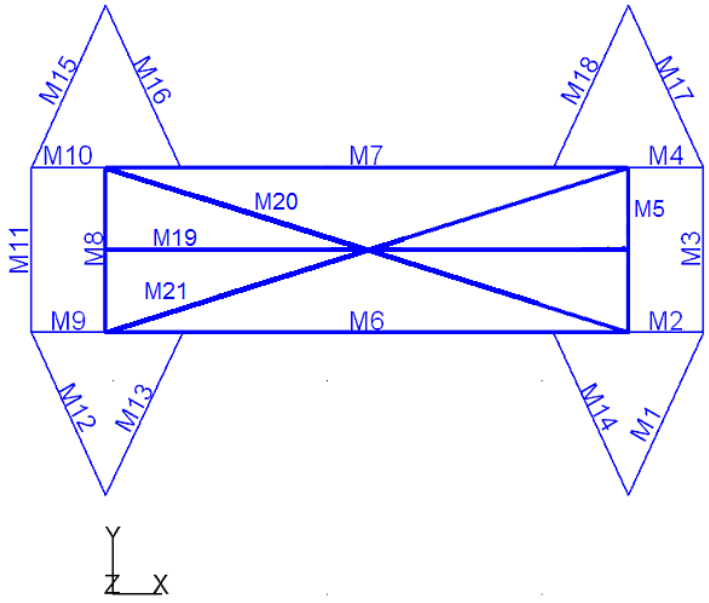

Figure A.3: Main chassis members and suspension A-arms

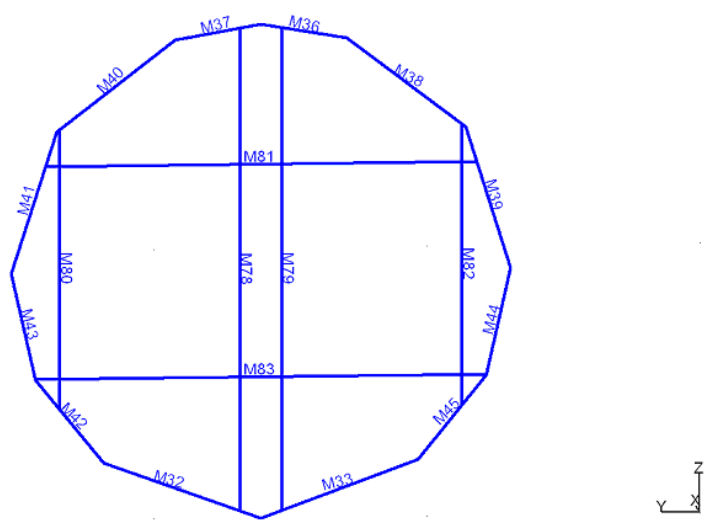

Figure A.4: Rear ring and suitport supports

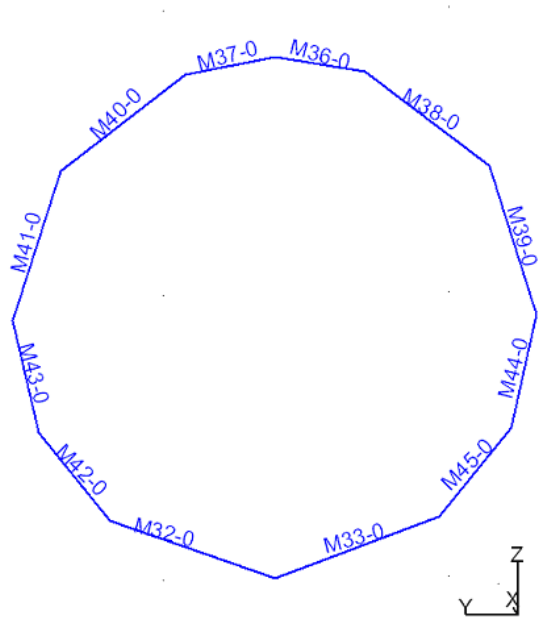

Figure A.5: Other ring sections

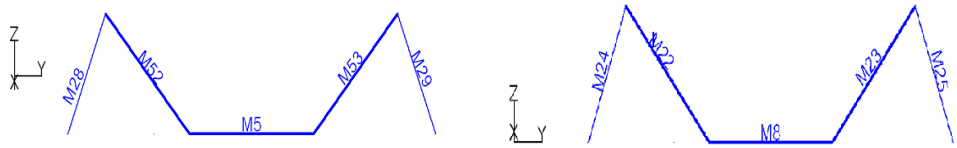

(a) Front

(b) Rear

Figure A.6: Front and rear sections

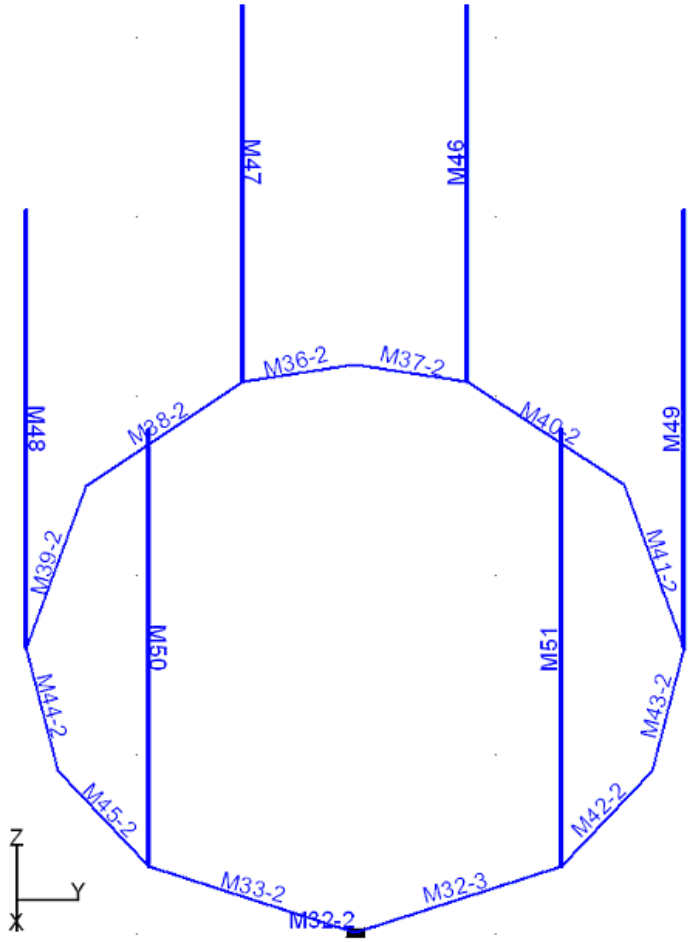

Figure A.7: Ring Struts

A.4 Table of Forces on Chassis (David McLaren, Aaron Cox)

Critical loading situations, and internal forces, torques, and moments, are shown in Tables A.2 - A.4 for every member in the flight rover chassis. Appendix A.3 contains figures illustrating the locations of each member.

Launch loads are the critical loading situation for most pieces. Some of them are sized by driving loads. The coordinate system is local to each piece; x is on an axis passing through the member, and y and z are perpendicular to it. Internal forces and moments are tabulated for each piece. V is the shear force, T is torque (equivalent to a moment about the center axis, Mx), and My/Mz are internal moments.

Table A.2: Chassis Forces

Name	Crit Load	Faxial (N)	Vy (N)	Vz (N)	T (N-m)	My (N-m)	Mz (N-m)
M1	Driving	-8800	22	60	-3	-50	-10
M2	Launch	-1820	-387	56	-51	28	140
M3	Launch	-2150	3240	89	24	-44	681
M4	Launch	-3540	1910	-75	-30	-38	-452
M5	Launch	-6080	362	643	59	119	296
M6	Launch	-19500	1240	-576	-291	74	261
M7	Launch	41000	1160	118	-131	118	-245
M8	Launch	11500	1330	110	-31	-38	-274
M9	Launch	1970	-906	64	-1	-38	-242
M10	Launch	1380	-32	40	-12	-37	105
M11	Launch	1180	-1890	-13	0	8	363
M12	Launch	218	189	-50	-18	-42	-119
M13	Launch	-355	-94	-46	-7	39	41
M14	Launch	14	-72	0	-63	0	-57
M15	Launch	90.5	-79	-53	25	-45	60
M16	Launch	-110	-44	-31	-8	26	-39
M17	Launch	-89	375	-14	13	-12	-228
M18	Launch	370	-180	3	-40	-3	-82
M19	Launch	-10300	-5940	-327	-237	-66	678
M20	Launch	-34900	-110	-86	-78	-114	103
M21	Launch	24900	164	159	-99	-109	142
M22	Launch	-1110	-1420	-2650	-48	-280	-178
M23	Launch	935	-1060	-4940	188	-464	-178
M24	Driving	-620	244	-1	0	5	153
M25	Driving	-812	-270	-5	0	7	-169
M28	Driving	686	276	15	-1	-8	173
M29	Driving	-659	-292	16	1	-10	-183

Table A.3: Chassis Forces

Name	Crit Load	Faxial (N)	Vy (N)	Vz (N)	T (N-m)	My (N-m)	Mz (N-m)
M32	Launch	-12300	1552	-471	124	-201	-299
M32-0	Launch	3030	-136	192	76	193	222
M32-1	Launch	3630	-8	186	-12	-127	211
M32-2	Launch	-680	19	-327	-11	-56	93
M32-3	Launch	4350	131	-315	-10	133	121
M33	Launch	13300	1738	-962	-62	-337	-303
M33-0	Launch	-1990	210	5	86	-97	80
M33-1	Launch	-2000	203	-512	3	231	109
M33-2	Launch	-2620	512	268	8	-99	178
M36	Launch	671	-1238	1730	-178	691	-162
M36-0	Launch	-380	226	3160	-43	920	43
M36-1	Launch	561	362	990	-22	287	-117
M36-2	Launch	273	-423	-365	-9	-85	-192
M37	Launch	695	-949	-1115	-88	190	-123
M37-0	Launch	-368	343	-3410	-56	-1073	133
M37-1	Launch	568	178	-1240	-17	-334	171
M37-2	Launch	-48	-462	-137	-12	-9	-84
M38	Launch	2860	316	-1880	-277	-811	71
M38-0	Launch	177	-113	1320	12	-570	23
M38-1	Launch	-728	234	971	5	-433	-70
M38-2	Launch	423	88	631	11	-247	-200
M39	Launch	-1370	-393	4367	-138	1230	-109
M39-0	Launch	205	164	1000	-29	526	41
M39-1	Launch	-662	-176	651	-3	283	41
M39-2	Launch	329	416	310	3	99	-169
M40	Launch	-4560	1400	-8770	541	2180	100
M40-0	Launch	2860	226	-1070	-72	543	212
M40-1	Launch	1290	-260	-209	26	112	135
M40-2	Launch	-675	-272	390	7	76	-235

Table A.4: Chassis Forces

Name	Crit Load	Faxial (N)	Vy (N)	Vz (N)	T (N-m)	My (N-m)	Mz (N-m)
M41	Launch	2780	-244	8270	-459	1930	100
M41-0	Launch	2400	-1410	-1390	-33	-598	-534
M41-1	Launch	873	-850	-529	63	-157	-429
M41-2	Launch	-704	319	-250	49	62	-235
M42	Launch	-11000	-5330	14400	-218	1650	-720
M42-0	Launch	2460	356	-955	37	-433	184
M42-1	Launch	1780	526	-1500	-34	-599	269
M42-2	Launch	643	588	-888	-21	-368	411
M43	Launch	-5230	266	-9390	369	2310	93
M43-0	Launch	2050	1410	-955	56	357	-528
M43-1	Launch	1370	1260	-1500	-30	591	-451
M43-2	Launch	316	812	-888	-13	338	176
M44	Launch	2650	907	-2740	75	644	90
M44-0	Launch	-453	174	517	62	-180	100
M44-1	Launch	-931	463	527	36	-199	146
M44-2	Launch	-418	619	329	17	-116	217
M45	Launch	10800	-5390	8540	186	1120	-711
M45-0	Launch	-483	-46	517	42	259	100
M45-1	Launch	-1040	2	527	26	237	146
M45-2	Launch	-649	370	329	8	153	364
M46	Launch	-8066	-4170	1780	-84	-950	2060
M47	Launch	-3892	-1920	-580	-93	-192	-813
M48	Launch	-6891	-1020	-1240	-88	575	551
M49	Launch	-17400	-3150	1180	-87	499	-642
M50	Launch	-12000	1091	-659	-73	348	266
M51	Launch	-19800	-1450	706	-114	271	548
M52	Launch	1070	-254	212	-95	-49	203
M53	Launch	-1980	761	-286	-87	61	183
M78	Launch	2400	-725	-915	105	-339	-192
M79	Launch	-2930	699	-727	70	275	-183
M80	Launch	-5680	2410	-11200	268	-1390	-654
M81	Launch	-1460	-6960	3700	516	-81	782
M82	Launch	3830	-2850	7280	-114	777	295
M83	Launch	2200	-8440	2800	-472	124	-519

A.5 Chassis Piece Sizes and Safety Margins (David McLaren)

Critical load type, thickness, inner and outer diameter, total element mass, and margin of safety are shown in Tables A.5 - A.7 for every member in the flight rover chassis. Appendix A.3 contains figures showing the location of each member. The majority of the pieces are sized by combined loads from internal forces and moments. A few are sized by buckling conditions. All pieces have a hollow, circular cross section. The final mass of the flight rover chassis is 163 kg.

Table A.5: Chassis Member Sizes

Name	Type	t (cm)	di (cm)	douter (cm)	m (kg)	MOS
M1	Buckling	0.5	1.0	2.0	0.53	0.15
M2	Combined	0.5	1.6	2.6	0.31	0.37
M3	Combined	0.9	2.4	4.2	1.9	0.31
M4	Combined	0.8	2.2	3.8	0.71	0.41
M5	Combined	0.7	2.0	3.4	1.2	0.35
M6	Buckling	0.8	2.8	4.4	6.0	0.29
M7	Combined	1.0	1.6	3.6	5.4	0.25
M8	Combined	0.8	1.6	3.2	1.3	0.27
M9	Combined	0.6	1.8	3.0	0.43	0.27
M10	Combined	0.5	1.4	2.4	0.28	0.44
M11	Combined	0.7	2.0	3.4	1.2	0.29
M12	Combined	0.5	1.4	2.4	0.68	0.32
M13	Combined	0.4	1.2	2.0	0.46	0.65
M14	Combined	0.4	1.2	2.0	0.46	0.68
M15	Combined	0.4	1.4	2.2	0.51	0.63
M16	Combined	0.4	1.0	1.8	0.40	0.53
M17	Combined	0.6	1.8	3.0	1.0	0.42
M18	Combined	0.4	1.4	2.2	0.51	0.47
M19	Combined	0.9	2.6	4.4	6.5	0.36
M20	Buckling	0.9	3.4	5.2	8.4	0.25
M21	Combined	0.8	1.6	3.2	4.2	0.4
M22	Combined	0.7	2.0	3.4	1.3	0.41
M23	Combined	0.8	2.2	3.8	1.6	0.33
M24	Combined	0.5	1.6	2.6	0.56	0.33
M25	Combined	0.6	1.4	2.6	0.64	0.29
M28	Combined	0.6	1.6	2.8	0.71	0.54
M29	Combined	0.6	1.6	2.8	0.71	0.45

Table A.6: Chassis Member Sizes

Name	Type	t (cm)	di (cm)	douter (cm)	m (kg)	MOS
M32	Combined	0.8	2.0	3.6	1.2	0.34
M32-0	Combined	0.7	1.8	3.2	0.91	0.31
M32-1	Combined	0.7	1.6	3.0	0.83	0.29
M32-2	Combined	0.5	1.4	2.4	0.00	0.52
M32-3	Combined	0.6	1.6	2.8	0.68	0.36
M33	Combined	0.9	2.0	3.8	1.4	0.31
M33-0	Combined	0.5	1.6	2.6	0.54	0.54
M33-1	Combined	0.6	2.0	3.2	0.81	0.43
M33-2	Combined	0.6	1.8	3.0	0.75	0.5
M36	Combined	0.9	2.4	4.2	0.81	0.28
M36-0	Combined	0.9	2.8	4.6	0.90	0.25
M36-1	Combined	0.7	1.8	3.2	0.48	0.3
M36-2	Combined	0.6	1.6	2.8	0.36	0.28
M37	Combined	0.6	1.8	3.0	0.39	0.41
M37-0	Combined	1.0	2.8	4.8	1.0	0.24
M37-1	Combined	0.7	2.0	3.4	0.51	0.26
M37-2	Combined	0.4	1.4	2.2	0.20	0.45
M38	Combined	0.9	2.6	4.4	1.5	0.23
M38-0	Combined	0.8	2.4	4.0	1.2	0.34
M38-1	Combined	0.7	2.2	3.6	0.95	0.25
M38-2	Combined	0.7	1.8	3.2	0.82	0.27
M39	Combined	1.0	3.2	5.2	2.0	0.33
M39-0	Combined	0.8	2.2	3.8	1.1	0.27
M39-1	Combined	0.6	2.0	3.2	0.73	0.32
M39-2	Combined	0.6	1.6	2.8	0.62	0.37
M40	Combined	1.2	3.8	6.2	2.8	0.26
M40-0	Combined	0.8	2.4	4.0	1.2	0.27
M40-1	Combined	0.6	1.6	2.8	0.62	0.49
M40-2	Combined	0.6	1.8	3.0	0.67	0.29

Table A.7: Chassis Member Sizes

Name	Type	t (cm)	di (cm)	douter (cm)	m (kg)	MOS
M41	Combined	1.2	3.4	5.8	2.6	0.21
M41-0	Combined	0.9	2.6	4.4	1.5	0.26
M41-1	Combined	0.8	2.0	3.6	1.0	0.26
M41-2	Combined	0.6	1.8	3.0	0.67	0.31
M42	Combined	1.2	3.4	5.8	1.9	0.24
M42-0	Combined	0.8	2.2	3.8	0.81	0.38
M42-1	Combined	0.8	2.6	4.2	0.92	0.3
M42-2	Combined	0.8	2.4	4.0	0.87	0.38
M43	Combined	1.3	3.6	6.2	2.2	0.23
M43-0	Combined	0.8	2.6	4.2	0.92	0.34
M43-1	Combined	0.9	2.6	4.4	1.1	0.37
M43-2	Combined	0.7	2.0	3.4	0.64	0.25
M44	Combined	0.9	2.4	4.2	1.0	0.36
M44-0	Combined	0.6	1.6	2.8	0.45	0.3
M44-1	Combined	0.6	1.8	3.0	0.49	0.29
M44-2	Combined	0.6	1.8	3.0	0.49	0.31
M45	Combined	1.1	3.0	5.2	1.5	0.21
M45-0	Combined	0.6	2.0	3.2	0.53	0.36
M45-1	Combined	0.6	2.0	3.2	0.53	0.34
M45-2	Combined	0.7	2.2	3.6	0.69	0.39
M46	Combined	1.3	3.6	6.2	13	0.24
M47	Combined	0.9	2.8	4.6	6.9	0.34
M48	Combined	0.9	2.8	4.6	6.9	0.36
M49	Combined	1.0	2.6	4.6	7.5	0.27
M50	Buckling	0.8	2.2	3.8	5.0	0.24
M51	Buckling	1.0	2.2	4.2	6.6	0.16
M52	Combined	0.6	1.6	2.8	0.87	0.26
M53	Combined	0.6	1.6	2.8	0.87	0.33
M78	Combined	0.7	2.2	3.6	3.1	0.37
M79	Combined	0.7	2.0	3.4	2.9	0.37
M80	Combined	1.1	3.4	5.6	4.4	0.32
M81	Combined	0.9	2.6	4.4	4.2	0.29
M82	Combined	0.9	2.8	4.6	2.9	0.34
M83	Combined	0.8	2.4	4.0	3.6	0.4

A.6 Materials (Ryan Levin)

A.6.1 Trade Studies

In order to build a successful space structure, many investigations into possible materials were conducted. The mass budget was the greatest concern at the beginning of our studies because any material would be ineffective if it were too heavy to launch. Material properties including density, elastic modulus, and yield strength were required to find out which materials had the possibility of becoming a part of the lunar rover. The chart in Figure A.8 is a summary of some of our selected materials which were investigated as well as a list of how we planned to use each one.

Material	Density (kg/m^3)	Young's Mod.(GPa)	Shear Mod.(GPa)	Poisson's Ratio	CTE (micrometers/K*m)	Shear Str.(MPa)	Yield Str.(MPa)	Ult. Str.(MPa)	Notes
Aluminum	2700	70	26	0.35	23.1	?	15	40	Unalloyed low tensile strength
Al. Alloy 6061-T6	2700	69	26	0.33	23.6	205	275	310	Weldable, heat treatable Wide use: aero, cycles, yachts
Ti. Alloy	4630	114	43	0.33	8.8	?	930	1070	
Carbon Epoxy	1600	70/70	5 (in-plane)	?	2.1	90 (in-plane)	?	600	**long/transverse values**
Graphite Epoxy	1522	264	5.5	0.33	.18/25.6	140	?	1600 (comp.) 1800 (tens.)	**long/transverse values**
HPFS (High Purity Fused Silica) glass	2201	72.7	31.4	0.16	0.57	70	?	54(Tensile Strength) 1140 (Compressive Strength)	?
Vitreloy	6100	93	35	0.35	10	?	1900	?	
Tempered Glass	2190	68.9	?	?	?	?	?	165(Compression)	?

Figure A.8: Material Properties

A.6.2 General Results

The rover chassis will be made of Aluminum Alloy 6061-T6, the pressure shell will be Graphite Epoxy, and the window will be made from a combination of High Purity Fused Silica (HPFS) glass and Vitreloy. The chassis is not made of Titanium Alloy due to a density nearly twice that of aluminum as well as a Young's modulus that did not help to compensate for the extra weight. Aluminum alloy was chosen over aluminum because its Yield Strength is almost 20 times that of aluminum. Graphite Epoxy was selected for the pressure shell because it is lighter than Aluminum (Alloy) and also incredibly stronger in terms of Ultimate Stress. The HPFS glass and Vitreloy were chosen for the window for their high Young's Modulus and while Vitreloy is very dense, it is essential for micrometeoroid protection.

A.7 Trade Study of Reactant Tank Materials (Aleksandar Nacev and Stephanie Petillo)

A.7.1 Overview

There are three options that were considered for tank materials for holding the cryogenic fuels: aluminum tanks, carbon fiber (Toray T300) composite tanks, and aluminum lined composite tanks. There was an in-depth analysis of the pressures experienced on the specific geometry of the tanks for the aluminum tanks and the composite tanks. From this analysis, it can be seen that the composite tanks are able to withstand the loaded pressures with a very reasonable safety factor. The composite tank also had a much lower mass requirement for withstanding the internal pressure compared to the aluminum tank. For these reasons, the aluminum tank was not chosen for a structural material. As for the aluminum lined tank, since the composite material is able to handle the load at the minimal manufacturing thickness, the inclusion of aluminum lining is not needed. Hence a pure composite tank was chosen.

A.7.2 Analysis of Pressure Load

Table A.8: Properties of Tanks

Property	**Aluminum**	**Composite**
$\rho \left[\frac{kg}{m^3}\right]$	2700	1800
Pressure Load $[MPa]$	2.41	2.41
Yield Strength $[MPa]$	20	3530
Minimum Thickness $[mm]$	30	3
Mass $[kg]$	115	7.02

The pressure load inside the cryogenic tanks was analyzed for the two tank materials: aluminum and composite. The material properties are seen in Table A.8. Figure A.9 shows the safety factor for the liquid hydrogen tank at the minimum thickness it can support. It can be seen that with the minimum thickness of 30 mm, the tank just barely reaches a safety factor of 1. The mass associated with this tank is 115 kg. It is important to note that the hydrogen fuel tanks are being analyzed and used as the worst case scenario. Since the liquid oxygen fuel tanks are stored at the same pressure, the larger of the two tanks (liquid hydrogen) will have the higher stresses.

Figure A.10 shows the safety factor for the composite fuel tanks. This safety factor, with a minimum thickness of 3 mm, is still high above the yield safety factor of 1. The thickness of 3 mm was chosen in this case due to manufacturing limits. Three millimeters is usually the thinnest that a carbon fiber composite can be made. The mass associated with a tank of this thickness and material is 7.02 kg. This tank is therefore much lighter than the aluminum version and it can still

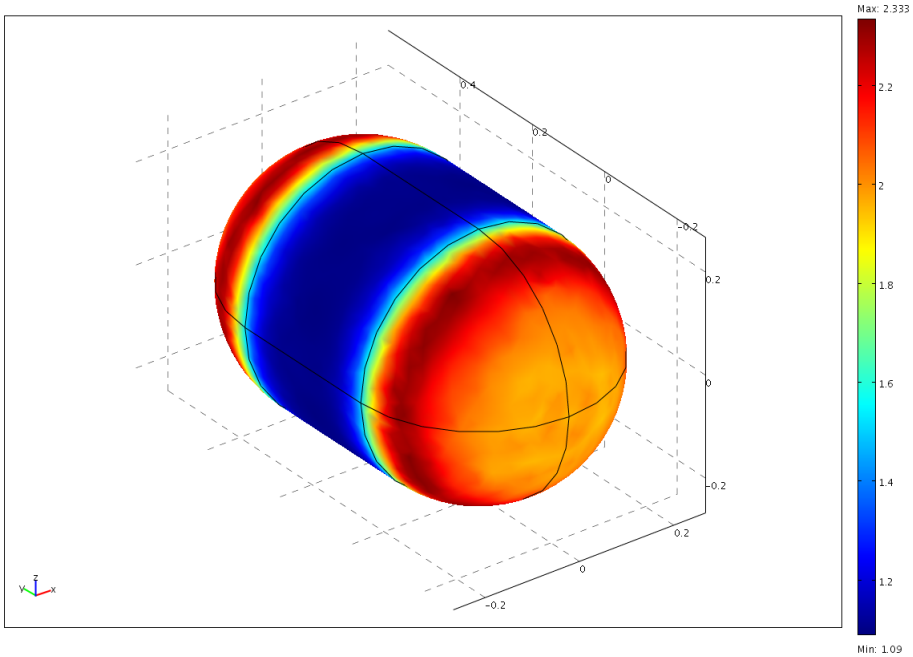

Figure A.9: Safety Factor for Aluminum Tank

withstand the internal cryogenic pressure with a very reasonable safety factor. Due to these factors, lining the composite tank with aluminum would not gain any additional advantage.

A.8 Trade Study of Power Generation Methods (Stephanie Petillo and Aleksander Nacev)

A.8.1 Overview

In determining how to generate power for the lunar rover, a variety of power supply methods are taken into consideration: fuel cells, solar arrays, and lithium-ion batteries. The primary concerns in selecting a power supply are keeping the mass carried by the rover (and Delta IV Heavy) as low as possible, while meeting the energy demand over each stage of the mission (tabulated throughout Section 6.3.1) and maintaining a constant source of power.

A.8.1.1 Solar Arrays

Even though the use of a solar array would only result in a mass of 39.4 kg, solar arrays do not work when there is no sunlight and would get quickly covered by dust on the lunar surface, requiring a backup power system to make sure the rover does not lose power at any point in time. They also do not stand up well under severe vibrations and require power-consuming motors to deploy

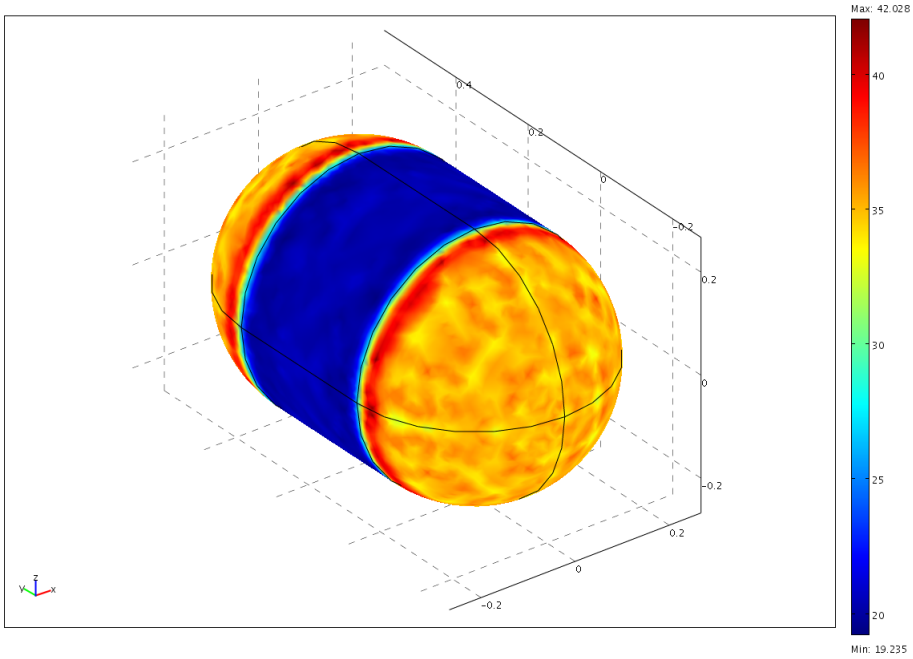

Figure A.10: Safety Factor for a Composite Tank

them. Solar arrays would also take up an area of about 6.6 square meters of planar space within the payload shroud, creating a much tighter fit for the rover in the shroud.

A.8.1.2 Fuel Cells versus Li-Ion Batteries

Although each stage of the mission could use a different type of power source, it is determined that the most efficient way to power the rover involves using only the PEM fuel cells from the Transfer Stage through the Sortie Mission Stage. This choice was based on the comparison of mass values and energy densities given in Table A.9 and to avoid the extra mass involved in creating a support system for a second type of power supply. This requires the least overall mass for power generation.

In comparing PEM fuel cells and Li-ion batteries, the much higher mass energy density of the fuel cell reaction over the batteries (2.647 kWhr/kg versus 0.16 kWhr/kg, respectively) dictates that the fuel cells are the only feasible power supply for the allowable loads on the rover.

Table A.9: Comparison of Power Supply Properties

	Li-ion Battery	Fuel Cells	Solar Array	Energy Req'd. (kWhr)
Mass Energy Density (kWhr/kg)	0.16	2.647	—	—
Mass Power Density (kW/kg)	1.8	—	0.045	—
Transfer Stage Mass (kg)	303	18.3	6.44	48.43
Desc. & Land. Stage #1 Mass (kg)	7.61	0.460	0.206	1.217
Desc. & Land. Stage #2 Mass (kg)	0.556	0.0336	5.18	0.089
Standby Stage Mass (kg)	575	34.8	0.0822	92.016
Sortie Mission Stage Mass (kg)	3888	235	39.4	622.157
Total Mass for all Stages (kg)	4774	289	39.4	763.909

Appendix B

Apollo Science (Matt Schaffer)

B.1 Apollo Science Packages (Matthew Schaffer)

B.1.1 Apollo 11 Experiments [11]

The experiments attributed as a part of the first deployed lunar science equipment consisted of three individual components:

- Passive Seismic Experiments Package
- Solar-wind Composition
- Laser Ranging Retroreflector

B.1.2 Apollo 12 Experiments [12]

Apollo 12 introduced Apollo Lunar Surface Experiments Package, which was an inclusive set of experiments which shared a single power source with the intent of collecting data for several years after the mission. The experiments included as a part of this package were:

- Lunar Surface Magnetometer
- Passive Seismic
- Solar-wind Spectrometer
- Suprathermal Ion Detector
- Cold Cathod Ion Gauge

The mission also included the solar-wind composition experiment, which was seen in the previous mission.

B.1.3 Apollo 14 Experiments [13]

Apollo 14 introduced the modular equipment transporter to carry equipment from the lunar module. It was a two-wheeled, hand-drawn cart capable of transporting up to 160 kg of science equipment.

The Apollo 14 science package included the following four experiments:

- Active Seismic
- Charged Particle Lunar Environment
- Passive Seismic
- Suprathermal Ion Detector

It also included two individually deployed experiments, which were seen in previous missions:

- Cold Cathode Ion Gauge
- Laser Ranging Retroreflector

B.1.4 Apollo 15 Experiments [14]

The Apollo Lunar Rover was introduced in Apollo 15. This greatly increased the distance astronauts could traverse and the weight they could carry on the surface. One way in which this is reflected is through the science package, which consisted of more experiments than any of the previous three missions.

These packaged experiments were:

- Heat Flow
- Lunar-surface Magnetometer
- Cold Cathode Gauge
- Solar-wind Spectrometer
- Suprathermal Ion Detector
- Lunar Dust Detector

As before, two separate experiments were included:

- Solar-wind Composition
- Laser Ranging Retroreflector

B.1.5 Apollo 16 Experiments [15]

Apollo 16 put a greater emphasis on sampling than previous missions, as a result the science package was smaller than in Apollo 15, containing the following experiments:

- Heat Flow
- Passive Seismic
- Active Seismic
- Lunar Surface Magnetometer

The mission did include a greater number of stand-alone experiments, most of which had not been attempted in former missions. These experiments included:

- Solar-wind Composition
- Far Ultra-violet Camera/Spectrograph
- Portable Magnetometer
- Cosmic Ray Detector

B.1.6 Apollo 17 Experiments [16]

As the final Apollo mission, several new experiments were introduced, that would have likely been followed-up on in the proceeding missions that were originally planned. As a result, issues that arose with the experiments throughout the mission could not be addressed and perfected, which was typically done in the prior missions.

The Apollo 17 experiments package included the following experiments:

- Heat Flow
- Lunar Seismic Profiling
- Lunar Surface Gravimeter
- Lunar Ejecta and Meteorites
- Lunar Atmospheric Composition

Several new stand-alone experiments were also performed:

- Surface Electrical Properties

- Lunar Neutron Probe
- Traverse Gravimeter
- Lunar Surface Cosmic Ray Experiment

B.1.7 Apollo Experiments Concluding Remarks

A common theme for Apollo was to repeat and improve on experiments several times throughout the program. In the interest of science, it broadened the range of data collected so that any analyses could be as complete and accurate as technologically possible. For the sake of the mission, it allowed NASA to pinpoint the sources of any complications and tweak them to as near-perfection as possible. This knowledge would then be used to prevent similar issues from occurring in future exploration programs and ultimately provides a foundation for the current plan to return to the moon in the near-future.

B.2 EVAs and Sampling

B.2.1 EVAs

Table B.1: EVA Duration^{+} and Distance Traversed

Mission	Distance (km)	EVA 1	EVA 2	EVA 3	Total Time
Apollo 11[11]	.24	2:24	N/A	N/A	2:24
Apollo 12[12]	2.0	4:00	3:50	N/A	7:50
Apollo 14[13]	3.3	4:49	4:20	N/A	9:09
Apollo 15[14]	27.9	6:33	7:12	4:50	18:35
Apollo 16[15]	27.0	7:00	7:00	5:00	19:00
Apollo 17[16]	35.0	7:12	7:37	7:15	22:04

+ All times given in the hh:mm format

Table B.1 shows the distance astronauts were able to cover and the time they spent on the lunar surface. With each mission, NASA knew more about what to expect of its astronauts and equipment capabilities on the extraterrestrial surface. The distance traveled on each mission was greatly increased with the introduction of the Lunar Rover on Apollo 15, eventually achieving a maximum distance of 35.0 km from the lander. TURTLE will continue this trend, with the capability of traveling a total of 50 km to and from the lander in a single sortie and 100 km by mission completion.

B.2.2 Example Apollo 17 Science Equipment List

Table B.2 shows the equipment that was used in taking samples for Apollo 17. Much of the equipment was also used in missions throughout Apollo with changes from astronauts' input after each mission.

Table B.2: Sampling Equipment Used During Apollo 17 [43]

Qty	Equipment	Mass/item (g)	Total Mass (g)
1	Cup-shaped Documented Sampling Bag Dispenser	358.1	358.1
6	Rectangular Document Sampling Bag Dispenser	445	2670
4	Sample Collection Bag	762	3048
4	Extra Sample Collection Bag	561	2244
2	Organic Sample Monitor	70.5	141.0
2	Apollo Lunar Sample Return Container	6700	13400
1	Core Sample Vacuum Container	492.3	492.0
1	Special Environment Sample Container	349.6	349.6
1	Drill System	13400	13400
5	Drive Tube	500	2500
2	Long Extension Handle	816.0	1632
1	Gnomon	272.0	272.0
1	Heavy-weight Hammer	1315	1315
1	Rake	1497	1497
1	Lunar Rover Soil Sampler	136.0	136.0
1	Sample Scale	227.0	227.0
1	Large Adjustable Scoop	590.0	590.0
2	32-inch Tongs	454.0	908
			45180

Appendix C

Interior

C.1 Interior Center of Gravity (Sara Fields)

Table C.1 shows the values used for the interior center of gravity calculation. All values measured from the geometric center of the cabin, at the start of the mission when the water tanks are empty and there are no spacesuits.

X-axis positive toward the rear

Y-axis positive toward the driver's side

Z-axis positive down

Results:

XCG: -13.55 cm

YCG: -4.75 cm

ZCG: 24.96 cm

Table C.1: Interior CG

C.G.	X (cm)	Y (cm)	Z (cm)	Mass (kg)
CHAIR	-66.15	0.00	26.10	5.00
LIOHCAN	-0.13	-32.39	56.70	4.60
LIOHCAN	16.38	-32.39	56.70	4.60
LIOHCAN	-0.13	-48.90	56.70	4.60
LIOHCAN	16.38	-48.90	56.70	4.60
LIOHCAN	7.24	-40.64	33.46	4.60
CLOTHES	36.70	-41.82	46.54	10.00
FOOD	23.75	41.82	46.54	20.00
HEATEXCHANGE	-83.31	0.00	-82.46	5.00
LIOHCAN	-45.21	-0.26	-78.65	4.60
COMPUTER	-71.88	49.66	55.94	7.50
COMPUTER	-71.88	19.18	55.94	7.50
DATASTORAGE	-71.88	34.54	55.94	10.00
IMU	113.92	0.01	67.55	7.00
OVERHEADLIGHT	18.29	0.00	-82.39	7.00
SINK	-23.81	36.83	38.35	10.00
FIRSTAID	-103.63	-78.35	-8.28	1.45
AED	-82.05	-82.56	-8.29	1.60
TOILETRIES	-8.17	23.51	62.29	0.50
TOILETRIES	-18.33	23.51	62.29	0.50
SUPPO2	-54.72	-78.28	-15.62	1.50
SUPPO2	-48.41	-78.30	-3.48	1.50
EXTINGUISHERPOTASS	-68.77	84.35	0.08	1.23
EXTINGUISHERFIREADE	-70.47	84.35	7.68	0.45
SUITPORT1	108.31	34.87	1.44	20.00
SUITPORT1MIRROR	108.33	-32.33	8.38	20.00
BEDCLOSED	0.00	-73.58	-11.37	7.50
BEDCLOSED	0.00	73.61	-11.37	7.50
WATERTANKABOVE	-0.50	0.00	-55.10	0.00
CIRCUITBREAKER	36.27	0.00	81.34	7.63
LIQUIDWASTE	-83.34	0.00	80.90	0.00
WIRINGCONDUIT	-17.92	0.00	66.92	1.00
COCKPITFRAME	-116.33	0.00	24.72	5.00
COMPUTERSCREEN	-118.76	42.82	-3.77	10.00
COMPUTERSCREEN	-118.77	0.00	-3.80	10.00
COMPUTERSCREEN	-118.77	-42.82	-3.80	10.00

LIGHTINGLOCKER	-83.31	-60.64	48.32	2.00
LOCKER	71.62	41.86	46.78	5.00
AIRLOCK	71.63	-41.64	46.61	5.00
SOLIDWASTE2	-27.78	0.00	81.20	0.00
AIRSYSDISTRIBUTOR	-119.25	0.00	-81.33	0.50
AIRSYSFAN	38.83	24.42	75.18	1.00
AIRSYSFILTER	-45.21	64.04	27.28	1.00
AIRSYSDISTRIBUTOR	111.40	24.42	81.98	0.50
TOILCHAIR	-26.39	-34.29	44.98	25.25
CHAIRTRACKS	-71.88	17.15	69.91	0.50
COMPUTER	-96.27	-31.24	56.19	7.50
COMPUTER	-96.27	-48.77	56.19	7.50
DATASTORAGE	-117.60	-36.20	55.94	10.00
AIRSYSDUCT2	-37.91	0.00	-81.20	0.50
AIRSYSDISTRIBUTOR	60.01	-29.59	-81.33	0.50
AIRSYSDISTRIBUTOR	60.20	29.40	-81.33	0.50
AIRSYSDISTRIBUTOR	-9.84	29.40	-81.33	0.50
AIRSYSDISTRIBUTOR	-9.84	-29.40	-81.33	0.50
AIRSYSDISTRIBUTOR	-63.50	29.40	-81.33	0.50
AIRSYSDISTRIBUTOR	-63.50	-30.67	-81.33	0.50
Totals:				293.21

C.2 Interior Storage Requirements (Sara Fields)

Table C.2 shows the dimensions of components stored inside the cabin, as provided by the POC, or point of contact. Some numbers may be out of date; if there is a conflict with numbers shown in the body of this paper, the numbers in the paper are correct.

Table C.2: Interior Storage Requirements

Component	Volume	Dimensions	Mass	Desired Location	POC
Suitport w/ PLSS (x2)	4.5 ft^3 each	2 x 3 x 0.75 (ft) each	150 kg	back of the rover side by side	James & Jason
Chair (x2)	1.5 ft^3	1.5 x 1.5 x 1.5 (ft)		At front	Sara
Bed (x2)		74 x 29 x 2 (in)		along each side wall	Sara
Internal Heat Exchanger		.6 x .4 x 0.05 (m)	5 kg	on ceiling ** 2/26	Stephanie, Alek
Ventilation Fans (x3)		9.5 x 11 x 6 (in) (x3)	4.05 lbs (x3)	one in each of 2 holes in tank for ventilation, and the 3rd placed internally for circulation	Stephanie
Power System Wiring		1.6 mm diam x 2.44 m x 20 wires	0.9028 kg	connects all components to fuel cells	AJ
Voltmeter and ammeter	3.2175e-4m^3	130 x 75 x 33 (mm)	242 g	Palm Size Digital LCD Multimeter/Voltmeter/ Ammeter Ohmmeter	AJ
Supplemental Oxygen (x2)	.293 ft^3 (each)	4.5 x 7.5 x 15 (in) each	6 lbs each	near seats	Jason Laing
First Aid Kit	.306 ft^3	11 x 6 x 8 (in)	1.45 kg	near seats	Jason Laing
AED	.0903 ft^3	8.25 x 6.875 x 2.75 (in)	1.6 kg	somewhere easily accessible	Jason Laing

Clothing Containment	.06 m^3 collapsible container	amorphous	up to 6.1 kg		Jason Laing
Used Clothing Container	.06 m^3 collapsible container	amorphous	up to 6.1 kg		Jason Laing
Trash Containment	.064 m^3 collapsible container	amorphous			Jason Laing
Fire Extinguisher: Potassium. Bicarbonate			2.75 lbs		Jason Laing
Fire Extinguisher: Fireade	16 oz.	2.5 diam x 10.375 (in)	.448 kg		Jason Laing
Toiletries Kit (x4)		approx. 3 x 7 x 6 (in) each	.5 kg each		Jason Laing
Toilet	1.431 ft^3	15 diam x 14 (in)	20.25 kg		Jason Laing
Computer (x4)	0.0135 m^3	30 x 30 x 15 (cm)	10 kg	Near the driving controls at the front	Joseph Lisee
IMU	0.00783 m^3	18 x 15 x 29 (cm)	7 kg	Near the center of the vehicle	Mike Levashov
waste water tank (full)	0.06544 m^3	amorphous	65 kg	near toilet, near washbasin	Ali Husain
potable water tank (full)	0.0958 m^3	amorphous	97.716 kg	near washbasin	Ali Husain
food (including packaging)	0.128 m^3	approximately box shaped	36.8 kg	anywhere convenient	Ali Husain
cooking/eating utensils	0.0028 m^3	approximately box shaped	1 kg	anywhere convenient	Ali Husain
washbasin	0.0135 m^3	box shaped	15 kg	near waste water tank	Ali Husain
LiOH canisters (x6)	0.00639 m^3each	0.1661 diam x 0.2949 (m) each	27.6 kg total	crew accessible, with space for one to be in air loop	Adam Mirvis

Appendix D

MATLAB Code

D.1 Air Handling (Adam Mirvis)

```
%Air Handling: Fan Power Calculation
clear all
clc

%Main variables

pp_O2 = 21.2783;    %kPa (from Atmosphere.m)
pp_N2 = 33.9064;
P_tot = pp_O2 + pp_N2;   %kPa

R = 8.314472;  %ideal gas constant, (m^3ůkPa)/(kgmolůK)
T = 298.15;     %temperature, K
M_O2 = 31.9988;      %grams/g-mole or kg/kg-mole, http://environmentalchemistry.com/yogi/referen
M_N2 = 28.01348;

O2_conc = pp_O2/(pp_O2+pp_N2);
M = O2_conc*M_O2 + (1-O2_conc)*M_N2;    %average molar mass of cabin air, kg/kgmole

density = (P_tot*1000*M)/(R*T);
viscosity = 1.78e-5;     %kg/(můs)

%--------

%Necessary flow rate to draw off CO2
```

```
pp_CO2_max = 0.4;                 %kPa, from NASA STD-3000
SF = 2.0;
pp_CO2 = pp_CO2_max/SF;

conc_CO2 = pp_CO2/P_tot          %concentration of CO2 in rover atmosphere

m_CO2_pppd = 1.0;    %kg CO2 produced per person per day (from Akin #10, slide 18)
mdot_CO2 = m_CO2_pppd*2/24/3600;   %output rate of CO2, kg/s
fa = 0.25;                          %adsorption fraction of lioh can
mdot = mdot_CO2/(fa*conc_CO2)          %required flow rate of cabin air, kg/s
ndot = mdot/M;                          %molar flow rate, moles/min
Vdot = ndot*R*T/(P_tot)           %volumetric flow rate, m^3/s (use everywhere in duct, assume i

%Exit area
A_ex = Vdot/0.2;        %total distributor exit area required
num_dist = 7;           %number of distributors used
A_ex_per = A_ex/num_dist    %area of each distributor

%--------

%LiOH

L_lioh = .295;       %length of LiOH segment, m
d_lioh = .022;       %diameter of LiOH segment, m
A_lioh = pi*(d_lioh/2)^2;    %area of LiOH segment, m^2

Re_lioh = Vdot*L_lioh/(A_lioh*viscosity);        %check Reynold's number to check laminar flow a
if Re_lioh<5200
   disp('Laminar flow assumption holds.')
else
   disp('Laminar flow assumption does not hold.')
end

r_lioh = viscosity*L_lioh/d_lioh^4;      %resistance kg/(m^4*s)
p_lioh = Vdot*r_lioh         %pressure gradient = flow rate*resistance %(desired flow rate is kn
```

```
%L_heat =        %heat exchanger
%A_heat =
%L_part =        %particle filter
%A_part =
%L_c =           %activated charcoal filter
%A_c =
```

D.2 Atmosphere (Adam Mirvis)

```
clear all

%VARIABLES

%Unit conversions (from http://digitaldutch.com/unitconverter/)
psi_per_atm = 14.695949;    %kPa is the standNed pressure unit for this file
kPa_per_atm = 101.325;
kPa_per_psi = 6.894757;
in_per_m = 39.370079;       %m is the standNed length unit for this file
cubic_cm_per_cubic_in = 16.387064;
cubic_ft_per_cubic_m = 35.314667;
J_p_kWh = 3600000;          %power, J/kWh

%Universal Gas Law constants
R = 8314;   %universal gas constant, J/kgmole-K
T = 298.15; %standard (room) temperature in K

%Molar masses of species
M_O2 = 31.9988;      %grams/g-mole or kg/kg-mole, http://environmentalchemistry.com/yogi/referen
M_N2 = 28.01348;
M_Ne = 20.18;
M_CO2 = 44.010;

%Rates of gas exchange (based on average person, will change for 95%ile males)
m_O2_pppd = 0.85;    %kg O2 consumed per person per day (from Akin #10, slide 8)
m_CO2_pppd = 1.0;    %kg CO2 produced per person per day (from Akin #10, slide 18)
```

```
%Other variables
t_total_press = 8*24;       %total pressurized vehicle hours
t_total_manned = 8*24;      %total manned vehicle hours. May need to subtract EVA hours - TALK T
V_cabin = 16.25;        %m^3, based on 5 days - max mission duration for one crew - TALK TO STRU
cabin_leak_rate = .01;   %Leak rate 1% percent per day, from Akin #10, slide 24
max_conc_O2_fire = .3;       %maximum concentration of oxygen for flammability safety, from NASA


%---------------


%ATMOSPHERIC COMPOSITION

%Oxygen partial pressure
pp_O2_min = .21*kPa_per_atm;        %minimum O2 partial pressure for productivity for an indefin
pp_O2_SF = 1;                       %safety factor (does activity level effect it?)
pp_O2 = pp_O2_min * pp_O2_SF;       %actual partial pressure of O2, kPa
pp_O2_psi = pp_O2/kPa_per_psi

%Nitrogen partial pressure
%pp_N2 = R_factor*P_O2_suit;     %kPa
%pp_N2_psi = pp_N2/kPa_per_psi
pp_N2_psi = 8 - pp_O2_psi       %re-solve for 8 psi atmosphere
pp_N2 = pp_N2_psi*kPa_per_psi;
P_O2_suit = 4.3*kPa_per_psi;    %EMU
R_factor = pp_N2/P_O2_suit         %from Akin lecture

%CO2 partial pressure
conc_CO2 = .00038;               %percentage of CO2 in Earth's atmosphere
pp_CO2 = conc_CO2*kPa_per_atm;     %partial pressure of CO2, kPa
pp_CO2_psi = pp_CO2/kPa_per_psi;

%Total Pressure
P_tot = pp_O2 + pp_N2 + pp_CO2;                 %total cabin pressure, kPa
P_tot_psi = P_tot/kPa_per_psi;
```

```
%Ratios
conc_O2 = pp_O2/P_tot
conc_N2 = pp_N2/P_tot

density_cabin = ((pp_O2*1000)*M_O2 + (pp_N2*1000)*M_N2);   %kg/m^3


%-------------


%CONSUMABLES MASSES

V_tot = V_cabin + 8*cabin_leak_rate;        %total volume of gas for pressurization, excluding r

n_N2 = ((pp_N2*1000)*V_tot)/(R*T);  %kgmoles of N2: Universal Gas Law: n=PV/RT
n_O2 = ((pp_O2*1000)*V_tot)/(R*T);  %kgmoles of O2

m_N2 = n_N2*M_N2;                %total mass of N2, kg
m_O2_pres = n_O2*M_O2;           %mass of O2 for pressurization, kg
m_O2_resp = m_O2_pppd*2*8;       %mass of O2 for respiration, kg
m_O2 = m_O2_pres + m_O2_resp;    %total mass of O2, kg


%-------------


%TRADE STUDY - GASEOUS STORAGE

storage_factor = 3;     %kg of tank plus gas per kg of gas (from Akin #10, slide 12)

m_N2_store = m_N2*storage_factor;    %mass of N2 with tank
m_O2_store = m_O2*storage_factor;    %mass of O2 with tank
m_store = m_N2_store + m_O2_store;   %mass of gases with tanks


%-------------
```

```
%TRADE STUDY - CRYOGENIC STORAGE

storage_factor_c = 1.5;    %kg of tank plus gas per kg of gas (average from Akin #10, slide 12)

m_N2_store_c = m_N2*storage_factor_c;    %mass of N2 with tank
m_O2_store_c = m_O2*storage_factor_c;    %mass of O2 with tank
m_store_c = m_N2_store_c + m_O2_store_c;     %total mass of gases + tanks

heat_vap = 210;   %kJ/kg required for vaporization (from Akin #10, slide 12)

m_N2_initial = m_N2*(V_cabin/V_tot);  %mass of N2 required for initial pressurization, kg
m_O2_initial = m_O2*(V_cabin/V_tot);  %mass of O2 required for initial pressurization, kg

Energy_press = heat_vap*(m_N2_initial + m_O2_initial);   %initial energy required to pressurize

m_N2_replace = m_N2 - m_N2_initial;  %mass of N2 to be replaced over course of mission, kg
m_O2_replace = m_O2 - m_O2_initial;  %mass of O2 to be replaced over course of mission, kg
m_replace = m_N2_replace + m_O2_replace;    %total mass of gas replaced during mission (to leaks

P_vap = heat_vap*m_replace/(t_total_press*3600);     %Constant power needed to vaporize gases, W


%-------------


%TRADE STUDY - LiOH CANISTERS

m_CO2 = m_CO2_pppd*2*(t_total_manned/24);    %total crew CO2 output, kg

m_CO2_per_m_LiOH = 0.75;    %from http://www.extendair.com/lit/lithiumdatasheet.pdf
m_LiOH_per_can = 3.9;       %kg
m_can = 4.6;                %kg
d_int_can = 0.0217;         %diameter of internal passage, m (determined from pixel measurement

m_LiOH = m_CO2/m_CO2_per_m_LiOH;    %total mass of LiOH without canister
cans = ceil(m_LiOH/m_LiOH_per_can);       %number of canisters needed
```

```
m_cans = cans*m_can;                %total mass of LiOH canisters


%-------------


%TRADE STUDY - SUPEROXIDES FOR CO2 REMOVAL AND O2 GENERATION

m_CO2_per_m_KO2 = 0.31;  %from Akin lecture #10, slide 13
m_O2_per_m_KO2 = 0.38;

m_O2_per_m_CO2 = m_O2_per_m_KO2/m_CO2_per_m_KO2;
m_O2_generated = m_CO2*m_O2_per_m_CO2;      %O2 generated by KO2 reactions

if m_O2_generated>m_O2          %mass of stored O2 saved by using KO2 system
    m_O2_saved = m_O2;
else
    m_O2_saved = m_O2_generated;
end

m_KO2 = m_CO2/m_CO2_per_m_KO2;  %mass of KO2 system, without packaging, for mission

KO2_LiOH_compare = (m_KO2 - m_cans) - m_O2_saved   %kg more mass required for KO2 system
%(because this number is positive even without KO2 packaging, LiOH is the more mass-efficient sy


%-------------


%POWER AND MASS TOTALS

%Gas storage + LiOH + fan
%Mass_g_kg = m_store + m_LiOH;
Mass = m_al + (m_O2 + m_N2)  %kg
Power = P_fan;                      %watts
Energy = Power*(t_total_manned*3600);   %Joules
Energy_kWh = Energy/J_p_kWh;             %kilowatt-hours
```

```
%Cryo storage + LiOH + fan
Mass_c_kg = m_store_c + m_LiOH;
Power_c_W = P_fan + P_vap;
Energy_c = Power_c_W*(t_total_manned*3600) + Energy_press;   %Joules
Energy_c_kWh = Energy_c/J_p_kWh;                             %kilowatt-hours


%-------------


%OTHER RESOURCES

%http://cermics.enpc.fr/~delNea/plongee/math_diving/math_diving.html
%http://human.space.edu/old/docs/HSSWG_2003.pdf
```

D.3 Gas Storage (Adam Mirvis)

```
%GAS STORAGE
%This program compares the storage mass and volume of steel and aluminum
%tanks at a range of pressures.

clc

%Universal Gas Law constants
R = 8314;   %universal gas constant, J/kgmole-K
T = 298.15; %standard (room) temperature in K

%Material properties
yield_steel = 690000;   %kPa, high strength steel (A514/A517)      http://en.wikipedia.org/wiki/
yield_al = 400000;
density_steel = 7.8;     %g/cm^3
density_al = 2.7;

%Storage pressure
P_tank = [2500:5000]/0.1450377;   %kPa
```

```
n_N2 = 0.2232;      %moles of N2 to be stored
n_O2 = 0.5652;      %moles of O2 to be stored
m_N2 = 6.2524;      %kg of N2 to be stored
m_O2 = 18.0855;     %kg of O2 to be stored

%Internal volume of tanks
V_N2tank_int = n_N2*R*T./(P_tank*1000);     %m^3
V_O2tank_int = n_O2*R*T./(P_tank*1000);

%internal radius of tanks
radius_int_N2 = ((3/4).*(V_N2tank_int./pi())).^(1/3);    %m
radius_int_O2 = ((3/4).*(V_O2tank_int./pi())).^(1/3);

%thickness of pressure shells - based on http://www.efunda.com/formulae/solid_mechanics/mat_mech
shell_thick_O2_steel = P_tank.*radius_int_O2./(2*yield_steel);
shell_thick_N2_steel = P_tank.*radius_int_N2./(2*yield_steel);
shell_thick_O2_al = P_tank.*radius_int_O2./(2*yield_al);
shell_thick_N2_al = P_tank.*radius_int_N2./(2*yield_al);

%external diameters of tanks
diameter_ext_O2_steel = 2*(radius_int_O2 + shell_thick_O2_steel);
diameter_ext_N2_steel = 2*(radius_int_N2 + shell_thick_N2_steel);
diameter_ext_O2_al = 2*(radius_int_O2 + shell_thick_O2_al);
diameter_ext_N2_al = 2*(radius_int_N2 + shell_thick_N2_al);

%total volume of tanks
V_steel_tot = (4/3)*pi()*(diameter_ext_O2_steel/2).^3 + (4/3)*pi()*(diameter_ext_N2_steel/2).^3;
V_al_tot = (4/3)*pi()*(diameter_ext_O2_al/2).^3 + (4/3)*pi()*(diameter_ext_N2_al/2).^3;

%volume of tank materials
V_steel_O2 = (4/3)*pi()*((diameter_ext_O2_steel/2).^3 - radius_int_O2.^3);
V_steel_N2 = (4/3)*pi()*((diameter_ext_N2_steel/2).^3 - radius_int_N2.^3);
V_steel = V_steel_O2 + V_steel_N2;      %m^3
V_al_O2 = (4/3)*pi()*((diameter_ext_O2_al/2).^3 - radius_int_O2.^3);
V_al_N2 = (4/3)*pi()*((diameter_ext_N2_al/2).^3 - radius_int_N2.^3);
V_al = V_al_O2 + V_al_N2;      %m^3
```

```
%masses of tanks
m_steel = (density_steel*1000)*V_steel;    %kg
m_steel_full = m_steel + m_N2 + m_O2;
m_al = (density_al*1000)*V_al;    %kg
m_al_full = m_al + m_N2 + m_O2;

%length of tanks
l_steel = diameter_ext_O2_steel+diameter_ext_N2_steel;
l_al = diameter_ext_O2_al+diameter_ext_N2_al;

%compare mass, volume and pressure for 3000 psi and 4500 psi tanks
mass_compare = (m_al_full(2001)-m_al_full(501))
vol_compare = (V_al_tot(2001)-V_al_tot(501))
l_compare = (l_al(2001)-l_al(501))

%slope of mass, volume, and length and funcs of pressure
mass_per_MPa_al = mass_compare*1000/(P_tank(2001)-P_tank(501))
vol_per_MPA_al = vol_compare*1000/(P_tank(2001)-P_tank(501))
l_per_MPA_al = l_compare*1000/(P_tank(2001)-P_tank(501))

figure(1)
title('Pressure vs. Total Tank Volume')
xlabel('Pressure (kPa)')
ylabel('Volume (m^3)')
hold on
plot(P_tank,V_steel_tot,'b')
plot(P_tank,V_al_tot,':')
legend('steel','aluminum')

figure(2)
title('Pressure vs. Total Tank Mass')
xlabel('Pressure (kPa)')
ylabel('Mass (kg)')
hold on
plot(P_tank,m_steel_full,'b')
plot(P_tank,m_al_full,':')
```

```
legend('steel','aluminum')

figure(3)
title('Pressure vs. Total Tank Size')
xlabel('Pressure (kPa)')
ylabel('Length (m)')
hold on
plot(P_tank,l_steel,'b')
plot(P_tank,l_al,':')
legend('steel','aluminum')
```

D.4 Window (Adam Mirivs)

```
% Window sizing code
% Adam Mirvis
% 3/25/08

% All human body sizes come from NASA STD-3000 Anthropometry and
% Biomechanics document at http://msis.jsc.nasa.gov/sections/section03.htm
% unless otherwise noted.

% All dimensions are in inches. Origin is the tip of the front endcap.

clear all;
clc;

% ~~~~ V A R I A B L E S ~~~~

    % ~~ BODY DIMENSIONS ~~

    % 1. 95th percentile male
        femur95 = 25.9;      % Buttock-knee length
        knee95 = 24.0;       % Knee height from floor, sitting
        eye95 = 34.2;        % sitting, eye height from seat
```

```
    seat95 = 21.9;       % length of seat (butt to back of knee, "buttock-popliteal")
    thigh95 = 7.5;       % thigh clearance
    elbow95 = 11.7;      % elbow rest height (above seat)
    foot95 = 11.5;       %foot length
    head95 = 8.3;        %length from front to back of head

% 2. 5th percentile female
    femur5 = 19.2;      % Buttock-knee length
    knee5 = 16.4;       % Knee height from floor, sitting
    eye5 = 26.8;        % sitting, eye height from seat
    seat5 = 14.9;       % length of seat (butt to back of knee, "buttock-popliteal")
    thigh5 = 4.4;       % thigh clearance
    elbow5 = 8.2;       % elbow rest height (above seat)
    foot5 = 8.4;        %foot length
    head5 = 6.6;        %length from front to back of head

% ~~ VIEWING ANGLES ~~

    lookdown = 20;  %degrees
    lookup = 5;
    lookside = 45;

% ~~ OTHER VARIABLES ~~

    seat_h = 18;    %height of seat above floor, assuming non-adjustable chair
    floor_h = 8;    %height of floor above bottom of cylinder
    driver_offset = 16;    %offset of center of driver's body to the left of centerline of c
    foot_offset = 8;    %distance of outside of foot from center plane of body (ESTIMATE, NO

    cabin_dia = 71; %cabin diameter
    cap_depth = 10; %from the end of the cylinder to the end of the endcap

% How far the driver can move their head to accomodate turns/terrain
    shiftside5 = 6;
    shiftside95 = 6;
    shiftforward5 = 0;
    shiftforward95 = 0;
```

```
        shiftdown5 = 6;
        shiftdown95 = 6;
        shiftforward5 = 6;
        shiftforward95 = 6;

% ----------------------------------------------------------------------

% ~~~~ C O M P U T A T I O N S ~~~~

% ~~ ENDCAP CURVATURE ~~

    cabin_rad = cabin_dia/2;
    cap_hyp = sqrt( cap_depth^2 + cabin_rad^2 );     %distance from edge of cylinder to center o
    theta1 = atan(cabin_rad/cap_depth);       %angle between vehicle centerline and cap_hyp
    theta2 = pi() - 2*theta1;    %angle from center of cap to edge of cap with vertex at the cen

    cap_rad = cap_hyp*sin(theta1)/sin(theta2);   %radius of curvature of endcap

 % ~~ DISTANCE FOOT EXTENDS INTO ENDCAP ~~

    floor_to_center = cabin_rad - floor_h;     %height from floor to center of cabin
    floor_extend = cap_depth - ( cap_rad - sqrt( cap_rad^2 - floor_to_center^2 ) );  %distance f

    floor_width_half = sqrt( cabin_rad^2 - floor_to_center^2);  %half the width of the floor

    floor_hyp = sqrt( floor_extend^2 + floor_width_half^2 );     %distance from edge of cylinder
    theta1 = atan(floor_width_half/floor_extend);       %angle between floor centerline and floo
    theta2 = pi() - 2*theta1;    %angle from center of cap to edge of cap with vertex at the cen

    floor_rad = floor_hyp*sin(theta1)/sin(theta2);   %radius of curvature of floor in endcap
    foot_to_center = driver_offset + foot_offset;   %distance from vehicle centerline to outside

    foot_extend = floor_extend - ( floor_rad - sqrt( floor_rad^2 - foot_to_center^2) );  %distan

% ~~ HEIGHT OF DRIVER'S EYE ABOVE CABIN CENTERLINE ~~

    center_to_eye95 = floor_h + seat_h + eye95 - cabin_rad;
```

```
    center_to_eye5 = floor_h + seat_h + eye5 - cabin_rad;

% ~~ WINDOW HEIGHT ~~

    %assume smaller drivers sit as far back from the window as larger ones
    cyl_to_eye95 = foot95 + seat95 - head95 - foot_extend;   %distance of driver's eye behind fr

%THIS SOLVE IS WRONG - THE CIRCLE BEING INTERSECTED SHOULD HAVE A RADIUS
%BASED ON HOW FAR IT IS SHIFTED LEFT OR RIGHT (DO 3D)
    %solve for intersections of sight lines with shell
    top = solve('y = tand(90-lookup)*(x-center_to_eye95) - (cyl_to_eye95 + cap_depth)',...
          'y = sqrt(cap_rad^2-x^2) - cap_rad');
    top = eval(top.x(1))   %solve for height of top of window above vehicle centerline

    bottom = solve('y = -tand(90-lookdown)*(x-center_to_eye5) - (cyl_to_eye95 + cap_depth)',...
          'y = sqrt(cap_rad^2-x^2) - cap_rad');
    bottom = eval(bottom.x(2))   %solve for height of bottom of window above vehicle centerline

    height = top - bottom       % height of window

% ~~ AVIONICS CLEARANCE ~~

    center_to_knee = cabin_rad - (thigh95 + seat_h + floor_h);        %distance of knee below ce
    avionics_clearance = center_to_knee + bottom     %clearance below window/above knee for avio

% ~~ DISTANCE FROM KNEE TO SHELL ~~

    cyl_to_knee95 = foot95 - (femur95 - seat95) - foot_extend;      %distance from knee to end o

    center_to_knee_diag = sqrt( (driver_offset + foot_offset)^2 + cyl_to_knee95^2 );     %distan
    cap_knee_depth = cap_depth - ( cap_rad - sqrt( cap_rad^2 - center_to_knee_diag^2 ) );    %de

    knee_depth = cyl_to_knee95 + cap_knee_depth    %distance from knee to shell

% ~~ WINDOW WIDTH (HEIGHT ADJUSTED) ~~

    %radius of shell curvature at top of window
```

```
top_extend = cap_depth - ( cap_rad - sqrt( cap_rad^2 - top^2 ) );  %distance from cylinder t
top_width_half = sqrt( cabin_rad^2 - top^2);  %half the width of the cabin at top of window
top_hyp = sqrt( top_extend^2 + top_width_half^2 );     %distance from edge of cylinder to ti
theta1 = atan(top_width_half/top_extend);       %angle between centerline and top_hyp
theta2 = pi() - 2*theta1;    %angle from center of cap to edge of cap with vertex at the cen
top_rad = top_hyp*sin(theta1)/sin(theta2);   %radius of curvature of shell at the level of t

%radius of shell curvature at bottom of window
bottom_extend = cap_depth - ( cap_rad - sqrt( cap_rad^2 - bottom^2 ) );  %distance from cyli
bottom_width_half = sqrt( cabin_rad^2 - bottom^2);  %half the width of the cabin at bottom o
bottom_hyp = sqrt( bottom_extend^2 + bottom_width_half^2 );     %distance from edge of cylin
theta1 = atan(bottom_width_half/bottom_extend);       %angle between centerline and bottom_h
theta2 = pi() - 2*theta1;    %angle from center of cap to edge of cap with vertex at the cen
bottom_rad = bottom_hyp*sin(theta1)/sin(theta2);   %radius of curvature of shell at the leve

%radius of curvature 1/4 of the way up the window
one_q = bottom + (top-bottom)*0.25
one_q_extend = cap_depth - ( cap_rad - sqrt( cap_rad^2 - one_q^2 ) );  %distance from cylind
one_q_width_half = sqrt( cabin_rad^2 - one_q^2);  %half the width of the cabin at one_q of w
one_q_hyp = sqrt( one_q_extend^2 + one_q_width_half^2 );     %distance from edge of cylinder
theta1 = atan(one_q_width_half/one_q_extend);       %angle between centerline and one_q_hyp
theta2 = pi() - 2*theta1;    %angle from center of cap to edge of cap with vertex at the cen
one_q_rad = one_q_hyp*sin(theta1)/sin(theta2);   %radius of curvature of shell at the level

%radius of shell curvature at middle of window
middle = bottom + (top-bottom)*0.5    %height of middle of window above center
middle_extend = cap_depth - ( cap_rad - sqrt( cap_rad^2 - middle^2 ) );  %distance from cyli
middle_width_half = sqrt( cabin_rad^2 - middle^2);  %half the width of the cabin at middle o
middle_hyp = sqrt( middle_extend^2 + middle_width_half^2 );     %distance from edge of cylin
theta1 = atan(middle_width_half/middle_extend);       %angle between centerline and middle_h
theta2 = pi() - 2*theta1;    %angle from center of cap to edge of cap with vertex at the cen
middle_rad = middle_hyp*sin(theta1)/sin(theta2);   %radius of curvature of shell at the leve

%radius of curvature 3/4 of the way up the window
three_q = bottom + (top-bottom)*0.75
three_q_extend = cap_depth - ( cap_rad - sqrt( cap_rad^2 - three_q^2 ) );  %distance from cy
three_q_width_half = sqrt( cabin_rad^2 - three_q^2);  %half the width of the cabin at three_
```

```
three_q_hyp = sqrt( three_q_extend^2 + three_q_width_half^2 );     %distance from edge of cy
theta1 = atan(three_q_width_half/three_q_extend);       %angle between centerline and three_
theta2 = pi() - 2*theta1;    %angle from center of cap to edge of cap with vertex at the cen
three_q_rad = three_q_hyp*sin(theta1)/sin(theta2);   %radius of curvature of shell at the le

right_turn_eye = driver_offset + shiftside5;   %farthest eye position to the outside
left_turn_eye = driver_offset - shiftside5;    %farthest eye position to the inside
cyl_to_eye_turn = cyl_to_eye95 - shiftforward5;   %closest eye gets to the cylinder

%solve for intersections of left/right sight lines with shell
    %top
left_top = solve('y = -tand(90-lookside)*(x+left_turn_eye) - (cyl_to_eye_turn + cap_depth)',
      'y = sqrt(top_rad^2-x^2) - cap_rad');
left_top = eval(left_top.x(2))

right_top = solve('y = tand(90-lookside)*(x+right_turn_eye) - (cyl_to_eye_turn + cap_depth)'
      'y = sqrt(top_rad^2-x^2) - cap_rad');
right_top = eval(right_top.x(1))

    %bottom
left_bottom = solve('y = -tand(90-lookside)*(x+left_turn_eye) - (cyl_to_eye_turn + cap_depth
      'y = sqrt(bottom_rad^2-x^2) - cap_rad');
left_bottom = eval(left_bottom.x(2))

right_bottom = solve('y = tand(90-lookside)*(x+right_turn_eye) - (cyl_to_eye_turn + cap_dept
      'y = sqrt(bottom_rad^2-x^2) - cap_rad');
right_bottom = eval(right_bottom.x(1))

    %one_q
left_one_q = solve('y = -tand(90-lookside)*(x+left_turn_eye) - (cyl_to_eye_turn + cap_depth)
      'y = sqrt(one_q_rad^2-x^2) - cap_rad');
left_one_q = eval(left_one_q.x(2))

right_one_q = solve('y = tand(90-lookside)*(x+right_turn_eye) - (cyl_to_eye_turn + cap_depth
      'y = sqrt(one_q_rad^2-x^2) - cap_rad');
right_one_q = eval(right_one_q.x(1))
```

```
        %middle
    left_middle = solve('y = -tand(90-lookside)*(x+left_turn_eye) - (cyl_to_eye_turn + cap_depth
          'y = sqrt(middle_rad^2-x^2) - cap_rad');
    left_middle = eval(left_middle.x(2))

    right_middle = solve('y = tand(90-lookside)*(x+right_turn_eye) - (cyl_to_eye_turn + cap_dept
          'y = sqrt(middle_rad^2-x^2) - cap_rad');
    right_middle = eval(right_middle.x(1))

        %three_q
    left_three_q = solve('y = -tand(90-lookside)*(x+left_turn_eye) - (cyl_to_eye_turn + cap_dept
          'y = sqrt(three_q_rad^2-x^2) - cap_rad');
    left_three_q = eval(left_three_q.x(2))

    right_three_q = solve('y = tand(90-lookside)*(x+right_turn_eye) - (cyl_to_eye_turn + cap_dep
          'y = sqrt(three_q_rad^2-x^2) - cap_rad');
    right_three_q = eval(right_three_q.x(1))

% ~~ DISTANCE BETWEEN WINDOW POINTS ON DOME ~~

%    y_left_top = cap_rad - sqrt( cap_rad^2 - left_top^2 - top^2 );              %distances of w
%    y_left_middle = cap_rad - sqrt( cap_rad^2 - left_middle^2 - middle^2 );
%    y_left_bottom = cap_rad - sqrt( cap_rad^2 - left_bottom^2 - bottom^2 );
%    y_right_top = cap_rad - sqrt( cap_rad^2 - right_top^2 - top^2 );
%    y_right_middle = cap_rad - sqrt( cap_rad^2 - right_middle^2 - middle^2 );
%    y_right_bottom = cap_rad - sqrt( cap_rad^2 - right_bottom^2 - bottom^2 );

%    sqrt( (left_bottom-right_bottom)^2 + (y_left_bottom-y_right_bottom)^2 )         %distance b


% TO DO

%- redo window width, design additional side windows
%- get reach data from anthropometry document


X = [-34:1:34];
```

```
Y_left = -tand(90-lookside)*(X+left_turn_eye) - (cyl_to_eye_turn + cap_depth);
Y = sqrt(cap_rad^2-X.^2) - cap_rad;axes()
Y_right = tand(90-lookside)*(X+right_turn_eye) - (cyl_to_eye_turn + cap_depth);
axis square
plot(X,Y)
hold on
plot(X,Y_left)
plot(X,Y_right)

Y_eyes = -(cyl_to_eye_turn + cap_depth)*ones(1,69);
plot(X,Y_eyes)
title('top view - eyes translate on horizontal line')
```

D.5 Terramechanics (Ugonma Onukwubiri)

```
close all
clear all
clc

b  = 0.30; %%wheel width meters
d  = 1.0; %%wheel diameter is 1 meters.
n  = 1.1%1.0;
h1  = .5; %%obstacle height
h2 = .015; %grouser height
nw = 4
gamma= 1.45 * (100)^2; % (g/m^2) soil density upperlimit ->1.45-1.55
l1 = 1.20; %length from front wheel to cg
l2 = 1.24; %length from back wheel to cg
Cb = 1040%0.0176*(100)*(100); %soil/wheel cohesion from Akin's notes in N/m^2
s  = 0.04;  %%wheel slip ratio
kc = 990%1400;    %kg/m^2
kphi =1528000 %.830*(100)*(100);  %kg/m^3
Mu_alpha = 11*(1/100)^2; %%soil adhesion
alpha = asin((d-2*h1)/d);
x  = 0.5*sqrt(d^2-(d^2 - 2*h1)^2);
cf = 0.05;  %%
```

```
K  = 0.018; %coefficient of soil slip in meter
W = 2000*9.8%1.63;
for nw=4:2:8
Ww = (2000*(1.63))/nw  %%Weight on wheel
%for b=0.1:0.005:0.50
    k  = (kc/b) + kphi ;
    z  = ((3*Ww)/(2*b*k*sqrt(d)))^(2/3)
    theta = acos(1 - ((2*z)/d));
    l = theta*(d/2) ;
    phiB = deg2rad(35); %rad
     %Compaction resistance
        Rc = 1/2*(kc + b*kphi)^(-1/3) * ((3*Ww)/(2*sqrt(d)))^(4/3)
     %Rolling resistance
        Rr = Ww*cf
     %Obstacle resistance
        fr = cf ;
        Rof = W*(l1+x)*(Mu_alpha-fr)*(fr*sin(alpha)+cos(alpha))/((cos(alpha) +...
        fr*sin(alpha) - Mu_alpha*sin(alpha))*(h1*(-Mu_alpha + fr) + l1 + l2 +...
        x));
        Ror= W*(l2-x)*(Mu_alpha-fr)*(fr*sin(alpha)+cos(alpha))/(cos(alpha) +...
        fr*sin(alpha) - Mu_alpha*sin(alpha))*(h1*(Mu_alpha - fr) + l1 + l2 + x)
        Ro=min(Rof,Ror);
      %Bulldozzing resistance
        Nc= 0.010; % Terzaghi's soil bearing capacity
        N_g= 0.014; % Terzaghi's soil besring capacity
        %%%%%%%%%%%%%%%%%%%%%%%%%%%%%
        Kc= (Nc-tan(phiB))*(cos(phiB)^2);
        Kg= ((2*N_g/tan(phiB))+1)*(cos(phiB)^2);
        lo= 2*sqrt((d-0.01)*0.01);%z*(tan((45*pi/180)-(phiB/2))^2);
        alph= acos(1-(2*z/d));

        Rb= (b*sin(alph+phiB)*((2*z*Cb*Kc)+((gamma)*(z^2)*Kg))/(2*sin(alph)*cos(phiB)))+...
        + (pi*(lo^2)*(gamma)*((90-(phiB*180/pi))/540))+ (Cb*pi*(lo^2)/180)+...
        Cb*(lo^2)*tan((pi/4)+(phiB/2))
        %%%%%%%%%%%%%%%%%%%%%%%%%%%%
 for Ng=2:2:8
     %Drawbar pull
```

```
        H = ((b*l*Cb*(1+((2*h2)/b))*Ng) + (Ww*tan(phiB)*(1+(.64*(h2/b)*(atan(b/h2))))))...
        *(1-(K/l)*(1-exp((-s*l)/K)))
        for slope=-20:0.1:20
      %Gravitional resistance
              Rg=Ww*sin(deg2rad(slope)); %%2 degree margin of safety..just in case!
              Rt=Rg+Rc+Rb+Rr+Ro
              D=H-Rg-Rc-Rb-Rr-Ro
             plot(slope,D, 'r') ;
            %axis([-20 20 0 600])
            legend('4 wheels')
            grid on ;
            hold on ;
        end
  xlabel('slope') ;
  ylabel('drawbar pull');
  title('drwabar pull vs slope for 4,6 & 8 wheels') ;
 end
end
```

Appendix E

Mock-up

E.1 Mock-up Structure (Ryan Levin)

E.1.1 Development

The mock-up saw many phases over the course of the semester. It began in two forms, a scaled foam block with most of the top half of the tank cut away to show the inside, and a full scale outer shell made of butchers paper.

The foam rover, shown in Figure E.1, is constructed using craft foam and is apporximately 1/12 scale. This model was mainly created to visualize the positioning of the suitports in reference to other interior items.

Figure E.1: Foam Rover

The paper model, shown below in Figure E.2, was built to be as close to full scale as possible. It is constructed using an external wooden frame to hang free floating PVC pipes that would hold the paper in place and give it its cylindrical shape. The paper met the floor at a point where we anticipated the rover floor to be in relation to the top of the rover. With this model, we were able

to use chairs to simulate a driving scenario and also find out that the original requested height of the floor of only six inches would not be enough to allow drivers to enter/exit the chairs.

Figure E.2: Paper Rover

E.1.2 Construction of the Final Iteration of the Mock-up

E.1.2.1 Search for a Shell

Construction of the final design began with finding an appropriate container to match the dimensions of the lunar rover. A water tank was the most desireable because of its inherant shape of being a cylinder. plastic-mart.com had a 71 in x 88 in tank which had two forklift holes around the side. We did not need this tank to hold water so they offered it to us for $500 including shipping, most other companies wanted $1500 for the product and shipping. The holes also worked out because they were on top of the rover due to the orientation of which place it. The tank can be viewed below in Figure E.3.

Figure E.3: Aerial View of the Tank

E.1.2.2 Support for the tank

The next step was to mount the tank and keep it from rolling. It was also brought up to the height of the lunar rover so that the suitports could be fully tested. One option at the time of construction was to build the mock-up directly onto a trailer which would give it easy mobility for long distance travel. This required a trailer and registration for the trailer through the University of Maryland. We met with manager of the University Motor Pool, who told us that all we could do is tell them what we were looking for and they would go about finding an appropriate trailer for us. This would take more time and money than we could afford so this option was abandoned.

The other option was to construct a cradle to seat the tank. There were too many possible configurations to be discusses in this report, but the final design included a series of ribs that would run the length of the tank. In order to keep the tank level and uniformly supported, the ribs would have to support the tank on the same level. There are five corrugations (or insets) in the tank which are evenly spaced, so five ribs were placed to match these corrugations. Each rib, shown below in Figure E.4, is constructed of a frame of 2"x4"s and then sandwiched between two sheets of 15/32" plywood. The plywood matches the contour of the tank while the 2"x4"s support the weight of the tank. The two angled 2"x4"s are tangent to the tank exactly where the floor joists are placed. The overall size of the rib is 62" length by 28" in height by 2.5" in width. The reason for not extending the ribs the entire diameter of the tank is that now we still have the option of transporting the rover via box truck and there will be no risk of the cradle causing problems if the door is only 6 feet wide.

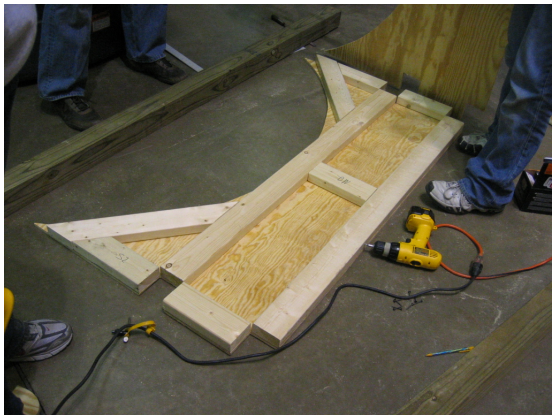

Figure E.4: Rib

The ribs are held together by a combination of 4"x4"s and plywood. 4"x4"s were inserted into the notches of the five ribs and all ribs were aligned into the corrugations in the tank before sheets of plywood were screwed into the ribs, and the 4"x4"s to hold the ribs in place. The idea of this operation can be seen in Figure E.5. The casters shown in E.5 bring the rover up to the height of the lunar rover, and provide eased mobililty, especially over rough surfaces.

Figure E.5: Cradle

E.1.2.3 Flooring

As mentioned earlier, the joists for the floor are supported directly by the frame. All joists run the length of the rover and vary in width to match the contour of the tank. The widest joist is eight inches wide. Except for the center joist, each joist had to be specially cut so that it could sit vertically and tangent to the tank. A wood screw is drilled through each of the joists, through the tank, and into each of the ribs to keep the ribs from sliding down the tank. Extra 2"x4" spacers are required to keep the three center joists from leaning and are affixed on each end of the rover. Finally, six equal square (24"x24") sheets of 15/32" plywood are placed on the joists. Pieces of scrap wood are screwed on underneath each sheet to keep the floorboards from moving side to side. Below is a view of the floor joists and one of the plywood floorboards.

Figure E.6: Floor Joists

E.1.3 Support for the Suitports

The 1/4" polyethylene wall is far too thin to support the weight of a human without collapsing, so it had to be reinforced with wood. A frame of 2"x4"s distribute the weight over the entire face of the tank end which is sufficient to hold the weight of someone sitting on the edge of a suitport as well as the weight of the suitport itself. Pictured below in Figure E.7 is a picure of this support as well as the suitport.

Figure E.7: Support

E.1.4 External Driving Platform

The External Driving Platform on the mock-up can be positioned into two of the four positions of the lunar rover. Unlike the lunar rover, however, all maneuvers with the platform must be done manually by clipping or unclipping the steel cables as opposed to electronically actuated. The steel cables clip to screw eyes which are attached to the Suitport Support. The platform sits 8 inches below the suitport, the upper section is 18 inches wide and the lower section is 28 inches wide. The platform is only one 54 inch long section while the actual rover will have two sections, one for each suitport. Below are pictures of each configuration.

E.1.5 Final Product

E.2 Development of Mock-up Interior (Kanwarpal Singh Chandhok)

Once the exterior of the mock-up was complete, and the tank was securely attached to the support structure, the interior of the cabin was developed. This task began with a list from all sub teams of the interior components that they have in the mock-up design. This included objects inside the cabin and above the floor; including but not limited to:

Figure E.8: External Driving Platform

Figure E.9: Final View

- instrument panel with monitors and computers
- chairs
- toilet
- sink
- water tank
- storage compartments
- storage canisters
- fire extinguisher and first aid kit
- heat exchanger
- cabin and emergency lighting

Items were then scaled down and made into a model of the cabin interior made of foam. This gave an idea of how the cabin would look with everything in place. The next step went into the actual development of a mock-up for each of these objects. The bigger objects, like the toilet, chairs, and instrument panel, were constructed with wood and existing structure (chair back rests). Smaller items were modeled with insulation foam of accurate shape and size. E.2 is a picture of the instrument panel along with the heat exchanger (top of roof), fire extinguisher (left side), and first aid kit (right side); The right side chair is folded down to allow for the bed to be opened.

Figure E.10: Cabin Interior Showing the Instrument Panel

The instrument panel supports were designed and built for the dome end cap and correct knee clearance height. The monitor supports were then cut and installed to allow for the monitors to

be securely mounted onto the instrument panel. There are a total of three monitors, which are all connected to a computer located under the instrument panel. The left monitor displays a sample user interface for the astronauts. The center monitor is connected to a camera located at the back of the rover and points towards the instrument panel. The right monitor shows video clippings from the Apollo missions.

Cabin lighting was also modeled in the mock-up using two eighteen inch fluorescent bulbs that are connected to an external AC outlet. The front window is also marked on the front end cap with the correct location and dimensions. Initially the chairs were kept on the floor at their positions, but after testing a pair of sliding rails was mounted to the driver chair base and the floor to allow the left chair to slide. There is also a bed installed in the mock-up. The passenger seat reclines its back rest and then the bed would fold from the wall on top of the chair. The bed would then open up and allow the astronauts to lie down. A hammock was tested for a comparison between the two sleeping methods. See Figure E.2

Figure E.11: Deployed Hammock Inside the Cabin

The installation of all of these components marked the completeness of the cabin interior and the mock-up was now ready for testing.

E.3 Instructions for Use of the Mock-up Suitport (Adam Mirvis)

E.3.1 Getting Into the Suit

1. Raise and secure the PCS.

2. Remove shoes and the contents of pockets, tuck shirt in, and tape pants around ankles or slip them inside socks. This keeps them from bunching up on ingress.

3. Start in the rover, lying on the flattened seat, feet towards the suit.
4. Slide feet into the suit below the chest strap.
5. Scoot forward and put body weight on heels on the ledge created by the external driving station.
6. Scoot forward until seated on the edge of the hatch. Be careful not to push the suit outward.
7. When lowering body into the suit, hold onto the wooden "actuator" on the left and the metal actuator track on the right, and lower body straight down in one smooth motion.
8. Be careful to get feet all the way to the bottom of the suit – they may need to be adjusted after getting arms in.
9. Slide arms through the straps, with the chest strap in front, and into the sleeves.
10. Pick up the actuator controller on right side and wait for instructions from the assistant inside the mock-up ([pulse/go] [up/down]/stop).
11. After the PCS is all the way down, wait for the assistant to get the top two PLSS hooks in place and instruct to go on EVA.
12. Reach to the sides, at head level, and unlatch the two sliding metal latches.
13. Step straight forward, being careful that the PLSS slides smoothly out of the PCS.
14. Simulate EVA.

E.3.2 Getting Out of the Suit

1. Back up to the rover, checking to make sure PLSS is aligned.
2. Slide the PLSS into the PCS and rest the bottom of the suit back on the block below the suitport.
3. Feel to the left and right at head level for the metal latches. Wiggle and gently push the suit until the latches are aligned, and close them. They may be easier to align one at a time.
4. Pick up the actuator controller, and wait for instructions from the assistant inside the mock-up.
5. Once the PCS is all the way up and has been secured, let go of the controller and slide arms out of sleeves and straps.

6. Reach back into the rover, and grab onto the wooden “actuator” on the left and the metal actuator track on the right.
7. Pull body up and sit on the edge of the suit hatch, with feet against the external platform for stability. Be careful not to push the suit outward.
8. Reach back to the seat and transfer body weight to sitting on the seat. Push at the sides of the seat to slide in further – don’t pull against the PCS.
9. Extract feet.
10. Lower and secure the PCS.

Figure E.12 shows two possible toilet designs for TURTLE. On the left is a self contained toilet, similar to what would be found in an RV or motorboat, and on the right is a toilet that could be incorporated as part of a more complicated water system. As of the publishing of this paper, the numbers referred to in this figure are out of date, but the concepts remain possibilities.

Toilet - Isolated Sewage Tank

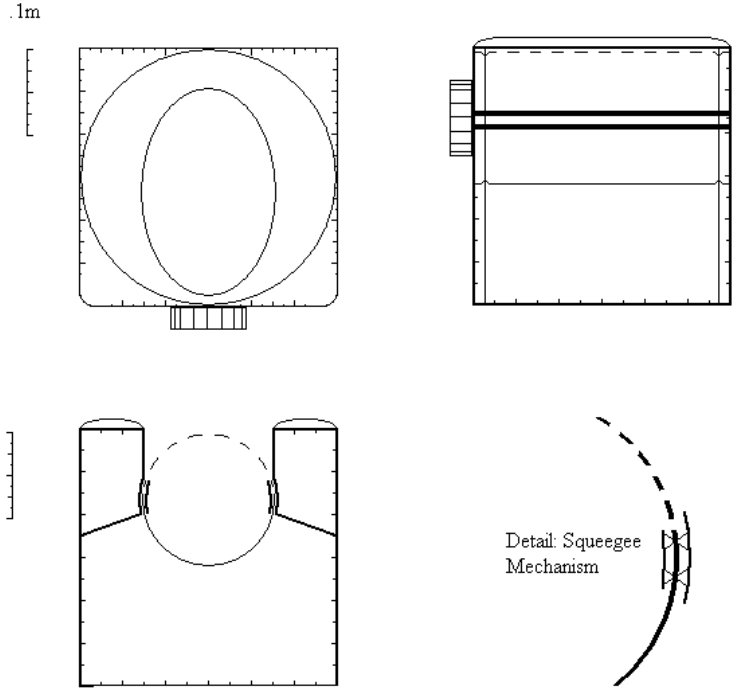

Dimensions: 30cm cube

Since our mission length is short, total waste will come to a volume of approximately .00288 m^3, or 2.88 L. This means that ease of use, not volume, is the primary design constraint. Thus, the seat is designed for comfortable sitting (relatively) as opposed to minimum volume. It's still compact though.

Based on aluminum with a density of 2700 kg /m^3, and a sheet metal volume of .001894 m^3, we get, (accounting for extra fittings,

m = 5.11 kg

Note the rotating half cylinder/squeegee mechanism - "flush" without water, keep odors in.

Toilet - Seat Attachment to Lower Sewage Bag

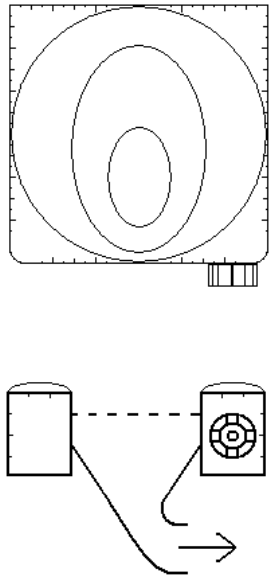

Dimensions: 30 cm sq. on top, 10 cm tall

This is mainly just an attachment to sit on top of the water tank, so it's not much more than a seat with a hole and a pipe fitting on it. Note the rolling shutter to keep pipe closed when not in use.

Based on the same metal properties as the other design, the metal volume is approximately .00109 m^3, and thus,

m = 2.725 kg

Figure E.12: Early Possible Toilet Designs

Appendix F

Outreach (Madeline Kirk)

Table F.1: Student Outreach Involvement

Name	Date	Hours	Event
David Berg	4/26/08	7	Maryland Day
Aaron Cox	3/28/2008	1	Open House
Adam Mirvis	4/26/2008	6.5	Maryland Day
Alek Nacev	4/26/2008	5	Maryland Day - SGT
	2/18/2008	2	Open House
Ali Husain	4/26/2008	4	Maryland Day
	3/7/2008	1	SSL tour group
	3/14/2008	1	WJHS Presentation
Ali-Reza Shishineh	4/26/2008	2	Maryland Day
Brian McCall	3/28/2008	1	Open House
David Gers	5/6/2008	1	Aero Advisory Board Presentation
	4/28/2008	6	Maryland Day (Aero booth)
	2/18/2008	1	Open House
	3/28/2008	3	Open House/Tours
	2/15/2008	1	Presentation and tour for high school students
	4/1/2008	1	Prospective Student Tour
David Mclaren	4/26/2008	2	Maryland Day
	4/4/2008	1	Open House
Andrew Ellsberry	4/13/2008	2	AIAA Campus Tour
	4/26/2008	5	Maryland Day
	4/23/2008	2	Parkland Middle School
	3/7/2008	1	SSL Tour
Enrique Coello	4/26/2008	2.5	Maryland Day
Hasan Oberoi	4/2/2008	2	HS Presentation
Jacob Zwillinger	4/7/2008	1	AIAA Campus Tour
	4/26/2008	3	Maryland Day

James Briscoe	4/26/2008	4	Maryland Day
Jason Laing	4/24/2008 4/26/2008 3/18/2008	0.5 6.5 1	AIAA GBM Presentation Maryland Day North County High School Presentation
Jason Leggett	4/4/2008	1	Open House
Jessica Mayerovitch	4/24/2008 4/18/2008	0.5 1	AIAA GBM Presentation Open House
Joseph Lisee	4/26/2008	3	Maryland Day SSL
Joshua Colver	4/26/2008	1	Maryland Day
KP Chandhok	4/18/2008	1	Open House
Madeline Kirk	4/24/2008 4/26/2008 4/25/2008 2/18/2008 4/4/2008 3/28/2008 3/7/2008 3/14/2008	0.5 7 4 1 1 2 1 1	AIAA GBM Presentation Maryland Day MLK Middle School Open House Open House Open House/SSL Tour SSL tour group WJHS Presentation
Matt Schaffer	4/4/2008	1	Open House
May Lam	4/26/2008	2.5	Maryland Day
Michael Levashov	4/7/2008 4/26/2008 4/23/2008	1 3 2	AIAA Campus Tour Maryland Day Parkland Middle School
Omar Manning	4/26/2008	1.5	Maryland Day
Ryan Levin	5/8/2008 4/4/2008	0.5 2	Aero Banquet Open House
Ryan Murphy	4/24/2008 4/25/2008 4/26/2008	0.5 4.5 7	AIAA GBM Presentation HS Presentation Maryland Day (Aero booth)
Sara Fields	4/26/2008	2.5	Maryland Day
Stephanie Petillo	4/26/2008 2/18/2008	3 1	Maryland Day Open House
Stuart Douglas	4/26/2008	2	Maryland Day
Tiffany Russell	4/2/2008	2	HS Presentation
Thomas Mariano	4/18/2008	1	Open House
Ugonma Onukwubiri	4/2/2008	2	HS Presentation
Zohaib Hasnain	4/26/2008 3/14/2008	1 1	Maryland Day WJHS Presentation
Total Hours		143	

Appendix G

Communications Link Budget (Andrew Ellsberry)

Appendix H

Display Setup Trade Study (Andrew Ellsberry)

Appendix I

Institutional Review Board - Human Testing (Ali Husain)

Bibliography

[1] Celestia 16k moon surface map VT. Online.

[2] Equipment cooling fans. McMaster-Carr Catalog.

[3] Landing site overview. Online.

[4] Lithium hydroxide extendair CO_2 absorbents. Online.

[5] Lunar orbiter: Impact basin geology.

[6] Micrometeoroid protection. Technical Report PD-EC-1107, NASA, http://www.klabs.org/DEI/References/design_guidelines/environment_series/1107.pdf.

[7] Mission overview.

[8] Thermodynamics: Gibbs free energy. Online.

[9] Thin-walled pressure vessels. Online.

[10] Tycho crater.

[11] Apollo 11 preliminary science report. Technical Report NASA-SP-214, NASA, http://www.history.nasa.gov/alsj/a11/as11psr.pdf, 1969.

[12] Apollo 12 preliminary science report. Technical Report NASA-SP-235, NASA, http://www.history.nasa.gov/alsj/a12/as12psr.pdf, 1970.

[13] Apollo 14 preliminary science report. Technical Report NASA-SP-272, NASA, http://www.history.nasa.gov/alsj/a14/as14psr.pdf, 1971.

[14] Apollo 15 preliminary science report. Technical Report NASA-SP-289, NASA, http://www.history.nasa.gov/alsj/a15/as15psr.pdf, 1972.

[15] Apollo 16 preliminary science report. Technical Report NASA-SP-315, NASA, http://www.history.nasa.gov/alsj/a16/as16psr.pdf, 1972.

[16] Apollo 17 preliminary science report. Technical Report NASA-SP-330, NASA, http://www.history.nasa.gov/alsj/a17/as17psr.pdf, 1973.

[17] Lunar orbiter: Impact crater geology. October 2000.

[18] Nuclear power in space. Online, 2003.

[19] Background: Meteoroid and debris models. August 2004.

[20] The vision for space exploration. Technical Report NP-2004-01-334-HQ, NASA, http://www.nasa.gov/mission_pages/constellation/news/index.html, February 2004.

[21] Commonly asked questions about radioisotope batteries – space batteries, July 2005.

[22] *Part 4: Lunar Architecture*. NASA, http://www.nasa.gov/mission_pages/exploration/news/ESAS_report.ht November 2005.

[23] *Part 5: Crew Exploration Vehicle*. NASA, http://www.nasa.gov/mission_pages/exploration/news/ESAS_rep November 2005.

[24] Safe handling of cryogens. Technical report, Harvard College, http://www-safety.seas.harvard.edu/services/cryo_general.html, February 2005.

[25] *Constellation Program Overview*, http://www.nasa.gov/mission_pages/constellation/news/index.html, October 2006.

[26] *In Information Needed to Make Radiation Protection Recommendations for Space Missions Beyond Low-Earth Orbit*, volume 163. National Council on Radiation Protection and Measurements, 2006.

[27] Fecunditatis basin. Online, September 2007.

[28] Kepler. Online, December 2007.

[29] Mars exploration rover mission: Technology. 2007.

[30] Aluminum 6061-t6. Online Database, May 2008.

[31] Celestia 3d space simulator, version 1.5.0. Online, January 2008.

[32] Characteristics of oxide glasses. Online Encyclopedia, 2008.

[33] Cost spreading. Online, May 2008.

[34] How fuel cells work. 2008.

[35] Learning curve calculator. Online, May 2008.

[36] Linear actuators, 2008.

[37] Nectaris basin. Online, February 2008.

[38] Seal master corporation, 2008.

[39] Specification sheets. 2008.

[40] Thomson. Online, March 2008.

[41] David L. Akin. Course overview/design project. August 2007.

[42] David L. Akin. Space life support. October 2007.

[43] Judith Haley Alton. Catalog of apollo lunar surface geological sampling tools and containers. Technical Report NASA-JSC-23454, NASA, http://www.lpi.usra.edu/lunar_resources/documents/LunarSampleToolCatalog.pdf, March 1989.

[44] D. Apostolopoulos. Analytical configuration of wheeled robotic locomotion. Online, April 2001.

[45] A.F. Barghouty. *Optimization of Crew Shielding Requirement in Reactor-Powered Lunar Surface Missions*. Marshall Space Flight Center, Hanover, MD, 2007.

[46] C. F. Beards. *Engineering Vibration Analysis with Application to Control Systems*. Halsted Press, 1996.

[47] M. G. Bekker. *Theory of Land Vehicle: The Mechanics of Vehicle Mobility*. University of Michigan Press, Michigan, 1956.

[48] M. G. Bekker. *Off-The-Road Locomotion*. University of Michigan Press, Michigan, 1960.

[49] Trudy Bell. Moonquakes. Online Magazine, March 2006.

[50] M. Blundell and D. Harty. *The Multibody Systems Approach to Vehicle Dynamics*. Elsevier, 2004.

[51] Jeanette M. Cardamone and Anand Purshottam Kanchager. Method of inhibiting the burning of natural fibers, synthetic fibers, or mixtures thereof, or fabric or yarn composed of natural fibers, synthetic fibers, or mixtures thereof, and products produced by such methods. Online, September 2007. United States Patent 7264637.

[52] D. Chung. Carbon fiber composites. Technical report, 1994.

[53] National Research Council Committee on the Scientific Context for Exploration of the Moon. *The Scientific Context for Exploration of the Moon: Final Report*. The National Academies Press, http://books.nap.edu/openbook.php?record_id=11954&page=1, 2007.

[54] J. Dixon. *The Shock Absorber Handbook*. Society of Automotive Engineers, 1999.

[55] Peter Eckart. *Spaceflight Life Support and Biospherics*. Microcosm Press/Klewer Academic Publishers, 1996.

[56] P. Edwards. Mass-spring-damper systems: The theory, 2008.

[57] Andrew Johnson et al. *LIDAR-based Hazard Avoidance for Safe Landing on Mars*. Jet Propulsion Laboratory, 4800 Oak Grove Drive, Pasadena, CA 91109, USA, 2001.

[58] Brian Pollard et al. *A Millimeter-wave Phased Array Radar for Hazard Detection and Avoidance on Planetary Landers*. Jet Propulsion Laboratory, 4800 Oak Grove Drive, Pasadena, CA 91109, USA, 2002.

[59] Dan Chang et al. *Miniature Coherent Velocimeter and Altimeter (MCVA) for Terminal Descent Control on Lunar and Planetary Landers*. Jet Propulsion Laboratory, 4800 Oak Grove Drive, Pasadena, CA 91109, USA, 2005.

[60] Yang Cheng et al. *Passive Imaging Based Hazard Avoidance for Spacecraft Safe Landing*. Jet Propulsion Laboratory, 4800 Oak Grove Drive, Pasadena, CA 91109, USA, 2001.

[61] D. J. Fox, Jr. G. F. Sykes, and C. T. Herakovich. Space environmental effects on graphite epoxy compressive properties and epoxy tensile properties. Technical Report NASA-TM-89297, July 1987.

[62] Boston Gears. *Theoretical Gear Equations*. http://www.bostongear.com, 2007.

[63] G. Genta. *Motor Vehicle Dynamics - Modeling and Simulation*. World Scientific, 1997.

[64] David Graziosi and Ryan Lee. I-suit advanced spacesuit design and improvements and performance testing. July 2003.

[65] Tom R. Halfhill. Tom's inflation calculator. Online Calculator, May 2008.

[66] B. R. Hawke, D. J. Lawrence, J. J. Gillis, D. T. Blewett, P. G. Lucey, C. A. Peterson, G. A. Smith, P. D. Spudis, and G. J. Taylor. Spectral anomalies in the imbrium region of the moon. http://www.lpi.usra.edu/meetings/lpsc2003/pdf/1545.pdf, March 2003.

[67] K. Hayashida and M. J. Suppanz. Space shuttle orbiter windshield system design and test. Technical Report NASA-CR-112234, NASA, November 1972.

[68] D. J. Heather and S.K. Dunkin. Clementine multispectral analysis of tsiolkovsky crater, lunar farside. March 1999.

[69] Carl T. Herakovich. *Mechanics of Fibrous Composites*. John Wiley & Sons, 1998.

[70] Ken Herkenhoff. Mars exploration rovers project: Microscopic imager. 2003.

[71] Hexcel Corporation. *Hex-Web, Tube-Core Energy Absorption Cylinder*, January 2004.

[72] Stephen J. Hoffman. Advanced eva capabilities: A study for nasa's revolutionary aerospace systems concept program. Technical Report TP-2004-212068, http://ston.jsc.nasa.gov/collections/TRS/_techrep/TP-2004-212068.pdf, 2004.

[73] Michael W. Hyer. *Stress Analysis of Fiber Reinforced Composite Materials*. McGraw-Hill, 1998.

[74] Jean-Bernard ITIER. A380 integrated modular avionics. presentation, 2007.

[75] A. Konradi J.W. Wilson, J. Miller and F.A. Cucinotta. Nasa conference publication 3360. In *Shielding Strategies for Human Space Exploration*, Hampton, VA, 1997. NASA Langley Research Center.

[76] Helen Lane and Dale Schoeller. *Nutrition in Spaceflight and Weightlessness Models*. CRC Press, Boca Raton, 2000.

[77] W.J. Larson and L.K. Pranke, editors. *Human Spaceflight: Mission Analysis and Design*. McGraw-Hill, New York, 1999.

[78] S. L. Lawson, A. P. Rodger, B. G. Henderson, S. C. Bender, and P. G. Lucey. Multispectral thermal image observations of the moon during total eclipse. http://www.lpi.usra.edu/meetings/lpsc2003/pdf/1761.pdf, March 2003. Lunar and Planetary Institute.

[79] Howard Lovatt. In-wheel motor for solar-powered electric vehicles: technical details. 2007.

[80] Donald A. Morrison and D. Ben J. Bussey. The apollo and korolev basins and the stratigraphy of the lunar crust. http://www.lpi.usra.edu/meetings/lpsc97/, March 1997.

[81] Francis Cucinotta Myung-Hee Kim and John Wilson. A temporal forecast of radiation environments for future space exploration missions. *Radiat Environ Biophys*, 46:95–100, 2007.

[82] NASA. *NASA-STD-3000: Man-Systems Integration Standards*. NASA, http://msis.jsc.nasa.gov/, 1995.

[83] NASA, http://ceh.nasa.gov/webhelpfiles/Cost_Estimating_Handbook_NASA_2004.htm. *Cost Estimating Handbook*, 2004.

[84] NASA. *NASA-STD-(I)-5001: Structural Design and Test Factors of Safety for Spaceflight Hardware.* NASA, http://standards.nasa.gov/released/NASA/NASA_STD_I_5001A_09_12_06.pdf, 2006.

[85] Clive R. Neal. The importance of establishing a global lunar seismic network. 2005.

[86] Human Energy Requirements: Report of a Joint FAO/WHO/UNU Expert Consultation. In food and nutrition technical report series, 2001.

[87] Joseph Ogando. The right stuff. *Design News Magazine*, 1994.

[88] Oliver Montenbruck and Eberhard Gill. *Satellite Orbits: Models, Methods and Applications.* Springer, 2000.

[89] Richard W. Orloff. Apollo 15 - the ninth mission: The fourth lunar landing. Technical Report NASA-SP-4029, NASA, http://history.nasa.gov/SP-4029/Apollo_15a_Summary.htm, September 2004.

[90] Jr. Philip Culbertson. Docking fixture and mechanism for a protective suit. Technical report.

[91] H. Rahnejat, M. Ebrahimi, and R. Whalley. *Multi-Body Dynamics: Monitoring and Simulation Techniques - II.* Professional Engineering Publishing Limited, 2000.

[92] R. Rajamani. *Vehicle Dynamics and Control.* Springer, 2006.

[93] Honeybee Robotics. Rat - rock abrasion tool. Online, 2003.

[94] Fred Schubert. Ideal anti-reflection coating. Technical report, Rensselaer Polytechnic Institute, 2007.

[95] David Smith, Maria Zuber, Mark Torrence, Jan McGarry, and Michael Pearlman. Laser ranging to the lunar reconnaissance orbiter (lro). October 2006.

[96] Paul D. Spudis and D. Ben J. Bussey. *Clementine Explores the Moon.* Lunar and Planetary Institute, http://www.lpi.usra.edu/publications/slidesets/clem2nd/clementine_index.shtml, 2 edition.

[97] Anthony Stentz. Optimal and efficient path planning for partially-known environments, May 1994.

[98] Thomas A. Sullivan. Catalog of apollo experiment operations. Technical Report NASA-RP-1317, Johnson Space Center, http://ares.jsc.nasa.gov/HumanExplore/Exploration/EXLibrary/docs/ApolloCat/apollo.htm, August 1993.

[99] T. Takata. Spectral analysis of volcanic features in aitken crater on lunar farside. http://www.lpi.usra.edu/meetings/LPSC98/pdf/1598.pdf, March 1998.

[100] Robert W. Thompson and Jr. Angelo V. Publiesse. *O-ring Closure Assembly.* UOP, Inc., http://books.google.com/patents?id=QI8tAAAAEBAJ&pg=PA5&lpg=PA5&dq=O-Ring+closure+assembly+4739899&source=web&ots=svaRPV9_oD&sig=oaOFBmqGrAhqouc8jrJPjeiBSRs April 1988.

[101] Stephen W. Tsai. *Composites Design.* Think Composites, http://composite.about.com/od/referencematerials/l/blnotes.htm#3, May 1988.

[102] United Launch Alliance, http://www.ulalaunch.com/docs/product_sheet/DeltaIVPayloadPlannersGuide200 *Delta IV Payload Planners Guide*, 2007.

[103] Mark Wade. Shuttle emu.

[104] Powell M.R. Waligora, J.M. and W.T Norfleet. The abaroferic hypothesis: a mechanism for reduction in risk of decompression sickness in microgravity environment. *Aviation, Space, and Environmental Medicine*, (64: 421).

[105] J. Y. Wong. *Theory of Ground Vehicle.* John Wiley & Sons, New York, 1994.

[106] Bill Wood. Technical Report NASA-JSC-09423, NASA, http://history.nasa.gov/apsr/Apollopt5-2.pdf, April 1975.

[107] Chuck Wood. Fertility central. *LPOD: Lunar Photo of the Day*, October 2004.

[108] Chuck Wood. Plato changes? *LPOD: Lunar Photo of the Day*, 2006.

[109] *AFDX Protocol Tutorial.* Condor Engineering Inc., Santa Barbara, CA 93101, 2005.

[110] *Passively Imaged, Multi-Cue HDA for Safe Landing.* http://marstech.jpl.nasa.gov, 2008.

[111] Warren C. Young. *Roark's Formulas for Stress & Strain.* McGraw Hill, 1989.